(NASA-TM-X-58190) CONTROL OF THERMAL BALANCE BY A LIQUID CIRCULATING GARMENT BASED ON A MATHEMATICAL REPRESENTATION OF THE HUMAN THERMOREGULATORY SYSTEM Ph.D. Thesis - California Univ., Berkeley (NASA) 63/54 20587

N77-19750
HC A24
MF A01
Unclas

JSC-11579

NASA TECHNICAL MEMORANDUM

NASA TM X-58190
October 1976

NASA

CONTROL OF THERMAL BALANCE BY A LIQUID CIRCULATING GARMENT BASED ON A MATHEMATICAL REPRESENTATION OF THE HUMAN THERMOREGULATORY SYSTEM

A Thesis Presented to the
Faculty of the Graduate Division of the
University of California at Berkeley
in Partial Fulfillment of the
Requirements for the Degree of
Doctor of Philosophy in Physiology

MAR 1977
RECEIVED
NASA STI FACILITY
INPUT BRANCH

NATIONAL AERONAUTICS AND SPACE ADMINISTRATION

LYNDON B. JOHNSON SPACE CENTER

HOUSTON, TEXAS 77058

1. Report No. NASA TM X-58190	2. Government Accession No.	3. Recipient's Catalog No.
4. Title and Subtitle CONTROL OF THERMAL BALANCE BY A LIQUID CIRCULATING GARMENT BASED ON A MATHEMATICAL REPRESENTATION OF THE HUMAN THERMOREGULATORY SYSTEM		5. Report Date October 1976 6. Performing Organization Code
7. Author(s) Lawrence H. Kuznetz		8. Performing Organization Report No JSC-11579
9. Performing Organization Name and Address Lyndon B. Johnson Space Center Houston, Texas 77058		10. Work Unit No. 986-15-KX-00-72 11 Contract or Grant No.
12. Sponsoring Agency Name and Address National Aeronautics and Space Administration Washington, D.C. 20546		13. Type of Report and Period Covered Technical Memorandum 14. Sponsoring Agency Code
15. Supplementary Notes		

16. Abstract

Test data and a mathematical model of the human thermoregulatory system were used to investigate control of thermal balance by means of a liquid circulating garment (LCG). The test data were derived from five series of experiments in which environmental and metabolic conditions were varied parametrically as a function of several independent variables, including LCG flowrate, LCG inlet temperature, net environmental heat exchange, surrounding gas ventilation rate, ambient pressure, metabolic rate, and subjective/obligatory cooling control. The resultant data were used to relate skin temperature to LCG water temperature and flowrate, to assess a thermal comfort band, to demonstrate the relationship between metabolic rate and LCG heat dissipation, and so forth. The usefulness of the mathematical model as a tool for data interpretation and for generation of trends and relationships among the various physiological parameters was also investigated and verified. Six conclusions are drawn.

17. Key Words (Suggested by Author(s))
Metabolism
Energy Levels
Liquid-Cooled Garment
Human Factors Engineering
Human Tolerances
Mathematical Models

18. Distribution Statement
STAR Subject Category:
54 (Man/System Technology and Life Support)

19. Security Classif (of this report)	20. Security Classif (of this page)	21 No of Pages	22 Price*
Unclassified	Unclassified	561	$13.50

*For sale by the National Technical Information Service, Springfield, Virginia 22151

NASA JSC

JSC Form 1424 (Rev Jul 74)

NASA TM X-58190

CONTROL OF THERMAL BALANCE BY A LIQUID CIRCULATING GARMENT BASED ON A MATHEMATICAL REPRESENTATION OF THE HUMAN THERMOREGULATORY SYSTEM

Lawrence H. Kuznetz
Lyndon B. Johnson Space Center
Houston, Texas 77058

CONTROL OF THERMAL BALANCE BY A LIQUID CIRCULATING GARMENT BASED ON A MATHEMATICAL REPRESENTATION OF THE HUMAN THERMOREGULATORY SYSTEM

Approved: Nello Pace
Lawrence Fatt
Robert Macey

Committee in charge

Lawrence D. Kingsley

CONTENTS

Section		Page
1	INTRODUCTION	1-1
	HISTORICAL DEVELOPMENT AND USE OF THE LCG	1-4
	HISTORICAL DEVELOPMENT AND USE OF THE MATHEMATICAL MODEL	1-11
	General Purpose	1-17
2	MATERIALS AND METHODS	2-1
	GENERAL	2-1
	FACILITIES, SUBJECTS, AND EQUIPMENT	2-2
	LIQUID CONDITIONING GARMENT	2-5
	TEST PROGRAM	2-6
	Series A	2-8
	Series B	2-10
	Series C	2-12
	Series D	2-14
	Series E	2-19
	INSTRUMENTATION, COMPUTATIONS, AND DATA MANAGEMENT	2-21
	MATHEMATICAL MODEL	2-27
	Active Thermoregulatory Control System	2-30
	Implementation of the Model and Generation of Trends	2-33
3	RESULTS	3-1
	SERIES A	3-1
	Heat Balance	3-1
	Transient Results	3-6
	LCG Heat Removal	3-7
	Sweating and Evaporative Heat Loss	3-12
	Skin Temperature, Rectal Temperature and Total Body Heat Storage	3-17
	Discussion of Errors	3-28
	SERIES B	3-33
	Heat Balance	3-33
	LCG Heat Removal	3-36
	Sweating and Evaporation Heat Loss	3-39
	Discussion of Errors	3-43
	SERIES C	3-47
	Heat Balance	3-48
	Transient Results	3-50
	LCG Heat Removal	3-52
	Sweating and Evaporation Heat Loss	3-55
	Skin Temperature, Tympanic Temperature, and Total Body Heat Storage	3-57

Section Page

SERIES D 3-66
Heat Balance 3-67
Transient Results 3-69
Steady-State Results 3-80

SERIES E 3-96

4 DISCUSSION 4-1

COMFORT CORRELATIONS 4-1
The Effects of the LCG on Thermal Comfort and Sweating 4-13
The Mathematical Model as an Index of Heat Strain 4-16
Accuracy of the Mathematical Model 4-24
Additional Model Development 4-27
Additional Applications of the Model 4-33

5 SUMMARY 5-1

6 BIBLIOGRAPHY 6-1

APPENDIX A — LEADING PARTICULARS OF THE APOLLO A7L SUIT, THE APOLLO LCG, AND TEST INSTRUMENTATION AND EQUIPMENT A-1

APPENDIX B — TECHNICAL DESCRIPTION OF THE MATHEMATICAL MODEL (80, 83, 125) B-1

APPENDIX C — PHYSIOLOGICAL RELATIONSHIPS AND EQUATIONS C-1

APPENDIX D — RAW DATA D-1

APPENDIX E — APOLLO EXPERIENCE REPORT AND LUNAR SURFACE MISSION RESULTS E-1

APPENDIX F — FORMULATION OF THE NEW MATHEMATICAL MODEL F-1

TABLES

Table		Page
3-1	SERIES A - CALCULATED DATA AND HEAT BALANCE (STEADY STATE) . . .	3-105
3-2	SERIES B - CALCULATED DATA AND HEAT BALANCE (STEADY STATE) . . .	3-137
3-3	SERIES C - CALCULATED DATA AND HEAT BALANCE	3-154
3-4	SERIES D - CALCULATED DATA AND HEAT BALANCE	3-182
3-5	STEADY-STATE HEAD CORE AND MEAN SKIN TEMPERATURES	3-212
3-6	COMPARISON OF REAL TIME MODEL PREDICTIONS WITH ACTUAL POST-EVA RESULTS	3-248
4-1	COMPARISON OF PREDICTED AND ACTUAL THERMAL DATA - SEA LEVEL AND ALTITUDE	4-66

FIGURES

Figure		Page
1-1	Responses of the human thermoregulatory system	1-19
2-1	Ventilation flow paths in the Apollo A7L suit	2-37
2-2	The total body heat balance equation	2-38
2-3	PLSS oxygen and water loop flowpaths	2-39
2-4	Apollo extravehicular mobility unit (EMU)	2-40
2-5	Liquid cooled undergarment	
	(a) Inside-out view showing cooling tubes	2-41
	(b) Full view	2-41
	(c) Close-up view of tube distribution	2-41
2-6	Live data pathways and flight monitoring and control system for Apollo missions	2-42
2-7	Lunar traverse paths for Apollo 15	2-43
2-8	Typical placement of skin temperature thermocouples	2-44
2-9	Discrete temperature distribution of mathematical model . .	2-45
2-10	Heat balance for internal body layers	2-45
2-11	The controlling system of the mathematical model	2-46
3-1	Predicted and actual body temperatures and heat storage vs time for cold LCG inlet temperatures and low metabolic rates (test 7)	3-106
3-2	Predicted and actual body temperatures and heat storage vs time for cold LCG inlet temperatures and high metabolic rates (test 11)	3-108
3-3	Predicted and actual body temperatures and heat vs time for moderate LCG inlet temperatures and low metabolic rates (test 4)	3-110
3-4	Predicted and actual body temperatures and heat storage vs time for moderate LCG inlet temperatures and high metabolic rates (test 6)	3-112

Figure		Page
3-5	Predicted and actual steady-state LCG heat removal vs metabolic rate, for various LCG inlet temperatures	3-114
3-6	LCG heat transfer coefficient vs LCG inlet temperature . . .	3-115
3-7	Ratio of LCG heat removal rate to metabolic rate vs LCG inlet temperature	3-116
3-8	Predicted and actual steady-state evaporative heat loss rate by active sweat vs metabolic rate, for various LCG inlet temperatures	3-118
3-9	Metabolic rate at which the onset of sweating occurs vs LCG inlet temperature	3-119
3-10	Ratio of evaporative heat loss rate by active sweat to metabolic rate vs LCG inlet temperature	3-120
3-11	Predicted and actual steady-state total evaporative heat loss rate vs metabolic rate, for various LCG inlet temperatures	3-122
3-12	Ratio of total evaporative heat loss rate to metabolic rate vs LCG inlet temperature	3-124
3-13	Rectal temperature and mean skin temperature vs LCG inlet temperature	3-126
3-14	Predicted and actual steady-state rectal and mean skin temperature vs metabolic rate for cool, moderate, and warm LCG inlet temperatures	3-128
3-15	Predicted and actual steady-state sweat rate and evaporative heat loss rate due to sweating vs mean skin temperature for LCG inlet temperatures of 7° and 16° C . .	3-130
3-16	Predicted and actual steady-state sweat rate and evaporative heat loss rate due to sweating vs rectal temperature for LCG inlet temperatures of 7° and 16° C . .	3-131
3-17a	Predicted and actual steady-state sweat rate and total evaporative heat loss due to sweating vs change in mean skin temperature	3-132
3-17b	Predicted and actual steady-state sweat rate and total evaporative heat loss due to sweating vs change in rectal temperature	3-133

Figure		Page
3-18	Actual and predicted steady-state active sweat rate and evaporative heat loss rate due to active sweating vs total body heat storage	3-134
3-19	Predicted and actual total body heat storage vs metabolic rate for steady-state conditions during test series A . . .	3-136
3-20	Predicted and actual steady-state LCG heat removal vs metabolic rate, for various LCG inlet temperatures	3-138
3-21	Ratio of LCG heat removal rate to metabolic rate vs LCG inlet temperature	3-140
3-22	Predicted total body heat storage vs metabolic rate for steady-state conditions during Series B	3-142
3-23	Predicted and actual steady-state evaporative heat loss rate by active sweat vs metabolic rate, for various LCG inlet temperatures	3-144
3-24	Active sweat rate and evaporative heat loss rate due to active sweat vs LCG inlet temperature for moderate metabolic rates (410 watts)	3-146
3-25	Ratio of evaporative heat loss rate by active sweat to metabolic rate vs LCG inlet temperature	3-147
3-26	Predicted and actual steady-state total evaporative heat loss rate vs metabolic rate, for various LCG inlet temperatures	3-148
3-27	Ratio of total evaporative heat loss rate to metabolic rate vs LCG inlet temperature	3-150
3-28a	Regression curve fit to test data for LCG heat removal rate and total evaporative heat loss rate vs metabolic rate	3-152
3-28b	Model error ($= \frac{\text{Test data-model predictions}}{\text{Metabolic rate}}$) vs metabolic rate for LCG and total evaporative heat loss rate predictions	3-152
3-29	Metabolic rate profile for test sequences 1 to 8	3-155
3-30	Metabolic rate profile for test sequences 9 and 10	3-156
3-31a	Head core (tympanic) temperature (upper curve) and mean skin temperature (lower curve) vs time for test sequences 1 to 8	3-157

Figure		Page
3-31b	Total body heat storage vs time for test sequences 1 to 8	3-157
3-32a	Head core (tympanic) temperature (upper curve) and mean skin temperature (lower curve) vs time for test sequences 9 and 10	3-158
3-32b	Total body heat storage vs time for test sequences 9 and 10	3-158
3-33	Predicted and actual steady-state LCG heat removal vs metabolic rate, for various LCG water flowrates	3-159
3-34	Ratio of LCG heat removal rate to metabolic rate vs LCG water flowrate	3-160
3-35	Predicted and actual total body heat storage vs metabolic rate for steady-state conditions during Series C	3-162
3-36	LCG heat transfer coefficient vs LCG water flowrate	3-164
3-37	Predicted and actual steady-state evaporative heat loss rate by active sweat vs metabolic rate, for various LCG water flowrates	3-165
3-38	Ratio of evaporative heat loss rate by active sweat to metabolic rate vs LCG water flowrate	3-166
3-39	Predicted and actual steady-state total evaporative heat loss rate vs metabolic rate, for various LCG water flowrates	3-167
3-40	Ratio of total evaporative heat loss rate to metabolic rate vs LCG water flowrate	3-168
3-41	Tympanic (head core) and mean skin temperature vs LCG water flowrate	3-170
3-42	Predicted and actual steady-state tympanic (head core) and mean skin temperature vs metabolic rate for various LCG water flowrates	3-172
3-43	Predicted and actual steady-state sweat rate and evaporative heat loss rate due to sweating vs mean skin temperature for various LCG water flowrates	3-174
3-44	Predicted and actual steady-state sweat rate and evaporative heat loss rate due to sweating vs tympanic (head core) temperature for various LCG water flowrates	3-175

Figure		Page
3-45	Predicted and actual steady-state sweat rate and evaporative heat loss rate due to sweating vs change in mean skin temperature for various LCG water flowrates	3-176
3-46	Predicted and actual steady-state sweat rate and evaporative heat loss rate due to sweating vs change in tympanic (head core) temperature for various LCG water flowrates	3-178
3-47	Actual and predicted steady-state sweat rate and evaporative heat loss rate due to active sweating vs total body heat storage	3-180
3-48	Metabolic rate profile for test 1	3-183
3-49	Metabolic rate profile for test 2	3-184
3-50	Metabolic rate profile for test 3	3-185
3-51	Metabolic rate profile for test 4	3-186
3-52	Metabolic rate profile for test 5	3-187
3-53	Metabolic rate profile for test 6	3-188
3-54	Metabolic rate profile for test 7	3-189
3-55a	Head core (tympanic) temperature (upper curve) and mean skin temperature (lower curve) vs time for test 1	3-190
3-55b	Total body heat storage vs time for test 1	3-190
3-56a	Head core (tympanic) temperature (upper curve) and mean skin temperature (lower curve) vs time for test 2	3-191
3-56b	Total body heat storage vs time for test 2	3-191
3-57a	Head core (tympanic) temperature (upper curve) and mean skin temperature (lower curve) vs time for test 3	3-192
3-57b	Total body heat storage vs time for test 3	3-192
3-58a	Head core (tympanic) temperature (upper curve) and mean skin temperature (lower curve) vs time for test 4	3-193
3-58b	Total body heat storage vs time for test 4	3-193
3-59a	Head core (tympanic) temperature (upper curve) and mean skin temperature (lower curve) vs time for test 5	3-194

Figure		Page
3-59b	Total body heat storage vs time for test 5	3-194
3-60a	Head core (tympanic) temperature (upper curve) and mean skin temperature (lower curve) vs time for test 6	3-195
3-60b	Total body heat storage vs time for test 6	3-195
3-61a	Head core (tympanic) temperature (upper curve) and mean skin temperature (lower curve) vs time for test 7	3-196
3-61b	Total body heat storage vs time for test 7	3-196
3-62a	LCG inlet temperature selected by test subject vs time for test 1	3-197
3-62b	Total body heat storage rate vs time for test 1	3-197
3-62c	LCG heat removal rate vs time for test 1	3-197
3-63a	LCG inlet temperature selected by test subject vs time for test 2	3-198
3-63b	Total body heat storage rate vs time for test 2	3-198
3-63c	LCG heat removal rate vs time for test 2	3-198
3-64a	LCG inlet temperature selected by test subject vs time for test 3	3-199
3-64b	Total body heat storage rate vs time for test 3	3-199
3-64c	LCG heat removal rate vs time for test 3	3-199
3-65a	LCG inlet temperature selected by test subject vs time for test 4	3-200
3-65b	Total body heat storage rate vs time for test 4	3-200
3-65c	LCG heat removal rate vs time for test 4	3-200
3-66a	LCG inlet temperature selected by test subject vs time for test 5	3-201
3-66b	Total body heat storage rate vs time for test 5	3-201
3-66c	LCG heat removal rate vs time for test 5	3-201
3-67a	LCG inlet temperature selected by test subject vs time for test 6	3-202

Figure		Page
3-67b	Total body heat storage rate vs time for test 6	3-202
3-67c	LCG heat removal rate vs time for test 6	3-202
3-68a	LCG inlet temperature selected by test subject vs time for test 7	3-203
3-68b	Total body heat storage rate vs time for test 7	3-203
3-68c	LCG heat storage rate vs time for test 7	3-203
3-69a	Total evaporative heat loss rate vs time for test 1	3-204
3-69b	Evaporative heat loss rate due to active sweat vs time for test 1	3-204
3-70a	Total evaporative heat loss rate vs time for test 2	3-205
3-70b	Evaporative heat loss rate due to active sweat vs time for test 2	3-205
3-71a	Total evaporative heat loss rate vs time for test 3	3-206
3-71b	Evaporative heat loss rate due to active sweat vs time for test 3	3-206
3-72a	Total evaporative heat loss rate vs time for test 4	3-207
3-72b	Evaporative heat loss rate due to active sweat vs time for test 4	3-207
3-73a	Total evaporative heat loss rate vs time for test 5	3-208
3-73b	Evaporative heat loss rate due to active sweat vs time for test 5	3-208
3-74a	Total evaporative heat loss rate vs time for test 6	3-209
3-74b	Evaporative heat loss rate due to active sweat vs time for test 6	3-209
3-75a	Total evaporative heat loss rate vs time for test 7	3-210
3-75b	Evaporative heat loss rate due to active sweat vs time for test 7	3-210
3-76	Metabolic rate, heat removal, and body heat storage rate for behavioral response to body heat storage and anticipatory behavioral response	3-211

Figure		Page
3-77	LCG heat transfer coefficient vs LCG inlet temperature	3-213
3-78	Predicted and actual steady-state LCG and total evaporative heat removal rates vs metabolic rate for hot, cold, and neutral environments and cold LCG inlet temperatures (7° to 9° C)	3-214
3-79	Predicted and actual steady-state LCG and total evaporative heat removal rates vs metabolic rate for hot, cold, and neutral environments and moderate LCG inlet temperatures (13° to 16° C)	3-216
3-80a	Predicted and actual steady-state LCG heat removal rate vs metabolic rate for hot, cold, and neutral environments, and warm LCG inlet temperatures (19° to 22° C)	3-218
3-80b	Predicted and actual steady-state total evaporative heat loss rate vs metabolic rate, for hot, cold, and neutral environments and warm LCG inlet temperatures (19° to 22° C)	3-218
3-81	Steady-state LCG and total evaporative heat removal rates vs net environmental heat gain, for constant metabolic rates and LCG inlet temperatures	3-220
3-82	Predicted change in LCG and total evaporative heat removal rates vs net environmental heat gain or loss, for constant metabolic rates and LCG inlet temperatures	3-222
3-83	Predicted and actual steady-state LCG heat removal, normalized to zero environmental effects, vs metabolic rate, for various LCG inlet temperatures	3-224
3-84	Ratio of LCG heat removal rate to metabolic rate vs LCG inlet temperature	3-225
3-85	Predicted and actual steady-state total evaporative heat loss rate, normalized to zero environmental effects, vs metabolic rate, for various LCG inlet temperatures	3-226
3-86	Ratio of total evaporative heat loss rate to metabolic rate vs LCG inlet temperature	3-227
3-87	Predicted and actual steady-state evaporative heat loss rate by active sweat, normalized to zero environmental effects, vs metabolic rate, for various LCG inlet temperatures	3-228

Figure		Page
3-88	Ratio of evaporative heat loss rate by active ·t to metabolic rate vs LCG inlet temperature	3-229
3-89a	Regression curve fit to test data for LCG heat removal rate vs metabolic rate	3-230
3-89b	Regression curve fit to test data for total evaporative heat loss rate vs metabolic rate	3-230
3-89c	Model error ($= \frac{\text{Test data - model predictions}}{\text{Metabolic rate}}$) vs metabolic rate for LCG and total evaporative heat loss rate predictions	3-230
3-90	Total body heat storage vs metabolic rate for steady-state conditions during Series D	3-232
3-91a	Predicted steady-state LCG heat removal rate, heat storage, and comfort band vs metabolic rate, for neutral environments (0 watts into suit) and various LCG inlet temperatures	3-234
3-91b	Predicted steady-state total evaporative heat loss rate, heat storage, and comfort band vs metabolic rate, for neutral environments (0 watts into suit) and various LCG inlet temperatures	3-235
3-92a	Predicted steady-state LCG heat removal rate, heat storage, and comfort band vs metabolic rate, for cold environments (72 watts out of suit) and various LCG inlet temperatures	3-236
3-92b	Predicted steady-state total evaporative heat loss rate, heat storage, and comfort band vs metabolic rate, for cold environments (72 watts out of suit) and various LCG inlet temperatures	3-237
3-93a	Predicted steady-state LCG heat removal rate, heat storage, and comfort band vs metabolic rate, for hot environments (126 watts into suit) and various LCG inlet temperatures	3-238
3-93b	Predicted steady-state total evaporative heat loss rate, heat storage, and comfort band vs metabolic rate, for hot environments (126 watts into suit) and various LCG inlet temperatures	3-239

Figure		Page
3-94	Predicted and actual steady-state LCG inlet temperatures selected for comfort vs metabolic rate, for net environmental heat exchange between 72 watts out of suit to 137 watts into suit	3-240
3-95	Predicted and actual steady-state LCG heat removal at comfort vs metabolic rate for net environmental heat exchange between 72 watts out of suit to 137 watts into suit	3-242
3-96	Predicted and actual steady-state total evaporative heat loss rate at comfort vs metabolic rate for net environmental heat exchange between 72 watts out of suit to 137 watts into suit	3-244
3-97	Real-time (live) Apollo EVA data, superimposed on a typical RTCC parametric curve of LCG heat removal rate vs metabolic rate for neutral environments (zero environmental heat exchange)	3-246
4-1	LCG inlet temperatures selected for comfort vs metabolic rate	4-42
4-2	LCG heat removal rate at comfort vs metabolic rate	4-44
4-3	Total evaporative heat loss rate at comfort vs metabolic rate	4-46
4-4	Active sweat rate at comfort vs metabolic rate	4-48
4-5	LCG water flowrate selected for comfort vs metabolic rate	4-50
4-6	Effect of LCG heat transfer coefficient upon LCG inlet temperature selected at comfort	4-52
4-7	Rectal temperature (upper curve) and zones of mean skin temperature at comfort (lower curve) vs metabolic rate, with LCG cooling	4-54
4-8	Comfort band with performance and tolerance limits	4-56
4-9	Active sweat rate vs metabolic rate for comfort, performance impairment and tolerance limits	4-57
4-10	Predicted LCG heating required for comfort at a metabolic rate of 200 watts in cold environment	4-58
4-11	Investigation study of the effects of head cooling	4-60

Figure		Page
4-12	Study of the thermoregulatory effects of the LCG upon skin bloodflow, shivering, and sweating	4-62
4-13	Predicted body heat storage vs time for average subjects running one mile every eight minutes in a hot, humid environment	4-63
4-14	Time required for skin temperature to reach pain threshold of 45° C vs intensity of incident environmental heat flux for various garment insulation properties	4-64
4-15	Effect of acute hypoxia (30 minutes) on the respiratory minute volume (100)	4-67
4-16	Steady-state body heat storage vs free air velocity in a zero-gravity environment	4-68

1. INTRODUCTION

The spiraling growth of technology over the last several decades has exposed man to increasingly hostile environments. These may range from the high external heat environments experienced in the ceramics, glass, metal, and rubber industries to the extremes of the space environment, in which low pressures, toxic materials, cosmic radiation, and extremes in temperature and humidity are commonplace.

A major problem in these environments occurs whenever heat input to the body differs markedly from heat dissipation. The resulting thermal stress can severely affect man's ability to perform useful work, and may, in fact, incapacitate him or prove fatal.

The ability of an individual to survive and work under these conditions depends, to a large extent, upon the type of protective equipment surrounding him. For most ground-based industrial applications, the problem is one of ambient temperature, in which the protective equipment must either remove or add just enough heat to balance the individual's heat input and heat output. For applications in the space environment, protection from near-vacuum pressures, toxic gases and ultraviolet or other cosmic radiation must be provided in addition to thermal protection.

The protective equipment required to shield man from these hostile environments consists of suits designed to essentially isolate the individual from his surroundings, in a manner similar to that of a thermos bottle. However, under such isolated conditions, even a moderate amount of metabolic activity would produce forced storage of metabolic heat. Consequently, an artificial cooling system must be provided in order to prevent rapid performance impairment and possible collapse due to excess body heat storage.

For applications involving low levels of metabolic activity, a ventilating gas circulated between the skin and the protective suit is adequate to remove the heat of metabolism by means of convective and evaporative heat transfer. The ventilating gas must also supply oxygen required for metabolism and remove metabolic waste products such as carbon dioxide and water vapor. However, for metabolic rates associated with most common activities, conventional body cooling by gas ventilation is inadequate (98). Even at low metabolic rates, the circulating gas provides cooling primarily through the mechanism of sweat evaporation rather than convection, and as such, leads to eventual heat stress and dehydration (3, 36, 145, 169). Furthermore, gas ventilation has a limited cooling capacity which cannot be increased without resorting to undesirably low gas inlet temperatures and high gas flow rates.

In the early 1960's, the Royal Aircraft Establishment (RAE) in London investigated and developed a new technique for circumventing the disadvantages of gas ventilation. They designed a garment which passed a liquid through many small tubes positioned against the subject's skin. The circulating fluid was capable of removing large quantities of metabolic heat by means of conductive heat transfer from the skin directly to the circulating liquid. This liquid conditioning garment (LCG) covered the entire body, with the exception of the hands, feet, and head, but the cooling tubes actually contacted less than 3% of the total body surface area. The entire garment weighed less than 2-1/2 lbs. Furthermore, because of the higher heat capacity and conductance of the liquid, the power requirement per unit of heat transferred decreased by several orders of magnitude when compared to gas ventilating systems. Since the early RAE investigations, a technology of LCG design and operation has gradually

evolved. The garment utilized in this experimental study is an outgrowth of this technology.

Although considerable information is available on liquid or conductive cooling in the physiological, medical, and engineering literature, it is often of a qualitative, rather than a quantitative nature. Specifically, very few attempts have been made to relate quantitatively the heat removal characteristics of the LCG to the various sensitive parameters of the human thermoregulatory system. The concepts of heat stress and thermal comfort have been described primarily in qualitative terms related to subjective observations of thermal sensation, and remain controversial subjects. Although several studies have been directed at relating LCG performance to skin temperature, rectal temperature or subjective comfort, a quantitative interrelationship between these and other physiological factors is lacking.

The research effort herein described was devoted to the development of such quantitative relationships. This was accomplished by means of an experimental test program in which several environmental and physiological factors were varied systematically in order to derive the most significant parametric relationships. It was also desired to establish a theoretical basis for the quantitative relationships in terms of the known behavior of the human thermoregulatory system. This required the development of equations, or a mathematical model, relating sweat rate, cutaneous blood-flow rate, and other physiological responses to various body and environmental temperatures. It was necessary that the equations fall within the framework of the known state-of-the-art behavior of human thermoregulation and yet reproduce, in a reasonable fashion, the parametric trends derived from the experimental results. The model provided a

mechanism for testing current theories of thermoregulation. Comparison of the model predictions with the experimental data served as a guideline by which to judge the validity of these theories. In addition, correlation of the mathematical model with the experimental results resulted in improved model accuracy. This, in turn, provided a means by which to investigate and explain the source of experimental results that were not immediately obvious.

HISTORICAL DEVELOPMENT AND USE OF THE LCG

The original purpose of the LCG was to remove metabolic heat which cannot be disposed of by normal environmental mechanisms. In accomplishing this task, the LCG acts to reduce heat strain and promote thermal comfort. In most instances, a ventilating gas supplies the necessary oxygen required for metabolism and removes metabolic waste products. It also removes a certain amount of heat from the skin, and an amount of heat from the respiratory tract during normal breathing that amounts to approximately 10% of metabolic heat generation (49). In order to be effective and maintain a zero body heat storage rate, the LCG is designed to remove the majority of heat attributed to metabolism plus any additional external heat loads from the environment.

The concept of a water cooled garment was first suggested by Billingham in 1958 (12). His work led to the development of a prototype suit by the RAF in 1962. Their initial interest was the protection of pilots in hot aircraft environments, but many other practical applications were ultimately considered. The garment was originally visualized as an extracorporeal circulatory system in which water passed through tubes in contact with the skin. The circulating water was warmed as it removed

body heat, and was then carried off to an external heat sink for cooling before returning to the LCG.

In 1964, theoretical studies on the RAE garment by Burton and Collier (25) showed that liquid cooling provided definite engineering advantages over gas cooling suits. Their computations showed that the higher heat capacity and thermal conductance of the liquid would result in more efficient heat transfer, lower system weight, and lower pumping power.

The first prototype LCG was constructed of 40 polyvinyl chloride tubes sewn into a suit of cotton underwear. Water was supplied to the wrists and ankles and conducted by manifolds to smaller tubes which distributed the flow over the limbs, where it picked up the majority of its heat, and was finally collected at outlet manifolds located at mid-thorax. Water flow was distributed to all parts of the body with the exception of the head, neck, hands and feet.

Experimental data analysis by Burton and Collier (26) showed that the design provided excellent heat transfer between the skin and the circulating water and that the LCG was comfortable even when high metabolic heat loads were imposed. Thermal comfort had been a subject of concern because the use of low water inlet temperatures at high metabolic rates resulted in large skin temperature gradients between regions of skin lying directly under the cooling tubes and adjacent sites between the tubes.

The prototype LCG was demonstrated by Burton and Collier for the National Aeronautics and Space Administration (NASA) in Houston, Texas in late 1964. This led to an extensive developmental and test program with the ultimate aim of applying the LCG to practical use.

The final version of the garment (and the one used for this experimental study) was constructed for NASA by the Hamilton Standard Corporation, Division of United Aircraft and was designated the Apollo-LCG. It featured 40 polyvinyl chloride tubes sewn into a cotton latex undergarment (see Figure 2-5). A nylon slip liner was placed between the garment and the skin to improve comfort and increase thermal conductance. Like the early RAE prototype, the Apollo-LCG provided cooling to all body areas except the head, neck, hands and feet. However, it featured a modified tubing distribution that was designed to provide local water flow in a manner proportional to body mass. In addition, water was both supplied and removed by manifolds located at mid-torso and was distributed in a loop pattern spreading from the torso to the extremities.

The Apollo-LCG was designed to accommodate average metabolic rates of 500 watts with peaks up to 600 watts. This constraint was imposed by the work tasks anticipated for activities on the lunar surface during NASA's Project Apollo. Sustained metabolic rates above these levels resulted in high body heat storage and considerable discomfort (149, 159).

Tests of the garment demonstrated that liquid cooling retarded sweating, increased subjective thermal comfort, and provided clear superiority over gas cooling in reducing signs of heat stress. These results were observed to be independent of whether the heat stress was induced by hot environments (2, 146) or high metabolic rates (112, 160). Other results showed that a wide range of combinations of water flow rate and inlet temperatures could be utilized to provide subjective comfort at any particular metabolic rate (83, 149); that heat exchange was greatest over working muscle groups such as the leg (37); and that cooling efficiency could be markedly reduced by placement of materials between the skin and the LCG tubing (73).

Since the introduction of the Apollo-LCG, other LCGs have been designed with improved cooling qualities. However, these remain largely of an experimental nature. Many of these garments are variations of the Apollo-LCG, tailored for specific tasks. For example, the current RAE suit has increased tubing length, producing more uniform flow with less pressure drop. This suit was designed for men doing mild work in hot environments such as overheated aircraft cockpits. The U.S. Air Force has developed an LCG vest covering the torso and upper thighs for use in flights over tropical climates. Experimental versions of the RAE suit have been tested for industrial use in glass factories, where furnace maintenance requires hard physical labor in the presence of high environmental heat loads. Because of these high radiant heat loads, it has been found that adequate comfort cannot be provided without the addition of cooling to the head and neck areas (68). Other concepts in LCG design have utilized partial LCGs such as head cooling caps, gloves or vests designed for specific work tasks.

The most recent innovations in LCG design have been based upon increased heat transfer from the skin to the LCG. This is accomplished by means of greater skin-tubing contact surface area or utilization of tubing material with increased thermal conductivity. Such designs permit the use of higher water inlet temperatures or lower water flow rates without decreasing the heat transfer efficiency of the garment. This lessens the likelihood of such physiological problems as shivering or vasoconstriction, while simultaneously decreasing power requirements. Examples of these advanced concept LCGs include the evaporative cooling garment designed by the McDonnell Douglas Corporation in Huntington Beach, California, and an LCG using a high conductance, heat-sealed plastic

material called FLEXITHERM, built by the Aerotherm Corporation in Mountain View, California.

The feasibility and capability of an LCG to maintain subjective human thermal comfort in stressful environments has been investigated in several studies. The first and most comprehensive review of these studies, and of LCG development in general, was performed by Nunneley in 1970 (98). She discussed the physiological effects of liquid cooling upon thermoregulation, the effects of variations in LCG design parameters, and the effects of regional or local body cooling. A more recent review of the literature was performed by Shvartz in 1972 (123). He investigated the ability of various LCG designs to reduce heat strain under different metabolic and environmental conditions.

Both of these reviewers concluded that the LCG was indeed capable of providing thermal comfort under a variety of stressful conditions. In addition, they emphasized that different areas of the body are more critical than other areas in the subjective determination of comfort. The lower body, especially the legs, requires high heat removal rates, thereby justifying a higher LCG tube density. It was also found that the head and neck areas are highly effective sites for LCG heat removal because these regions lack a significant vasoconstriction mechanism (98, 99). The latter finding has done much to spur the recent interest in head cooling (33, 99, 163, 164, 165, 166), which had been largely ignored in the past.

In 1972, Shitzer, Chato, and Hertig (119, 120) also studied the effects of regional cooling on human subjects working at various metabolic rates. They employed a modified Apollo-type LCG and observed that various body areas required different cooling rates for comfort, with the thigh and neck regions demanding the lowest inlet water temperatures. They also

performed an analytical investigation to determine the effects of variable LCG tube spacings, heat flux rates, metabolic rates and peripheral blood flow rates upon the temperature profile throughout a small cross section of human tissue approximated by a rectangular slab or a circular cylinder. Based upon this analysis, they concluded that the peripheral blood flow effect is important in determining the local skin temperature, that closer spaced LCG tubes would yield a more uniform skin temperature, and that the highest temperature in the body probably occurs within the muscle tissues at elevated metabolic rates. In an earlier, similar study, Buchberg and Hurrah (21) performed a theoretical analysis of the efficiency of liquid cooling through polyvinyl chloride tubes as a function of the skin-tubing contact surface area. These two analytical investigations are noteworthy because they represent the first attempts to apply mathematical and theoretical principles to the interactions between the human physiological system and the LCG.

Other experimental studies performed with whole or partial body cooling have further demonstrated the ability of the LCG to maintain subjective thermal comfort at high metabolic rates in hot environments (30, 32, 117, 124, 126, 140, 163). Included in the studies were advanced concepts for automatic control of LCG cooling. In these experiments, LCG inlet temperature was adjusted based upon measurements of heart rate, sweat rate, skin temperature, or other physiological parameters.

Such investigations have provided the impetus for the application of the LCG to many diverse uses, including laboratory studies for the exact control of skin temperature in cardiovascular research (109, 110, 111). For the latter application, an Apollo-LCG modified to cover the head, hands and feet imposed a constant skin temperature across the body while

permitting continuous monitoring of various physiological processes, including cardiac output by means of heart catheterization. These experiments clearly established that high skin temperatures are associated with substantial increases in cardiac output, with the largest percentage of the increase going to the peripheral circulation.

In other applications, LCGs have been used to cool racing car drivers in the presence of high engine heat (87), to cool surgeons during delicate operations that would be obstructed by high perspiration rates (87), and to subcool patients during neurosurgery (83). They are also under consideration for heating divers descending to great depths, where high conductive heat loss to the water is a severe problem (101, 158).

One final application of the LCG is noteworthy in that it pertains directly to some of the experiments that constitute this investigation. By covering the entire body with an Apollo-type LCG modified to cover the head, hands and feet, and then thermally isolating the man from his environment, the LCG has been used as a calorimeter for the direct determination of metabolic heat output (157). Subjects dressed in the LCG were covered with an outer insulating garment and performed measured quantities of external work at known metabolic rates. By using a thermal chamber to minimize environmental heat exchange, a close match was achieved between metabolic heat production and LCG heat removal plus mechanical work. However, these studies leave something to be desired in that they imposed an unnatural constraint on the subject by eliminating convective and evaporative heat removal. That is, the outer insulating garment usually consisted of a rubberized or neoprene suit that permitted sweating but essentially eliminated evaporation of sweat and convection heat transfer.

To date, there has been no comprehensive quantitative [illegible]ing LCG performance to sweat rate, metabolic rate and [illegible] loss

rate under comfort and off-comfort conditions. Such a study would permit the calorimetric use of an LCG to determine metabolic rate without inhibiting the normally occurring processes of convective, evaporative and radiative heat transfer.

Part of the difficulty of performing such an investigation can be traced to the complexity and inherent inaccuracy of techniques for measuring the convective, evaporative and radiative heat loss from exercising subjects wearing an LCG. However, for the experimental study that comprised the present research effort (described subsequently in Section 2), a new approach has been utilized. A mathematical model of the human thermoregulatory system was combined with a detailed environmental model including the effects of the LCG, and then used in conjunction with experimental data to determine parametric relationships between LCG performance and metabolic rate. In addition to providing a calorimetric method for estimating metabolic rate, this technique also permits accurate predictions of sweat rate and evaporative heat loss rate for comfort and off-comfort conditions, while simultaneously offering a quantitative means of assessing thermal comfort.

HISTORICAL DEVELOPMENT AND USE OF THE MATHEMATICAL MODEL

It was mentioned earlier that Buchberg and Hurrah (21), followed later by Shitzer, Chato and Hertig (118, 119), deduced important physiological characteristics of LCG performance by using mathematical and theoretical principles to simulate the interactions between the human physiological system and the LCG. However, their analyses were inadequate in one very important respect: they failed to account for the variable and dynamic effects of the human thermoregulatory system. Furthermore,

since they were only concerned with analyzing a small region of tissue, they did not consider the effects of other body regions a distance away.

These effects cannot be ignored, since every region of the body contributes to the total body heat balance which, in turn, influences important thermoregulatory system parameters such as sweating, peripheral circulation and shivering. As a consequence of this property of feedback control exhibited by human thermoregulation, the local heat balance of every region of the body affects every other region. Any theoretical analysis of human heat loss is therefore incomplete unless it accounts for such interactions.

Of course, it may be argued that many of these interactions are quite complex and poorly understood. However, a considerable body of knowledge about these effects has been accumulated in recent years through various research programs. Consequently, the major mechanisms of human thermoregulation are fairly well known. Examples of those mechanisms are shown in Figure 1-1.

While it is true that many of the pathways shown are quite complex, it is also true that the validity of any theoretical or mathematical analysis of human thermoregulation depends greatly upon the extent to which it faithfully reproduces these physiological processes. The most efficient way to account for these processes, and yet simultaneously learn more about them, is by the use of a mathematical model of the human thermoregulatory system.

An essential element of the present research effort has been the development and utilization of such a model. The use of this model has been beneficial in three important respects: first, it has enhanced the interpretation and understanding of the physical processes affecting

the experimental results; secondly, the quantitative accuracy of the model has been evaluated and improved by comparison with the test data. This has resulted in a high degree of confidence in the ability of the model to predict the thermal response of man to his environment. Finally, the model predictions, in conjunction with the test data, constituted an effective tool with which to investigate the ability of the LCG to control heat stress. These results were used to establish physiological trends that provided insight into the behavioral response of man to heat stress.

The development and utilization of mathematical models of biological systems is not a new phenomena. Scientists have been intrigued and fascinated by the workings of the human thermoregulatory system since the 18th Century, when the French chemist Lavoisier established the fact that the human body generates heat (116). It has been known for many years that the thermoregulatory system was capable of maintaining a fairly constant deep body temperature under a wide range of environmental conditions by dissipating or preserving heat. The early attempts to understand this behavior consisted of observing the thermal response of individuals under natural and laboratory controlled conditions. However, this approach soon reached a point of diminishing return, and it was clear that more sophisticated methods of study were required. It was from this need that the concept of the mathematical model was derived.

The first mathematical model of human thermoregulation to appear in the literature was introduced by Burton in 1934 (22). By utilizing the principles of conservation of mass and energy, he appears to have been the first to apply the equations of heat transfer and thermodynamics to the human body. His analysis considered the body as a single homogeneous

entity within a control volume. It was from this approach that the familiar total body heat balance equation was formulated.

In 1945, a new approach emerged, whereby the body was divided into two concentric shells, each at a uniform temperature (44). The inner shell constituted the core and was designated the deep body or rectal temperature, while the outer shell was assigned the average skin temperature. This core and skin technique provided satisfactory solutions for simple problems and remained popular until the late 1950s. However, it soon became obvious that the 2-shell approach had three basic shortcomings. Firstly, by approximating the entire body as a single inner segment surrounded by an outer segment, it failed to account for the physiological differences between separate regions of the body. Thus, the interactions between the arms, legs, head, hands and feet, etc., were neglected and instead, approximated by one overall segment. Secondly, by approximating the continuous temperature profile between the skin and the deep body with a discrete temperature profile consisting of only 2 temperatures, significant errors would arise when a large temperature difference existed between the skin and the air. Finally, this method failed to account for the various sensing and control mechanisms of the thermoregulatory system. As a consequence of these insufficiencies, the 2-shell approach was inadequate to handle all but the simplest of problems.

With the advent and availability of high speed digital and analog computers in the late 1950s and early 1960s, the restraints which had prevented the correction of the above inadequacies were removed. It became possible to implement advanced mathematical techniques on computers, which, beforehand, could not be practically utilized in hand calculations. These methods permitted the solution of the complex, simultaneous differential

heat transfer equations that resulted from consideration of the effects of several distinct body compartments, multiple layers of tissue within each compartment, and the sensory and motor responses of the human thermoregulatory control system.

With the availability of advanced computational techniques, many investigators embarked on the development of more sophisticated mathematical models. Several excellent reviews of these models are available in the literature. The interested reader is directed to the works of Chato and Hertig (34), Shitzer, Chato and Hertig (118), Fan et al. (48), and Shitzer (116) for a more comprehensive historical overview and technical description of the major mathematical models developed through 1972. In the forefront of the research in this area has been the J. B. Pierce Foundation Laboratory at the Yale University School of Medicine. Since 1961, Drs. J. Stolwijk and J. Hardy of this institution have been intensively investigating the responses of the human thermoregulatory system by the use of mathematical models in close connection with an experimental program (138-138). Their approach is described in the following summary (116):

> "The human body is represented by three (or more) cylinders: the head, the trunk and the extremities. Each cylinder is divided into two or more concentric layers to represent anatomical and functional differences in so far as they are of primary importance in thermoregulation. Heat flow between adjacent layers is by conduction, and all layers exchange heat with the environment by convection with a central blood compartment. All three skin layers exchange heat with the environment by conduction, convection, radiation and evaporation. Signals which are proportional to temperature deviations in the brain and to deviations in average skin temperature are supplied to the regulator portion of the model. The regulator then causes evaporative heat loss, heat production by shivering, or changes in the peripheral blood flow to occur in the appropriate location in the body. If a proposed mechanism of thermoregulation is expressed in quantitative form, it describes the relationships between the input signals and the resulting thermoregulatory

response; the model can be used to compare the quantitative response resulting from a proposed mechanism with the responses obtained by measurement. A number of experimental results are compared with prediction furnished by the mathematical model using a regulator with an output which is proportional to the product of the input signals"

The mathematical model utilized in the experimental program described in the present dissertation is based largely upon the Stolwijk-Hardy concept. The evolution of the model has been taking place since 1965 at NASA's Johnson Space Center in a developmental program concurrent with the research of Stolwijk and Hardy.

The model initially consisted of the 2-shell concept discussed earlier. A set of thermoregulatory control mechanisms was added, followed by the growth of the model to 3, 6, and finally 10 cylinders, representative of the various body elements. The current model has a separate cylindrical element for the head, the trunk, each arm, each leg, each hand and each foot. The number of concentric layers within each cylinder has also increased from 2 to 4, with a separate region for the inner core surrounded by layers of muscle, fat and skin.

Characterization of the thermoregulatory system has become increasingly more sophisticated as research provided more information on the nature of the primary physiological processes. The current model utilizes the latest sensory-motor pathways identified by the J. B. Pierce Foundation and consists of dynamic feedback and interplay between all of the body elements and layers. This includes the effects of interactions between all body regions with a central blood compartment which contacts these regions. Each of the 10 skin layers exchanges heat with the environment by conduction, convection, evaporation and radiation.

A considerable effort has been spent in developing the equations describing these heat transfer mechanisms and correlating them with experimental data (80, 83, 85). The current model is capable of accounting for the heat transfer effects of surrounding garments ranging from an undergarment to a multilayered space suit. This includes the simulation of the LCG, which constitutes an important part of this research study. The model can also account for the effects of variations in the properties of the surrounding environmental gas, as well as variations in ambient pressure, temperature, humidity, gas flowrate and incident environmental radiation. Finally, heat exchange between the environment and the respiratory tract is also considered by incorporating empirical relationships derived from previous experimental studies or from the literature. A more detailed description of the mathematical model follows subsequently in Section 2.

General Purpose

The mathematical model described above was used in conjunction with the results of an experimental program to generate important physiological information. A calorimetric technique was found to relate the heat dissipated by the LCG to the metabolic rate, sweat rate and thermal comfort of human subjects. It was found that individuals controlled their LCG cooling in such a way as to minimize sweating according to a predictable relationship. A quantitative assessment of thermal comfort was investigated and a study of the behavioral and physiological responses to off-comfort environmental conditions was pursued. The accuracy of the model was improved by adjustment of several model parameters that ultimately resulted in better agreement with the test data, and conversely, the correlated model was used as a tool to study unusual experimental

results. Finally, this effort culminated in the formulation of a new, second generation mathematical model, with improvements designed to correct the major inadequacies illuminated by this study.

A description of the detailed experimental procedures utilized to deduce the above findings now follows in Section 2. The actual results are shown and examined in detail in Section 3. However, the analysis of many of these results is quite complex and time consuming. Therefore, for the reader who does not wish to pursue this level of detail, the major findings and practical applications of these findings, are summarized in the discussion of Section 4.

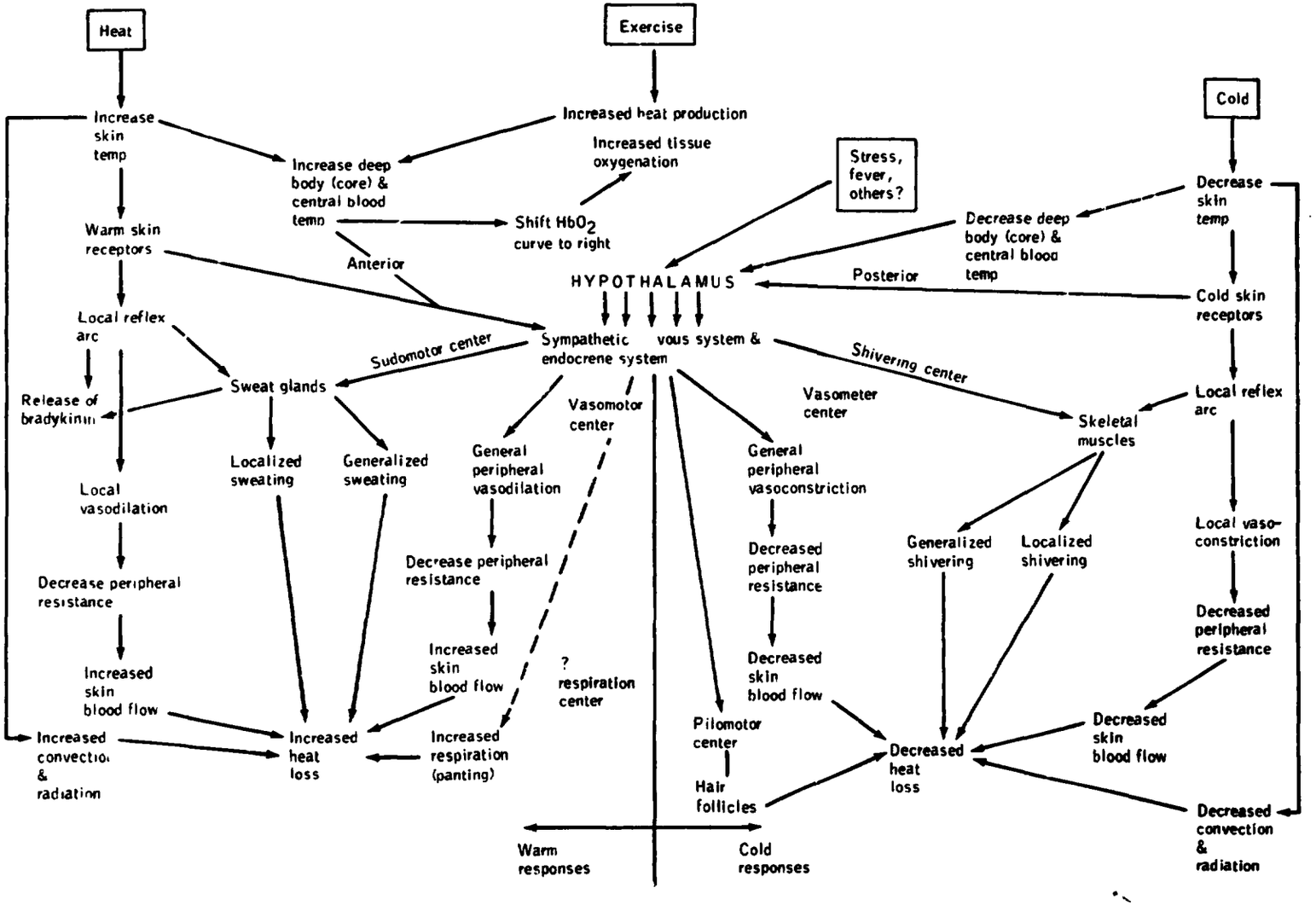

Figure 1-1.- Responses of the human thermoregulatory system.

2. MATERIALS AND METHODS

GENERAL

The experiments herein described were conducted to provide information in several vital areas. From an engineering standpoint, the primary objective was to demonstrate the capability of NASA's portable life support system equipment to meet the design specifications required for extravehicular activity (EVA) on the lunar surface. From a physiological standpoint, these tests were conducted to ensure that man could satisfactorily perform scientific tasks while exposed to the harsh environmental stress of space.

Although the primary justification for these experiments was to provide confidence that the life-support equipment could thermally support the first Apollo lunar landing missions, by utilizing the data in a systematic and orderly fashion, it was possible to investigate the physiological response of the human thermoregulatory system under stress. The internal heat of metabolic activity can lead to thermal stress when man is sealed in the impermeable cocoon of a space suit. Under these conditions, body heat cannot be efficiently dissipated to the environment by conventional heat rejection mechanisms. However, thermal comfort can be provided by the use of a liquid conditioning garment (LCG) in conjunction with a forced oxygen ventilation system.

The following experiments provide considerable data on the performance of human subjects while wearing an LCG to reject metabolic heat as contrasted with the more conventional mechanisms of convective, evaporative and radiative heat removal. In addition, these data were used to correlate and verify a mathematical model of the human thermoregulatory system,

which was used, in turn, to establish trends in the physiological response of man to thermal stress.

FACILITIES, SUBJECTS, AND EQUIPMENT

All of the experiments, with the exception of Series E, were conducted at the facilities of NASA's Johnson Space Center, in Houston, Texas, for environments ranging from room temperature to simulated lunar surface conditions. Hypobaric thermal vacuum chambers were utilized to simulate the desired space environments. These consisted of the 8-foot diameter hypobaric chamber of the Crew Systems Division laboratories and the Chamber B facility of the Space Environment Simulation Laboratory. The hypobaric chambers provided the capability of controlling the ambient temperature, humidity, pressure and ultraviolet and infrared radiation to the desired requirements of each test series (6, 46, 47, 88, 129). This included the capability to vary ambient pressure from sea level to below 10 torr and to control external space suit temperatures to limits as extreme as ± 122°C.

The test program consisted of 5 series of tests in which subjects exercised at prescribed metabolic rates for periods of time ranging from 30 min to 7 hrs, while wearing an LCG for conductive cooling. For Series A, B, C, and D, thirteen healthy adult males, all of whom were either NASA test subjects or astronauts, were used in the experiments. For Series E, 12 healthy adult males, all of whom were NASA astronauts, were used as subjects.

For the sea-level test series (Series A), subjects wore the snug-fitting LCG under an artic coverall garment designed to minimize heat loss to the environment. A small area of the face was exposed to the room temperature environment.

For the hypobaric experiments (Series B, C and D), and for Series E, subjects wore the LCG under the Apollo A7L space suit. This full pressure suit provided pressure integrity, oxygen, ventilation, and thermal protection (46). The oxygen ventilation flow path through the A7L suit was normally directed to the head, flowing initially across the oral-nasal area, then over the torso and limbs, and finally, to the hands and feet. This flow path provided convective and evaporative heat removal and prevented the buildup of carbon dioxide in the facial area. The ventilating gas was then collected in ducts located near the hands and feet and directed out of the suit through appropriate manifolding (See Figure 2-1).

For the tests conducted in the 8-foot diameter hypobaric chamber (Series B and C) the outlet gas exiting the suit was then directed, by means of umbilicals, to condensing heat exchangers, contaminant control filters and pumps within the chamber facility Here, the temperature, humidity and flowrate were controlled to the desired requirements of each test, and carbon dioxide and other contaminants were removed. This conditioned oxygen was then returned to the suit by means of a suit inlet umbilical.

For the test sequences conducted in the Chamber B Space Environment Simulation Laboratory (Series D), and for Series E, the outlet gas exiting the suit was directed to the NASA portable life support system (PLSS). The PLSS was worn on the back of a suited subject in "knapsack" fashion and attached to the A7L suit by means of a harness-umbilical arrangement. Because the PLSS was designed to operate in the 1/6 gravity environment of the lunar surface, it became necessary to relieve 5/6 of its weight during Series D, in order for the test subjects to experience realistic

weight constraints and stand upright comfortably. This was accomplished by means of a counterweight mechanism (46).

The PLSS conditioned the suit outlet gas temperature and humidity by making use of a porous plate sublimator that utilized the low pressure sublimation thermodynamics of a vacuum (7, 63, 75). Heat was rejected and moisture was removed when the suit outlet gas was indirectly exposed to an ice layer formed on the surface of the sublimator. The ice was formed when water supplied by a feedwater storage tank within the PLSS was exposed to vacuum conditions on the exterior surface of the sublimator plate. The ice layer removed the heat from the ventilating gas (and also from the circulating outlet water of the LCG) and, in so doing, sublimated directly to a vapor. As the ice layer sublimated away, it was continually replaced by the freezing of water supplied from the feedwater storage tank.

The amount of feedwater in the feedwater tank was one of the major life support system consumables of the PLSS, and since it was used primarily to cool the suit oxygen and LCG water exiting the suit, its usage rate was directly proportional to the metabolic rate of the test subject (82). This can be seen from the total heat balance equation shown in Figure 2-2 and by examination of the PLSS oxygen and LCG water loop flow paths (Figure 2-3). Here, most of the heat of metabolism is dissipated to the LCG or by sensible convection or latent evaporation of body moisture to the circulating oxygen. These, in turn, find their way into the PLSS oxygen and LCG water circuits. The conditioned gas and LCG water leaving the PLSS then return to the suit inlet with the temperature, humidity and flowrate controlled to the desired requirements necessary for metabolic heat removal.

Removal of metabolic end products, primarily CO_2, was also accomplished in the PLSS by passing the ventilating gas through a cannister containing lithium hydroxide and activated charcoal. The internal components and flow paths for the PLSS are shown in more detail schematically in Appendix A.

The PLSS, together, with the LCG, and the Apollo A7L space suit with its oxygen ventilation system, comprise what is referred to as the extravehicular mobility unit (EMU). This is shown in Figure 2-4 and Appendix A, Figures A5-A7. Leading particulars of the EMU and the Apollo A7L space suit are also shown in Appendix A. Additional details on the construction and design of the EMU may be found in References 30 and 46.

LIQUID CONDITIONING GARMENT

The LCG was originally developed to provide conductive cooling for men resting or mildly active in hot environments (12). It was then modified to meet the needs of NASA in which individuals were required to work strenuously while isolated from direct heat exchange with the outside environment.

For Series A-E, the liquid conditioning garments used were the standard Apollo-type LCGs. The garment consisted of a network of polyvinyl chloride (PVC) tubing stitched to the inside surface of the open mesh cotton garment (see Figure 2-5). A lightweight nylon comfort layer was used to separate the tubing network from the skin surface. The LCG incorporated 91 meters of PVC tubing fabricated with an ID of 1.6 mm and OD of 3.2 mm. The tubes were sewn to the inside of the cotton undergarments and covered the skin area with the exception of the head, neck, hands and feet. When fully charged with water, the LCG weighed about 1 kgm.

The water flow to the LCG was supplied through a temperature regulating system located either in the chamber facility (Series A, B, and C) or in the PLSS (Series D and E). The water temperature for all tests was varied between 7 and 26°C depending upon test requirements. For Series A, B, and C, water temperature was controlled by an external heat exchanger in the chamber facility according to a predetermined profile. For Series D and E, a 3-position, check-stop diverter valve located on the PLSS, permitted the subject to select cold, moderate or warm inlet water temperatures, in accordance with his own subjective comfort. This valve controlled the inlet water temperature by diverting a portion of the water flow around the PLSS sublimator.

The LCG water flowrate was controlled to 109 liters/hr for all tests, with the exception of Series C where flowrate was varied between 0 to 82 liters/hr. The inlet and outlet LCG water temperatures were measured by thermistors for all tests.

The LCG water flowrate was measured with a rotometer in all cases except Series D and E, where it was regulated by the PLSS to a fixed, calibrated flow of about 109 liters/hr. Other pertinent details about the LCG may be found in Appendix A, and information concerning the manufacturers and descriptions of the LCG and other equipment used in these experiments are listed in Table A3 of Appendix A.

TEST PROGRAM

The test program followed in these experiments was organized in such a fashion as to maximize the physiological information gained about the performance of human subjects working in LCGs, and yet still provide enough data to correlate and validate the mathematical model of the human thermoregulatory system. Each of the test series was conducted under

unique conditions, yet similar enough to the oth. test series to permit parametric analysis of the results.

For example, Series A was conducted in a room temperature environment, with subjects wearing an insulating coverall garment designed to limit convection and radiation loss. There was no air ventilation flow across the skin and all runs were made at sea level pressure. LCG flowrate was constant and LCG inlet temperature was varied.

Series B was conducted in a vacuum environment below 10 torr. Subjects wore an Apollo A7L space suit with gas ventilation consisting of oxygen circulating at 170 liters/min. The suit was pressurized to 195 torr. LCG flowrate was again constant and LCG inlet temperature was varied. The chamber environment was kept near room temperature in order to minimize radiative interchange with the environment.

Series C was performed at a reduced pressure of 259 torr. The chamber temperature was again neutral to eliminate radiation heat transfer between the subjects and the ambient environment. The subjects again wore the Apollo A7L suit over the LCG. However, in this case, the circulating flowrate of the oxygen ventilating system was almost doubled to 331 liters/min. The suit was maintained at the ambient pressure of 259 torr, so that no differential pressure existed between the suit and the environment. For Series C, the LCG flowrate was varied while the inlet temperature was maintained constant. This permitted direct comparison with other tests for which the flowrate was fixed and the inlet temperature was varied.

Series D and E were conducted in a vacuum environment with all critical life-support system functions being controlled by the PLSS. The ambient pressure was below 10 torr, but subjects wore the A7L suit

pressurized to 195 torr. The oxygen ventilation system was regulated by the PLSS to a circulating flow of 170 liters/min. The LCG flowrate was again constant at 109 liters/hr and the inlet temperature was varied. However, in these tests, the inlet temperature was selected entirely in accordance with subjective comfort, as opposed to the other test series in which either temperature or flowrate was varied according to a predetermined, parametric profile. For Series D, the chamber environment was varied in a parametric fashion from very hot to very cold. This permitted the additional benefit of providing comparative data with the previous test series in which the surrounding environments were thermally neutral.

For Series E, the lunar environment and the life-support equipment used were similar to Series D. However, on the lunar surface, the effect of gravity was only 1/6 as great as the 4 Earth-based test series.

Additional details of the experimental methods and procedures for each test series will now be presented.

Series A

The Series A experiments consisted of 11 test sequences in which 5 subjects were exercised at metabolic rates ranging from rest to vigorous activity (100 to 620 watts) while wearing an LCG under an arctic clothing assembly in a room temperature environment. All tests were conducted at sea-level pressure. The tests were all 2 to 3 hours in duration and steady-state data were collected during the final 30 - 60 minutes of each sequence. All tests were conducted using an LCG water flow of 109 liters/hr and an inlet temperature of either 7 or 16°C.

Metabolic rates were measured by collecting gas samples at approximately 5 min intervals in Douglas bags. Oxygen consumption and carbon

dioxide production rates were determined from these samples by using a Tissot spirometer, followed by chemical analysis using the Scholander technique (115). These values were used to determine a respiratory quotient and metabolic rate (see Appendix C, Figure C1). The metabolic rate was controlled by varying the speed of a motor-driven treadmill.

A biomedical harness was utilized to measure several body skin temperatures. These included temperature measurements for the forehead, chest, arms, legs, back, hands, and feet. Copper-constantan thermocouples were used for the measurements. A rectal temperature thermistor and ECG sensors were also included in the biomedical harness to measure rectal temperature and heart rate. Thermistors were used to measure LCG inlet and outlet water temperatures and a rotometer was used to measure LCG water flowrate. All of the above temperatures were recorded at intervals of 5 minutes or less and used to determine LCG heat removal, total body heat storage and heat storage rate (See equations 3, 4, and 5, Section 2).

A human balance with an accuracy of ±5 grams was used to measure the subjects pre-test and post-test weights. These data were used to determine sweat rate and evaporative heat loss (See sample calculation, Appendix C).

Due to the nature of the tasks performed, subject mechanical work was very small and neglected in the results.

All of the raw data for Series A, including environmental and metabolic conditions, are presented in Table D1 of Appendix D. The results calculated from these data, including the overall body heat balance, are shown in Table 3-1 of Section 3.

Series B

Series B consisted of a group of 4 tests, each comprising 4 to 7 separate test sequences in which 2 subjects were exercised at metabolic rates from moderate to vigorous activity (256 to 556 watts). The subjects wore the Apollo A7L space suit, which provided gas ventilation, over the LCG. All tests were conducted in the 8-foot diameter hypobaric chamber of the Crew Systems laboratories at the Johnson Space Center. The chamber pressure was essentially a vacuum at 10 torr or less while the suit pressure was regulated to 195 torr pure oxygen.

All test sequences were 30 minutes in duration and data were collected continuously. Steady-state conditions were recorded at the conclusion of each 30 minute test sequence. All tests were conducted using an LCG water flowrate of 109 liters/hr and an inlet temperature that was varied between 7 and 25°C according to the predetermined profile shown in Table D2 of Appendix D.

The ventilating gas through the A7L suit was supplied by the chamber environmental equipment and consisted of pure oxygen circulated at 170 liters/min and maintained at a temperature of 20°C and a dewpoint of 4°C. The suit outlet gas was collected and delivered to the chamber environmental conditioning equipment by means of umbilicals. CO_2 and humidity were removed and the temperature, dewpoint and flowrate controlled to the suit inlet conditions previously specified. Heat added to the LCG by the exercising subject was also removed by the chamber environmental conditioning equipment. The circulating oxygen and LCG water were then delivered back to the suit inlet by a return umbilical.

The oxygen and LCG inlet and outlet temperatures were measured by thermistors and were recorded continuously. The oxygen and water flowrates

were also measured, as was the suit inlet and outlet dewpoint. The latter measurements were utilized to determine LCG, convective, and evaporative heat removal rates on a continuous basis during the test (equations 5, 6 and 7, Section 2). The equilibration of these values was used as an indication of steady-state.

Metabolic rates were measured by comparing the subjects heart rate, measured with ECG sensors, with a predetermined calibration curve of heart rate versus metabolic rate. The calibration curve was determined prior to the test by utilizing bicycle ergometry apparatus to measure oxygen consumption, carbon dioxide production, and heart rate at various controlled resistance workloads. The apparatus also included a turbine flowmeter and a mass spectrometer to measure respiratory flowrate and respiratory gas composition (O_2 and CO_2). This information was then combined to determine a calibration curve for each subject to be used during the test (see equation 1 and Figures C1 and C2, Appendix C). The metabolic rate during an experiment was controlled by varying the subject's step rate on a Harvard step test until his heart rate equilibrated at a point representing a desired work level, as determined from the calibration curve.

The duration of each sequence in this test series was from the onset of exercise until the outlet gas temperature, dewpoint and LCG outlet water temperature reached steady-state. This was approximately 30 minutes for each test sequence. The use of the space suit outlet conditions as a monitor for the achievement of steady-state was necessitated because body temperatures were not measured during this test series.

The chamber environment was neutral with no imposed heat load. The chamber wall and air temperature were about 27°C and it was assumed

that radiation heat transfer through the Apollo space suit was small. As in all other test series, subject mechanical work was negligible and not considered in the heat balance.

All of the raw data for Series C, including environmental and metabolic conditions, are presented in Table D2 of Appendix D. The results calculated from these data, including the overall body heat balance, are shown in Table 3-2 of Section 3.

Series C

Series C consisted of a sequence of 10 tests in which 2 subjects exercised at constant metabolic rates ranging from moderate to vigorous activity (352-586 watts). The subjects wore the A7L space suit over the LCG, which provided gas ventilation. All tests were conducted in the 8-foot diameter hypobaric chamber of the Crew Systems Division laboratories at the Johnson Space Center. The chamber pressure was regulated to 259 torr absolute and the suit pressure was also controlled to 259 torr, so that there was no pressure differential between the suit and the chamber. The chamber environment remained near room temperature throughout each test sequence, and radiation exchange between the subject and the chamber was minimal.

All test sequences were 30 minutes in duration and data were collected continuously. Steady-state data were recorded at the conclusion of each test sequence after body temperatures had reach equilibrium. All tests were conducted using a constant LCG inlet water temperature of 17 - 19°C with a variable water flowrate that ranged between 0 to 82 liters/hr, according to the predetermined profile shown in Table D3 of Appendix D. The water temperature and flowrate were supplied and controlled by heat exchangers and pumps within the chamber environmental control equipment.

The flowrate was varied in such a fashion as to permit parametric examination of the cooling effects of variable LCG flow at constant metabolic rates. In order to accomplish this, the flowrate was increased sequentially in a stepwise fashion for a low metabolic rate. This sequence sequence was then repeated at a higher metabolic rate, and so on.

The ventilating gas through the A7L suit was supplied by the chamber environmental control equipment, as in Test Series B, and consisted of pure oxygen circulated at 331 liters/min. The suit inlet temperature was controlled between 22 - 27°C and the inlet dewpoint was kept between 7 and 8°C. The suit outlet gas and LCG water were collected and delivered to the chamber environmental conditioning equipment by means of oxygen and LCG water umbilicals. CO_2 and humidity were then removed and the temperature, dewpoint and flowrate were regulated to the suit inlet conditions previously specified. The conditioned oxygen and LCG water were then delivered back to the suit inlet by a return umbilical. Oxygen and LCG water inlet and outlet temperatures were measured by thermistors and recorded continuously. Oxygen inlet and outlet dewpoints and oxygen and LCG water flowrates were also measured and continuously monitored. These measurements were used to compute LCG, convective, and evaporative heat loss rates (see equations 5, 6, and 7, Section 2).

Metabolic rates were measured and controlled by varying the subject's step rate on a Harvard step test in accordance with a predetermined calibration of metabolic rate versus step rate. The pre-test calibration was performed by collecting gas samples for each subject while he was stepping at a given rate on the Harvard step under conditions similar to those imposed during the test. The gas samples were then analyzed for O_2 and CO_2 by the method described in series A, and an RQ and metabolic

rate determined for each step rate. By repeating this process for a series of step rates, several data points were determined and used to generate calibration curves such as Figure C3 of Appendix C.

A biomedical harness was used to measure several body skin temperatures. These included temperature measurements for the forehead, chest, abdomen, back, calf, forearm, hand, and thigh. Copper-constantan thermocouples were used for these measurements. Tympanic membrane temperature was also measured by means of an ear probe thermistor. The latter measurements were recorded continuously and used to calculate mean skin temperature, and total body heat storage and heat storage rate (equations 2, 3, and 4, Section 2). ECG sensors were also included in the biomedical harness for measurement of heart rate.

Due to the nature of the tasks performed, subject mechanical work was very small and neglected in the heat balance.

All of the raw data for Series C, including environmental and metabolic conditions, are presented in Table D3 of Appendix D. The results calculated from these data, including the overall body heat balance, are shown in Table 3-3 of Section 3.

Series D

Series D consisted of a group of 7 tests in which 4 subjects worked at metabolic rates ranging from rest to vigorous activity (143-615 watts). The subjects wore the A7L space suit over the Apollo-LCG and also carried a portable life-support system (PLSS) on their back in "knapsack" fashion. The PLSS provided oxygen, ventilation, and conditioned LCG water to the suit. All tests were conducted in the Space Environment Simulation Laboratory (SESL), hypobaric chamber B, at the Johnson Space Center. The chamber pressure was maintained at 10 torr or less throughout

each test sequence, while the suit pressure was regulated to 195 torr, pure oxygen, by the PLSS.

The thermal environment of the chamber was adjusted for each test to simulate the various environmental conditons anticipated during lunar surface explorations. The high incident radiation environments expected during the lunar day were simulated by carbon-arc solar lamps utilizing xenon vapor, and by infrared heaters. The cold conditions expected during lunar night were simulated by circulation of liquid nitrogen through the chamber walls. The net environmental heat exchange resulting from these severe chamber environments ranged from extremes of 137 watts into the suit to 72 watts out of the suit. The primary factor in the limitation of the radiative heat exchange to these values was the insulation characteristics of the A7L space suit. The suit wall was comprised of seven layers of beta cloth, Kapton, and aluminized mylar, which provided effective insulation from thermal radiation and environmental temperature extremes.

The tests ranged in duration from about 4 to 7 hours each, and data were collected continuously over each test period. The LCG water flowrate was regulated by the PLSS to about 109 liters/hr and the LCG inlet temperature was controlled by the subject in accordance with his own comfort throughout each test. This was accomplished by means of a 3-position diverter valve located on the PLSS. The inlet temperatures selected by the test subjects in this manner ranged from 6 to 30°C. During each test, the subject was requested to evaluate his feelings of comfort and thermal sensation. This included sensory estimations for individual areas such as the limbs or extremities, as well as whole body sensations. All test subjects were experienced in the use of the LCG and associated equipment.

The ventilating gas through the A7L suit was supplied by the PLSS and consisted of pure oxygen circulated at 170 liters/min and maintained at a temperature and dewpoint of approximately 25°C and 10°C, respectively. The suit outlet gas and LCG water were collected in separate umbilicals and delivered to the PLSS for conditioning. The PLSS oxygen ventilating circuit first resupplied any oxygen lost by metabolic consumption or leaks. The suit outlet gas then passed through a contaminant control assembly where carbon dioxide was removed by chemical reaction with lithium hydroxide. Odors and foreign particles were filtered out by an activated charcoal filter. The oxygen was then circulated to a porous plate sublimator, which cooled it, and then to a wicking water separator, which removed the evaporated moisture of metabolism. The cooled, dry oxygen was then passed to a fan/motor assembly, which forced it into the suit inlet at the conditions previously specified. The PLSS recirculating liquid transport loop directed the LCG outlet water to the PLSS sublimator where the heat added by metabolism was then dissipated by sublimation as previously described. The cooled LCG water was then circulated to a pump/motor assembly, which pumped it into the LCG at a flowrate of about 109 liters/hr. The temperature of the inlet water was controlled by diverting part or all of the water flow around the porous plate sublimator. This was done manually by the subject by means of the PLSS water diverter valve, which could be turned to a MIN, INTERMEDIATE, or MAX position for warm, moderate or cool water temperatures.

The PLSS also contained all of the other life support system consumables and equipment required for EVA. This included oxygen, feedwater for heat rejection by sublimation, communication and telemetry equipment, electrical power, and operating controls and displays. The PLSS was

attached to the A7L suit by means of a harness, and during Series D, 5/6 of its weight was relieved from the test subject by means of a counter-weight device.

The suit inlet and outlet oxygen and water temperatures were measured by thermistors and recorded continuously. These measurements were used to calculate convective and LCG heat removal rates (equations 5 and 6, Section 2). The evaporated water of metabolism was collected in the PLSS water separator and measured at the conclusion of each test. This was used to determine the total evaporative heat loss over the duration of each test (equation 3, Appendix C). The instantaneous evaporative heat loss rate was not measured directly due to the failure of dewpoint sensors, however, it was determined by a heat balance technique that will be described in the Series D test results. The net environmental heat exchange into or out of the suit was determined by an engineering heat balance analysis performed on the PLSS at the conclusion of each test. This analysis was based upon subtraction of the amount of feedwater used to reject metabolic heat from the total amount of feedwater used (equation 14, Appendix C).

The metabolic rate profile for each test was designed to simulate the actual workloads required for the various tasks and experiments to be performed on the lunar surface. The metabolic rate was controlled by varying the step rate on a Harvard step test in accordance with a predetermined calibration of metabolic rate versus step rate for each subject. The pre-test calibration was performed by a procedure identical to that of Series C. In addition, the metabolic rate was estimated on a real-time basis by using the LCG heat removal rate and inlet temperature data and the PLSS oxygen usage rate data (82, 147). This information, along with heart rate data, was used to alter the step rate, if deviations

from the calibration curve were indicated. As a final check on the metabolic rate, a chemical analysis of the lithium hydroxide canister in the PLSS was performed at the conclusion of each test to determine CO_2 production. This, combined with the total amount of oxygen used in the PLSS oxygen tank for metabolic consumption provided an RQ and total metabolic expenditure for each test (Figure C1, Appendix C). This was then compared to the other metabolic rate methods to determine a final metabolic rate profile for each test.

A biomedical harness was used to measure several body skin temperatures (see Figure A4, Appendix A). These included forehead, upper chest, lower back, bicep, hand, foot, and thigh temperatures. Copper-constantan thermocouples were used for these measurements. An ear probe thermistor was also used to measure tympanic membrane temperature. The latter measurements were recorded continuously and used to calculate mean skin temperature, total body heat storage, and heat storage rate (see equations 2, 3 and 4, Section 2). Silver chloride ECG sensors were also included in the biomedical harness and used to measure heart rates and monitor ECG. The heart rate data was used with a previously determined heart rate versus metabolic rate calibration curve (Figure C2, Appendix C). as determined in the manner described for Series B. This information was used, along with the other real-time indicators of metabolic rate, to evaluate deviations from the step rate calibration curve and make appropriate adjustments to the step rate.

As in Series A, B, and C, subject mechanical work was negligible and not considered in the results.

All of the raw data for Series D, including environmental and metabolic conditions are presented in Table D4 of Appendix D. The results calculated

from these data, including the overall total heat balance for each test, are shown in Table 3-4 of Section 3.

Series E

Series E consisted of the EVAs (extravehicular activities) that occurred on the lunar surface for the 6 manned Apollo lunar missions. During the Apollo program, a total of 28 EVAs were conducted by 12 different NASA astronauts. Lunar surface activities and experiments were performed by astronauts while wearing an Apollo-LCG, an A7L space suit and a PLSS (portable life-support system) identical to that used for Series D.

Conditions on the lunar surface proved to be similar to those of Series D with ambient pressures of 0 torr and net environmental heat exchange between 72 watts out to 137 watts into the suit.

Space suit ventilation and LCG operating conditions were also the same as Series D, and the astronauts selected LCG inlet temperatures in accordance with their own comfort.

The EVAs ranged in duration from about 4 to 7 hours each, and data were transmitted continuously from the PLSS during that time. The data included LCG inlet temperatures, LCG temperature differential (ΔT), PLSS sublimator outlet gas temperature, PLSS feedwater pressure, PLSS battery current and voltage, A7L space suit pressure, astronaut ECG, and PLSS oxygen bottle pressure. In addition, the astronauts were periodically requested to subjectively evaluate their feelings of thermal comfort.

The PLSS contained all of the life-support system consumables and equipment required for EVA. This included oxygen, feedwater for heat rejection by sublimation, communication and telemetry equipment, a battery for electrical power, and operating controls and displays.

The PLSS was attached to the A7L suit by means of a harness. A counterweight device such as used in Series D was not required since the lunar gravity was only 1/6 that on Earth.

All of the PLSS telemetry data were transmitted to the Mission Control Center at the Johnson Space Center in Houston for processing (Figure 2-6). The LCG inlet and outlet water temperatures received in this way were used to calculate LCG heat removal rates (equation 5, Section 2). This information was then used as input into a real-time computer program that included parametric curves generated from analysis of the results and model predictions of Series A-D. This provided the basis for the determination of astronaut metabolic rate, heat storage and heat stress, sweat rate, and consumables usage rates as they occurred. This information was also used to determine the metabolic cost of performing various work tasks on the lunar surface, and to monitor general physiological performance and safety. Finally, based upon the predicted consumable usage rates determined from the parametric correlations, the EVA task and experiments were modified on a real-time basis so as to permit the optimum utilization of the limited supply of consumables available. This included modifications to the traverse paths and stay times at particular geologic sites (Figure 2-7), which allowed completion of those experiments with the highest priority. Additional details on this phase of the experimental program are presented in Section 3, and in Appendix E.

The net environmental heat exchange into or out of the suit was determined by pre-mission engineering predictions based upon the expected lunar environment and the A7L space suit insulation properties. This was checked and, if necessary, adjusted after such EVA, based upon a heat balance analysis of the amount of PLSS feedwater used (see equation 14, Appendix C).

The metabolic rate profile for each EVA was controlled by the actual workloads required for the various tasks and experiments performed on the lunar surface. The rates were calculated by using the LCG heat removal data in the real-time computer program described above. The PLSS oxygen usage rate data and astronaut heart rate data were also used to determine the final real-time metabolic rate, as described subsequently in Section 3, Series E Results. The oxygen usage rate was determined from the telemetry data of PLSS oxygen bottle pressure and the astronaut heart rate was determined from ECG data. Silver chloride ECG sensors incorporated into the biomedical harness worn under the A7L suit were used to transmit the data.

As in previous test series, subject mechanical work was neglible and not considered in the results. The pertinent raw data for Series E are presented in Tables E1 and E2 of Appendix E. The results calculated from these data are shown in Table 3-6 of Section 3. The A7L suit environmental conditions, including all flowrates and inlet temperatures, etc., and surrounding (lunar) environmental heat exchange may be assumed to be the same as those for Series D unless otherwise specified.

INSTRUMENTATION, COMPUTATIONS, AND DATA MANAGEMENT

The physiological measurements recorded during Series A, B, C, D, and E consisted of various skin temperatures, rectal temperature, tympanic membrane temperature, and heart rate. These measurements were made continuously over the duration of each test. Other physiological parameters, measured during the pretest calibrations, consisted of respiratory minute volume and respiratory gas compositions (O_2 and CO_2).

Other pertinent measurements taken during the experiments consisted of LCG water flowrate, LCG water inlet and outlet temperature, suit gas

inlet and outlet dewpoints temperatures and suit ventilation flowrate. In the absence of dewpoint measurements, subject weight loss was recorded to determine evaporative heat loss.

The skin temperatures were measured with copper-constantan thermocouples and were arranged in various locations over the body. Typical arrangements as used in Series D, are shown in Figure 2-8. The skin temperatures measurements were used to determine the mean weighted skin temperature (MWST) as follows:

$$MWST = K_1T_1 + K_2T_2 + K_3T_3 + \ldots\ldots K_nT_n \qquad (2)$$

where the proportioning factors (K_1, K_2, ...K_n) are weighted according to the relative surface area of each body region (43). These weighting factors are shown in Appendix B, Table 3. The skin temperatures that were inoperative during a particular test were eliminated from the calculation of MWST and the other weighting factors were increased equally to compensate so that the weight factors used always added up to 100%.

Rectal temperature was measured in Series A using a linear precision thermistor, and tympanic membrane temperature was measured in Series C and D with a similar device, fitted to the subject's ear canal. Total body heat storage (QSTOR) was then determined by multiplying the rise in core and skin temperatures by their appropriate heat capacitances, as follows:

$$QSTOR = \sum_{\text{all I}} C(I)\,[T(I) - T(I)_{\text{Initial Value}}] \qquad (3)$$

where the heat capacitances (C(I)'s) for each body area are shown in Appendix B, Table 1, and the initial values of core and skin temperatures ($T(I)_{\text{Initial Value}}$) were measured at the start of each test. The heat

storage rate (STORAT) was then found by dividing the change in body heat storage over a particular time interval by the time interval. Thus,

$$STORAT = QSTOR/\Delta t \qquad (4)$$

During tnese experiments, STORAT was used as a means of monitoring the instantaneous direction of heat transfer between the subject and his environment. When it approached zero, the test subject was assumed to have reached steady-state conditions.

In order to determine metabolic rate, it was necessary to take respiratory measurements (minute volume, O_2, CO_2) while the subject was being calibrated at a particular heart rate or step rate prior to the test. The one exception was in Series A where respiratory measurements were made during the test.

Oxygen consumption, CO_2 production and minute volume were found by using Douglas Bags to collect the samples, a Tissot spirometer to measure respiratory volumes and the Scholander chemical analysis technique to measure O_2 and CO_2. When available, an alternative technique was used, whereby a turbine flowmeter was utilized to determine respiratory volumes and a mass spectrometer or Beckman gas analyzer was utilized to find O_2 and CO_2 composition. Oxygen and CO_2 measurements were then used to compute RQ, and metabolic rate was determined from Figure C1, Appendix C. Heart rates were monitored during all tests by silver-chloride ECG sensors incorporated in a biomedical harness with the skin and core temperature sensors. Work loads were imposed during the calibrations by the use of a Harvard Step (Series C and D), a Collins bicycle ergometer (Series B), or a motor-driven treadmill (Series A). Typical calibration curves derived in the above manner are shown in Appendix C, Figures C2-C4.

The heat removal rate of the LCG was determined by measuring the water flowrate ($\dot{M}_w$) and inlet and outlet temperatures. Turbine flowmeters were used to measure LCG water flowrate and linear precision thermistors recorded LCG inlet and outlet water temperatures. This information was used in the following equation to find LCG heat removal rate (QLCG):

$$QLCG = \dot{M}_w \cdot C_{P_w} \cdot (T_{wout} - T_{win}) \quad \text{or} \quad \dot{M}_w \cdot C_{P_w} \cdot \Delta T_w \tag{5}$$

where C_{p_w} is the heat capacity of the LCG water.

The amount of metabolic heat removed by sensible convection from the body (QCONV) was determined by measuring the ventilation flowrate through the A7L suit ($\dot{m}g$) and the suit gas inlet and outlet temperatures. This information was used in the following equation to determine convection heat loss:

$$QCONV = \dot{m}g \cdot c_{p_g} \cdot (T_{gout} - T_{gin}) \tag{6}$$

where C_{p_g} is the heat capacity of the suit oxygen. Suit oxygen flowrate was measured with a "Voluflow" mass flowmeter and suit inlet and outlet temperatures were measured with linear precision thermistors.

The amount of metabolic heat removed by evaporation heat loss was determined from measurements of suit inlet and outlet dewpoint temperature and suit ventilation flowrate, or deduced from measurements of subject weight loss. Suit inlet and outlet dewpoint measurements were made with Cambridge or Hastings dewpoint sensors, based upon the principle of fogging or defogging of a polished mirror by a thermoelectric refrigerator or heater circuit. The suit gas flowrate was measured as before with a mass flowmeter. These data were utilized in the following equation to

determine total evaporative heat loss rate (QEVAP):

$$QEVAP = \dot{m}g \cdot h_{fg} \cdot (W_{gout} - W_{gin}), \quad (7)$$

where W_{gout} and W_{gin}, the specific humidity of the suit outlet and inlet gases, are found from their respective dewpoints by means of psychrometric charts (104) and h_{fg} is the latent heat of evaporization of water vapor. For the tests in which dewpoint senscrs were not used or inoperative, total evaporative heat loss was determined by weighing the subject before and after the test with a Buffalo or Toledo human balance. Subject weight loss was then used to determine evaporative heat loss as shown in the sample calculation of Appendix C.

The total evaporative heat loss was used to determine evaporative heat loss due to active sweat (QSWT) and active sweat rate (SR). Total evaporative heat loss is compiised of three components: evaporative loss through the respiratory tract (QR), evaporativ. loss due to passive diffusion of moisture from the skin (SD), and heat loss due to evaporation of sweat (QSWT). Therefore,

$$QSWT = QEVAP - QR - QD, \quad (8)$$

and

$$SR = QSWT/h_{fg} \quad (9)$$

where expressions for QR and QD were derived from empirical results from several sources (49, 50, 80, 103) and are found in Appendix C. A sample calculation of QSWT and SR is also demonstrated in Appendix C.

The determination of radiation heat loss is a complex function of many factors, including surface properties of garments, skin and surrounding

walls, garment insulation characteristics, geometrical view factors between the subject and the surroundings, etc. For this reason, a separate engineering analysis accounting for these various factors was performed to evaluate QRAD (84). A detailed description of this anlysis is beyond the scope of this text but is summarized in Appendix B.

Other measurements made that were pertinent to these experiments included environmental (chamber or room) temperatures and environmental and internal suit pressures. The former were measured by copper-constantan thermocouples while the latter were measured with variable reluctance type pressure transducers. A complete list of the major equipment and instrumentation used in these experiments, including a brief functional description and list of manufacturers, appears in Table A3 of Appendix A.

The recording, collection, display, and monitoring of test data were controlled by a computing system incorporating analog signal receiving and conditioning instruments, analog-to-digital conversion equipment, a sequential data sampling device, digital tape transports, card readers, card punchers, typewriters, high speed printers, and assorted special equipment. Three separate computer systems were utilized to process the data, with a total available memory capacity in excess of 65,536 13-bit words. The data handling system was capable of processing more than 3000 analog data measurements separately and sampling then at a rate of 1 sample per second per measurement.

The raw data collected were displayed on cathode ray tubes (CRTs) in the test control room area as they were being sampled (See Figures E1 and E2, Appendix E). The data were also simultaneously recorded on paper and magnetic tape, and were typed on high speed printers at periodic intervals. All performance parameters of interest, including the computations of body

heat storage, and LCG, convective and evaporative heat removal rates, were computed on line, on a real-time basis to permit constant surveillance of the condition of the subject and the progress of the test. To facilitate this, real-time electronic plotting capability was included for various test sequences. At the conclusion of each test series, the computed data stored on magnetic tapes were further analyzed and used to produce final computer-generated plots of the raw data.

MATHEMATICAL MODEL

The mathematical model utilized in this study represents the end product of several years of developmental research. The earliest model was an extremely simplified 2-node version which assumed that the human thermal system could be adequately represented by subdivision into two segments consisting of a core layer and a skin layer. It soon became obvious that this assumption was inadequate for all but the simplest conditions. Over the years, more body segments were added and the physiological reponses that were simulated became increasingly sophisticated. The current model that has evolved utilizes 41 separate body compartments to describe the human thermal system.

The fundamental basis of this or any other model in which heat and energy are exchanged is the first law of thermodynamics. Simply stated, the first law says that for any substance, the difference between the heat gained (either from the environment or by internal production) and the heat lost (by transfer to the environment) is equal to the change in the internal energy of the substance plus the net mechanical work done.

The human body may be considered in the same manner as a heat engine. That is, heat is produced ($\dot{Q}MET$) by the oxidation of fuel (food) for energy, and heat is dissipated by conduction, convection, radiation, and

mass transfer trnasfer at the skin surfaces. In man, the mass transfer of 3 components: evaporation of sweat ($\dot{Q}$SWEAT), heat loss through the respiratory tract ($\dot{Q}$LUNG LATENT) and passive mass diffusion. Heat produced in excess of that which can be dissipated will be stored in the tissues ($\dot{Q}$STOR) with a resulting rise in body temperatures. In addition, a small amount of energy can be transferred from the body to the environment in the form of mechanical work. A heat balance performed on the total body, treating the skin surface as the external boundary, is shown in Figure 2-2. Consideration of the individual thermodynamic terms discussed above results in the familiar total body heat balance equation shown at the bottom of Figure 2-2 (equation 1).

To describe the internal temperature distribution within the body, a similar type of heat balance is performed on an element of tissue, rather than over the entire body. The mathematical model divides the body into 10 elements: head, trunk, right and left arms, right and left hands, right and left legs, and right and left feet. Each consists of a core, muscle, fat, and skin layer. Considering the central blood as a separate element, there are 41 distinct compartments, and each compartment is assumed to be at a uniform temperature having a discrete temperature distribution (see Figure 2-9).

Again, considering the first law of thermodynamics, heat is generated in each compartment by metabolism ($\dot{Q}$MET), and is transmitted by convective heat transfer to the bloodstream ($\dot{Q}$CONV), and by conduction to adjacent compartments ($\dot{Q}$COND). For skin compartments, convection heat transfer to a surrounding gas stream ($\dot{Q}$SEN), radiation to the environment ($\dot{Q}$RAD), latent evaporation ($\dot{Q}$LAT), and conduction to a thermal undergarment ($\dot{Q}$UG) are all considered as avenues of heat dissipation. In addition, conduction

heat transfer to the cooling tubes of an LCG ($\dot{Q}LCG$) is also considered. A typical heat balance for the internal body layers is shown in Figure 2-10, and the general equations for the core, muscle, fat, and skin layers of each major body compartment are as follows:

- Core

$$(\text{Mass} \cdot C_p)_{\text{core}} \quad \frac{dT\text{core}}{dt} = QMET_{\text{core}} - QCOND - QCONV \qquad (10)$$

- Muscle

$$(\text{Mass} \cdot C_p)_{\text{muscle}} \quad \frac{dT\text{muscle}}{dt} = QMET_{\text{muscle}} + QCOND - QCOND' - QCONV' \qquad (11)$$

- FAT

$$(\text{Mass} \cdot C_p)_{\text{fat}} \quad \frac{dT\text{fat}}{dt} = QMET_{\text{fat}} + QCOND' - QCOND'' - QCONV'' \qquad (12)$$

- Skin

$$(\text{Mass} \cdot C_p)_{\text{skin}} \quad \frac{dT\text{skin}}{dt} = QMET_{\text{skin}} + QCOND'' - QCONV''' - QRAD - QSEN - QLAT - QLCG, \qquad (13)$$

where the $\frac{dT}{dt}$ terms represent the change in temperature with respect to time and C_p is the heat capacity of the particular body layer.

A very significant fact is derivable from the previous discussion. In order to understand the heat transfer processes within the human body, a detailed understanding of the physiological processes of sweating and blood-flow regulation is required. Both of these processes greatly affect the temperature field. They both vary significantly as a function of certain body temperatures, and they are also under the control of the central nervous system. Consequently, in order to correctly describe the transient thermal response of man to his environment, two distinct, and yet interrelated processes must be understood--the heat transfer characteristics of the passive human body (the controlled system) and the active thermoregulatory control of the central nervous system (the

controlling system). The passive system has been described in the previous paragraphs and a discussion of the active control system follows.

Active Thermoregulatory Control System

The human body is capable of regulating the amount of heat that is transferred to the environment. It does so through four primary physiological mechanism:

(1) Sweat production
(2) Shivering
(3) Vasodilatation)
) Blood-flow Control
(4) Vasoconstriction)

The controlling system for each mechanism consists of three separate parts (See Figure 2-11). The first part is the detecting system which records the thermal state of the passive system. The second part utilizes this information in an integrator which serves as an amplifier or an attenuator to produce appropriate effector commands. The third part receives the effector commands and processes them into appropriate action at the periphery (sweat glands, muscles, arteries, veins).

Detector

Research has shown that thermal control signals have been generated by local temperature changes from a reference, and by the rate of change of local temperatures. Consequently, the stimulus from the detector part of the controller which describes the thermal state of the passive sytem for all four control mechanisms is of the form:

$$ERROR(I) = (T^t(I) - TSET(I) + \frac{(T^t(I) - T^{t-1}(I)}{\Delta t}) \cdot (A(I) \qquad (14)$$

Where $T^t(I)$ is the temperature of the sensitive thermoreceptors of body compartment I at time t, A(I) is a constant and TSET(I) is a reference temperature.

Integrator

The integrator part of the control system functions by modifying the ERROR signal for each mechanism. It is most probable that this signal is modified by a central control signal from the brain and by a local control signal from the skin-environment interface. Dr. J. Stolwijk of the J. B. Pierce Foundation, suggests that the central control signal would most simply be proportional to the ERROR(I) term for the tissue region representing the hypothalamic area of the brain. Furthermore, it is likely that this signal be positive for sweating or vasodilatation commands where heat transfer at the skin surface is to be augmented, and negative for shivering or vasoconstriction commands where heat transfer at the skin surface is to be attenuated. Thus, the central signal is of the form:

```
CEN SWT = SWT1 X ERROR(1)          SWEATING
CEN SHIV = SHIV1 X ERROR(L)        SHIVERING                    (15)
CEN DIL = DIL1 X ERROR(1)          VASODILITATION
CEN STRICT = STRICT1 X ERROR(1)    VASOCONSTRICTION
```

Where the index I = 1 is for the hypothalamic region of the head, and SWT1, SHIV1, DIL1, and STRICT1 are gain constants.

It is convenient to assume that the control signals for each skin segment are of the same form. Since all the local signals must be summed to produce one final local contribution to the integrated signal, the skin input may be characterized as:

```
LOC SWT = SWT2 X     (A(J)•ERROR(J))        SWEATING
LOC SHIV = SHIV2 X     (A(J)•ERROR(J))      SHIVERING
LOC DIL = DIL2 X     (A(J)•ERROR(J))        VASODILITATION      (16)
LOC STRICT = STRICT2 X     (A(J)•ERROR(J))  VASOCONSTRICTION
```

Where A(J)'s are local constants for each skin region, ERROR (J)'s

are local skin error signals and SWT2, SHIV2, DIL2, and STRICT 2 are overall local gain constants.

Based on this discussion, the most generalized integrator signals would have a local contribution, a central contribution, and a combination of both. Thus, for example:

$$\begin{aligned}
&\text{SWEAT} = \text{CEN SWT} + \text{LOC SWT} + \text{SWT3 (LOC SWT X CEN SWT)} \\
&\text{SHIVER} = \text{CEN SHIV} + \text{LOC SHIV} + \text{SHIV3 (LOC SHIV X CEN SHIV)} \\
&\text{DILAT} = \text{CEN DIL} + \text{LOC DIL} + \text{DIL3 (LOC DIL X CEN DIL)} \\
&\text{STRICT} = \text{CEN STRICT} + \text{LOC STRICT} + \text{STRICT3 (LOC STRICT X CEN STRICT)}
\end{aligned} \tag{17}$$

Effector

The third part of the control system processes the integrator signal into an appropriate response to be delivered to the periphery for effector action. Thus, the SWEAT signal is proportioned into several peripheral sweat commands based on the density of sweat glands, and the SHIVER signal is proportioned into several local heat generation terms in the muscle region based upon muscle density. The vasoconstriction and vasodilatation terms are similarly proportioned into various contributions to the local blood flow, $(\dot{m}_I)_b$. In addition the blood flow is also modified due to increases or decreases in metabolic activity level (q_m). Thus

$$(\dot{m}_I)_b = \frac{B(I) + [C(I) \text{ X DILAT}] + [E(I) \text{ X } q_m(I)]}{1 + [D(I) \text{ X STRICT}]}$$

Where B(I) is a basal blood-flow rate for tissue element I, C(I), D(I) and E(I) are weight ratios for element I and $q_m(I)$ is the local heat generation term.

Through control of local heat generation, blood flow, and sweat rate, the active thermoregulatory control system interfaces with the passive system.

A more detailed description of the mathematical model, including the various physical properties and control parameters utilized, is presented in Appendix B. In addition, there are various options that are available within the model for evaluating the thermal response of man to different activity levels, various environmental conditions, and for several protective garment configurations, ranging from simple clothing to a complex space suit. For interested readers, a description of these additional capabilities is available in documented references of the mathematical model computer program and in the program user's manual (80, 94, 127).

The mathematical model described here was transformed into magnetic tape for use on a digital computer to support this experimental program. The computer program (94) is written in Fortran V for the Univac 1108 computer with the EXEC II or EXEC 8 operating systems. However, the program is compatible with other computer systems such as the IBM 360 series, and is available on request to any interested party.

Implementation of the Model and Generation of Trends

The mathematical model described above was used to investigate the experimental results of Series A-E and as a means to predict physiological trends in human performance. In addition, comparison of the model predictions with the test data permitted a "tuning" of the model which resulted in improved accuracy.

To accomplish the above tasks, computer simulations were run for each test series. The test conditions for each experiment were used as

input to the model and the resulting computer output was then compared to the experimental data. The input consisted of various environmental parameters versus time, read into the computer program in tabular input form. These included ambient pressures, temperatures, and dewpoints; garment, LCG and suit insulation properties; and incident radiation heat fluxes, and other similar parameters. The metabolic rate profile was also entered as input for each experiment.

The computer model output consisted of the various human physiological responses of interest. These included body temperatures, including skin and core temperatures, mean skin temperature, total body heat storage, heat storage rate, sweat rate, evaporative, convective and radiative heat loss rates, and LCG heat removal rate. Shiver rate and skin blood-flow rates were also available for examination and were frequently used to explain particular experimental results. Other output parameters of interest were LCG water and suit gas outlet temperatures, suit outlet dewpoint temperatures, space suit or garment temperatures, etc. A sample of the input-output format for a typical computer program run is shown in Appendix B.

The model predictions for each experiment were hand-plotted graphically with the test data superimposed. Although this was done as a function of time for many of the parameters, the steady-state results were of primary interest for these experiments. The process of "tuning" the model to bring it into closer agreement with the test data was in inexact process at best; heavy reliance was placed on intuition and previous experience in using the model. All adjustments of physiological or physical parameters within the model were constrained within the bounds of current knowledge.

Comparisons of the model results and test data exhibited good accuracy for almost all physiological parameters. Errors were not large enough to warrant modifications to the active thermoregulatory control system equations. However, improvements in the predictions of individual skin temperatures were achieved with modifications to the passive, controlled system equations. The actual adjustments that were made to the model to improve its predictions are explained in more detail in Sections 3 and 4.

After the model was correlated in the manner described above, the results of each test were again superposed with the predictions to produce the final results shown in Section 3. Comparison of the model predictions with the test data provided one other benefit. It illuminated many of the inadequacies of the current model and formed the groundwork for a new model that will be described subsequently.

One of the most significant applications of the model in this experimental program was in the derivation of correlations demonstrating the physiological response of man while wearing an LCG to maintain comfort. These correlations are presented in Section 4. The experimental results were first plotted independently, and a regression analysis and curve fitting to the data were performed. This included an error analysis in which only statistically significant data were included. Comfort envelopes were then generated by the model describing the predicted behavior of the same physiological parameter. These comfort envelopes were superposed over the experimental results. The degree to which the data and regression curves fell within the predicted envelopes provided a theoretical basis for the physiological behavior observed during the tests and provided additional confidence in the test results and the

model itself. Further details on the procedures employed for the above results are presented in Section 4.

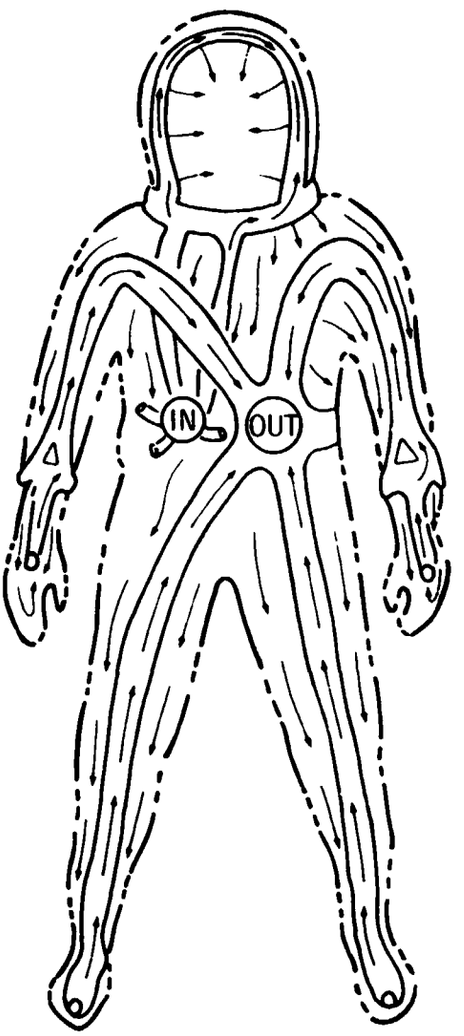

Figure 2-1.- Ventilation flow paths in the Apollo A7L suit.

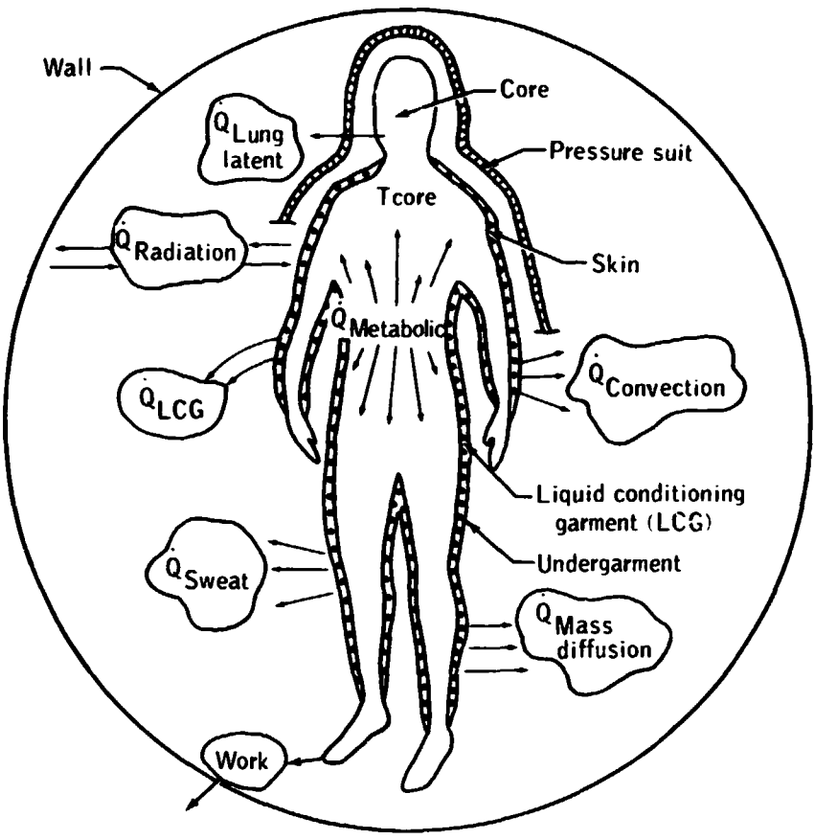

$$\underbrace{\dot{Q}_{Metabolic}}_{\text{Heat produced}} - \underbrace{\left(\dot{Q}_{Convection} + \dot{Q}_{Mass\ diffusion} + \dot{Q}_{Sweat} + \dot{Q}_{Lung\ latent} + \dot{Q}_{Radiation} + \dot{Q}_{LCG}\right)}_{\text{Heat dissipated}} = \underbrace{\dot{Q}_{Stored}}_{\text{Heat stored}} + \text{Work} \quad (1)$$

Figure 2-2.- The total body heat balance equation.

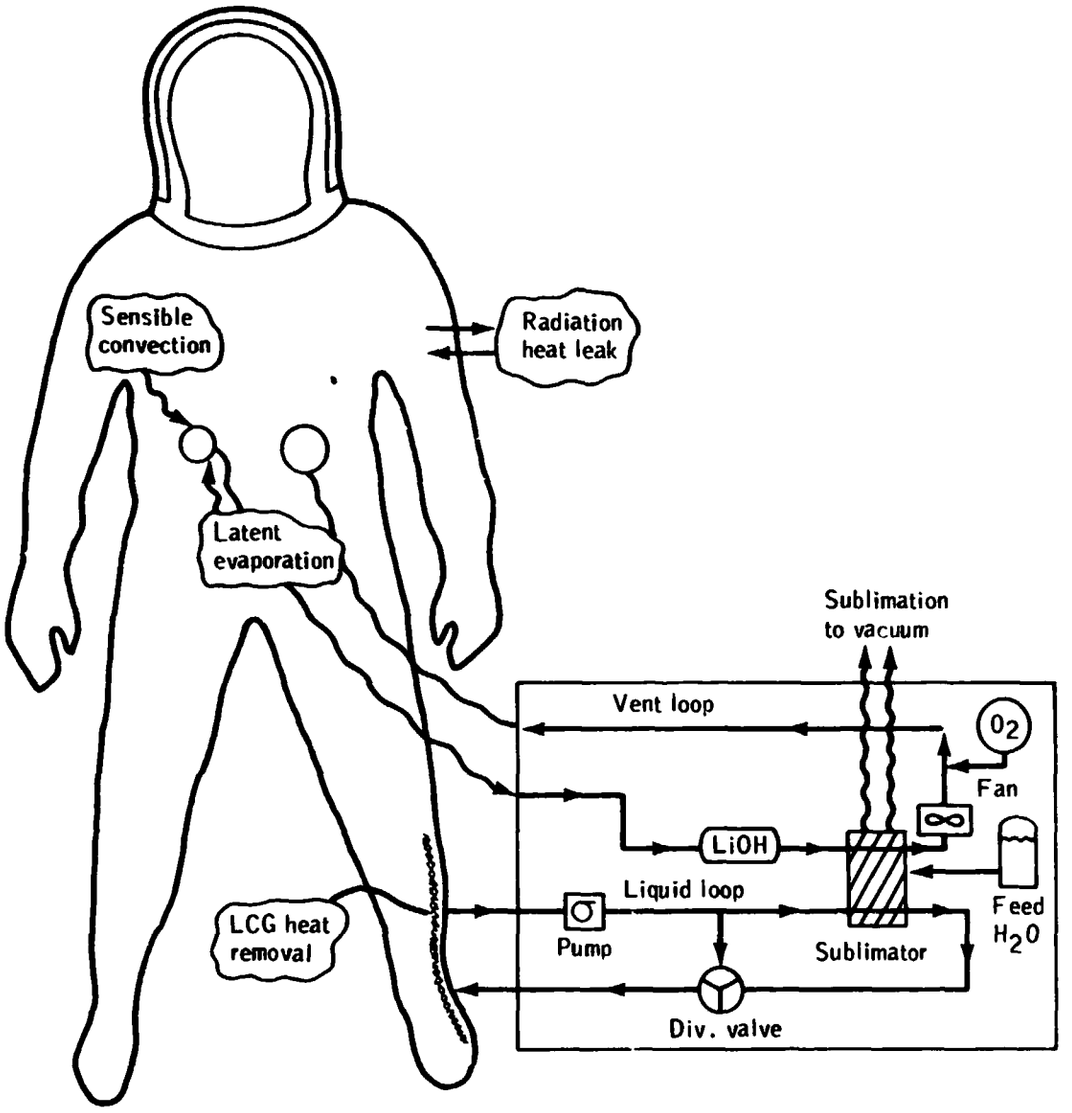

Figure 2-3.- PLSS oxygen and water loop flowpaths.

Figure 2-4.- Apollo extravehicular mobility unit (EMU).

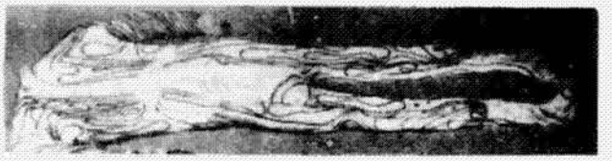

(a) Inside-out view showing cooling tubes.

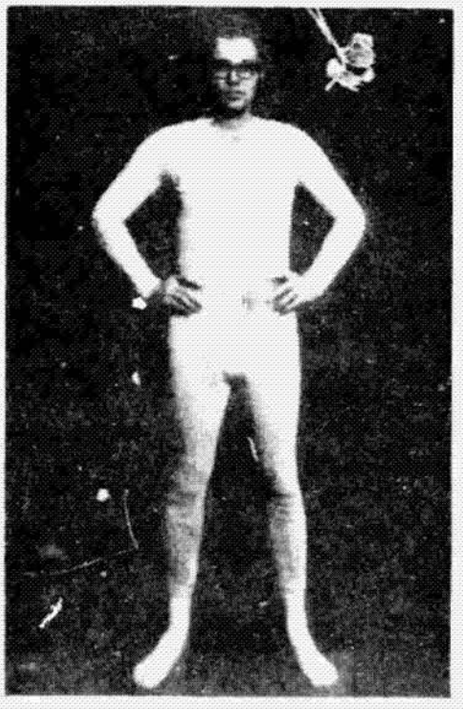

(b) Full view.

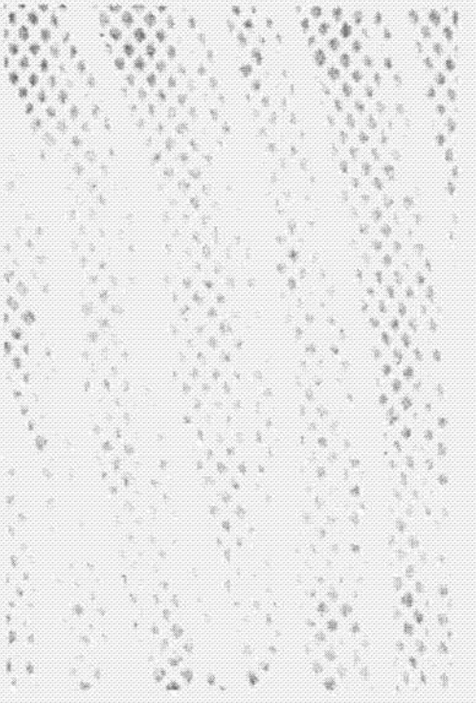

(c) Close-up view of tube distribution.

Figure 2-5.- Liquid cooled undergarment.

REPRODUCIBILITY OF THE
ORIGINAL PAGE IS POOR

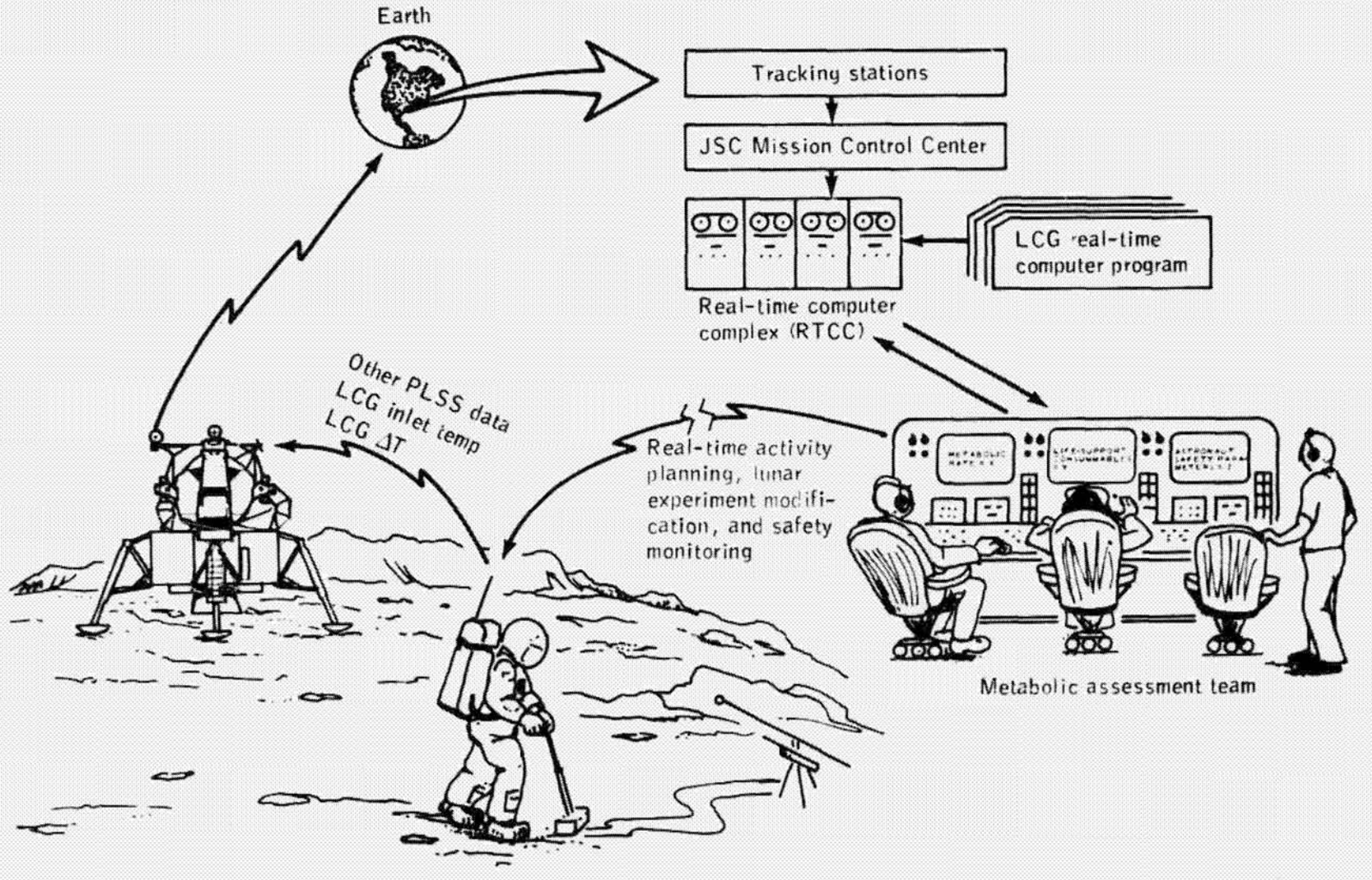

Figure 2-6.- Live data pathways and flight monitoring and control system for Apollo missions.

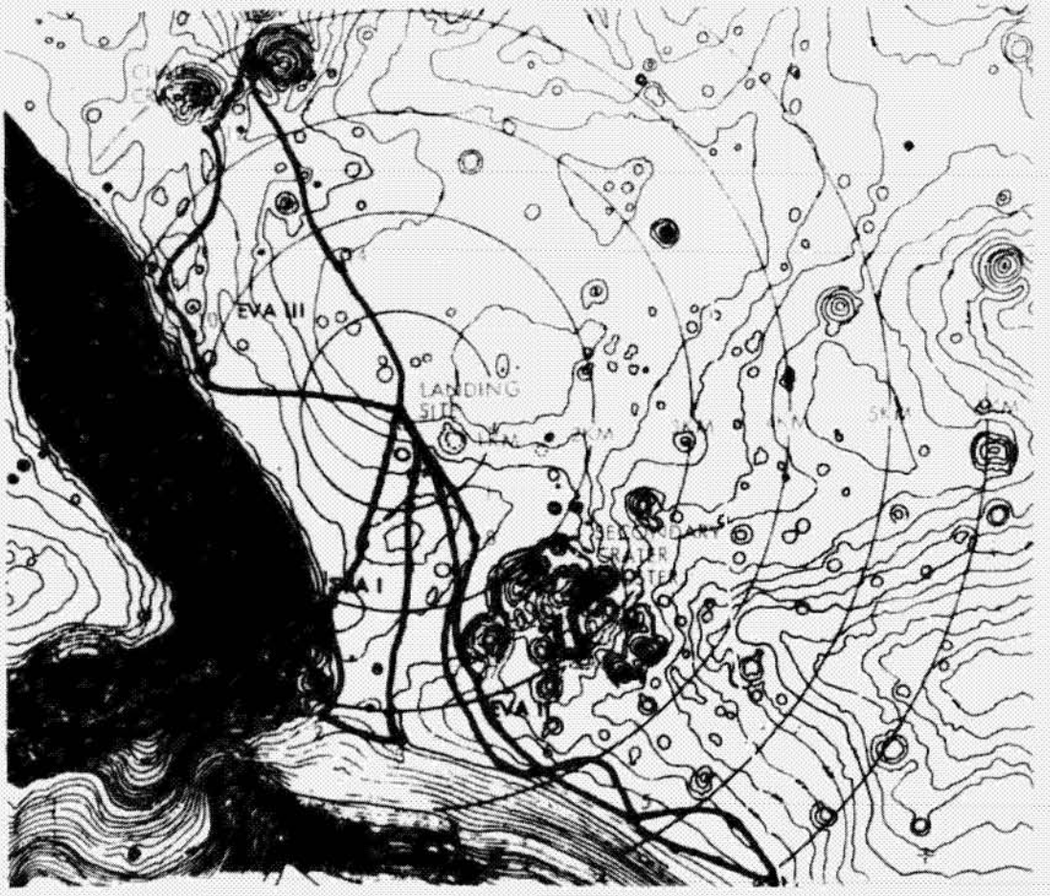

Figure 2-7.- Lunar traverse paths for Apollo 15.

REPRODUCIBILITY OF THE
ORIGINAL PAGE IS POOR

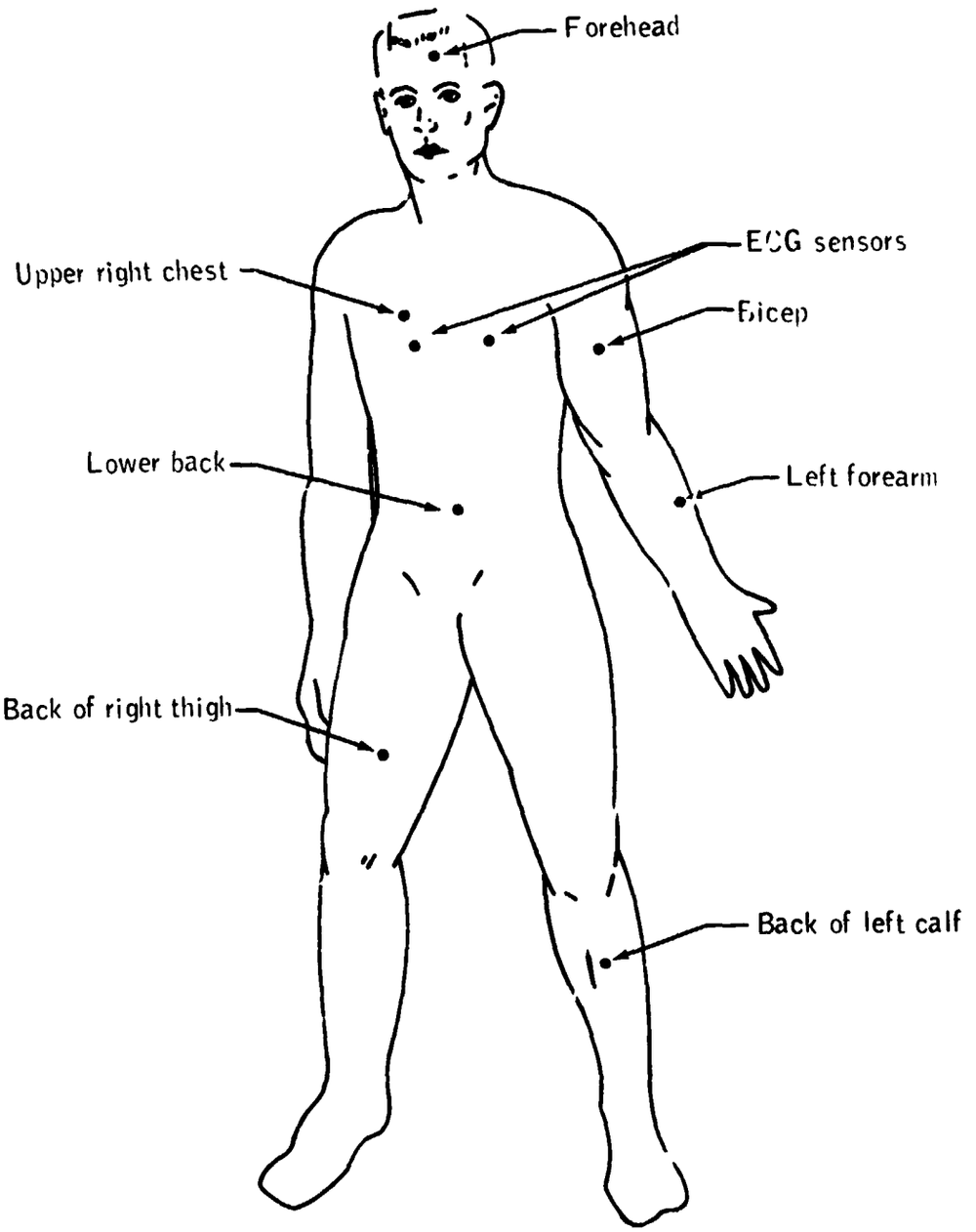

Figure 2-8.- Typical placement of skin temperature thermocouples.

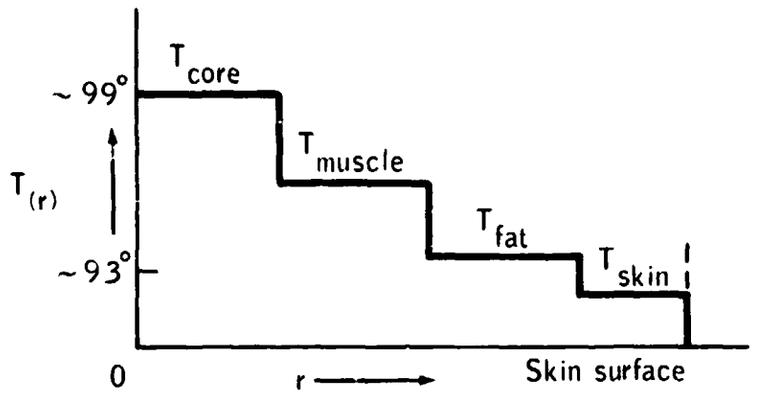

Figure 2-9.- Discrete temperature distribution of mathematical model.

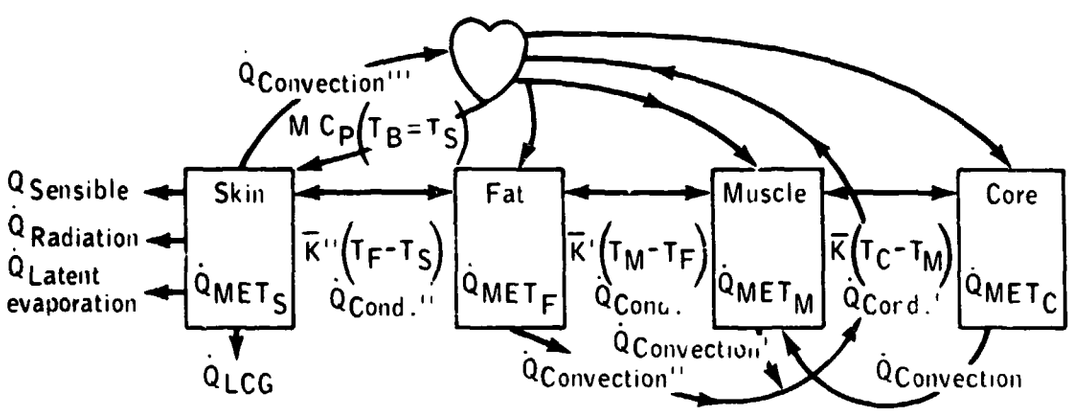

Typical heat balance for skin segment

$$K''\left(T_{fat}-T_{skin}\right)+MC_P\left(T_{blood}+T_{skin}\right)+\dot{Q}_{Metabolic\ generated}$$
$$-\dot{Q}_{radiation}\ -\dot{Q}_{sensible}\ -\dot{Q}_{latent\ evaporation}\ -\dot{Q}_{LCG}$$
$$=\left(Mass_{skin}\right)\left(CP_{skin}\right)\frac{dT_{skin}}{dt}$$

Figure 2-10.- Heat balance for internal body layers.

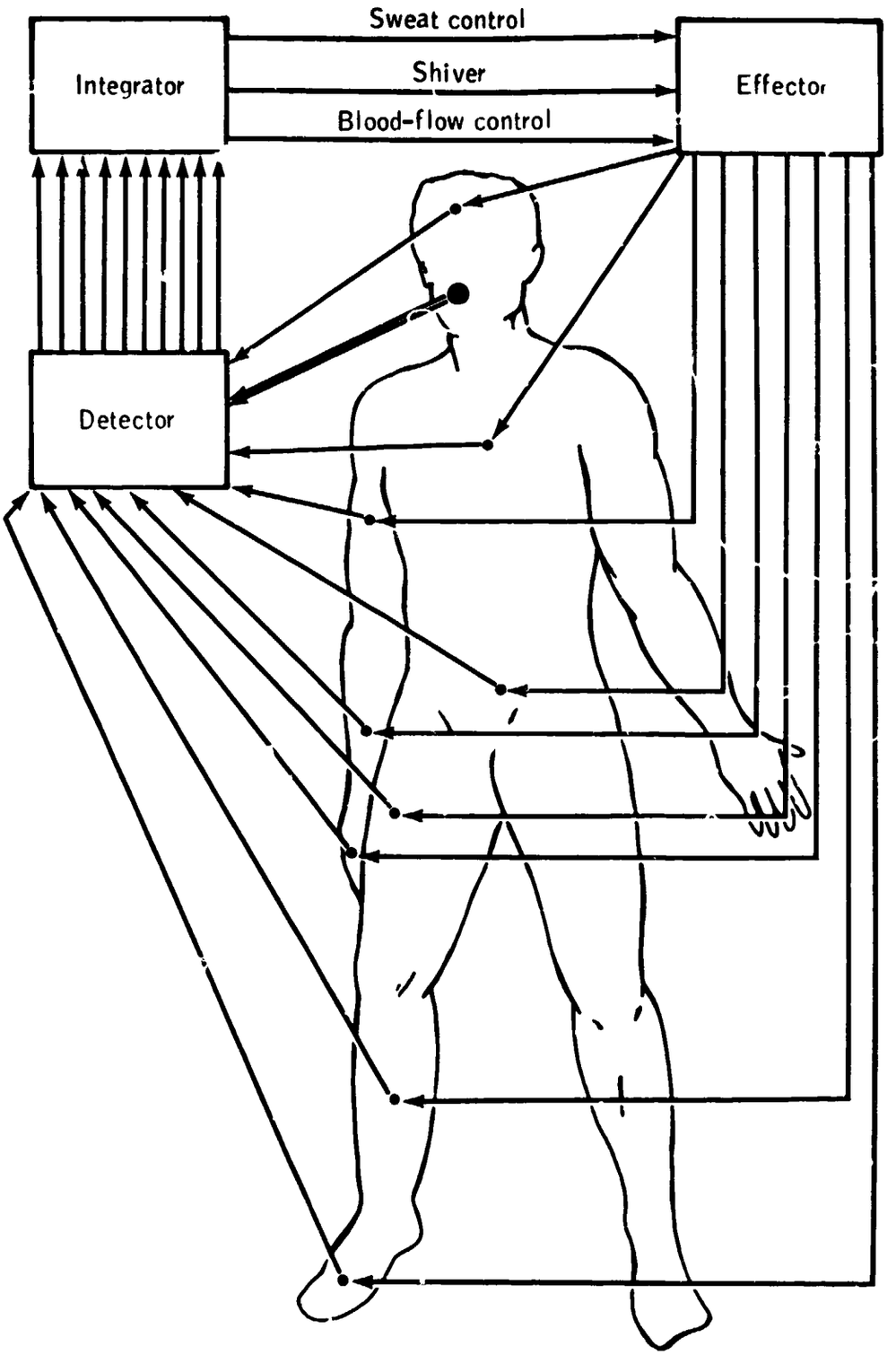

Figure 2-11.- The controlling system of the mathematical model.

3. RESULTS

SERIES A

Series A was conducted in a room temperature environment, with subjects wearing an insulating coverall garment designed to limit convection and radiation heat loss. There was no air ventilation flow across the skin and all tests were conducted at sea-level pressure. The Apollo-LCG was worn under the outer garment and the water flowrate was fixed at 109 liters/hr while the water temperature was varied.

The metabolic rate for each test sequence was controlled by varying the speed of a motor-driven treadmill and is shown in Table D1 of Appendix D. The raw, steady-state data for each of the test conditions is also shown in Table D1.

Heat Balance

Table 3-1 presents the calculated steady-state results and heat balance data for Series A. The basis of the heat balance shown in Table 3-1 is the heat balance equation (see equation 1, Figure 2-2). All terms in this equation were determined as indicated by the footnotes of Table 3-1, with the exception of shiver rate, which could not be measured, and mechanical work rate, convection, and radiation heat loss, which were all assumed negligible. Mechanical work rate was neglected because the nature of the exercise profiles of Series A produced no external work other than friction, which was small. This was the case for all of the exercise profiles considered in this study. Convection and radiation heat loss were neglected because the physical characteristics of the arctic coverall overgarment (no gas ventilation and low thermal conductance) were assumed to insulate the test subject effectively from heat transfer by these mechanisms.

The results show the expected relationship between heat production and heat loss. That is, for a constant LCG inlet temperature (7 or 16°C), total evaporation heat loss, heat loss through the LCG, and total heat loss all increase as metabolic heat production increases.

The HEAT BALANCE row shows the difference between heat production and heat loss. From the heat balance equation, this difference may be attributed to the rate of heat storage (or shivering). It should be noted that this value is negative for all tests with the exception of Test 5, which indicates that heat removal was generally greater than metabolic heat production. Negative heat balance values are often indicative of cool or cold testing conditions, while positive values signify warm conditions.

Further information is provided by the TOTAL HEAT STORAGE row. These values show the direction of changes in skin and rectal temperatures over the duration of each test. Here, negative values indicate a drop in body temperatures, while positive values signify an increase. It is observed that body temperatures decreased for low metabolic rates at both LCG inlet temperatures, but became higher and eventually positive as metabolic rate increased. This suggests that test conditions were cool or cold at the low metabolic rates, but became warm as work rate was increased. This was indeed the case as test subjects visibly shivered in Tests 1, 2, and 3, and subjectively noted cold sensations in Tests 7, 8, and 9.

In order to more fully assess the heat balance equation, it was necessary to determine the final heat storage rate at the end of each test. This was found from the change in body temperatures measured over the final 30 - 60 min. Ideally, for true steady-state conditions, this value

would be close to zero, indicating that body temperatures were not changing while the various heat production and heat loss measurements were being recorded. However, due to subject fatigue and discomfort resulting from cold conditions (often accompanied by shivering); and the long duration of many of the test sequences in Series A, it was possible to reach a true steady-state in only 5 of the 11 tests. Predictably, these tests were at the higher metabolic rates, for which shivering or cold discomfort was not a factor (Tests 4, 5, 6, 10, and 11).

For those tests in which a true steady-state was not obtained, a precise accounting of all of the terms in the heat balance equation is difficult because equilibrium conditions were not reached. However, additional insight can be provided by subtracting the FINAL HEAT STORAGE RATE row from the HEAT BALANCE row. Theoretically, the difference between these two values, designated the HEAT DEFICIT row, should be the shiver rate, since it is the only unknown term left in the heat balance equation. However, in practicality, the heat deficit also represents any errors made in the determination of the individual heat production, heat loss or heat storage rate terms. As mentioned previously, the failure to reach true steady-state for several of the tests causes complications by introducing another term into the heat balance equation (i.e., heat storage rate). Error may result if the heat storage rate is much different from zero because this indicates that body temperatures, and therefore evaporation rate, LCG heat removal, and total heat loss, were changing at the time they were measured, despite the fact that they appeared to be in equilibrium.

It is observed that the heat deficit values are all negative, ranging between -4 to -91 watts. If no errors were present, it would be expected

that the largest negative values would be at the lowest metabolic rates for each LCG inlet temperature. This would then be associated with shivering or subjective cold sensations and also with an overall drop in body temperatures and negative total body heat storage. Furthermore, in the absence of errors, the heat deficit should become more positive as metabolic rate increases until it approaches zero at about the same time that total body heat storage approaches zero. This is because shivering or cold sensation should only persist for decreased body temperatures (and negative heat storage). However, the heat deficit values of Table 3-1 do not uniformly display this trend, indicating the presence of errors in some terms of the heat balance.

The most likely sources of error may be traced to the determinations of heat storage rate, evaporative heat loss and radiation heat loss. The final heat storage rate may vary for each test condition depending on the time interval utilized in its determination. However, any value significantly different from zero indicates non-equilibrium conditions which are a likely source of error. Evaporative heat loss values are another likely source of error because they were determined from subject weight loss (see sample calculation, Appendix C). In this determination, it is assumed that all sweat was evaporated. In fact, any sweat that was not evaporated ("runoff sweat") would contribute to weight loss but not to heat loss, since unevaporated sweat does not constitute heat removal. Therefore, the use of subject weight loss to determine evaporative heat loss rates can cause error because the latter values may be too large.

The third, most likely source of error, is the determination of radiation heat loss. Based upon the low thermal conductance of the arctic overgarment, it was assumed that radiation interchange with the environment

was negligible. However, as will be seen subsequently, the most pronounced effect of cold LCG inlet water temperatures is to lower the average skin temperature. This effect, combined with the low water temperatures inside the LCG itself, acts to drop the inside surface of the overgarment nearest the skin below that of the external environment. This could then provide an effective "sink" for radiation heat transfer from the environment to the skin or the LCG. In either case, the result would be an overly large heat removal rate, which would, in turn, result in a negative heat deficit. This effect would be most pronounced for the lowest skin and LCG inlet water temperatures, but may be present for the other test conditions.

Based upon the heat deficit values found in this test series, and the limits of radiation heat leak commensurate with the physical properties of the arctic covergarment, a value of 30 watts appears to be a reasonable estimate of the actual radiation heat transfer from the environment into the man/suit system. Although this value probably changes for each test condition (being somewhat larger at the lower metabolic rates and smaller at the higher metabolic rates), it represents an average which would enhance the heat balance calculations, and yet is quite reasonable. It should also be noted that the effect would be less significant for higher LCG inlet temperatures, since the "sink" temperature would more closely approach that of the environment.

Finally, it should be observed that the actual heat deficits are probably a consequence of a combination of the above factors, rather than any one in particular. It is likely that shivering and errors in evaporation heat loss, heat storage rate and radiation heat loss all combined to produce the negative heat deficit values of Table 3-1.

Transient Results

Typical results for the transient response of skin and rectal temperatures are shown in Figures 3-1 to 3-4. The 4 tests shown represent the data for 2 different metabolic rates (one low and one high) each at the 2 LCG inlet water temperatures utilized (7°C and 16°C).

The most immediate observation about these data is that for the lower LCG inlet temperature, all body temperatures were observed to decrease over the duration of the test for the lower metabolic rate (Figure 3-1). However, for the same inlet temperature at the higher metabolic rate (Figure 3-2), the rectal temperature, and the temperature of the arms and legs are shown to significantly increase while the forehead undergoes little change and the chest drops markedly.

At the higher LCG inlet temperature, the results are somewhat similar, except elevated in all cases. That is, at the lower metabolic rate (Figure 3-3), there is little change in most of the body temperatures, with the chest, arms and legs showing slight decreases. For the higher metabolic rate (Figure 3-4), all temperatures are observed to increase except the chest, which decreases.

In general, those skin temperatures in which the LCG is in contact with the skin initially decrease as the test begins. However, as time progresses, the regions in which muscle action was minimal (such as the chest or the back) continue to drop, while the regions of vigorous muscular activity (such as the arms and legs) begin to increase as the heat produced by the nearby muscles reaches the skin surface. The lag time required for this to occur appears to be in the order of 30 to 45 min, a result forecast by the mathematical model (solid lines). The coldest

skin temperatures monitored were those of the chest and the thigh, while the warmest was the forehead, which was not in contact with the LCG.

The predictions of the mathematical model are shown in Figures 3-1 to 3-4 as solid lines. In general, there is reasonable agreement with the test data. The most accurate predictions are for rectal and mean skin temperature, and for total body heat storage. Differences between predictions and actual results for several individual skin temperatures were greater. These variations are a consequence of several complex phenomena and will be discussed subsequently, after other results are examined.

The bulk of the information gained from this test series is derived from analysis of the steady-state results. These are shown for all 11 test conditions in Table 3-1, and beginning with Figure 3-5, an analysis of the heat removal characteristics of the LCG.

LCG Heat Removal

Figure 3-5 shows the heat removal capability of the liquid conditioning garment (LCG) at various metabolic rates and water inlet temperatures. The LCG heat removal rate is determined from equation 5 of Section 2. Test data using LCG inlet water temperatures of 7° and 16°C are shown, along with the the data of Santamaria (112) for higher temperatures of 23-26°C.

The results indicate that the LCG heat removal rate is a nearly linear function of metabolic rate, for metabolic rates between 100 and 620 watts. The slopes of the lines for 7°C and 16°C are approximately equal (slope = change in LCG heat removal per unit change in metabolic rate ($\sim$ 0.4)), with the cooler inlet water temperature curve displaced

predicted results from the mathematical model are shown by

the solid lines, and agreement between the test and predicted results is fairly good.

At first glance, differences between the test and predicted results appear to be attributable to the heat transfer coefficient between the skin and the LCG (See Equation 10, Appendix C). The model assumes a fixed heat transfer coefficient (Figure 3-6), whereas the actual heat transfer coefficient may vary considerably from test to test for various reasons. One of these is the actual fit of the LCG. For these tests, all 5 subjects used the same LCG, although the subjects differed in physical size. Thus, the efficiency of the LCG was not the same from subject to subject.

Another important variable is the degree of wetness of the underliner that separates the tubes of the LCG. The liner must be fully wet from perspiration in order to establish a maximum conductive path between the tubes. This acts to increase the effective surface area of the LCG in much the same manner as fins act to increase the effectiveness of a heat exchanger. If the liner is not fully wet, the heat transfer coefficient and the LCG heat removal rate will vary depending upon the degree of wetness. The fact that the test data did not exhibit significant variations, and that the predicted results were lower than the actual data by a nearly constant amount indicates that the heat transfer coefficient used by the model may be low, resulting in slightly less heat removal than observed in the tests.

For the highest inlet temperatures, the original raw data of Santamaria showed considerable scatter in heat transfer coefficient values. Furthermore, the values were generally lower than those observed in this test series. For this reason, the use of Santamaria's experimental data

(112) was limited to heat transfer coefficient values between 10 and 25 watts/°C, results consistent with the Apollo-type LCGs used in Series A-E. Also, slight differences in test conditions, and in the outer cover garment used by the test subjects contributed to differences between the results of Santamaria and the predicted results. However, the important point is that the trends shown by these data are basically in agreement with the predicted results.

The results of this test series indicate that a considerable percentage of the metabolic heat generated was absorbed by the LCG. This was especially true at the colder inlet temperature where 100% or more of the metabolic heat produced was removed by the LCG for metabolic rates below 440 watts. For such conditions, there was an overall negative heat balance and test subjects were subjectively cold, with frequent shivering. The negative heat balance was manifested by negative heat storage values. These were calculated using equation 3 of Section 2, and determined for each subject over the duration of each test. They are indicated by the numbers located near each data point of Figure 3-5.

Additional insight may be gained by replotting the results of Figure 3-5 in terms of the percentage of metabolic heat production removed by the LCG (LCG heat removal/metabolic rate) vs. LCG inlet temperature. This is shown in Figure 3-7. It is noted that there was a very sharp increase in LCG heat removal from 30% to over 100% of the metabolic heat production as LCG inlet temperature decreased from 29°C to 7°C. Furthermore, most of the data fall within a fairly narrow band, which is shown bounded by the lines representing model predictions of 585 and 234 watts. The fact that the observed data for a wide range of metabolic rates fall into a narrow band illuminates the feasibility of using this relationship

as a means of predicting metabolic rate from LCG performance. It can be seen that if the LCG heat removal and inlet temperature are known, an estimate of metabolic rate can be determined from the data of Figure 3-7.

Obviously, if the band of data were narrower, these estimates would be more accurate. Considerable scatter is introduced as a consequence of the fact that many of the test points in this series consisted of off-comfort conditions. That is to say, the subjects were not permitted to control the LCG inlet water temperature in order to maintain comfort. As a consequence, many of the test conditions were too cold. Most of the data scatter in the band of Figure 3-7 occurs in the region of colder LCG inlet temperatures and is associated with subjects who were too cold and frequently shivering.

Shivering results from depressed skin and rectal temperatures, which cause a reflex involuntary contraction of the skeletal musculature. The mechanism of detection and control is by means of thermoreceptors in the skin and hypothalamus (8,15). The involuntary muscular contraction causes increased heat production which is indistinguishable from the heat of metabolism. Consequently, shivering is an off-comfort condition that can produce thermal effects which will cause variations in data from values expected under comfort conditions.

In fact, any off-comfort condition which results in significant thermoregulatory adjustments, such as vasodilatation, vasoconstriction, extreme sweating or shivering, will alter the means by which the body dissipates heat and therefore change the normally linear relationship that exists between heat production and heat loss at comfort. It will be shown later that if subjects are permitted to regulate the LCG inlet temperature in order to maintain thermal comfort over a wide range of

metabolic rates, that the scatter in LCG heat removal data is much less, with the resulting improvement in metabolic rate estimates from LCG performance.

It should also be noted that there is very good agreement between the computer model predictions and test data, emphasizing the capability of the mathematical simulator to predict accurately the heat removal characteristics of the LCG in response to the various test conditions.

From the apparent linearity of Figure 3-5, it might be concluded that an incremental increase in the heat produced by the muscles will reach the skin and be removed in a linear fashion by the LCG. However, it is necessary to observe relationships between skin temperature, LCG performance, and other factors in order to clarify this hypothesis.

The data of Santamaria show the same trends as the observed test data, but with a considerably lower LCG heat removal rate. This is a consequence of the higher inlet water temperatures and the reduced temperature gradient between the skin and the LCG water. Since the gradient represents the driving force for heat transfer between the skin and the LCG, it is expected that higher inlet water temperatures would result in decreased heat removal by the LCG. If there are no other means available for removing the excess heat that cannot be removed by the LCG at the higher inlet temperatures, body temperatures and heat storage will rise. This is supported by the increase in the heat storage values shown in Figure 3-5 for progressively warmer inlet water temperatures at constant metabolic rates. For example, at a metabolic rate of approximately 440 watts, heat storage increases from -37 to +32 to above 88 (predicted) watt-hours as LCG inlet temperature increases from 7 to 16 to 24-26°C.

Sweating and Evaporative Heat Loss

The consequence of decreased LCG heat removal is an increase in skin and rectal temperatures and body heat storage. Since active sweat rate is directly controlled by the increase in core and skin temperatures, it would be anticipated that this would lead to an increase in sweat rate and evaporation heat loss. The computer model utilizes the following relationship, developed by Stolwijk and Hardy (136) to characterize active sweating: $SWEAT = K_i (T_{skin_i} - T_{skin_{i(o)}}) + K_{si} (T_{skin_i} - T_{skin_{i(o)}}) \cdot (T_{core} - T_{core_{(o)}}) + K_c (T_{core} - T_{core_{(o)}})$ (See equation 17, Section 2). Other investigators relate the rate of change of skin and rectal temperatures to sweat rate; however, in all cases, a rise in body temperatures and heat storage is associated with an increase in active sweat rate.

The expected relationships between sweating and the decreased LCG heat removal at high inlet temperatures are shown in Figure 3-8. Total evaporative heat loss was calculated from total weight loss for each test condition as shown in the sample calculation in Appendix C. This was then converted into evaporation heat loss from active sweat by subtracting out empirical expressions for evaporation heat loss by passive diffusion and by respiration (equations 5 and 7, Appendix C). The results are plotted in Figure 3-8 as a function of metabolic rate, and demonstrate that the sweating response is not initiated unless metabolic energy production is sufficiently high to exceed LCG heat removal rate. For higher LCG inlet temperatures, the sweat glands and active sweating are more easily stimulated, even at resting metabolic rates. However, as the LCG inlet temperature decreased to 16°C and then to 7°C, it required progressively higher metabolic rates of 229 and 410 watts to excite the sweating

response. This is shown in Figure 3-9, which presents the metabolic rate at which active sweating first occurred at each LCG inlet temperature, as taken from Figure 3-8. From Figure 3-8, the data for 24-26°C inlet temperatures show the highest sweat rates, whereas the data for 7°C inlet temperatures show the lowest. In all cases, for a given metabolic rate, sweating was reduced as LCG inlet temperature was decreased, and was dramatically less than it would have been without the LCG.

Agreement between the test data and the model predictions of Figure 3-8 is fairly good. Predicted values tend to be slightly higher than the test data for the higher metabolic rates. However, this is anticipated from the total heat balance equation since LCG heat removal predictions were slightly less than the test data values, while the other heat loss factors in the equation were relatively constant.

Inaccurate estimations of radiation heat exchange can also lead to differences between the model predictions and test data. To produce the predictions shown, the mathematical model utilizes the environmental conditions of each test as input and then computes radiation and convection heat loss between the subject and his surroundings. These calculations suggest that convective loss is unlikely, but a small amount of radiative interchange is probable. Of course, this depends largely upon the insulation properties assumed for the arctic coverall overgarment. The heat balance data of Table 3-1 also indicate that radiation heat exchange from the environment to the subject may have occurred. This "leak," although small (on the order of 30 watts), would also partially explain the constant error found between the predicted and actual results.

Another source of error is the utilization of body weight loss to calculate evaporative heat loss rate and sweat rate for each test sequence.

In addition to inaccuracies due to unevaporated sweat, the empirical expressions for evaporative heat loss through the respiratory tract and for passive skin diffusion that must be subtracted from the total evaporative heat loss data to arrive at sweat rate are approximations with a certain degree of error.

The data of Figure 3-8 (both predicted and test) display a near rectilinear relationship between active sweating and metabolic rate. This is partially because there was no active sweating for any of the cases in which the subjects were cold or shivering; and also because sweat rates, in general, were very low, indicative of little, if any, heat stress. Since shivering or high sweat rates would lead to discontinuous or non-rectilinear results, it is reasonable to expect rectilinearity in the absence of heat stress.

Another observation about the data of Figure 3-8 is that heat removal by active sweating constitutes a far smaller percentage of the total heat removal than does LCG heat removal. This can be more clearly seen by replotting the data as the ratio of heat removal by active sweating to total metabolic rate, as a function of LCG inlet temperature (Figure 3-10) and comparing results with Figure 3-7. Here it can be seen that at water temperatures between 7 and 16°C, active sweat heat removal rate varies from 0 to 16% of the total metabolic heat production, as compared with 60 to 100% for the LCG heat removal. At the higher inlet temperatures, data from Santamaria show a greater range of sweat heat removal with values between 10 and 37% of the total metabolic rate.

The data scatter at high inlet temperatures implies that under these conditions, sweat rate is driven or controlled more by metabolic rate. This is emphasized by the higher percentage of sweat heat loss rates at

the higher metabolic rates, as contrasted with the low LCG temperature data in which metabolic rate makes little difference in percent heat loss. Under the latter conditions, sweat rates are very low and appear to be driven or under the control of the LCG. However, in order to ascertain that this is truly the case, it will be necessary to examine sweat heat loss rate as its dependence upon skin and rectal temperatures and heat storage. This will be done subsequently.

The band of data relating sweat heat loss rate and LCG inlet temperature, especially at the lower inlet temperatures, also raises the possibility of using these results as a means of predicting active sweat rate from LCG performance. It can be seen that if Figure 3-5 or 3-7 is utilized to predict metabolic rate from LCG inlet temperature and LCG heat removal, then Figure 3-8 or 3-10 can be coupled to this to predict active sweat heat loss rate (and active sweat rate). Of course, in order for such a predictive scheme to be valid, it must be shown that the trends demonstrated by these results are repeatable for many other tests over a wide range of conditions. It is to this end that much of this thesis is directed.

It should be emphasized that heat loss by active sweating is only one of three ways that the body utilizes to lose heat by evaporative heat transfer. Sweating is a reflex response of the thermoregulatory system to rising body temperatures and heat stress. However, the body also loses heat by evaporation of water through the respiratory tract, and by continuous passive diffusion of water through the skin.

Evaporation heat loss by diffusion depends upon a diffusion coefficient, and the water vapor pressures of the air and at the skin surface. It may be calculated using equation 7 of Appendix C. This relationship is in basic agreement with data from Fanger (50) and other investigators (57)

and the results for a typical case are shown in Figure C6 of Appendix C. It is seen that evaporation heat loss by diffusion at comfort decreases with metabolic rate and represents a rather negligible percentage of the total evaporation heat loss. The slight decrease shown is due to increased peripheral vascoconstruction, and decreased skin temperature and saturation vapor pressure at the skin surface, associated with the progressively lower LCG water temperatures utilized at the higher metabolic rates.

On the other hand, evaporation heat loss through the respiratory tract is quite significant, especially at higher metabolic rates. Evaporation heat loss by respiration is calculated in the mathematical model by equation 5 or Figure C5 of Appendix C. This expression is shown to be dependent upon metabolic rate and the water vapor pressures of the air and in the respiratory tract. Heat loss is related to the volume of air exchanged in the lungs, and is predicated on the observation that air inspired through the respiratory tract at ambient environmental conditions will be expired at temperatures near deep body temperature and saturated at 100% humidity. The heat loss expression relates the volume of air exchanged to metabolic rate and also includes other effects, such as hyperventilation in response to hypoxia (see Figure C4 of Appendix C). Although equation 5, Appendix C is a simplification of a complex process, the results are in good agreement with observations of respiration heat loss by other investigators (50).

Figure 3-11 presents the total latent evaporation heat removal rate as a function of metabolic rate for the various LCG inlet water temperatures used. The total evaporation heat loss represents the summation of active sweat heat loss (Figure 3-8), evaporation heat loss by passive diffusion, and evaporation heat loss through the respiratory tract. It

is determined from total subject weight loss for each test condition (see sample calculation of Appendix C). Figure 3-11 shows that total evaporation heat loss is considerably greater than the heat loss by active sweating alone.

This is shown more graphically in Figure 3-12, which presents the data of Figure 3-11 as the ratio of total evaporative heat loss to metabolic rate, as a function of LCG inlet water temperature. Here it is observed that total evaporation heat loss removes as much as 52% of the total metabolic heat load produced for the higher LCG inlet temperatures (249 watts are removed by evaporation heat loss at a metabolic rate of 472 watts for an LCG inlet water temperature of 24°C). However, for the lower inlet water temperatures, this percentage is still much smaller than the LCG heat removal, usually amounting to approximately 25% of the total heat produced.

Skin Temperature, Rectal Temperature and Total Body Heat Storage

In order to understand more fully the effects of the LCG upon thermo-regulation, it is instructive to look at such physiological parameters as skin temperature, rectal temperature, heat storage and sweat rate. Figures 3-13 and 3-14 show the steady-state response of mean skin and rectal temperature to LCG inlet water temperature and metabolic rate for this test series. Mean skin temperature is calculated by weighted values of at least five skin temperatures (see equation 2 of Section 2). The weight factors are proportioned to relative body mass and only steady-state temperatures are considered.

From the steady state data of Figure 3-13, representing a composite of all metabolic rates between 117 and 615 watts, it can be seen that

rectal temperature remained nearly constant for all water inlet temptures between 7 and 26°C, while mean skin temperature showed a dramatic linear increase, with a gradient of 0.32°C change in mean skin temperature per 1°C change in inlet temperature. At the lower LCG inlet temperatures (7 and 16°C), skin temperature is controlled by the LCG water temperature rather than metabolic rate. This is evident because these data points represent a wide range of metabolic rates between 352 - 615 watts. At the higher inlet temperatures, the same conclusion is not as obvious because metabolic rates were generally lower and did not vary as widely.

It is suspected that skin temperature at the higher inlet temperatures would be more a function of metabolic rate (that is, heat production) than at lower LCG temperatures. This is shown to some extent by Figure 3-14, which shows the variation of mean skin and rectal temperatures as a function of metabolic rate. The higher inlet temperature data of Santamaria suggest a more direct increase in average skin temperature in response to metabolic rate than does the lower LCG temperature data. However, more data points at higher metabolic rates are necessary to justify this trend since this data only represented metabolic rates between 205 and 293 watts.

Comparing Figures 3-13 and 3-14, it should be noted that the variation of skin temperature in response to metabolic rate for a constant LCG water temperature (Figure 3-14) is not as dramatic as the variation of skin temperature as a function of LCG water temperature for all metabolic rates (Figure 3-13). This again emphasizes that skin temperature is more under the control of the LCG water temperature, especially at the lower water temperatures. As seen in Figure 3-13, rectal temperature appears to decrease somewhat because metabolic rate, and thus heat production, generally varied inversely with inlet temperature. On the other hand,

Figure 3-14 indicates a rectilinear increase in body temperature with metabolic rate. The slope of the curve fit to the data is 0.0035°C/watt and appears independent of LCG inlet temperature. In fact, it has been demonstrated (97) that rectal temperature varies directly in response to metabolic rate and is largely independent of heat loss at the skin surface.

In Figure 3-14, the predicted (mathematical model) results are shown as solid lines, and agreement with the actual data points is reasonable. There is very good agreement between predicted and actual rectal temperatures, while predicted mean skin temperatures are generally lower than actual results. Variations between predicted and actual mean skin temperature may be traced to individual subject variations from test to test (5 different subjects were used), to difficulties in measuring skin temperatures accurately due to the proximity of the skin thermocouples to the LCG water tubes with resultant possible biasing, and to shortcomings and simplifications of the thermal model itself.

The model predictions of mean skin temperature appear to deviate from the actual results by almost the same amount (2-3°C) for each LCG inlet water temperature. This raises the possibility that the model may be underpredicting the heat production that occurs in various tissues at a given metabolic rate, which would lead to lower predicted skin temperatures in certain areas, and a low mean skin temperature. This will be discussed further in the subsequent analysis of the transient results. However, another likely possibility is that the model may be overly restricting peripheral blood flow circulation, especially at cooler skin temperatures. This could be caused by oversimulation of vasoconstriction, or, perhaps, undersimulation of vasodilatation.

Since both of these physiological control functions are characterized in the model by complicated expressions containing set-point temperatures and gain constants (see equation 17, Section 2), it would be difficult to ascribe such errors to the model without considerably more data and analysis than are available from the present test series. However, those factors should not be overlooked as a possible source of error.

The fact that the model under-predicts mean skin temperature sheds added light on the interpretation of the results plotted in Figures 3-5 and 3-8. Differences in the predicted and actual results of these curves were traced to possible errors in the heat transfer coefficient or the radiation heat exchange properties used by the model. Now it appears that underprediction of skin temperature may also be a significant source of error, since the driving force for heat transfer to the LCG is the temperature difference between the LCG water and the skin. These factors will be examined subsequently in more detail; however, for the data of Figure 3-14, the predicted behavior of the mathematical model has some value in interpretation of the trends shown by the test data.

The S-shape of the 7°C curve in Figure 3-14 probably results in part from vasoconstriction effects which are predicted by the model for skin temperatures below 24°C at metabolic rates below 360 watts, and were noted by Webb (155). At these metabolic rates and water temperatures, skin temperature is depressed, and vasoconstriction and shivering with increased heat retention by the deep body is predicted. For this reason, the skin temperature remains constant at very low metabolic rates (dashed line). The heat reaching the skin is restricted because the peripheral blood-flow remains reduced until the metabolic rate increases enough to drive the skin temperature up by means of conduction of heat from the deep body.

As metabolic rate increases beyond 360 watts, shivering ceases, and heat production and skin blood-flow eventually increase until peripheral circulation is fully restored and active sweating is initiated. For the test data shown, this appears to occur at a metabolic rate of approximately 400 watts for the 7°C water temperature, in agreement with the results of Figure 3-9. As metabolic rate is increased further, the skin temperature continues to increase as vasodilatation and active sweating develop.

As metabolic rate increases beyond 440 watts, the rise in skin temperature ceases. The mathematical model predicts that this occurs because the active sweat response is large enough to offset the increased metabolic heat production, and evaporation heat loss maintains the skin at nearly constant temperature. Thus, skin temperature does not appreciably rise because the heat removed by the LCG and by evaporation are adequate to remove all of the heat of metabolism.

The shape of the 16°C inlet-water temperature curve is somewhat different in appearance. Here the model predicts vasoconstriction effects only at the lowest metabolic rates. From the test data, the onset of active sweating occurred at 220 watts (see Figure 3-9). Skin temperature is not depressed as much as for the lower water temperature case, and continues to rise as metabolic rate increases. This, coupled to increases in core temperature, results in larger sweat rates, sufficient to remove the heat of metabolism. The higher sweat rates are required because LCG heat removal is less at the higher inlet temperature and must be supplemented by evaporative heat loss.

Core temperature, skin temperature, peripheral vasodilitation and sweating continue to rise until the last is high enough to balance total heat production with total heat loss. This occurs before the skin is

fully wetted, in a zone in which sweat rate can be greatly increased with only slight increases in skin temperature. The result is a near-constant plateau in skin temperature, which occurs at lower metabolic rates than for the data of the 7°C case.

Skin temperature ultimately resumes its increase at higher metabolic rates (dashed line) because LCG heat removal, sweating, and evaporative heat loss are eventually insufficient to maintain a steady-state heat balance. At this point, the skin is fully wetted, and body heat storage, core temperature, and skin temperature must all rise until the latter is sufficiently high to raise the vapor pressure of water at the skin surface. This augments evaporative heat loss enough to offset the increased metabolic rate but requires a much greater rise in skin temperature than the previous zone.

The behavior of the 16°C curve again suggests that as inlet temperature increases, skin temperature becomes influenced more by metabolic rate and less by the LCG. The data of Santamaria for the 24-26°C water temperatures seem to reinforce this idea further, but again, more data points at higher metabolic rates are needed.

As mentioned previously, the rectal temperatures displayed in Figure 3-14 show a general increase with metabolic rate. There was no appreciable difference between the data for 7 or 16°C water temperatures. This general increase is associated with an increase in heat production accompanied by active sweating in order to maintain a proper total heat balance at the higher metabolic rates. This is the trend predicted by the mathematical model, and agreement with the test data in this case is excellent.

As mentioned previously, the dependence of active sweating upon skin temperature and core temperature is well known (8, 15, 49, 65, 107, 139). This relationship was observed in the present test series and is seen in Figures 3-15, 3-16, 3-17 and 3-18.

Figure 3-15 indicates a general increase in the active sweat rate as skin temperature increases from 24 to 32°C, and Figure 3-16 shows a substantial increase in active sweat rate with a rise in rectal temperature from 36.5°C to 38.5°C. Thus, sweat rate appears to be more sensitive to a change in rectal temperature than a change in skin temperature, as emphasized by the greater slope of Figure 3-16 compared to Figure 3-15.

This is demonstrated in another way by Figure 3-17, which relates the change in average skin and rectal temperatures measured over the duration of each test to active sweat rate. Here, increases in average skin temperatures on the order of 5-6°C are required to produce the same equivalent sweat rates as an increase of 1.5°C in rectal temperature. It is this type of observation that has led physiologists to the conclusion that the response of the thermoregulatory control system (in this case, sweating) to changes in skin temperature constitute a less sensitive, "fine tuning" type of control, while adjustments in response to changes in deep body (or hypothalamic) temperature are associated with a more sensitive homeostatic control mechanism (101).

Concerning the model predictions shown in Figures 3-15 and 3-16, it is seen that the model results show the same trends as the data. The separate predictions for 7° and 16°C LCG inlet temperatures illustrate the fact that sweating depends upon both skin and core temperature. Thus, for example, it is possible to have the same sweat rate for low skin temperatures and high rectal temperatures as for high skin temperatures

and lower rectal temperatures. It is noted that for the skin temperature curve, the onset of sweating is predicted to occur considerably before it actually did. The same discrepancy is present, although much less noticeable,in the rectal temperature curve. Thus, the model predicts the occurrence of sweating at lower skin or rectal temperatures than was actually observed; and also predicts higher sweat rates for a given skin or rectal temperature.

These findings may explain why predictions of sweat heat loss rate and total evaporative heat loss rate (Figures 3-8 and 3-11) were good despite the fact that skin temperature was underpredicted. In other words, the model simulations of skin temperature (Figure 3-14) and sweat rate (Figures 3-15, and 3-16) deviate from the actual results in an opposing fashion. The total effect is that the heat balance is generally accurate because errors in predictions of skin temperature and predictions of the effects of skin temperature upon sweating tend to cancel one another out. The data of Figure 3-17, on the other hand, show much better agreement between the actual and predicted change in skin and rectal temperatures versus sweat rate. Thus, the model appears to be better at predicting the effect of a change in skin or rectal temperature upon sweating than in relating the absolute skin or rectal temperature to sweating.

In light of the above, it would seem that some of the set-point temperatures used in the equations characterizing sweat in the model (equations 14-17, Section 2) may be too low, while the gain constants utilized appear to be accurate. This would lead to a premature predicted onset of sweating, yet with a correct slope and an accurate prediction of the effect of changes in skin and rectal temperature upon sweating.

Modifying the set-point temperatures in accordance with the above, while simultaneously decreasing the model's vasoconstriction function (or increasing vasodilatation), would probably produce a rise in skin temperatures with little effect upon sweating, thus bringing predictions more into agreement with actual results. However, due to the complex dynamic interactions of the model (the sweating function indirectly interacts with the vasoconstriction function, etc.), these changes may not produce the results that appear obvious from first glance. Furthermore, many other factors have been mentioned in the test itself which could contribute to the observed errors, and it is likely that a combination of these factors is responsible. Consequently, it will be necessary to examine more results, and possibly perform more tests, before a pattern emerges that would reasonably justify and guide modification to the controlling parameters of vasodilatation, vasoconstriction and sweating in the model.

Perhaps a more useful means of evaluating the sweating response is by the computation of total body heat storage. Total heat storage is a measure of the change in body heat from the beginning to the end of a particular test. It reflects the change in both skin and rectal temperatures (see equation 3, section 2) as measured over a specified time period.

The variation of active sweat rate with body heat storage is shown along with model predictions in Figure 3-18. In relating body heat storage to sweating, variations and scatter in skin temperature data tend to be damped out, as rectal temperature is more heavily weighted in the calculation of heat storage. Consequently, the predictions of active sweat rate versus total body heat storage are in very good agreement with actual results (since predictions of rectal temperature were more accurate).

Figure 3-18 also shows a strong linear relationship between active sweat rate and heat storage, with a slope of about 1.3 g/watt-hr^2. It should be noted that the model predicts some dependence of the heat storage-sweat rate curve upon LCG inlet temperature. This is because different combinations of changes in skin and rectal temperatures can produce the same value of heat storage, but slightly different sweat rates.

The use of heat storage has the additional advantage of providing a quantitative means of assessing thermal comfort. By relating the subjective responses of test subjects to measured values of body heat storage, the Environmental Physiology Laboratory at the Johnson Space Center of the National Aeronautics and Space Administration has postulated a comfort band for test subjects wearing an LCG. This band varies linearly from 0 ± 19 watt-hrs stored body heat at a metabolic rate of 146 watts to 40 ± 19 watt-hrs stored body heat at a metabolic rate of 586 watts. Heat storage values above the upper limits of the band represent off-comfort warm conditions and values below the lower limit represent off-comfort cold conditions.

The band was determined by noting that subjects generally were comfortable if sweat rates were limited between 0 to 100 g/hr for metabolic rates of 146 to 586 watts respectively. The heat storage for each sweat rate was determined, and it was this value that was associated with thermal comfort at each metabolic rate. Furthermore it was found from the literature (18) that subjective feelings of comfort varied from individual to individual at each environmental condition.

The variance in subjective comfort was correlated with a range of ± 0.3°C in rectal temperature. The variation in rectal temperature at comfort was then related to a variance in heat storage of $\pm$ 19 watt-hours

(see equation 3, Section 2). Thus, the comfort band was derived from a value of heat storage associated with a sweat rate observed at comfort at a particular metabolic rate; plus a variation in heat storage which accounts for differences in the subjective feeling of comfort experienced by various individuals.

It is possible to show that this comfort band can be superimposed on curves of sweat heat-loss (such as Figure 3-8) in such a way as to demonstrate that under comfort conditions, a subject wearing an LCG would limit his sweat heat-loss rate to a very small percentage of the total metabolic heat production. He would do so by controlling the inlet water temperature of the liquid cooled garment. By superimposing the comfort band on the data for LCG heat removal, it would also be possible to predict the inlet temperature that would be selected and the amount of heat that must be removed by the LCG in order to optimize comfort.

This concept will be demonstrated for subsequent tests, but can be shown in another way by Figure 3-19. Here, total body heat storage is presented as a function of metabolic rate and LCG inlet temperature for each test. The predictions of the mathematical model are indicated by the solid lines and the comfort band is shown superimposed on the data.

Figure 3-19 shows that the heat storage curve for the 16°C inlet water temperature is well above that for the colder 7°C water, at the same metabolic rate. If this is then referred to Figure 3-18, it is easily seen that the sweat rate is higher for the higher inlet temperature. Thus, body heat storage is a most convenient parameter with which to relate active sweat rate to metabolic rate and LCG inlet temperature.

From Figure 3-19, it is also seen that many of the test points lie outside of the comfort band. As mentioned previously, subjects had no

control over the LCG inlet temperature, and, in fact, most data points were on the cold side of comfort with frequent shivering. This is shown very well by Figure 3-19, and is supported by the subjective comments of the test subjects. It should be noted, however, that since relatively few data points were within, or were above the warm limit of the comfort band, additional test data would be desirable. Tests in which the subjects regulated the inlet water temperature to maintain thermal comfort under a variety of environmental conditions will be presented subsequently and will underscore the utility of this comfort band technique as a means of assessing thermal comfort.

Discussion of Errors

The results of Figure 3-19 illustrate the usefulness of the mathematical model as a tool for predicting heat storage and thermal comfort. Overall agreement between the test data and the predicted results is excellent. There is some scatter for the more negative heat storage region; however, this is understandable because the mathematical model is not well correlated for extreme cold or shivering conditions, primarily because of the scarcity of test data, and also because the test data are very difficult to evaluate for shivering subjects. On the other hand, agreement in the regions of heat storage near comfort is very good.

It should also be pointed out that although model predictions of core and individual skin temperature may deviate from test data to a greater extent than does predictions of heat storage, the utility of the model lies more in its ability to predict heat storage and thermal comfort than in its ability to forecast various skin and rectal temperatures. Differences between actual and predicted rectal and skin temperatures may occur for a variety of reasons, not the least important of which are the many

oversimplifications inherent in the mathematical model. These oversimplifications and proposed methods of improvement are discussed subsequently. However, it should be noted that if total body heat storage predictions are more accurate than those of individual skin and rectal temperatures, it simply suggests that the model is partitioning the production and dissipation of heat among the various body compartments less accurately than it is computing the total body heat balance.

This is seen to be the case for several of the transient results presented in Figures 3-1 to 3-4. All four tests showed reasonably good agreement between actual and predicted rectal temperature, average skin temperature and heat storage, and in most cases the mathematical model predictions were slightly lower than the test values.

Comparison of predicted and actual individual skin temperatures shows that the chest had the greatest deviation for all four tests considered. This may have occurred through overprediction by the model of the percentage of the total heat removed by the LCG from the chest. More specifically, if the percentage of the total water flowrate assigned to the chest area of the LCG is too high, then predicted chest skin temperature will be too low.

The agreement between actual and predicted chest skin temperature would be improved simply by reducing the proportion of total LCG flowrate that goes to the chest area. In addition, the mathematical model treats the entire torso area as one region. That is, the chest, back, upper thighs and groin are lumped into a so-called trunk or chest area. It can be seen from Figure 3-1 that there can be a considerable difference in temperature between the chest and the back. Therefore, oversimplification of the model in this respect results in inaccurate representation of the chest skin area. In future versions, the torso will be divided into discrete

regions, thus permitting greater accuracy. This will be described in more detail in Section 4.

While the differences between predicted and actual skin temperatures are less for other areas, such as the arms, legs a forehead, in some cases, they are substantial. It is suspected that these differences arise, at least in part, from the lumped parameter techniques employed by the current model. Future versions will use a more accurate finite-difference approach that will account for heat transferred in two spatial dimensions.

As mentioned previously, other possibilities for the differences observed between actual and predicted skin temperatures include inaccuracies in the vasoconstriction/vasodilatation expressions utilized by the model, and underpredictions of local heat production in various tissues. In the case of the former, changing the set points or gain constants of the equations of vasodilatation or vasoconstriction in such a way as to increase localized peripheral blood-flow would result in an increase in the predicted local skin temperature. This would appear to be especially applicable to the chest area.

From the transient data in Figures 3-1 to 3-4, it will be noted that agreement between predicted and actual heat storage is quite good despite wide variations in several skin temperatures. This occurs for two reasons: Firstly, heat storage is more heavily dependent upon rectal or core temperature (for which there was good agreement between predicted and actual results). More important, however, is the fact that heat storage is found from the change in rectal and skin temperatures, rather than from their absolute values, and the model was more accurate at predicting the changes that occurred in various body temperatures than it was at predicting the temperatures themselves.

This suggests that the set-point parameters used in the vasoconstriction terms may have been too low, or those of the vasodilatation terms too high. If additional analysis shows a consistent pattern, the individual skin temperatures which show the largest deviation from actual results may dictate a modification of the set-point parameters for the vasoconstriction or vasodilatation terms that control blood-flow to those specific regions in the model.

As regards the possibility that the model is underpredicting local heat generation, there are insufficient data at hand to evaluate this idea critically. However, some comments are in order.

The model determines total heat generation by assigning a basal metabolic rate to all body tissues, and augments this by increasing the metabolic rate of the muscles so that total heat production adds up to the metabolic rate required to perform a specific task. The percentage increase for each muscle region is proportional to the relative size of the muscle.

In the current version of the model, there is no attempt to partition the heat production of various muscles according to the specific task being performed. In other words, the percentage increase in the heat production of the muscles does not consider the fact that different muscles are used more than others for different tasks. Since all tasks for the present study required similar types of exercise, this shortcoming did not impair the usefulness of the model. However, for widely variant types of muscular activity, it will be necessary to account for this factor in future versions of the model.

In addition, the model assumes that the other body organs generate a constant amount of heat (basal) that is invariant during exercise.

There is evidence to suggest this may not be the case. Hodgdon (90) observed cyiical changes in internal body temperatures of primates, and Webb (157) reported cyclical changes in the heat storage of human subjects which may be attributable to a 24-hr rhythm in heat generation by various body organs. In any case, far more work is required before the nature of the local heat production terms can be fully understood, and this is certainly a possible source of error in the model which could explain differences between predicted and actual body temperatures.

To conclude the analysis, some observations about the behavior of the transient data in Figures 3-1 to 3-4 are appropriate. The time constant for most of the temperatures appears to be on the order of 30 to 60 min; however, this is subject to variation, depending on the severity of the test conditions. For example, for the tests shown in Figures 3-2 and 3-3, most of the temperatures had approached their steady-state values approximately 30 min after the start of the test. However, both of these tests were for conditions within the comfort band. On the other hand, some temperatures in Figure 3-1 still had not approached steady state after 180 min of testing. The latter test was conducted under off-comfort cold conditions. Therefore, it may be concluded that the time required for body temperatures to reach near steady-state values (time constant) varies with the severity of the test, being shorter for conditions near thermal comfort, and longer for off-comfort conditions.

Finally, although the mathematical model generally tracked the test data well, there was some dispersion during the initial minutes of testing. This is attributed to the difficulty in initializing the model to the exact starting conditions that prevailed for each test sequence, and to the simplified finite difference technique used by the model, which necessitated the relatively long time steps used for each iteration.

SERIES B

Series B was conducted in a vacuum environment below 10 torr. All subjects wore a NASA-Apollo AFL space suit over the Apollo-LCG. The suit provided gas ventilation, consisting of pure oxygen, circulating at 170 liters/min. The LCG water flowrate was maintained constant at 109 liters/hr and the LCG inlet water temperature was varied between 7 and 25°C. The suit inlet gas and dewpoint temperatures were kept relatively constant, as was the AFL suit pressure, which was maintained at 195 torr, absolute. These conditions were selected because they reasonably duplicated those that were to be provided by the PLSS during lunar surface explorations.

The chamber environment was kept near room temperature in order to minimize radiative interchange with the environment.

The metabolic rate for each test was controlled by varying the step-rate on a Harvard step test until the subject's heart rate matched a point on a predetermined calibration curve. The metabolic rate profile for each test is shown in Table D2 of Appendix D.

Heat Balance

Table 3-2 presents the calculated results and heat balance data for Series B. The raw test data are shown in Table D2 of Appendix D. Two observations should be made concerning the data of Series B which tend to detract from the accuracy of the heat balance calculations.

First, it should be noted that subject body temperatures were not measured in this test. Consequently, total body heat storage and heat storage rate could not be determined. This meant that the determination of physiological steady-state for each test sequence could not be ascertained

directly. Instead, suit outlet environmental parameters were used to judge steady-state, and this indirect method is less accurate.

Second, the use of heart rate versus metabolic rate calibration curves for each subject (see Figure C2, Appendix C) has been shown to be the least accurate method of controlling the real-time metabolic rate to a desired profile (147). In addition, the heart rate data itself became erratic during several sequences of the test series and it became necessary to modify the pre-planned metabolic profile.

Despite these shortcomings, an accurate heat balance was obtained on all but 5 of the sequences of Series B. The heat imbalance in these 5 cases all occurred for the coldest LCG inlet water temperatures, and can probably be attributed to the failure to reach adequate steady-state conditions or to shivering.

Another factor contributing to the inaccuracy of the heat balance was the estimate of radiation heat loss, especially at the lower LCG inlet water temperatures. As was shown in the results of Series A, skin temperature decreases linearly as LCG inlet water temperature decreases. At these low skin temperatures, radiation heat transfer from the environment into the man-suit system is possible and the magnitude of this mechanism can only be estimated. For Series A, radiation heat loss was assumed to be negligible through the Arctic coverall garment. However, the heat balance data and subsequent analysis with the mathematical model suggested an actual heat input by radiation. Consequently, for Series B, radiation heat transfer was estimated to be 30 watts into the suit at the colder LCG inlet water temperatures (7 and 12°C) and negligible for the higher LCG inlet temperatures. This estimate was judged to be reasonable with respect to the thermal properties of the space suit.

It is possible that other factors, such as additional heat input from overhead lamps used in the chamber, coupled to the inherent difficulty in accurately assessing the thermal properties of a complex, multi-layered garment such as the Apollo space suit, may well have contributed to errors in radiation heat loss. However, the absolute magnitude of the resulting error was still small when compared to the total heat production or total heat loss for most sequences of this test series.

The calculated data of Table 3-2 point out another interesting effect of the LCG. It would be expected that the ventilating gas provided by the suits used in Series B would allow a significant amount of heat to be removed by convection heat transfer, a heat loss mechanism which was not available in Series A. However, from the computations of convective heat loss in Table 3-2 (see equation 6, section 2), it is evident that heat loss by convection is also negligible in Series B, despite the presence of a ventilating gas with a significant flowrate. The only explanation for this phenomenon is that the gas, with its limited heat capacity, is cooled by the cooling tubes of the LCG by means of countercurrent heat exchange. In effect, the convective heat removal of the ventilating gas is converted to conduction heat removal of the LCG. This is evidently the case because convection heat loss is significant in a space suit without an LCG.

One final note on the heat balance computations of Table 3-2 is in order. As mentioned earlier, in the 5 cases in which a heat balance could not be obrained, the heat deficit could be attributed to shivering, failure to reach steady-state, or errors in the prediction of radiation heat exchange. However, unlike Series A, there were no subjective comments from the test subjects to indicate that shivering was a major factor. Although this does not preclude the possibility that shivering occured, it

tends to place more emphasis on the other two factors as the primary contributors to the heat balance deficits.

Despite the lack of a complete heat balance, the data from Series B are informative. It is still possible to compare these data with mathematical model predictions. Furthermore, in cases where conditions overlap, the results can also be compared with those from Series A. This is possible because convection heat transfer is negligible in both test series and also because radiative heat exchange is about the same order of magnitude. Examination of the test data reveals that the results from Series B show the same general trends obtained by the mathematical model, and seen in Series A.

LCG Heat Removal

Figure 3-20 shows the LCG heat removal rate as a function of subject metabolic rate for LCG inlet water temperatures ranging between 7 to 26°C. As in Series A, the same general trend of an increase in LCG heat removal for an increase in metabolic rate as a constant inlet water temperature was observed. Also as seen in Series A, the cooler LCG inlet temperature curves are displaced upwards from, but have approximately the same slope as the warmer inlet temperatures.

The predicted results for Series B are shown by the solid lines, and as in Series A, the model predicts less LCG heat removal than was actually observed. However, unlike Series A, the difference between predicted and observed results is not constant. At lower metabolic rates, agreement between predicted and actual results is relatively good. However, at higher metabolic rates and colder inlet temperatures, the test data (dark symbols) deviate considerably from predicted results. This is especially noticeable for the 7 and 12°C inlet water temperature cases.

It is also significant that for 7°C inlet temperatures, the data of Series B demonstrate greater LCG heat removal rates than the corresponding data of Series A (open symbols). In Series A, the difference between predicted and actual results was approximately constant, with the slopes being the same. This was ultimately attibuted to errors in estimates of radiative interchange, differences in the predicted and actual LCG heat transfer coefficients, and model skin temperature underpredictions. In Figure 3-20, there is good agreement at the lower metabolic rates but increased deviation in the higher metabolic rate range. Thus, the differences in Series B cannot be associated simply with errors in estimation of heat transfer coefficient or radiative exchange.

It is possible, however, that the discrepancy may be related to the observation that a steady-state was not always reached when cold inlet temperatures were imposed at high metabolic rates. In other words, the test subject may have been overcooled with depressed skin temperatures and suppressed sweating. If the test conditions had been longer in duration, it is likely that LCG heat removal would have decreased and sweating increased.

Figure 3-21 presents the data of Figure 3-20 replotted as the percentage heat removal of the LCG (LCG heat removal/metabolic rate) versus LCG inlet temperature. This graph has the effect of normalizing the deviations seen in Figure 3-20. As in Series A, there is a very sharp increase in percentage LCG heat removal as the inlet temperature decreases. Heat removal varied from 50% of metabolic rate at the highest inlet temperature to 118% at the coldest. The percentage heat removal is also observed to be higher for lower metabolic rates at the same inlet temperature. Agreement between predicted and actual results is generally good despite

the differences that exist at higher metabolic rates and colder inlet temperatures. It is also seen from Figure 3-21 that the data of Series B falls in the same range and shows the same trend as that of Series A. However, there appears to be more heat removal, especially at the lower inlet temperatures.

Although the subjects in this test had no control over the LCG inlet temperature, they tended more towards sensations of comfort or warm, with no incidence of shivering, rather than the cool conditions of Series A. This is supported by the model predictions shown in Figure 3-22.

Although heat storage was not measured, the values predicted by the mathematical model for the conditions of Series B indicate that most of the test points were probably within or on the warm side of the comfort band.

As mentioned previously, it appears that if test subjects are permitted to control the inlet water temperature to maintain comfort, heat removal by the LCG (and also heat removal by evaporation of active sweat) should fall within a fairly narrow band that forms the basis of a means of predicting metabolic rate from LCG performance. This does not mean to imply that the band would possess the same characteristics as found in Figures 3-20 and 3-21 of the present test series. Indeed, it should be stressed that many of the data points in both Series A and B are off-comfort points, and errors arising from shivering, uncertainties over the LCG heat transfer coefficient, and determinations of metabolic rates, radiation heat exchange and total body heat balances will almost certainly bias these results. This is expecially true for Series B, where lack of body temperature and heat storage data limit error analysis. However, despite these shortcomings, the trends demonstrated thus far support the predictions of the mathematical model.

One final note about Figures 3-20 and 3-21 concerns itself with the difference observed in the predictions and results of Series A and B at low LCG inlet temperatures; namely, that LCG heat removal was greater in Series B. In conjunction with the analysis of the heat balance data of Table 3-2 presented earlier, the higher LCG heat removal observed in Series B can be explained by a failure to reach physiological steady state, or greater than predicted radiation heat exchange (owing to cool skin temperatures and uncertain space suit thermal properties). Shivering is also a possibility but is less likely considering the shorter duration of each sequence in Series B and the scarcity of subjective comments.

Sweating and Evaporation Heat Loss

The removal of heat by evaporation of active sweat is shown in Figure 3-23 as a function of metabolic rate and LCG inlet temperature. For Series B, heat loss by active sweating was found by subtracting respiratory and skin diffusion heat loss from total evaporative heat loss. (See equations 5 and 7, Appendix C.) Total evaporative heat loss was calculated from the gas flowrate through the Apollo suit and the inlet and outlet dewpoint temperatures (see equation 7, Section 2).

The trends shown in Figure 3-23 are the same as observed in Series A (open symbols) and as predicted by the mathematical model. Sweat rate generally increased in a linear fashion as metabolic rate increased at a constant LCG inlet temperature.

Agreement between the test data and model predictions is reasonably good. As in Series A, the model generally overpredicts sweat heat loss; a result expected from the total heat balance equation (equation 1) since LCG heat loss is generally underpredicted. The deviations shown in

Figure 3-20 are also present in Figure 3-23. That is, differences between predicted and test results are larger at higher metabolic rates and colder LCG inlet temperatures. However, it should be noted that the differences in Figure 3-21 are not as great as those observed in Figure 3-20. This suggests that greater-than-predicted radiation heat leak into the space suit at lower LCG inlet temperatures is a likely possiblity. Space suit design testing indicates that a significant percentage of the thermal radiation entering an Apollo A7L suit may be transferred to the LCG duri the transient period preceding attainment of physiological steady-state.

The LCG may remove a large quantity of heat in cooling down the space suit a l surroundings. This amount of heat comes from the environment rather than from the man and may bias the test data higher than the predictions. Coupled to the fact that skin temperature and sweating are depressed at low LCG inlet temperatures, the increased environmental and radiation leak would lead to larger errors in predictions of LCG heat removal than in predictions of evaporative heat loss. However, radiation heat loss probably cannot explain all of the differences observed between the predicted and actual results of Figure 3-23, and as mentioned previously, these errors undoubtedly result from a combination of factors.

The results of Figure 3-23 show fairly good agreement with those of Series A (open symbols). The trends are the same and the magnitude of the sweat heat-loss rate is similar for both test series. It should be emphasized that in Series A, body weight loss was used to calculate evaporative heat loss, while in Series B, space suit inlet and outlet dewpoint tempera-tures were utilized directly, a more accurate method. In addition, it was assumed that all sweat was evaporated. However, post-test inspection revealed that some moisture was retained in the Apollo space suit. This

trapped moisture could partially explain why values of sweat and total evaporative heat loss rates for Series B were lower than predicted by the mathematical model. Despite these errors, the results of Series A and B are similar, indicating that in the case of Series A, weight loss is an acceptable means of assessing sweat rate; and also that unevaporated sweat, although a likely source of error, was not appreciably different for either test.

The data of Series B also show the trend of decreased sweat rates as the LCG inlet temperature decreases for a given metabolic rate. This is shown very nicely in Figure 3-24, were agreement with predicted results is excellent. Furthermore, the predicted onset of sweating is shown to increase from 293 to 396 watts as inlet temperature drops from 12 to 7°C (Figure 3-23). Both of these results are in agreement with previous trends seen in Series A.

Figure 3-25 presents the heat removal by evaporation of active sweat as a percentage of metabolic heat production for various LCG inlet temperatures. Comparing this to Figure 3-21, it is again obvious that heat removal by active sweating constitutes a far smaller percentage of the total heat removal than does LCG heat removal. Maximum values of sweat heat removal ranged from 5% of the total metabolic heat production at the coolest inlet temperature to 35% of the total at the warmest inlet temperature. These results agree very well with the model predictions and also with the data of Series A. The test points fall within a band which increases as a function of LCG inlet temperature. The fact that these data have less scatter at the warmer inlet temperatures than the data of Series A is probably because metabolic rates were uniformly low in Series B under these conditions. In any case, one of the most significant

results emerging from the study thus far is that the LCG limits sweating considerably, and in a predictable fashion.

Total evaporative heat loss rate is shown as a function of metabolic rate and LCG inlet temperature in Figures 3-26 and 3-27. As mentioned previously, total evaporative heat loss rate is determined from the inlet and outlet dewpoint temperatures and gas flowrate according to equation 7 of Section 2. Total evaporative heat loss represents the sum of evaporative heat loss by active sweat, by diffusion from the skin surface, and through the respiratory tract. Heat loss by diffusion and respiration are determined from the empirical expressions found in Appendix C. Figures 3-26 and 3-27 show that total evaporation heat loss is considerably greater than heat loss by active sweating alone, but follows the same trends. Heat removal rate varied from about 10% of metabolic rate at the lower inlet temperatures to 45% at the highest inlet temperature. The dependence upon LCG inlet temperature is not surprising since the largest component of total evaporative heat loss is due to active sweating (diffusion and respiration heat loss are not appreciably dependent upon LCG performance). The results of Figures 3-26 and 3-27 also show good agreement with the mathematical model predictions, and with the results of Series A.

In view of the influence of active sweating upon total evaporative loss, the same errors noted earlier for the active sweating relationships are present in Figures 3-26 and 3-27. These factors contribute to most of the deviations seen between the actual results of Series B and the predictions of the mathematical model, or with the results of Series A.

Discussion of Errors

As noted previously, certain discrepancies observed between the results and predictions of Series B appear to be dependent upon metabolic rate and inlet temperature. These discrepancies were observed in both LCG heat removal and evaporative heat loss (although more significant in the former due to a probable increase in radiation heat exchange at the colder inlet temperatures). Some insight into the cause of the differences is derived from Figure 3-28a, where LCG and total evaporative heat loss rate (dark and open symbols) are shown for different metabolic rates and LCG inlet temperatures. A regression curve fit through the data shows a steep increase in LCG heat removal as metabolic rate is increased. The curve is second order and described by the following equation: LCG heat removal = 114 - .062 (met. rate) + .0013 (met. rate)^2. The accuracy of the curve fit is good, with a correlation coefficient of 0.82. In subsequent data reduction, it will be shown that the curve fit can be improved significantly if certain constraints are considered.

The LCG heat removal increased sharply with metabolic rate because colder inlet temperatures were utilized as metabolic rate increased. The colder inlet temperatures not only had the effect of increasing LCG heat removal, but also decreased skin temperatures and consequently, reduced sweating. The reduced sweat rate is exemplified by the almost asymptotic behavior of the evaporative heat removal curve (dashed line). The curve fit to these data was also second order and described by the equation: Evaporative heat loss = -182 + 1.397 (met. rate) - .0016 (metabolic rate)^2.

The accuracy of this curve fit is not as good as that for LCG heat removal, the correlation coefficient being only 0.39. The reasons for this are complex and will be reviewed in Section 4 along with data reduction techniques for improvement of the correlation.

Figure 3-28b shows the difference between the test data of Series B and the mathematical model predictions. Errors are shown as a percentage of metabolic heat production for LCG heat removal (dark symbols) and total evaporative heat loss (open sysbols). Curve fits to the data are also shown (solid and dashed lines). The results show that at high metabolic rates the model underpredicts LCG heat removal by as much as 20% and overpredicts evaporative heat loss by roughly 15%. The largest errors occur at the coldest inlet temperatures and are largely attributable to the transient overcooling effect discussed earlier. All errors appear to be lower at the lower metabolic rates and increase slightly with heat production.

The curves of Figure 3-28b suggest that these differences depend upon both inlet temperature and metabolic rate rather than one or the other exclusively. A most reasonable explanation for this behavior can be traced to the characterization of vasodilatation, vasoconstriction, and sweating by the mathematical model. As noted in Series A, differences between actual and predicted skin temperatures may be caused by inaccurate simulations of these terms in the model. If this were the case, the model could predict lower skin temperatures for the colder LCG inlet temperatures since, for example, decreased peripheral blood-flow would restrict the transfer of heat to the skin surface. Furthermore, elevated sweat rate predictions could be a consequence of oversimulation of the sweating terms.

The differences seen in Figure 3-28b indicate that as metabolic rate increases, the model is not providing enough peripheral blood-flow to the extremities when the LCG inlet temperatures are low. Thus, the colder LCG inlet temperatures would appear to overly depress skin temperature.

This would result in predictions having less LCG heat removal (due to a lower driving force between the skin temperature and LCG water temperature). The overpredictions of active sweat and evaporative heat loss are less severe. They may be due in part, to a slightly higher rise in core temperature resulting from less peripheral circulation.

The inadequate peripheral circulation at lower inlet temperatures and higher metabolic rates could be a consequence of inaccurate simulation of the interaction between vasoconstriction and vasodilatation characterized by the model. The model depicts vasoconstriction and vasodilatation as being dependent upon various set-point temperatures and gain constants (see equation 17, Section 2). This is probably an oversimplification, since these values depend upon many complex parameters and vary even from individual to individual, a factor not taken into account by the model. In light of this, it is easy to see how variations in skin blood-flow could lead to the types of errors seen in Series B. For example, a low gain constant for vasodilatation could cause low predicted skin blood-flow at higher metabolic rates for all LCG inlet temperatures, while a high peripheral set-point could cause low circulation at lower LCG inlet temperatures for all metabolic rates. A combination of both factors could cause the largest errors to occur at high metabolic rates and low inlet temperatures.

The task of accurately characterizing the physiological phenomena of sweating, vasoconstriction, and vasodilatation is a formidable one. Considering all of the factors involved, the results produced by the model are quite acceptable. It should also be emphasized that some of the deviations seen in Series B were not noted in Series A. For example, differences between predicted and actual LCG and evaporative heat removal

in Series A were constant while those in Series B were not. The deviations in LCG heat removal at 7°C and high metabolic rates were greater in Series B than in Series A. It is probable that physiological steady-state was not attained for some of the conditions of Series B. This may have resulted from the shorter duration of each test. In any event, the model predictions are steady-state values, and do not simulate well the over-cooling effect which occurs in the transient. The latter also emphasizes that inadequacies in defining peripheral blood-flow may be only one of many possible sources of error. In other words, the discrepancies seen in both Series A and B are the result of a combination of many factors, and analysis of many additional tests would be required for a complete explanation.

In concluding the consideration of Series B, a final observation is in order. The data of Figure 3-28a point out another interesting factor that has not yet been considered. The results show that there is no characteristic difference between the responses of the 2 subjects tested under the same conditions. Variation in the results from the same subject tested at 2 nearly identical test conditions (repeat points) is about the same as exists between the 2 subjects at the same approximate test condition. The differences that do exist can be ascribed to variations in physical conditioning, fatigue, and test conditions. In other words, the test results appear to be reproducible with different subjects.

It should be noted, however, that both test subjects were of approximately the same weight and build. It would be more instructive to have subjects who were more anthropomorphically dissimilar. This points out another source of error between the model and the test results. At present, the model utilizes physiological data for an "average man". This

"average man", compiled from the data of several sources (42, 43, 134) is 70 kg in weight and 173 cm in height. There is no provision to vary the input characteristics of the model to account for specific physical characteristics of individuals. Obviously, differences between predicted and actual results would be expected for individuals whose physical characteristics differ markedly from the data of the "average man" used by the mathematical model. It is intended that future versions of the model be modified to accept a means of matching the input data more closely to individual physical characteristics such as height, weight, general body shape, body density, etc. Darling and coworkers (38) have had some success in making such modifications to an early version of the Stolwijk-Hardy model and additional work is forthcoming.

SERIES C

Series C was performed in a hypobaric chamber at a reduced pressure of 259 torr. The pressure in the A7L suit was also maintained at 259 torr. The chamber environment was kept neutral to eliminate radiation heat transfer between the subjects and the ambient environment. All subjects wore the Apollo A7L suit over the LCG, with a circulating oxygen flowrate of 331 liters/min.

The LCG water flowrate was varied between 0-82 liters/hr while the LCG inlet temperature was kept constant. The suit inlet gas temperature and dewpoint were also kept relatively constant.

The metabolic rate for each test sequence was controlled by varying the step rate on a Harvard step test in accordance with a predetermined calibration of metabolic rate versus step rate for each subject. The metabolic rate profile for each test sequence is shown in Figures 3-29 and 3-30.

Table 3-3 presents the calculated results and overall heat balance data for Series C. The raw data is shown in Table D3 of Appendix D.

Heat Balance

The data from Series C show the effect of parametrically varying LCG water flowrate at a constant inlet temperature, as contrasted with the previous test series in which the inlet temperature was varied and the flowrate kept constant. The heat balance data (Table 3-3) illustrate that for a constant metabolic rate, LCG heat removal increased with flowrate. However, the effect was not as dramatic as that of previous test series in which the inlet temperature was varied. In fact, the LCG heat removal will subsequently be shown to approach asymptotic limits as flowrate increases beyond 55 liters/hr. The data of Table 3-3 also show that as the LCG flowrate increased at a given metabolic rate, evaporative heat removal by active sweating decreased. This is expected since increased flowrate results in greater LCG heat removal which acts to lower skin temperature, increase conductive heat loss and decrease active sweating. It was observed that the largest sweat rates occurred with no LCG water flow. In fact, there was more sweating at a metabolic rate of 352 watts with no LCG cooling than at a metabolic rate of 586 watts with an LCG flowrate of 55 liters/hr and a relatively high inlet temperature of 17°C. This underscores the powerful influence of the LCG upon thermoregulatory sweating.

Table 3-3 also shows that convective heat removal through the ventilating gas in the suit was almost negligible. Although this trend was seen in Series B, it was not expected for this test series. Convective heat loss was predicted to be significant for Series C because the ventilating

gas was circulated at nearly twice the flow of the previous test series (331 liters/min); and also because LCG cooling was limited since inlet water temperatures were relatively high at 17 - 19°C. However, the heat balance data show negligible convective loss, including the 2 cases where there was no LCG cooling (zero water flowrate). This somewhat paradoxical result is explained by examining the radiation heat loss data.

It is seen that environmental heat loss out of the suit was significantly larger than experienced in either Series A or B. These large heat loss values (up to 62 watts) mean that any heat that might have been transferred from the subject's skin to the gas stream by convection was ultimately lost to the environment by radiation. The environmental heat loss data for Series C were determined by using the insulation properties of the A7L space suit and the environmental conditions in the hypobaric chamber (22°C wall and air temperature) as input to the mathematical model. The model then predicted values for radiation heat loss.

Although the same procedure had been used for the previous test series, the radiation heat loss predictions for Series C were much larger. This occurred because the insulation properties of the space suit require the ambient pressure to be close to a vacuum in order to be most effective. For Series C, the ambient pressure was 259 torr, as opposed to 10 torr as in Series B. Consequently, the suit insulation was not as effective and more heat was conducted through the suit and radiated to the chamber walls.

This interesting fact was discovered because initially, utilization of the vacuum properties of suit insulation resulted in negligible radiation loss and large errors between predictions and test values of LCG heat removal and evaporative heat loss. Furthermore, use of these low radiation heat loss values in the heat balance data of Table 3-3 produced low values

in the TOTAL HEAT LOSS row. This led to large positive values for the HEAT BALANCE row, which, in turn, resulted in excessively large heat deficit values.

It was suspected that the large heat deficit results were caused by errors in the computed values of heat storage rate, or by errors in radiation heat loss (since there was no observable shivering). The former computations were suspect, due to the slow response of changes in skin and ear canal temperatures, coupled to the rather short duration of each test sequence (30 min). However, consultation with the manufacturer of the NASA-A7L space suit, in conjunction with detailed engineering analysis of its thermal properties, revealed a much larger than expected suit conductance for environments at significant ambient pressures (259 torr). It was decided that the latter was probably most responsible for the high heat deficit values.

Utilization of the higher suit conductance properties at 259 torr resulted in the large radiation heat loss values shown in Table 3-3. Using these data in the heat balance increased the TOTAL HEAT LOSS row and substantially reduced the HEAT DEFICIT row to the values shown. The latter quantities are more in keeping with the corresponding data of other test series. The heat deficits shown are relatively small and are largely attributable to errors in heat storage rate determinations (for positive heat deficits), small, unavoidable variabilities in radiation heat loss estimates (for negative heat deficits), or simply errors in the data for LCG, convective, or evaporative heat loss.

Transient Results

The results for the transient response of mean skin and tympanic temperatures and total body storage are shown for Series C in Figures 3-31

and 3-32. The response of the individual skin temperatures are shown in Figures D1 through D4 in Appendix D. These results revealed only slight variation in head core temperature but considerable change in individual and mean skin temperature. The maximum values of mean skin temperature, head core temperature and body heat storage occurred at or near the test sequences in which there was no water flow and consequently no LCG cooling, while the minimum values of mean skin temperature occurred during the sequences in which water flow was a maximal 82 liters/hr.

In general, the mathematical model predictions track the transient data very well. For predictions of individual skin temperatures, the results are not quite as good (see Figures D1 - D4, Appendix D). Here, the model shows a definite tendency to underpredict the trunk skin temperature (dotted line). These predictions were as much as 3°C lower than any of the abdomen, back or chest skin temperature test data that are equivalent to the model's trunk skin prediction. Incidentally, the occasionally wide differences between the test values of abdomen, back and chest temperature noted in several of the test sequences further illustrate the need to divide the model into more segments in the trunk region if greater accuracy is to be achieved. The model (dotted line) also shows a tendency to overpredict leg skin temperature (when compared to the test data for calf or thigh temperature). Again, significant differences between the test values of calf and thigh temperatures point out the shortcoming of approximating the entire leg region in the model with one segment.

The model inaccuracies described in the previous paragraph follow identical observations that were made for model predictions of Series A (Figures 3-1 to 3-4). These inaccuracies and their correction are the subject of a subsequent discussion. Also in keeping with previous

observations during Series A, the forehead and hand skin temperatures were observed to be the warmest, while the abdomen and thigh temperatures were the coldest.

One final note about the model predictions and test data concerns itself with the relative frequency of changes. Examination of the transient behavior of the ear canal and mean skin temperature and heat storage data shows much faster response by the model predictions than by the test data. This is especially observable over the 7-hr period comprising the first 8 test sequences (Figure 3-31), where gradient changes are much more pronounced for the model than for the test data. The conclusion to be drawn here is that this fault probably lies with the lag time associated with the skin and tympanic thermocouples utilized for this test. The difficulty of properly insulating and placing a skin thermocouple, plus the tendency for tympanic thermocouples to work loose all contribute to a slow response time. This is especially likely in view of the rapid progression of test sequences that occurred (30 min per sequence). It is this slow response time that makes the computation of heat storage rate from the test data values of ear and skin temperatures susceptible to error over the relatively brief duration of each test sequence.

LCG Heat Removal

Figures 3-33 and 3-34 show LCG performance as a function of metabolic rate and water flowrate. For Series C, LCG heat removal was controlled by varying the water flowrate with a constant inlet water temperature (17 - 19°C), rather than the reverse procedure used in all other test series. This was done to determine if any substantial differences existed between the two methods. The subjects had no control over the selected water flowrate. In effect, each subject worked at a constant metabolic

rate for 30 min with a given flowrate. These conditions were then repeated for 3 other flowrates ranging between 0 to 82 liters/hr. Subjects were generally either warm or near comfort.

This observation was verified by using the heat storage data and the previously developed comfort zone to assess thermal comfort (Figure 3-35). Figure 3-35 also indicates that for each metabolic rate, a unique range of LCG flowrates would be required to maintain heat storage and thermal comfort within acceptable limits. However, it is difficult to evaluate this relationship fully since the test data were frequently changing at the conclusion of some of the 30-min test sequences. Final heat storage rates in several cases were still significant, indicating the likelihood that total body heat storage would have increased further had each sequence been longer in duration.

Figure 3-33 shows the expected trend of increased LCG heat removal with increases in metabolic rate for a given water flowrate. However, as contrasted with the corresponding curves for Series A and B, the data appear to be approaching a limit at the higher metabolic rates. Thus, this method of heat removal may not be as efficient as that of temperature control. It is noted that the higher water flowrate curves are displaced upward from the lower flowrate curves in a manner similar to that for the colder inlet water temperature curves of Figures 3-5 and 3-20. However, it is also observed that the heat removal (both predicted and actual) for the highest metabolic rate of 586 watts is not substantially greater at a flowrate of 82 liters/hr than it was at 55 liters/hr. This implies that for constant inlet water temperatures of 17 - 19°C, no appreciable benefit from LCG cooling is derived from flowrates greater than 55 liters/hr. This is clearer from Figure 3-34, which shows the percentage of metabolic heat

removed by the LCG as a function of water flowrate. Here, it is observed that at the 2 higher metabolic rates, LCG performance begins to approach a limit somewhat below 60% of total heat removal for flowrates beyond 55 liters/hr.

The method could be improved significantly by using inlet temperatures lower than the 17 - 19°C utilized for this test. The effectiveness of LCG heat removal at these relatively high inlet temperatures is reduced below that of Series A or B, especially at the higher metabolic rates. The maximum LCG heat removal amounted to less than 60% of metabolic heat production, as contrasted with values of up to 120% noted in the corresponding data from Series A and B (see Figures 3-7 and 3-21). The reason for the decreased effectiveness can be traced to the flow dependence of the LCG heat transfer coefficient (Figure 3-36). The heat transfer coefficient for constant flow, variable inlet temperature control was shown to be constant at 23 watts/°C for inlet temperatures up to 17°C (See Figure 3-6). However, for the lower flowrates and constant inlet temperatures of Series C, Figure 3-36 shows a reduced heat transfer coefficient which asymptotically approaches the constant flow, variable inlet temperature value as the flowrate approaches 109 liters/hr. In other words, the LCG does not remove the body heat as effectively for the variable flow case as it did for the variable inlet temperature case.

The predictions of the mathematical model are shown as solid lines in Figures 3-33 and 3-34, and agreement with the actual data is very good. In Figure 3-34, the predictions fall within a fairly narrow band for flowrates between 27 to 82 liters/hr at metabolic rates from 352 to 586 watts. This suggests the possibility of using such curves to predict metabolic rate, given LCG heat removal and flowrate. However, a useful relationship would require substantially more data.

Sweating and Evaporation Heat Loss

The removal of heat by evaporation of active sweat is shown as a function of metabolic rate and LCG water flowrate in Figures 3-37 and 3-38. As in Series B, this is determined from the suit ventilation flowrate and inlet and outlet dewpoint data (equation 7, Section 2). Sweat rate is then found by deducting empirical expressions for respiratory evaporative and skin diffusion heat loss (equations 5 and 7 Appendix C) from total evaporative heat loss.

The trends shown in Figure 3-37 illustrate the inverse relationship that exists between LCG heat removal and active sweat rate. The highest sweat rates occurred for the zero water flow tests in which there was no LCG cooling. The next highest sweat rates occurred for the minimum water flow case of 27 liters/hr. The lowest sweat rates were observed for flowrates of 55 and 82 liters/hr, with very little difference between the two. The latter finding supports the contention that for inlet water temperatures of 17-19°C, only minimal benefit is derived from LCG flowrates greater than 55 liters/hr.

The usefulness of the LCG in reducing sweating is also apparent from Figure 3-37. The sweat heat removal rates shown for the no-cooling, zero water flow sequences are far in excess of any values that have thus far been observed. This may be seen more easily in Figure 3-38, which shows the percentage of metabolic heat removed by evaporation of sweat as a function of LCG flowrate. At zero flowrate, sweat evaporation constitutes 45 to 55% of the removal of total heat production. These high values are contrasted with sweat heat removal ratios below 25% for all previous test data in which there was sufficient LCG cooling.

The model predictions, shown as solid lines in Figures 3-37 and 3-38 also show excellent agreement with the test data. The noticeable tendency

to overpredict evaporation rates that was observed in Series A and B (Figure 3-28b) is absent in this case. As mentioned previously, erroneous values of suit insulation properties initially predicted negligible radiation loss, with consequent errors in predictions of sweating and evaporation heat loss. However, correcting the suit insulation properties to the appropriate values for a pressure environment greatly reduced the errors and also improved the heat balance data of Table 3-3.

The predictions and data of Figure 3-38 also show the large effect that even a small amount of LCG cooling can provide. The band bounded by the model predictions has a very steep negative gradient at the lower flowrates, demonstrating a linear reduction in sweating that amounts to 0.84 - 1.0 watts/liter/hr of water flow for flowrates between 0 and 27 liters/hr. However, as water flow is increased beyond 55 liters/hr, the gradient largely disappears and approaches zero, another reflection of the fact that the latter flowrate appears to be optimum for these test conditions. At the high flowrates, sweat heat removal amounts to less than 25% of metabolic heat production.

Figures 3-39 and 3-40 show total evaporative heat removal, including respiratory and skin diffusion heat loss, as a function of metabolic rate and LCG water flowrate. As previously discussed, total evaporative heat loss is determined directly from the suit gas flowrate and dewpoint data. All of the trends observed on the curves are similar to those for evaporative heat loss by active sweat alone, except that they are greater in magnitude. Total heat removal by evaporation amounts to 65 to 70% of metabolic rate for the no-cooling test sequences, and exponentially decreases to 25 to 35% at the higher water flowrates. As in the case for sweat evaporation alone, total evaporative heat removal for the no-cooling tests exceeds all previous corresponding data from Series A and B,

but approaches the same minimum values as LCG flowrate increases. It should be noted that for the test sequences in which there was no LCG cooling, the remainder of the metabolic heat generated in the body is dissipated primarily in the form of radiation loss or increased body heat storage.

Skin Temperature, Tympanic Temperature, and Total Body Heat Storage

The effects of LCG cooling upon thermoregulation, sweating, and comfort are more easily interpreted when augmented by physiological data for the steady-state responses of skin temperature, head core temperatures and body heat storage. For Series C, these data are presented in Figures 3-41 through 3-47. In comparable cases, results agree favorably with the equivalent data of Series A, although the latter test utilized inlet water temperature as the independent variable, rather than water flowrate. Mean skin temperature was determined in Series C by using the final skin temperatures at the conclusion of each test sequence, multiplying each by its appropriate weighting factor, and combining these values into an overall mean skin temperature (see equation 2, Section 2). Total body heat storage was found by combining skin temperatures and core temperature (in this case, tympanic temperature) in the manner described in test series A and equation 3 of Section 2.

Figure 3-41 shows the effect of water flowrate upon head core temperature and mean skin temperature. The data represent metabolic rates of 352 to 586 watts. It is observed that the tympanic temperature remains nearly constant and is independent of water flowrate, while the mean skin temperature decreases asymptotically as water flowrate increases. The independence of head core temperature from water flowrate is comparable to Figure 3-13 of Series A, where rectal temperature was shown to be

independent of water inlet temperature. These findings are in keeping with Nielson's original studies showing that deep body temperatures reach a plateau in the steady-state associated directly with the level of metabolic rate, despite the presence of strong surface cooling at the skin from the LCG (97, 161).

The decrease in mean skin temperature with increasing flowrate is similar to the decrease observed with lower inlet temperatures from Series A (Figure 3-13). However, the latter relationship was rectilinear, whereas the Series C data exhibit a more gradual decrease that asymptotically approaches a value slightly above 30°C. As might be expected, this asymptote value is the same that is found from Figure 3-13 of Series A for the corresponding inlet temperatures used in Series C (17 - 19°C). The gradually decreasing change in skin temperature with flowrate change as opposed to the steeper rectilinear effect with inlet temperature change again reflects the more effective, precise control of the latter method of LCG cooling.

From Figure 3-41, it is also apparent that mean skin temperature is controlled primarily by the LCG, rather than metabolic rate. This is concluded from the fact that the data encompass a wide range of metabolic rates (352 - 586 watts), yet seem to be largely independent of the latter. Figure 3-42 shows some increase in mean skin temperature with metabolic rate at constant flowrates, but the dependence is not strong.

These results are similar to the findings of Series A, which also showed mean skin temperature to be controlled primarily by inlet water temperature rather than metabolic rate. This is reasonable because increased body heat produced by metabolism occurs internally at the cellular level and is dissipated,in part, by convective heat transfer to the

blood-stream and the surrounding tissues before finally being transferred to the skin surface for removal. This constitutes a type of insulating boundary between metabolic heat production and its ultimate removal at the skin. On the other hand, the LCG imposes a direct boundary condition at the skin surface. Furthermore, metabolic heat generated internally requires a lag time to reach the skin surface, whereas conduction of heat between the LCG and the skin is immediate. The lag time simply means that the skin temperature data will not reflect increases in metabolic rate over a short duration test as rapidly as it will reflect changes in LCG flowrate.

It is interesting to note that the skin temperature predictions of the mathematical model are in generally good agreement with the test data. The differences that are present are probably the result of the slow response time of the skin temperature thermocouples described previously. By contrast, the model results in Series A exhibited a marked tendency to underpredict the test data. This can be attributed to several factors.

First, the underpredictions of Series A were most noticeable at very low water inlet temperatures of around 7°C, where cold stress, vasoconstriction effects, and associated model errors are most likely to occur. Underpredictions at the higher inlet temperatures utilized for this test series (17 - 19°C) were not as significant.

Secondly, the radiation heat loss in Series A was not as well defined as in Series C, and the model has demonstrated that incorrect estimates of the latter can lead to underpredictions of skin temperature.

Thirdly, analysis of these and other test data suggested that the amount of heat extracted from different regions of the body by the LCG was simulated incorrectly. Modifications made to the model resulted in improvements in skin temperature predictions, and were utilized for the

model predictions in this and subsequent test series. They account, in part, for the improved accuracy.

Finally, the results expressed here are after 30 min of testing, at which time several test sequences showed significant heat storage rates, indicating unsteady-state conditions. It is possible that had each sequence been continued for a longer duration, as in Series A, underpredictions proportional to the degree of deviation from comfort may have occurred. Such underpredictions were observed for some of the individual skin temperatures such as the chest or the back, but were not reflected in the mean skin temperature due to equivalent overpredictions for the temperature of the leg.

The data and predictions for tympanic (head core) temperature are also shown in Figure 3-42 and agree very well. They demonstrate the expected increase with metabolic rate predicted by Nielson and also observed in Series A. It appears that as long as a heat balance is reached, deep body temperatures rise primarily in response to metabolic rate and are largely insensitive to the boundary conditions at the skin surface.

The dependence of active sweating upon skin temperature, core temperature and heat storage is shown in Figures 3-43 through 3-47. As in Series A, test data and model predictions demonstrate an increase in sweat rate directly proportional to all three parameters. Figure 3-43 shows an average gradient of 107 g/hr per °C increase in mean skin temperature. This is in agreement with the results of Benzinger (8), and comparable to the results from Series A for the same approximate inlet temperatures (shown as flagged symbols).

As in Series A, the data exhibit some dependence upon different LCG cooling rates. The highest flowrate data show the largest sweat rates for

a given skin temperature. This is similar to Series A where the lowest inlet temperature data showed higher sweat rates at a given skin temperature.

This result is explained by the fact that as LCG cooling increases (either by increasing the flowrate or decreasing the inlet temperature), a higher metabolic rate, and consequently, a higher core temperature is required to maintain a constant skin temperature. It is the increase in core temperature that causes the higher sweat rates at increased LCG cooling rates for the same skin temperature. It is also worth noting that the effect is much less apparent from the flowrate dependent data of Series C (where data and predictions are more closely bunched for the different flowrates) than the inlet temperature dependent data of Series A (Figure 3-15). This is another manifestation of the greater sensitivity to LCG cooling by temperature control as compared to flowrate control.

One final observation about Figure 3-43 is that the model predictions are in better agreement with the test data than for the corresponding results of Series A. This can be traced to the improved predictions in individual skin temperatures for Series C that were previously discussed.

Figure 3-44 shows the increase in active sweat rate in proportion to increased deep body (tympanic) temperature. The average gradient of the predictions and data is 350 g/hr sweat rate per °C increase in tympanic temperature. Therefore, the influence of tympanic temperature upon sweating is over 3 times as great as that of mean skin temperature. This is in keeping with the results of Benzinger (8), Stolwijk and Hardy (133-139),and Wyss (172). The more powerful, coarse control of sweat rate effected by deep body temperature as opposed to the less influential, fine control by skin temperature was also observed and discussed in Series A.

The results of Figure 3-44 also exhibit some dependence of active sweat rate upon LCG cooling, with the lowest flowrates showing the highest sweat rates at a given tympanic temperature and the highest flowrate showing the lowest sweat rates. However, the correlation is less than that of the previous figure. This is because low flowrates (or high inlet temperatures) result in higher skin temperatures for the same core temperature, and therefore, higher sweat rates. However, this has a lesser influence on sweat rate than does elevated core temperatures at the same skin temperature.

The predictions of the mathematical model demonstrate somewhat lower sweat rates than the test data of Figure 3-44 for the same tympanic temperature. However, this may be the result of inaccuracies in the ear probe sensor used in this test. The model predictions are for head core temperature, which under ideal conditions, should be nearly identical to deep body or rectal temperature (89, 90). However, tympanic thermocouples have a tendency to lag actual head core temperature by as much as 0.5°C, especially if they are not fitted painstakingly, or if they work partially loose. Consequently, the tympanic temperature results are often low, which would explain the discrepancy between predictions and data. If the test data was displaced to the right by about 0.5°C, it would fall almost directly on the predictions.

Thermocouple inaccuracy is also suspect because the data of Series A showed equivalent sweat rates at higher rectal temperatures (Figure 3-16). Although rectal temperature was not measured in Series C, it should not differ greatly from head core temperature, and the results of Series A show closer agreement with the model predictions of Figure 3-44 than the Series C test data.

Finally, results from Benzinger's temperature regulation studies (8) are superposed on Figure 3-44 (as a dashed line) and show closer agreement to the model predictions for no LCG cooling than the Series C test data. The no-cooling case is used for comparison because Benzinger's results were derived for a nearly constant skin temperature without an LCC.

Of course, another possibility exists that the errors described above are associated with the short duration of each test sequence, combined with frequent unsteady-state conditions. Such transients are often difficult to correlate and prone to error.

The preceding results are presented in another light by Figures 3-45 and 3-46, which show sweat rate as a function of the change in skin temperature and or tympanic temperature as measured over the duration of each test sequence, rather than the absolute value at the endpoint. All of the same trends observed in the preceding figures are apparent. Furthermore, it is seen that to produce the same sweat rate, a change in mean skin temperature approximately 5 to 10 times as large as that of tympanic temperature is required.

Agreement between the test data and model predictions is again quite good, demonstrating the ability of the model to simulate the changes in body temperature and their effects upon sweating. The results also show that mean skin temperature decreased over the duration of every test sequence with the exception of the no-cooling case. Conversely, tympanic temperature always increased. This trend was also observed for Series A, and is a consequence of the powerful skin cooling effect of the LCG, and the relative independence of core temperature from LCG cooling, as discussed earlier. The other implication of the observation is that the LCG must have lowered the skin temperature below the peripheral thermostatic

set-point for local sweating. This would have the effect of inhibiting sweating by limiting its response only to changes in core temperature or rates of change of core and skin temperature. The response to levels of skin temperature above the local set-point would be nonexistent.

The combined effect of both tympanic and mean skin temperature is illustrated in Figure 3-47, which presents sweat rate as a function of total body heat storage. In the determination of total body heat storage, increases in skin temperature are less significant than increases in core temperature. Therefore, since it was shown earlier that the relationship between the core temperature and sweat rate is not greatly affected by LCG cooling, it is not surprising that Figure 3-47 exhibits minimal dependence on LCG cooling. The model predictions are bunched closely together for the different LCG flowrates, and agree well with the test data. There was somewhat more dependence shown by the equivalent figure for Series A (Figure 3-18), primarily because skin temperatures were depressed to a greater extent as a result of the low inlet temperatures used (7°C).

The good agreement of test data and model predictions, coupled to the minimal effect of LCG flowrate, combine to make Figure 3-47 a good method of assessing sweat rate as a function of thermal stress. If the amount of heat stored by the body under certain environmental and metabolic conditions can be determined, and related to thermal comfort, it can then be associated with a given sweat rate.

This can be demonstrated by using the results of Figure 3-35, which show body heat storage as a function of metabolic rate for various LCG flowrates. It is seen that for the same metabolic rate, body heat storage increases as LCG flowrate decreases. This is the same trend that was observed in Series A for increasing inlet temperatures (Figure 3-19). It is caused by reduced LCG cooling, culminating in elevated body temperatures.

In Figure 3-35, the test data and model predictions are in reasonable agreement, with the exception of the no-cooling case where the model predictions are consistently higher. These deviations are probably caused by unsteady-state test conditions. Positive heat storage rates at the conclusion of the no-cooling test sequences indicate that the heat storage values were still rising and would have approached the model predictions if time had been extended.

Figure 3-35 serves to point out the utility of the model in predicting body heat storage in response to metabolic work loads and LCG performance. The increased heat storage values from Figure 3-35 that result at lower flowrates can be combined with Figure 3-47 to show the strong influence that heat storage exerts upon sweat rate. For example, from Figure 3-35, at a metabolic rate of 469 watts, reducing the LCG flow from 82 to 27 to 0 liters/hr resulted in an increase in body heat storage of 30 to 58 to 72 watt/hr. Utilizing these values in Figure 3-47 shows that this caused active sweating to increase steeply from 163 to 235 to 410 g/hr.

It should be noted that total heat storage and sweat rates for the conditions of no LCG cooling were considerably larger than any other corresponding data from this or the preceding test series. The high sweat rates experienced at both the 27 liters/hr and no-flow LCG cases are both well above the comfort levels of 100 g/hr specified by Webb. In support of this, the test subject complained of feeling sticky and uncomfortably warm at the conclusion of these test sequences. On the other hand, the sweat rates observed for LCG flows in excess of 55 liters/hr were markedly reduced and associated with subjective feelings of comfort.

The latter findings can also be used to illustrate the application of the heat storage based comfort band. The band is shown as the cross-

hatched zone in Figure 3-35. It is observed that the heat storage data for the higher LCG flowrates are within or quite close to the comfort band. However, as flowrate decreases, the data show values above the comfort band in the uncomfortably warm or hot region. With increasing deviation from the band, the mathematical model predicts rising sweat rates well above 100 g/hr (Figure 3-47). These predictions are verified since test subjects did sweat at higher rates and felt uncomfortably warm.

It is also observed that the comfort band can be used to forecast the degree of LCG cooling required to maintain comfort. For example, at the lower metabolic rates, low flowrates of 27 liters/hr are acceptable. However, as metabolic rate increases beyond 420 watts, higher flowrates are required to stay within the comfort band. This relationship will be examined in more detail subsequently, in Series D.

SERIES D

Series D was conducted in a vacuum environment with all critical life support system functions being controlled by the PLSS. The ambient pressure was below 10 torr but subjects wore the A7L suit, which was pressurized to 195 torr. The oxygen ventilation system was regulated by the PLSS to a circulating flow of 170 liters/hr, while the LCG water flowrate was regulated to about 109 liters/hr.

The LCG inlet water temperature was selected in accordance with subjective comfort. This was accomplished by the subject turning the PLSS LCG water diverter valve to 1 of 3 positions - Min, Intermediate, or Max cooling.

For Series D, the hypobaric chamber environment was varied in a parametric fashion from very hot (137 watts into the A7L suit) to very

cold (72 watts out of the suit). The metabolic profile was designed to simulate the actual workloads required for the various tasks and experiments to be performed on the lunar surface and was controlled by varying the subject's step rate on a Harvard Step.

Table 3-4 presents the calculated results and heat balance data for Series D. (The raw test data are shown in Table D4 of Appendix D). The data of Table 3-4 are presented in terms of total, rather than steady-state or average rate values, since the most accurate heat balance analysis utilized post-test determinations of such total values as metabolic heat production from total oxygen consumption and carbon dioxide production, and evaporative heat loss from total water collected. Coincidentally, the instantaneous values of metabolic rate and total evaporative heat loss rate integrated over time agree favorably with the total values measured in the post-test analysis. Therefore, any conclusions drawn from the overall heat balance are, in most instances, equally applicable at any given time during each test.

Heat Balance

As was the case for Series A, B, and C, the largest portion of the heat removal was through the LCG, as shown by the LCG HEAT REMOVAL row of Table 3-4. In this case, however, the LCG heat removal was controlled according to subjective comfort rather than imposed upon the test subject. As in previous test series, convective heat removal was negligible, a tendency consistent with the use of an LCG as the primary mechanism of heat transfer. Also from Table 3-4, it is seen that evaporative heat loss is significant, although considerably less than LCG heat removal.

The single most distinguishing characteristic of Series D is the magnitude of the net heat exchange between the subject and the ambient

environment. Whereas in previous test series, radiation heat exchange was relatively small, the data of this test demonstrated average values between 72 watts out of the suit to 137 watts into the suit. In fact, in most cases, the net environmental heat exchange was in the same order of, and often exceeded, the total evaporative heat removal for the duration of each test.

The HEAT BALANCE row of Table 3-4 shows the difference between heat production and heat loss for the duration of each test. In all cases but Test 2 (which had a cold environment) the difference was positive, indicating the likelihood that some heat was stored by the test subject. The actual body heat storage, as determined by skin and tympanic temperature measurement, is shown in the next row. This shows that heat storage was actually negative for 3 of the 7 tests. However, it should be kept in mind that the values are quite small, especially considering the extended duration of each test.

Some insight into the difference between the heat balance and the body heat storage values may be gained by examining the numerical difference between the two, shown in the HEAT DEFICIT row. As in previous tests, the heat deficit represents errors in the estimations of heat production, heat loss or heat storage, or more simply stated, unexplained heat. In this case, all values are very small or positive. It can be stated with some confidence that the largest source of the heat deficit comes from slight underestimations of the total heat removal.

Specifically, the method of determining total evaporative heat loss is subject to some small error. Table D4 shows the total subject weight loss and the evaporated water collected over the duration of each test. These data show that in every case, the former exceeded the latter. It

was assumed that the difference between the two was unevaporated water that would not enter into the heat balance (runoff sweat). However, it is likely that some amount of this runoff was actually evaporated and then recondensed inside the suit and never collected. Therefore, this would lead to underestimations of total evaporative heat removal, and thus total heat removal. This would then explain the positive heat deficit values for Series D. Conversely, the determination of evaporative heat loss from weight loss alone was a significant source of error in Series A which resulted in negative heat deficit values.

The data of Table 3-4 indicate that the overall heat balances for Series D were quite accurate. The heat deficit values are all small considering the duration of the tests (from 3.2 to 7.0 hr). In fact, the largest error recorded was an average rate of 36 watts for Test 3. The total body heat storage for test subjects was also small and showed no particular trend. This is probably the result of LCG inlet temperature selection by the subject in response to his comfort.

Transient Results

Typical results for the transient response of head core (tympanic) and mean skin temperature are shown in Figures 3-55 to 3-61 (dashed lines). The mean skin temperatures shown represent a weighted average of all of the skin temperatures recorded for each particular test (see equation 2, Section 2). These individual skin temperatures are shown in Appendix D in Figures D5-D11. The total body heat storage calculated from the core and skin temperatures (see equation 3, Section 2) is also shown at the bottom of Figures 3-55 to 3-61.

From these data, it can be seen that mean skin temperature decreased significantly in each case from the beginning of each test, while head

core temperature showed far less change. The results are understandable in view of the fact that head core and skin temperatures are primarily driven by 2 factors: metabolic rate and LCG inlet temperature. The metabolic rate profile for each test (Figures 3-48 to 3-54) may be overlayed on the corresponding Figures 3-55 to 3-61 to show that the maximum head core temperatures generally occurred at or near the points of maximum metabolic rate for each test. Similarly, the minimum head core temperatures match up nicely with minimum metabolic rates. In a similar fashion, it can be shown that the minimum mean skin temperatures occurred at or near the maximum metabolic rates, and the higher skin temperatures occurred near the lowest metabolic rates.

This apparently contradictory result can be explained in terms of the results from Series A and C, which showed that LCG inlet temperature is a more significant driver of mean skin temperature than is metabolic rate. Therefore, it is also important to examine the profile of LCG inlet temperature for Series D. This is shown at the top of Figures 3-62 to 3-68 for each of the 7 tests of Series D. The corresponding metabolic rate profile for each test is shown by the dotted profile at the bottom of these figures.

From these data, it is seen that the minimum LCG inlet temperatures for each test were selected by the subject at times generally corresponding to the points of maximum metabolic rate; and that maximum LCG inlet temperatures were selected for lower metabolic rates. This, then is the primary reason for the occurrence of the inverse relationship between metabolic rate and mean skin temperature that was previously noted.

The behavior exhibited by the data of the previous curves is easier to understand when considered in light of the physiological responses

brought into play. As the metabolic profile shown for each test was implemented, the heat produced by the muscles of the working test subject varied accordingly. This heat was then either conducted away from the muscles towards the skin, or dissipated into the nearest available blood supply nourishing and removing wastes from the muscles.

The heat reaching the blood would very quickly be distributed throughout the bloodstream (a consequence of the fact that the entire blood volume of approximately 5 liters is circulated completely around the body about once a minute or faster). Indeed, some of this heated blood would perfuse the tympanic membrane of the ear and be recorded as a spike in head core temperature. Some of the same blood supply to the head would pass to the hypothalamic region of the cerebral cortex where it could trigger a variety of thermoregulatory responses such as sweating, vasodilatation, and the perception of heat or discomfort.

The heat conducted across the tissues away from the muscles would ultimately find its way to the thermoreceptors of the skin, which in turn would elicit thermoregulatory responses by means of neural control. These responses would be similar to and yet distinct from those of the hypothalamus (central versus local control). The perception of heat or discomfort might then act as a stimulus to the test subject, thereby causing him to initiate the behavioral response of regulating the LCG inlet temperature. This would result in an increase in the heat removal through the LCG and act to return the skin and hypothalamic temperatures back toward the comfort level, thus maintaining homeostasis.

The above responses are illustrated by the heat storage curves in Figures 3-62 to 3-68. Despite the fact that conditions such as metabolic rate and environment varied markedly during each test and from test to test,

the actual body heat storage was controlled and limited to relatively small positive and negative values around zero throughout each test. In other words, the test subjects regulated their LCG performance to maintain comfort, as manifested by drops in skin temperature associated with increases in head core temperature at higher metabolic rates; and increases in skin temperature associated with decreases in head core temperature at lower metabolic rates.

Although the test data of Figures 3-62 to 3-68 generally follow the patterns described above, this is not always the case. Exceptions result from the fact that there is a definite lag time required (shown in Series A to be in the order of 0.5 hours) for heat generated by the muscles to reach the skin thermoreceptors by conduction.

Another explanation is that the subjects for each test had prior knowledge of the metabolic profile to be followed for that particular test. Consequently, some preferred to regulate their LCG heat removal immediately before beginning a high work rate level (anticipatory behavioral response), while others waited until the heat was actually generated, distributed to the blood supply and skin, and finally perceived as heat before regulating their LCG cooling (behavioral response to heat storage). In some instances, a subject actually preferred to store a considerable amount of heat before making an LCG diverter valve change.

These factors, coupled to the rapid transients in metabolic rate that occurred for each test, make it difficult to interpret the results accurately at any given time instant for any particular test. However, for longer periods of time during each test, the time-integrated values almost always display the trends described above.

The predictions of the mathematical model are also shown in the above figures as solid lines (with the exception of Tests 6 and 7, where transient predictions were not made due to the similarity of the testing conditions with Tests 2 and 4). In general, predictions of head core temperature are excellent with a slight tendency to underpredict; predictions of mean skin temperature are generally lower than the actual data, but still very accurate; and predictions of total body heat storage are generally lower than the data, the latter resulting from the underpredictions of core and skin temperature.

The individual skin temperature predictions are shown in Figures D5-D11 in Appendix D. The chest and thigh temperatures were occasionally underpredicted, but showed no consistent trend; back temperature was often significantly different from upper chest temperature; hand, foot, and forehead temperatures had the least error and were the warmest (a consequence of the fact that they were not cooled by the LCG). Chest, thigh and back temperatures were the coolest. The latter trends were also exhibited by the data and predictions of Series A and C. The underpredictions of mean skin temperature in Figures 3-55 to 3-61 can be traced primarily to underpredictions of thigh or chest temperature, a trend seen in previous test series that will be discussed in more detail subsequently.

Due to the rather transient nature of each of the 7 tests, it is difficult to draw any conclusions about the accuracy of the predicted versus the actual time lag between heat production and heat loss. Suffice it to say that the transient behavior of the predictions generally follows the data, with major changes in predicted body temperatures or heat storage occurring at about the same time as that of the test data.

The center and lower curves of Figures 3-62 to 3-68 show the total body heat storage rate and LCG heat removal rate respectively, as a function of time for each of the 7 tests, with the metabolic profile of each test superposed (as dotted lines) over the LCG heat removal curve. The predicted results are also shown (as solid lines) and agreement is again quite good. The heat storage rates were determined by calculating the slope of the total heat storage curves (Figures 3-55b to 3-61b) taken between successive times.

The heat storage rates are generally shown to vary above and below zero, an indication that the subjects attempted to achieve physiological steady-state by adjusting their LCG cooling to try to balance their heat removal against their metabolic heat production. This does not mean that all of the data shown represent physiological steady-state conditions. In fact, most of the points in the heat storage rate curve lie somewhat above or below the zero line, and many data points cross the zero-rate line with a large slope.

This suggests that more often than not, the subjects would tend to overcorrect in attempting to balance their heat production by using the LCG, which is indicative of poor perception of instantaneous thermal comfort, but good perception for longer time periods. The latter can be shown by observing that the heat storage rates integrated over time approach zero for longer time periods (the areas above and below the zero heat storage rate line are approximately equal).

The distinction is important because in order to isolate true steady-state points from each of the 7 transient tests, it becomes imperative to establish a firm set of criteria with which to judge these points. The criteria will be discussed subsequently, when steady-state data from all

of the tests are compared to model predictions, for the purpose of recognizing trends observed in the previous Series A, B, and C.

Several trends are immediately obvious from the LCG heat removal curves of Figures 3-62 to 3-68. The LCG heat removal rate superposed over the metabolic rate profile quite clearly demonstrates that the largest portion of metabolic heat production is removed by the LCG. If all 7 tests are compared, it can also be seen that as the net environmental heat exchange into the suit increased, the amount of the metabolic heat removed by the LCG generally increased. This is shown by comparing Figures 3-63c and 3-67c (for the cold environmental conditions of Tests 2 and 6) with Figures 3-65c and 3-68c (for the hot environmental conditions of Tests 4 and 7).

It can be surmised that as the environmental heat into the space suit increased, a certain amount of it found its way into the LCG, thus biasing the LCG heat removal in a fashion not necessarily the same as that from metabolic heat. In fact, the influence of environmental heat on the LCG is different from that of metabolic heat and will be examined later.

As mentioned earlier, the variations in LCG heat removal rate for any given test in which the ambient environment was constant are directly sensitive to adjustments in LCG inlet temperature. From Figures 3-62 to 3-68, it can be seen that high metabolic rates generally coincided with low LCG inlet temperatures selected by the test subject, which caused high LCG heat removal rates. Conversely, low metabolic rates coincided with higher LCG inlet temperatures which, in turn, caused lower LCG heat removal rates. There are exceptions to this observation, but they may be traced to the rapidity with which many of the transients occurred, or to a variation in the method with which some of the test subjects regulated their LCG

(anticipatory behavior response versus behavioral response to excess body heat storage). The latter is especially noticeable if one compares the results of Test 5 and to a lesser extent Test 2 (Figures 3-66 and 3-63) with those of Tests 3 and 4 (Figures 3-64 and 3-65).

In Tests 2 and 5 the changes in LCG diverter valve position, the decreases and increases in LCG inlet temperature and the corresponding increases and decreases in LCG heat removal coincide almost identically with the times of the abrupt increases and decreases in metabolic rate. This is a classic example of an anticipatory behavioral response.

On the other hand, the results of Tests 3 and 4 often show changes in LCG inlet temperature and LCG heat removal clearly lagging behind metabolic rate, a condition indicative of a behavioral response to the stimulus of high body temperatures or excess heat storage. The latter is associated with the delay time required for the heat generated by the muscles to reach the skin and hypothalamic thermoreceptors by conduction and internal convection. This may have resulted from the test subject temporarily forgetting to keep track of the planned metabolic profile; or simply preferring to store heat before adjusting his LCG cooling.

Coincidentally, the amount of heat stored by a test subject before he made an adjustment in LCG cooling was usually limited to a narrow band within $\pm$ 50 watt-hr (see Figures 3-55 to 3-61), a fact which supports the use of a comfort band based upon heat storage as a means of quantitatively assessing thermal comfort. The one exception to this is in Test 5 (Figure 3-59b), where it is suspected that the tympanic temperature probe worked loose, resulting in a below-normal reading of head core temperature and thus body heat storage.

Figures 3-69 to 3-75 show the actual and predicted transient response of total evaporative heat loss rate (upper curve) and evaporative heat loss by active sweat (lower curve). Since dewpoint sensors were inoperative for Series D, it was necessary to determine the evaporative heat loss rates by a heat balance computation. Utilizing a heat balance equation (equation 13, Appendix C), and the known values of net average environmental heat load, metabolic rate, LCG heat removal rate, and body heat storage rate, it was possible to calculate transient evaporation loss for each test. The evaporation heat loss rate by active sweat was then found by subtracting the empirical relationships previously described for diffusion and respiratory heat loss (equations 5 and 7, Appendix C).

The largest source of error in this type of computation is the assumption that the instantaneous environmental heat exchange did not appreciably differ from the net average environmental heat exchange as determined by post-test analysis of the PLSS. However, the assumption is not too bad considering that all of the inner and outer space suit temperatures that were measured reached a steady-state shortly after exposure to the test environment. Other sources of error in the computation were the assumption of no s ivering in the heat balance equation, errors in the accuracy of measured body temperatures which affect the heat storage rate, and errors in the metabolic rate profile.

Despite these sources of error, it was possible to check the accuracy of the computational technique by integrating the total evaporative heat loss rate curves over time and comparing the totals with the total evaporative heat removed over the duration of each test as determined from measurements of the collected water separated out by the PLSS (Table D4, Appendix D). The comparison (Table D5, Appendix D) demonstrates that the

computational technique described above provides a reasonable estimate of evaporative heat loss rates for Series D.

The results of Figures 3-69 to 3-75 show that the total evaporative heat loss rates vary considerably over the duration of each test. This is a reflection of the changing heat storage rates that occur when the subject attempts to regulate the LCG inlet temperature to maintain his comfort. In some instances, the evaporation rates are quite high and account for a substantial amount of the metabolic heat dissipation. This often occurs during the lag time between the onset of a high metabolic rate and the subsequent adjustment in LCG cooling. However, it will be later shown that evaporation rates during the steady-state points of each test are comparable to those seen in previous test series, and in fact are usually substantially lower than LCG heat removal rates.

The evaporative heat loss by active sweating is also shown to vary over the course of each test. However, it usually accounts for only a small portion of metabolic heat dissipation In fact, in many instances, there is no active sweating at all. This is apparently a manifestation of the use of the LCG to maintain comfort by minimizing sweating. The mathematical model predictions are also shown, and in most cases, agreement with the data is good.

One final observation should be made about the predictions of LCG heat removal and evaporative heat loss. Despite the occurrence of rapid transients during each of the tests, the model predictions tracked the changes exhibited by the test data in a reasonable fashion. Although the rapidity of the transients makes it difficult to detect any trends in model accuracy, it appears that LCG heat removal is slightly underpredicted, a trend which has been repeatedly observed in other tests. On the other

hand, predictions of evaporative heat loss do not display any consistent error.

These and similar trends could be examined in a more rigorous fashion if steady-state data for each of the tests were isolated and compared to model predictions. In pursuit of this objective, it was necessary to establish 2 sets of criteria with which to judge steady-state data. These are listed as follows:

1. Steady-state data for each test are identified by times during which the following 4 conditions prevailed:
   a. The body heat storage rate was approximately zero; and the slope of the heat storage rate curve was also approximately zero.
   b. The LCG inlet temperature was approximately constant.
   c. The metabolic rate was approximately constant.
   d. The LCG heat removal rate was approximately constant.

OR

2. Intervals during each test for which the time-integrated values of body heat storage rate were zero.

For the second set of criteria, the corresponding LCG and evaporative heat removal rates were considered to be the time-averaged values for the same time interval. However, this was not always the case for the corresponding metabolic rates. If the subject regulated his LCG by an anticipatory behavioral response, then the time of metabolic heat production and LCG and evaporative heat removal were identical to the time required for the integrated value of body heat storage to approach zero. If, on the other hand, the subject regulated his LCG by responding to the stimulus of body heat storage associated with the lag time between heat-production and

heat sensation, then the time required to remove the heat of metabolism by LCG and evaporative cooling in order to produce an integrated value of zero body heat storage was somewhat longer than the time of sustained metabolic heat production.

This procedure is summarized by the hypothetical example shown in Figure 3-76. Here the time-averaged metabolic rates (the shaded areas under the upper curves divided by the time period A) are identical. However, for the case of a behavioral response to body heat storage, the time interval required for the integrated heat storage rate curve (dashed line) to approach zero (interval B) is longer than the equivalent time for the case of an anticipatory behavioral response (interval A). The difference occurs because for the heat-storage regulated response, it required a longer time interval to remove the heat produced by metabolism than for the anticipatory behavioral response (center curves). This longer time interval is the result of an obligatory period of forced body heat storage that occurs as a consequence of the lag time (C), and an equivalent period of destorage that occurs after the cessation of metabolic work.

By utilizing the above 2 sets of criteria, it was possible to isolate steady-state data for each test. These data, with their associated time periods are presented in Appendix D in Table D6.

Steady-State Results

Table 3-5 presents the steady-state predicted and actual head core and mean skin temperatures determined in the manner described above. The data are arranged for warm, moderate, and cool LCG inlet temperatures, as a function of metabolic rate.

As in previous test series, the warmest and coolest skin temperatures occurred at the highest and lowest inlet temperatures respectively. That

is, LCG inlet temperature has a greater effect on skin temperature than does metabolic rate. On the other hand, the head core temperatures showed no apparent dependence on LCG temperature. Tympanic temperatures were about the same for the warmer LCG inlet range as for the colder range. This trend was also observed in Series A and C.

The predictions of the mathematical model agree quite well with the steady-state data. As suggested by the transient data, head core predictions are very close to the actual data, while mean skin predictions are also close but usually lower. Contrary to Series A, the error in skin temperature predictions does not appear to be dependent upon LCG inlet temperature or metabolic rate. This may be a consequence of the fact that Series A was more of an off-comfort test than Test Series D.

Figure 3-77 shows the LCG heat transfer coefficient for the steady-state data. The value used as input for the mathematical model was taken from the solid line. The heat transfer coefficient was determined from mean skin temperature and LCG water temperature and flowrate according to equation 10 in Appendix C. The values shown are in good agreement with those of other test series. Differences between the assumed heat transfer coefficient and the actual values resulted primarily from individual variations in LCG fit among test subjects. These variations are sources of error that influence predictions of LCG heat removal; however, in most cases, the effect is slight.

Figures 3-78 to 3-80 show predicted and actual steady-state LCG and total evaporative heat removal as a function of metabolic rate for cool, moderate, and warm LCG inlet temperatures, respectively. Each curve shows the effect of parametrically increasing the net environmental heat exchange from the maximum loss to the ambient environment (67-72 watts out) to the

maximum gain from the environment (117-137 watts in). As indicated by the data, LCG and evaporative heat removal rates expectably increased as metabolic rate increased. Concerning the predictions of the mathematical model, LCG heat removal rates are occasionally underpredicted, although less frequently than observed in other test series. Total evaporative heat loss rate predictions are good with no obvious trend in the errors. Evaporative heat removal is observed to be substantially less than LCG heat removal at the lower LCG inlet temperatures, and comparable for the highest inlet temperatures.

Both the LCG and evaporative heat removal rates are shown to increase as the net heat exchange from the environment increases. At the same metabolic rate and LCG inlet temperature, the results for the hottest and coldest ambient environments differ significantly. This makes it difficult to compare all the results of the cold environment tests directly with those for the hot environments. Direct comparison of the steady-state results of Series D with previous test series is also difficult. It would therefore be desirable to quantitate the effect of environmental heat exchange upon the LCG and upon evaporative heat loss in order to provide a mechanism for direct comparison of all tests, independent of the environment.

Although it would have been more desirable to use actual test data to determine and quantitate the environmental effect, the number of steady-state data points that existed for varied ambient environments at the same metabolic rate and the same LCG inlet temperature were few. Furthermore, although environmental effects were significant, they were still small enough such that slight variations in testing conditions would have made it difficult to rigorously analyze and isolate this effect from others

which may have occurred (such as variations in experimental procedure, metabolic rate or LCG inlet temperature). Consequently, it was decided to use the mathematical model to quantitate the environmental effect in order to eliminate the influence of factors which might bias the test results.

Figure 3-81 shows the effect of increasing the net heat gain from the environment for 3 representative conditions. Predictions of LCG and total evaporative heat loss are shown for a high metabolic rate with a low LCG inlet temperature, a moderate metabolic rate with a moderate inlet temperature, and a low metabolic rate with a high inlet temperature. The available corresponding steady-state data points are also shown, and agreement with the predictions is reasonable. Both LCG and evaporative heat loss rates appear to increase rectilinearly with environmental heat gain. The relationship for LCG heat removal is not visibly different from that for evaporative heat loss.

Figure 3-82 shows the results of the previous curve presented as the change in environmental heat gain or loss (using zero heat-exchange as the reference) versus the corresponding change in heat removal. It is the slope of the lines in Figure 3-82 that provides the desired relationship between the effect of environmental heat exchange and heat removal. Despite the fact that conditions varied considerably from a high metabolic rate at a low inlet temperature to a low metabolic rate at a high inlet temperature, the slopes derived from Figure 3-82 varied by only $\pm$ 5%. The LCG heat removal is shown to absorb (or lose) approximately 40% of the net environmental heat exchange into (or out of) the suit, while the total evaporative heat loss changes by about 60%.

In other words, environmental heat influences the sweating and evaporative heat loss mechanism slightly more than it does LCG heat removal.

Therefore, environmental heat gets in (or out) of the LCG in a fashion unlike that of metabolic heat. Although LCG heat removal has been shown to account for anywhere between 45 to 118% of metabolic heat production (depending upon metabolic rate and inlet temperature), it only accounts for 40 $\pm$ 5% of environmental heat exchange. This conclusion is in agreement with independent engineering analyses of the LCG using manikins with heaters.

These results can be used to eliminate the effect of the environment from all of the steady-state test data of Series D, which permits all of the data to be transformed to the condition of a thermally neutral environment and thus compared in the same fashion as previous test series. It also permits direct comparison of these data with the data of previous test series in order to substantiate or invalidate previous trends.

Figure 3-83 shows LCG heat removal rate as a function of metabolic rate for various LCG inlet temperatures. The data shown are the steady-state values of Table D6 of Appendix D with the environmental effects subtracted in the manner described above.

As in other test series, the same general trend of an increase in LCG heat removal for an increase in metabolic rate at a constant inlet temperature is observed. Also, as expected, the cooler inlet temperature data shows more heat removal than the warmer inlet temperature data for similar metabolic rates.

The mathematical model predictions shown (solid lines) are for conditions of zero environmental heat exchange. Agreement with the actual data is good, especially for the lower and moderate metabolic rates. At higher metabolic rates there is some underprediction. However, unlike other test series, no consistent pattern of error is discernible (such as increasing

underpredictions at high metabolic rates and low inlet temperatures). In fact, the agreement of test and predicted data at the higher metabolic rates for inlet temperatures of 6-9°C is very good.

Figure 3-84 presents the data of Figure 3-83 replotted as the percentage of metabolic heat production removed by the LCG (LCG heat removal/metabolic rate) versus LCG inlet temperature. The data are grouped for low, moderate, and high metabolic rates and bounded by predictions for metabolic rates of 293 and 615 watts. As in other tests, there is a sharp increase in percentage heat removal as the inlet temperature decreases. Actual heat removal varied between 43 to 90% of metabolic heat production, depending upon inlet temperature and metabolic rate. These results are entirely consistent with previous trends, and the data of Figure 3-84 generally fall within the band defined by the predictions. Deviation does occur at the higher inlet temperatures, but some of it may be attributable to the fact that the LCG heat transfer coefficient decreases and differs somewhat from that used by the model at higher inlet temperatures. Alternatively, this error may simply be a consequence of the technique used for eliminating environmental effects from the data. In any case, the data and predictions confirm the relationships deduced from previous tests, and the errors appear less severe and more random.

Total evaporative heat loss is shown as a function of metabolic rate and LCG inlet temperature in Figure 3-85. The individual values were determined from the heat balance computation outlined earlier. The trends shown are the same as observed in previous test series, and as predicted by the mathematical model (dashed lines). Evaporation heat loss increased almost rectilinearly as metabolic rate increased at a constant inlet temperature, and evaporation rates were greater for higher LCG inlet tempera-

tures at the same metabolic rate. Agreement between test and predicted data is generally good, with no obvious trend in the differences that do occur. Unlike Series A or B, the mathematical model does not exhibit a tendency to overpredict evaporative heat loss at higher metabolic rates, although this occurs somewhat in the 14-17°C temperature range.

Figure 3-86 depicts the total evaporative heat loss rate as a percentage of metabolic rate and shows the expected trend of an increase in evaporation rates as LCG inlet temperature increases. As with LCG heat removal, the evaporative heat loss data fall nicely within the band bounded by model predictions of 293 and 615 watts. It is also observed that for inlet temperatures below 17°C, total evaporative heat loss rates represent a lower portion of metabolic heat removal than LCG heat removal rates. Evaporation heat loss varies between 10 and 50% of metabolic heat production (as opposed to 43 to 90% for LCG heat removal). It should also be noted that for the same LCG inlet temperature, a greater percentage of evaporative heat loss is expected for higher metabolic rates than lower metabolic rates, whereas for LCG heat removal, the reverse is true.

Figures 3-87 and 3-88 show the heat loss by evaporation of active sweat as a function of metabolic rate and LCG inlet temperature. These steady-state data were determined by subtracting the empirical relationships for diffusion and respiratory heat loss from total evaporative heat loss. Sweating is shown to constitute a far smaller channel of heat removal than LCG heat loss. The evaporation of active sweat varies almost rectilinearly with metabolic rate for constant LCG inlet temperatures, and agreement with the predicted data (dashed lines) is good. However, these results were to be expected since the data of Figures 3-87 and 3-88 were

derived from total evaporative heat loss data, and consequently, should exhibit the same trends.

It is observed in several instances that evaporative sweat heat loss is zero or very low. This probably resulted from the use of the LCG to eliminate or limit sweating in order to maintain comfort. For example, for cold inlet temperatures between 6 and 9°C, the onset of sweating did not occur until metabolic rates greater than 440 watts were achieved. In fact, most of the sweat heat removal rates were limited below 150 watts for all combinations of metabolic rate and LCG inlet temperature, and evaporative heat removal by active sweat rarely exceeded 35% of the metabolic heat production.

Figure 3-88 also shows the data generally falling within the narrow band defined by predictions of 293 and 615 watts. This implies that the subjects regulated LCG cooling in order to limit sweating, and presumably to maintain thermal comfort. Such a conclusion can be tested by performing a regression analysis and curve fit to the data of Figures 3-83 and 3-85. This is shown in Figure 3-89. The predictions of the mathematical model are also shown for reference on the clear overlay.

If the data are examined without the overlay, it is observed that there is a strong correlation between metabolic rate and LCG heat removal (dark symbols of top graph). The least squares curve fit through the data is a second order curve with a correlation coefficient of 0.90. The second order curve fit had a better correlation than a linear fit, but a third order fit did not significantly improve the correlation. The steepness of the curve indicates the strong dependence upon LCG cooling to maintain comfort as metabolic rate increased.

On the other hand, the total evaporative heat removal (open symbols of middle graph) did not increase nearly as much with metabolic rate. In fact, after a slight increase, it leveled off and approached an asymptotic value of about 150 watts. The best least squares curve fit to the data (dashed line) has a correlation coefficient of 0.65. There is probably more data scatter and less of a correlation primarily because of the errors inherent in the computational techniques used to extract total evaporative heat loss rate from the raw test data. However, the salient point is that LCG heat removal is regulated in such a fashion (presumably in response to thermal comfort) as to limit sweating and evaporation in the manner shown by Figure 3-89. The evaporation heat loss rate approaches a limit because the cold LCG inlet temperatures selected at high metabolic rates (6-13°C) depress skin temperature and, therefore, local sweating signals. The regulation of the LCG heat removal is accomplished by varying the inlet temperature.

If the clear overlay is now superposed over Figure 3-89, it can be seen that the LCG regression curve intersects the lines of constant LCG inlet temperature (top curve) at specific metabolic rates. Assuming that the subjects regulated their LCG cooling in accordance with their own comfort, this demonstrates that ideally, at each metabolic rate, there is a unique inlet temperature that will be selected. (In actuality, there is a range of inlet temperatures, due to individual variations in comfort.)

It is the selection of a unique comfort inlet temperature at each metabolic rate that results in the limitation of sweating demonstrated by Figure 3-89b. This implies that there is a definite relationship between the limitation of sweating and thermal comfort. Such a relationship is well established in environmental physiology. For example, studies by

Webb and Fanger (49, 155) have related thermal comfort to the limitation of sweat rate.

The uniqueness of the results of Figure 3-89 is the relationship that exists between LCG cooling and sweat rate, which permits far greater metabolic rates to be achieved at comfort while wearing an LCG. It should be mentioned that the LCG correlation of Figure 3-89a could have been improved if a detailed error analysis were performed, and the points with a large standard error omitted. However, another method exists for refining the correlation.

If the equivalent regression curves of Series B (Figure 3-28a) are compared with those of Figure 3-89, it is noted that the equations of corresponding curves are different. Furthermore, the regression curves of Series D have a higher correlation coefficient than the equivalent curves of Series B. The difference may be attributed to the fact that in Series D, the test subjects were permitted to vary their LCG cooling in response to metabolic rate, environmental conditions, and presumably, thermal comfort. Therefore, it has been assumed that all of the data of Series D represent comfort conditions. However, many investigators feel that over short time periods, man is a poor judge of his own thermal comfort. Consequently, it would be useful to examine the body heat storage data of Series D in relation to the comfort band that has been postulated to relate thermal comfort to heat storage. This would provide a good indication of the validity of the comfort assumption for Series D.

Figure 3-90 presents total body heat storage as a function of metabolic rate for all of the steady-state data points. The comfort band is also shown with the data. It is observed that almost all of the data points fall within the comfort zone. However, there are several points

that lie significantly outside of the band (shown circled). If these are truly off-comfort points, they would bias the correlations of Figure 3-89 because of the non-rectilinear or discontinuous thermoregulatory effects that occur under off-comfort conditions.

It will subsequently be shown in Section 4 that the correlations of LCG heat removal and evaporation heat loss can be improved further by including only those points which fall in the comfort zone. The points which fall outside of the comfort band of Figure 3-90 may well represent conditions during which the test subject was not aware of his own comfort. This is a distinct possibility, considering the transient nature of the tests in Series D. However, it is equally likely that these results represent errors in the experimental procedure, such as body temperature sensor error, or in the selection process for determining steady-state points.

Nonetheless, it is observed that most of the data fall within the comfort band and follow the same trend of an increase with metabolic rate. This is in contrast to previous test series where LCG inlet temperatures were imposed upon, rather than selected by, test subjects and much of the heat storage data was outside the comfort zone. (see Figures 3-19, 3-22 and 3-35).

It should be mentioned that most of the steady-state data of Series D were found by integration of raw data over relatively long, rather than short, time periods; and that subjective comments of uncomfortable conditions by the test subjects were uncommon. Therefore, the initial assumption that subjects regulated LCG cooling in response to thermal comfort was reasonable. Consequently, the data of Figure 3-90 also strongly

support the validity of the proposed comfort band concept as a means of quantitating thermal comfort.

In light of the results expressed in Figures 3-89 and 3-90, the influence of heat storage on the limitation of sweating, and the control of LCG cooling becomes clear. Test subjects regulated their LCG cooling in such a way as to keep body heat storage within the comfort zone, thereby limiting sweating and evaporative heat loss in the manner shown by Figure 3-89. It is also noteworthy to recall that the comfort zone was based upon a rectal temperature tolerance and a limitation of sweating. The data of Figure 3-89b show equivalent sweat rates well within the limits of other conventional techniques of assessing comfort as related to sweat rate.

It has been previously stated that the accuracy of the predictions of the mathematical model depends upon the degree of comfort associated with a particular set of test conditions. For off-comfort conditions, such as encountered in many of the tests in Series A and B, the model shows a general tendency to underpredict LCG heat removal and overpredict evaporative heat loss (Figure 3-28). The model errors can be traced to the difficulty of simulating the thermoregulatory system responses that become more pronounced as an individual deviates further from comfort. Therefore, it would be expected that the model errors seen in these previous test series would be reduced for Series D, where comfort was achieved for almost all test points.

This is observed to be the case from the data on the bottom curve of Figure 3-89. Here, errors in the model predictions of LCG heat removal (dark symbols) and total evaporative heat loss rate (open symbols) are shown as a percentage of metabolic rate, for all steady-state test points.

A hand-drawn curve fit through the error data is also shown (solid line for LCG error, dashed line for evaporative heat loss).

These data show no trend in either LCG or evaporative heat loss error. In both cases, errors rarely exceed 10% of metabolic rate. Unlike previous test series, there is no trend indicating dependence upon metabolic rate or LCG inlet temperatures, and the error appears random. This is in contrast to Series A and B, where errors were positive for LCG heat removal and negative for evaporative heat loss (Figure 3-28b). Furthermore, the errors of Series A and B were generally larger and showed a tendency to increase with metabolic rate. However, these results are expected since thermoregulatory responses such as cutaneous blood-flow regulation and sweating are greater at higher metabolic rates.

The error analysis data of Figure 3-89, coupled to the reasonably good predictions of skin temperature, rectal temperature and heat storage, emphasize the validity of the mathematical model as a valuable tool for accurately simulating the overall response of the human thermoregulatory system, especially for comfort conditions. It has also been shown that the heat storage based comfort band is a useful method of quantitating the thermal comfort of subjects wearing an LCG.

It now becomes possible to combine these two tools in such a way as to provide the following results:

1. Predictions of the manner in which an LCG is regulated to maintain comfort.
2. Prediction and verification of the LCG heat removal relationship demonstrated by Figure 3-89a.
3. Prediction and verification of the sweat limitation relationship demonstrated by Figure 3-89b.

4. Generation of a method of predicting metabolic rate from LCG heat removal rate.

The results described above are derived by superposing the comfort band over the steady-state LCG and evaporative heat loss predictions of the mathematical model. This is shown in Figures 3-91 to 3-93 for neutral, cold, and hot ambient environments, respectively. In each case, the chamber and space suit environmental conditions were input to the model, and metabolic rate and LCG inlet temperature were input that were varied parametrically. Steady-state predictions of LCG heat removal, evaporative heat loss and total body heat storage were then generated.

Predictions of LCG heat removal (solid lines) and total evaporative heat loss (dashed lines) are shown as a function of metabolic rate. Lines of constant LCG inlet temperature corresponding to 5, 10, 16, 21, and 27°C are also shown. The total body heat storage predictions appear as numbers lying alongside the solid and dashed lines at metabolic rates of 146, 234, 352, 469, and 586 watts. The comfort band was then superposed on the LCG and evaporative heat loss predictions simply by connecting the appropriate values of comfort heat storage at each metabolic rate.

The result is a band of predictions that intersects lines of constant LCG inlet temperature at values of LCG heat removal and total evaporative heat loss rates that conform to the comfort zone. For the LCG heat removal curves, values above the band correspond to cold conditions (accompanied by shivering for high negative heat storage values) and values below the band correspond to uncomfortably hot conditions (accompanied by excessive sweating for high positive heat storage values). For the evaporative heat loss curves, the reverse is true.

The striking thing about these bands is that they have the same appearance as the data and regression curves of Figure 3-89. Specifically, the predicted comfort bands of Figures 3-91 to 3-93 show a strong rectilinear or second order dependence of LCG heat removal versus metabolic rate and a near-constant value of total evaporative heat loss rate that asymptotically approaches values similar to those of Figure 3-89b.

It should be noted that the variation between the bands from Figure 3-91 to Figure 3-93 reflects the effect of the changing environment upon comfort. That is, at each metabolic rate, as the net heat exchange from the environment increases, the LCG inlet temperature predicted for comfort decreases and the LCG heat removal increases. This is shown by the upward movement of the LCG comfort band as the environmental heat goes from heat loss to heat gain. Consequently, the effect of the additional heat input from the environment upon sweating and evaporative heat loss is minimized, since LCG cooling can be adjusted to compensate for it. In fact, it is suspected that there would have been no effect of the environment upon sweating at all, had the PLSS cooling system been designed so that the test subject could select any LCG inlet temperature desired, instead of one of 3 discrete temperatures: cool, medium, or warm.

The preceding observations are summarized in Figures 3-94 to 3-96, where the comfort bands for LCG inlet temperature, LCG heat removal, and total evaporative heat loss, respectively, are shown as a function of metabolic rate, and compared to the steady-state test data. Each curve shows the predicted comfort band for environments ranging from cold (net 72 watts out of suit) to hot (net 137 watts into suit).

It may be seen from Figures 3-94 and 3-95 that both the predictions and the test data demonstrate selection of decreased LCG inlet temperatures

and increased LCG heat removal for increased environmental heat exchange at constant metabolic rates or for increased metabolic rates at constant environmental heat exchange. Consequently, the total evaporative heat loss is limited for all conditions, as shown by Figure 3-96. There is no significant trend in the evaporative heat loss data that reflects environmental effects and the data show only a slight increase with metabolic rate before approaching a limit.

The predicted bands of Figures 3-94 to 3-96 contain nearly all of the test data and thus provide confidence in the ability of the model to predict the LCG inlet temperature, LCG heat removal and evaporative heat loss necessary for comfort at each metabolic rate for a range of environmental conditions.

Before concluding the analysis of Series D, several additional comments are in order. It can be observed from Figure 3-93 (predictions for the hot environment) that the selection of even the coldest LCG inlet temperature does not achieve comfort at metabolic rates of 586 watts or greater. This reflects the fact that the Apollo-LCG was designed for peak heat removal efficiency at metabolic rates below 586 watts in a neutral environment. At high metabolic rates and hot environmental conditions, LCG heat removal performance is inadequate and comfort cannot be maintained. This could be improved by modifying the existing LCG design to increase the effective contact surface area between the LCG and the skin, thereby increasing the heat transfer coefficient; or by the application of other LCG concepts, such as a head cooling garment. Designing an improved LCG is only one of the many uses for which the mathematical model can be applied as a valuable research tool and will be discussed in Section 4.

Another factor that should be mentioned is that the current model does not have any provision for muscle fatigue associated with sustaining high metabolic rates for long periods of time. Such a physiological performance degradation would affect the test data, but not the model predictions. Therefore, errors that occur at high metabolic rates in Figures 3-91 to 3-96 may be partly attributable to this factor.

Finally, it can now be seen that the model predictions form the basis of a method of predicting metabolic rate from LCG performance. For example, if the net radiative heat exchange for a particular environment is known, and the LCG inlet temperature and heat removal rate at equilibrium are measured, this information may be utilized in the parametric data of Figures 3-91 to 3-93 to predict metabolic rate and quantitate comfort with surprising accuracy. This is the method that was employed to determine astronaut metabolic rates for all of the Apollo lunar surface explorations and is described in the next section for Series E.

SERIES E

In order to allow adequate physiological assessment of the astronaut on the lunar surface, to determine the rate of utilization of life-support system consumables, and to provide information for activity scheduling for real-time and subsequent mission planning, it was necessary to estimate accurately the metabolic rate in real-time for each EVA. This was accomplished by integrating 3 independent methods that utilized all of the available telemetry data that was transmitted from the PLSS. These data were received and processed as input parameters into the Real Time Computer Complex (RTCC) of the Mission Control Center at the NASA/Johnson Space Center. The data were then used in real-time computer programs utilizing

the 3 independent methods, to present 3 independent metabolic rates. These rates were examined by a metabolic assessment team, and a best, integrated value was chosen. The 3 methods utilized were based upon PLSS telemetry data of astronaut heart rate, astronaut oxygen consumption, and astronaut LCG inlet temperature and LCG heat removal. The procedures that were utilized, including general background, results, accuracy, and significance are reported in detail in the Apollo Experience Report - Assessment of Metabolic Expenditures (Appendix E).

The LCG method that was used involved the utilization of the parametric predictions shown in Figures 3-91 to 3-93 of Series D. These and similar predictions were implemented on the RTCC. The PLSS telemetry data of LCG heat removal and inlet temperature were transmitted from the lunar surface and used as input to the RTCC computer program, which then provided real-time estimates of astronaut metabolic rate during each EVA, based upon LCG performance (Figure 2-6).

The method may be illustrated by examining some of the real-time results of the Apollo missions (see Table E2, Appendix E) superimposed on parametric curves typical of those used on the RTCC computer program. Figure 3-97 shows the live data with the parametric predictions and comfort band utilized for those EVAs during which the net environmental heat exchange was approximately zero. This was usually the case for the EVAs that occurred when the sun angle was low, and the lunar surface temperatures were neither excessively hot or cold, such as EVA 1 of Apollo 11, EVA 2 of Apollo 12, EVA 1 of Apollo 15, and EVA 1 of Apollo 17 (see Table E1, Appendix E). For those EVAs that occurred during hotter or colder surface conditions, other parametric predictions similar to Figures 3-92 or 3-93 were used.

As the real-time data of LCG inlet temperature and heat removal rate were received, they were instantaneously cross-plotted on the curve as shown. Because the parametric curves specify a unique relationship between LCG heat removal rate and metabolic rate for each LCG inlet temperature, an estimate of metabolic rate was continuously available from the data, and was displayed on Flight-monitor consoles to the metabolic assessment team (Figures E1 and E2, Appendix E).

Furthermore, the overall thermal comfort of the astronauts was assessed by observing the extent that the live data fell above or below the comfort band. If the real-time data deviated well-below the comfort band for prolonged periods of time (20 minutes or longer) this indicated that the astronaut was probably using an LCG inlet temperature that was too high for the specific task he was performing. Since such a condition could lead to excess body heat storage and performance impairment, it was one of the critical safety factors monitored closely by the metabolic assessment team and the flight surgeon.

Conversely, if the data deviated above the comfort band, this was indicative of inlet temperatures that were too cold. It was important to detect these conditions because they could lead to peripheral vasoconstriction, negative heat storage and performance impairment.

In the event that the real-time data fell significantly above or below the comfort band (circled points) and was unchanged or stable for longer than 20 minutes, the metabolic assessment team alerted the flight surgeon, who, on several occasions, requested that the astronaut change his LCG-diverter valve setting to increase or decrease his LCG cooling. This means of safety monitoring was deemed necessary because the nature of the scientific tasks and the tight schedule required during an EVA often led to conditions whereby an astronaut was not aware of his own thermal comfort.

In addition to the real-time estimates of metabolic rate and astronaut thermal comfort it was also important to keep track of the cumulative energy expenditure and peak energy requirements during the EVA. The RTCC computer program provided this by integrating the instantaneous values of metabolic rate over time, and by recording peak energy expenditures in memory.

During the actual EVA, the flight surgeon had to be ready at all times to make recommendations concerning the advisability of continuing or deviating from an activity in the mission plan. His principal concerns were the reserve capacity of the astronauts and their physiological status. The physiological status was based upon a variety of factors, some of which were historical in nature, and some of which were real-time.

The historical factors included such things as the extent of deconditioning resulting from 3 days of weightlessness during translunar coast, the individual response observed during pre-mission training for specific activities, the pre-flight physical condition of each astronaut, and the amount of exercise, sleep and fatigue observed prior to the EVA.

The real-time factors included instantaneous metabolic rate and cumulative and peak energy demands. Data on excessively high heart rates, ventilation rates and heat storage were also recorded and related to instantaneous and peak energy demands as part of the total consideration of crew status.

Data on cumulative energy expenditures were important by themselves in that they were directly applied in the determination of the consumables usage rates and reserve status. The usage rate of these consumables (oxygen, sublimator feedwater supply, lithium hydroxide, and battery) was the determining factor in the useful life of the PLSS on the lunar surface

and was closely related to the cumulative metabolic energy expenditure. This was particularly significant in the case of the sublimator feedwater reserve, which provided LCG, convective and PLSS equipment cooling, because there was no direct measurement of the feedwater supply.

The instantaneous and cumulative metabolic energy expenditures also provided essential information for the lunar surface activity planners who had constructed a schedule of crew activities based upon pre-flight estimations of the metabolic rate and the time required to perform each activity. These planners were responsible for modifying the activities and scientific tasks in real-time if the actual metabolic data deviated from the pre-flight predictions.

As mentioned earlier, 3 independent methods were utilized by the metabolic assessment team to determine a final, integrated metabolic rate. This procedure was decided upon because earlier studies indicated several sources of uncertainty in each method when used individually. The heart rate and oxygen consumption methods and their associated errors are discussed in detail in the Apollo Experience Report, Appendix E.

The calorimetric, LCG method described above proved to be a most accurate and reliable indicator, despite the fact that the available calorimetric data from the PLSS was limited to LCG inlet and outlet temperature and suit gas inlet temperature.

The standard by which the accuracy of the LCG method was judged was a post-EVA heat balance analysis of the total life-support system consumables remaining in the PLSS at the conclusion of the EVA. Primarily, the amount of PLSS feedwater remaining, coupled to an estimate of environmental heat exchange, provided an accurate determination of the cumulative metabolic expenditure. This calorimetric approach was valid because the

PLSS feedwater was used in the sublimator to reject the heat of the LCG and the convective and evaporative heat of metabolism (see Figure 2-3). Therefore, the total amount of PLSS feedwater used was directly proportional to the total astronaut energy expenditure. The usage of feedwater and other PLSS consumables of interest are presented in Table E1 of Appendix E.

The accuracy of the LCG program was judged by integrating the real-time estimates of metabolic rate over time for the EVA duration and comparing this cumulative metabolic expenditure with the post-EVA heat balance analysis of the PLSS based upon feedwater usage. These results are presented in Table 3-6. The results show surprising accuracy, generally greater than 90%, and further serve to validate the trends demonstrated by the test data and the mathematical model in Series D.

The errors associated with the LCG method in Table 3-6 result from several uncertainties in the data and in the method itself. Ideally, the most accurate measurement of metabolic rate by direct calorimetry would require measurement of LCG heat removal, sensible and latent heat removal by the surrounding gas stream, net environmental heat exchange into or out of the pressure suit, and energy dissipated as mechanical work. However, the available PLSS telemetry data were limited to LCG heat removal (LCG inlet and outlet temperatures) and suit gas inlet temperature.

Fortunately, the largest portion of metabolic heat production was removed by the LCG, and the mathematical model of human thermoregulation described in Section 2 was used to estimate the types of heat removal that were not directly measured. However, each of these estimates had uncertainties associated with them that contributed to the total error.

A second source of error was the fact that the estimate of metabolic rate was dependent upon proper selection of the LCG inlet temperature by the astronaut in accordance with his thermal comfort. If an improper inlet temperature was selected, thereby causing subcooling, or inadequate cooling with heat storage, the total heat removal was unequal to metabolic heat production. However, in this case the estimate was still useful because it provided an index of deviation from comfort that was used as a means of monitoring crew safety. In this case, consumables usage rate estimates were not effected since they depended upon accurate determinations of total heat removal rather than metabolic rate. Furthermore, errors of this type were usually diminished or eliminated as the EVA grew longer in duration since the astronauts would almost always correct their LCG cooling to maintain thermal comfort as time accumulated.

A third source of error occurred during the transient period following a change in the position of the LCG diverter valve. After such change was made, the LCG inlet temperature changed rapidly and required several minutes to stabilize. During such periods, the LCG heat removal rate alone was used to estimate metabolic rate, by determining the intersection of the LCG heat removal rate with the comfort band. This procedure was based upon the fact that the LCG heat removal data did not change as rapidly as the inlet temperature and that over large time periods, the average LCG heat removal rate was proportional to thermal comfort in the manner shown by Figure 3-95. This is described in more detail in the Apollo Experience Report, Appendix E.

A fourth source of error occurred during transient periods following a step-rate change from one metabolic rate to another. As previously mentioned, the parametric predictions of Figures 3-91 to 3-93 represent steady-

state results during which metabolic rate and total heat removal were invariant. For short time periods over which the latter 2 quantities were actually changing, the LCG method was inaccurate by nature of its steady-state assumption. However, for longer time periods, the results again averaged out to compensate and provided accurate mean and cumulative results. The time required to dampen out such errors was on the order of 20 to 30 minutes, approximately the same length of time observed for the lag time between heat production and heat dissipation (see Series A Results).

The consequence of this lag time error was that the response of the LCG method in estimating metabolic rate was slow. However the estimates were observed to begin to respond almost immediately to a change in metabolic rate.

A final source of error was the inherent inaccuracy of the LCG heat removal data. This was dependent upon the accuracy of the LCG inlet and outlet temperature measurements and the assumption of a constant LCG water flowrate.

Despite the sources of error described above, the LCG method of estimating metabolic rate provided accurate real-time estimates judged at least equal to or better than the other independent methods. When integrated with the other 2 methods, these results provided the metabolic assessment team with the most complete and accurate information available for monitoring and guiding the progress of the EVA.

The metabolic team received all incoming raw data, processed the data in accordance with the best real-time estimates for values of the unmeasurable factors involved, used the result obtained from each of the individual methods to provide correction factors for the other methods

(such as LCG flowrate, net environmental heat exchange or suit oxygen leak rate) and finally provided one integrated value for the flight surgeon.

It was realized that this process could be iterative, and that updates could cause retrospective changes in values as the EVA progressed. However, after completion of the mission and post-flight analysis of the data, a better basis for planning future lunar traverses was established.

Accordingly, the results from the Apollo 11 mission were used to plan rest periods and establish limits on heart and respiratory rates for Apollo 12. These results led to an extension of the lunar surface stay-time on Apollo 12 without loss of confidence. Similarly, the experience and information gained from preceding missions were incorporated into planning subsequent missions.

For example, it was discovered that the LCG method would provide accurate estimates of average metabolic rate but could not produce accurate results for time periods less than 20 minutes. Conversely, the heart rate method was sensitive to minute-by-minute changes in metabolic rate, but was very inaccurate. By correlating these methods together, it was ultimately possible to produce accurate minute-by-minute prediction of metabolic rate which were then associated with individual activities of short duration, such as walking, running, digging lunar samples or deploying lunar surface experiments (147).

As the knowledge and information base gained from these methods increased, the confidence level of each mission increased. The ultimate result was that the stay-times, useful work accomplished and knowledge gained on the lunar surface was increased and a high [illegible] was provided with optimum safety.

TABLE 3-1.- SERIES A - CALCULATED DATA AND HEAT BALANCE (STEADY-STATE)

TEST/SUBJECT	1/T.W.	2/J.W.	3/R.H.	4/R.H.	5/M.C.	6/J.W.	7/F.D.	8/R.H.	9/R.H.	10/R.H.	11/J.W.
Duration, min.	100	120	120	150	180	150	180	120	180	120	120
LCG inlet temp., °C	16	16	16	16	16	16	7	7	7	7	7
Heat Produced											
1. Metabolic rate, watts	117	228	254	342	433	589	360	413	452	491	618
Heat Loss											
1. Evaporation heat loss, watts											
a. By respiration and diffusion[1]	29	44	46	58	69	88	60	66	71	76	86
b. By active sweating[2]	0	0	5	32	32	75	5	3	16	53	53
Total Evaporative Heat Loss[3]	29	44	51	90	101	163	65	69	87	129	145
2. Convection and radiation heat loss, watts[4]	0	0	0	0	0	0	0	0	0	0	0
3. LCG heat loss, watts[5]	232	241	266	274	297	386	392	423	423	452	524
Total heat loss, watts	261	285	317	364	398	596	457	492	510	581	669
Heat balance = heat produced - total heat loss, watts (also equal to heat storage rate and/or shiver rate, 6	-144	-57	-63	-22	+35	-7	-97	-79	-58	-90	-51
Total heat storage over duration of test, watt-hrs[7]	-77	-46	-96	+5	+32	+62	-118	-23	-37	-4	+14
Final heat storage rate, watts[8]	-53	-23	-28	+2	+1	-4	-51	-18	-46	-4	-4
Heat deficit = heat balance - final heat storage rate, watts	-91	-34	-35	-20	-34	-4	-45	-59	-10	-86	-47

1. See Eqns. 5, 6 and 7, Appendix C. 2. Sweat heat loss = total evap. - (respiration + diffusion). 3. From total weight loss - see sample calculation appendix C. 4. Assumed negligible based on physical characteristics of overgarment. 5. See Eqn. 5, Section 2. 6. See Eqn. 1, Figure 2-2. 7. See Eqn. 3, Section 2. 8. See Eqn. 4, Section 2.

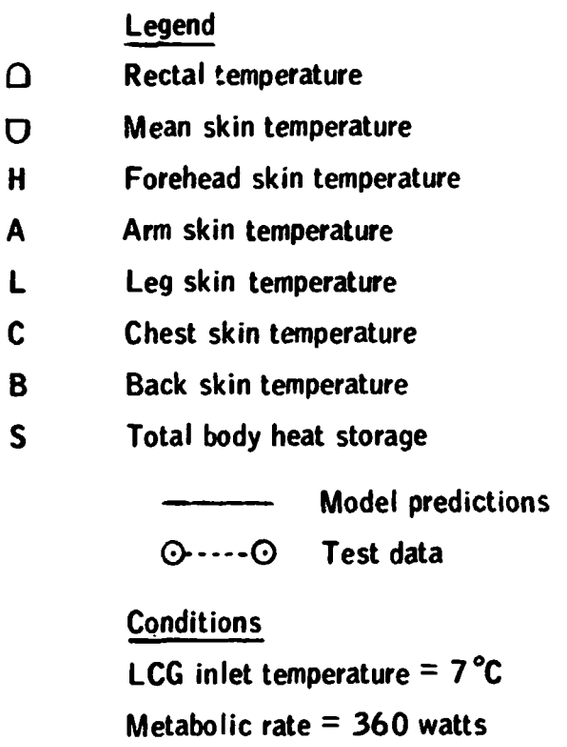

Figure 3-1.- Predicted and actual body temperatures and heat storage vs time for cold LCG inlet temperatures and low metabolic rates (test 7).

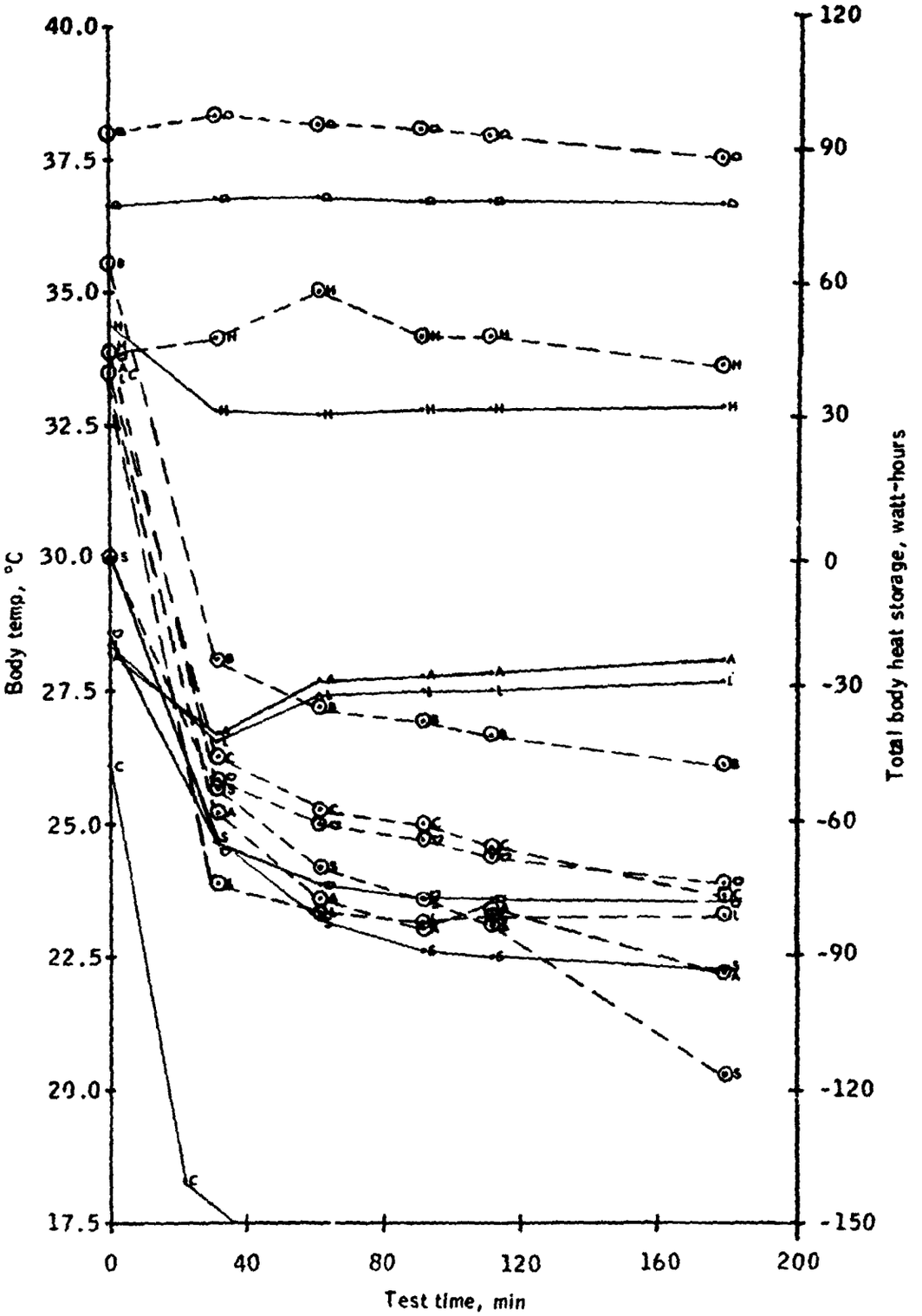

Figure 3-1.- Concluded.

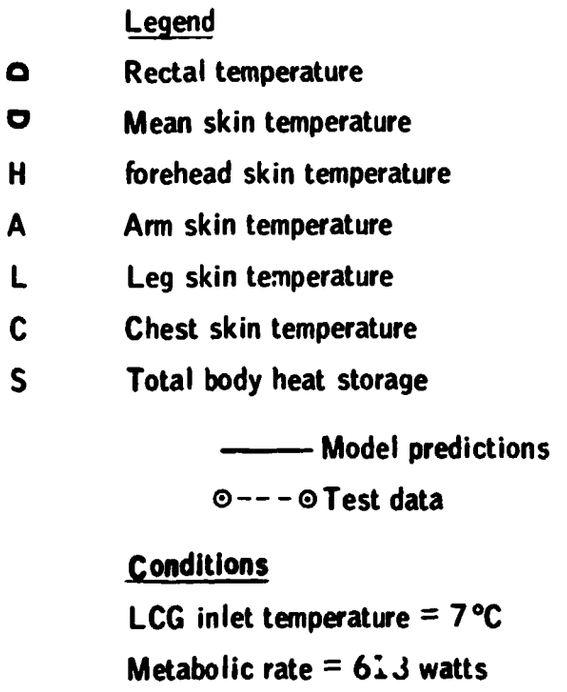

Figure 3-2.- Predicted and actual body temperatures and heat storage vs time for cold LCG inlet temperatures and high metabolic rates (test 11).

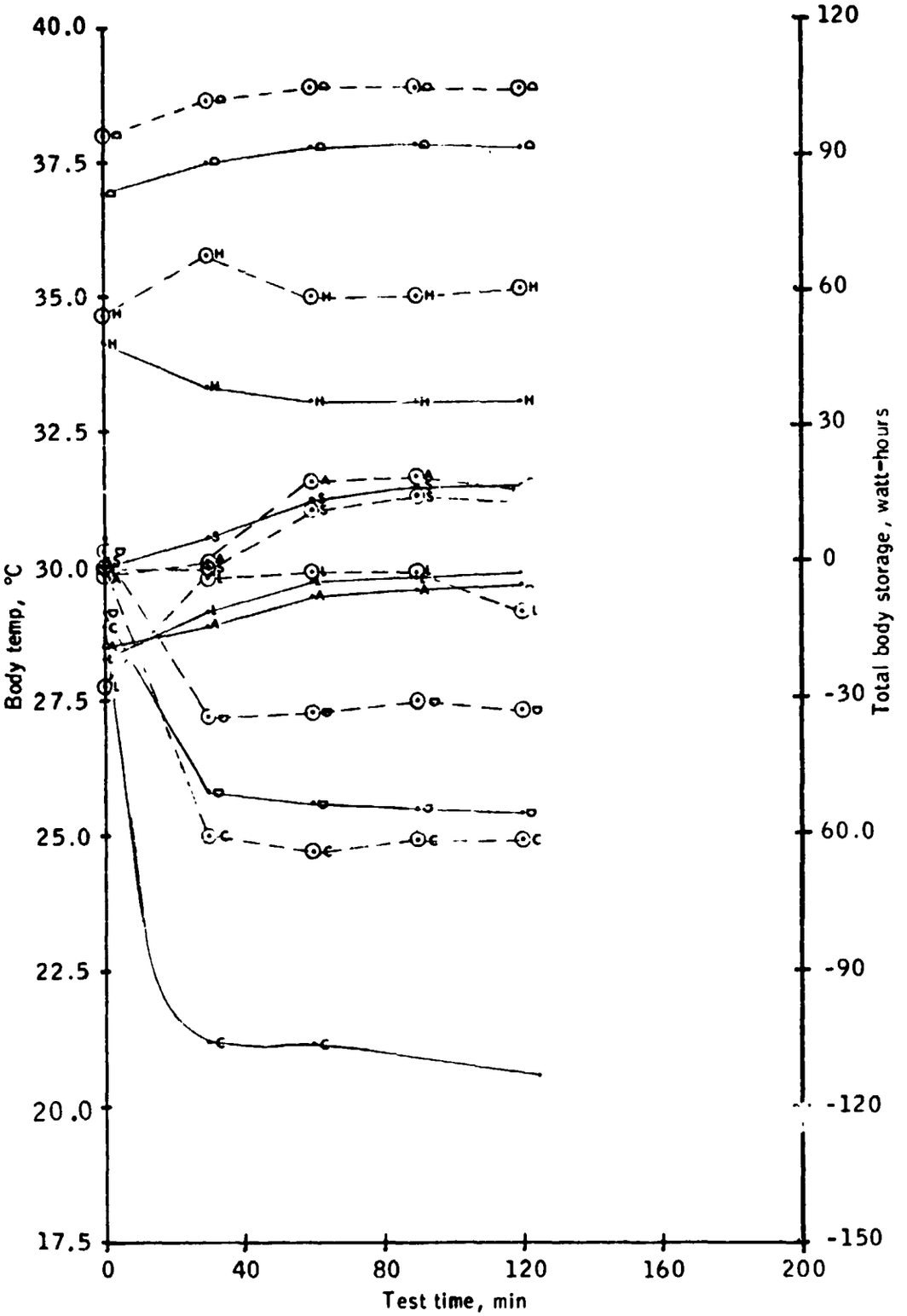

Figure 3-2.- Concluded.

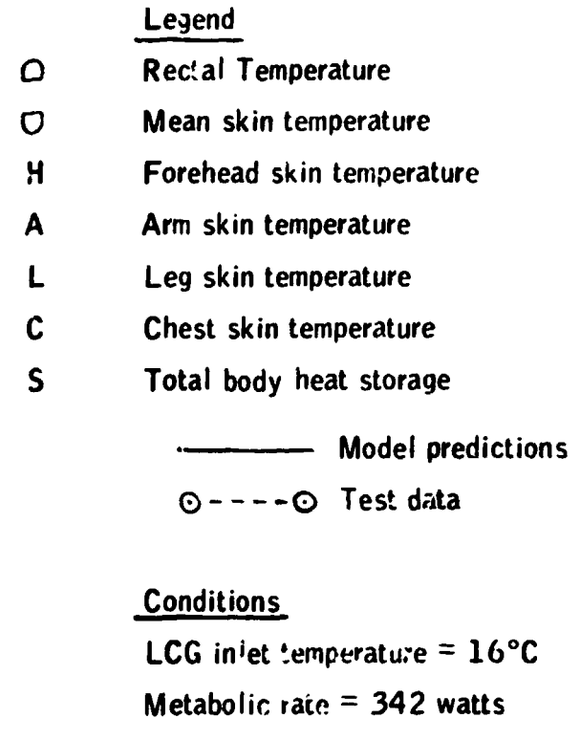

Figure 3-3.- Predicted and actual body temperatures and heat vs time for moderate LCG inlet temperatures and low metabolic rates (test 4).

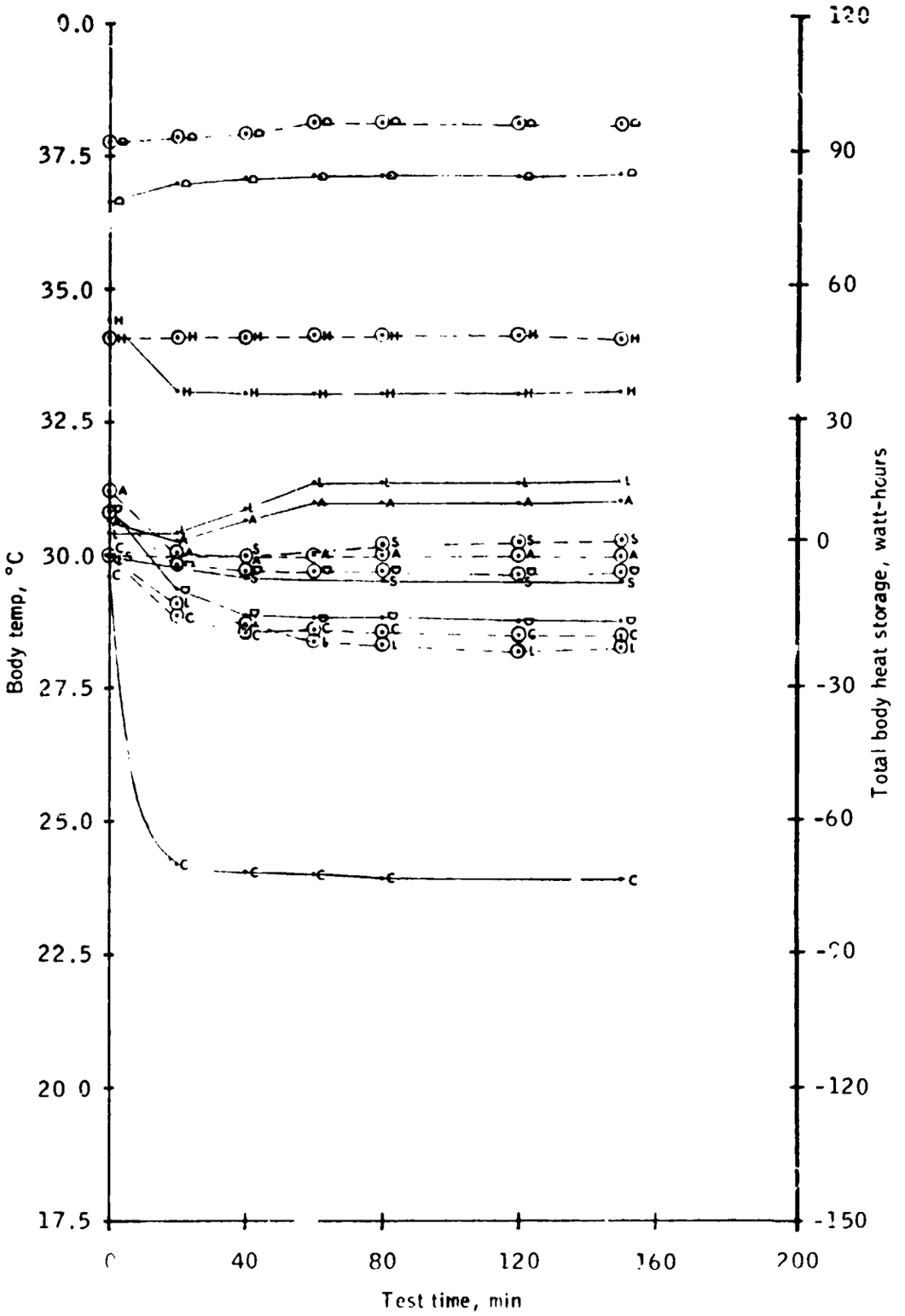

Figure 3-3.- Concluded.

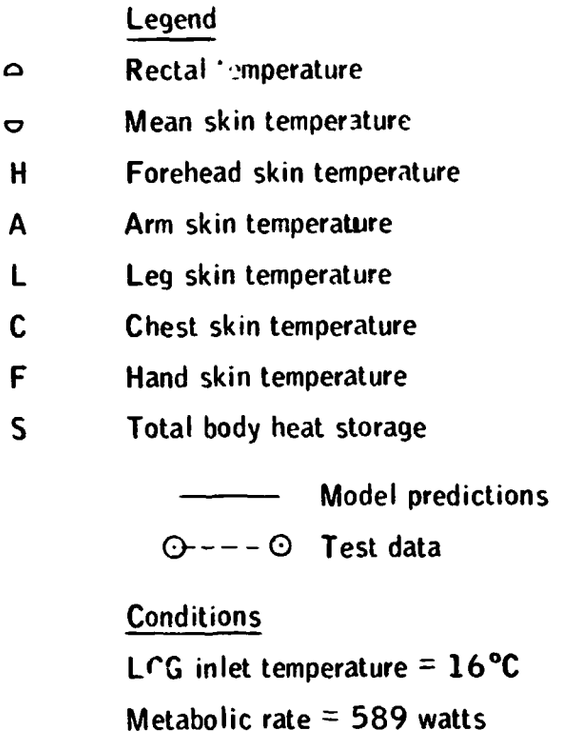

Figure 3-4.- Predicted and actual body temperatures and heat storage vs time for moderate LCG inlet temperatures and high metabolic rates (test 6).

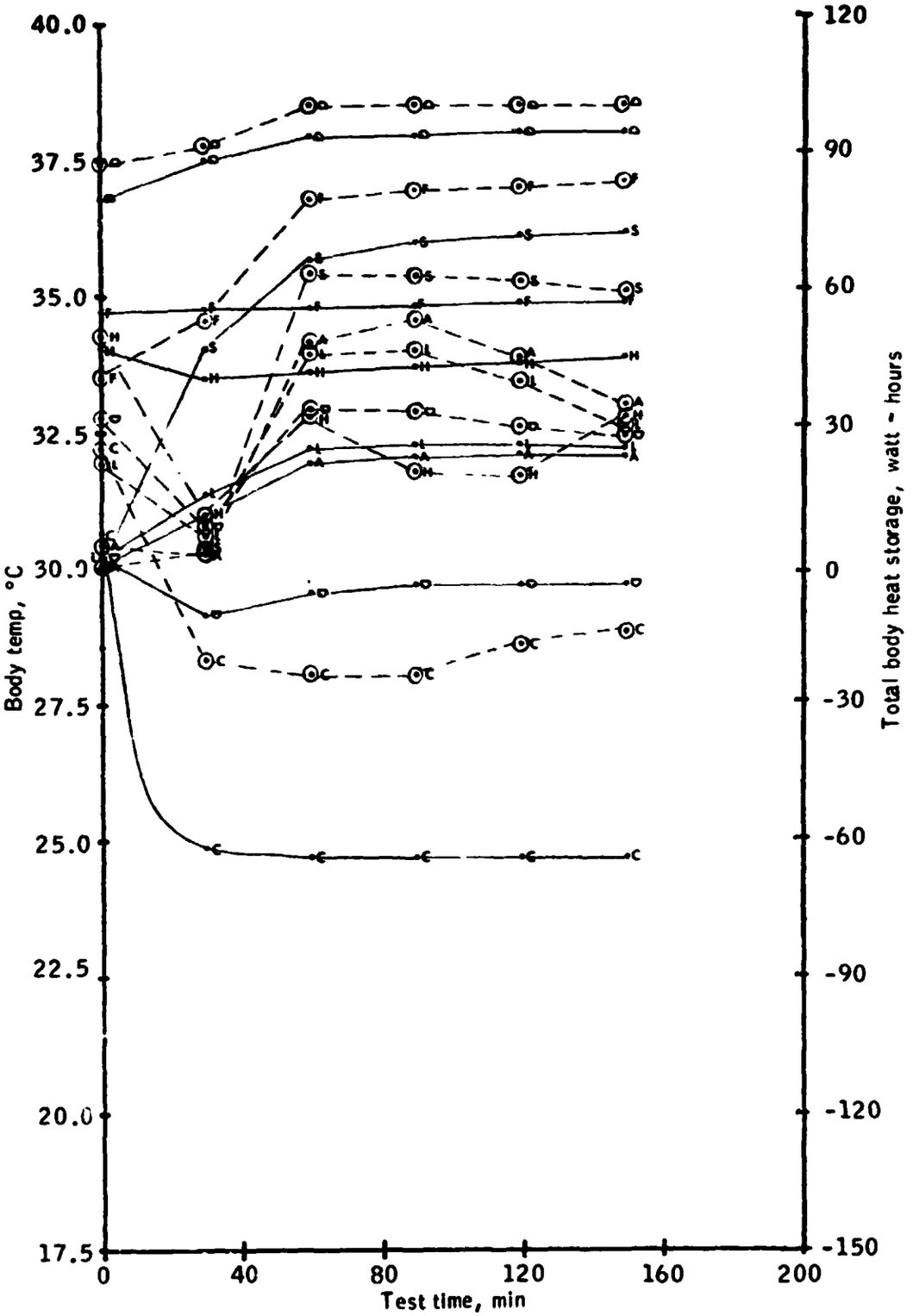

Figure 3-4.- Concluded.

Legend

Parameter	Test data symbol	Test condition	Mathematical model prediction
LCG heat removal rate	◇	LCG inlet temp = 7°C	——— 1.
	○	=16°C	——— 2.
	△	=24-26°C	——— 3.

Notes: Numbers near data points indicate total body heat storage. Values in parenthesis are predictions

Flagged data points (◇, ○, △) are from Santamaria (112)

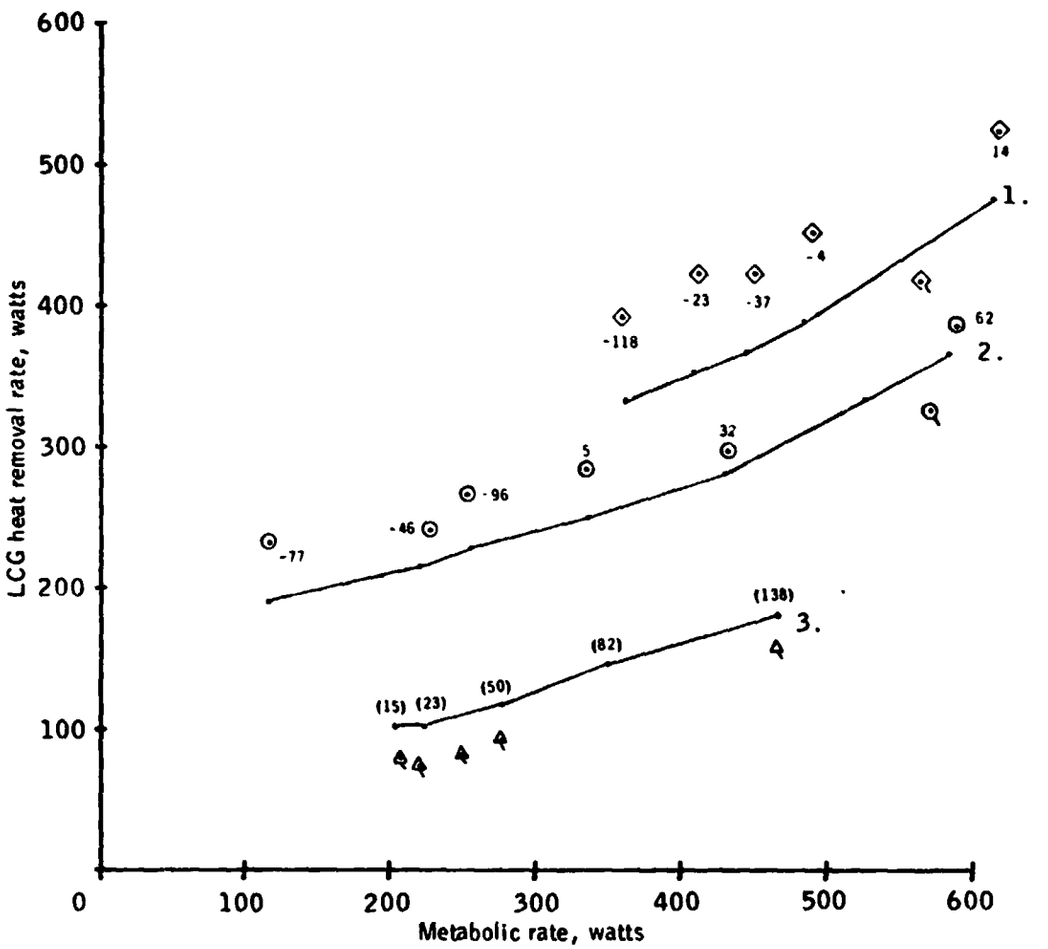

Figure 3-5.- Predicted and actual steady-state LCG heat removal vs metabolic rate, for various LCG inlet temperatures.

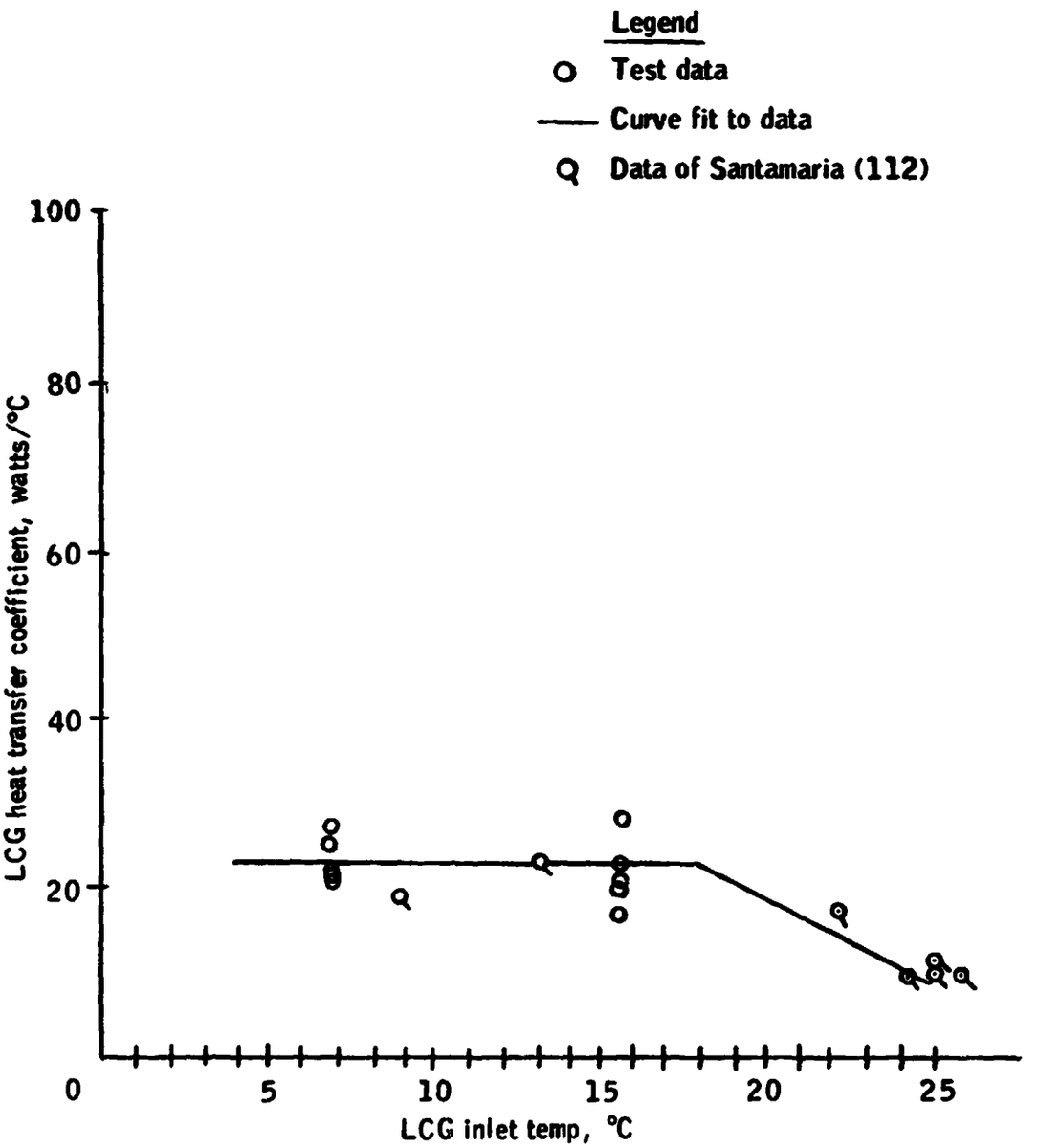

Figure 3-6.- LCG heat transfer coefficient vs LCG inlet temperature.

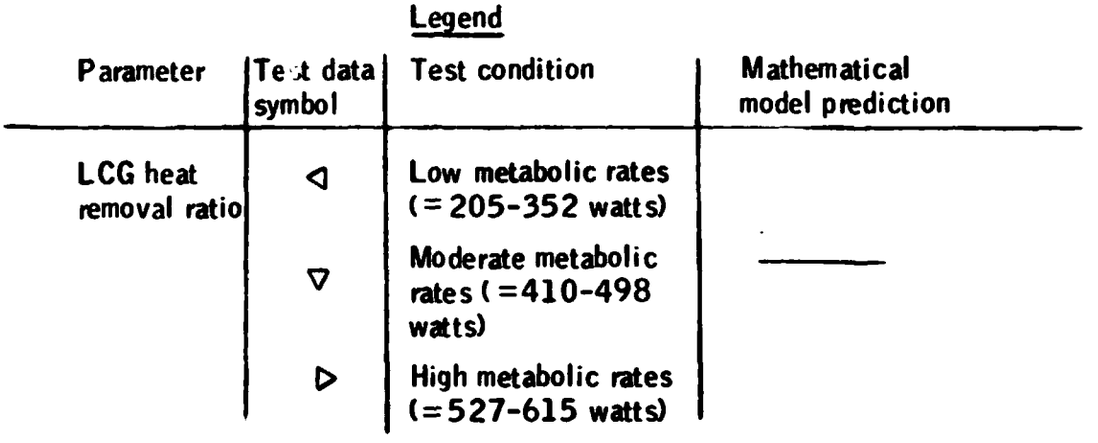

1. Model prediction for metabolic rate of 234 watts

2. Model prediction for metabolic rate of 586 watts

Note: Flagged data (◁, ▽ , ▷) are from Santamaria (112)

Figure 3-7.- Ratio of LCG heat removal rate to metabolic rate vs LCG inlet temperature.

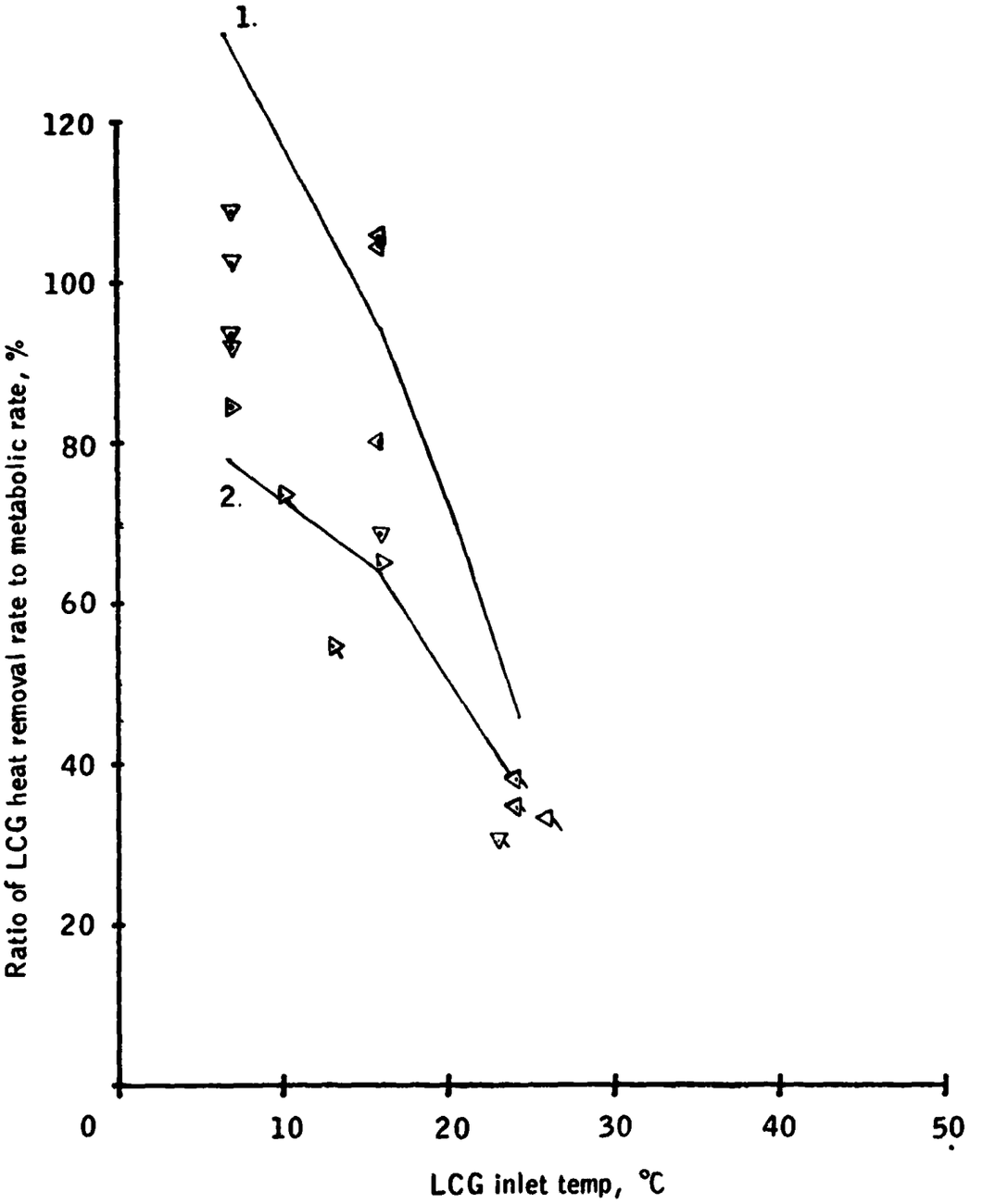

Figure 3-7.- Concluded.

Legend

Parameter	Test data symbol	Test condition	Mathematical model prediction
Evaporative heat loss rate by active sweat	◇	LCG inlet temp 7°C	——— 1.
	○	16°C	——— 2.
	△	24-26°C	——— 3.

Notes: Numbers near data points indicate total body heat storage. Values in parenthesis are model predictions.

Flagged values (◇, ○, △) are from Santamaria (112)

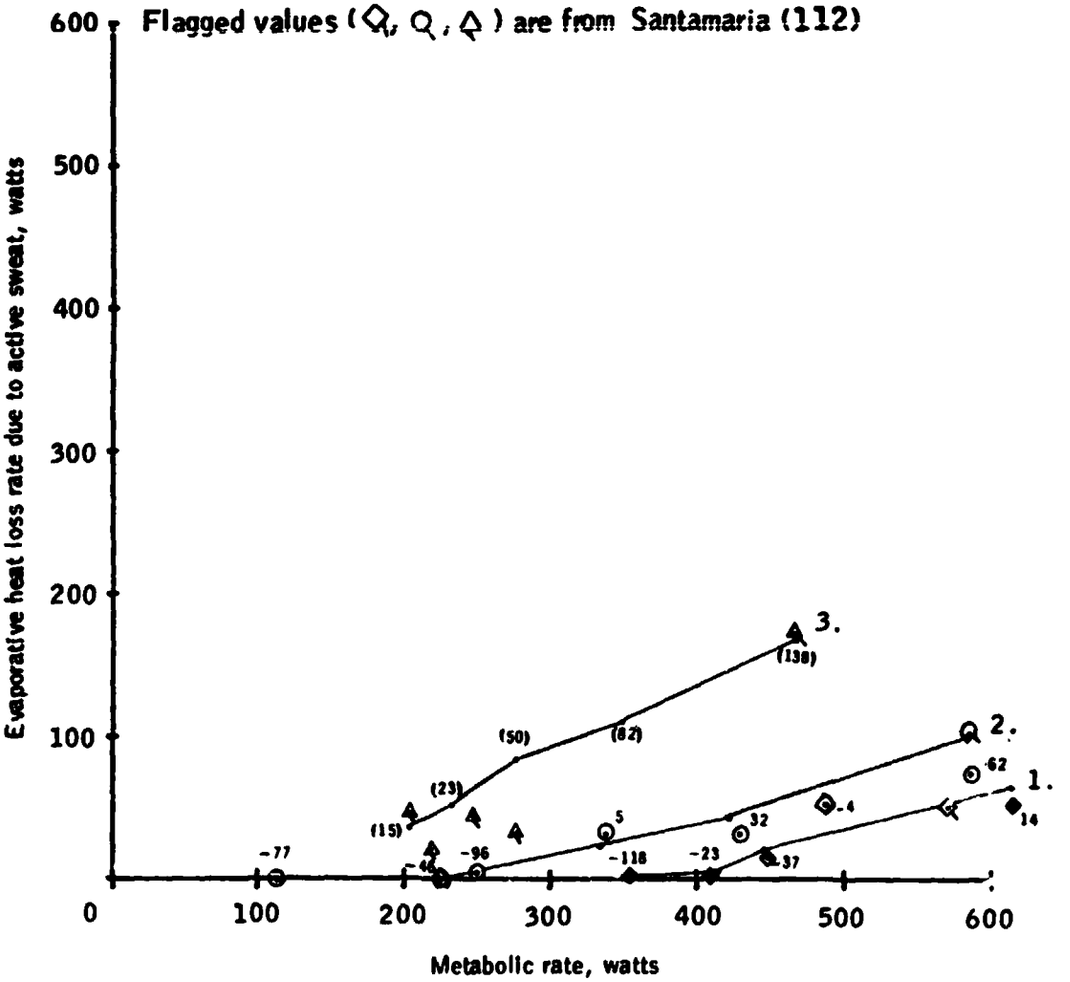

Figure 3-8.- Predicted and actual steady-state evaporative heat loss rate by active sweat vs metabolic rate, for various LCG inlet temperatures.

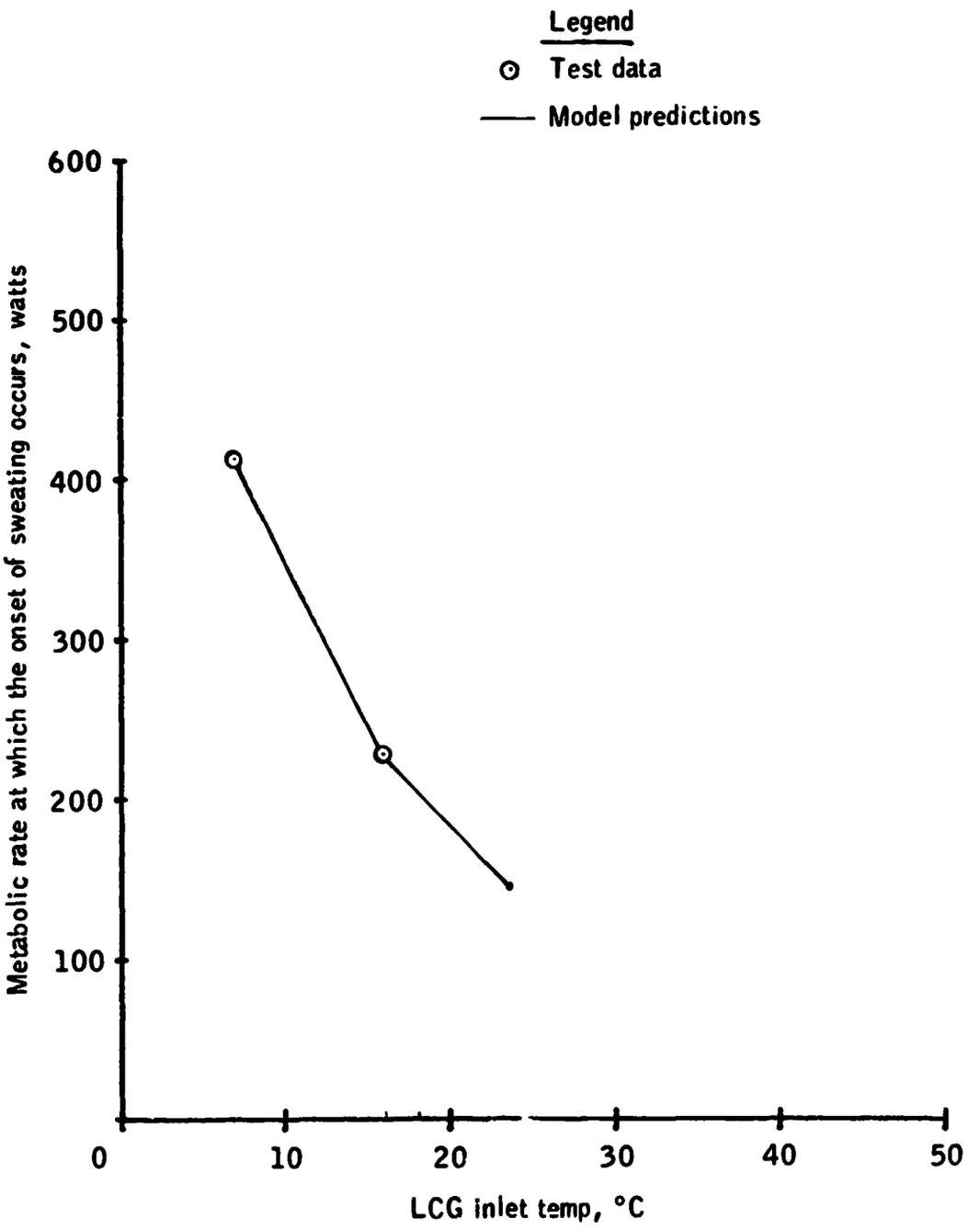

Figure 3-9.- Metabolic rate at which the onset of sweating occurs vs LCG inlet temperature.

Legend

Parameter	Test data symbol	Test condition	Mathematical model prediction
Sweat heat loss ratio	◁	Low metabolic rates (= 205-352 watts)	
	▽	Moderate metabolic rates (410-498 watts)	————
	▷	High metabolic rates (= 527-615 watts)	

1. Model prediction for metabolic rate of 234 watts

2. Model prediction for metabolic rate of 586 watts

Note: Flagged data (◁,▽ ,▷) are from Santamaria (112)

Figure 3-10.- Ratio of evaporative heat loss rate by active sweat to metabolic rate vs LCG inlet temperature.

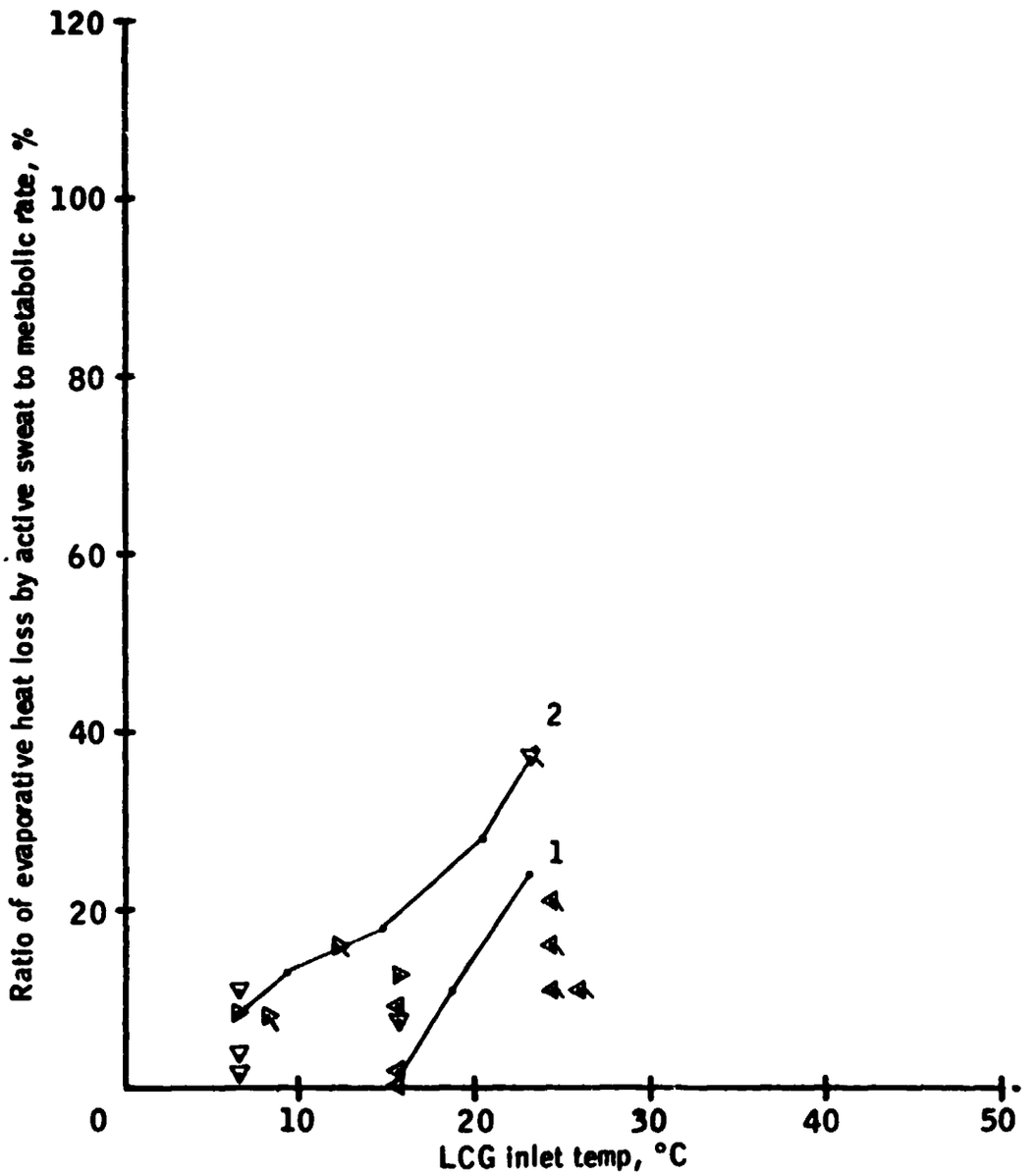

Figure 3-10.- Concluded.

Legend

Parameter	Test data symbol	Test condition	Mathematical model prediction
Total evaporative heat loss rate	◇	LCG inlet temp = 7°C	——— 1.
	○	= 16°C	——— 2.
	△	= 24-26°C	——— 3.
Evaporative heat loss rate by respiration only			——— 4.

Note: Flagged data (◇, ○, △) are from Santamaria (112)

Figure 3-11.- Predicted and actual steady-state total evaporative heat loss rate vs metabolic rate, for various LCG inlet temperatures.

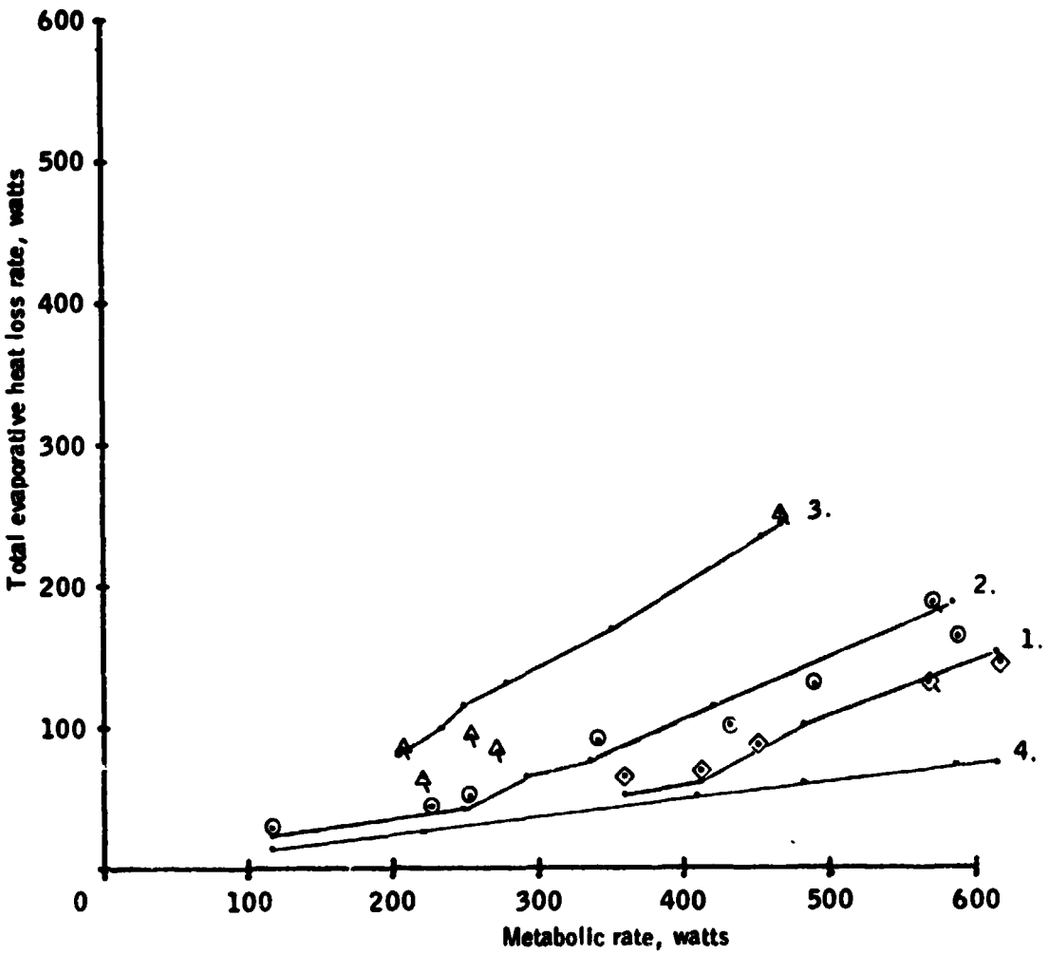

Figure 3-11.- Concluded.

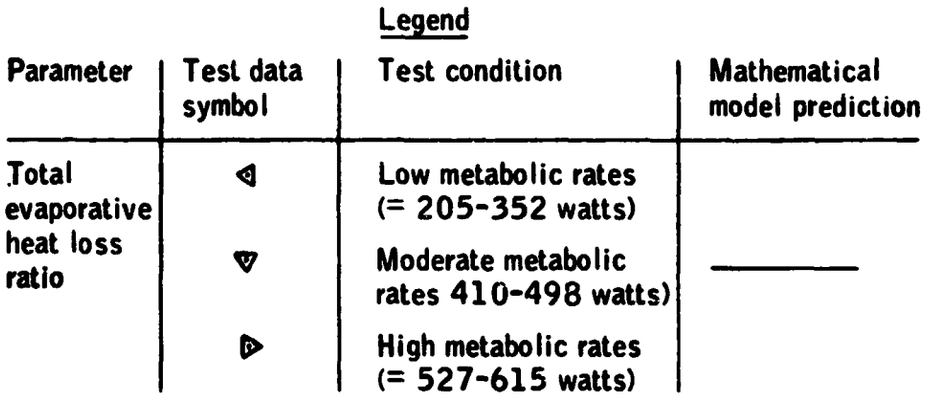

1. Model prediction for metabolic rate of 234 watts

2. Model prediction for metaboli ate of 586 watts

Note: Flagged ata (◁, ▽ , ▷) are from Santamaria (112)

Figure 3-12.- Ratio of total evaporative heat loss rate to metabolic rate vs LCG inlet temperature.

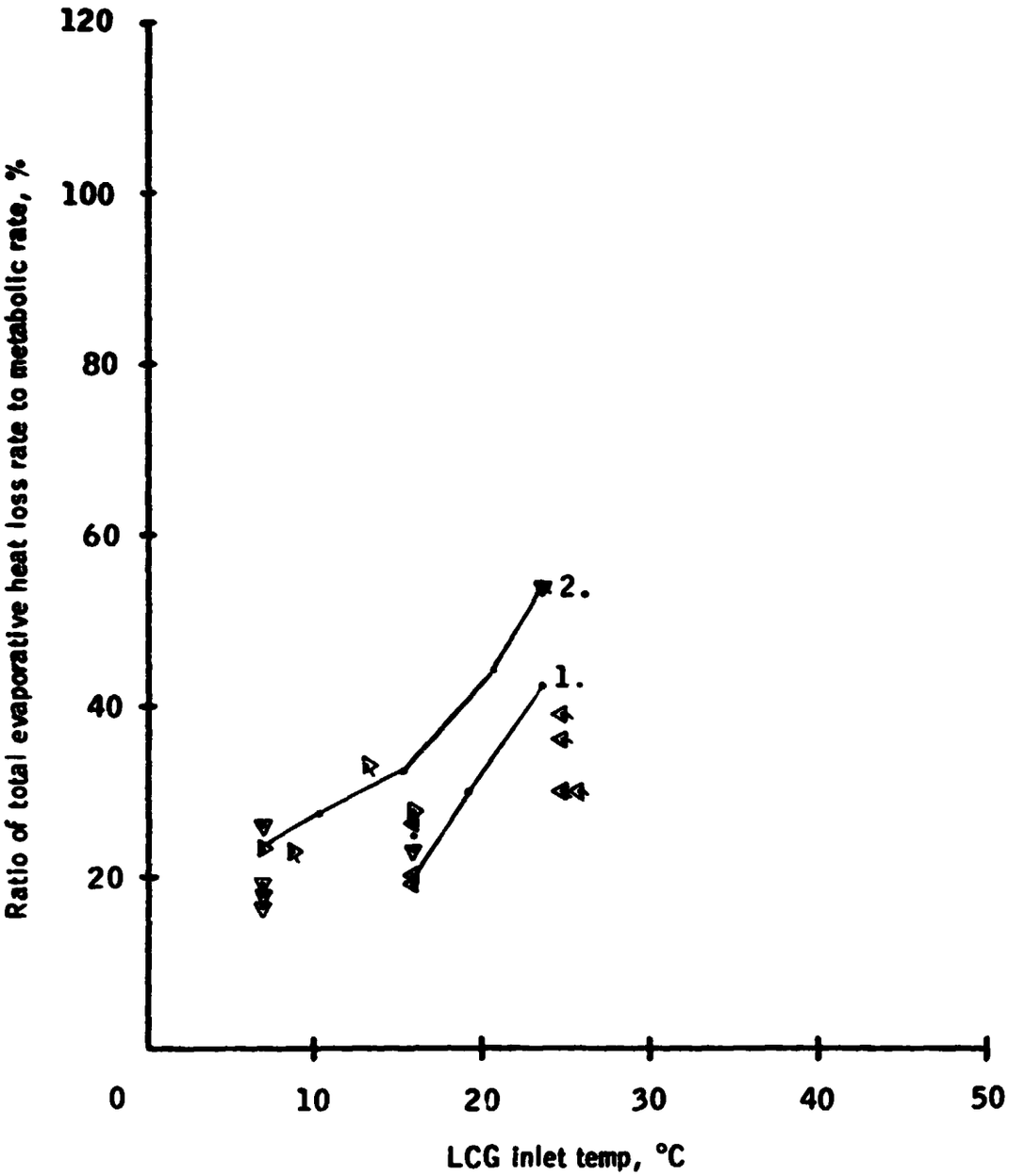

Figure 3-12.- Concluded.

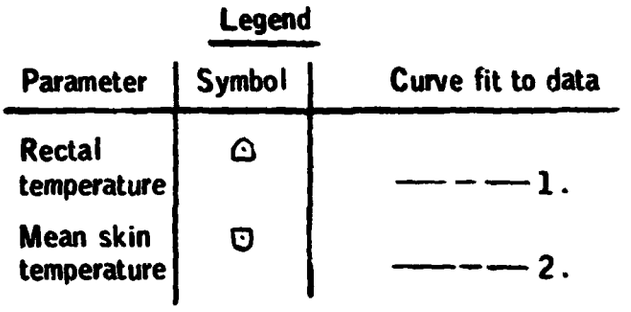

Figure 3-13.- Rectal temperature and mean skin temperature vs LCG inlet temperature.

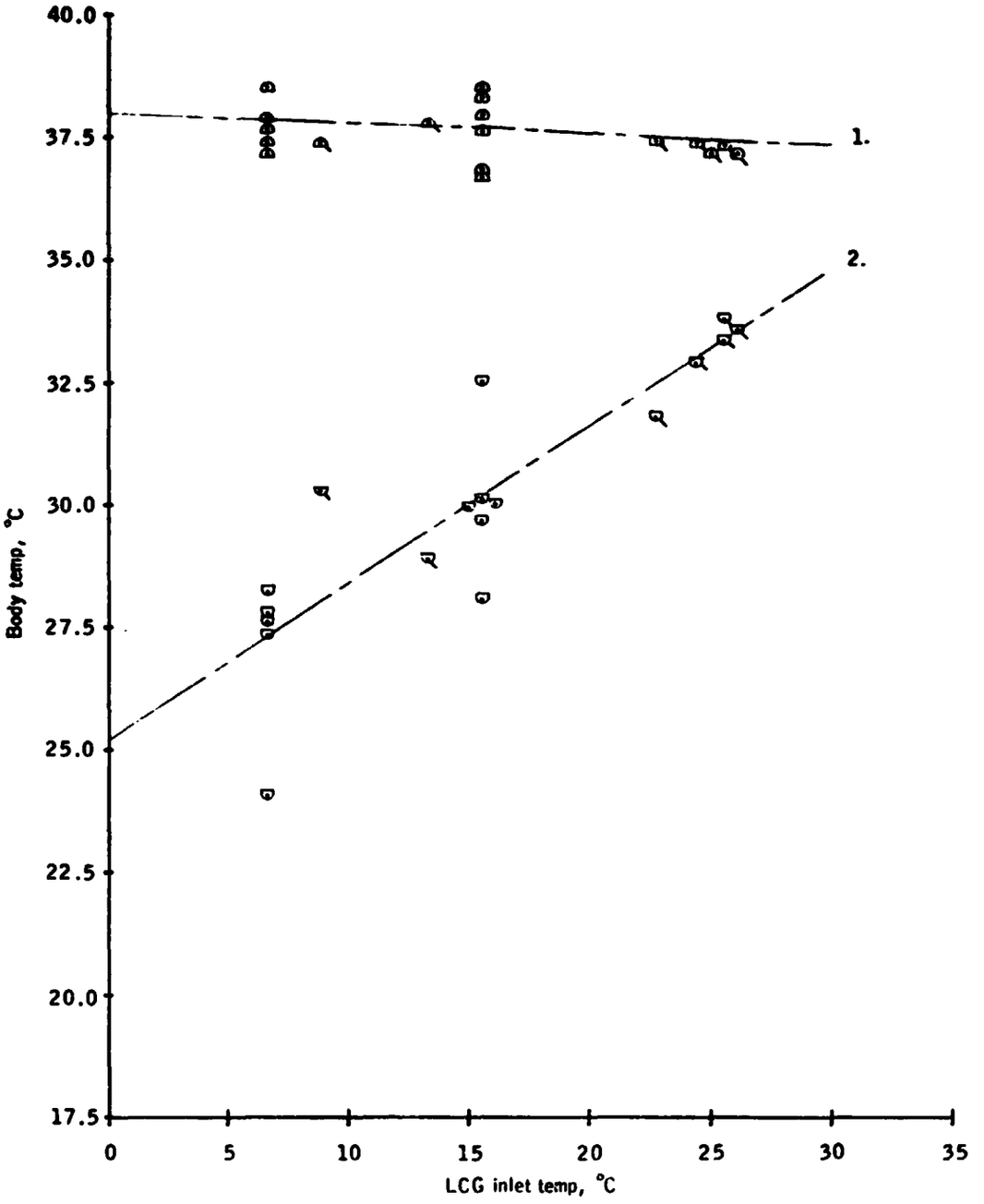

Figure 3-13.- Concluded.

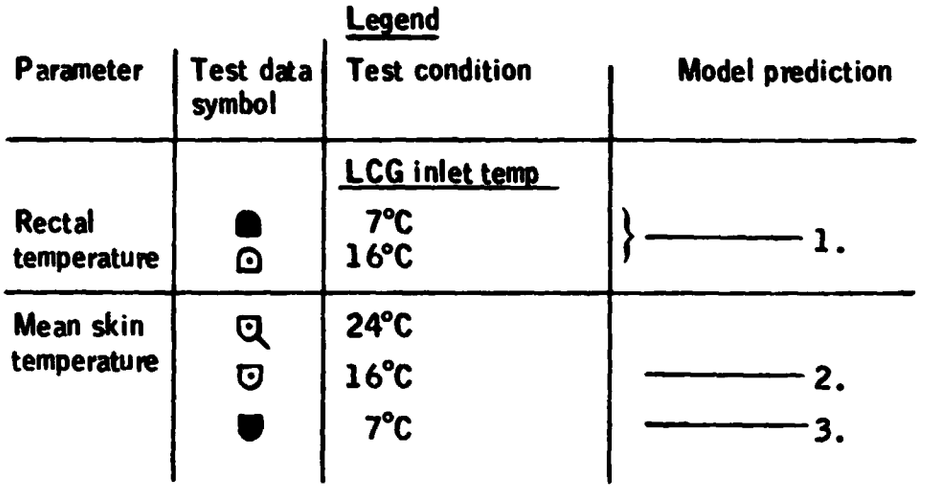

Figure 3-14.- Predicted and actual steady-state rectal and mean skin temperature vs metabolic rate for cool, moderate, and warm LCG inlet temperatures.

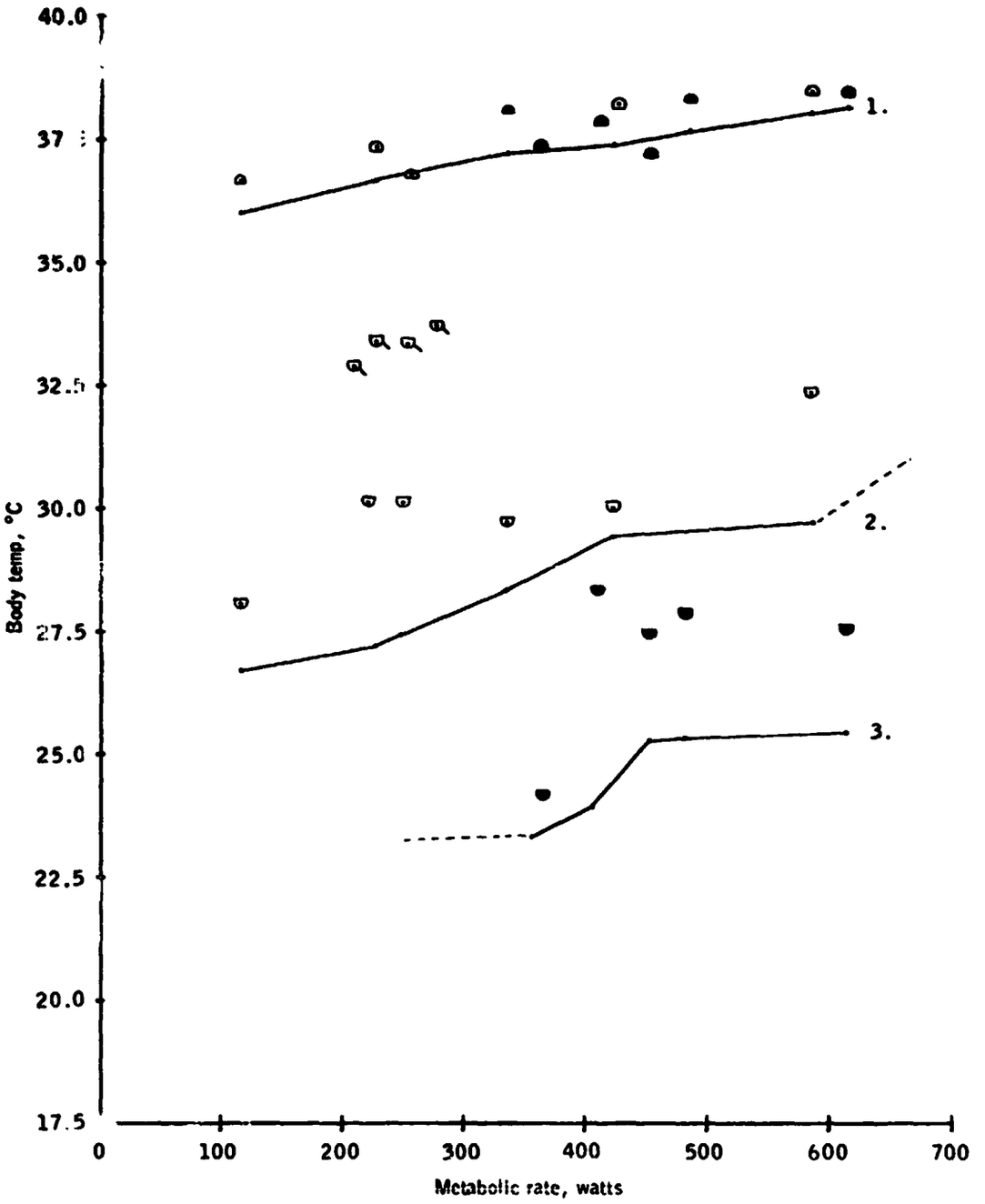

Figure 3-14.- Concluded.

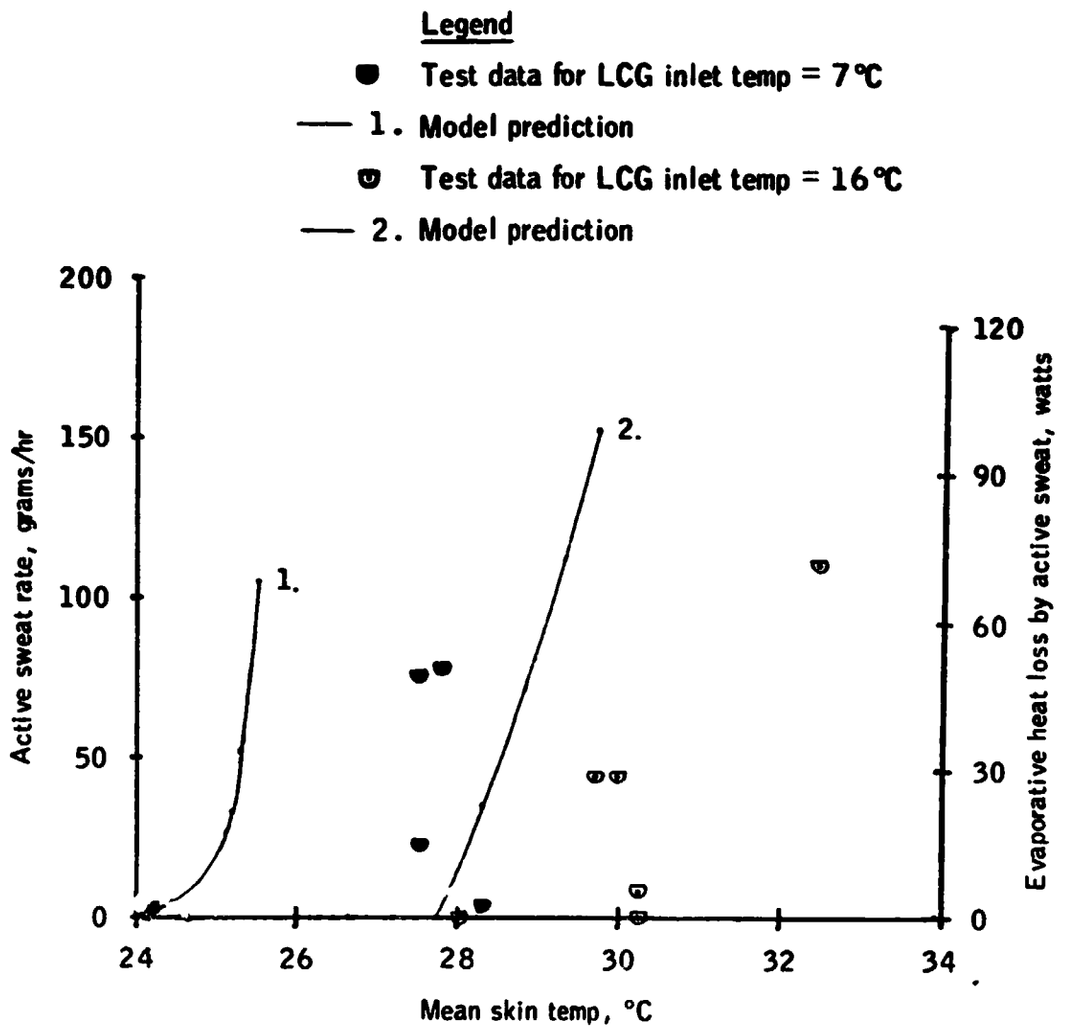

Figure 3-15.- Predicted and actual steady-state sweat rate and evaporative heat loss rate due to sweating vs mean skin temperature for LCG inlet temperatures of 7° and 16° C.

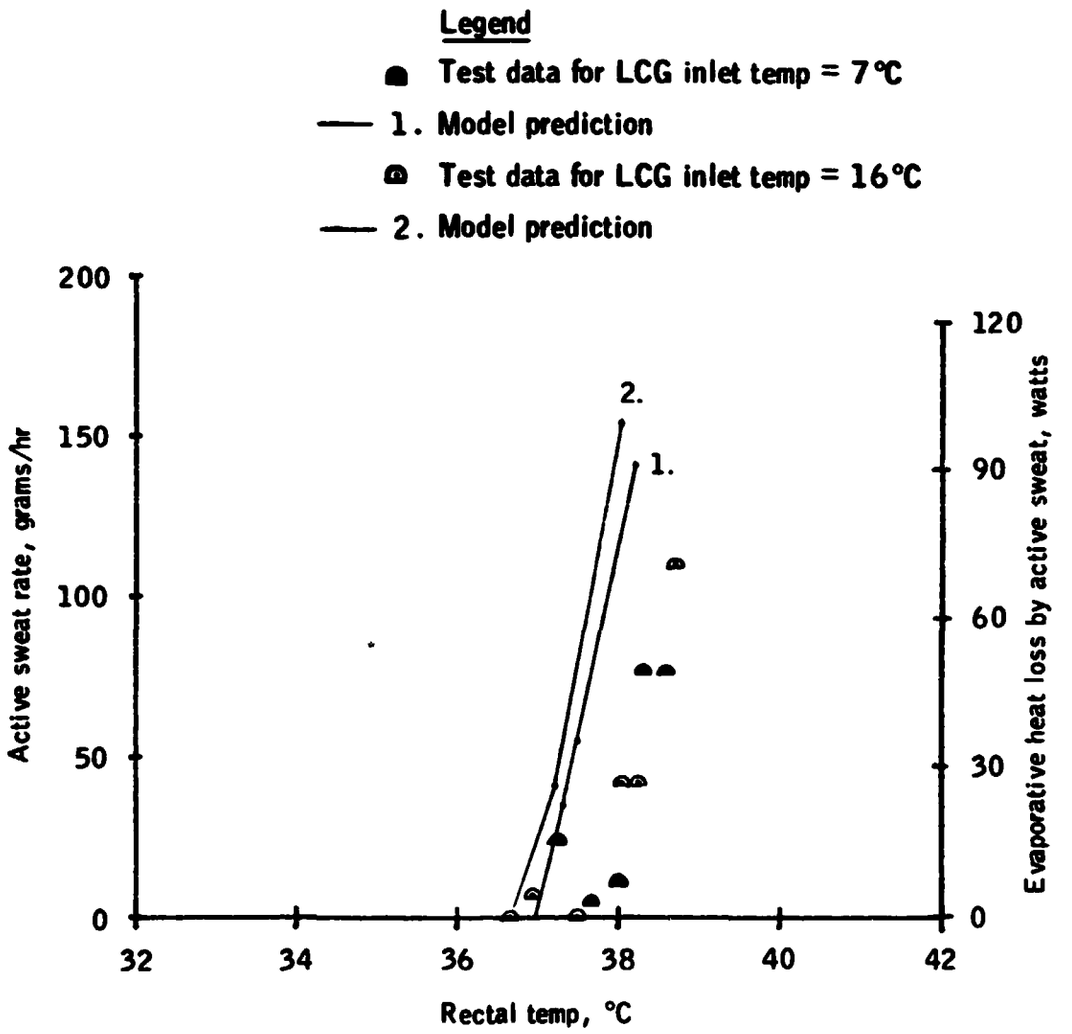

Figure 3-16.- Predicted and actual steady-state sweat rate and evaporative heat loss rate due to sweating vs rectal temperature for LCG inlet temperatures of 7° and 16° C.

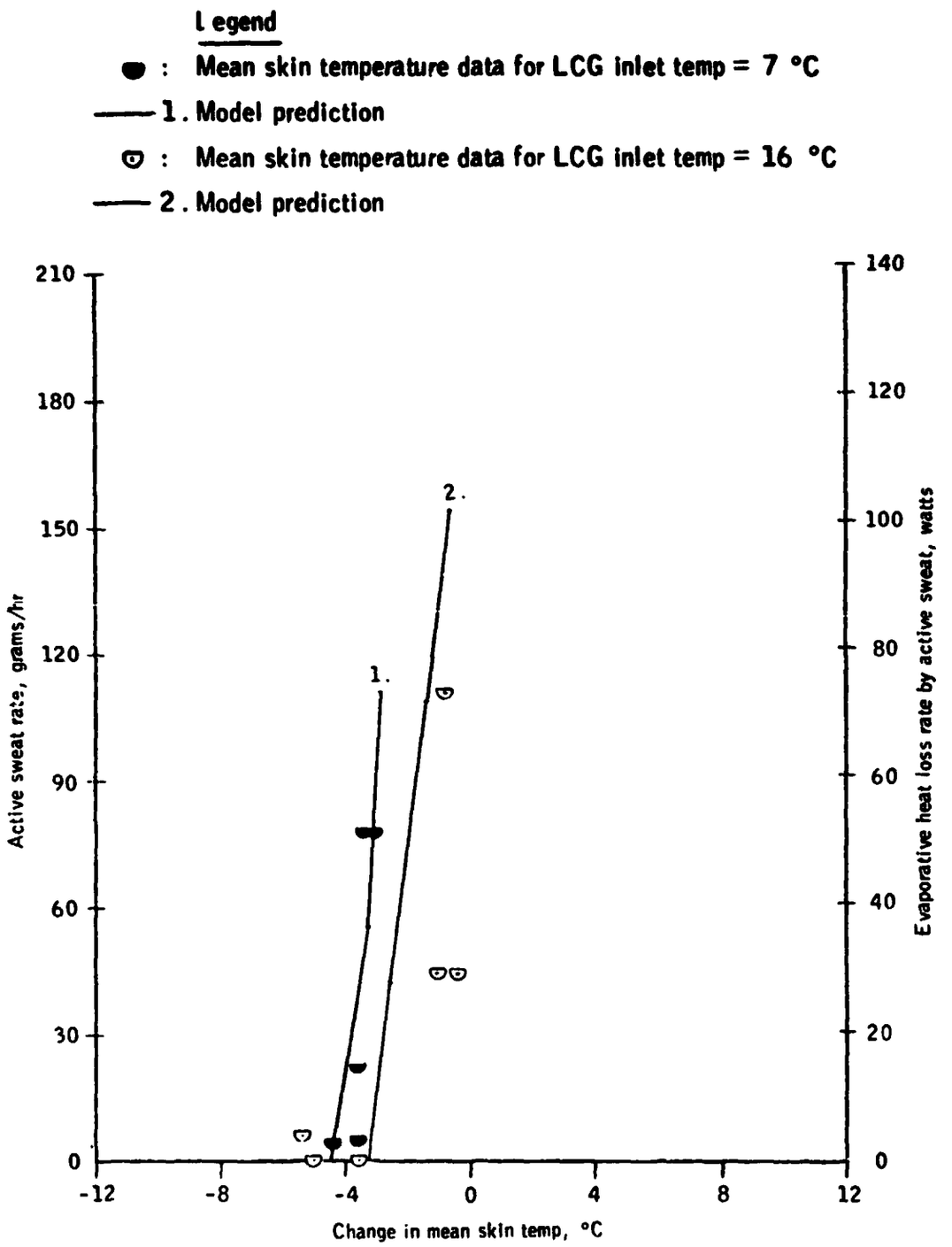

Figure 3-17a.- Predicted and actual steady-state sweat rate and total evaporative heat loss due to sweating vs change in mean skin temperature.

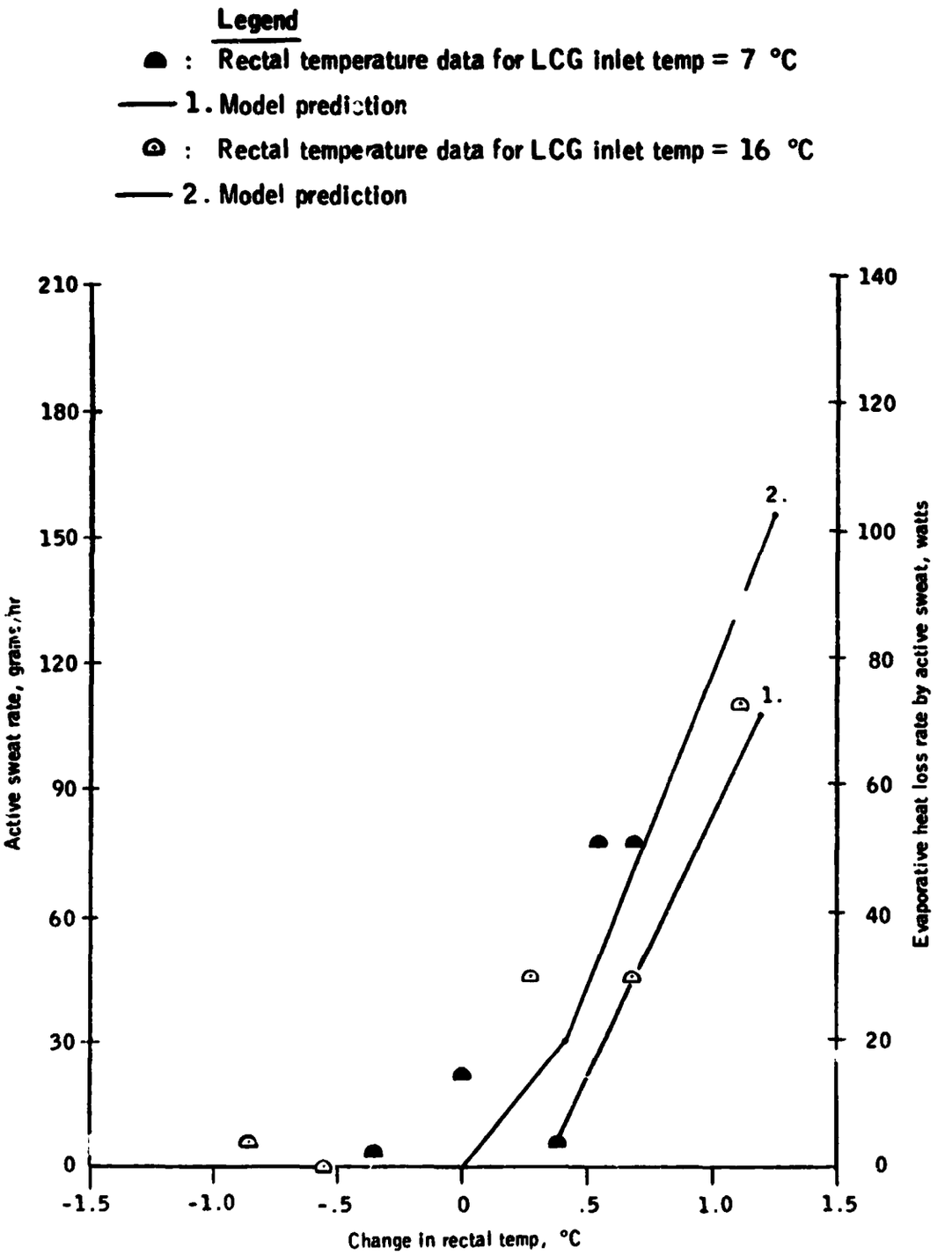

Figure 3-17b.- Predicted and actual steady-state sweat rate and total evaporative heat loss due to sweating vs change in rectal temperature.

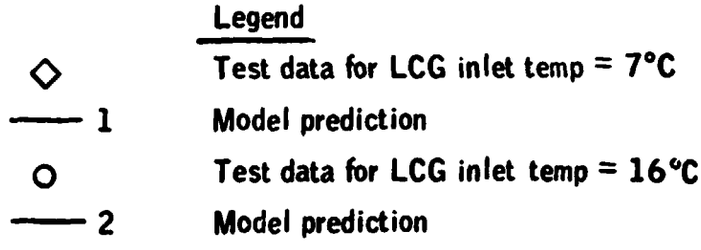

Figure 3-18.- Actual and predicted steady-state active sweat rate and evaporative heat loss rate due to active sweating vs total body heat storage.

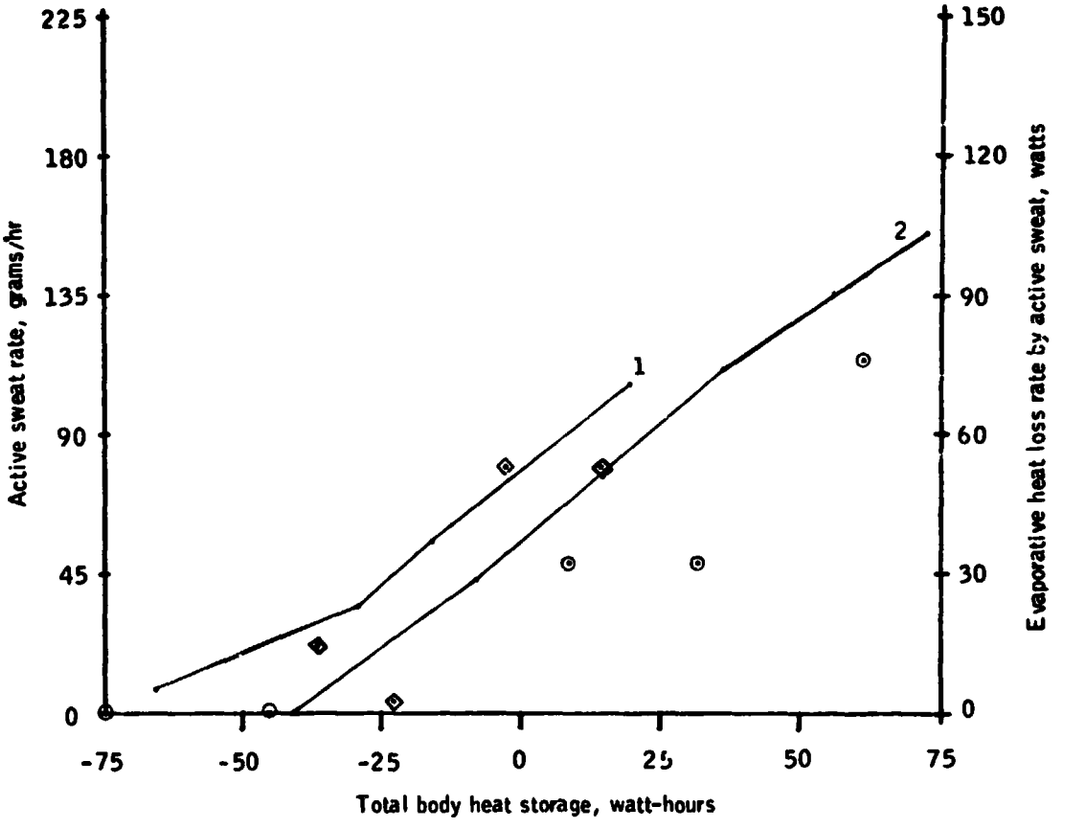

Figure 3-18.- Concluded.

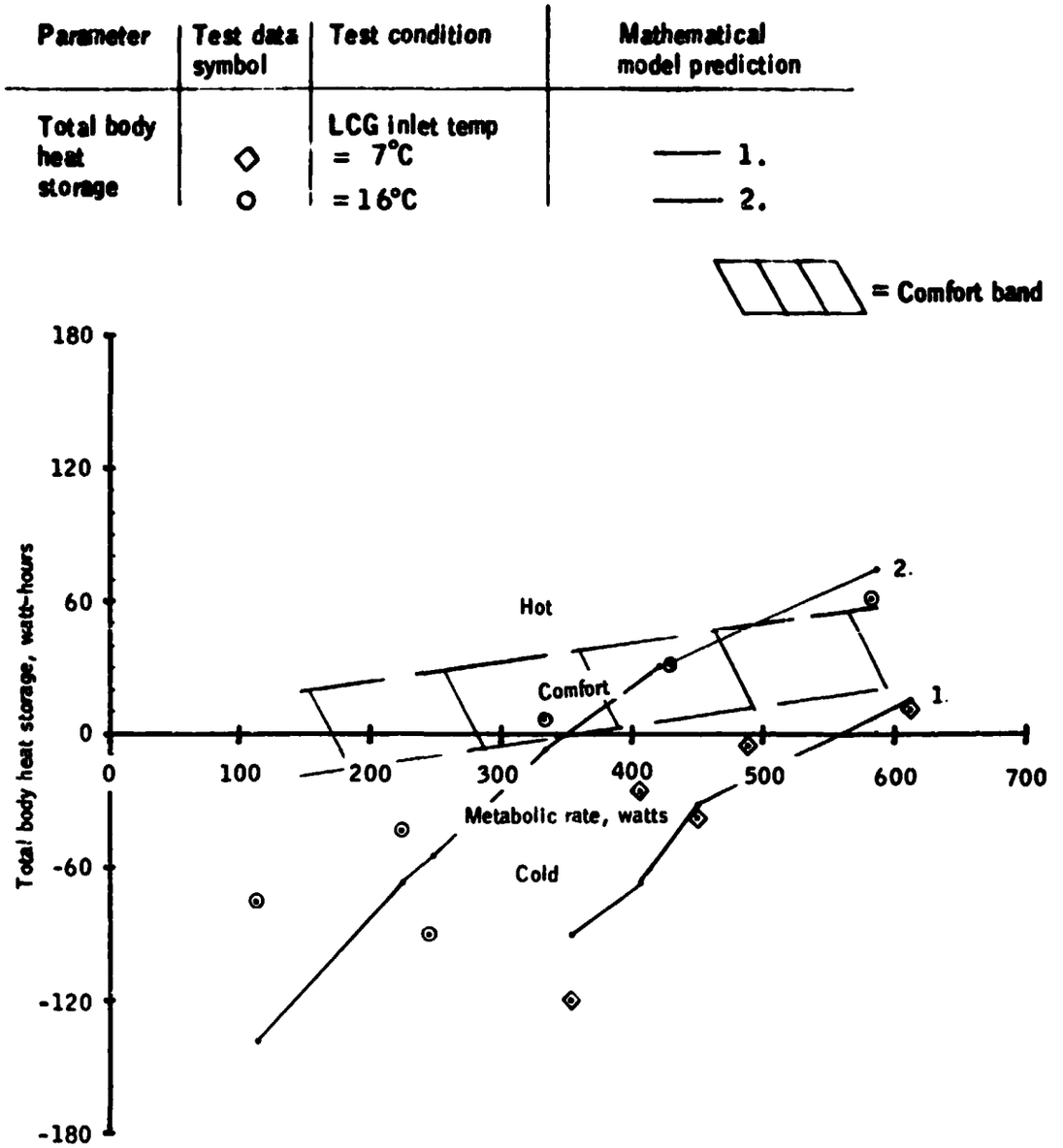

Figure 3-19.- Predicted and actual total body heat storage vs metabolic rate for steady-state conditions during test series A.

TABLE 3-2.- SERIES B - CALCULATED DATA AND HEAT BALANCE (STEADY STATE)

TEST/SUBJECT	1/J.W.					2/J.W.							3/C.L.					4/C.L.			
TEST CONDITION	A	B	C	D	E	A	B	C	D	E	F	G	A	B	C	D	E	A	B	C	D
LCG Inlet Temperature, °C	25	18	12	12	18	7	13	13	19	19	25	18	7	13	18	24	19	18	23	26	18
Heat Produced																					
1. Metabolic rate, watts	336	467	535	410	293	528	293	556	308	440	351	497	440	322	296	346	483	278	276	308	467
Heat Lost																					
1. Evaporation heat loss, watts																					
a. By respiration and diffusion[1]	41	54	61	48	37	60	37	63	38	51	43	57	45	40	37	42	56	35	35	38	54
b. By active sweating[2]	104	19	47	45	38	24	38	66	70	101	110	88	0	21	62	103	104	9	49	107	40
Total Evaporation Heat Loss[3]	145	145	107	93	75	84	75	128	107	151	151	145	44	60	97	145	159	44	93	145	93
2. Convection heat loss, watts[4]	3	3	0	0	-1	-2	-3	2	-1	3	3	2	-5	-2	-1	6	3	-7	-1	4	1
3. Radiation heat loss, watts[5]	0	0	-29	-29	0	-29	-29	-29	0	0	0	0	-29	-29	0	0	0	0	0	0	0
4. LCG heat loss, watts[6]	190	321	458	404	219	562	265	456	200	285	197	351	517	322	198	196	321	239	182	159	375
Total Heat Loss, watts	337	467	536	467	293	615	337	556	308	440	351	497	528	351	296	346	483	278	276	308	467
Heat balance = heat produced - total heat loss (also equal to heat storage rate and/or shiver rate)[7]	0	0	0	-59	0	-88	-15	0	0	0	0	0	-88	-29	0	0	0	0	0	0	0

1. See Eqns. 5, 6 and 7, Appendix C
2. Total evap. - (respiration + diffusion)
3. See " . 7, Section 2
4. See . . 6, Section 2
5. Based on properties of Apollo spacesuit
6. See Eqn. 5, Section 2
7. From total heat balance equation - See Eqn. 1, Figure 2-2

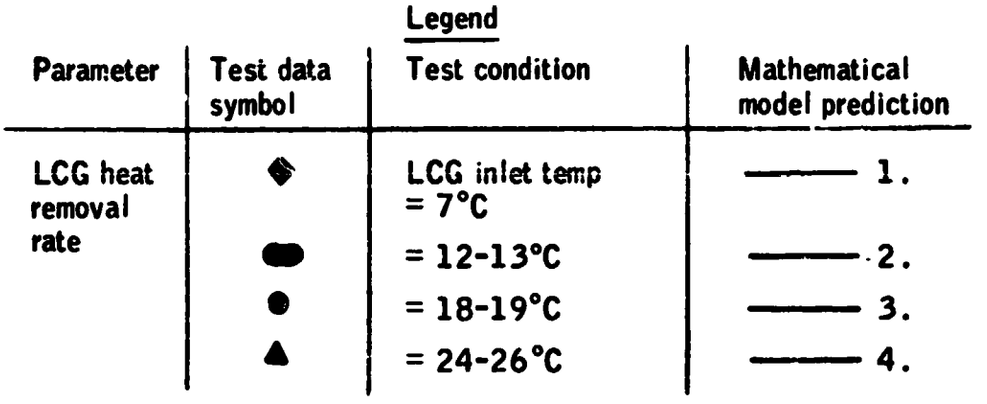

Figure 3-20.- Predicted and actual steady-state LCG heat removal vs metabolic rate, for various LCG inlet temperatures.

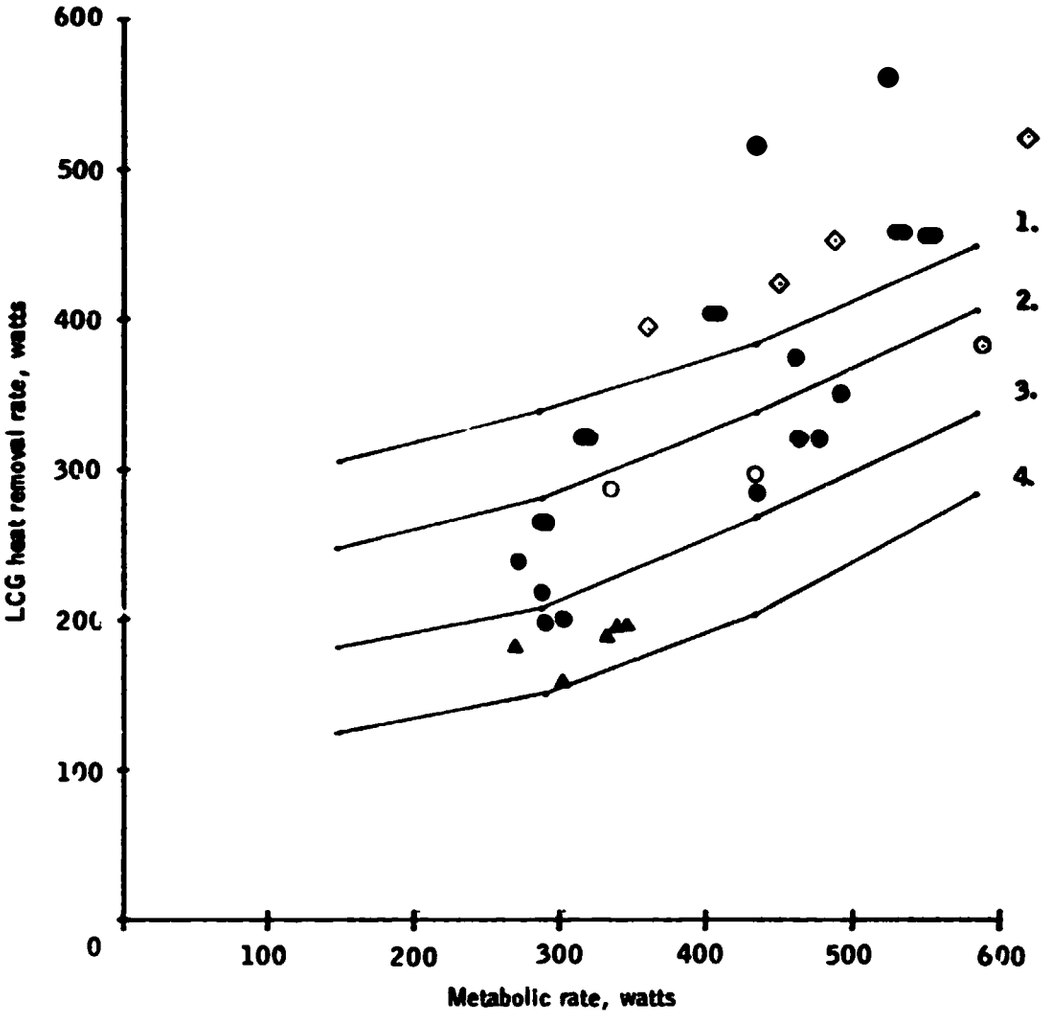

Figure 3-20.- Concluded.

Legend

Parameter	Test data symbol	Test condition	Mathematical model prediction
LCG heat removal ratio	◀	Low metabolic rates (= 278-351 watts)	
	▼	Moderate metabolic rates (410-497 watts)	———
	▶	High metabolic rates (= 528-586 watts)	
	◆	Repeat points- low and moderate metabolic rates	

1. Model prediction for metabolic rate of 293 watts
2. Model prediction for metabolic rate of 586 watts

Note: Open symbols (◁ , ▽ , ▷) indicate data of Series A.

Figure 3-21.- Ratio of LCG heat removal rate to metabolic rate vs LCG inlet temperature.

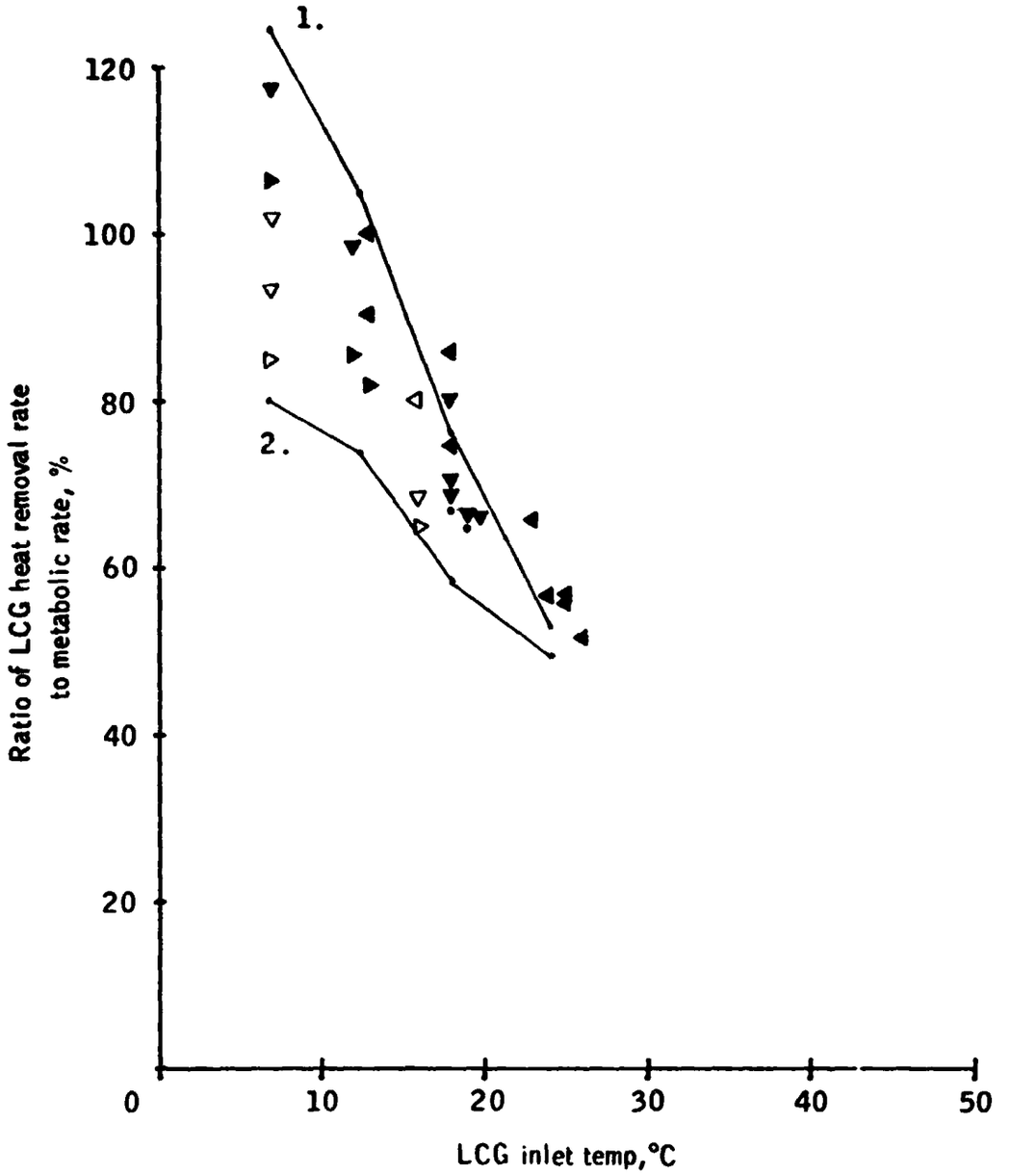

Figure 3-21.- Concluded.

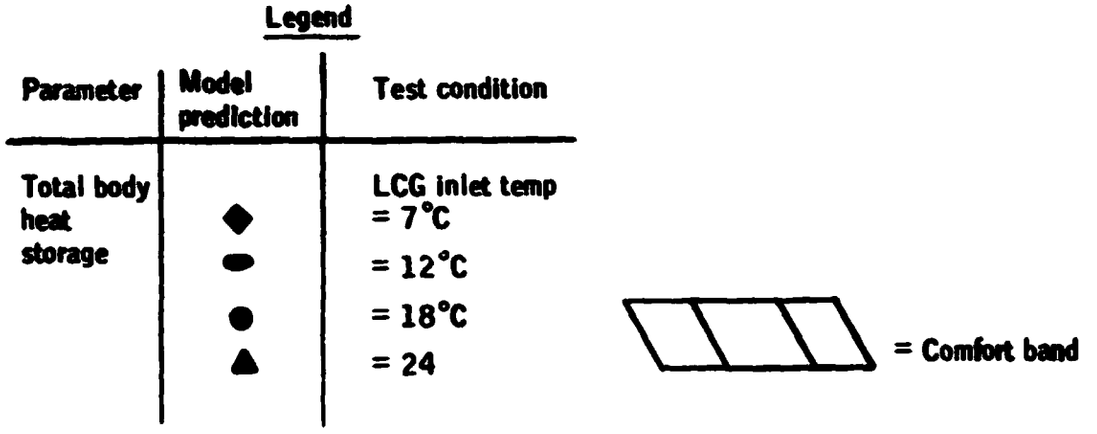

Figure 3-22.- Predicted total body heat storage vs metabolic rate for steady-state conditions during Series B.

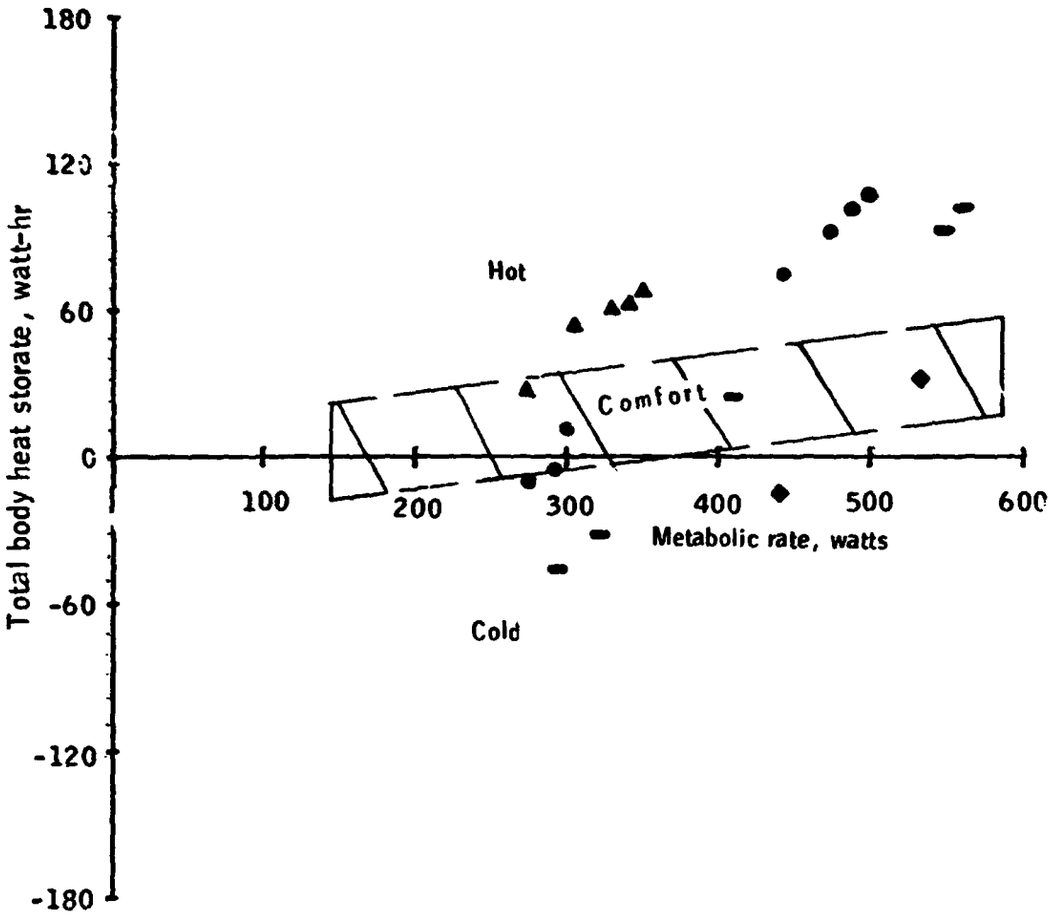

Figure 3-22.- Concluded.

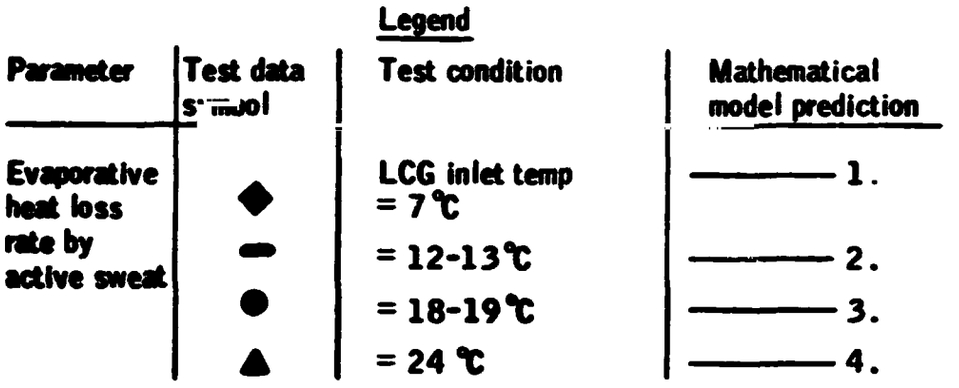

Figure 3-23.- Predicted and actual steady-state evaporative heat loss rate by active sweat vs metabolic rate, for various LCG inlet temperatures.

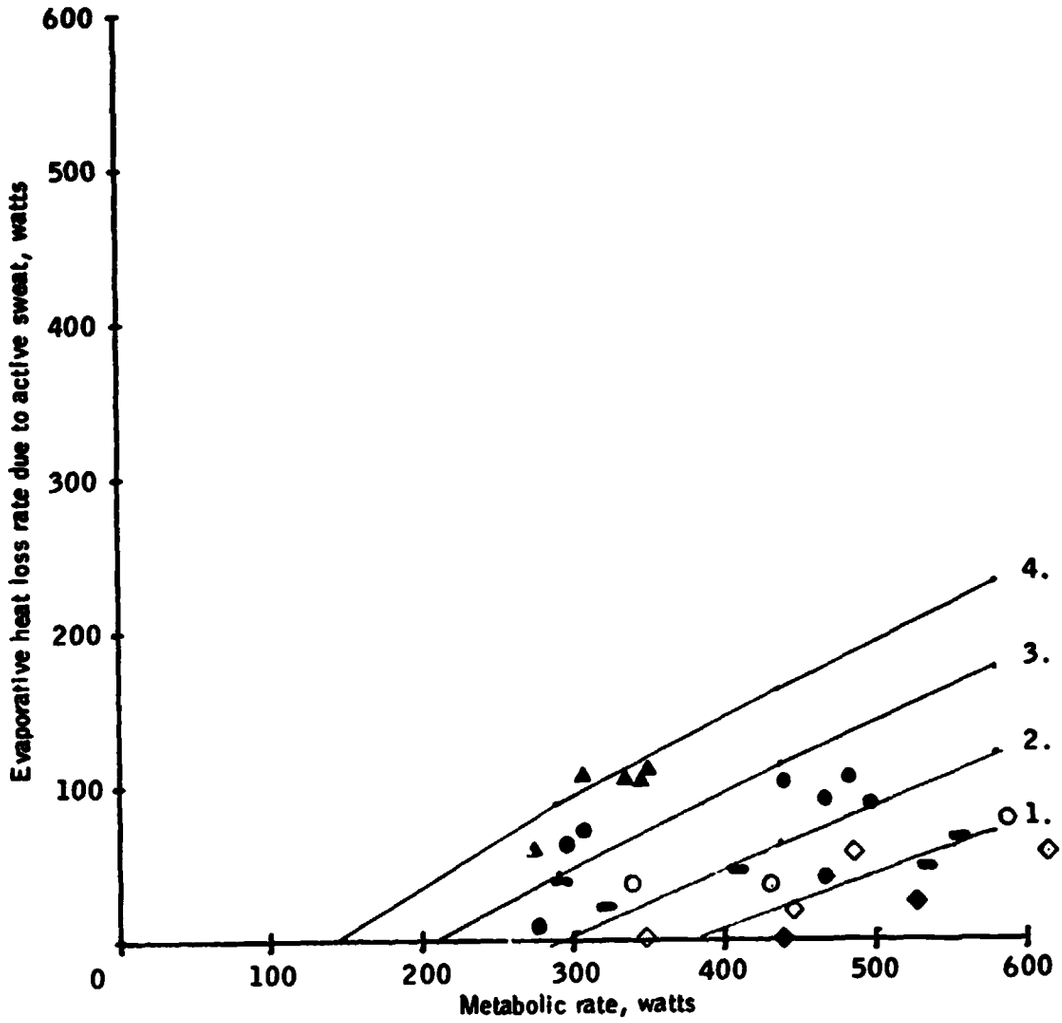

Figure 3-23.- Concluded.

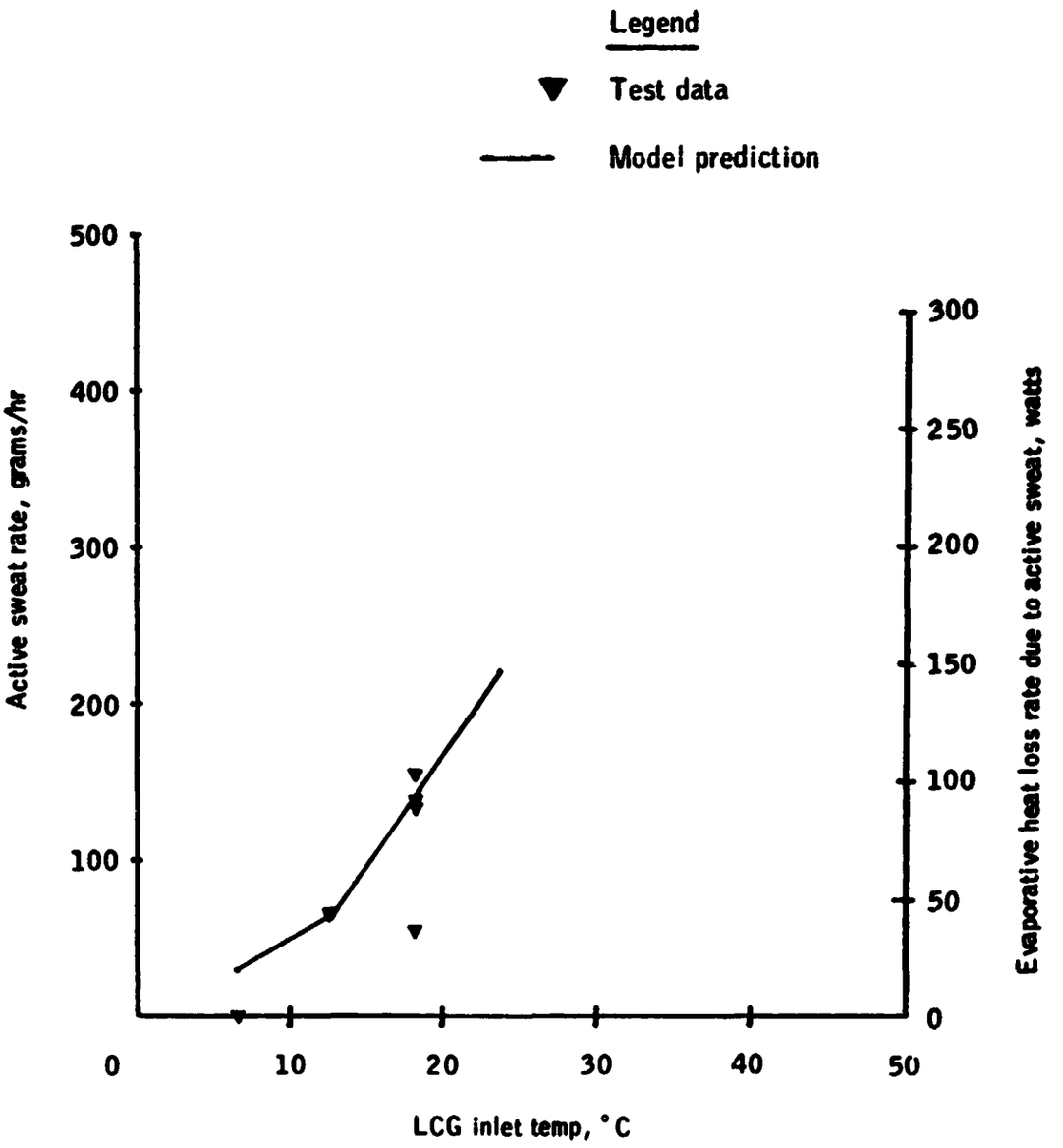

Figure 3-24.- Active sweat rate and evaporative heat loss rate due to active sweat vs LCG inlet temperature for moderate metabolic rates (410 watts).

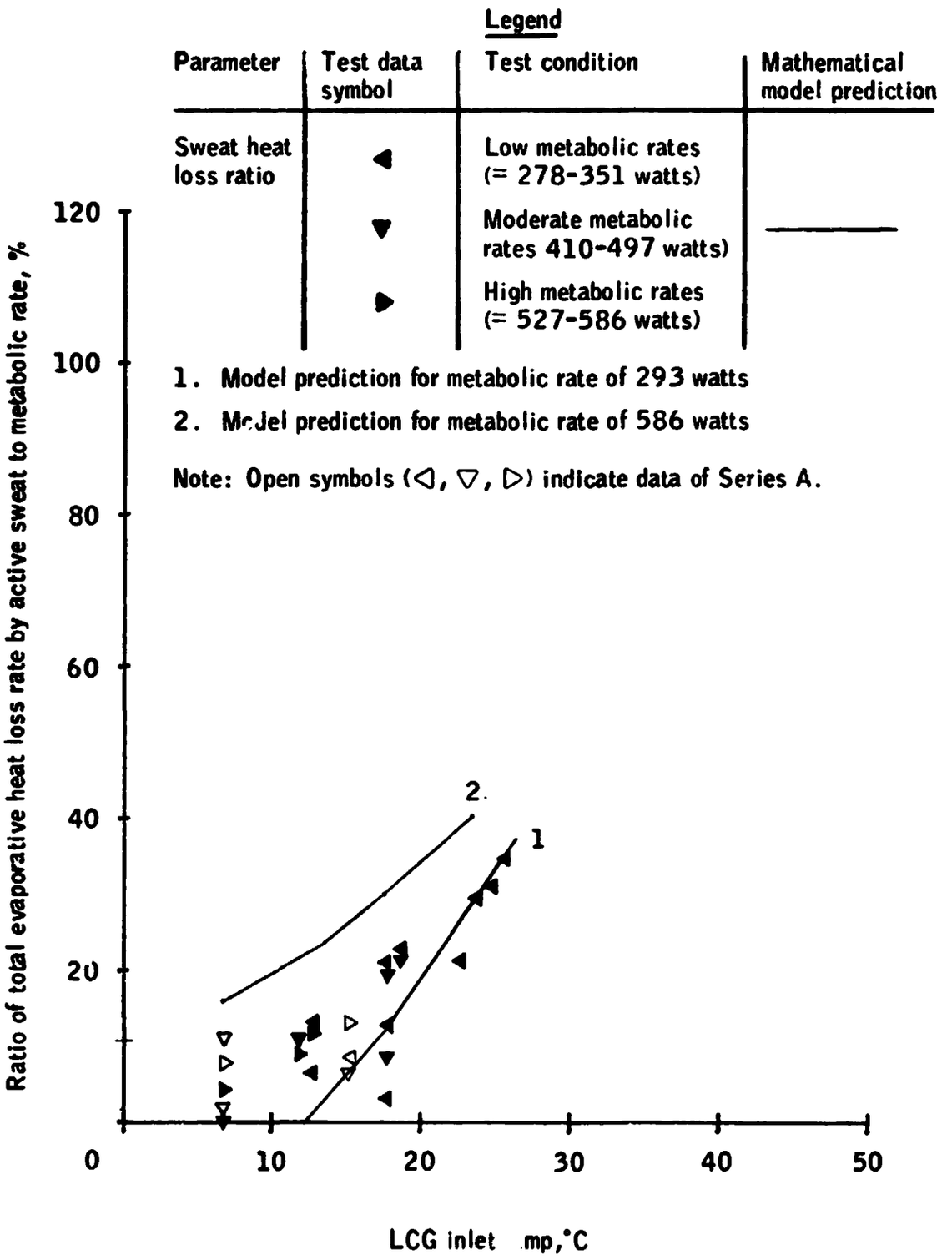

Figure 3-25.- Ratio of evaporative heat loss rate by active sweat to metabolic rate vs LCG inlet temperature.

Legend

Parameter	Test data symbol	Test condition	Mathematical model prediction
Total evaporative heat loss rate	●	LCG inlet temp = 7°C	——— 1.
	▬	= 12-13°C	——— 2.
	●	= 18-19°C	——— 3.
	▲	= 24°C	——— 4.
Evaporative heat loss rate due to respiration only			——— 5.

Note: Open symbols (◇, ▭, ○, △) indicate data of Series A.

Figure 3-26.- Predicted and actual steady-state total evaporative heat loss rate vs metabolic rate, for various LCG inlet temperatures.

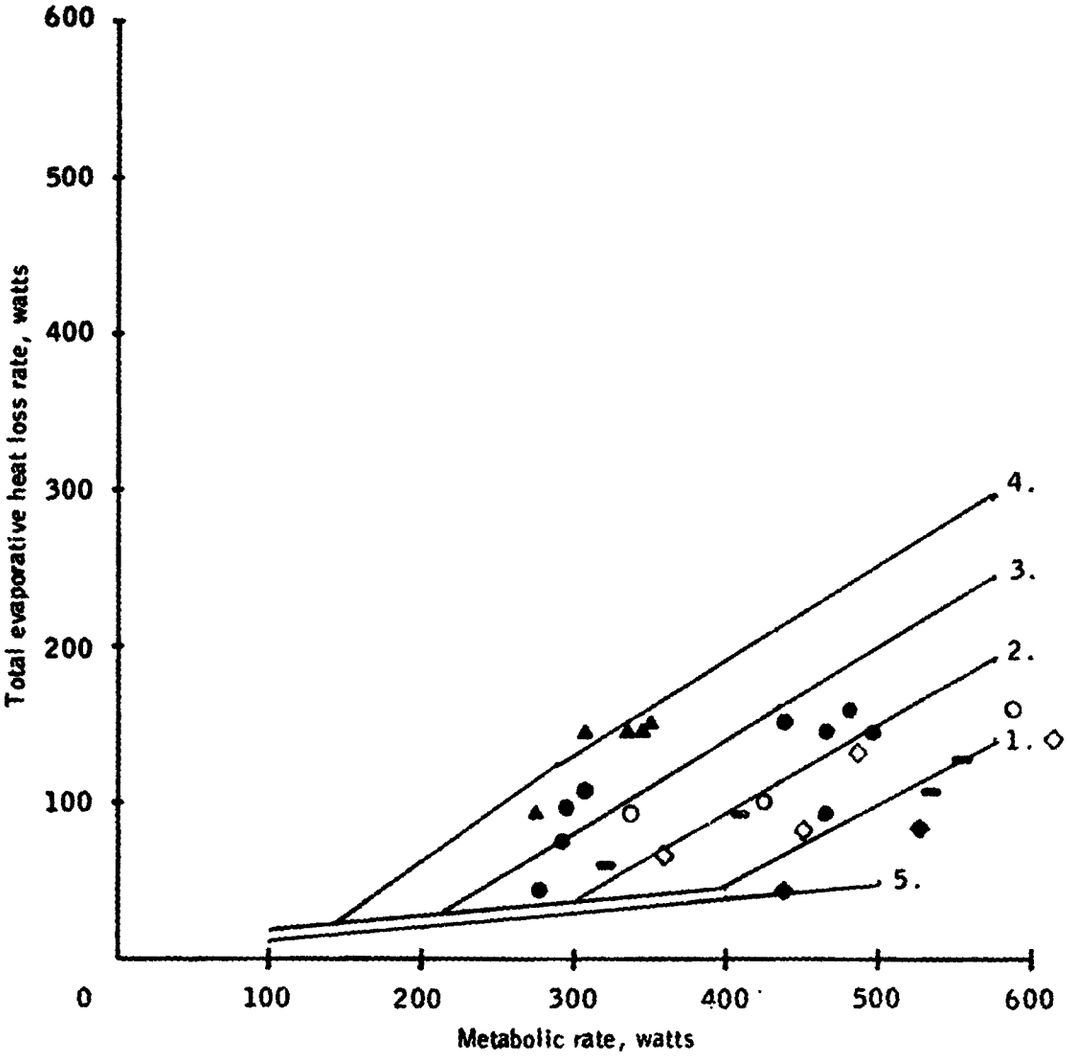

Figure 3-26.- Concluded.

Legend

Parameter	Test data symbol	Test condition	Mathematical model prediction
Total evaporative heat loss ratio	▽	Low metabolic rates (=278-351 watts)	
	◁	Moderate metabolic rates (= 410-497watts)	———
	▷	High metabolic rates (= 527-586 watts)	

1. Model prediction for metabolic rate of 293 watts

2. Model prediction for metabolic rate of 586 watts

Note: Open symbols (◁, ▽, ▷) indicate data of Series A.

Figure 3-27.- Ratio of total evaporative heat loss rate to metabolic rate vs LCG inlet temperature.

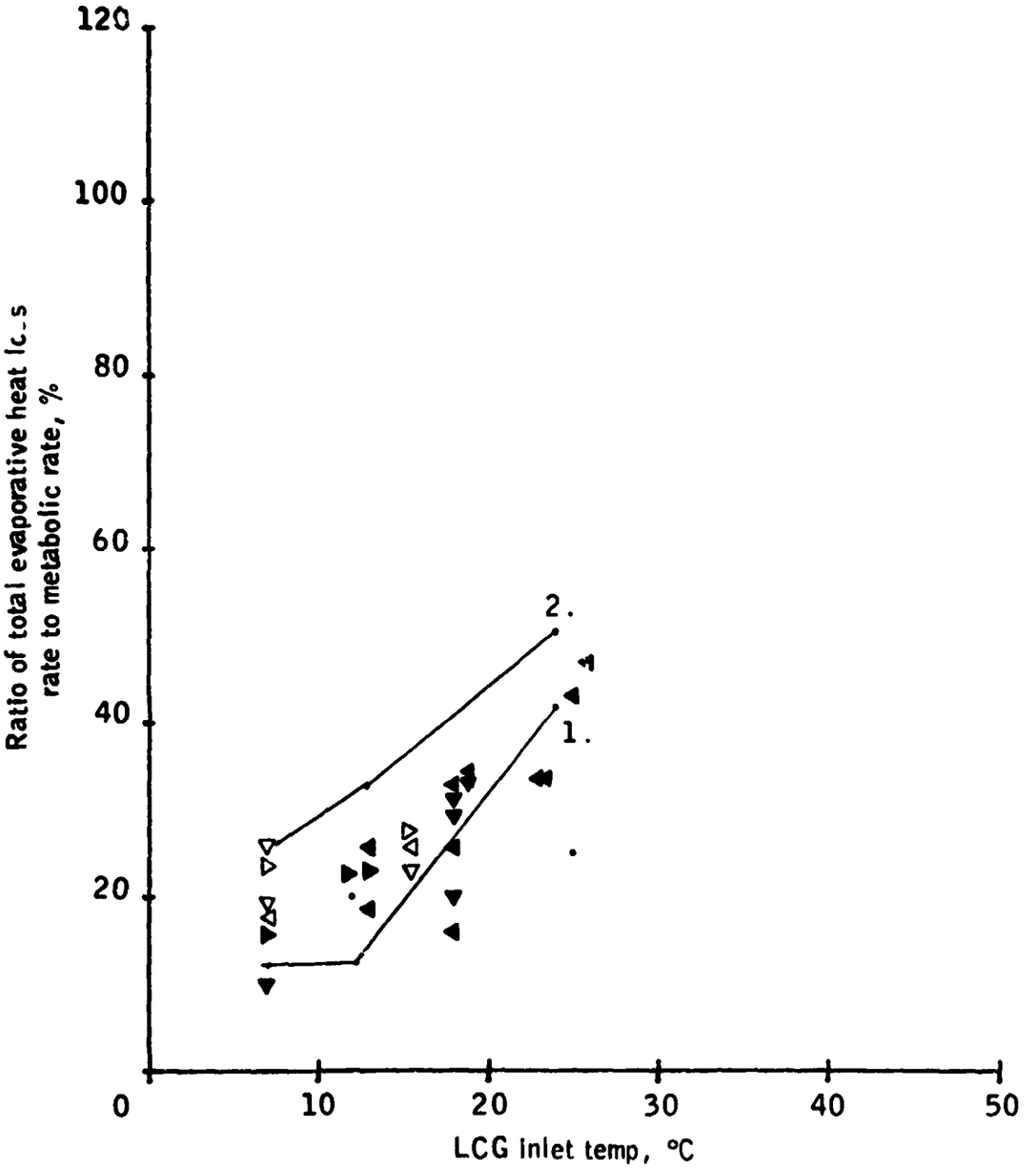

Figure 3-27.- Concluded.

Legend

Parameter	Test data symbol	Test condition: LCG inlet water temp	Test condition: Test subject
LCG heat removal rate	◆	7°C	J.W.
	◆	7°C	C.L.
	⬬	12-13°C	J.W.
	⬬	12-13°C	C.L.
	●	18-19°C	J.W.
	●	18-19°C	C.L.
	▲	24°C	J.W.
	▲	24°C	C.L.
Total evaporative heat loss	◇	7°C	J.W.
	◇	7°C	C.L.
	⬭	12-13°C	J.W.
	⬭	12-13°C	C.L.
	○	18-19°C	J.W.
	○	18-19°C	C.L.
	△	24°C	J.W.
	△	24°C	C.L.

Regression curve fit to LCG heat removal data

Symbol: ————

Type of fit: Second order

Correlation coefficient: .82

Equation of curve:

$Y = 1.4 - .062X + .0013X^2$

Regression curve fit to total evaporative heat loss data

Symbol: — — — —

Type of fit: Second order

Correlation coefficient: .39

Equation of curve:

$Y = -182 + 1.397X - .0016X^2$

Figure 3-28a.- Regression curve fit to test data for LCG heat removal rate and total evaporative heat loss rate vs metabolic rate.

Legend

Parameter	Test data symbol	Test condition: LCG inlet temp	Parameter	Test data symbol	Test condition: LCG inlet temp
Error in model predictions of LCG heat removal	●	= 7°C	Error in model predictions of total evaporative heat loss	◇	= 7°C
	⬬	= 12-13°C		⬭	= 12-13°C
	●	= 18-19°C		○	= 12-13°C
	▲	= 24°C		△	= 24°C
	—				

———— : Curve fit to LCG error

— — — — : Curve fit to total evaporative heat loss error

Notes: Positive error indicates under-prediction; negative error indicates over-prediction.
Flagged values (◆, ●, ▲, etc) indicate data of Series A.

Figure 3-28b.- Model error ($= \frac{\text{Test data-model predictions}}{\text{Metabolic rate}}$) vs metabolic rate for LCG and total evaporative heat loss rate predictions.

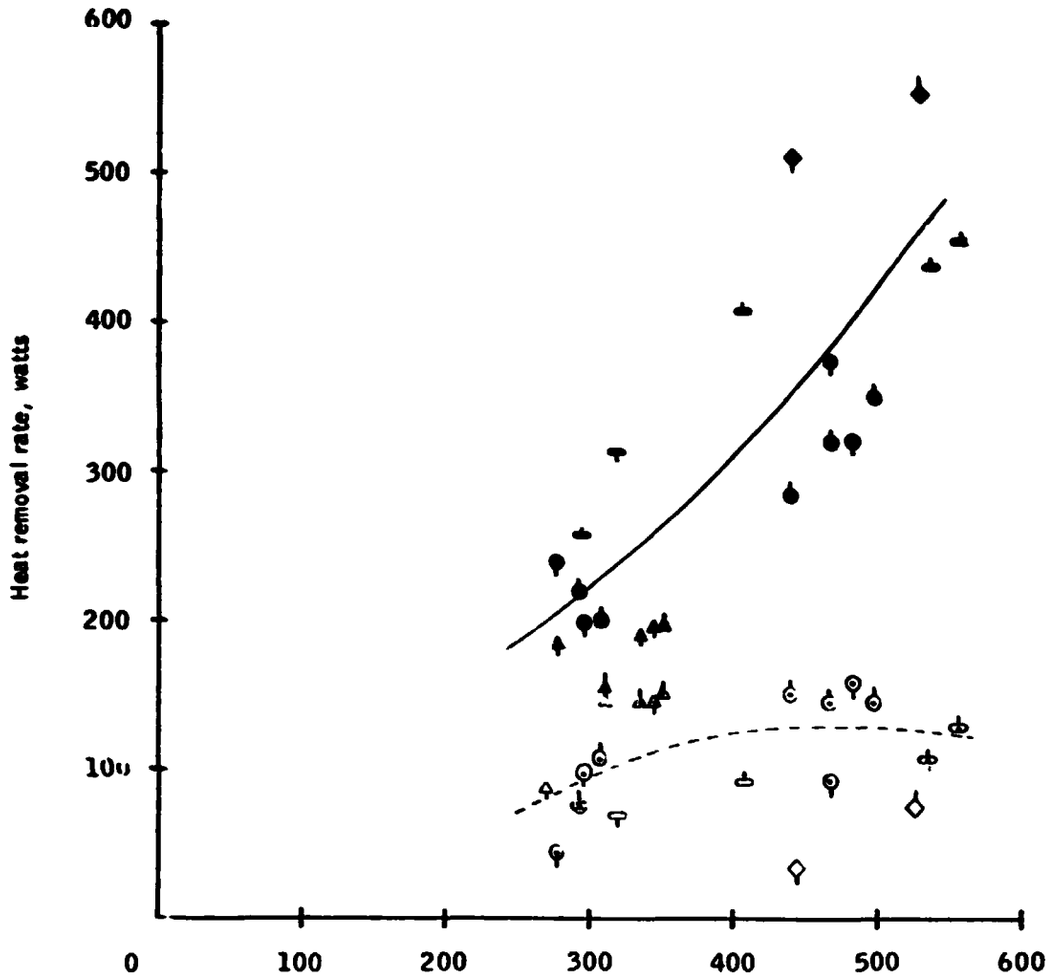

Figure 3-28a.- Concluded.

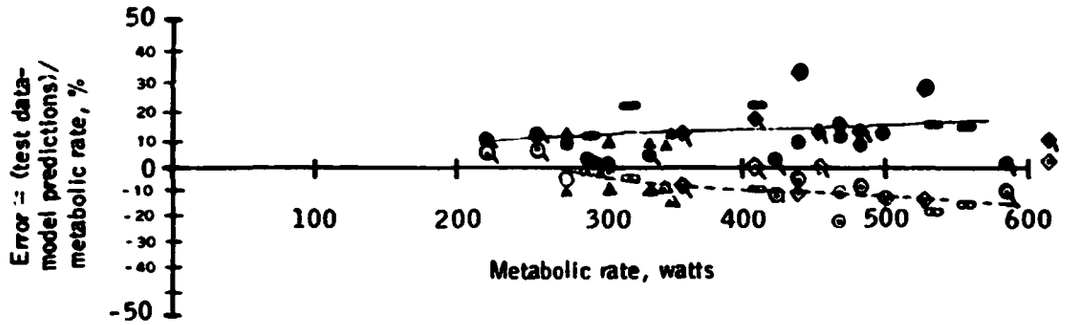

Figure 3-28b.- Concluded.

TABLE 3-3.- SERIES C - CALCULATED DATA AND HEAT BALANCE

TEST/SUBJECT	1/J.B.	2/J.B.	3/J.B.	4/J.B.	5/J.B.	6/J.B.	7/J.B.	8/J.B.	9/J.M.	10/J.M.
Duration, min.	30	30	30	30	30	30	30	30	30	30
LCG flowrate, liters/hour	0	27	55	82	0	27	55	82	55	82
LCG inlet temp., °C	-	@19	@19	@18	-	@10	@19	@18	@17	@17
Heat Produced										
1. Metabolic Rate, watts	352	352	352	352	469	469	469	469	586	586
Heat Loss										
1. Evaporation heat loss, watts										
a. By respiration and diffusion(1)	50	50	50	50	62	62	62	62	73	73
b. By active sweating(2)	170	70	70	37	267	155	120	110	137	110
Total Evaporative Heat Loss(3)	220	120	120	87	329	217	182	172	210	183
2. Convection heat loss, watts(4)	10	8	7	6	11	1	4	1	8	9
3. Radiation heat loss, watts(5)	58	49	42	42	62	53	45	45	44	43
4. LCG heat loss, watts(6)	0	110	175	210	0	163	213	260	309	327
Total Heat Loss, watts	288	287	343	345	402	434	444	478	571	562
Heat balance = heat produced - total heat loss, watts (also equal to heat storage rate and/or shiver rate)(7)	64	65	9	7	67	35	25	-9	15	24
Total heat storage over duration of test, watt-hrs(8)	48	27	30	5	70	59	59	30	65	70
Final Heat Storage Rate, watts(9)	24	14	15	3	35	30	30	15	32	35
Heat deficit = heat balance - final heat storage rate, watts	40	51	-6	4	32	5	-5	-24	-17	-11

1. See Eqns. 5, 6 & 7, Appendix C. 2. See Eqn. 8, Section 2. 3. See Eqn. 7, Section 2. 4. See Eqn. 6, Section 2. 5. See Eqn. 2.18, Appendix B. 6. See Eqn. 5, Section 2. 7. See Eqn. 1, Figure 2-2.
8. See Eqn. 3, Section 2. 9. See Eqn. 4, Section 2.

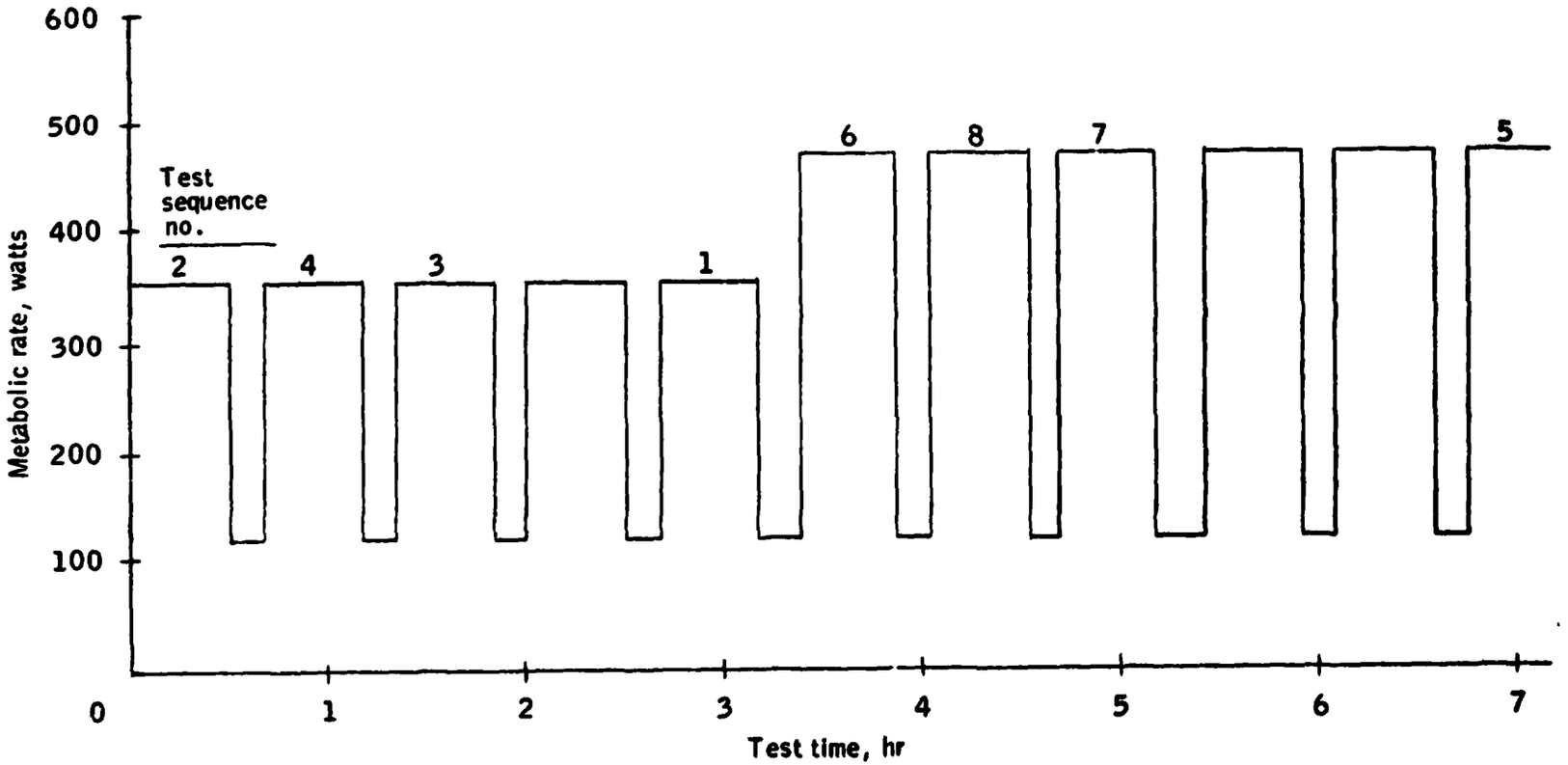

Figure 3-29.- Metabolic rate profile for test sequences 1 to 8.

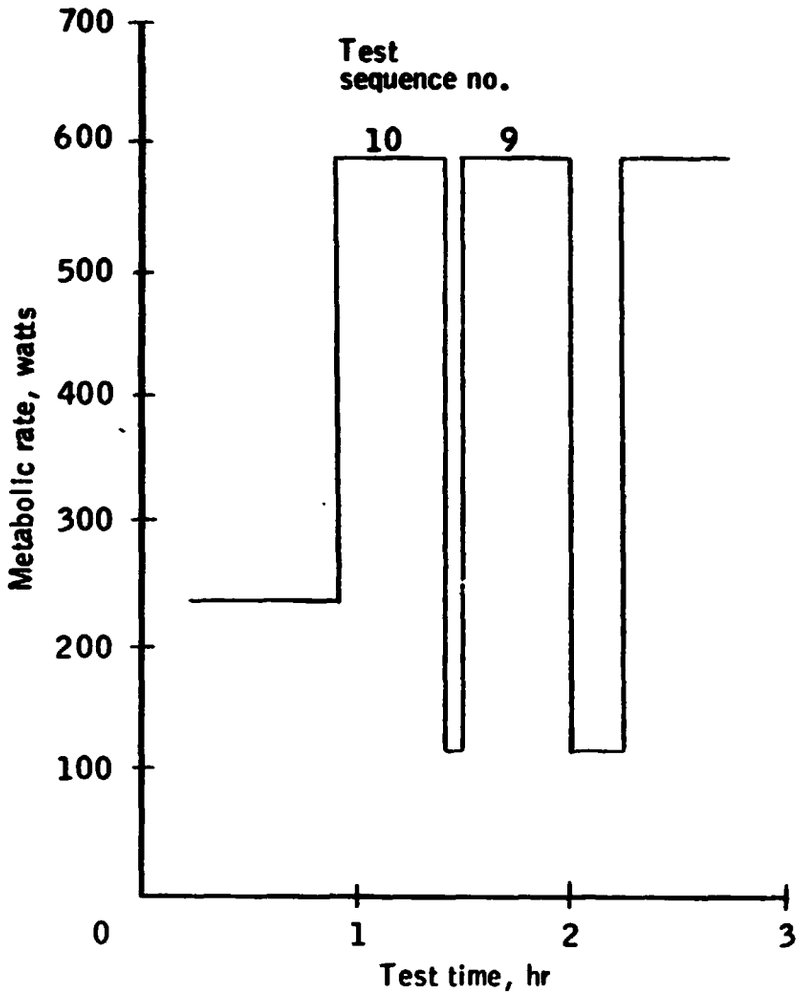

Figure 3-30.- Metabolic rate profile for test sequences 9 and 10.

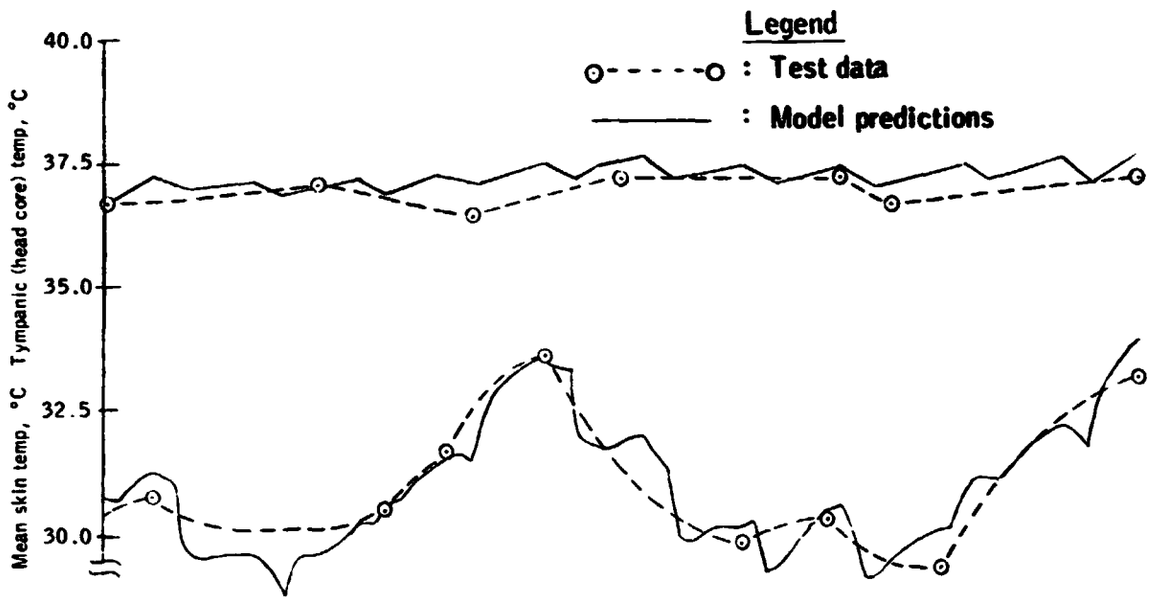

Figure 3-31a.- Head core (tympanic) temperature (upper curve) and mean skin temperature (lower curve) vs time for test sequences 1 to 8.

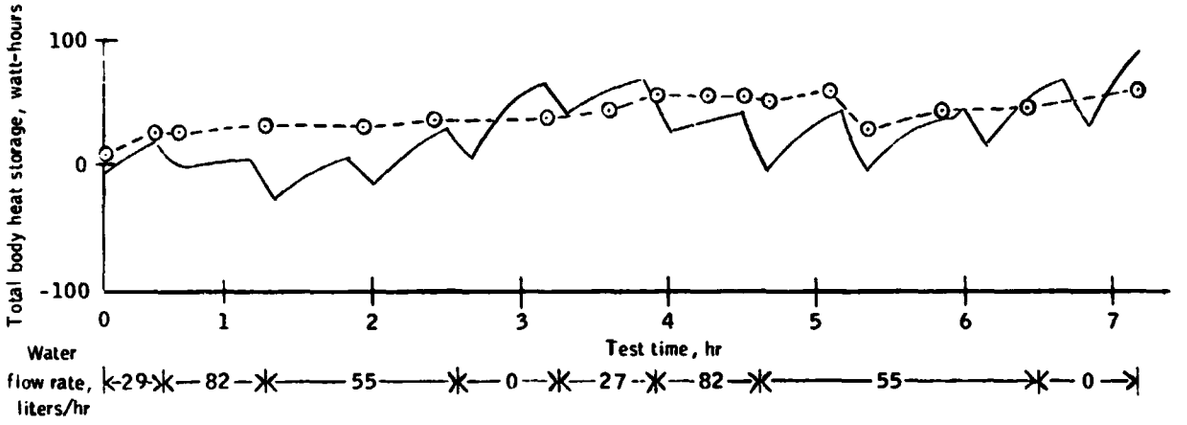

Figure 3-31b.- Total body heat storage vs time for test sequences 1 to 8.

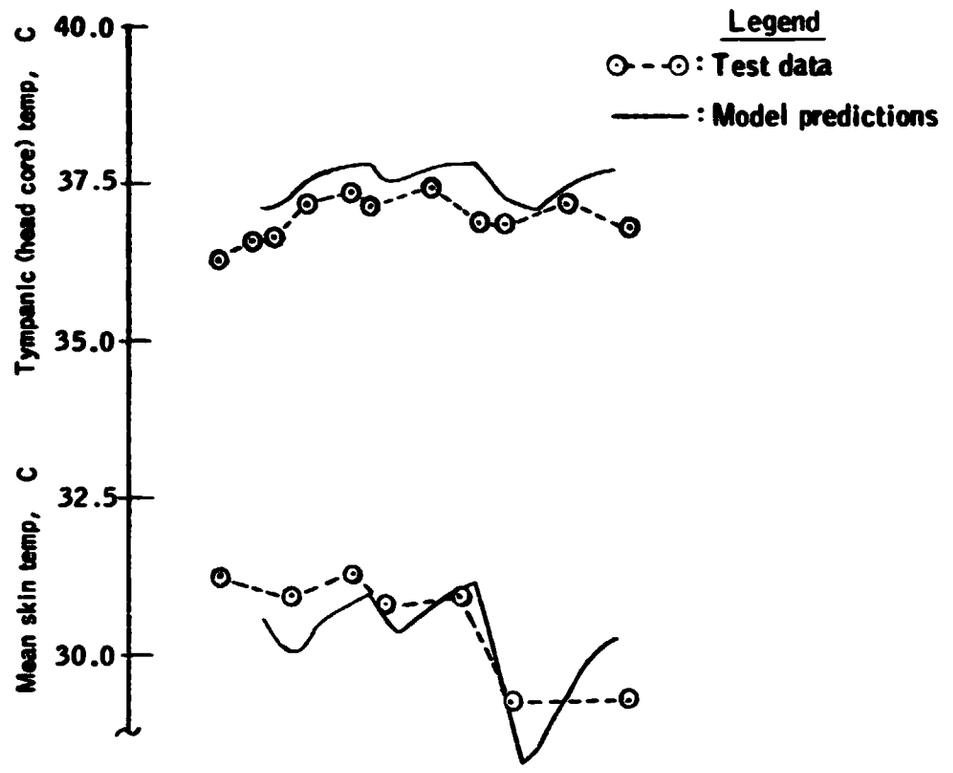

Figure 3-32a.- Head core (tympanic) temperature (upper curve) and mean skin temperature (lower curve) vs time for test sequences 9 and 10.

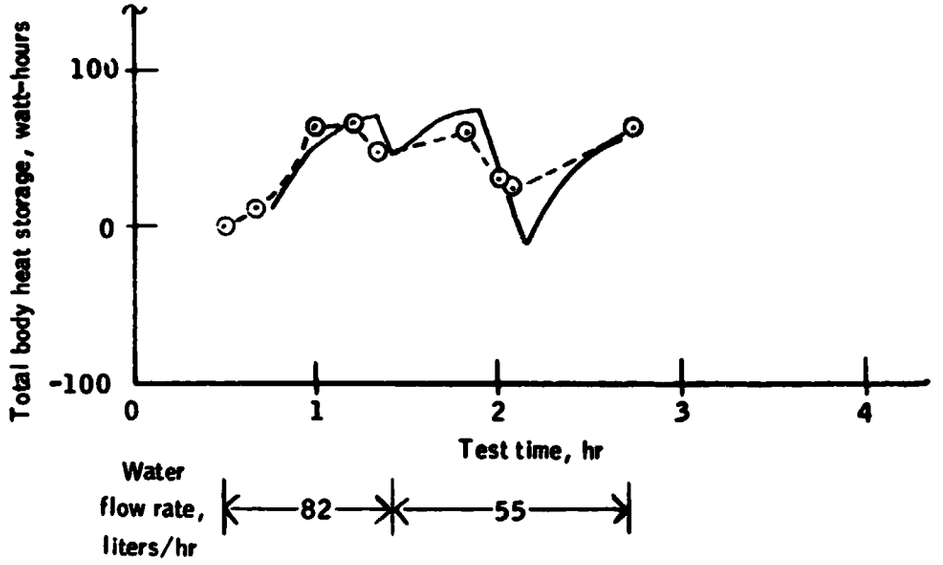

Figure 3-32b.- Total body heat storage vs time for test sequences 9 and 10.

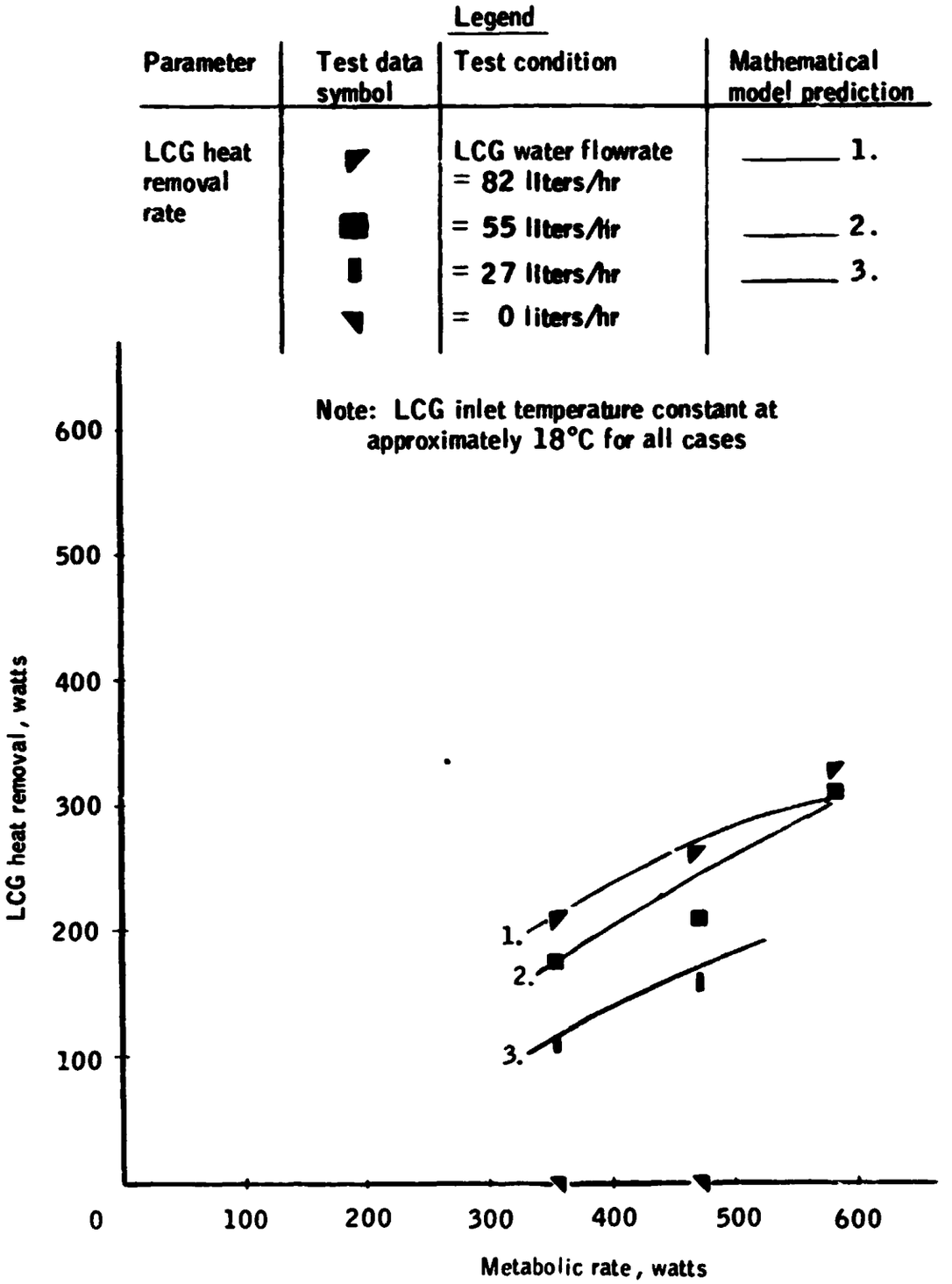

Figure 3-33.- Predicted and actual steady-state LCG heat removal vs metabolic rate, for various LCG water flowrates.

Legend

Parameter	Test data symbol	Test condition	Mathematical model prediction
LCG heat removal ratio	◁	Low metabolic rates (352 watts)	_____1.
	▽	Moderate metabolic rates (469 watts)	_____2.
	▷	High metabolic rates (=586 watts)	_____3.

Figure 3-34.- Ratio of LCG heat removal rate to metabolic rate vs LCG water flowrate.

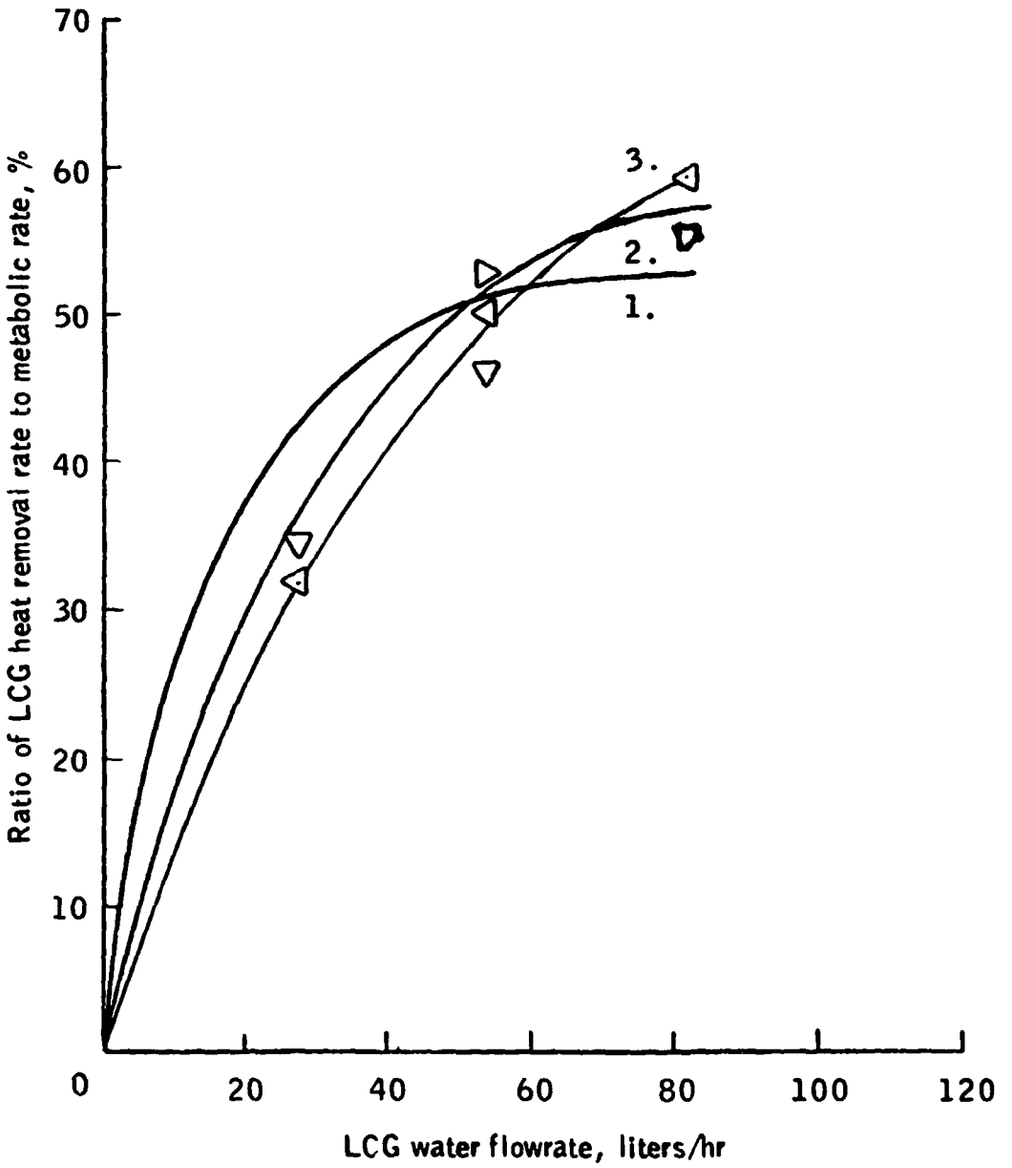

Figure 3-34.- Concluded.

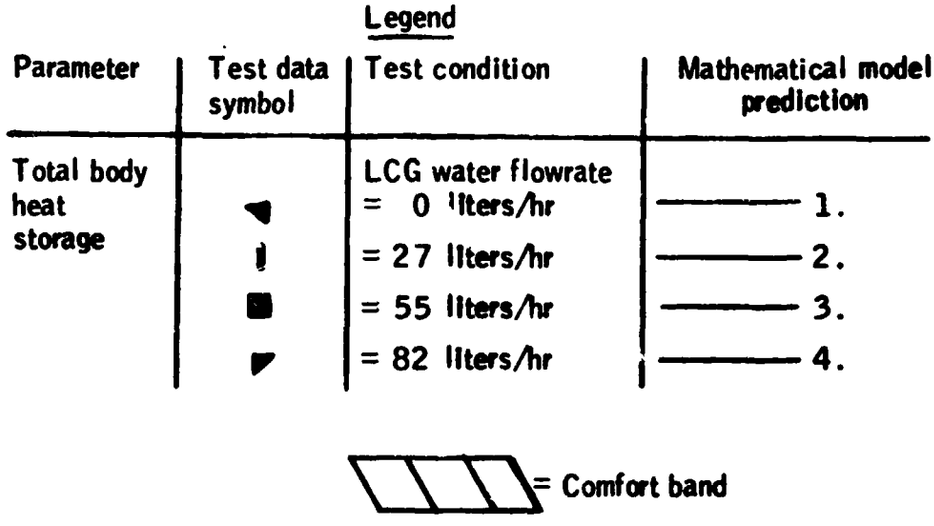

Figure 3-35.- Predicted and actual total body heat storage vs metabolic rate for steady-state conditions during Series C.

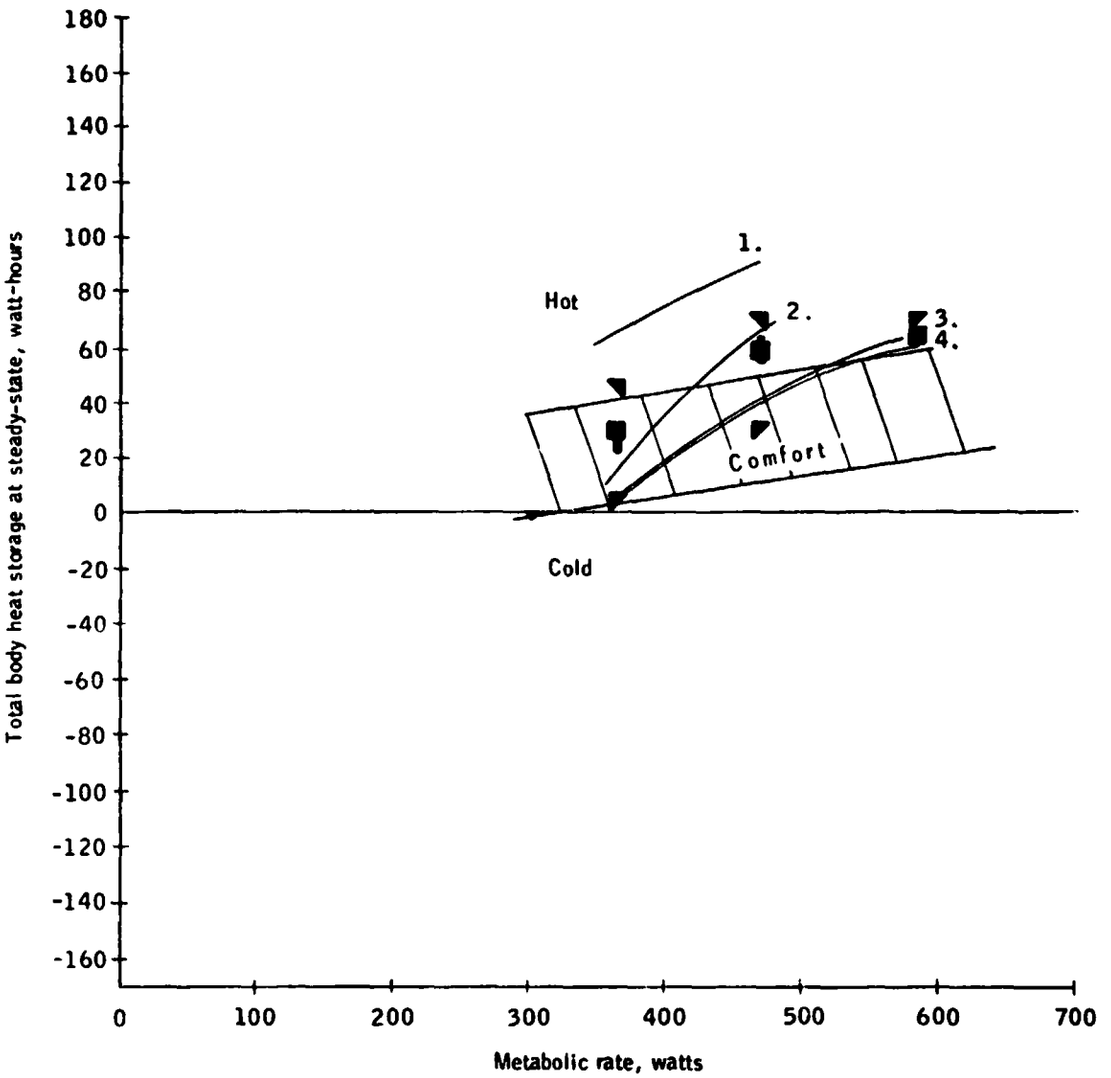

Figure 3-35.- Concluded.

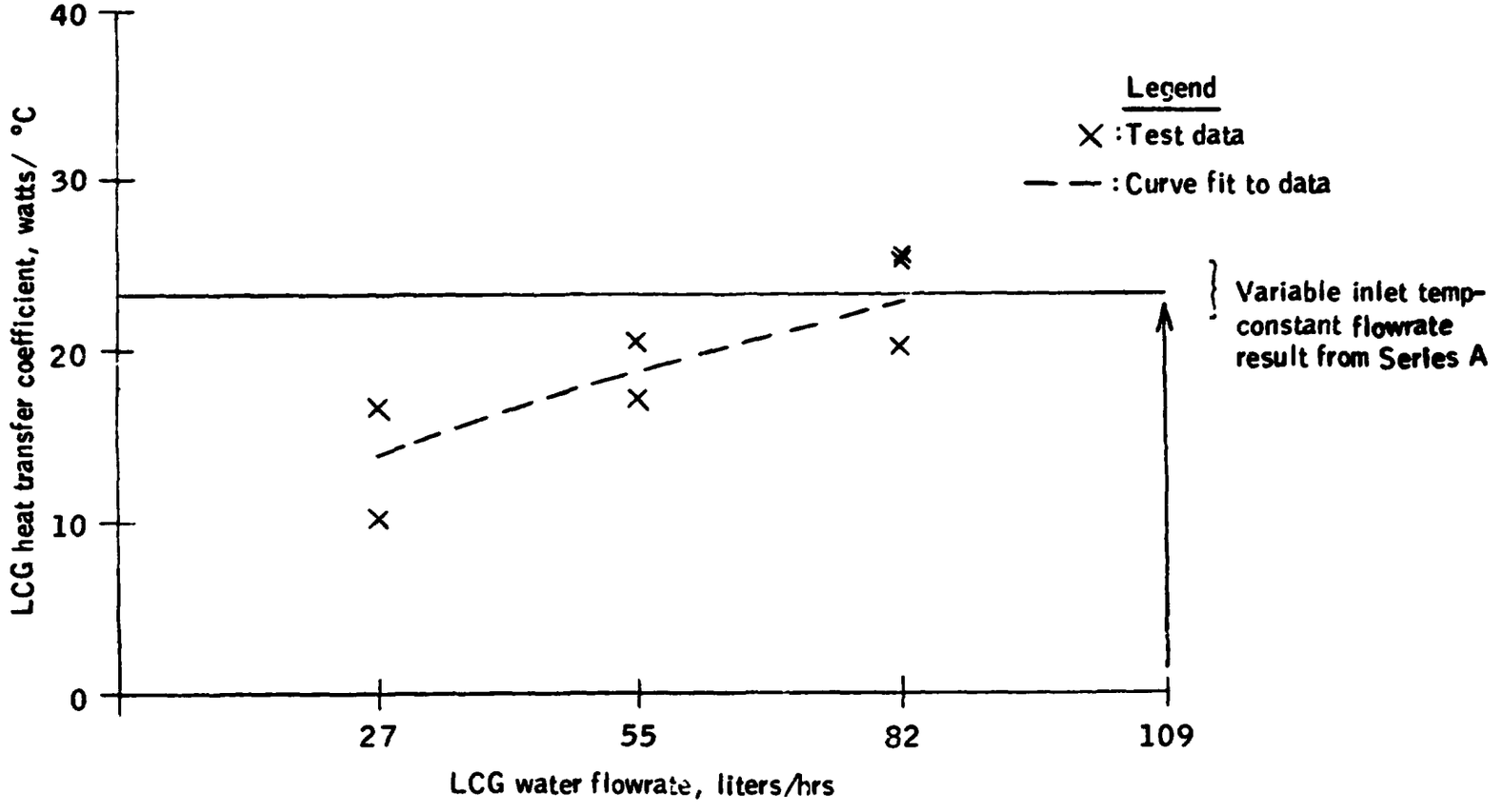

Figure 3-36.- LCG heat transfer coefficient vs LCG water flowrate.

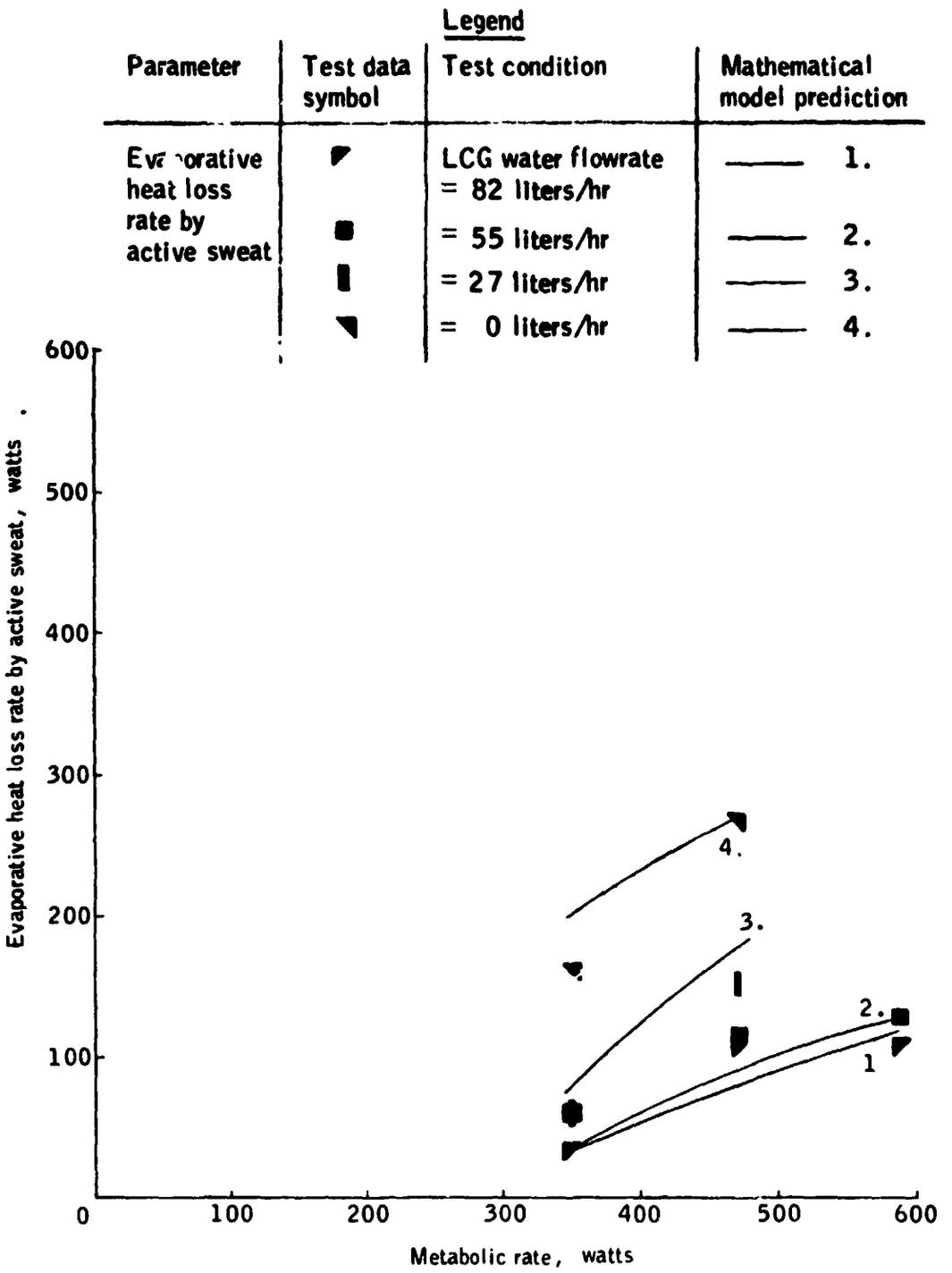

Figure 3-37.- Predicted and actual steady-state evaporative heat loss rate by active sweat vs metabolic rate, for various LCG water flowrates.

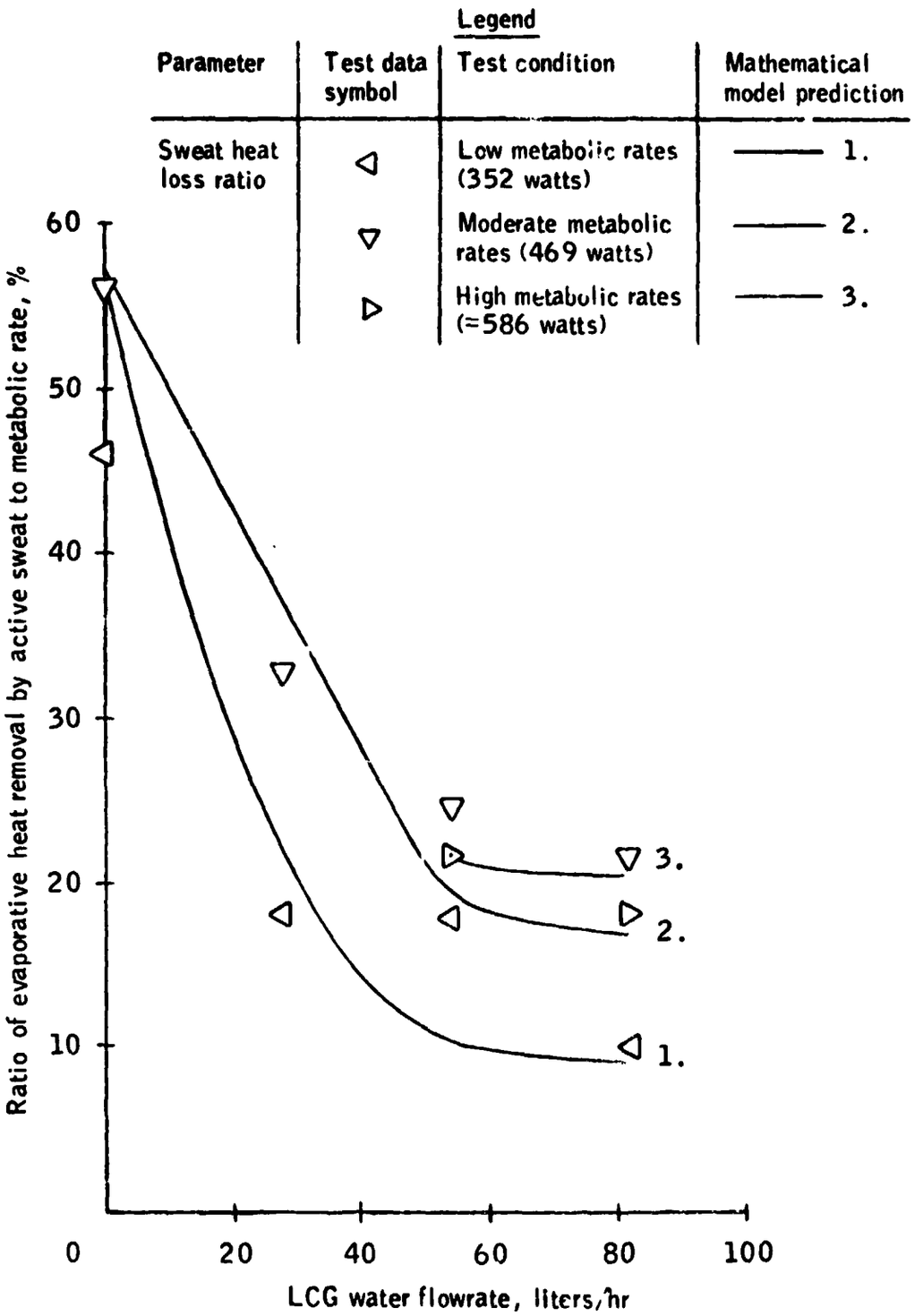

Figure 3-38.- Ratio of evaporative heat loss rate by active sweat to metabolic rate vs LCG water flowrate.

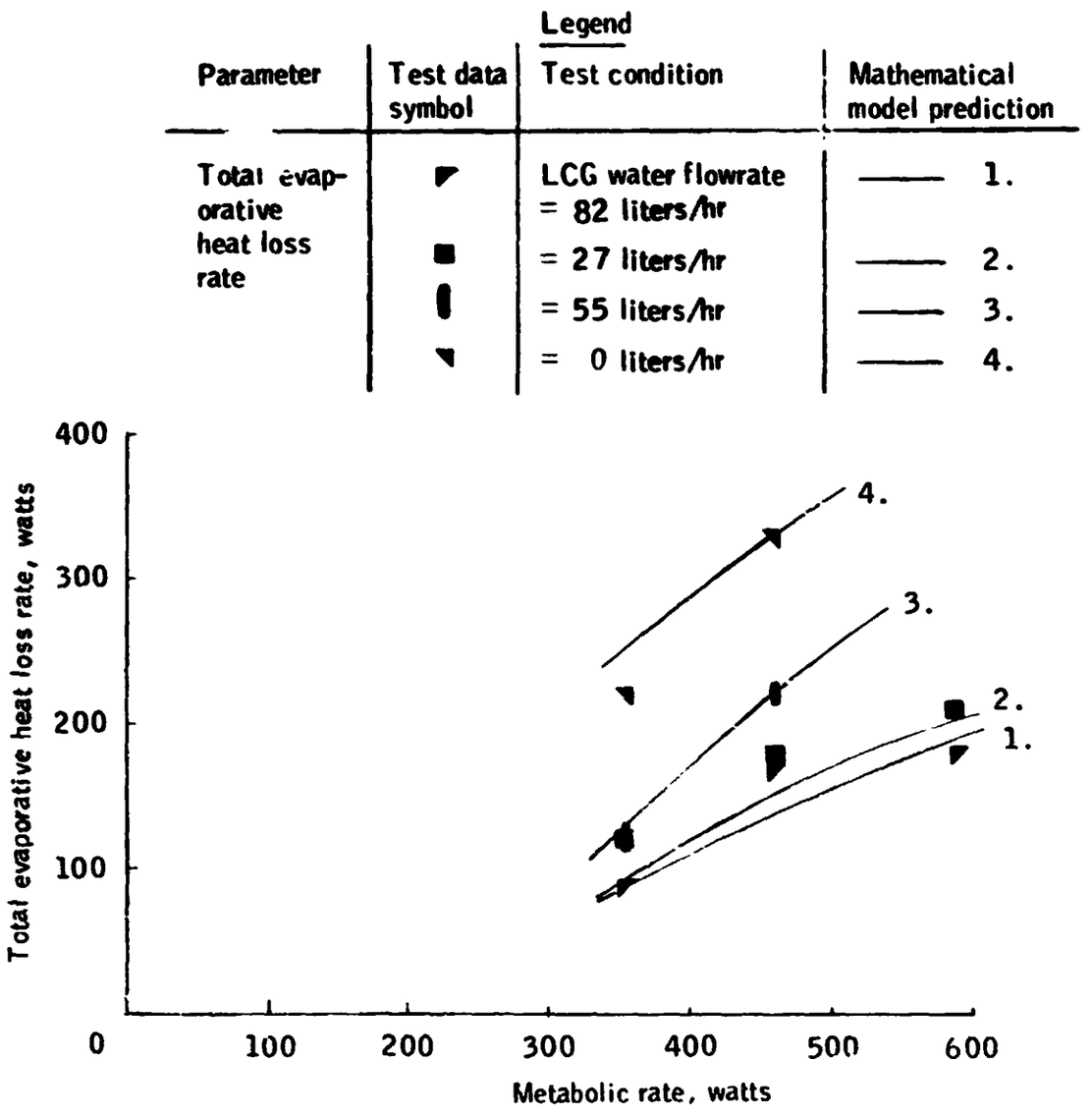

Figure 3-39.- Predicted and actual steady-state total evaporative heat loss rate vs metabolic rate, for various LCG water flowrates.

Legend

Parameter	Test data symbol	Test condition	Mathematical model prediction
Total evaporative heat loss ratio	◁	Low metabolic rates (352 watts)	_____1.
	▽	Moderate metabolic rates (469 watts)	_____2.
	▷	High metabolic rates (=586 watts)	_____3.

Figure 3-40.- Ratio of total evaporative heat loss rate to metabolic rate vs LCG water flowrate.

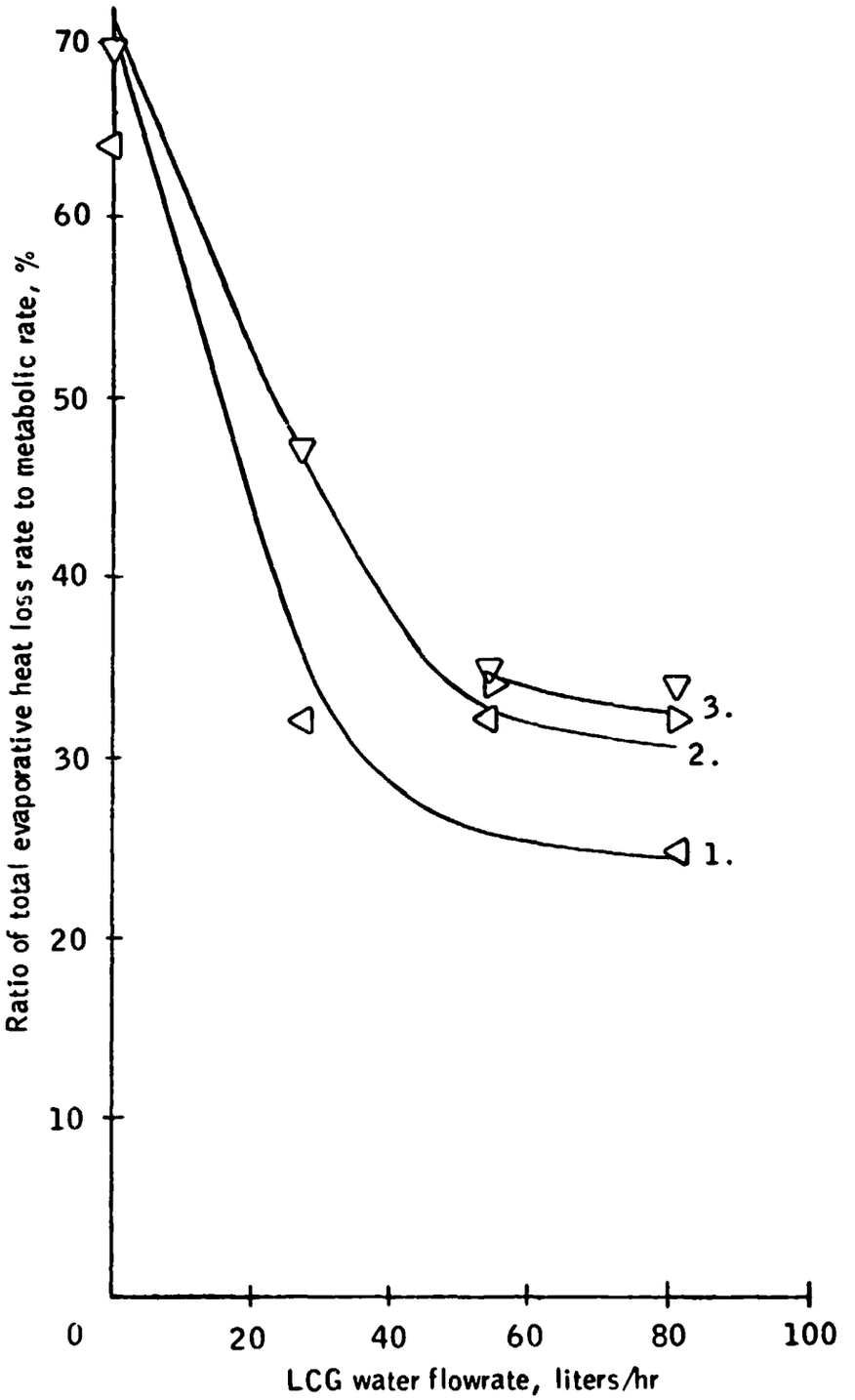

Figure 3-40.- Concluded.

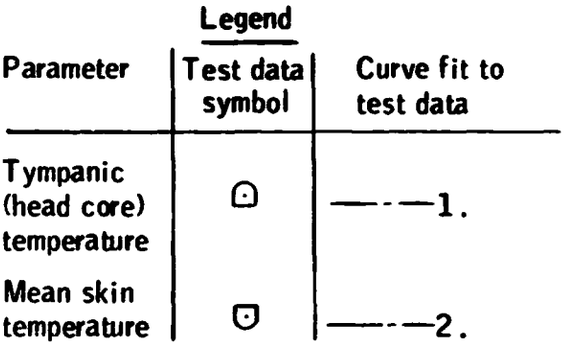

Figure 3-41.- Tympanic (head core) and mean skin temperature vs LCG water flowrate.

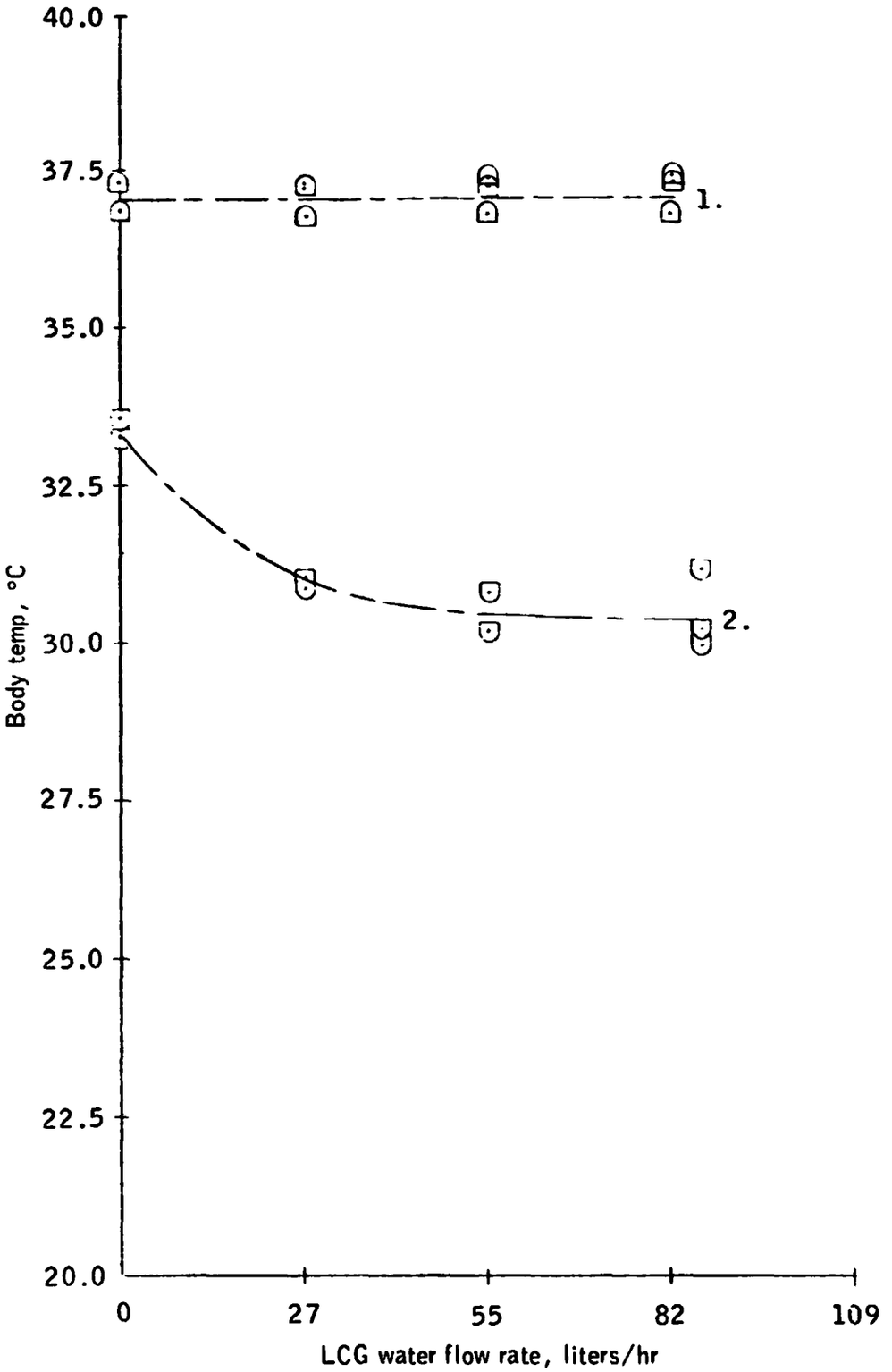

Figure 3-41.- Concluded.

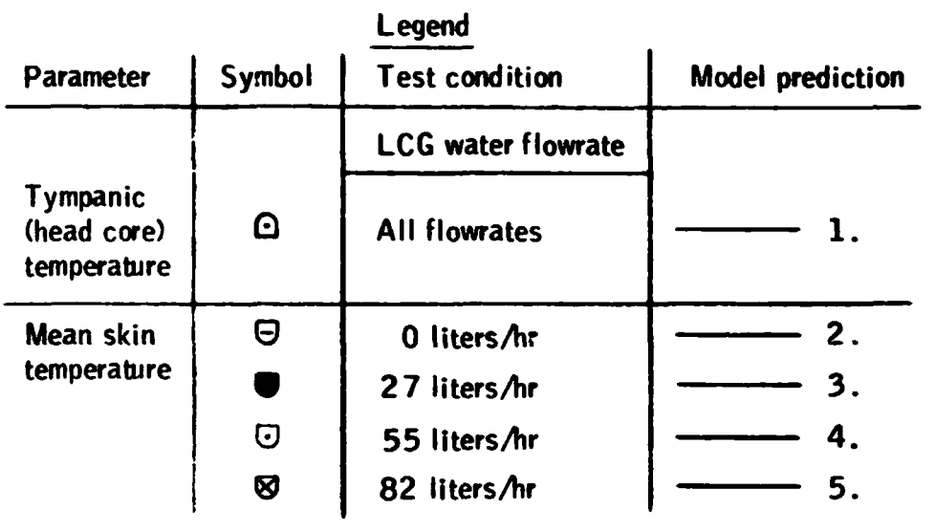

Figure 3-42.- Predicted and actual steady-state tympanic (head core) and mean skin temperature vs metabolic rate for various LCG water flowrates.

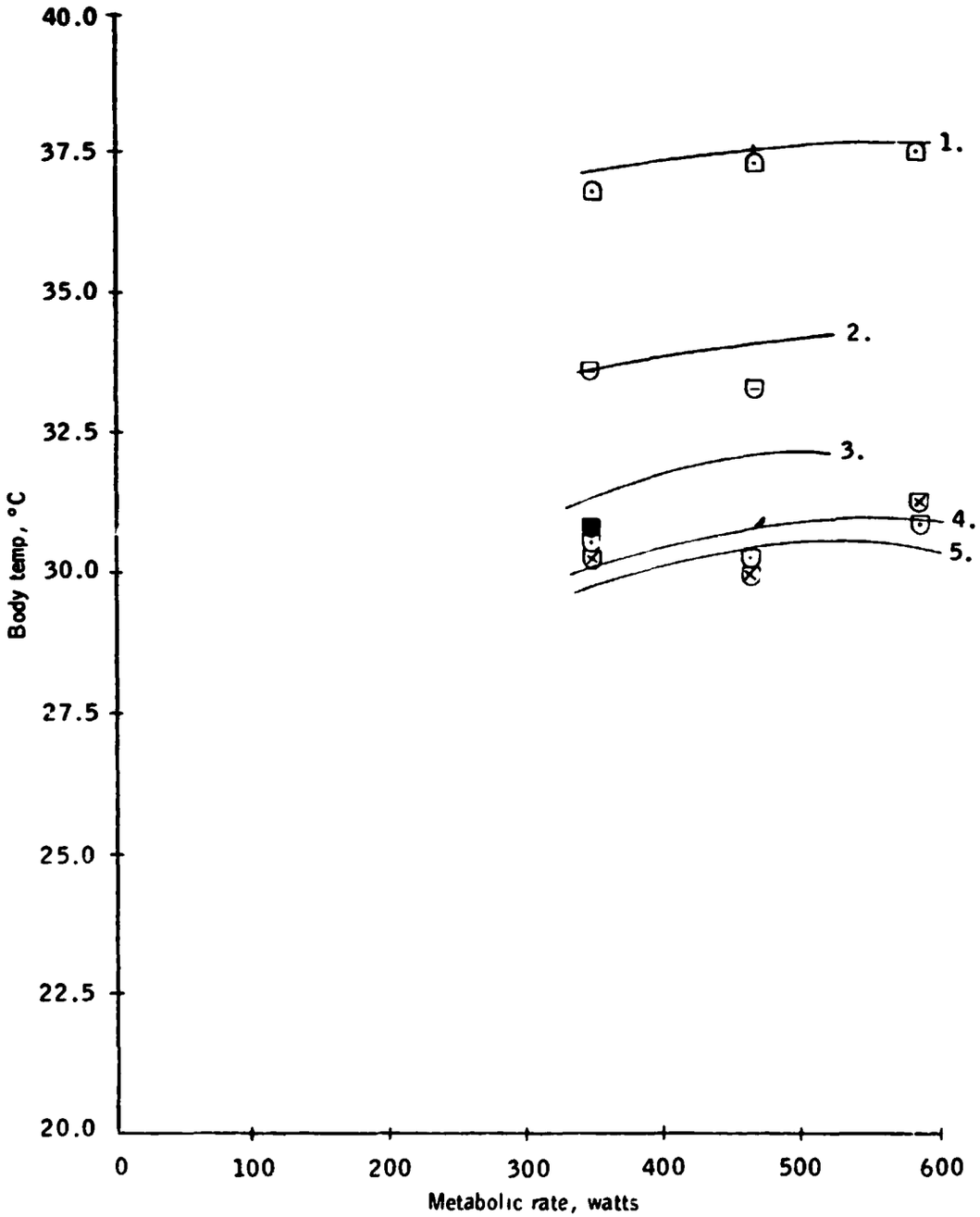

Figure 3-42.- Concluded.

Legend

Parameter	Symbol	Test condition	Model prediction
		LCG water flowrate	
Sweat rate (and sweat heat loss rate)	⊖	0 liters/hr	——— 1.
	●	27 liters/hr	——— 2.
	⊙	55 liters/hr	——— 3.
	⊗	82 liters/hr	——— 4.

Note: ● = data of Series A for LCG flowrate of 109 liters/hr

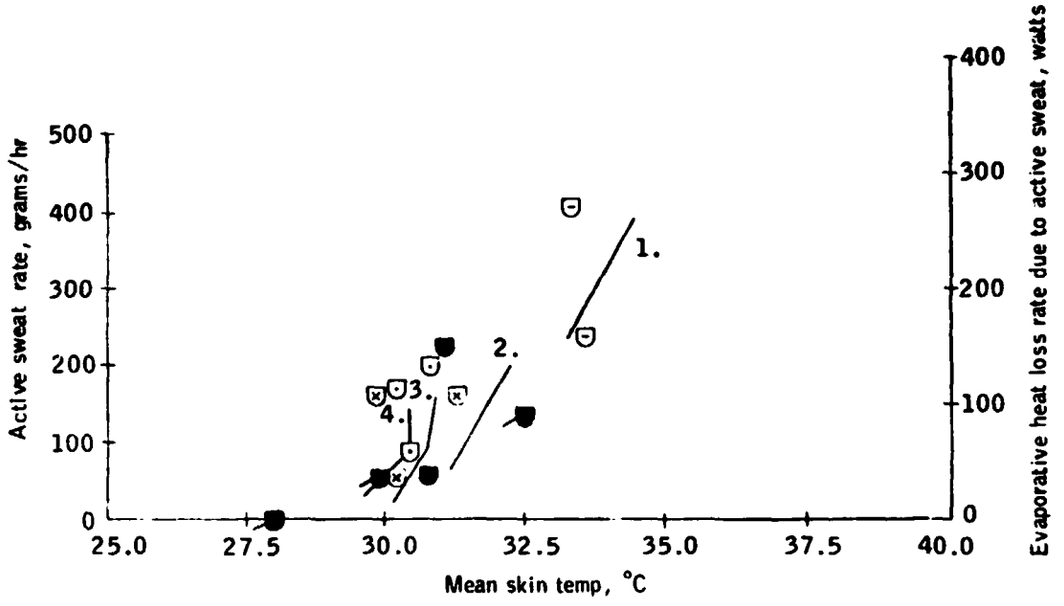

Figure 3-43.- Predicted and actual steady-state sweat rate and evaporative heat loss rate due to sweating vs mean skin temperature for various LCG water flowrates.

Legend

Parameter	Symbol	Test condition	Model prediction
		LCG water flowrate	
Sweat rate (and sweat heat loss rate)	⊖	0 liters/hr	——— 1.
	●	27 liters/hr	——— 2.
	⊙	55 liters/hr	——— 3.
	⊗	82 liters/hr	——— 4.

Note: - - - = data of Benzinger for no skin cooling (8).

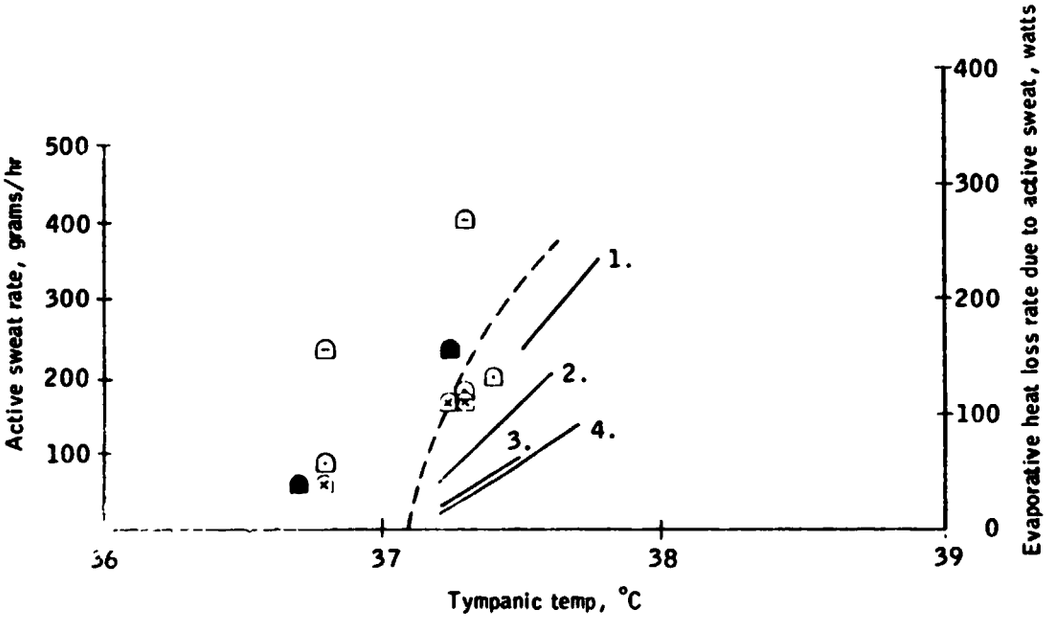

Figure 3-44.- Predicted and actual steady-state sweat rate and evaporative heat loss rate due to sweating vs tympanic (head core) temperature for various LCG water flowrates.

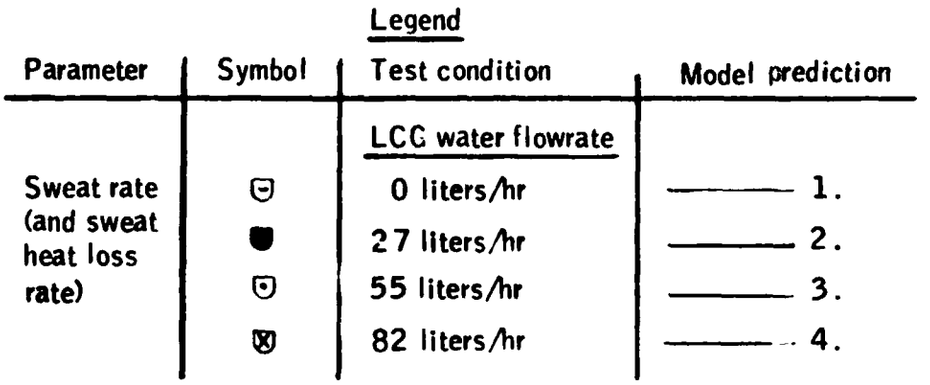

Figure 3-45.- Predicted and actual steady-state sweat rate and evaporative heat loss rate due to sweating vs change in mean skin temperature for various LCG water flowrates.

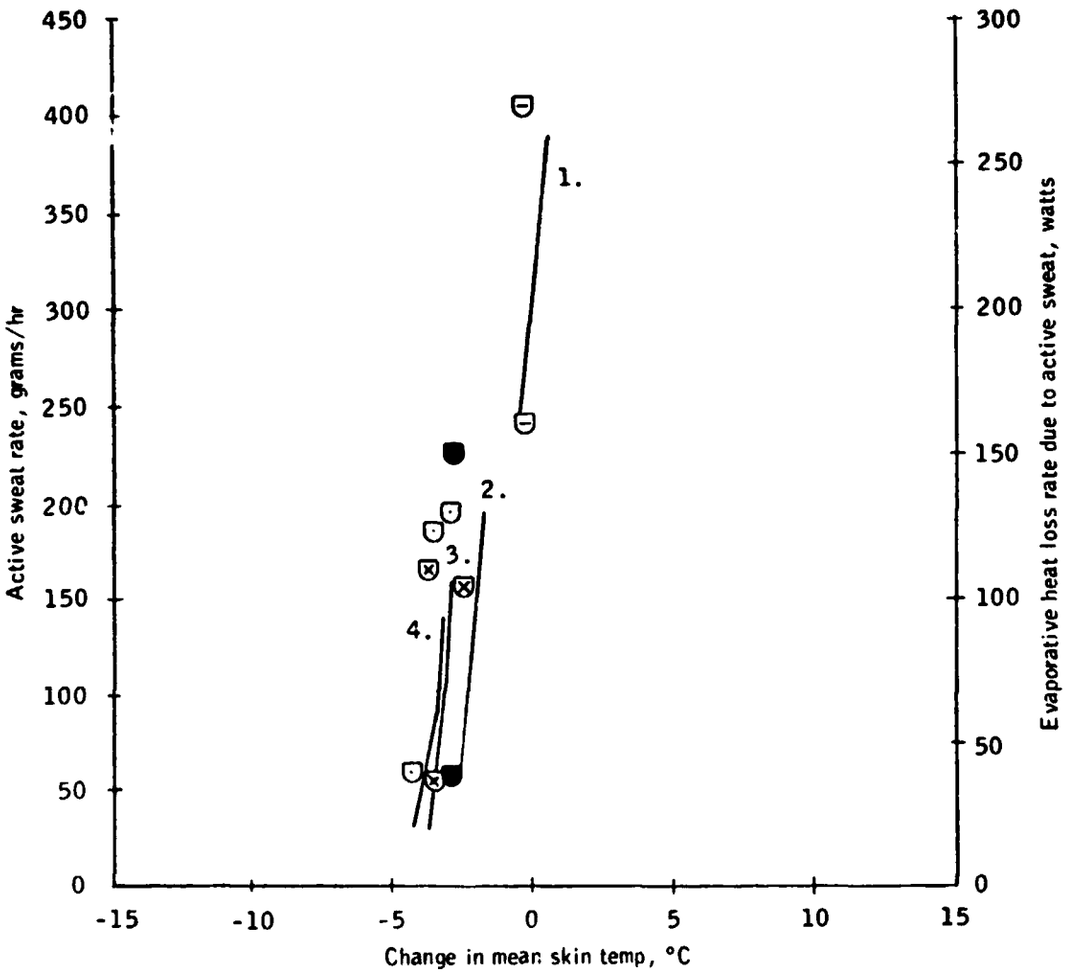

Figure 3-45.- Concluded.

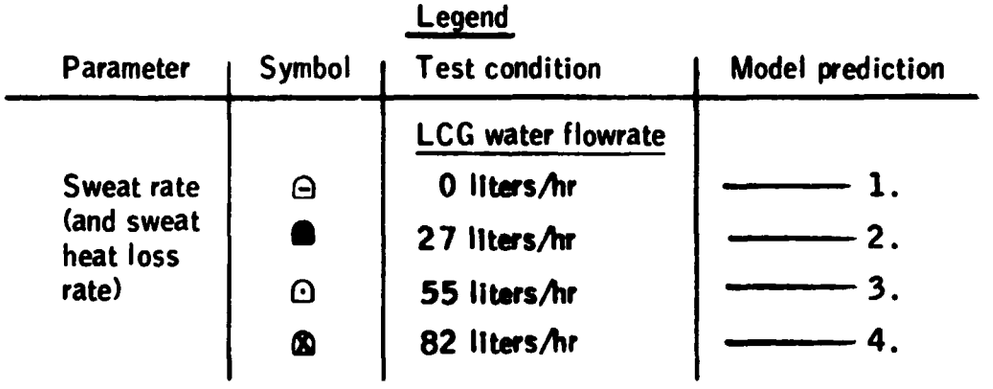

Figure 3-46.- Predicted and actual steady-state sweat rate and evaporative heat loss rate due to sweating vs change in tympanic (head core) temperature for various LCG water flowrates.

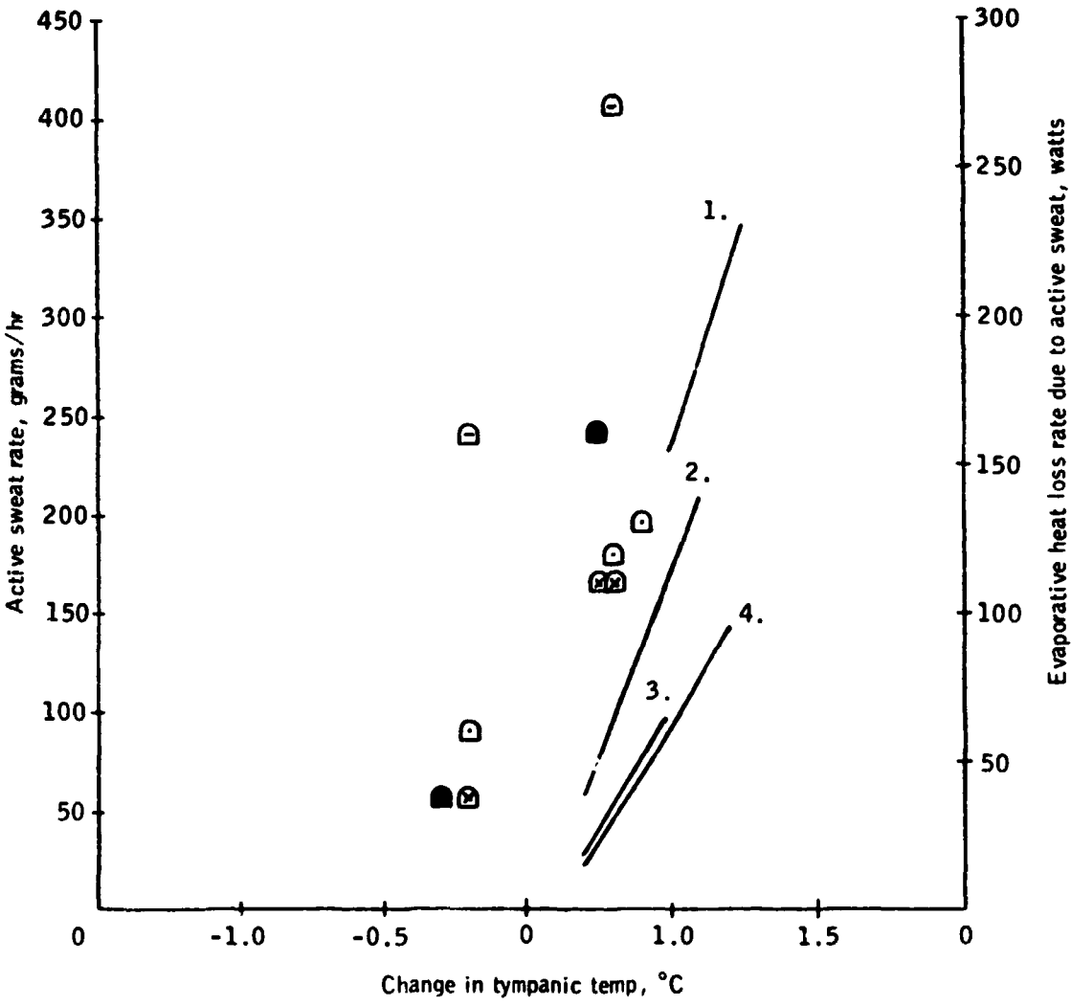

Figure 3-46.- Concluded.

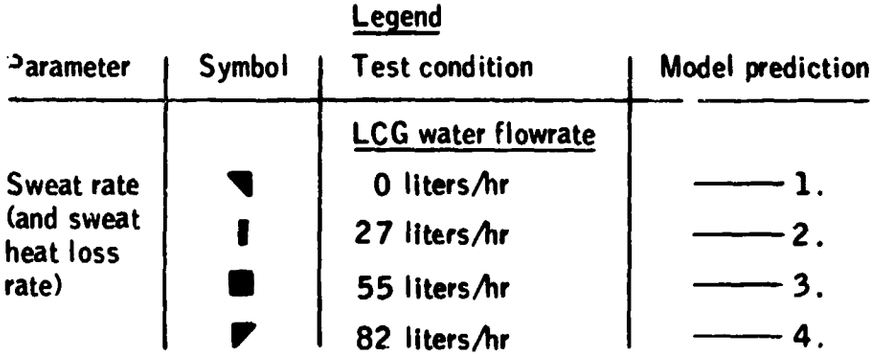

Figure 3-47.- Actual and predicted steady-state sweat rate and evaporative heat loss rate due to active sweating vs total body heat storage.

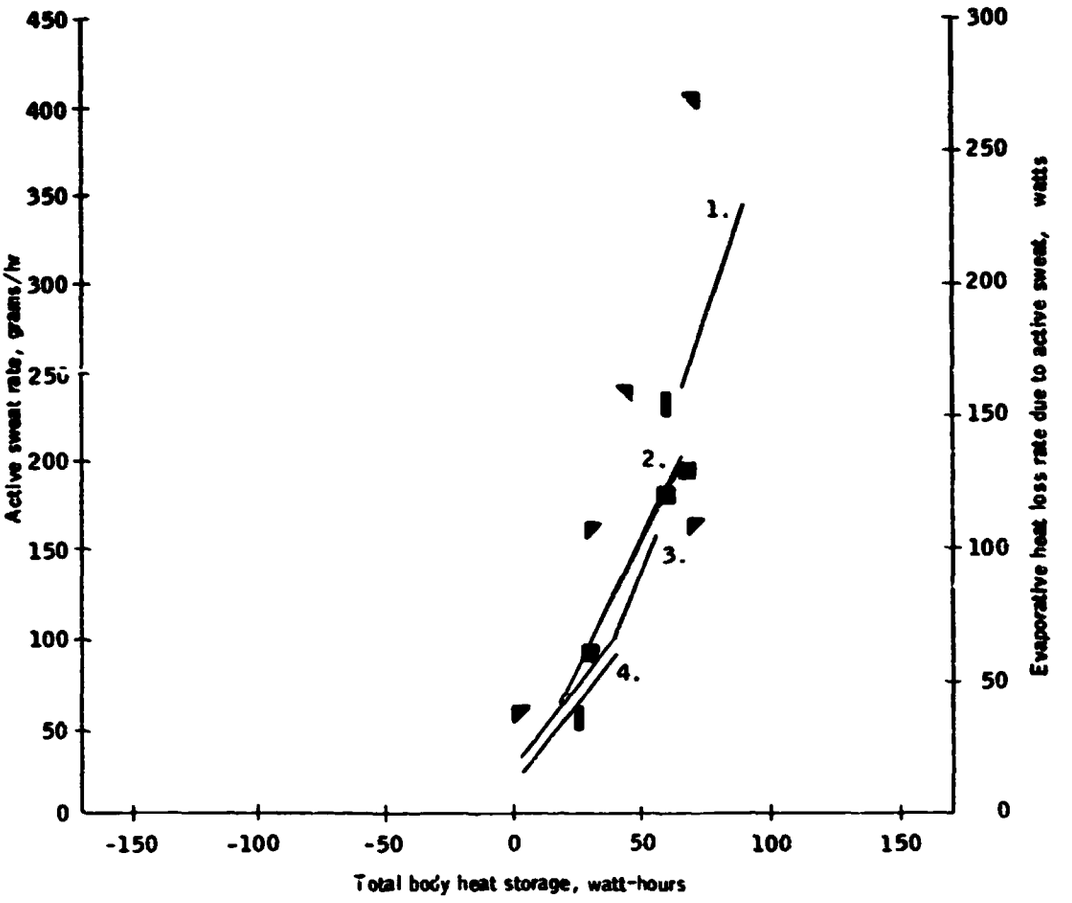

Figure 3-47.- Concluded.

TABLE 3-4.- SERIES D - CALCULATED DATA AND HEAT BALANCE

TEST SUBJECT	1/D.S.	2/F.H.	3/J.M.	4/J.M.	5/J.M.	6/J.M.	7/K.M.
Duration, hrs.	6.98	6.97	3.17	3.43	3.93	3.62	3.52
Average LCG inlet temperature selected, °C	19	22	13.5	11.5	17	23	13
Total Heat Produced							
1. Metabolic heat produced over duration of test, watt-hrs.	2133	1943	1330	1402	1122	1313	1620
Total Heat Loss							
1. Evaporation heat loss, Watt-hrs							
a. By respiration & diffusion(1)	284	266	167	175	152	168	199
b. By active sweating(2)	470	300	91	83	22	227	226
Total Evaporative Heat Removed Over Duration of Test, watt-hrs(3)	754	566	258	258	174	395	425
2. Total convective heat removed over duration of tests, watt-hrs(4)	4	-8	12	20	0	10	23
3. Net environmental heat exchange over duration of test, watt-hrs(5)	547 into suit	445 out of suit	205 into suit	404 into suit	137 out of suit	261 out of suit	480 into suit
4. Total LCG heat removed over duration of test, watt-hrs(6)	1887	955	1172	1486	774	598	1597
Total heat removed over duration of test, watt-hrs	2098	1958	1237	1360	1085	1264	1565
Heat balance = total heat produced - total heat removed, watt-hrs(7)	+35	-15	+93	+42	+37	+46	+55
Body heat storage at end of test, watt-hrs(8)	+35	-30.5	-27.5	+19	-30	+9.7	+53
Heat deficit = heat balance - body heat storage, watt-hrs	0	+15.5	+115.5	+23	+67	+36.3	+2

1. See Eqns. 5, 6 & 7, Appendix C. 2. See Eqn. 8, Section 2; 3. See Eqn. 3, Appendix C; 4. See Eqn. 6, Section 2. 5. See Eqn. 14, Appendix C; 6. See Eqn. 5, Section 2; 7. See Eqn. 1, Figure 2-2. 8. See Eqn. 3, Section 2.

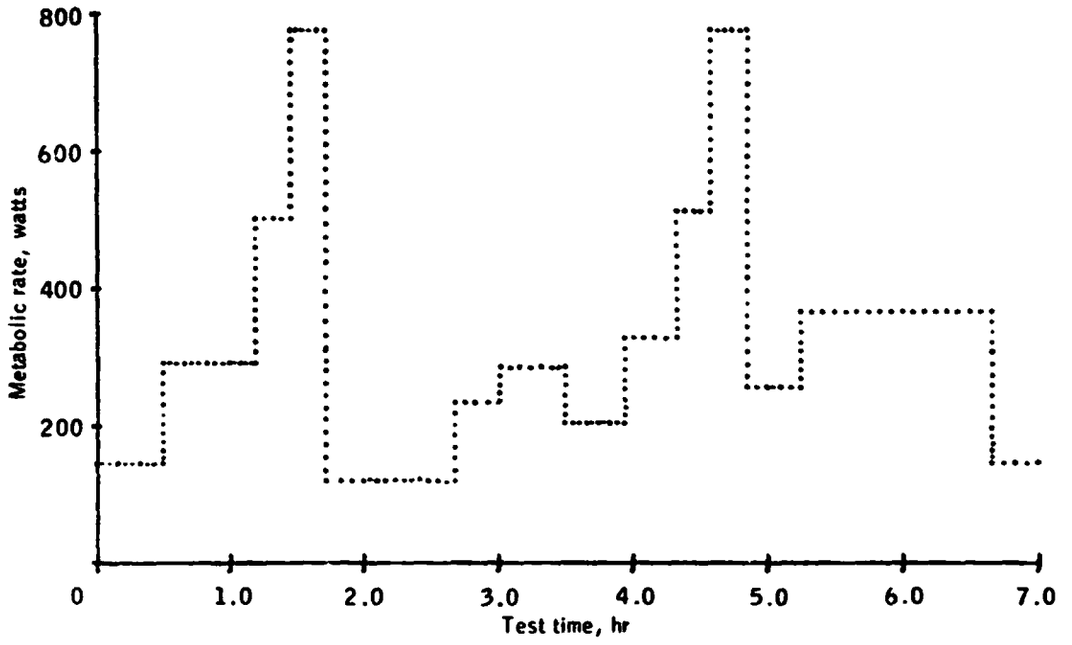

Figure 3-48.- Metabolic rate profile for test 1.

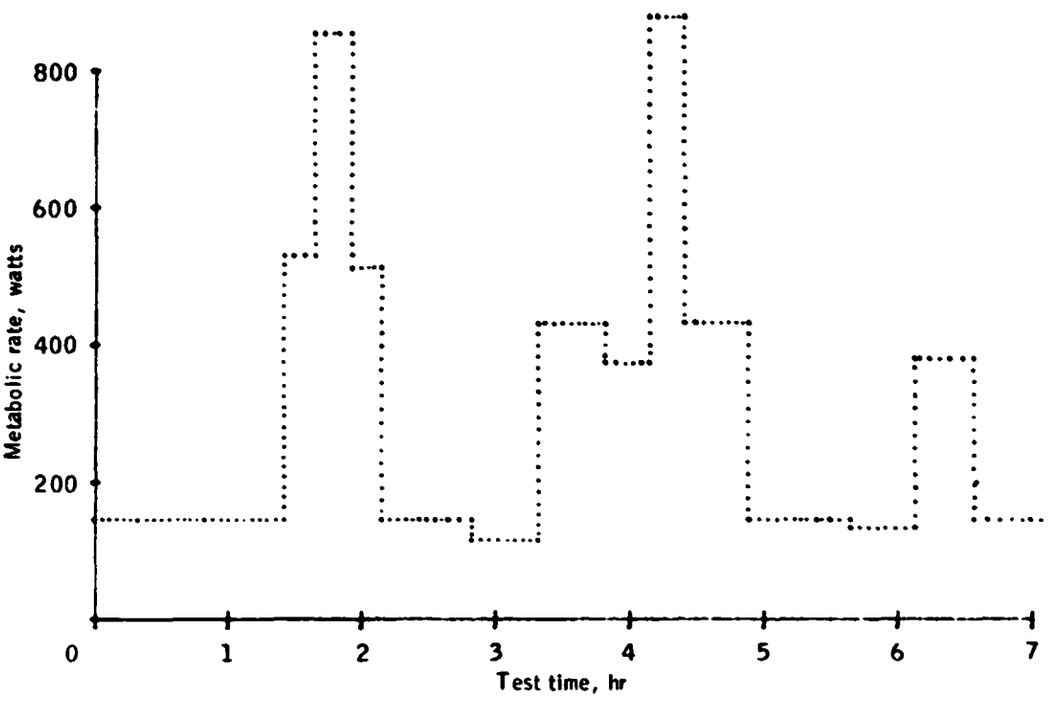

Figure 3-49.- Metabolic rate profile for test 2.

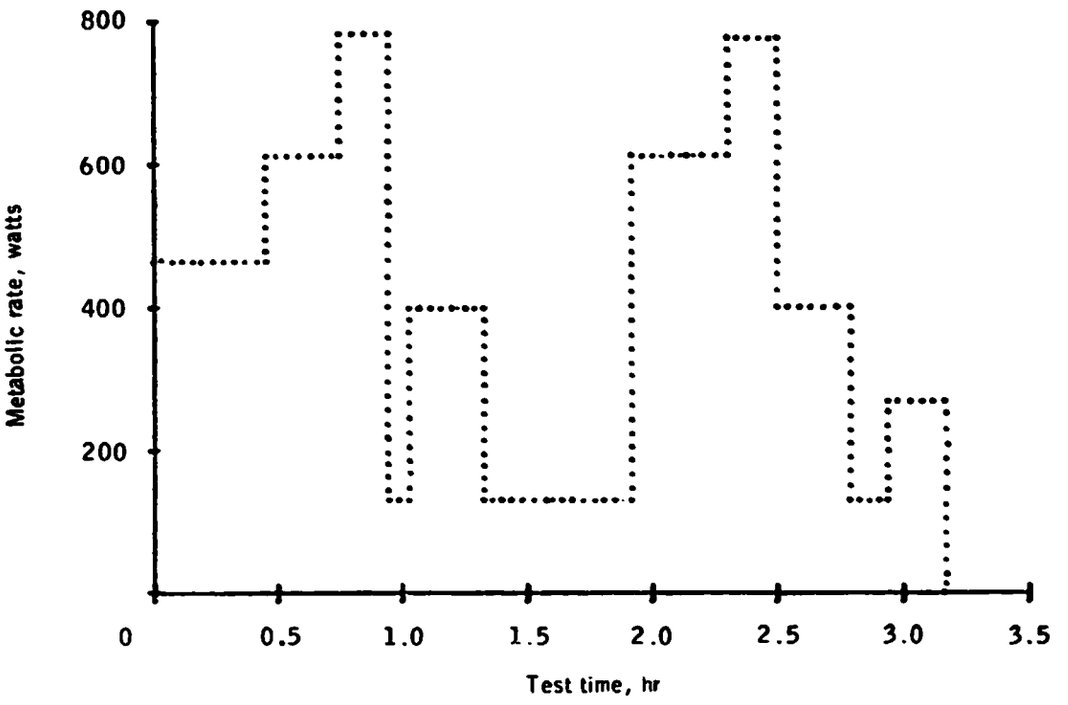

Figure 3-50.- Metabolic rate profile for test 3.

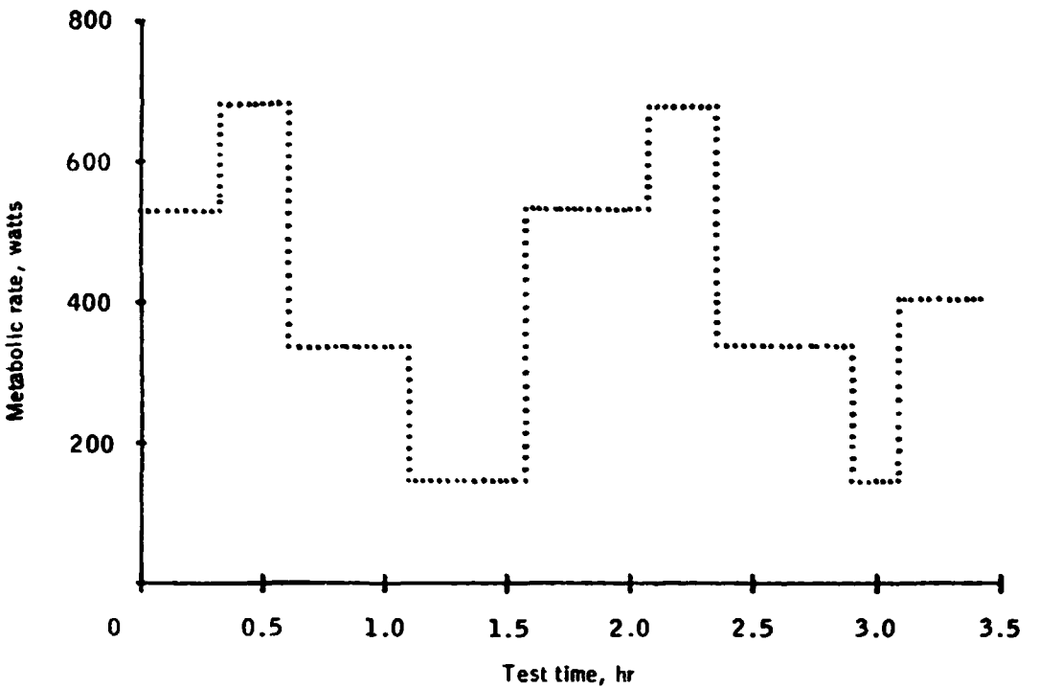

Figure 3-51.- Metabolic rate profile for test 4.

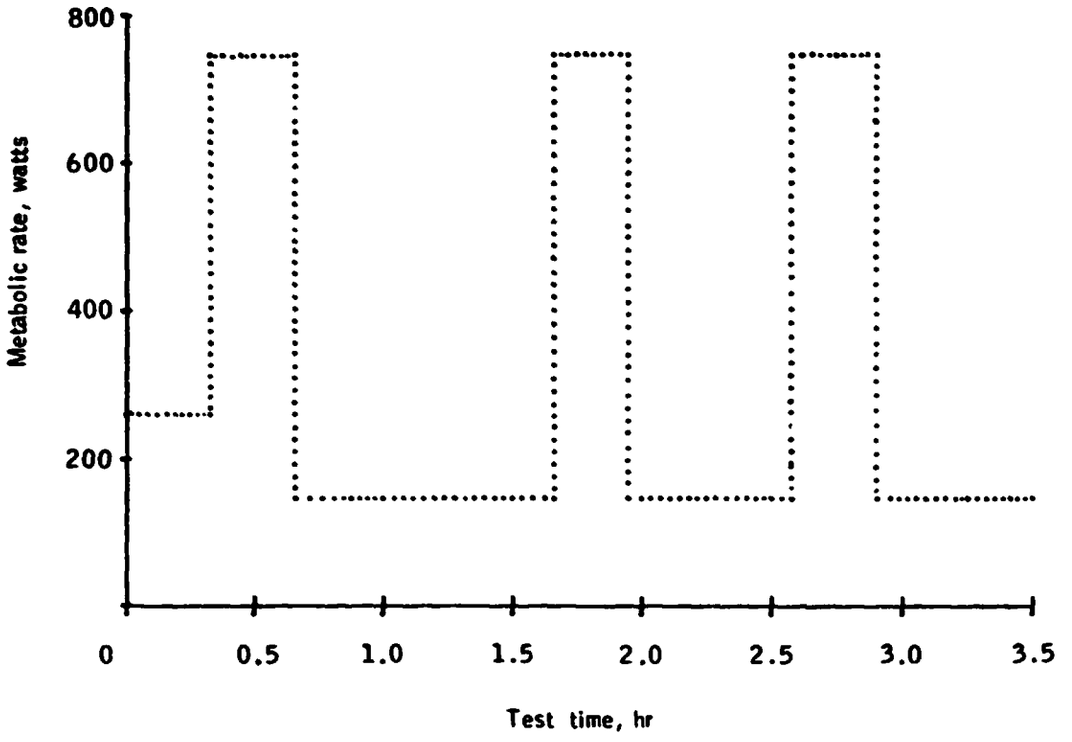

Figure 3-52.- Metabolic rate profile for test 5.

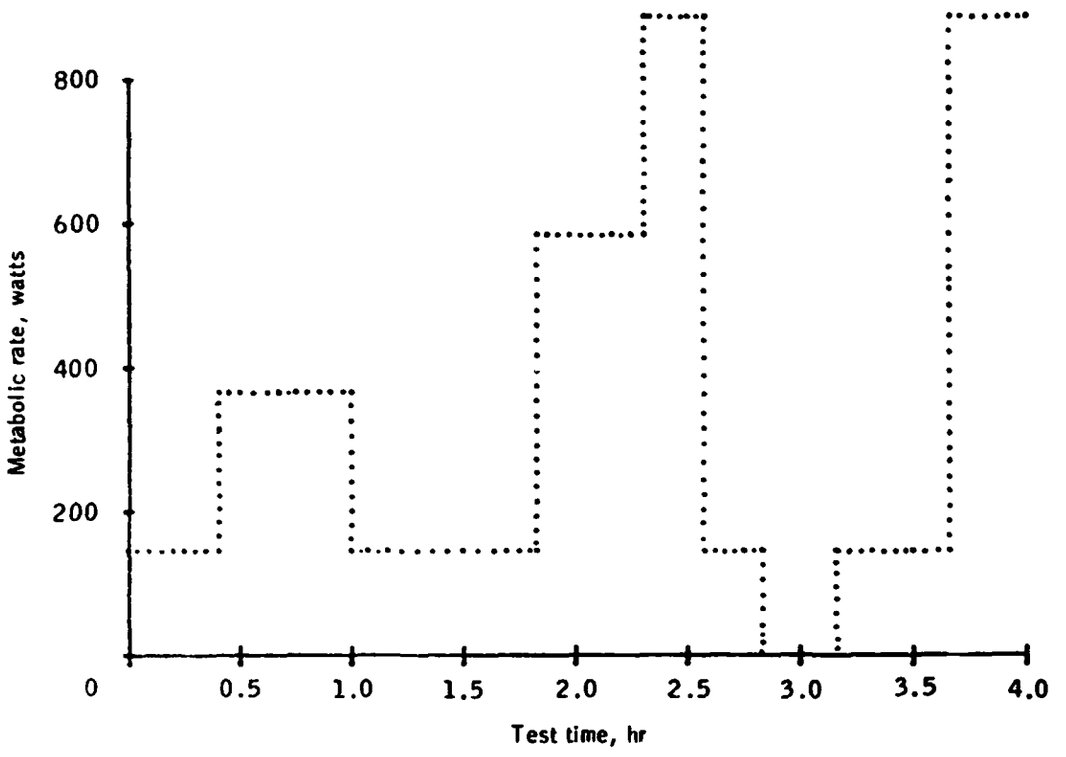

Figure 3-53.- Metabolic rate profile for test 6.

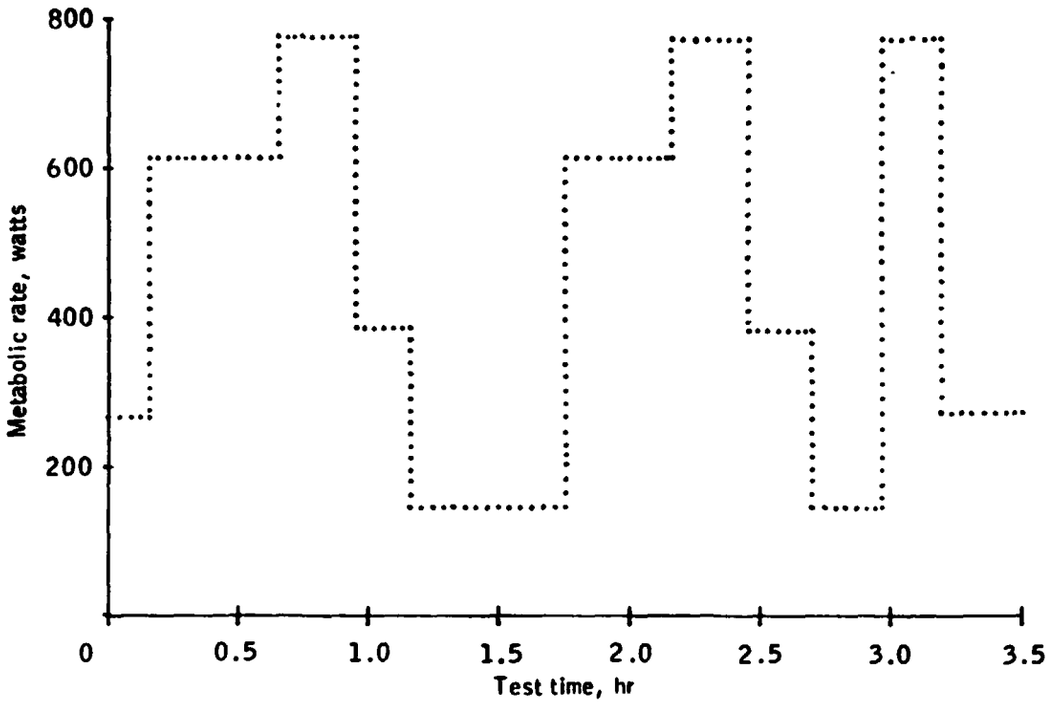

Figure 3-54.- Metabolic rate p ofile for test 7.

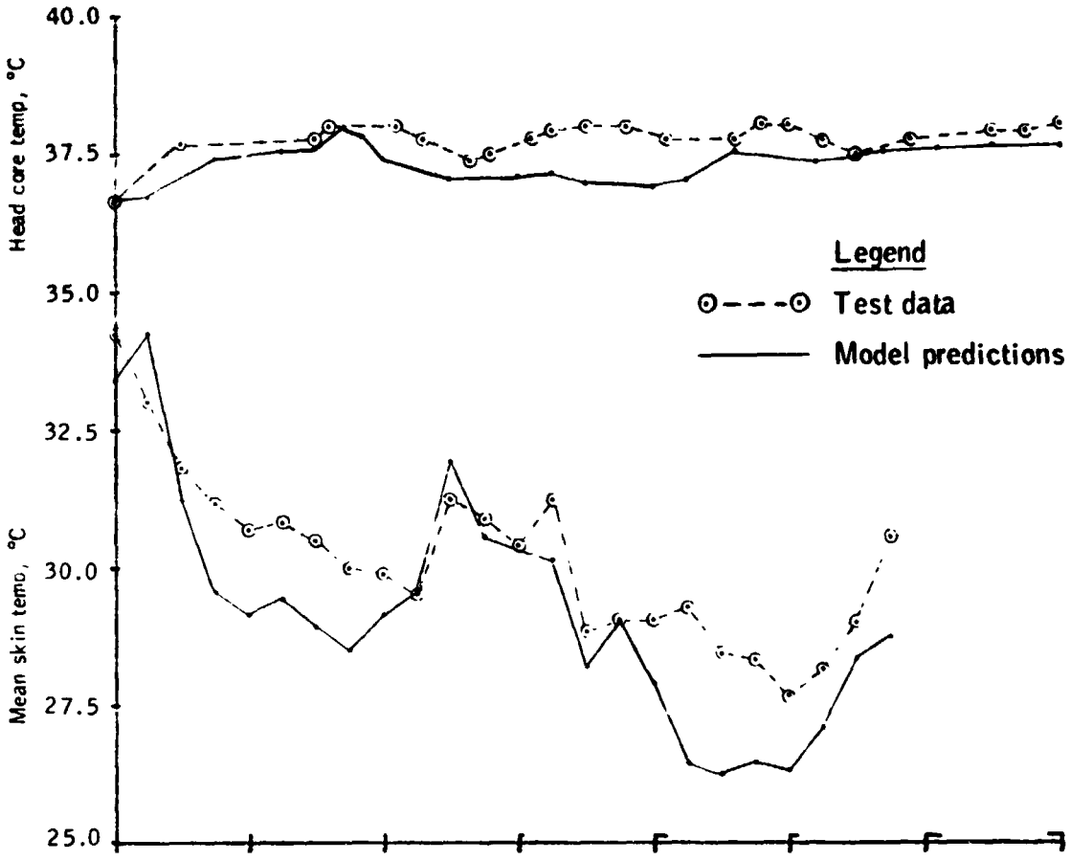

Figure 3-55a.- Head core (tympanic) temperature (upper curve) and mean skin temperature (lower curve) vs time for test 1.

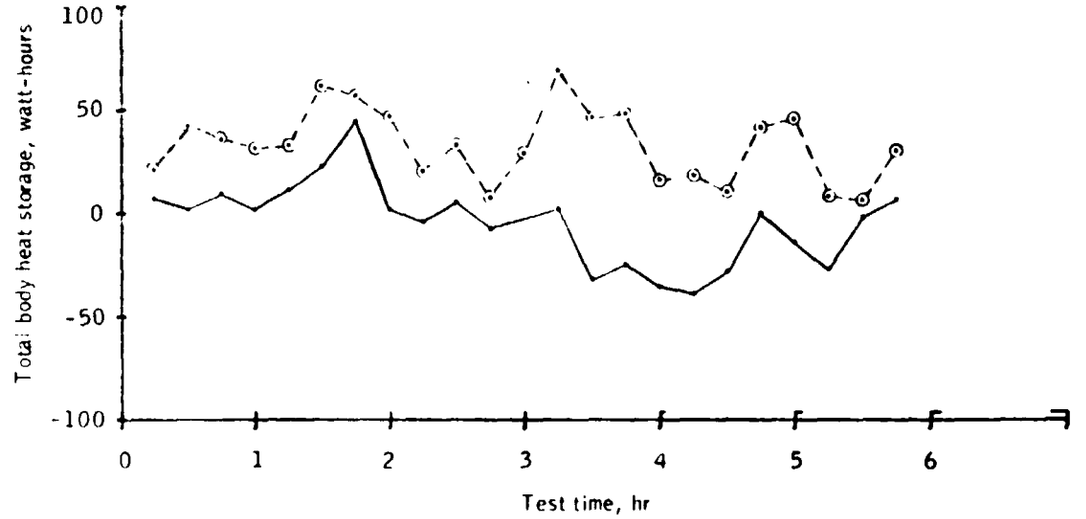

Figure 3-55b.- Total body heat storage vs time for test 1.

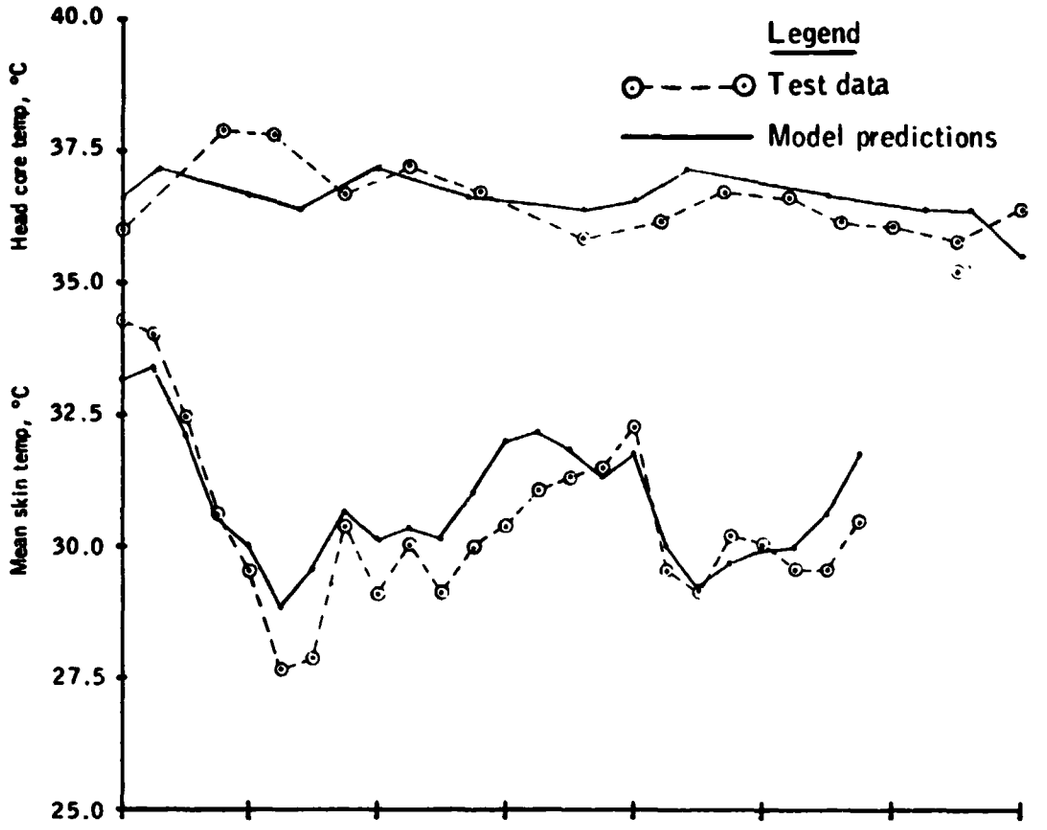

Figure 3-56a.- Head core (tympanic) temperature (upper curve) and mean skin temperature (lower curve) vs time for test 2.

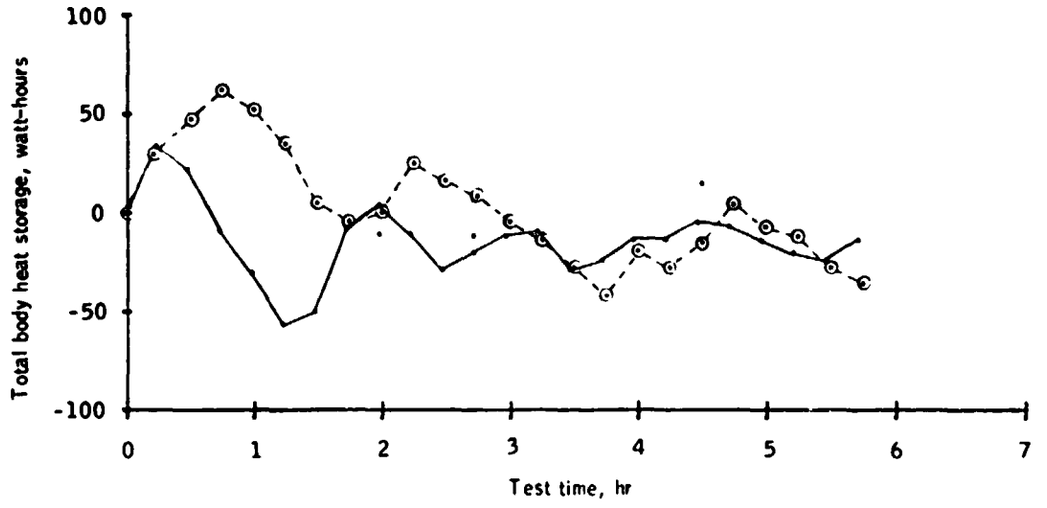

Figure 3-56b.- Total body heat storage vs time for test 2.

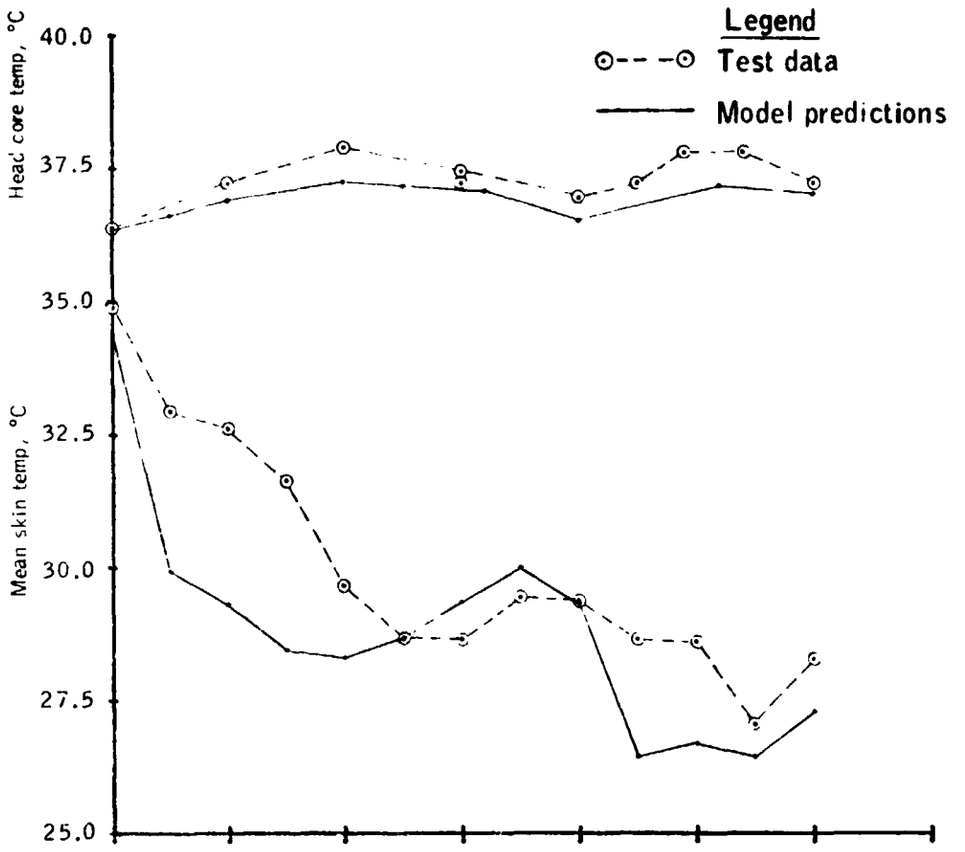

Figure 3-57a.- Head core (tympanic) temperature (upper curve) and mean skin temperature (lower curve) vs time for test 3.

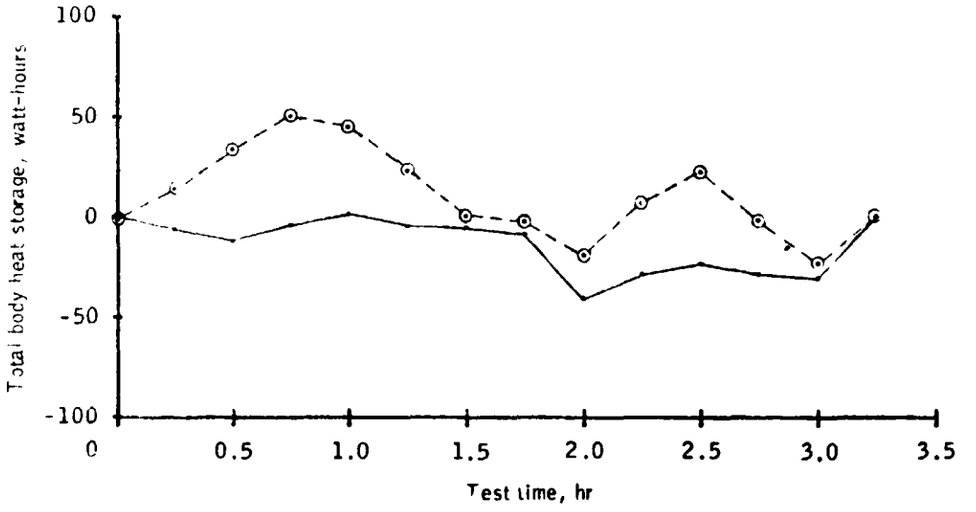

Figure 3-57b.- Total body heat storage vs time for test 3.

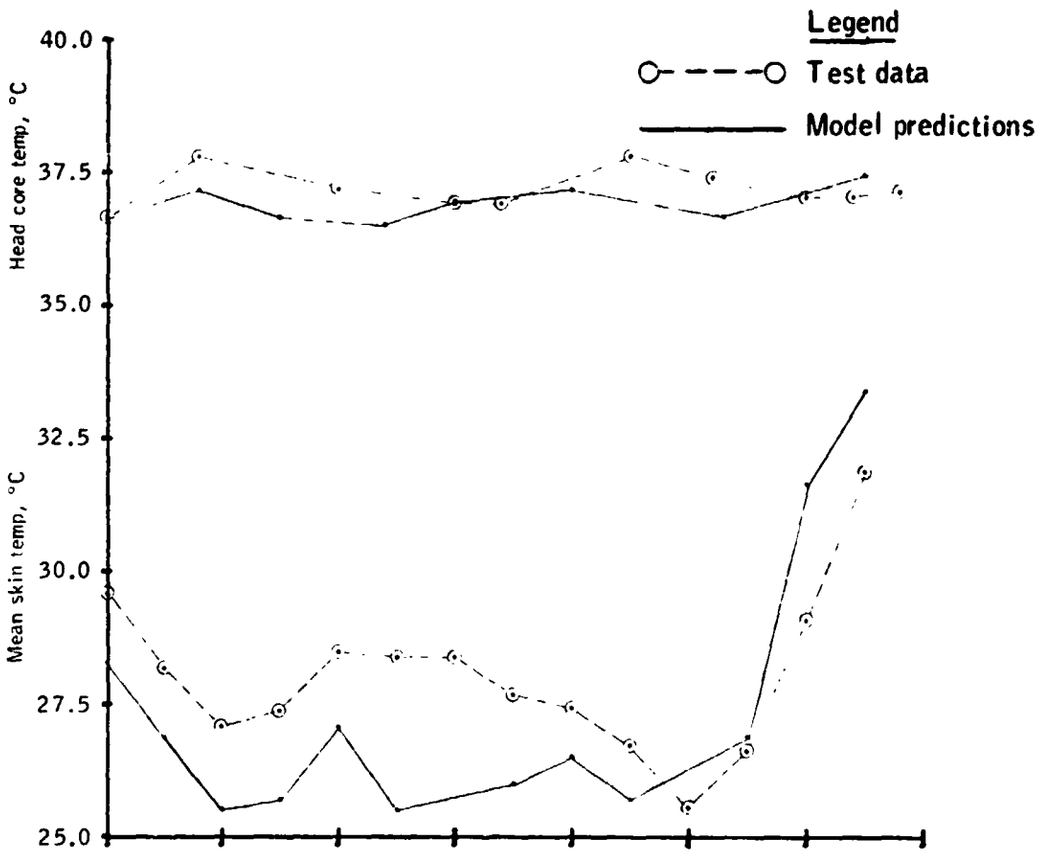

Figure 3-58a.- Head core (tympanic) temperature (upper curve) and mean skin temperature (lower curve) vs time for test 4.

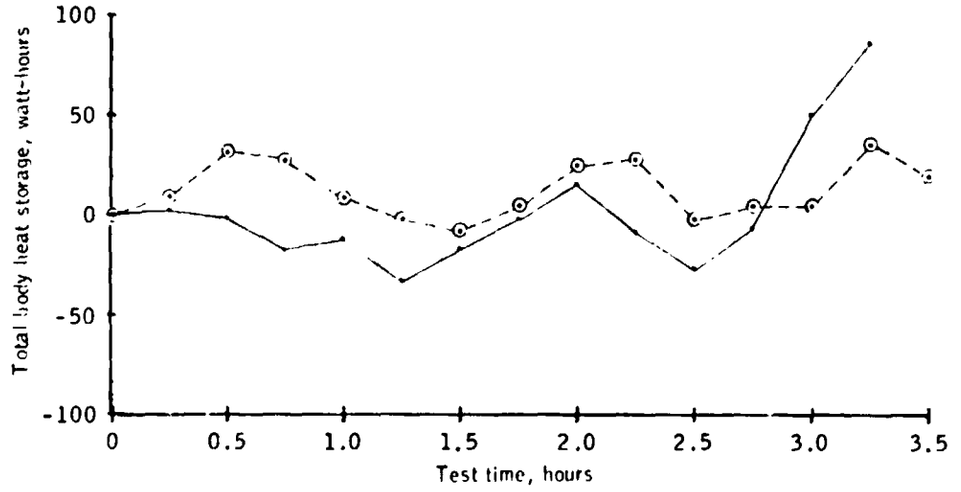

Figure 3-58b.- Total body heat storage vs time for test 4.

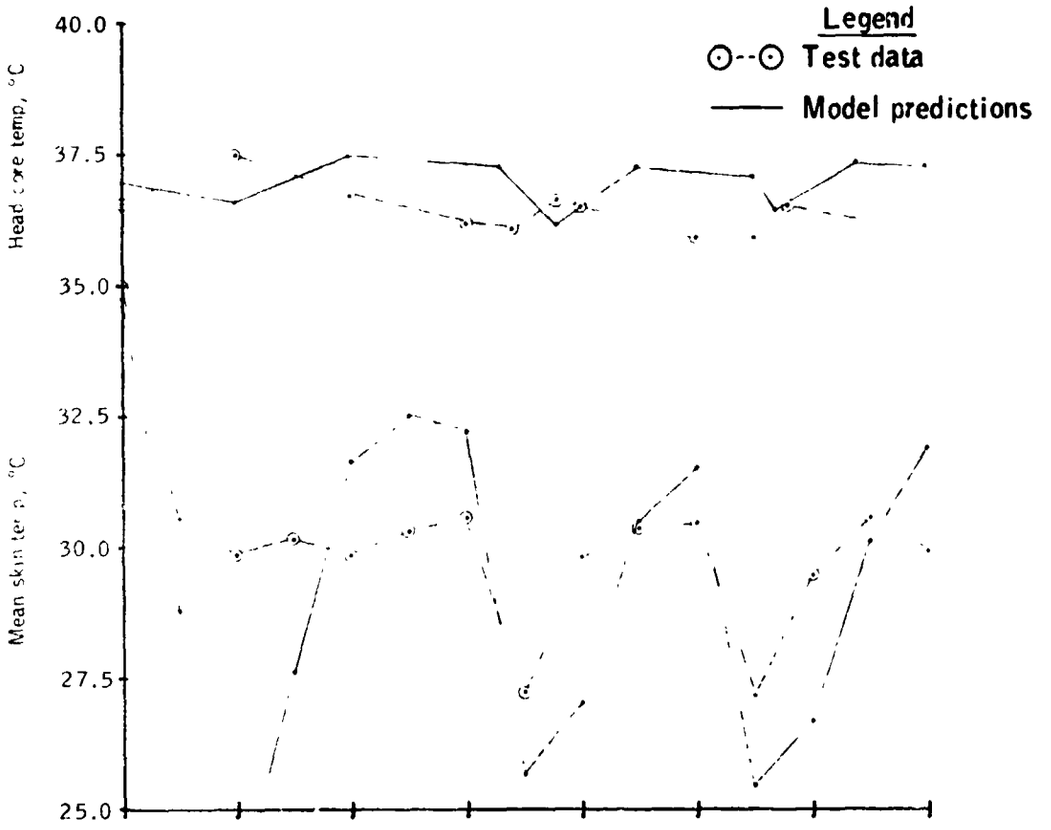

Figure 3-59a.- Head core (tympanic) temperature (upper curve) and mean skin temperature (lower curve) vs time for test 5.

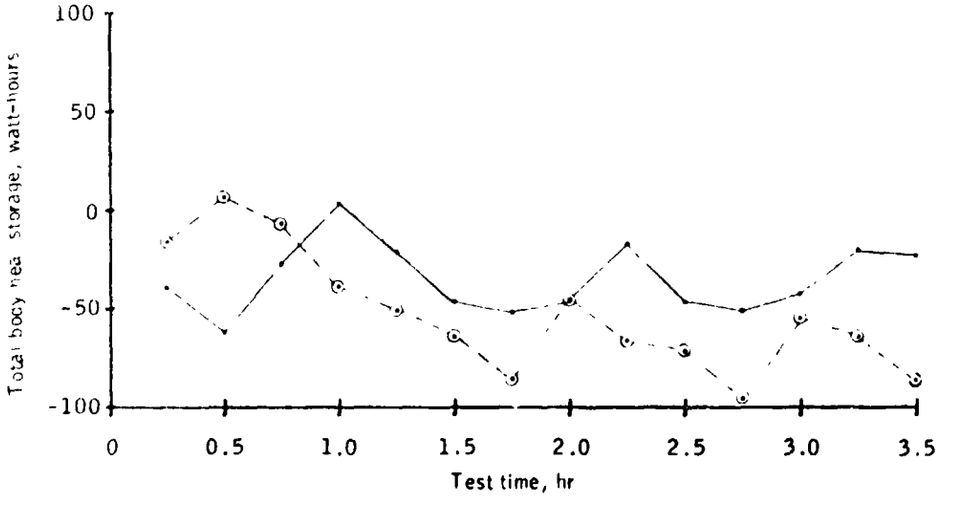

Figure 3-59b.- Total body heat storage vs time for t . 5.

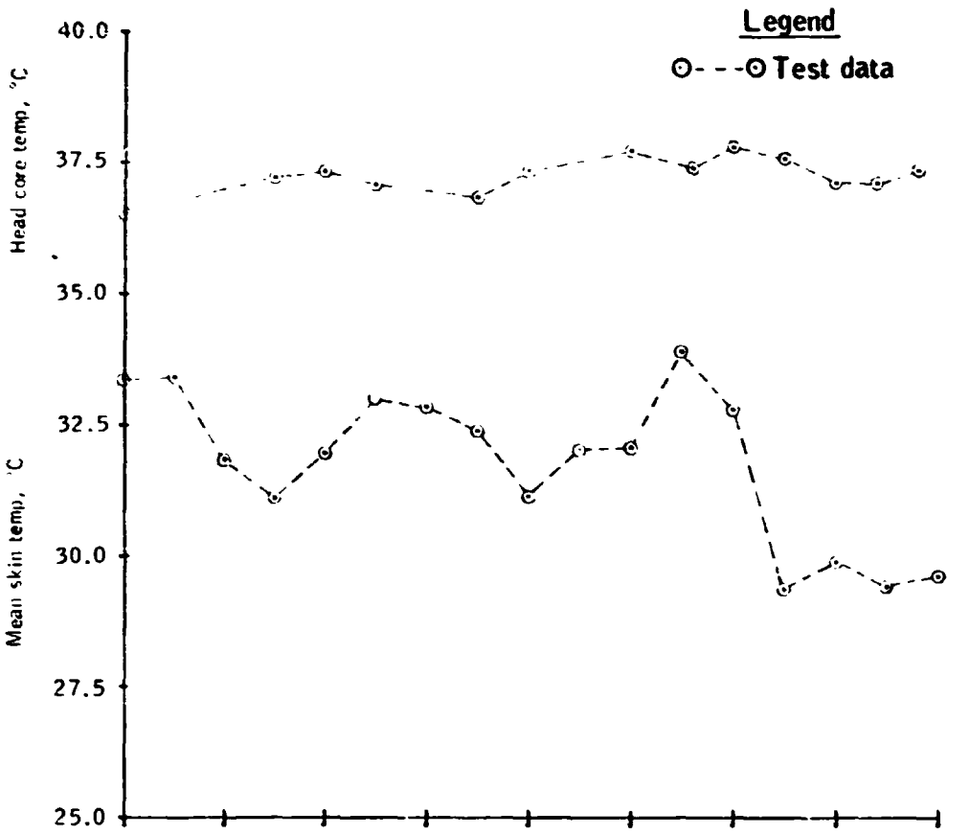

Figure 3-60a.- Head core (tympanic) temperature (upper curve) and mean skin temperature (lower curve) vs time for test 6.

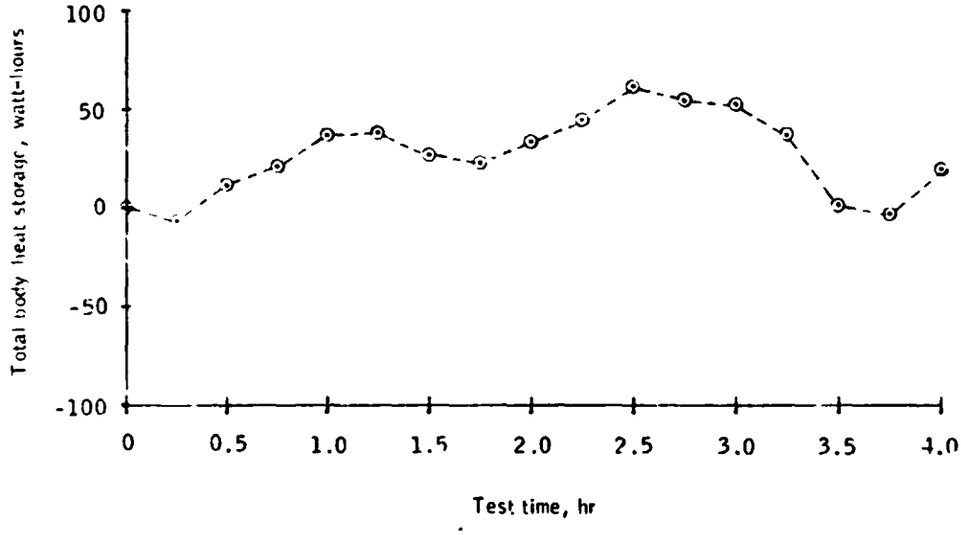

Figure 3-60b.- Total body heat storage vs time for test 6.

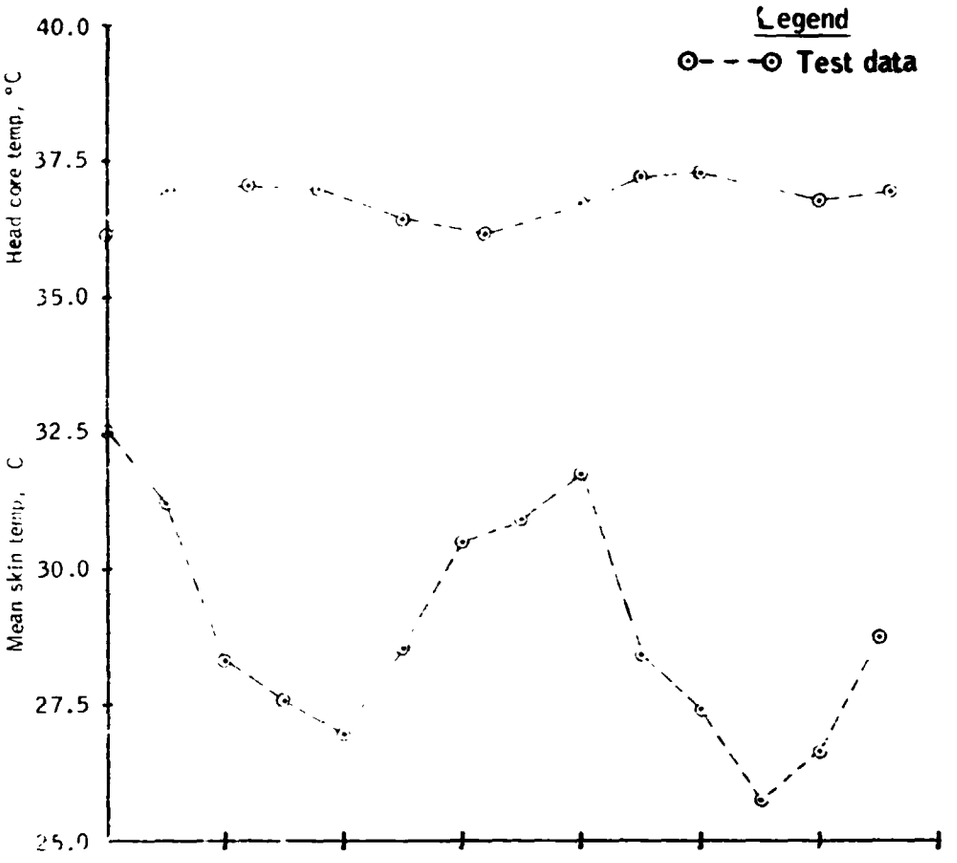

Figure 3-61a.- Head core (tympanic) temperature (upper curve) and mean skin temperature (lower curve) vs time for test 7.

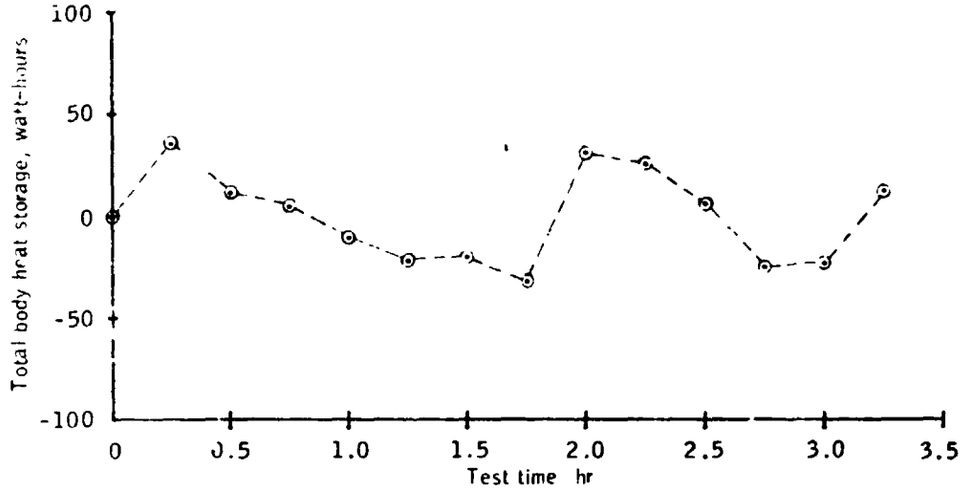

Figure 3-61b.- Total body heat storage vs time for test 7.

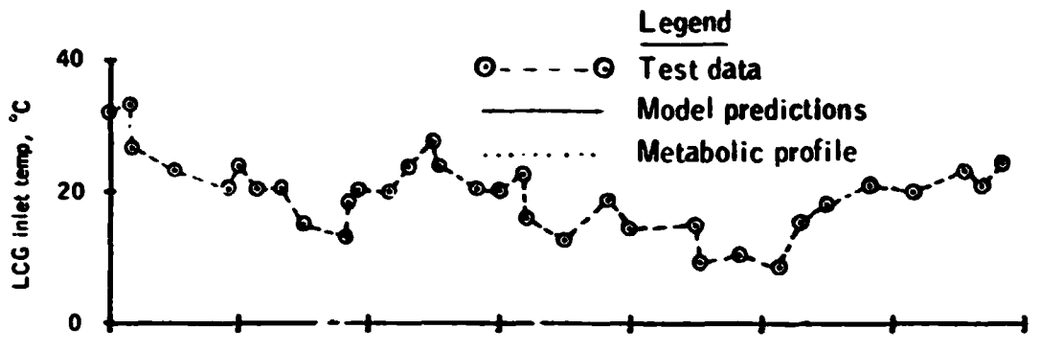

Figure 3-62a.- LCG inlet temperature selected by test subject vs time for test 1.

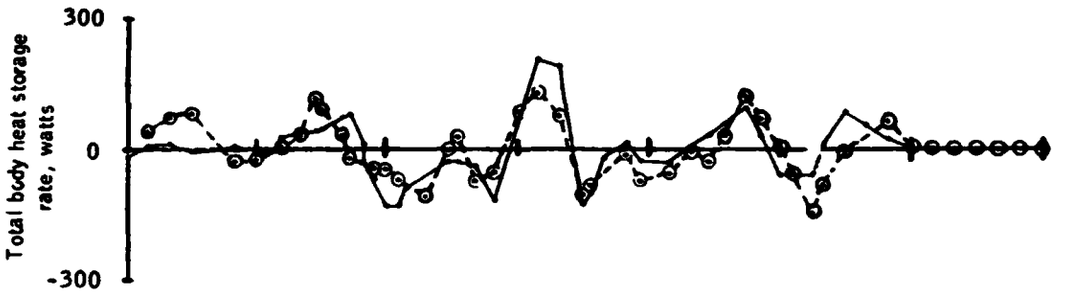

Figure 3-62b.- Total body heat storage rate vs time for test 1.

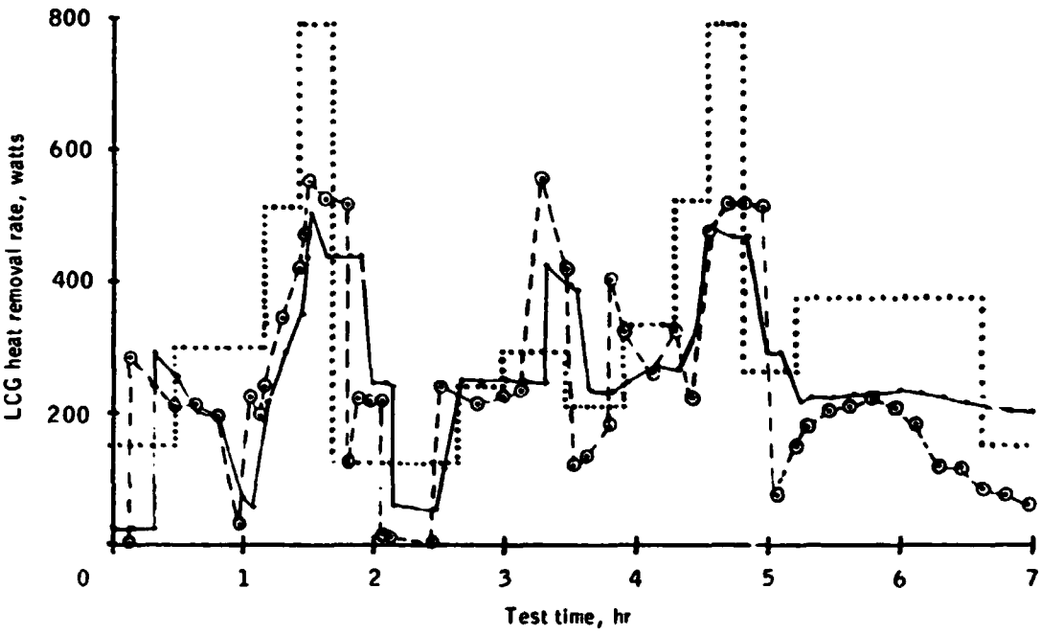

Figure 3-62c.- LCG heat removal rate vs time for test 1.

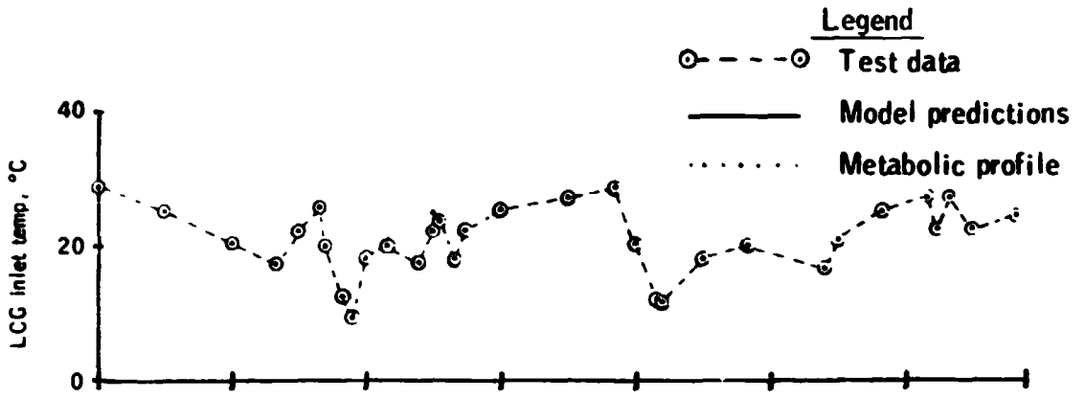

Figure 3-63a.- LCG inlet temperature selected by test subject vs time for test 2.

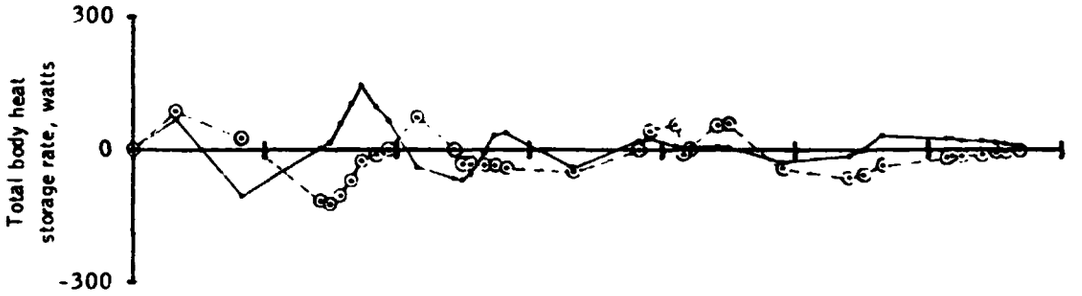

Figure 3-63b.- Total body heat storage rate vs time for test 2.

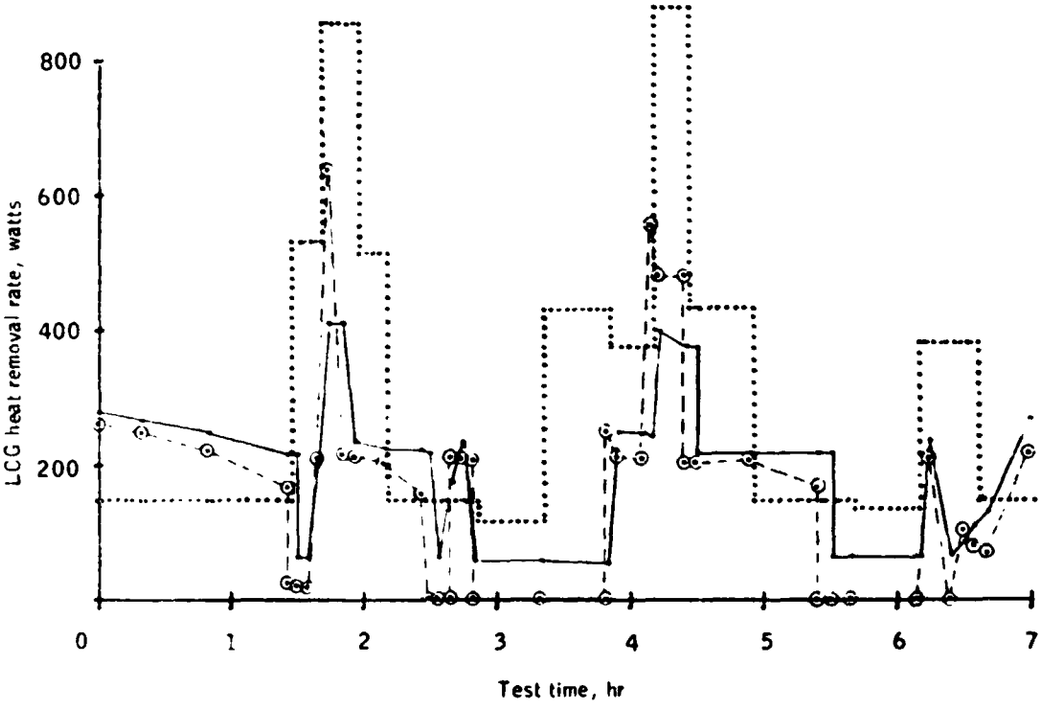

Figure 3-63c.- LCG heat removal rate vs time for test 2.

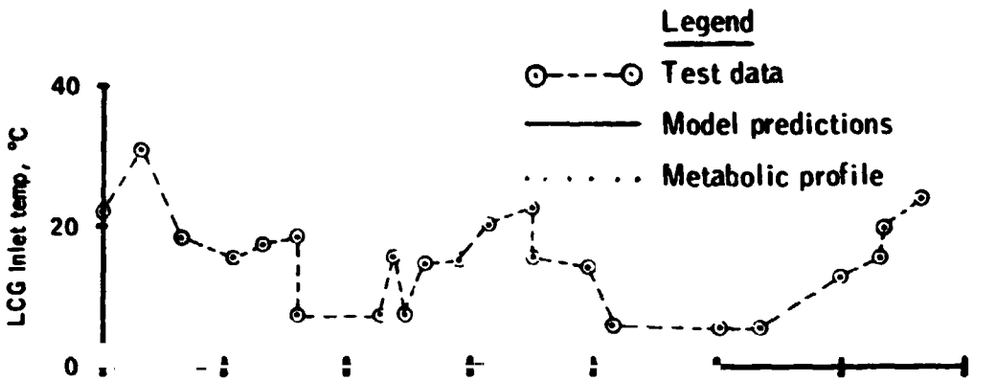

Figure 3-64a.- LCG inlet temperature selected by test subject vs time for test 3.

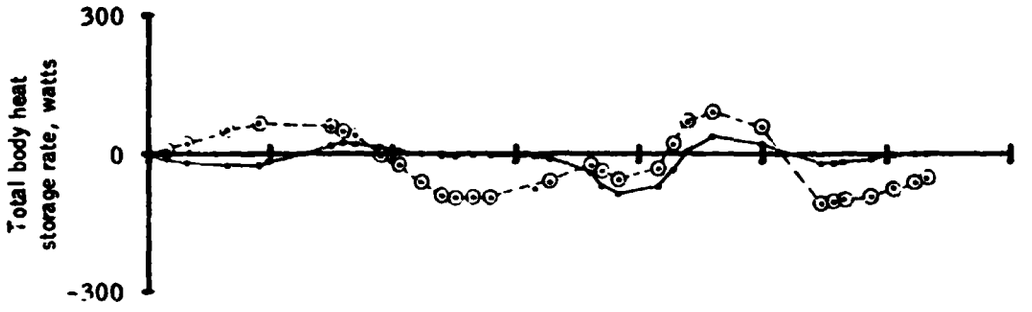

Figure 3-64b.- Total body heat storage rate vs time for test 3.

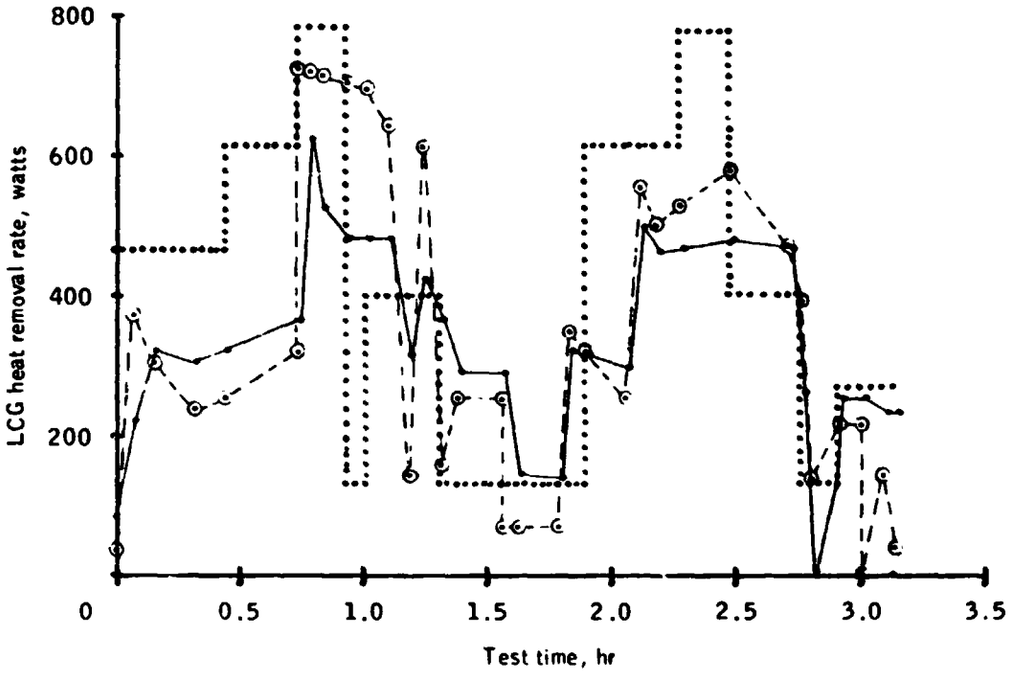

Figure 3-64c.- LCG heat removal rate vs time for test 3.

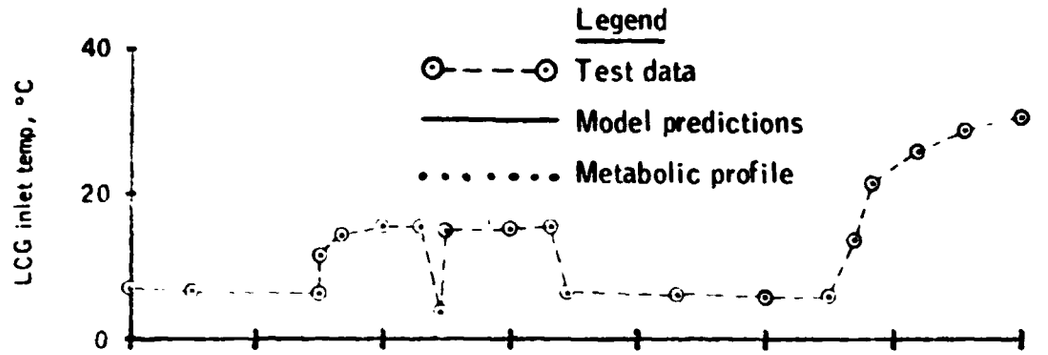

Figure 3-65a.- LCG inlet temperature selected by test subject vs time for test 4.

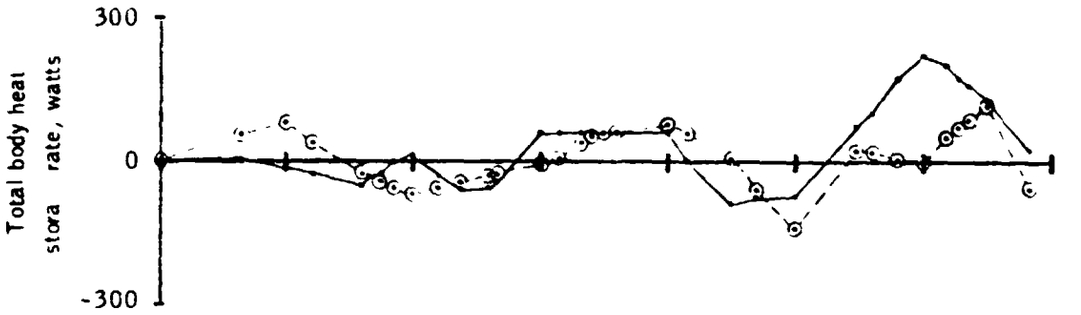

Figure 3-65b.- Total body heat storage rate vs time for test 4.

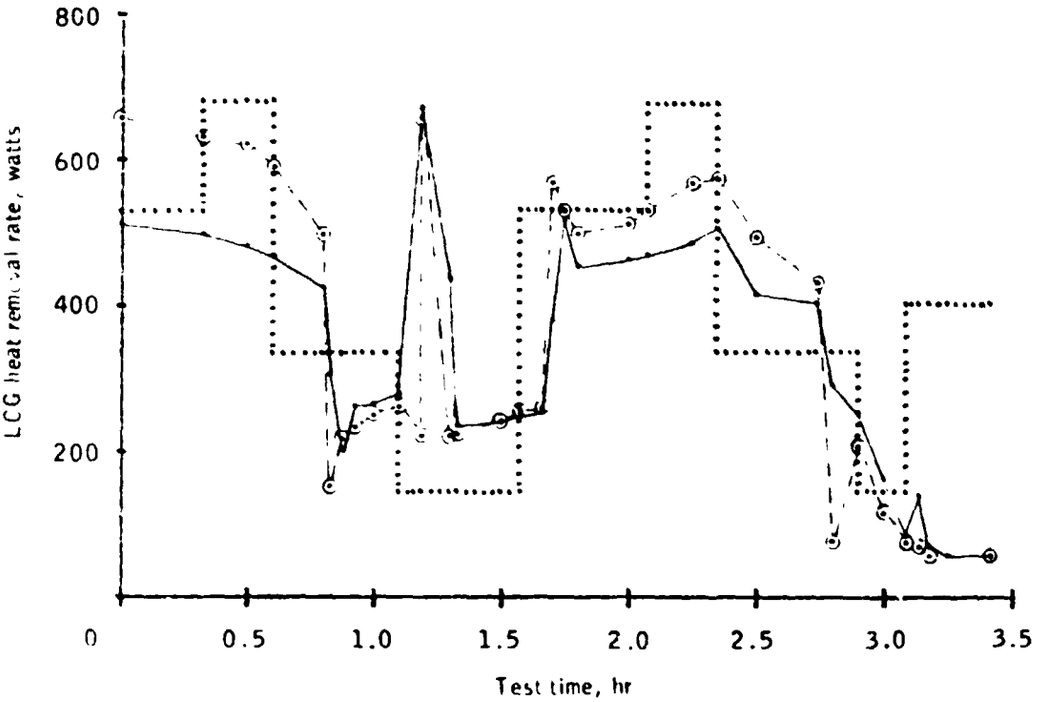

Figure 3-65c.- LCG heat removal rate vs time for test 4.

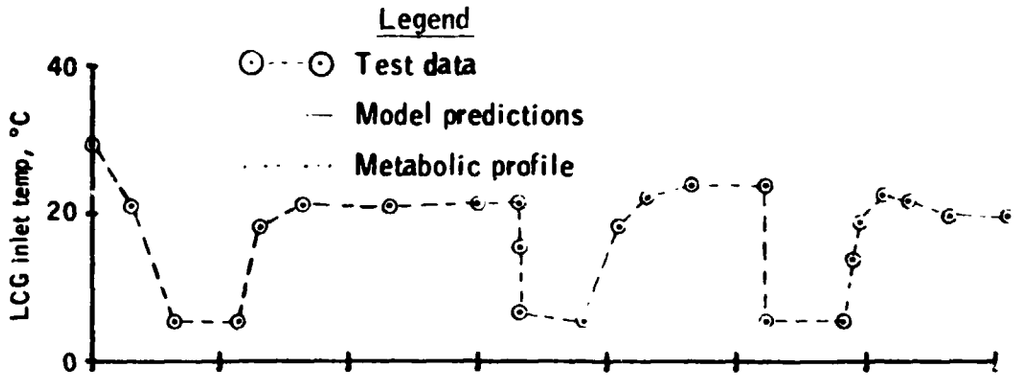

Figure 3-66a.- LCG inlet temperature selected by test subject vs time for test 5.

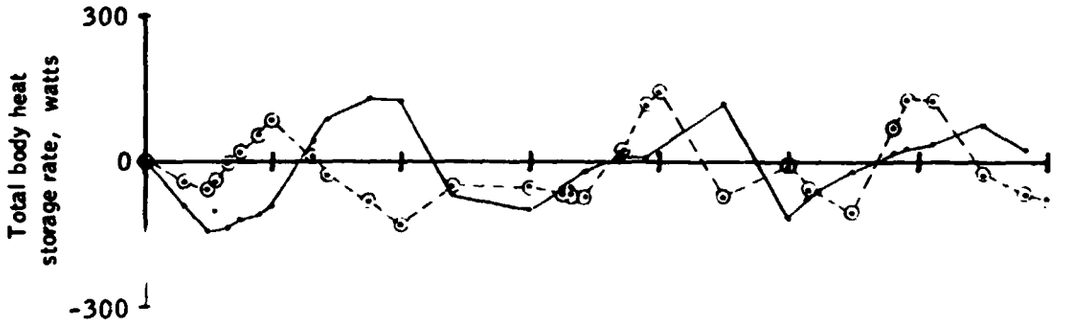

Figure 3-66b.- Total body heat storage rate vs time for test 5.

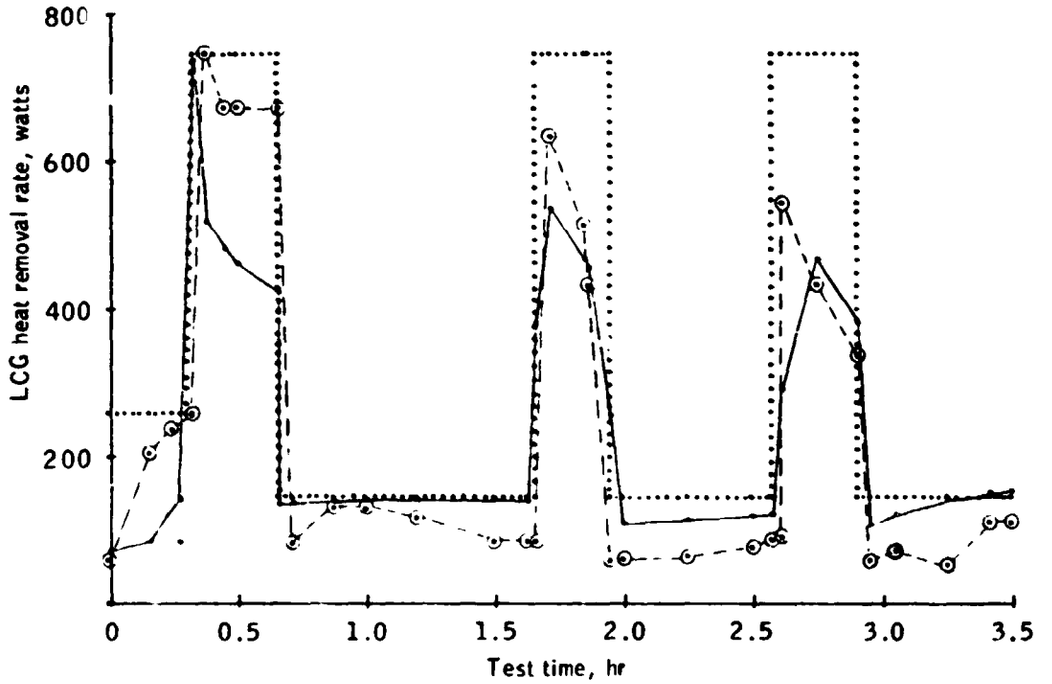

Figure 3-66c.- LCG heat removal rate vs time for test 5.

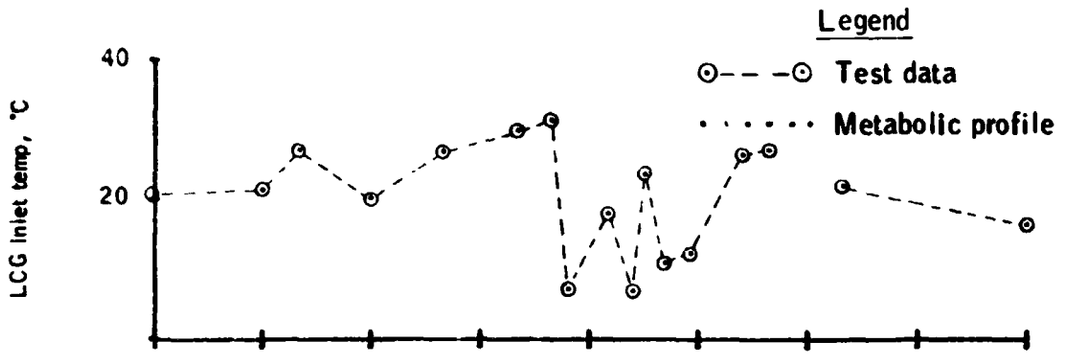

Figure 3-67a.- LCG inlet temperature selected by test subject vs time for test 6.

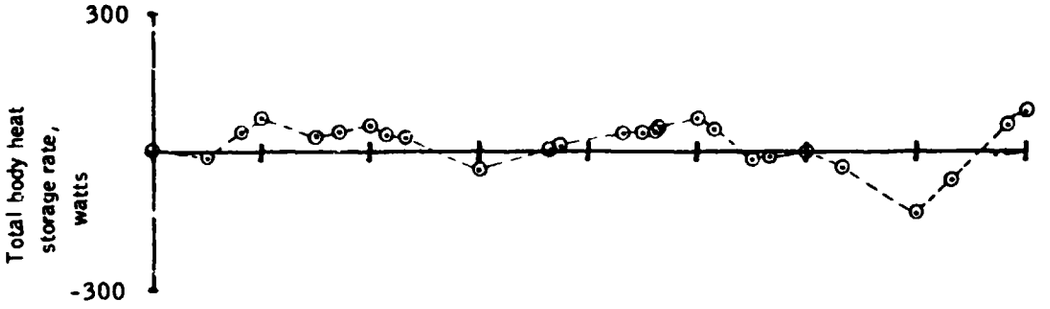

Figure 3-67b.- Total body heat storage rate vs time for test 6.

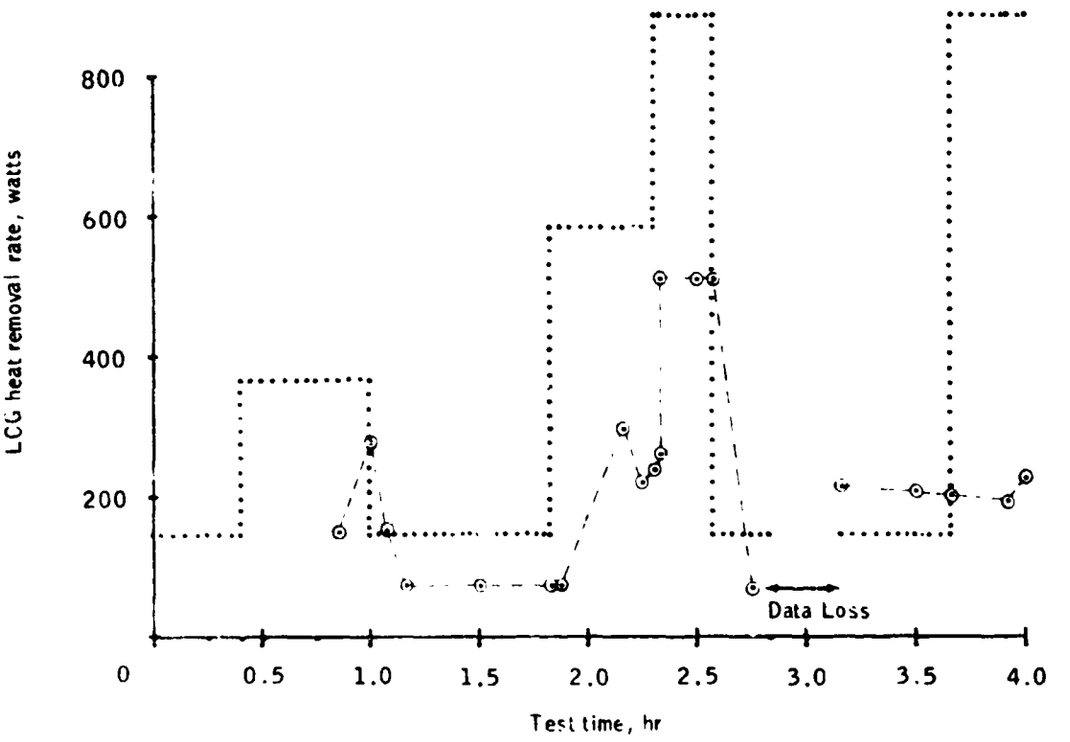

Figure 3-67c.- LCG heat removal rate vs time for test 6.

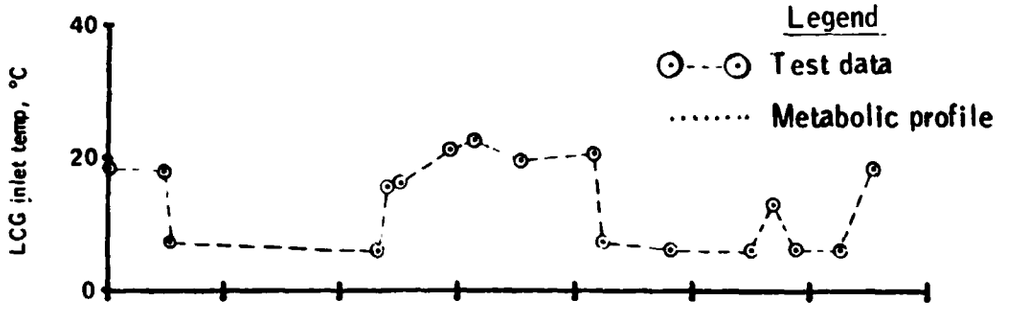

Figure 3-68a.- LCG inlet temperature selected by test subject vs time for test 7.

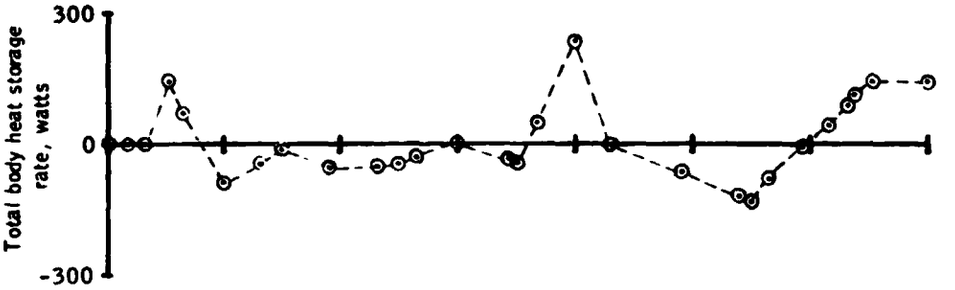

Figure 3-68b.- Total body heat storage rate vs time for test 7.

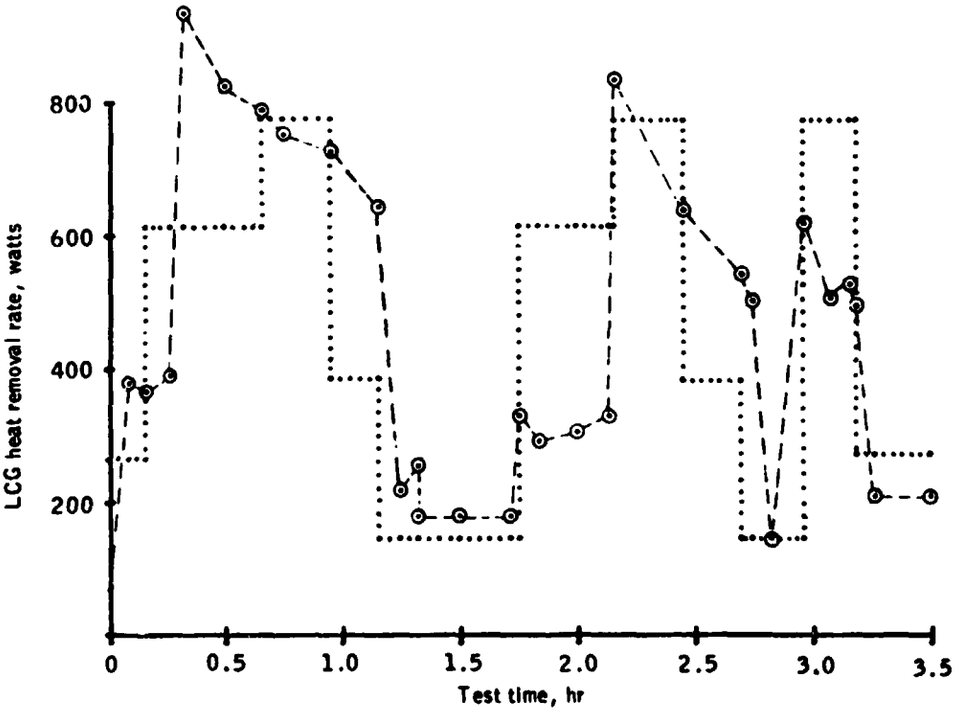

Figure 3-68c.- LCG heat storage rate vs time for test 7.

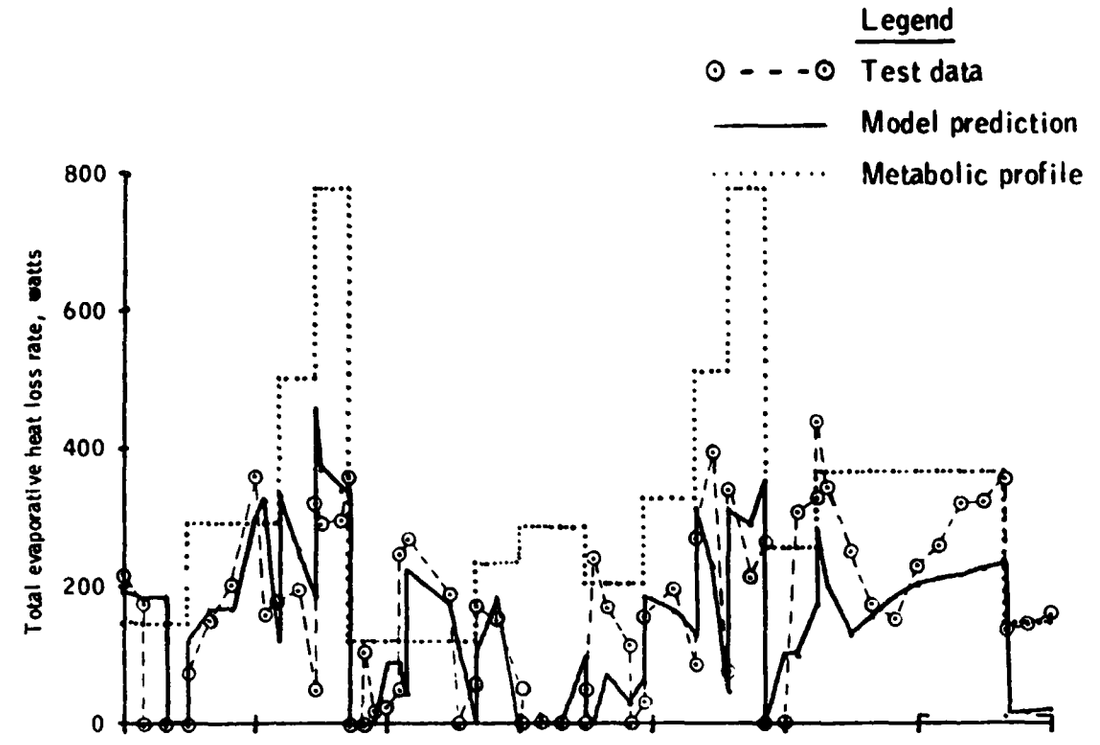

Figure 3-69a.- Total evaporative heat loss rate vs time for test 1.

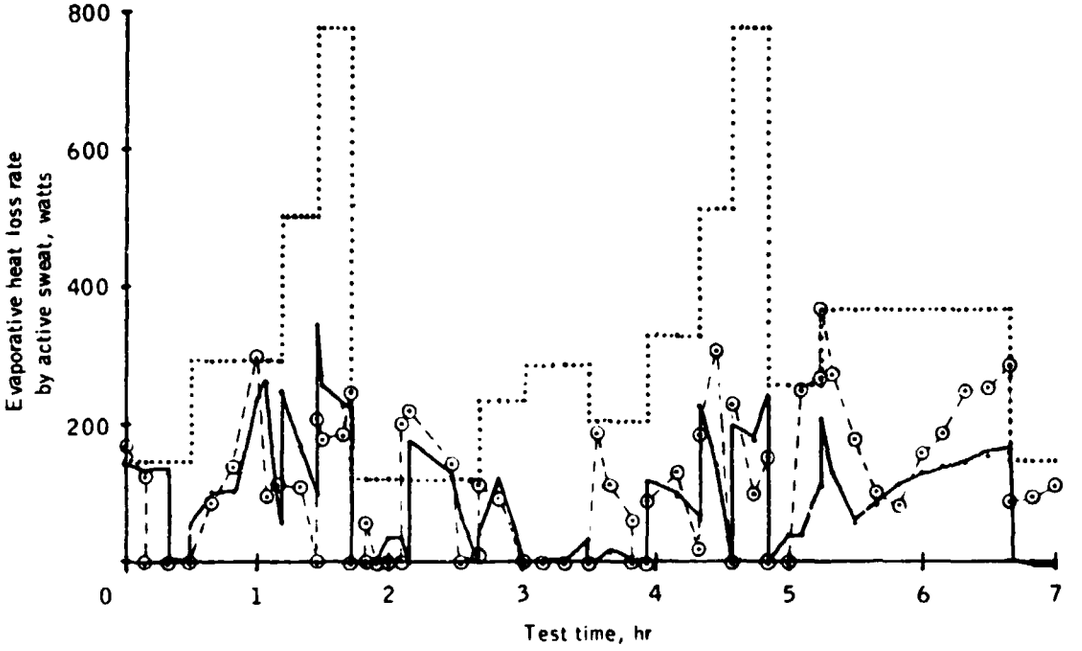

Figure 3-69b.- Evaporative heat loss rate due to active sweat vs time for test 1.

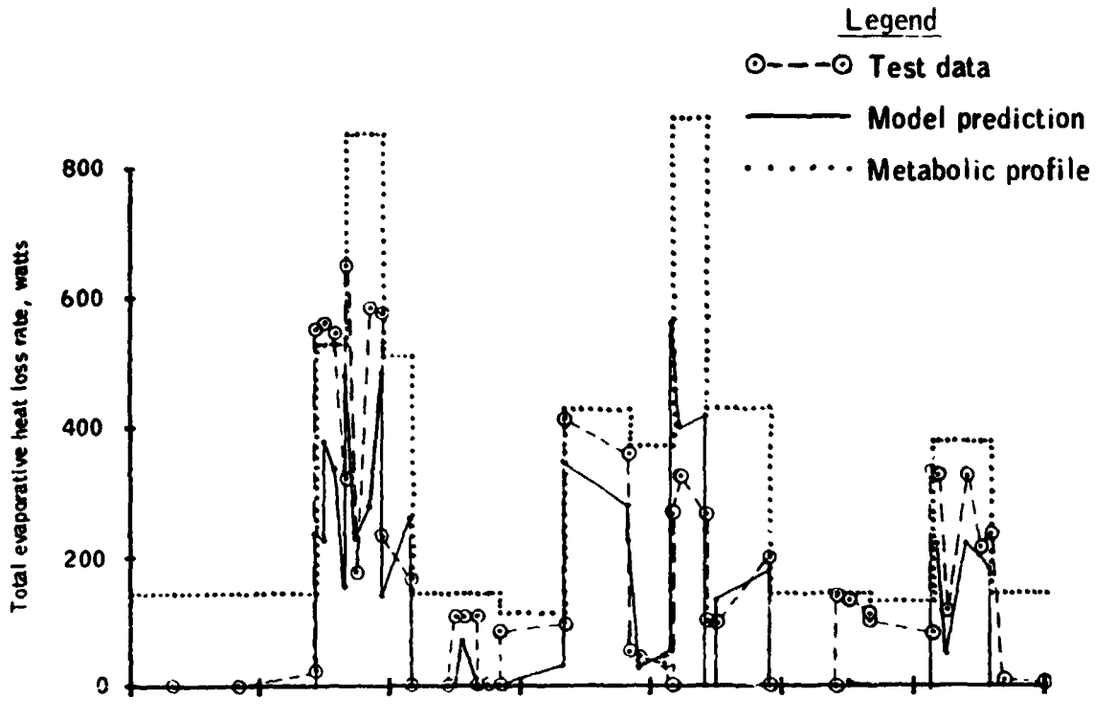

Figure 3-70a.- Total evaporative heat loss rate vs time for test 2.

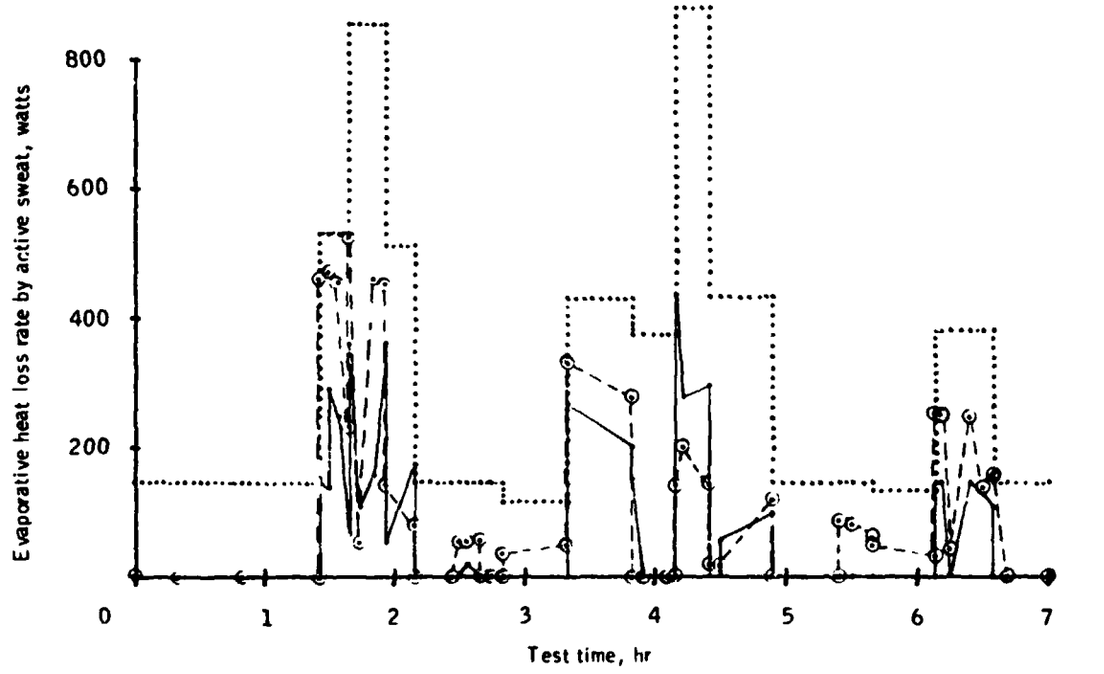

Figure 3-70b.- Evaporative heat loss rate due to active sweat vs time for test 2.

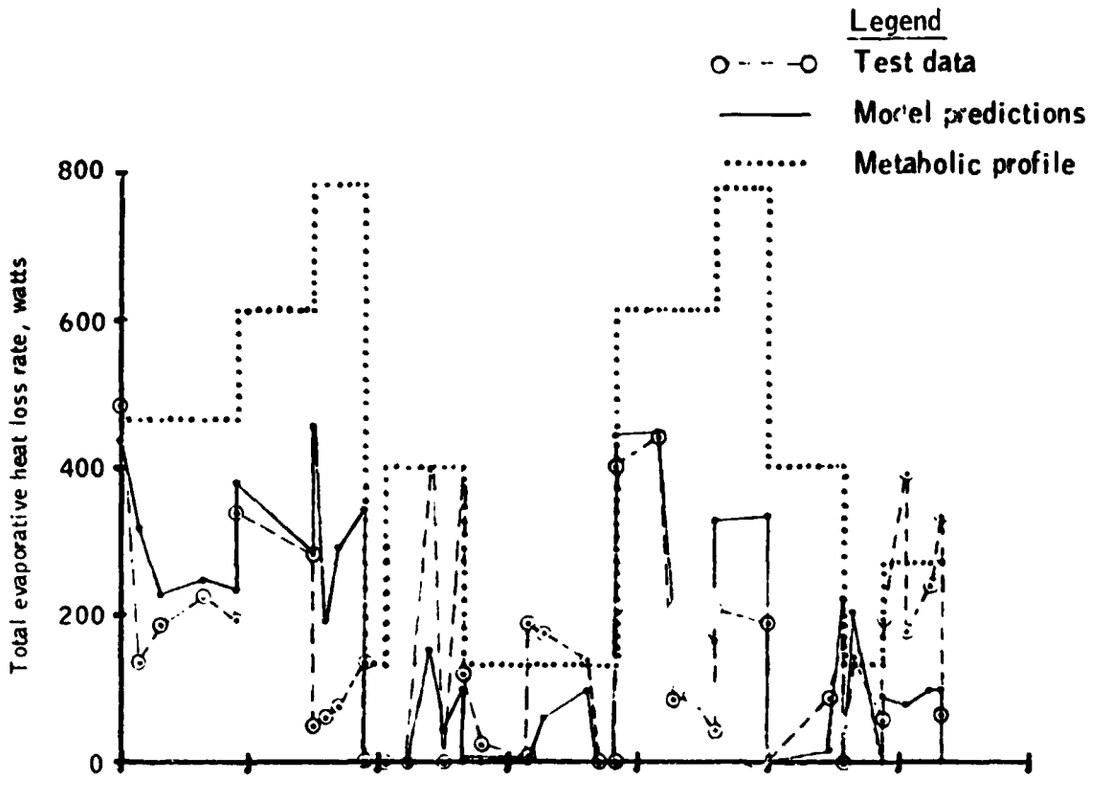

Figure 3-71a.- Total evaporative heat loss rate vs time for test 3.

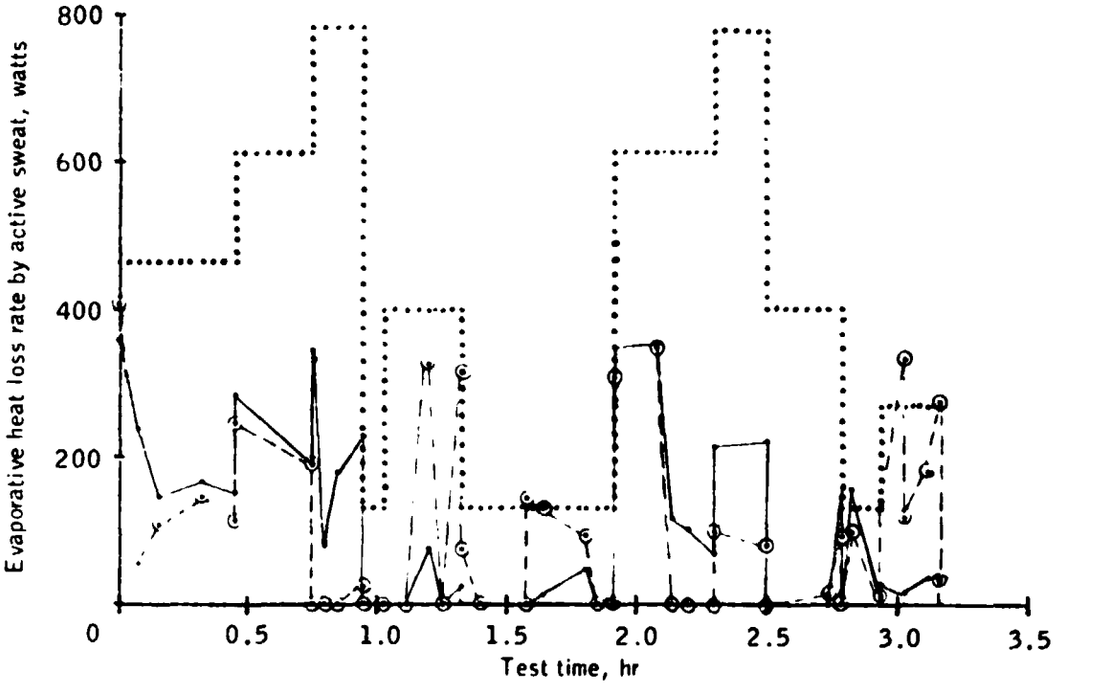

Figure 3-71b.- Evaporative heat loss rate due to active sweat vs time for test 3.

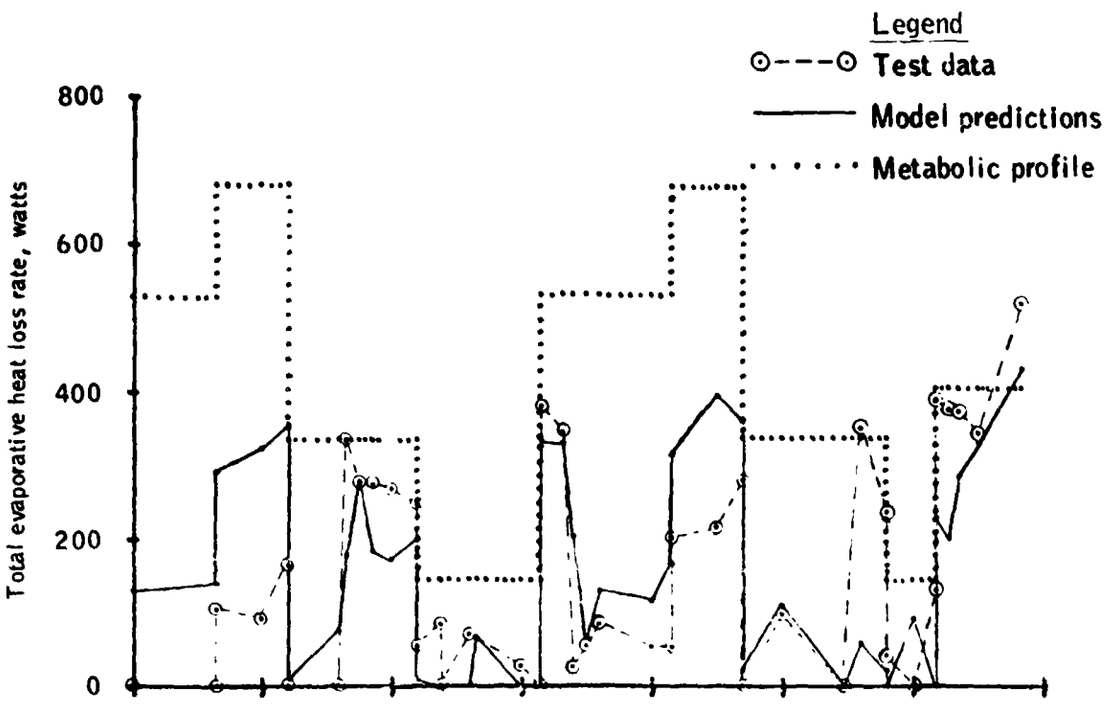

Figure 3-72a.- Total evaporative heat loss rate vs time for test 4.

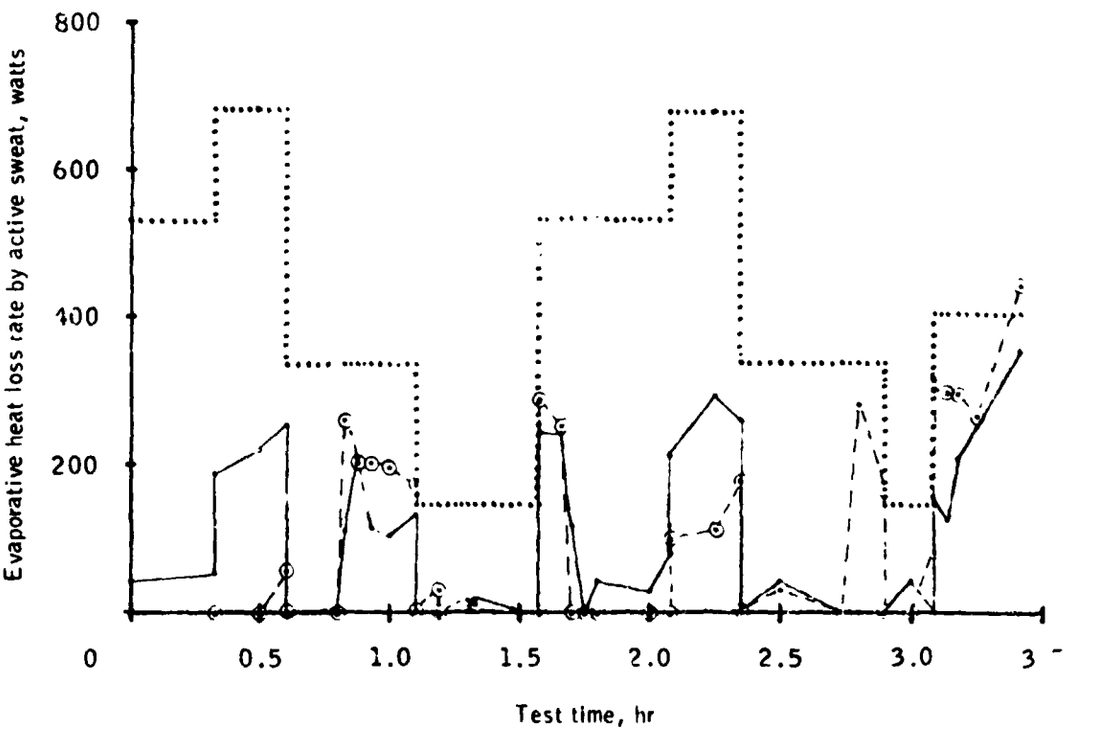

Figure 3-72b.- Evaporative heat loss rate due to active sweat vs time for test 4.

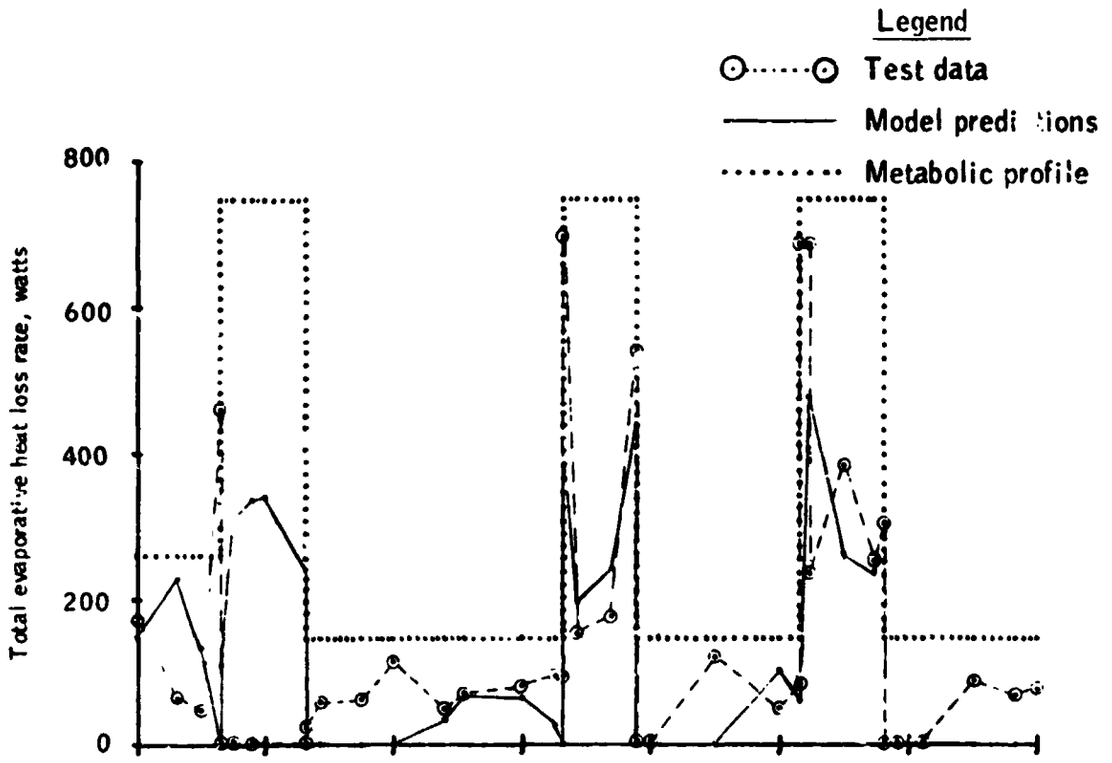

Figure 3-73a.- Total evaporative heat loss rate vs time for test 5.

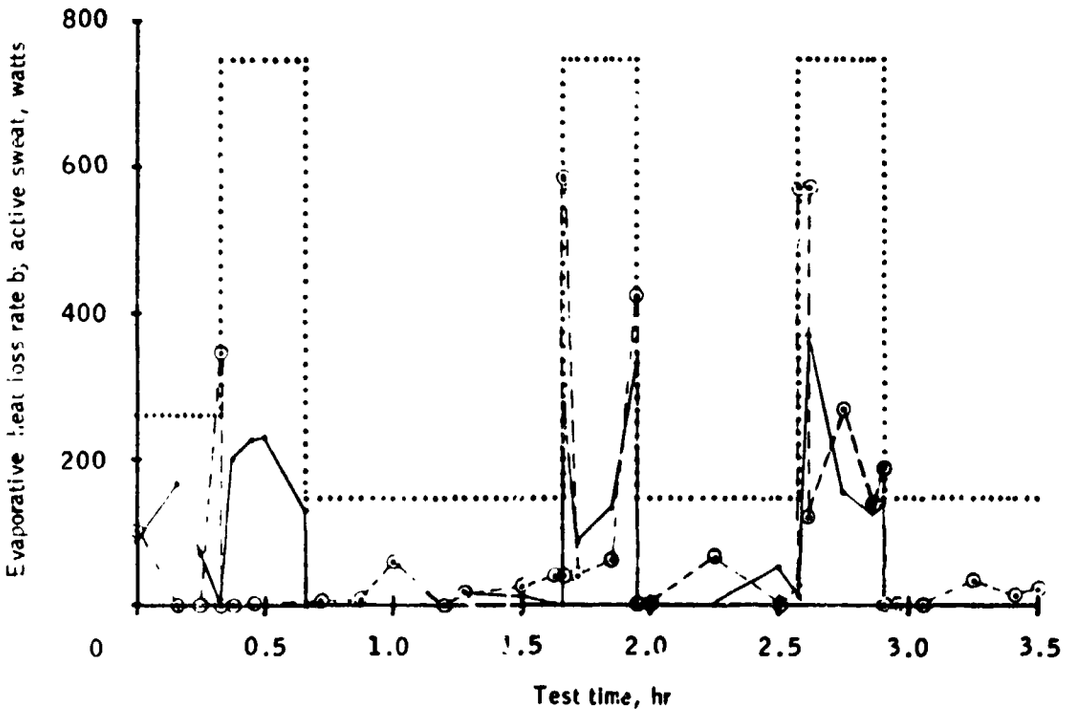

Figure 3-73b.- Evaporative heat loss rate due to active sweat vs time for test 5.

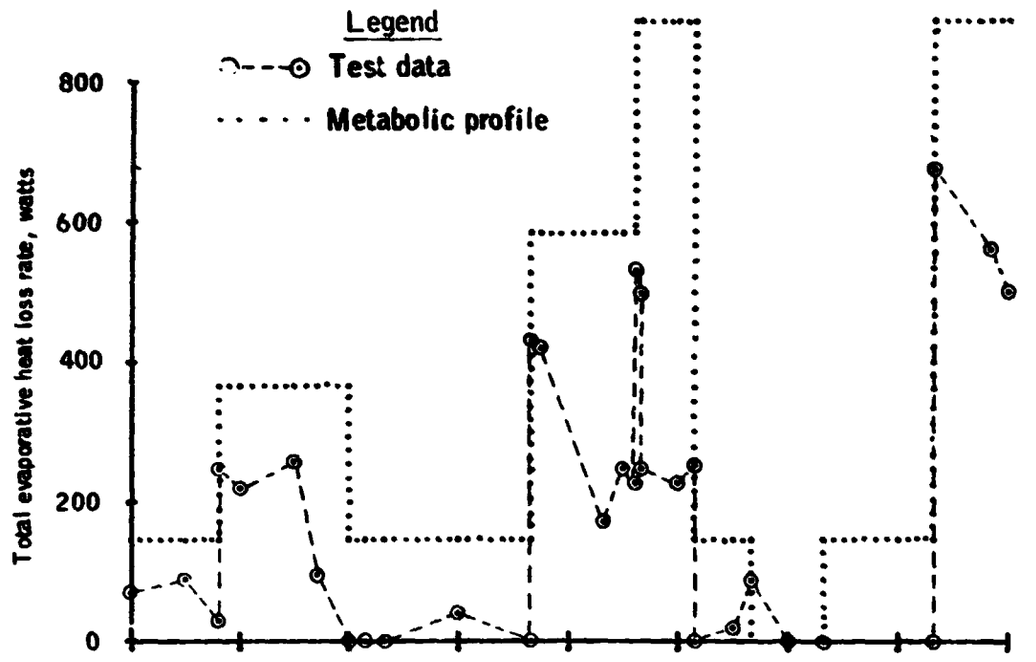

Figure 3-74a.- Total evaporative heat loss rate vs time for test 6.

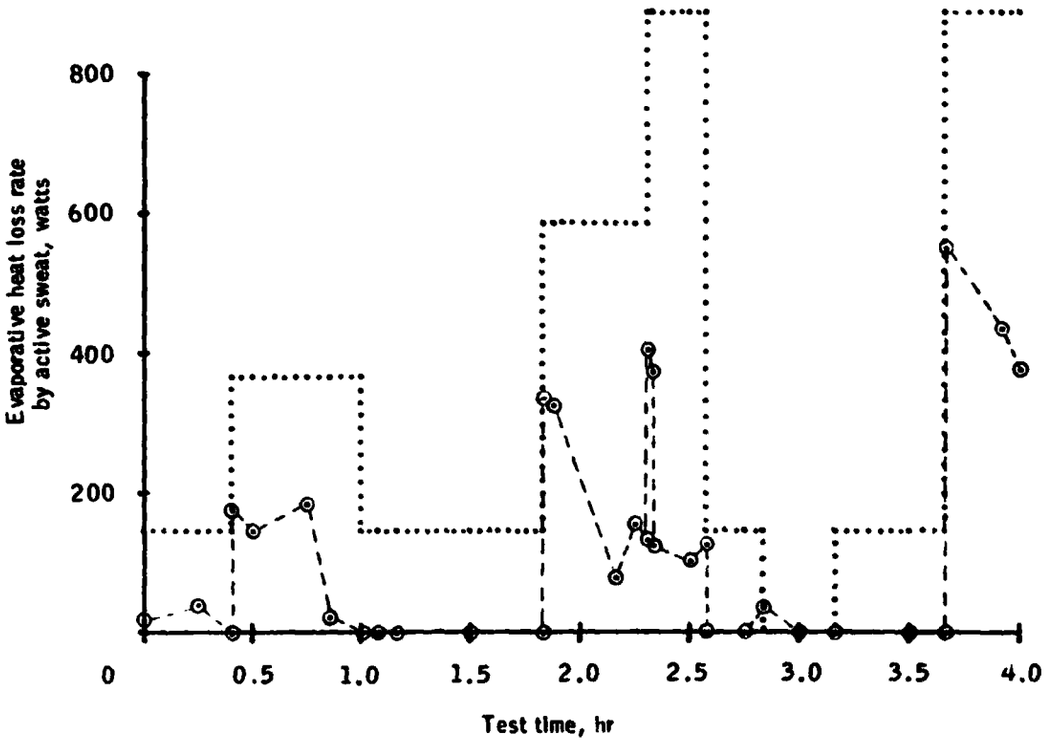

Figure 3-74b.- Evaporative heat loss rate due to active sweat vs time for test 6.

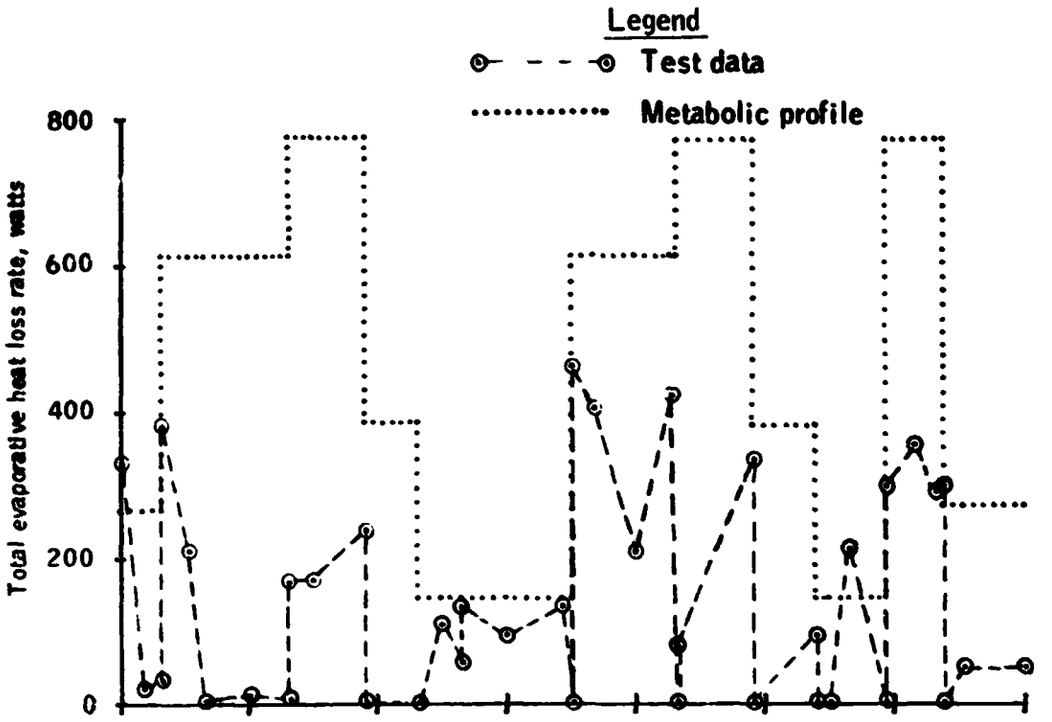

Figure 3-75a.- Total evaporative heat loss rate vs time for test 7.

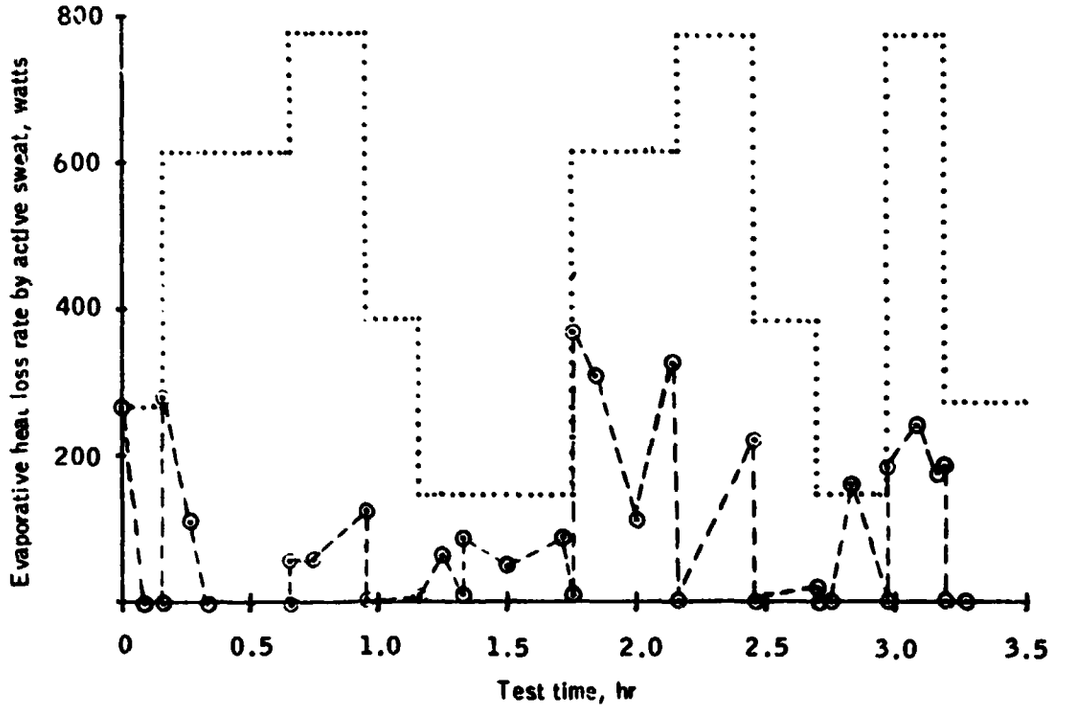

Figure 3-75b.- Evaporative heat loss rate due to active sweat vs time for test 7.

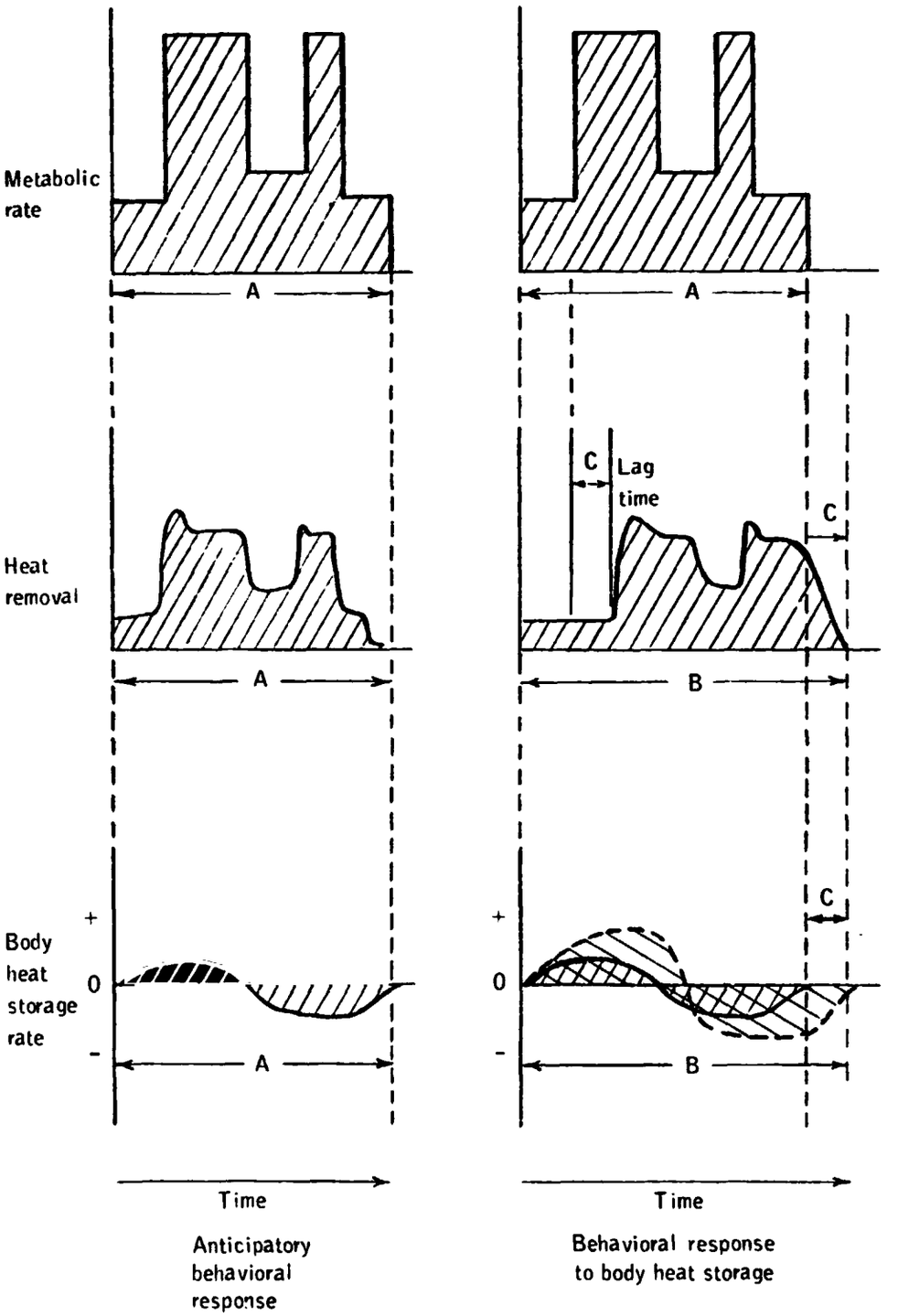

Figure 3-76.- Metabolic rate, heat removal, and body heat storage rate for behavioral response to body heat storage and anticipatory behavioral response.

TABLE 3-5.- STEADY STATE HEAD CORE AND MEAN SKIN TEMPERATURE

A = Actual
P = Predicted

TEST CONDITIONS	DATA	METABOLIC RATE, WATTS 100	150	200	250	300	350	400	450	500	550	600	650
Warm LCG Inlet Temperatures 18-22°C	LCG Inlet Temperature °C		21			21	19	21	21	18	19		
	Mean Skin Temperature A		30			31^{2}	31^{7}	33	30^{3}	31	29		
	Mean Skin Temperature P		32^{5}			30	31	-	30	31	30		
	Head Core Temperature A		36^{5}			37^{5}	37^{8}	37^{4}	36^{8}	36^{3}	36^{8}		
	Head Core Temperature P		37^{4}			37^{3}	37^{5}	-	36^{9}	36^{9}	36^{8}		
Moderate LCG Temps. = 13-16°C	LCG Inlet Temperature, °C		14			15	14	16		13	16	13	
	Mean Skin Temperature A		28.5			30^{2}	27^{8}	28^{8}		28^{6}	31^{8}	32	
	Mean Skin Temperature P		25.6			26^{7}	26^{1}	27^{9}		27	29^{8}	-	
	Head Core Temperature A		36.8			37^{5}	37^{4}	36^{7}		37^{5}	37	37^{4}	
	Head Core Temperature P		36.8			37^{3}	37^{6}	37^{3}		37^{4}	36^{8}	-	
Cold LCG Inlet Temps = 7-11°C	LCG Temperature °C									6	9	11	7	6
	Mean Skin Temperature A									21^{3}	27^{8}	28^{8}	28^{5}	28^{7}
	Mean Skin Temperature P									26	26^{2}	-	27^{5}	27^{0}
	Head Core Temperature A									37^{3}	37^{6}	36^{6}	37^{5}	37^{9}
	Head Core Temperature P									37^{3}	37^{3}	-	37	37^{2}

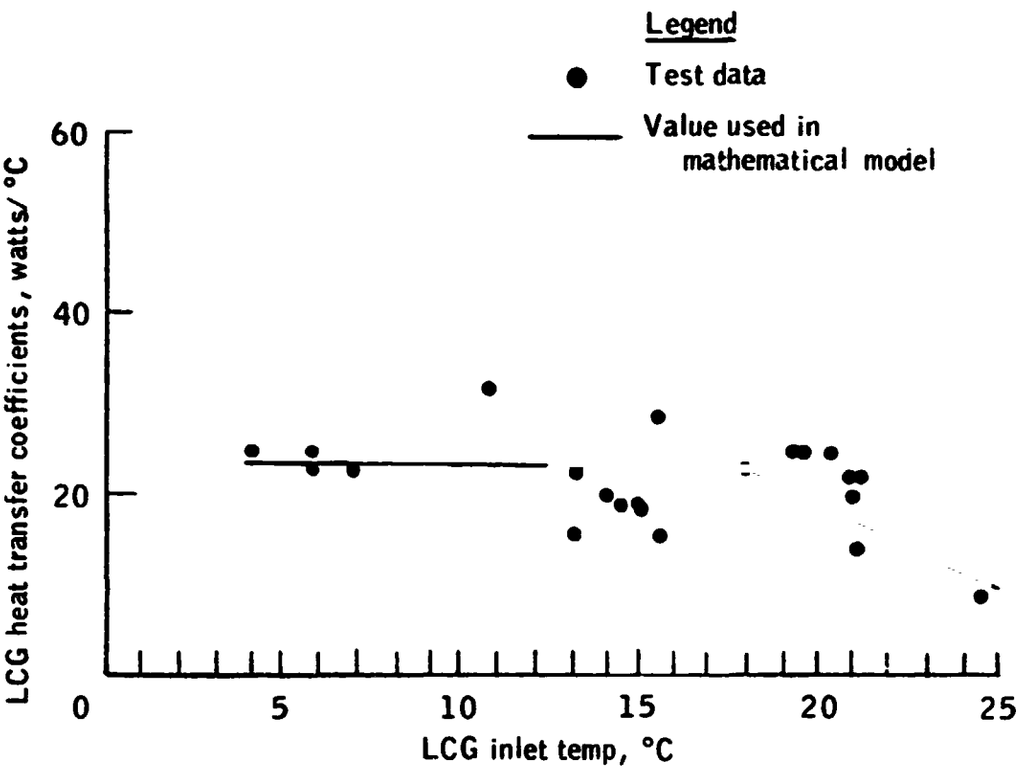

Figure 3-77.- LCG heat transfer coefficient vs LCG inlet temperature.

Legend

Parameter	Test data symbol	Test condition	Mathematical model predictions
LCG heat removal	●	Net environmental heat gain = 65 - 79 watts into suit	——— .
	●	Net environmental heat gain = 117 - 137 watts into suit	
Total evaporative heat loss	○	Net environmental heat gain = 65 - 79 watts into suit	- - - - .
	○	Net environmental heat gain = 117 - 137 watts into suit	

1. Model prediction for environmental heat gain of 126 watts into suit
2. Model prediction for environmental heat gain of 0 watts
3. Model prediction for environmental heat loss of 72 watts out of suit

Figure 3-78.- Predicted and actual steady-state LCG and total evaporative heat removal rates vs metabolic rate for hot, cold, and neutral environments and cold LCG inlet temperatures (7° to 9° C).

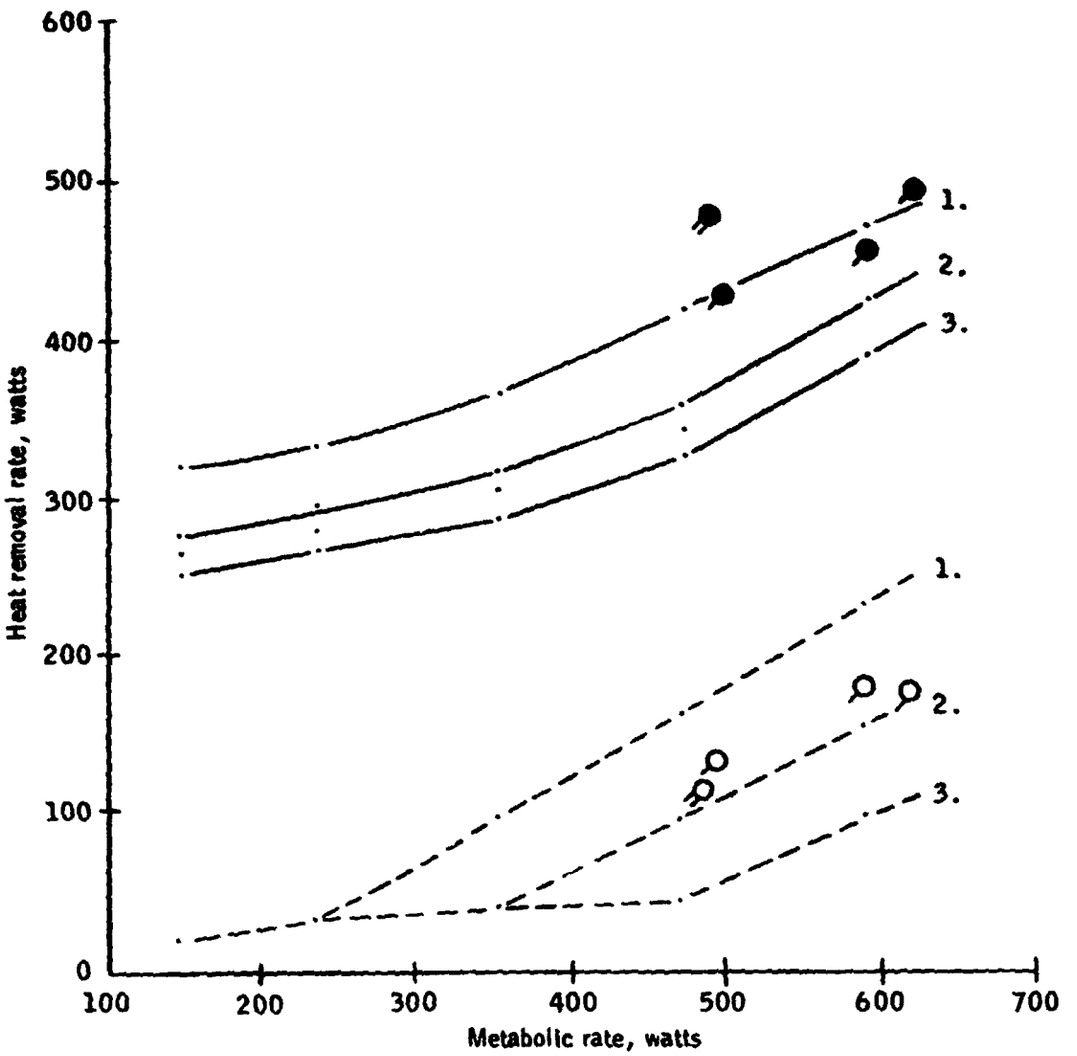

Figure 3-78.- Concluded.

Legend

Parameter	Test data symbol	Test condition	Mathematical model predictions
LCG heat removal	●	Net environmental heat loss = 67-72 watts out of suit	————
	●	Net environmental heat loss = 35 watts out of suit	
	●	Net environmental heat gain = 65-79 watts into suit	
	●	Net environmental heat gain = 117-137 watts into suit	
Total evaporative heat loss	○	Net environmental heat loss = 67-72 watts out of suit	- - - - - - -
	○	Net environmental heat loss = 35 watts out of suit	
	○	Net environmental heat gain = 65-79 watts into suit	
	○	Net environmental heat gain = 117-137 watts into suit	

1. Model prediction for environmental heat gain of 126 watts into suit
2. Model prediction for environmental heat gain of 0 watts
3. Model prediction for environmental heat loss of 72 watts out of suit

Figure 3-79.- Predicted and actual steady-state LCG and total evaporative heat removal rates vs metabolic rate for hot, cold, and neutral environments and moderate LCG inlet temperatures (13° to 16° C).

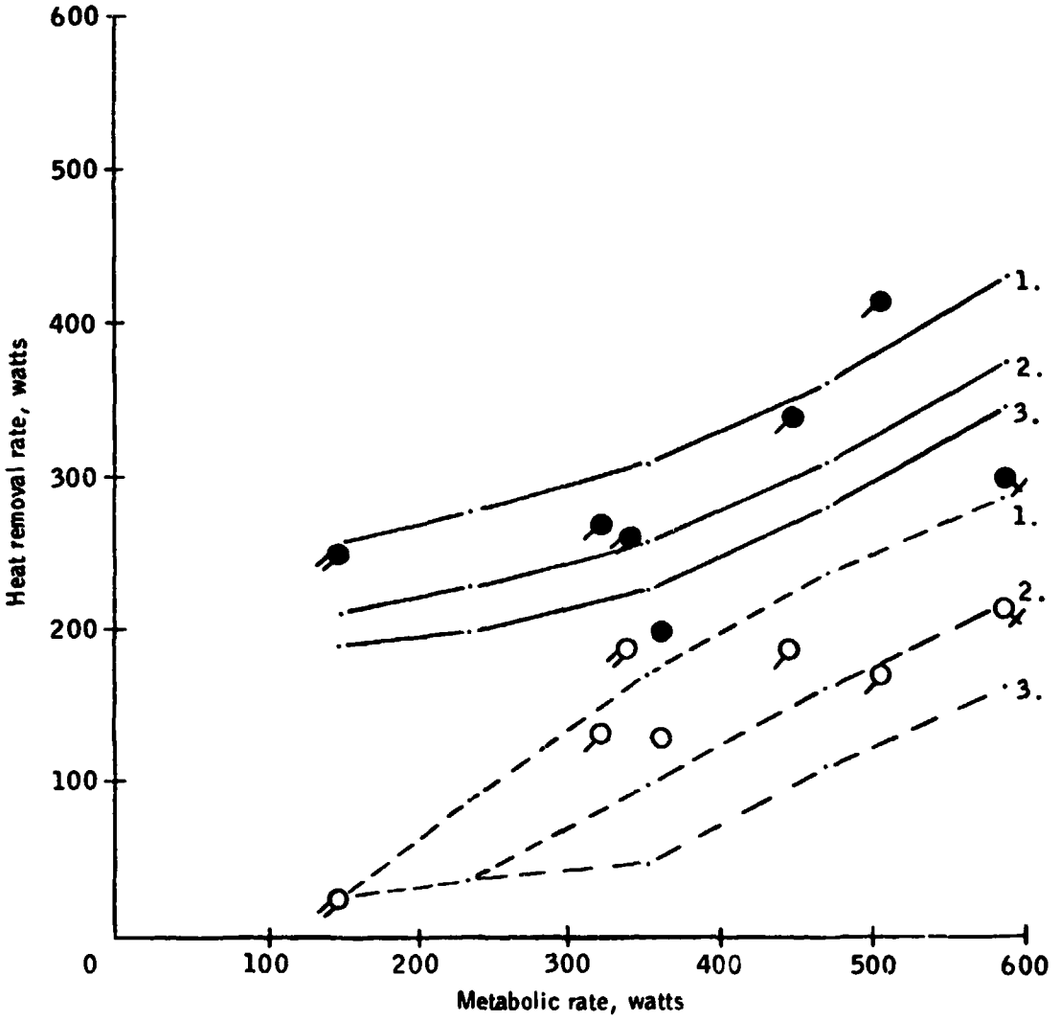

Figure 3-79.- Concluded.

Legend

Parameter	Test data symbol	Test condition	Mathematical model predictions
LCG heat removal		Net environmental heat loss = 67-72 watts out of suit	——— .
		Net environmental heat loss = 35 watts out of suit	
		Net environmental heat gain = 65-79 watts into suit	
		Net environmental heat gain = 117-137 watts into suit	
Total evaporative heat loss		Net environmental heat loss = 67-72 watts out of suit	- - - - - - .
		Net environmental heat loss = 35 watts out of suit	
		Net environmental heat gain = 65-79 watts into suit	
		Net environmental heat gain = 117-137 watts into suit	

1. Model prediction for environmental heat gain of 126 watts into suit
2. Model prediction for environmental heat gain of 0 watts
3. Model prediction for environmental heat loss of 72 watts out of suit

Figure 3-80a.- Predicted and actual steady-state LCG heat removal rate vs metabolic rate for hot, cold, and neutral environments, and warm LCG inlet temperatures (19° to 22° C).

Figure 3-80b.- Predicted and actual steady-state total evaporative heat loss rate vs metabolic rate, for hot, cold, and neutral environments and warm LCG inlet temperatures (19° to 22° C).

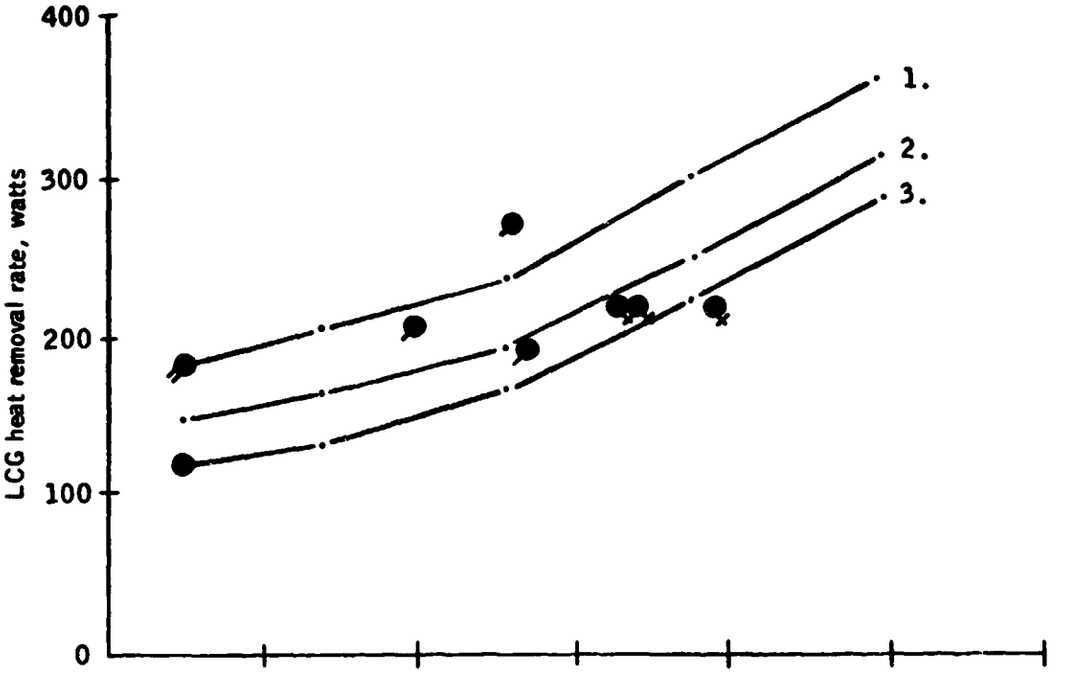

Figure 3-80a.- Concluded.

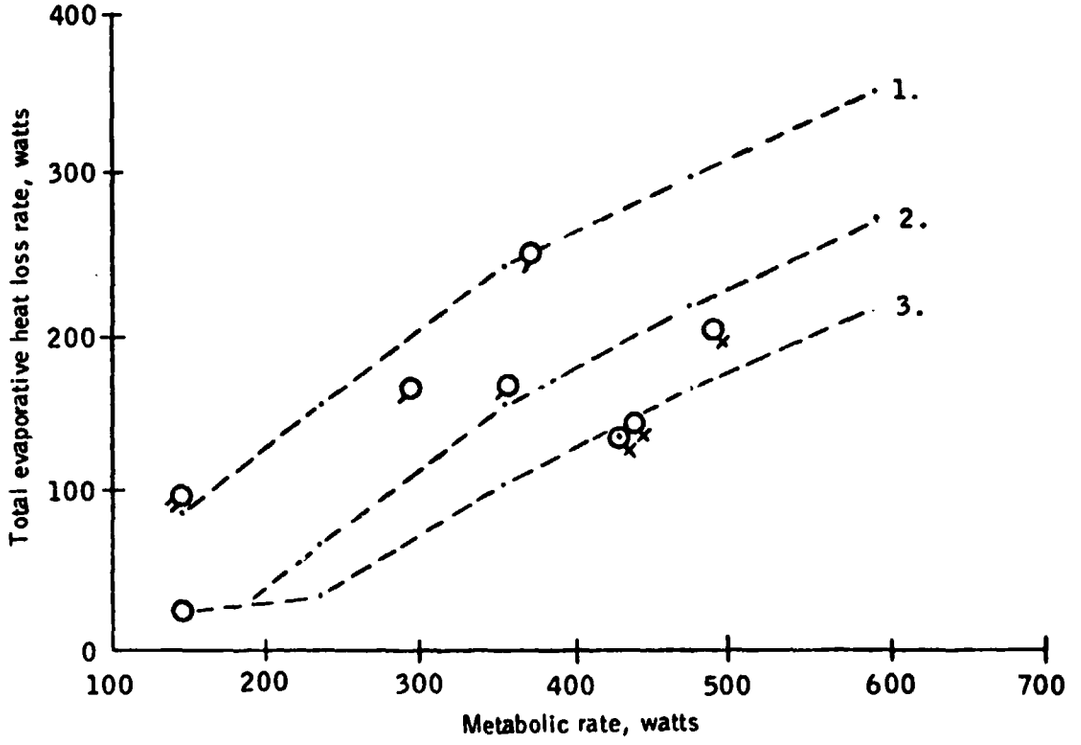

Figure 3-80b.- Concluded.

Legend

Parameter	Test data symbol	Test condition	Mathematical model predictions
LCG heat removal	●	Metabolic rate = 583 watts, LCG inlet temp = 7°C	—— 1.
	●	Metabolic rate = 340-358 watts, LCG inlet temp = 14-16°C	— — 2.
	▲	Metabolic rate = 146 watts, LCG inlet temp = 21°C	—— 3.
Total evaporative heat loss	◇	Metabolic rate = 583 watts, LCG inlet temp = 7°C	----- 1.
	○	Metabolic rate = 340-358 watts, LCG inlet temp = 14-16°C	----- 2.
	△	Metabolic rate = 146 watts, LCG inlet temp = 21°C	----- 3.

Figure 3-81.- Steady-state LCG and total evaporative heat removal rates vs net environmental heat gain, for constant metabolic rates and LCG inlet temperatures.

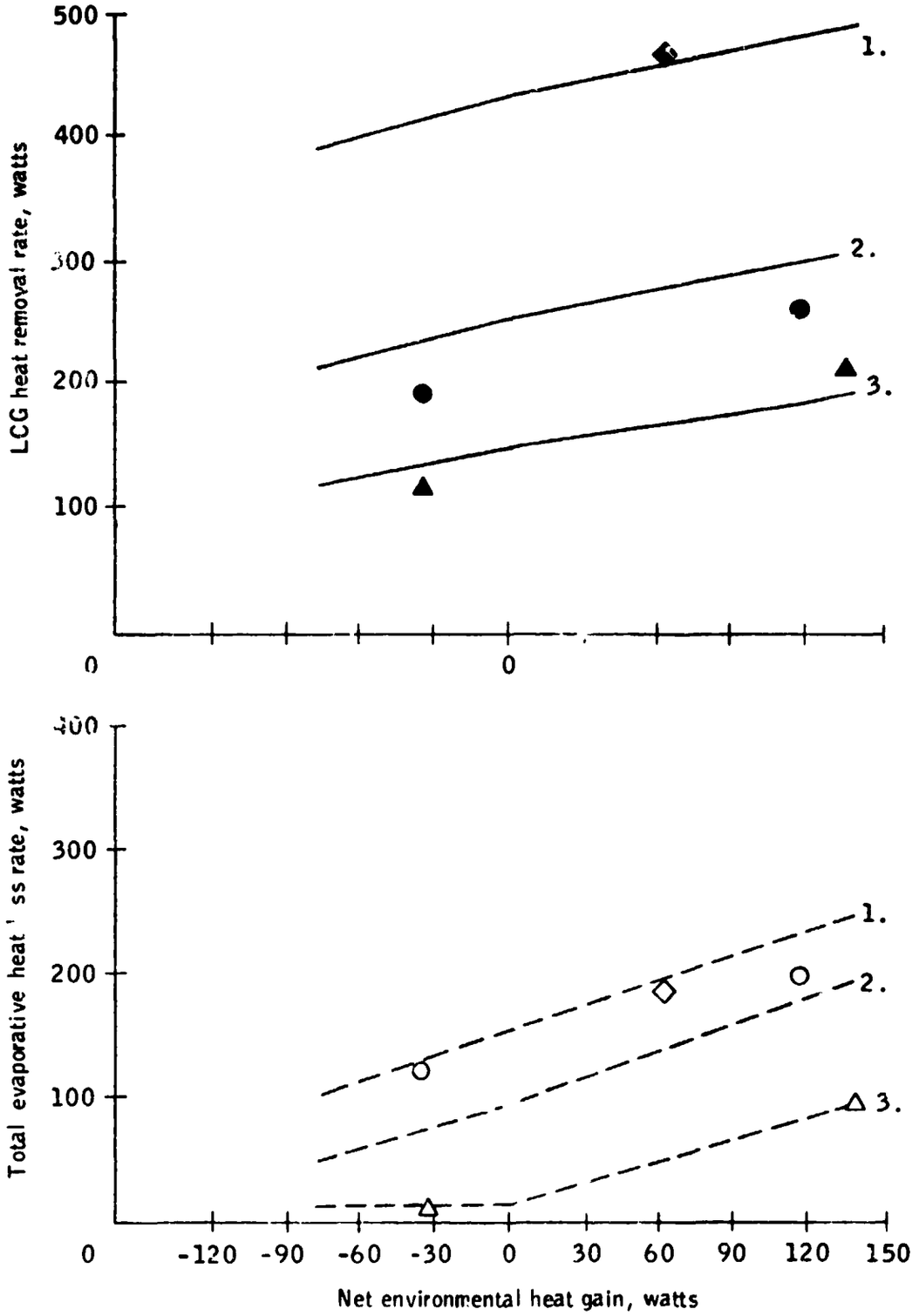

Figure 3-81.- Concluded.

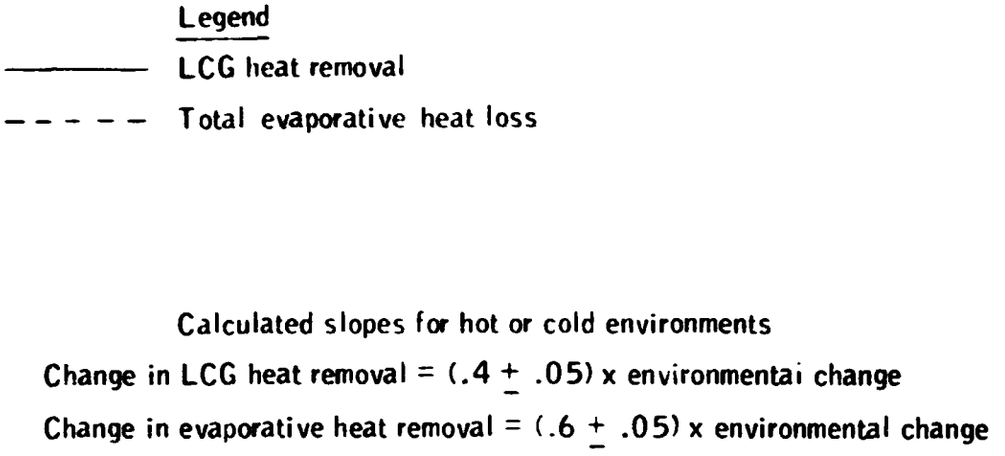

Figure 3-82.- Predicted change in LCG and total evaporative heat removal rates vs net environmental heat gain or loss, for constant metabolic rates and LCG inlet temperatures.

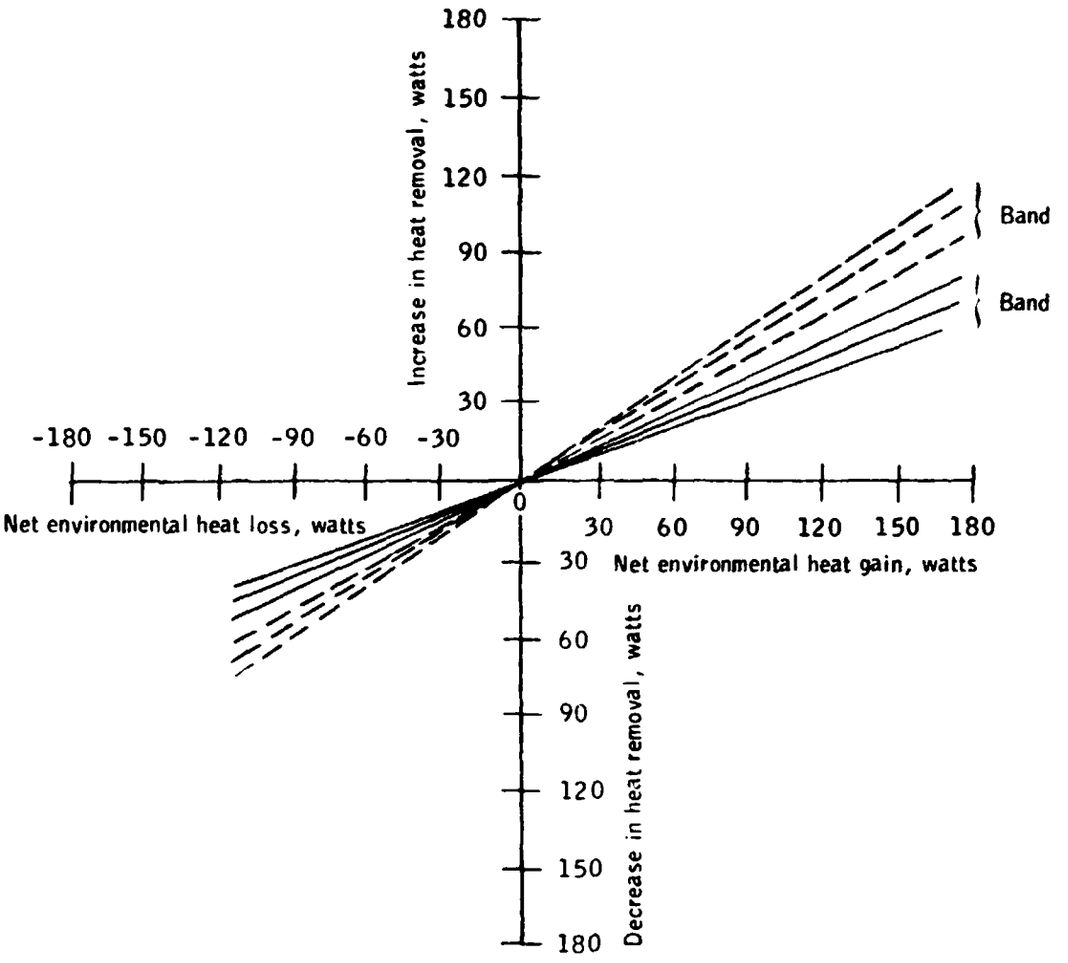

Figure 3-82.- Concluded.

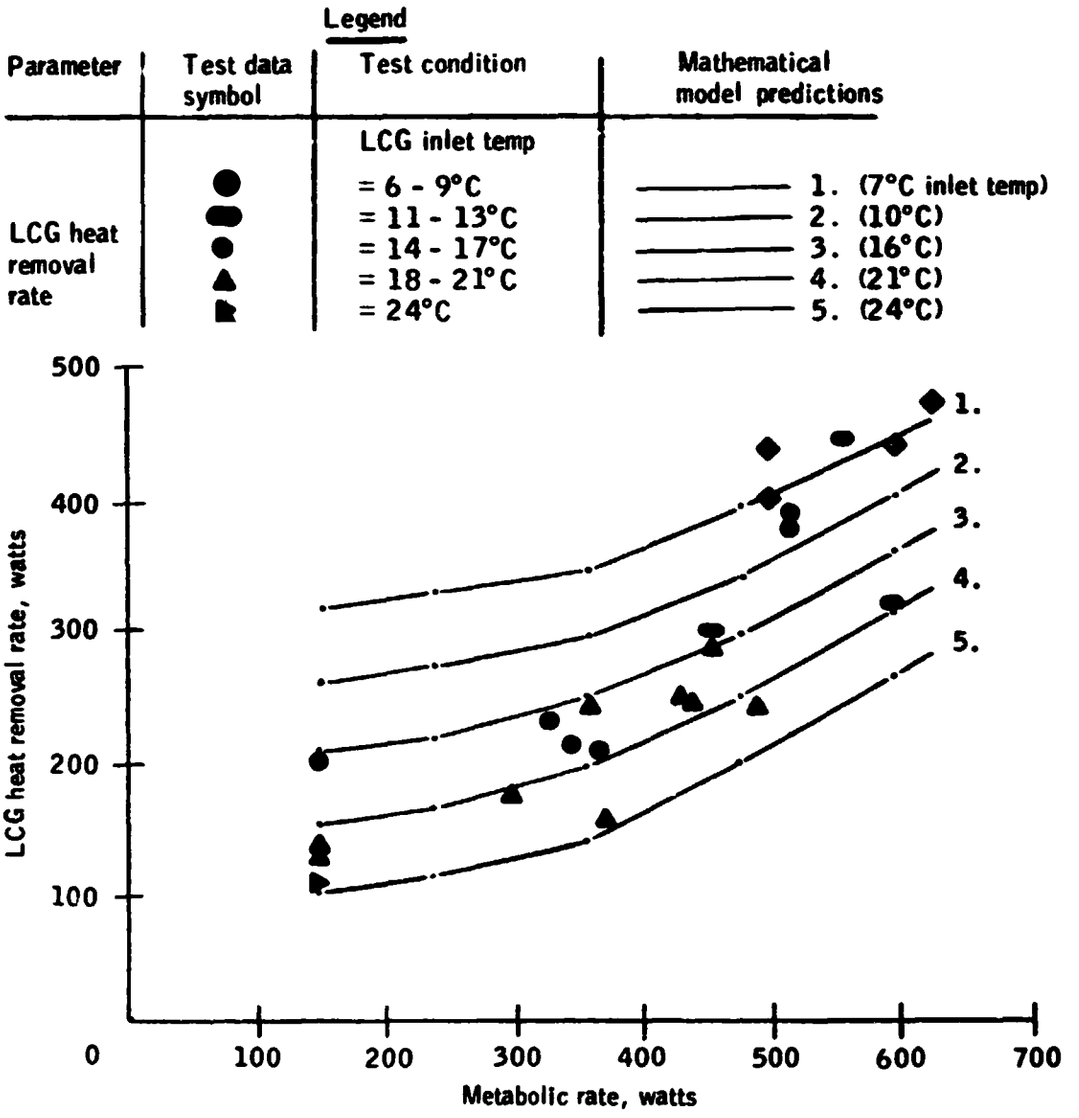

Figure 3-83.- Predicted and actual steady-state LCG heat removal, normalized to zero environmental effects, vs metabolic rate, for various LCG inlet temperatures.

Legend

Parameter	Test data symbol	Test condition	Mathematical model predictions
LCG heat removal ratio	◀	Low metabolic rates (= 293 - 366 watts)	
	▼	Moderate metabolic rates (= 425 - 513 watts)	———
	●	High metabolic rates (= 527 - 615 watts)	

1. Model prediction for metabolic rate of 293 watts
2. Model prediction for metabolic rate of 586 watts

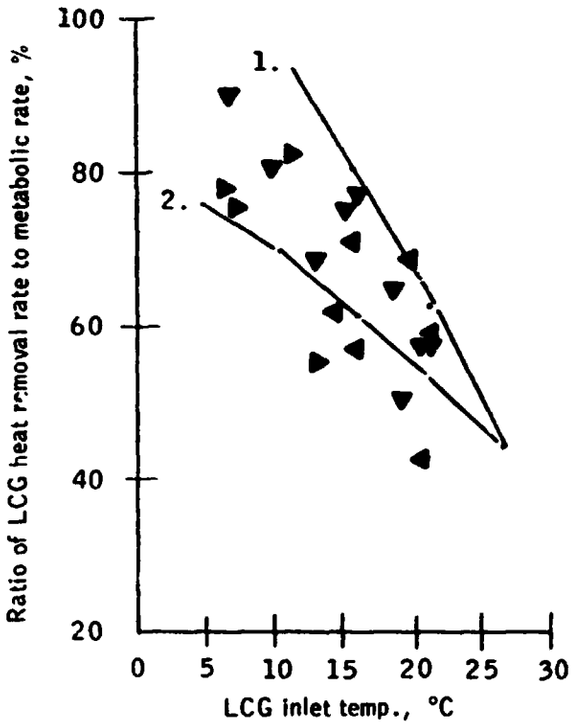

Figure 3-84.- Ratio of LCG heat removal rate to metabolic rate vs LCG inlet temperature.

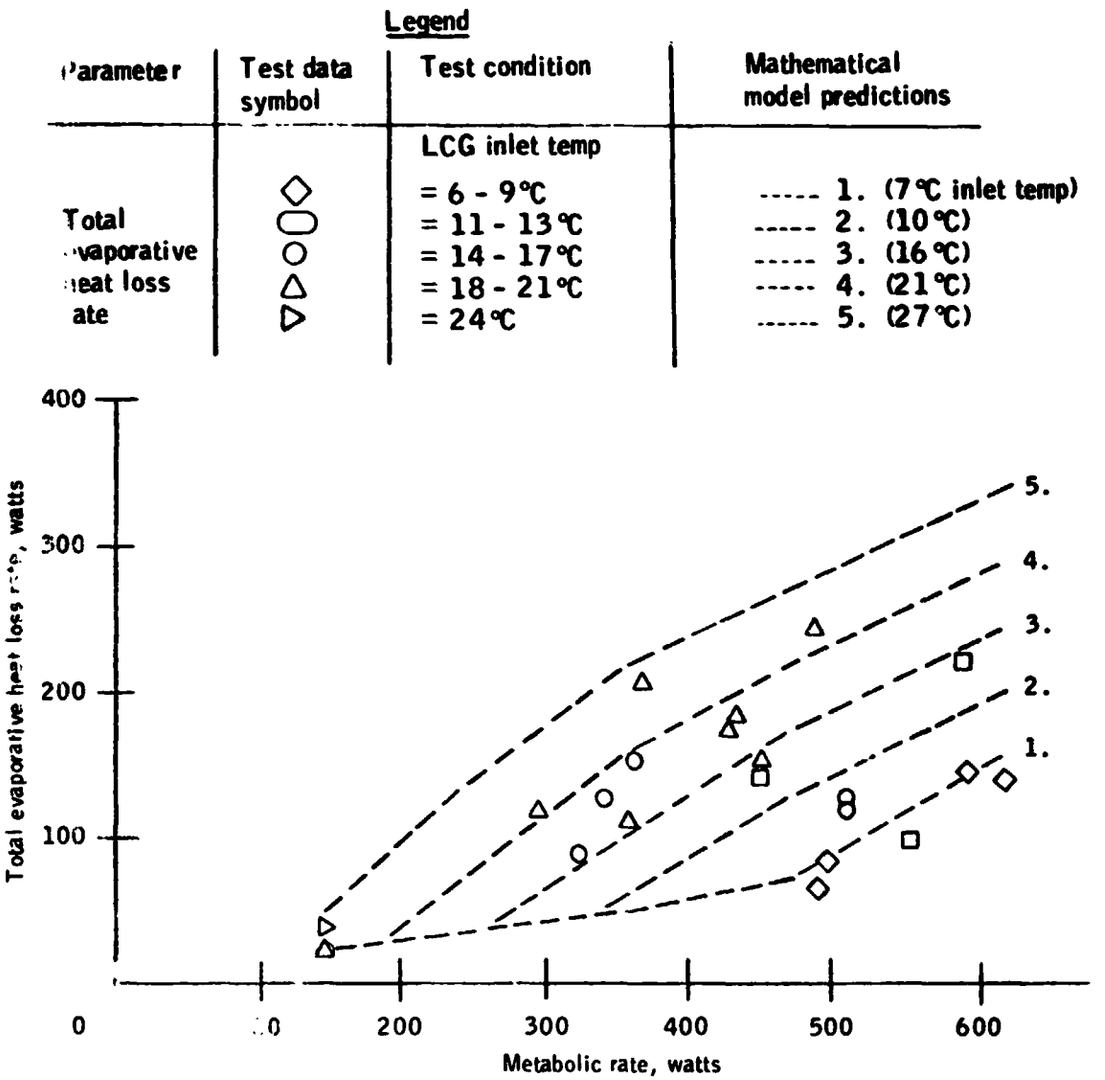

Figure 3-85.- Predicted and actual steady-state total evaporative heat loss rate normalized to zero environmental effects, vs metabolic rate, for various LCG inlet temperatures.

Legend

Parameter	Test data symbol	Test condition	Mathematical model predictions
Total evaporative heat loss ratio	◁	Low metabolic rates (= 293 - 366 watts)	
	▽	Moderate metabolic rates (= 423 - 513 watts)	------
	▷	High metabolic rates (= 527 - 615 watts)	

1. Model prediction for metabolic rate of 293 watts
2. Model prediction for metabolic rate of 586 watts

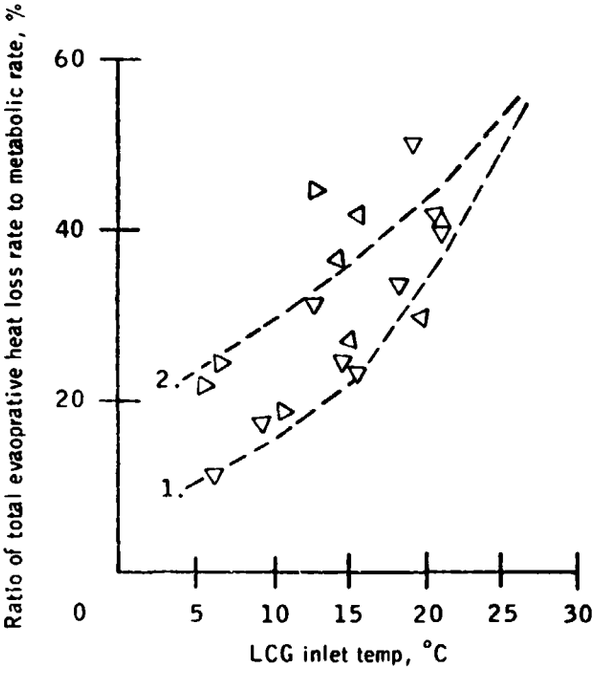

Figure 3-86.- Ratio of total evaporative heat loss rate to metabolic rate vs LCG inlet temperature.

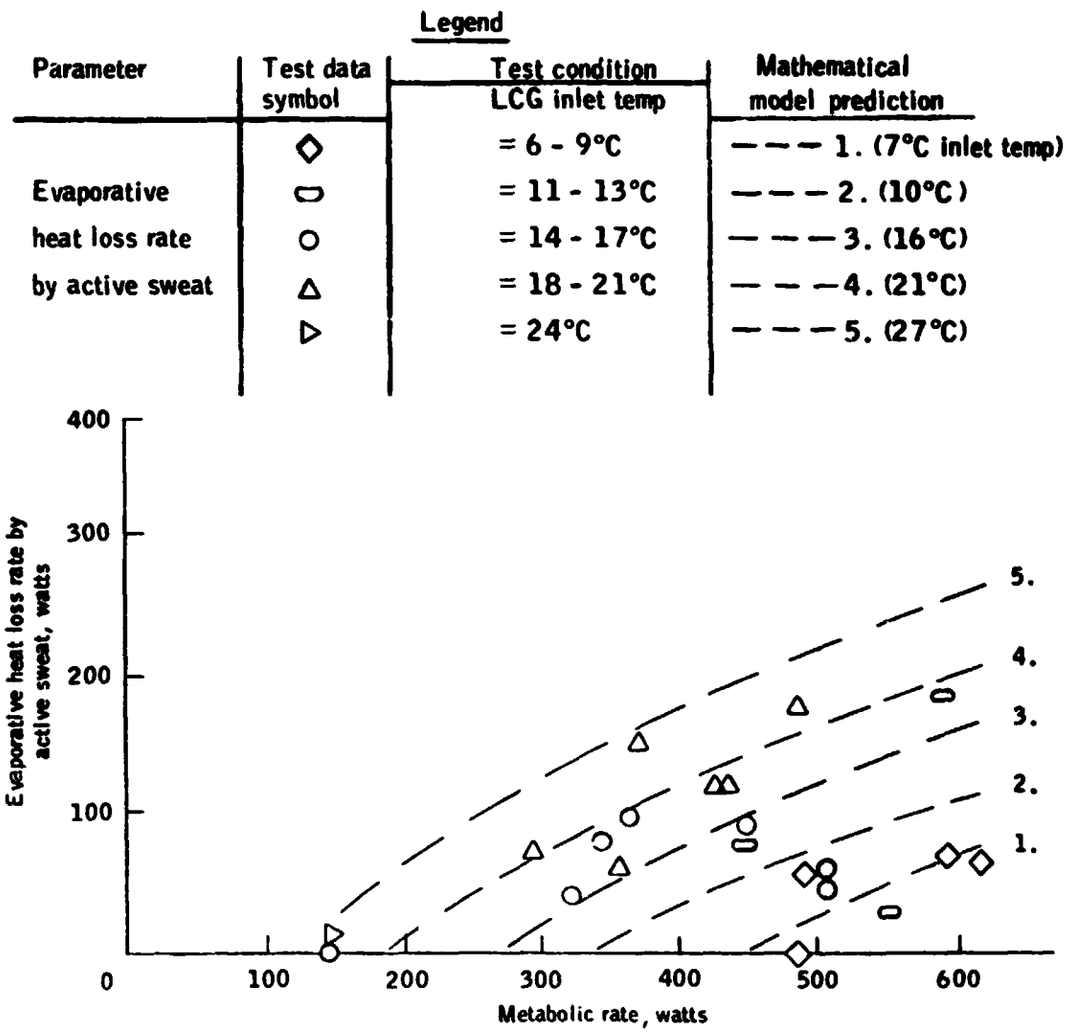

Figure 3-87.- Predicted and actual steady-state evaporative heat loss rate by active sweat, normalized to zero environmental effects, vs metabolic rate, for various LCG inlet temperatures.

Legend

Parameter	Test data symbol	Test condition	Mathematical model prediction
Sweat heat loss ratio	◁	Low metabolic rates (= 293 - 366 watts)	— —
	▽	Moderate metabolic rates (= 425 - 513 watts)	
	▷	High metabolic rates (= 527 - 615 watts)	

1. Model prediction for metabolic rate of 293 watts
2. Model prediction for metabolic rate of 586 watts

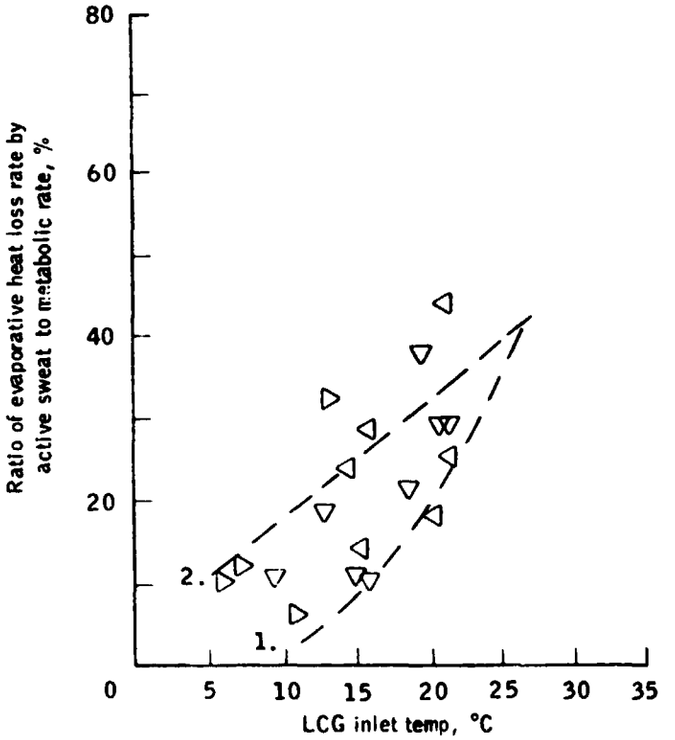

Figure 3-88.- Ratio of evaporative heat loss rate by active sweat to metabolic rate vs LCG inlet temperature.

Regression curve fit data

Type of fit: Second order
Correlation coefficient: .90
Equation of curve:

$$Y = 93.2 + .034X + .00093X^2$$

Figure 3-89a.- Regression curve fit to test data for LCG heat removal rate vs metabolic rate.

Regression curve fit data

Type of fit: Second order
Correlation coefficient: .65
Equation of curve:

$$Y = -55 + .81X - .008X^2$$

Figure 3-89b.- Regression curve fit to test data for total evaporative heat loss rate vs metabolic rate.

Legend

Parameter	Test data symbol	Test condition	Parameter	Test data symbol	Test condition
		LCG inlet temp			LCG inlet temp
Error in model predictions of LCG heat removal	♦	= 6-9°C	Error in model predictions of total evaporative heat loss	◊	= 6-9°C
	▬	= 11-13°C		⬭	= 11-13°C
	●	= 14-17°C		○	= 14-17°C
	▲	= 18-21°C		△	= 18-21°C
	▶	= 24°C		▷	= 24°C

——— : Curve fit to LCG error

------ : Curve fit to total evaporative heat loss error

Note: Positive error indicates under-prediction; negative error indicates over-prediction.

Figure 3-89c.- Model error ($= \frac{\text{Test data - model predictions}}{\text{Metabolic rate}}$) vs metabolic rate for LCG and total evaporative heat loss rate predictions.

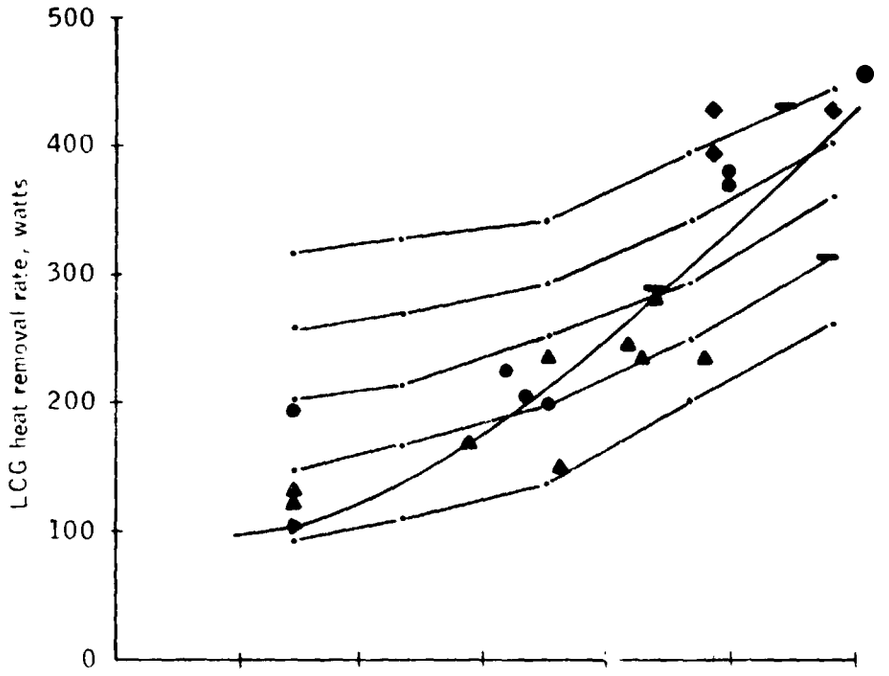

Figure 3-89a.- Concluded.

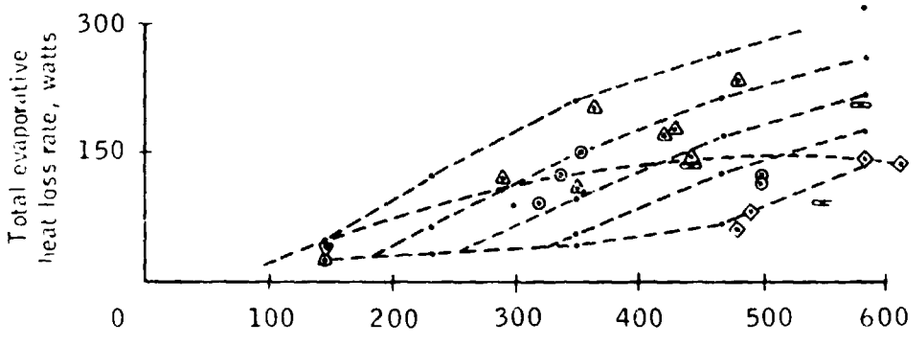

Figure 3-89b.- Concluded.

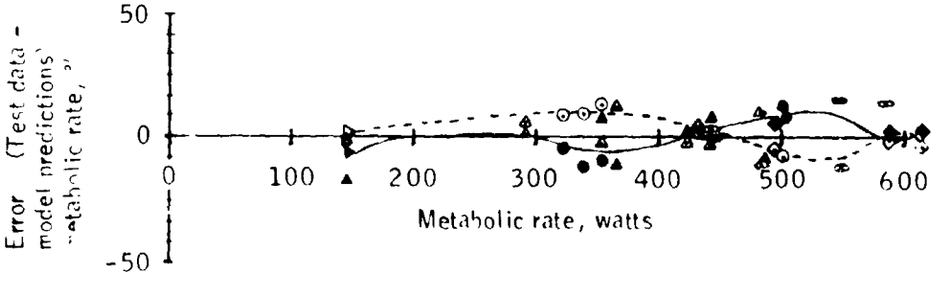

Figure 3-89c.- Concluded.

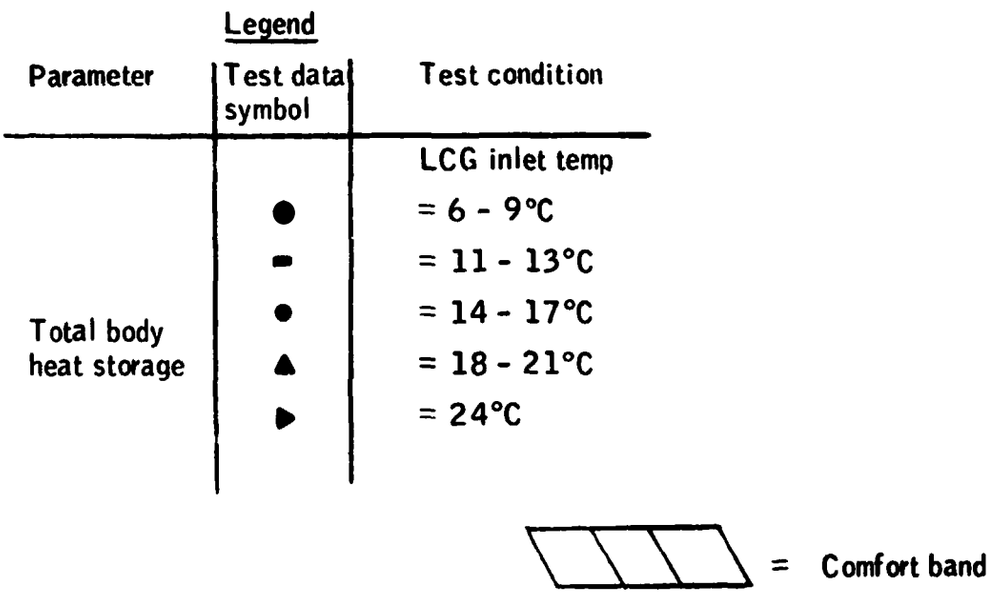

Figure 3-90.- Total body heat storage vs metabolic rate for steady-state conditions during Series D.

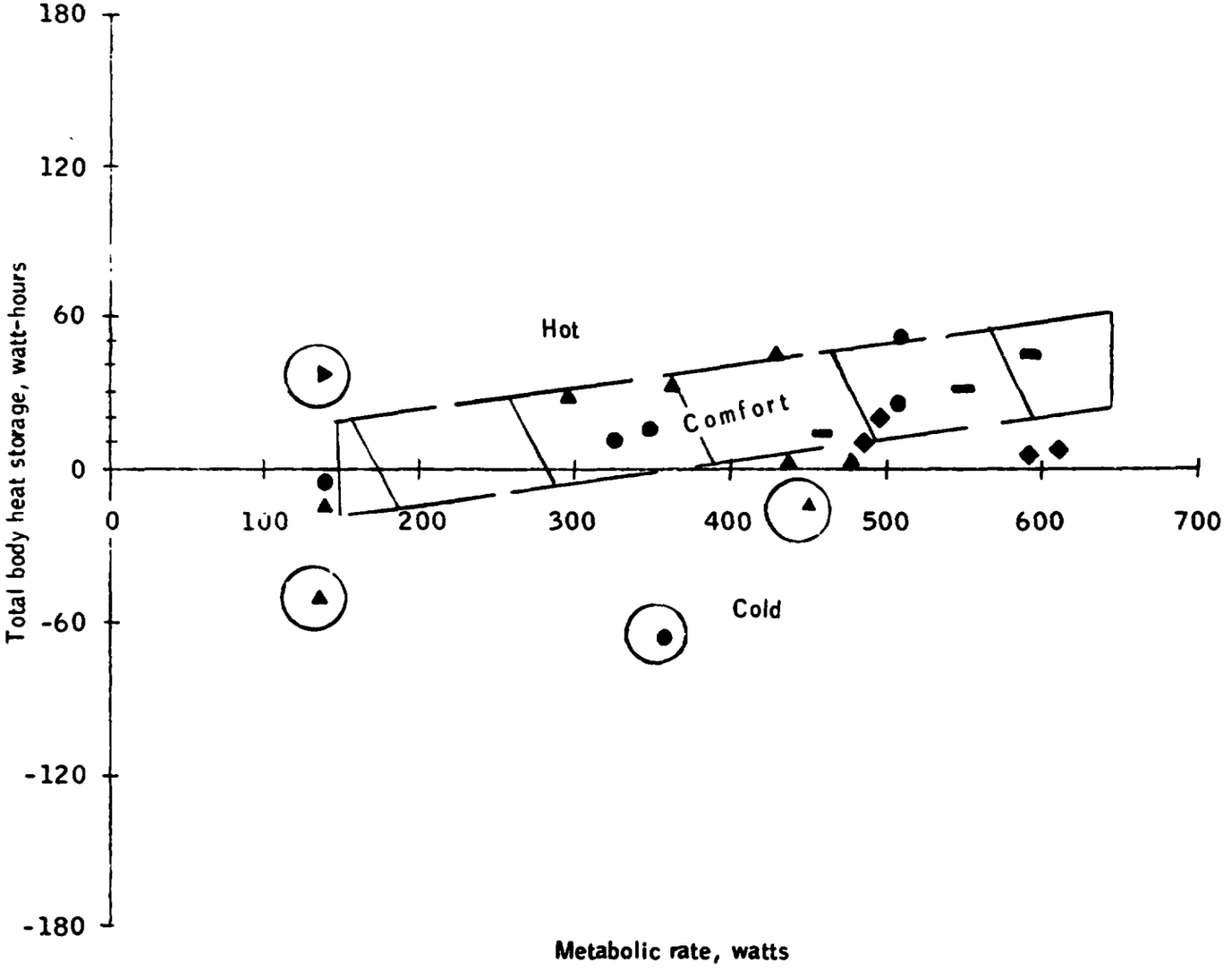

Figure 3-90.- Concluded.

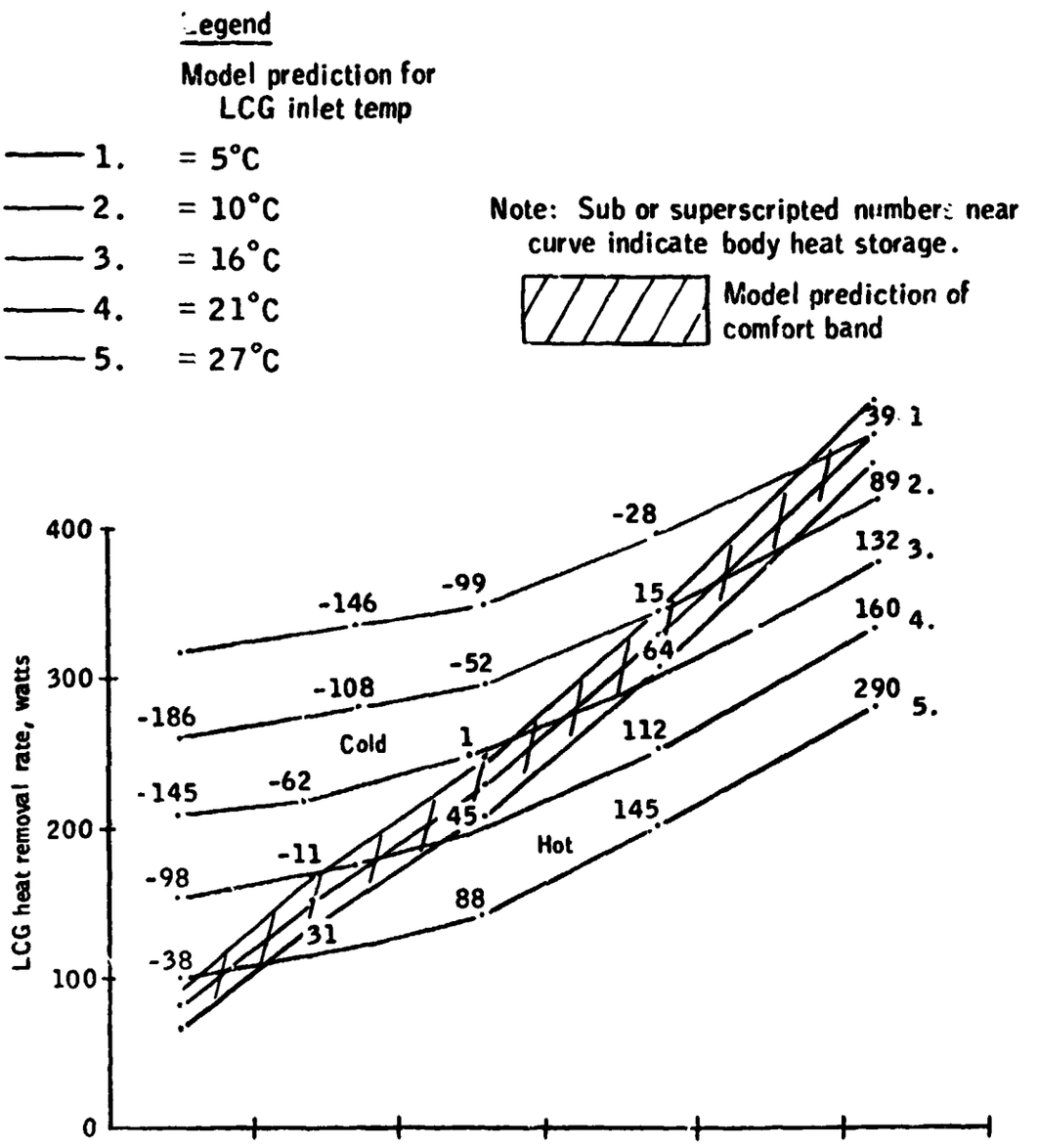

Figure 3-91a.- Predicted steady-state LCG heat removal rate, heat storage, and comfort band vs metabolic rate, for neutral environments (0 watts into suit) and various LCG inlet temperatures.

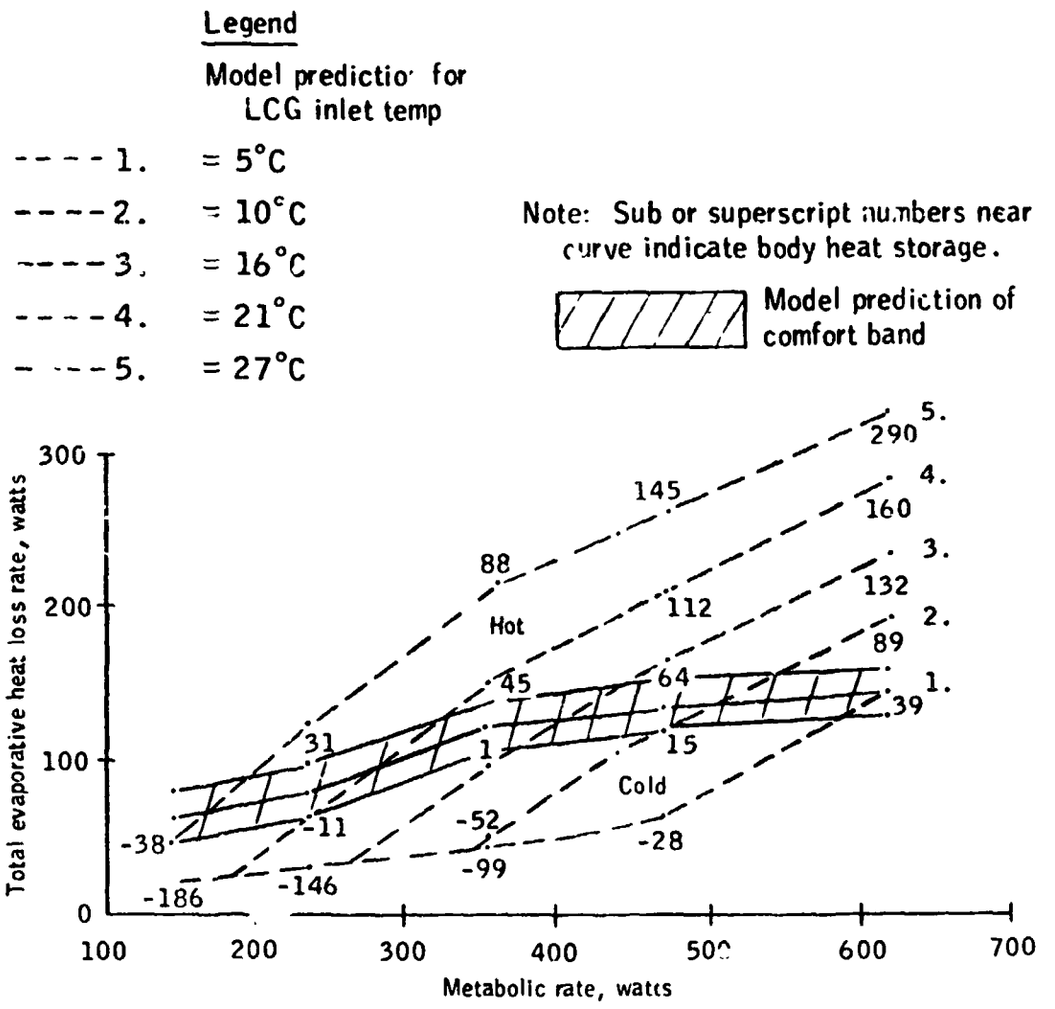

Figure 3-91b.- Predicted steady-state total evaporative heat loss rate, heat storage, and comfort band vs metabolic rate, for neutral environments (0 watts into suit) and various LCG inlet temperatures.

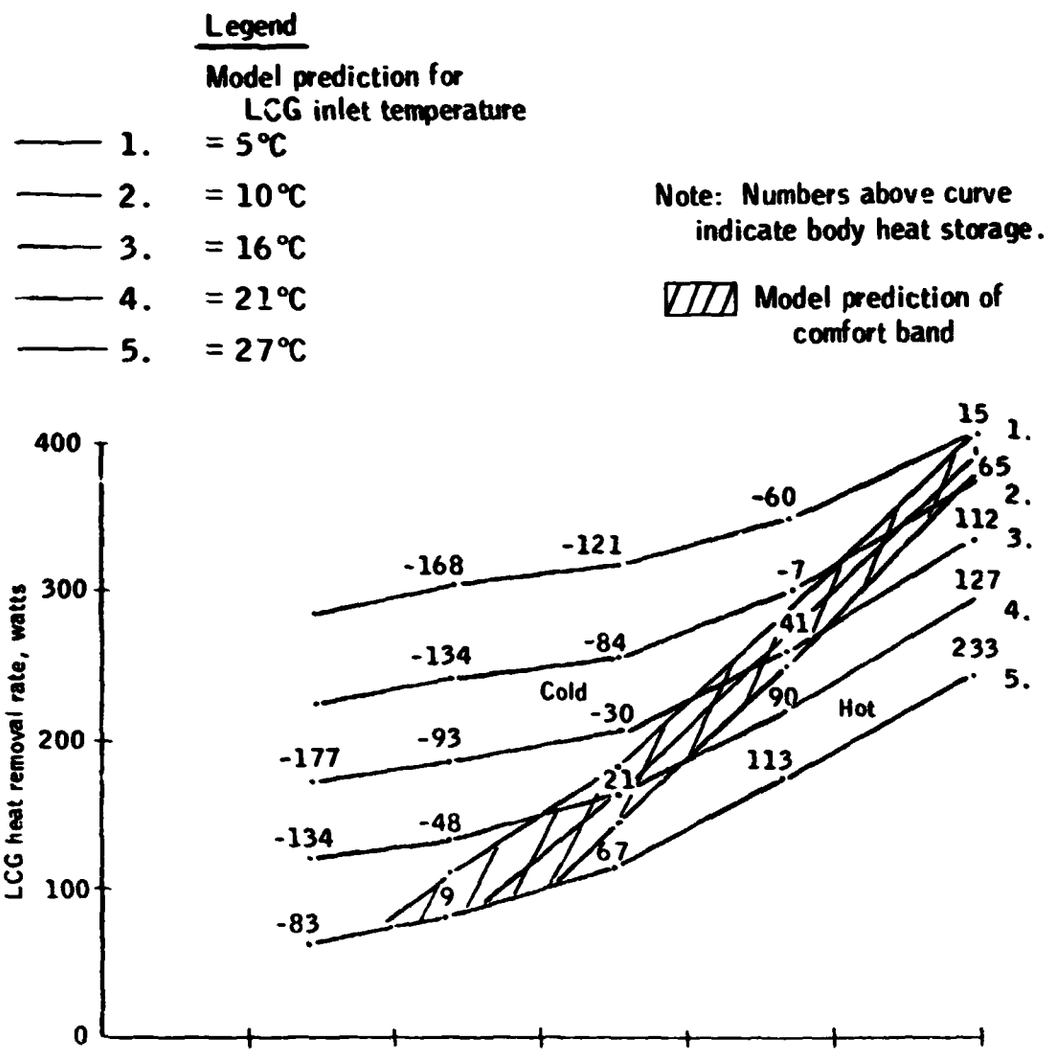

Figure 3-92a.- Predicted steady-state LCG heat removal rate, heat storage, and comfort band vs metabolic rate, for cold environments (72 watts out of suit) and various LCG inlet temperatures.

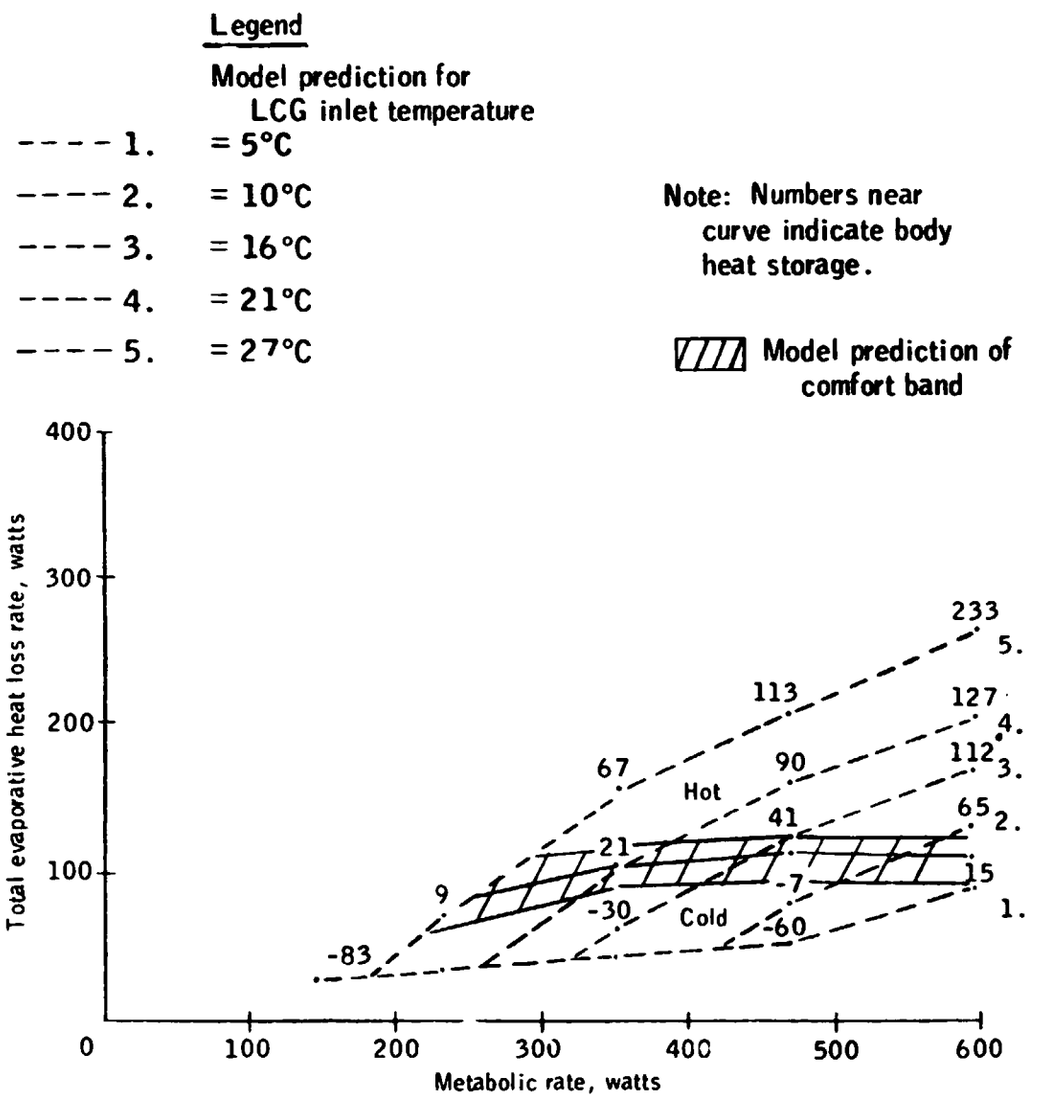

Figure 3-92b.- Predicted steady-state total evaporative heat loss rate, heat storage, and comfort band vs metabolic rate, for cold environments (72 watts out of suit) and various LCG inlet temperatures.

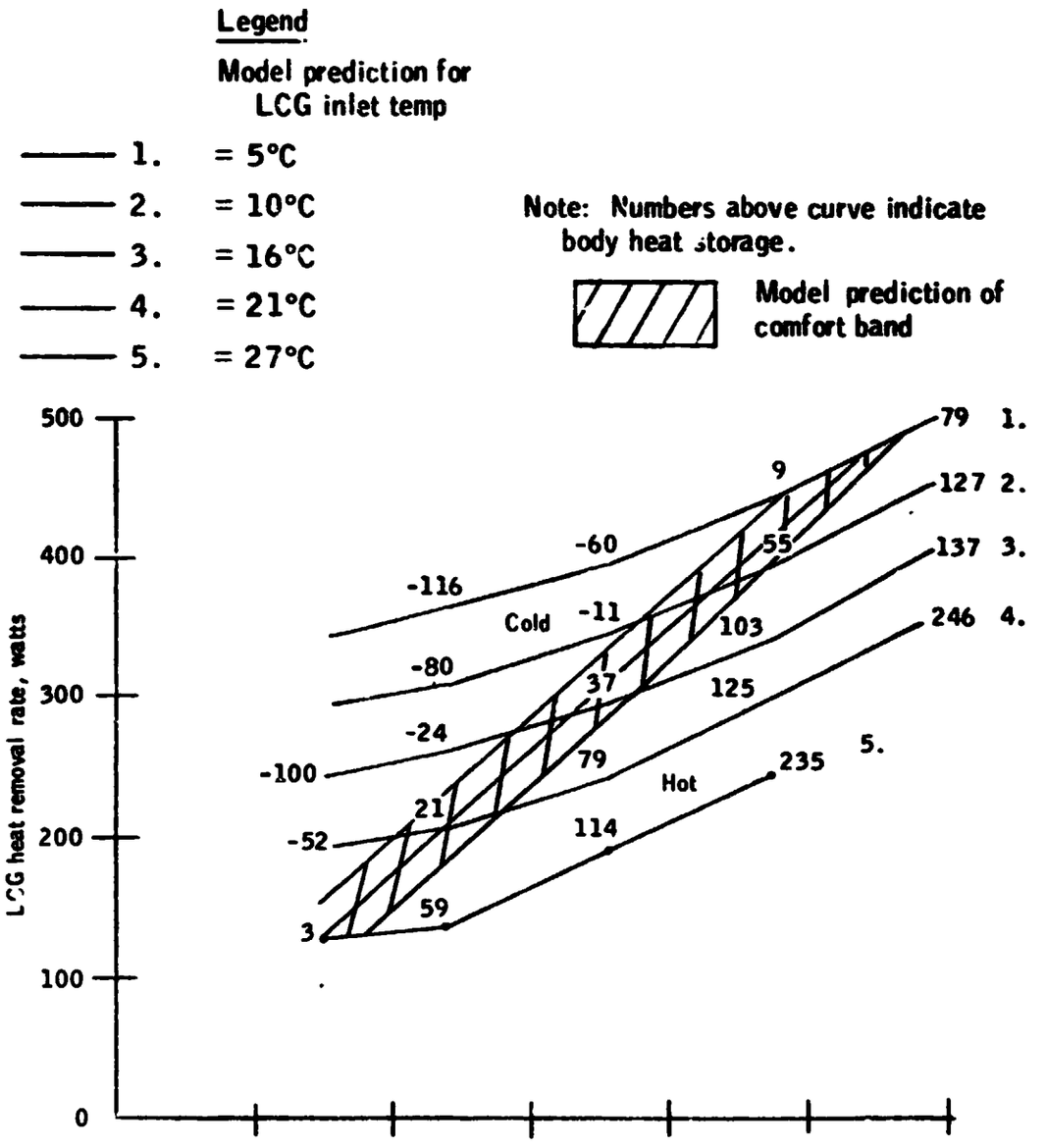

Figure 3-93a.- Predicted steady-state LCG heat removal rate, heat storage, and comfort band vs metabolic rate, for hot environments (126 watts into suit) and various LCG inlet temperatures.

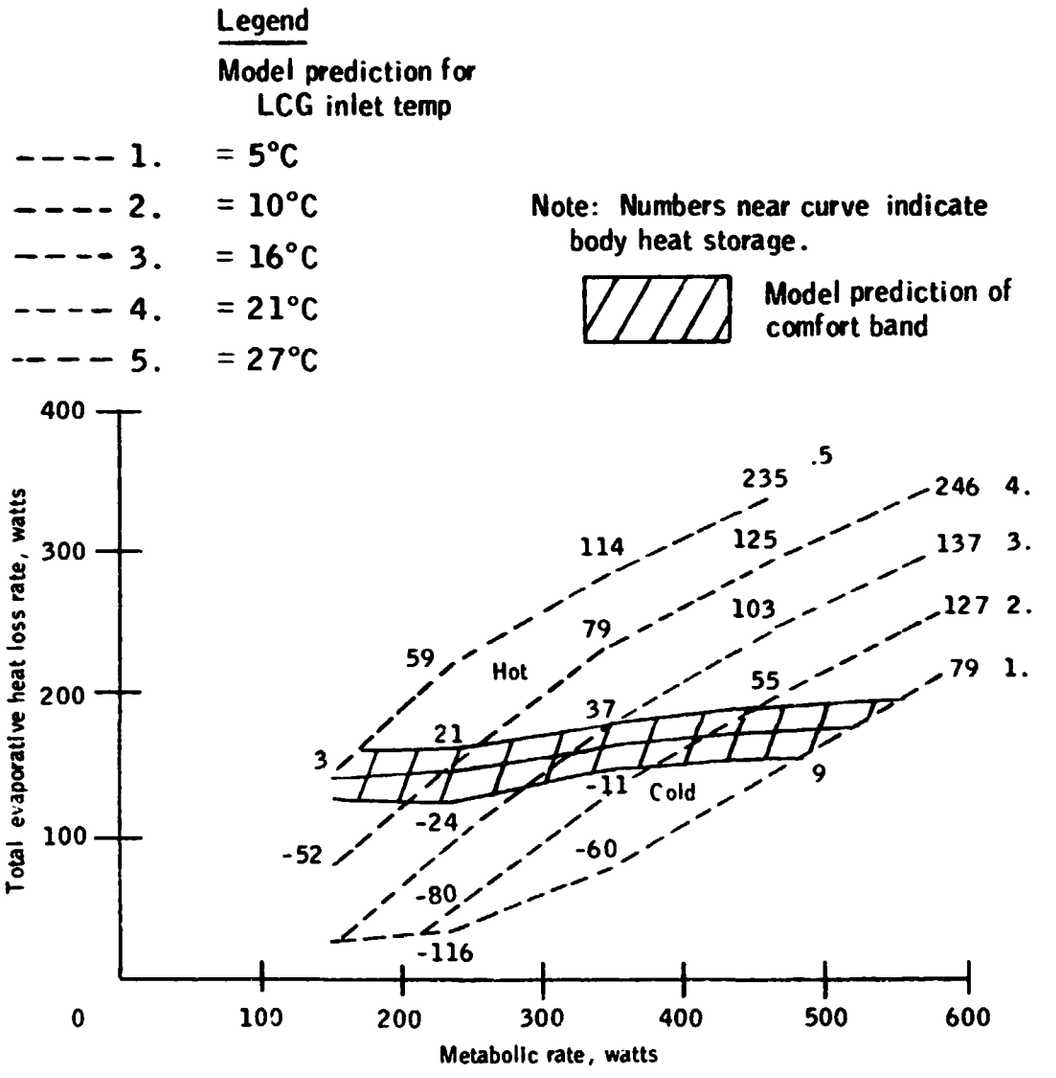

Figure 3-93b.- Predicted steady-state total evaporative heat loss rate, heat storage, and comfort band vs metabolic rate, for hot environments (126 watts into suit) and various LCG inlet temperatures.

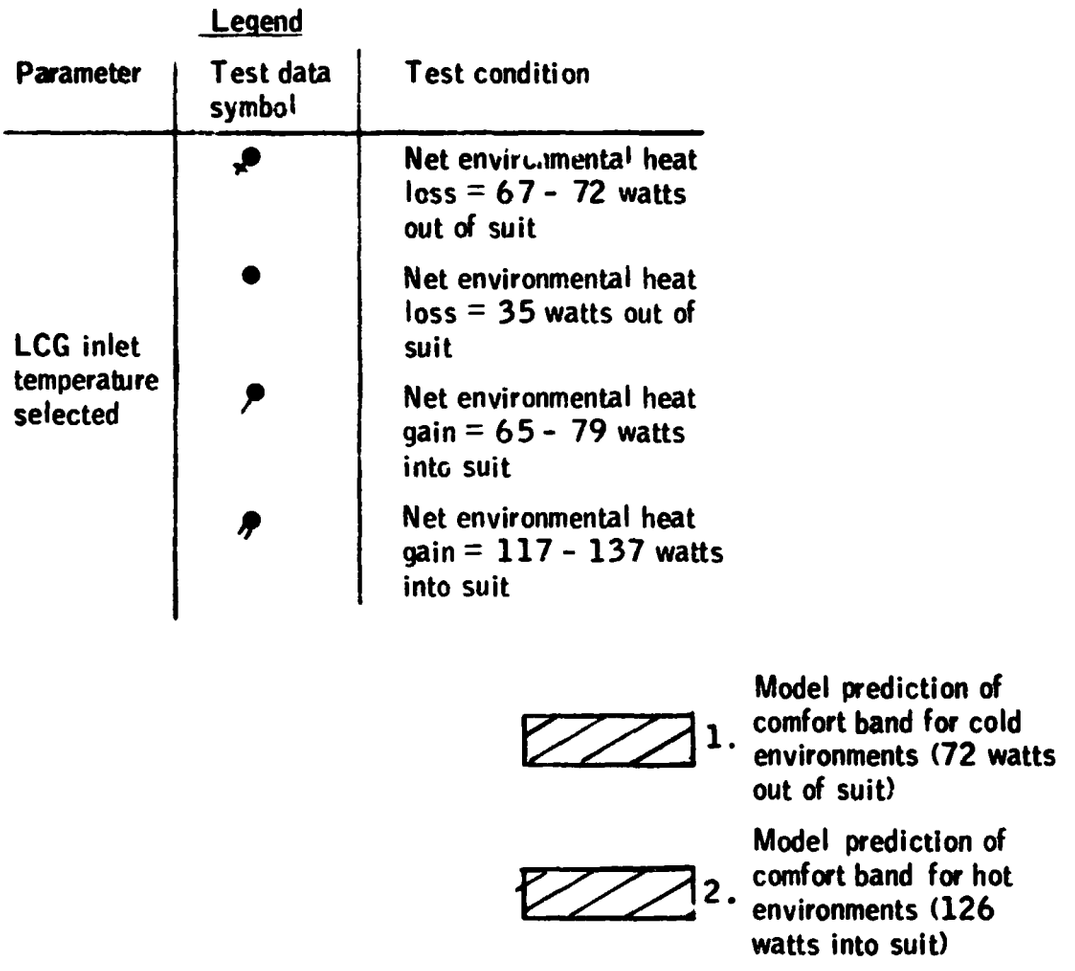

Figure 3-94.- Predicted and actual steady-state LCG inlet temperatures selected for comfort vs metabolic rate, for net environmental heat exchange between 72 watts out of suit to 137 watts into suit.

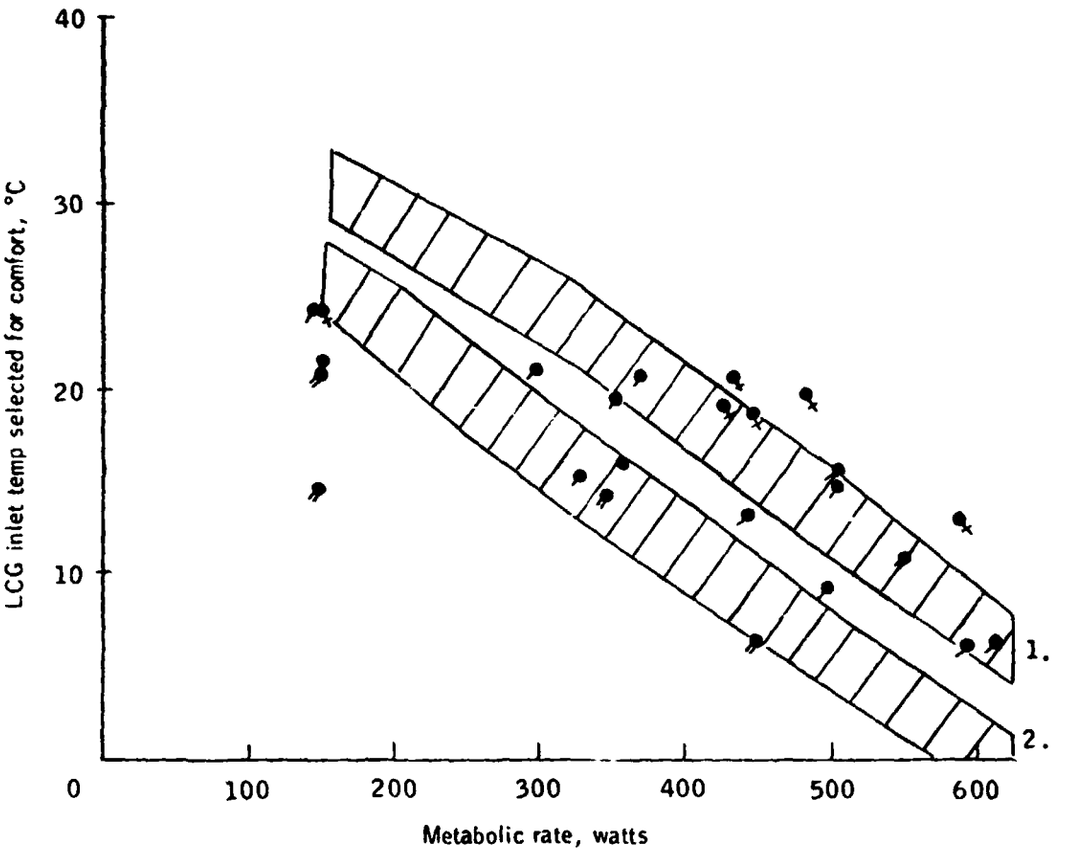

Figure 3-94.- Concluded.

Legend

Parameter	Test data symbol	Test condition
LCG heat removal rate at comfort		Net environmental heat loss = 67 - 72 watts out of suit
		Net environmental heat loss = 35 watts out of suit
		Net environmental heat gain = 65 - 79 watts into suit
		Net environmental heat gain = 117 - 137 watts into suit

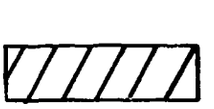

1. Model prediction of comfort band for hot environments (126 watts into suit)

2. Model prediction of comfort band for neutral environments (0 watts into suit)

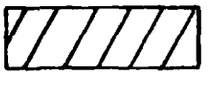

3. Model prediction of comfort band for cold environments (72 watts out of suit)

Figure 3-95.- Predicted and actual steady-state LCG heat removal at comfort vs metabolic rate for net environmental heat exchange between 72 watts out of suit to 137 watts into suit.

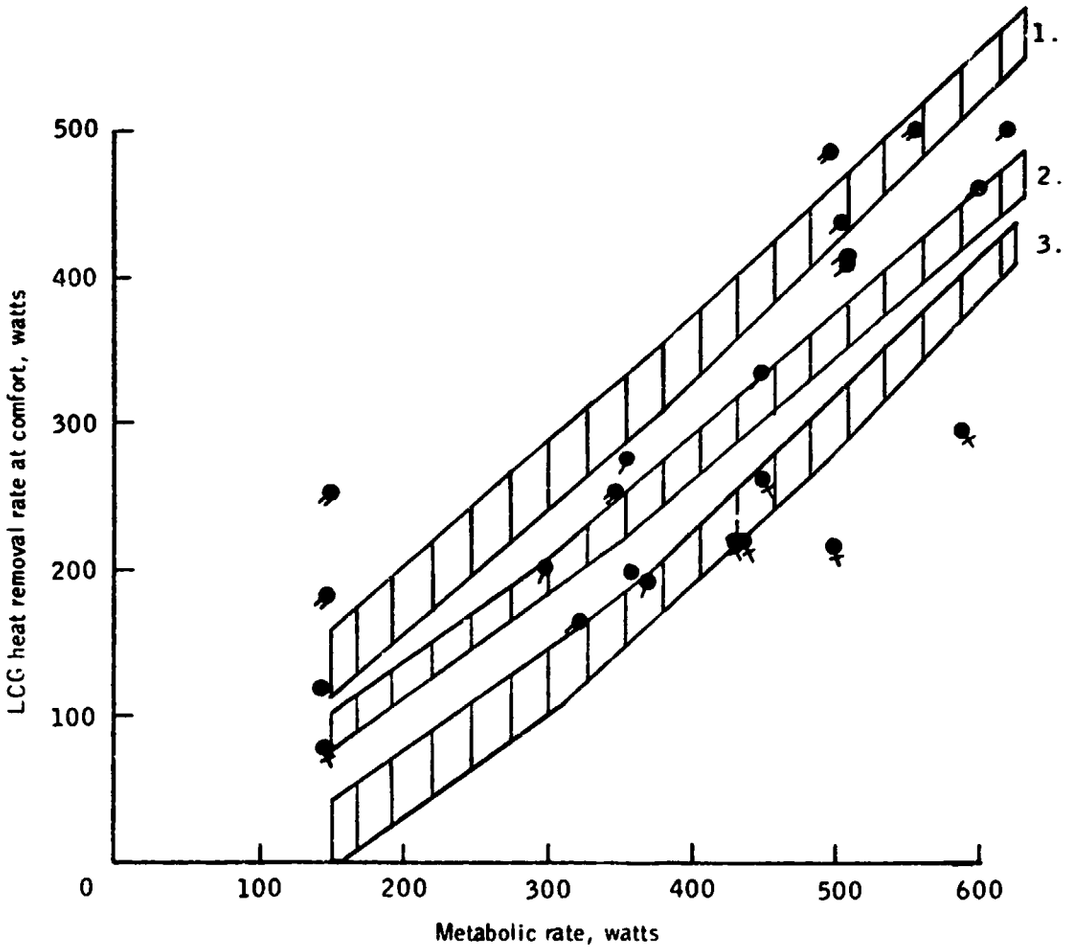

Figure 3-95.- Concluded.

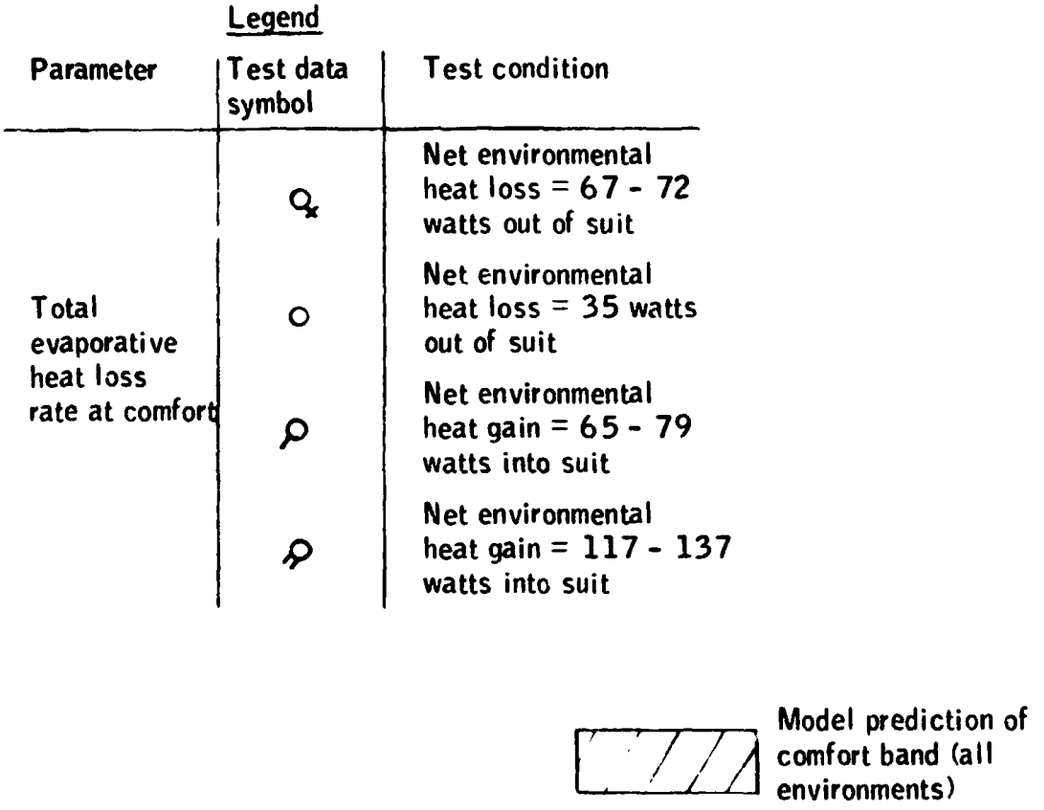

Figure 3-96.- Predicted and actual steady-state total evaporative heat loss rate at comfort vs metabolic rate for net environmental heat exchange between 72 watts out of suit to 137 watts into suit.

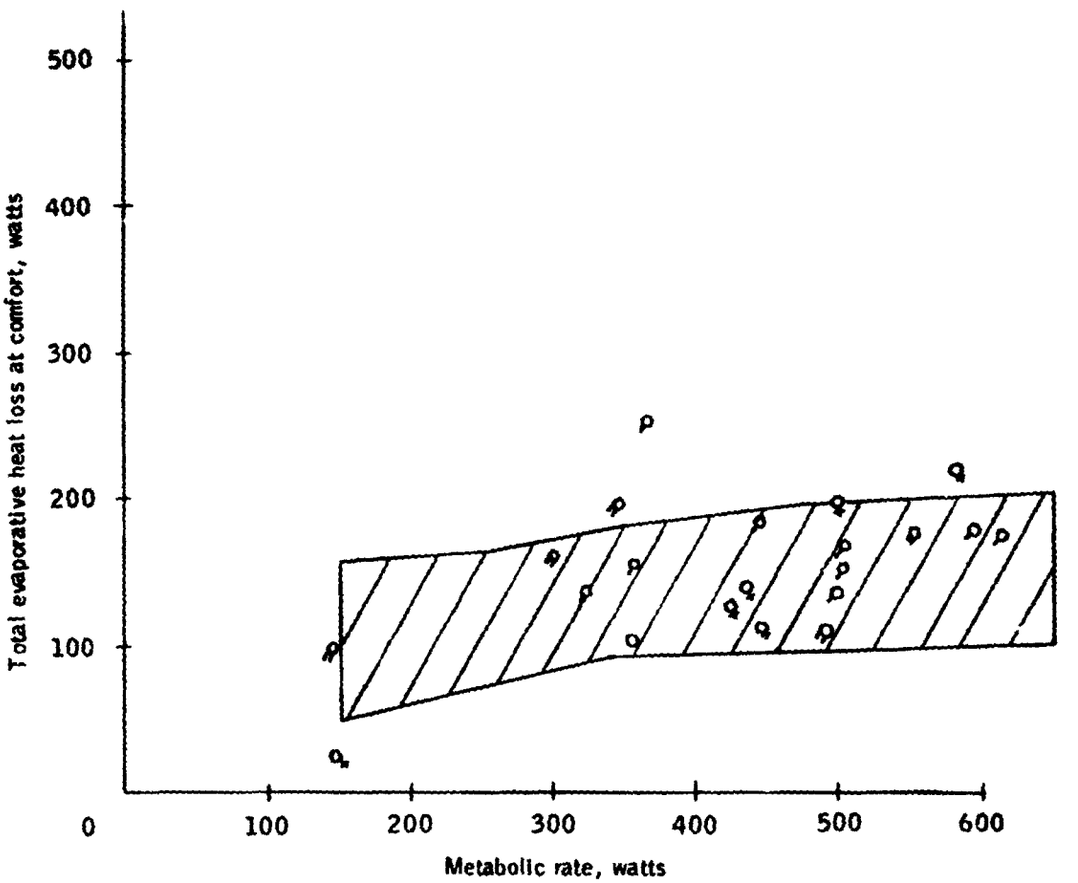

Figure 3-96.- Concluded.

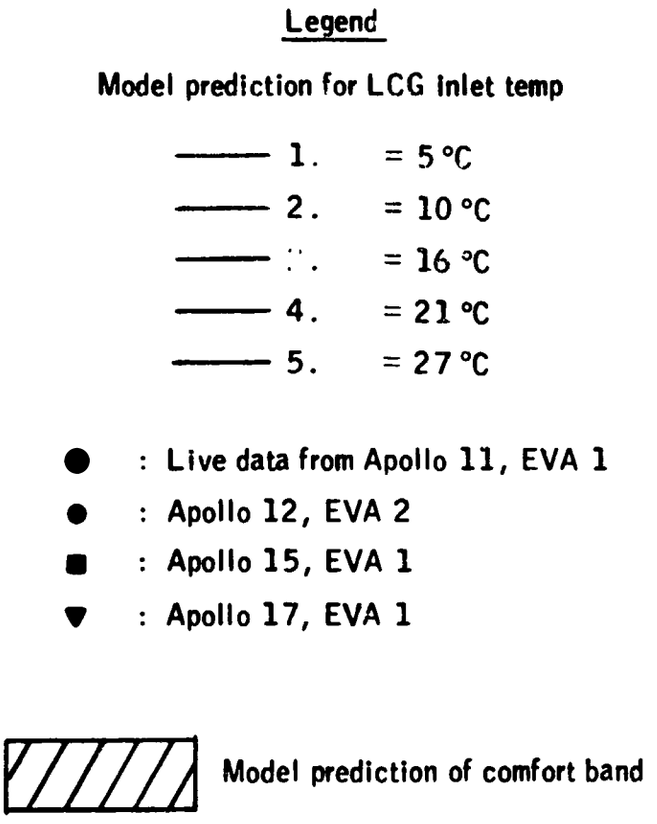

Figure 3-97.- Real time (live) Apollo EVA data, superimposed on a typical RTCC parametric curve of LCG heat removal rate vs metabolic rate for neutral environments (zero environmental heat exchange).

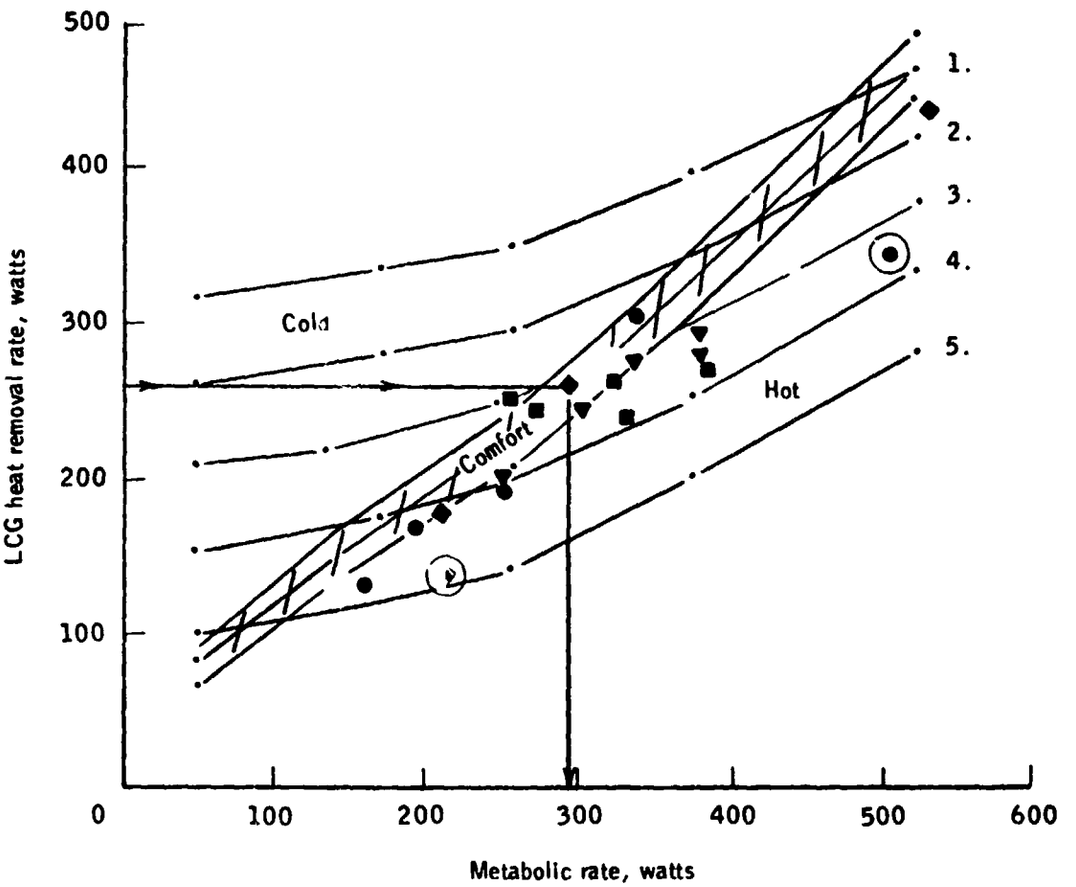

Figure 3-97.- Concluded.

TABLE 3-6.- COMPARISON OF REAL TIME MODEL PREDICTIONS WITH ACTUAL POST-EVA RESULTS

Apollo Mission No.	EVA No.	Astronaut	Average Metabolic Rate, BTU/hr (watts)		Error, Percent
			Predicted by LCG method, BTUs/Hr (watts)	Actual Result (From Heat Balance)	
11	1	N. Armstrong (CDR)	800 (234)	900 (264)	- 11.1
		E. Aldrin (LMP)	1295 (379)	1200 (352)	+ 7.9
12	1	C. Conrad (CDR)	999 (293)	975 (286)	+ 2.5
		R. Gordon (LMP)	1061 (311)	1000 (293)	+ 6.1
	2.	C. Conrad (CDR)	696 (204)	875 (256)	- 20.0
		R. Gordon (LMP)	1069 (313)	1000 (293)	+ 6.9
14	1	A. Shepard (CDR)	875 (256)	800 (234)	+ 9.4
		E. Mitchell (LMP)	849 (249)	930 (273)	- 8.7
	2	A. Shepard (CDR)	883 (259)	910 (267)	- 2.9
		E. Mitchell (LMP)	1034 (303)	1000 (293)	+ 3.4
15	1	D. Scott (CDR)	1138 (333)	1100 (322)	+ 3.5
		J. Irwin (LMP)	1042 (305)	980 (287)	- 6.3
	2	D. Scott (CDR)	1110 (325)	1000 (293)	+ 11.0
		J. Irwin (LMP)	832 (244)	810 (237)	+ 2.7
	3	D. Scott (CDR)	1017 (298)	1030 (302)	- 1.3
		J. Irwin (LMP)	726 (213)	810 (237)	- 10.4
16	1	J. Young (CDR)	914 (268)	870 (255)	+ 5.1
		C. Duke (LMP)	1096 (321)	1010 (296)	+ 8.5
	2	J. Young (CDR)	760 (223)	780 (229)	- 2.5
		C. Duke (LMP)	903 (265)	830 (243)	+ 8.7
	3	J. Young (CDR)	887 (260)	810 (237)	+ 9.5
		C. Duke (LMP)	876 (257)	820 (240)	+ 6.8
17	1	E. Cernan (CDR)	1026 (301)	1090 (319)	- 5.9
		J. Schmitt (LMP)	1089 (319)	1080 (316)	+ 0.1

TABLE 3-6.- CONTINUED

Apollo Mission No.	EVA No.	Astronaut	Average Metabolic Rate, BTU/hr (watts)		
			Predicted by LCG method, BTUs/Hr (watts)	Actual Result (From Heat Balance)	Error, Percent
17 (contd.)	2	E. Cernan (CDR)	851 (249)	820 (240)	+ 3.7
		J. Schmitt (LMP)	923 (270)	830 (243)	+ 11.2
	3	E. Cernan (CDR)	1018 (298)	930 (273)	+ 9.5
		J. Schmitt (LMP)	1011 (296)	940 (275)	+ 7.6
				Average	+ 6.5%
				Error	- 7.9%

CDR = Mission Commander

LMP = Lunar Module Pilot

4. DISCUSSION

COMFORT CORRELATIONS

The relationships that have thus far been developed between LCG cooling, evaporative heat loss, and other physiological parameters represent results for both comfort and off-comfort conditions. It now remains to refine the results, by making use of comfort zone guidelines, to d ive a final series of expressions for LCG performance and sweating at comfort. This can be accomplished by using only the data points associated with thermal comfort. They are determined primarily by selecting test points of Series A-D for which total body heat storage falls near or within the comfort band of Figures 3-19, 3-22, 3-35, and 3-90. This includes almost all of the data of Series D and considerable data from the other test series.

The data points used for the final correlations are shown in Table D7 of Appendix D. The final correlations were made by performing a regression curve fit and error analysis (159) on the comfort points, in which data points with a standard error greater than 2 S.E. were rejected. The regression curve and data were then compared with the predictions of the mathematical model. Th se results are shown in Figures 4-1 to 4-4. All of the relationships shown are for zero net environmental heat exchange. Environmental effects upon LCG and evaporative heat removal data have been eliminated by the procedure outlined in the Series D results.

Figure 4-1 shows the data and regression curve fit for LCG inlet temperatures selected at comfort vs. metabolic rate. The comfort band

prediction of the mathematical model is shown by the clear overlay preceding Figure 4-1. The regression curve fit is second order and the equation of the curve is:

$$T_{inlet} = -3.33 \times 10^{-5} (Met.Rate)^2 - .0118 (Met.Rate) + 25.1.$$

The correlation coefficient is 0.89 and the standard error of the fit is $\pm$2.6°C.

The scatter in the data is attributable to the fact that selection of inlet temperature was usually limited to a coarse range of cool, moderate or warm rather than a fine range. Also, it was not possible to adjust inlet temperature data for environmental effects as was done for heat removal data. Nevertheless, the regression curve falls nicely within the band predicted by the mathematical model, except at the lowest metabolic rates (146 watts).

The reason for variation at low metabolic rates and high inlet temperatures can be traced to the cooling characteristics of the LCG. As mentioned in the Series A results, the Apollo-LCG efficiency depends upon the formation of a sweat layer in the nylon mesh that connects the LCG tubes. The sweat layer forms a conductive pathway between LCG tubes that acts to increase the heat transfer coefficient. Since minimal sweating would be expected from subjects who begin working at low metabolic rates and high inlet temperatures, it follows that the conductive pathway would be reduced under these conditions, with a resulting drop in the LCG heat transfer coefficient. This is the trend shown by the data of Figures 3-6 and 3-77 at high inlet temperatures.

On the other hand, if the subject selects high inlet temperatures at low metabolic rates following exercise periods at high work rates, a sweat

layer and conductive pathway between LCG tubes may already have been established. This would result in a higher LCG heat transfer coefficient and more heat removal. The variability that can result from these factors makes it difficult to identify valid test points at very low metabolic rates. Consequently, many of the later data were not utilized in the correlations.

The results of Figure 4-1 show that at constant LCG flowrates of 109 liters/hr, inlet temperatures selected by test subjects will decrease almost rectilinearly as metabolic rates increase. The effect of decreased inlet temperatures will be an increase in LCG heat removal to compensate for the increased heat production at higher metabolic rates. If LCG inlet temperatures are fixed, increased LCG heat removal can also be achieved by providing higher LCG flowrates. (For reference purposes, mathematical model predictions are shown in Figure 4-5 for fixed LCG inlet temperatures of 7 and 17°C with variable water flowrates.)

The results of Figure 4-1 provide a guideline for achieving thermal comfort over a wide range of metabolic rates for subjects wearing an LCG. The comfort inlet temperature correlation shown here is supported by the data of other researchers (also shown in Figure 4-1), despite some wide variations in their testing conditions.

The control of inlet temperature (or flowrate) to maintain comfort at different metabolic rates can be achieved by subject control, as in the PLSS, or by means of an automatic controller based on any signal proportional to metabolic rate. Subject control of inlet temperature offers the advantage of simplicity. However, factors such as preoccupation with other work tasks, or inexperience with LCGs can result in gross errors in cooling control, with discomfort and thermal stress (23, 26, 30, 98, 156).

These errors are not always immediately reversible. For example, the control of inlet temperature in response to heat storage noted in Series D can lead to transient periods of high body heat storage and discomfort. Conversely, overcooling at work onset may produce vasoconstriction and decreased heat extraction with cold discomfort which persists long after a lesser cooling level is resumed (87, 148, 159).

A major problem with subjective cooling control is timing. Webb (153) found that there is a temporal dissociation between heat production and heat output to the LCG. There is a delay following a step change in work rate before heat output reaches a new level. Webb (156) also found that while oxygen uptake and heart rate showed almost immediate stabilization to levels appropriate to the new metabolic rate, skin temperature, rectal temperature, and LCG heat removal were considerably slower; in some instances requiring nearly an hour to reach their new equilibrium values. These findings are consistent with the results of Series A, were the delay time was observed to be 30 min to over 1 hr, depending upon the degree of deviation from thermal comfort. The delay represents an obligatory period of heat storage after the onset of a new metabolic rate and an equal period of destorage at the termination of work. This suggests that there is a resetting of the set-points of the regulatory system, enabling the body to run warmer as metabolic rate rises (97, 153, 159, 160).

The thermal control problems noted above may be lessened if the subject controls his cooling by an anticipatory behavioral response as noted in Series D, or by the use of an automatic control system. Figures 4-1 and 4-5 may be used as a guide in the design of an automatic controller that would continuously monitor metabolic rate and adjust LCG inlet temperature or flowrate accordingly.

Several researchers have investigated automatic LCG cooling control and various prototype units have been built employing principles similar to that described above. Physiologic signals used in automatic cooling control have included oxygen uptake (140, 161), heart rate (141), skin temperature (92, 130, 131, 141, 156), and sweat rate (87, 160).

Chambers (31, 32) built and tested an automatic controller that varied LCG inlet temperature in a manner inversely proportional to evaporative heat loss. He used a simplified 3-node (skin, muscle, core) electrical analog model to correlate his results. Extracting the LCG inlet temperature data of Chambers, and plotting it against metabolic rate instead of sweat rate, permits a direct comparison with the results of Figure 4-1. Chambers' results superimposed in this way show excellent agreement.

Crocker, Jennings and Webb (37) supplied varying LCG inlet temperatures to test subjects in response to their subjective feelings of comfort while wearing an Apollo-type LCG at atmospheric pressure. Their results are also consistent with Figure 4-1.

Webb and coworkers (155, 156) built several automatic LCG controllers that varied LCG inlet temperature in response to oxygen consumption, heart rate, skin temperature, rectal temperature, and LCG, or total heat removal rate. They also used a 3-node biothermal model to correlate their data. Some of Webb's results are shown in Figure 4-1. Again, the results demonstrate the same trends.

Before concluding the discussion of Figure 4-1, two additional points should be made. Firstly, the relationship shown between LCG inlet temperature (also LCG flowrate) and metabolic rate has been derived based upon an examination of body heat storage at comfort. In other words,

Figure 4-1 expresses the relationship between inlet temperature and metabolic rate for body heat storage values constrained to the heat storage based comfort zone. Therefore, the type of LCG cooling control expressed here is proportional to total body heat storage, a factor not yet considered in LCG controller design.

Secondly, these results represent equilibrium or steady-state conditions. No attempt has been made to predict the LCG inlet temperature selected for comfort under dynamic conditions. The latter has been a topic of investigation by Webb (162).

Figure 4-2 expresses the LCG heat removal rate required to maintain comfort for various metabolic rates. This relationship is the same, irrespective of the mechanism used to remove the heat in the LCG. That is, it is equally valid for constant LCG flowrates at variable inlet temperatures or constant inlet temperatures at variable flowrates. The regression curve fit is second order and the equation of the curve is:

$$\text{LCG heat removal required for comfort} = .00063\ (\text{Met.Rate})^2 + .257\ (\text{Met.Rate}) + 73.5.$$

The correlation coefficient for the curve is 0.96 and the standard error is $\pm$31 watts. It should be noted that the correlation is even more accurate than that of Figure 3-89a. This is a consequence of the error analysis and the deletion of data points that fall out of the comfort zone.

The predictions of the mathematical model for zero environmental heat exchange were shown in Figure 3-91a and are reproduced for convenience in the clear overlay preceding Figure 4-2. Again, it can be seen that the regression curve falls within the prediction band of the mathematical model. The latter result is truly noteworthy because it means that the manner in which a test subject regulates his LCG for comfort can be

accurately predicted by the mathematical model. In other words, the relationship expressed by the regression curve fit can be predicted on a theoretical basis. The model does this by utilizing calculations of body heat storage, combined with the comfort zone that has been developed here.

The results of 3 other investigations in which LCG heat removal was adjusted (either automatically or manually) according to subjective comfort are also shown in Figure 4-2. Chambers, Blackaby and Miles (32) controlled inlet temperature in a manner inversely proportional to evaporative heat loss while using mean skin temperature and subjective comments to evaluate comfort. Their data agree well with the results expressed here. Troutman (140, 141) and Webb (155, 156) automatically controlled LCG inlet temperature in response to several physiological parameters and used the limitation of sweating below 100 g/hr as an index of thermal comfort. Their data also show good agreement with the present results, although they both used a modified Apollo-type LCG.

It is interesting to note that the data of Troutman, Webb, and Chambers are in agreement with Figure 4-2, despite the fact that their experiments were conducted at atmospheric pressure. Apparently, pressure has little effect upon LCG heat removal. This is predicted from theoretical considerations of the heat transfer equations, although a slight effect resulting from increased evaporative heat loss and decreased skin temperatures at altitude is a possibility.

It is observed from Figure 4-2, that at higher metabolic rates, the relationship between LCG heat removal and metabolic rate is very nearly rectilinear. In order to achieve the high LCG heat removal rates required at high metabolic rates, it is necessary to use low LCG inlet temperatures. However, if inlet temperature becomes too low, it supresses

skin temperature enough to cause vasoconstriction (87, 148, 159). This results in reduced LCG heat removal at the skin surface. Such an off-comfort effect would be manifested by the LCG heat removal curve "tailing off" and becoming asymptotic at higher metabolic rates. It should therefore be realized that the rectilinearity of Figure 4-2 at high metabolic rates is, in itself, an indicator of thermal comfort.

Thermal comfort at high metabolic rates is predicated upon the adequacy of the LCG design to remove heat efficiently under these conditions. For example, it has been stated that the tube design of the Apollo-LCG has been optimized to accommodate peak metabolic rates of around 600 watts. Therefore, it would be expected that the LCG heat removal curve would become asymptotic if metabolic rates were in excess of this value. The result would be inadequate thermal comfort. Such a condition could be prevented by a modified LCG utilizing a greater contact surface area with the skin. Such an LCG could also utilize higher inlet temperatures to remove equivalent amounts of heat, thereby reducing the possibility of vasoconstriction.

The design of such an improved LCG is an example of the potential usefulness of the mathematical model. Figure 4-6 shows the predicted LCG inlet temperature required for comfort vs. metabolic rate, for LCGs of varying efficiency. The efficiency is expressed by the overall LCG heat transfer coefficient, which is a function of tube conductivity, contact surface area, tube shape, tube spacing, water flowrate and other parameters. As indicated by Figure 4-6, an LCG designed with heat removal characteristics superior to an Apollo-LCG could utilize significantly higher inlet temperatures.

The latest version of the mathematical model is currently being refined to permit parametric adjustment of the many factors affecting the LCG heat transfer coefficient, in order to achieve a desired level of LCG efficiency and thermal comfort commensurate with any particular set of metabolic and environmental requirements. Such an improvement will ultimately allow one to "tailor the LCG to the job" without the necessity for costly design and testing studies.

Figure 4-3 shows the final correlation between total evaporative heat loss rate and metabolic rate. The regression curve fit through the data is second order and the equation describing evaporative heat loss at comfort is:

$$\text{Total evaporative heat loss rate at comfort, watts} = -.00074(\text{Met.Rate})^2 + .818\ (\text{Met.Rate}) - 79.5.$$

The correlation coefficient for this fit is 0.88 and the standard error is $\pm$23 watts. It is observed that the correlation is significantly improved over the corresponding curve in Series D (Figure 3-89b). However, it is still not as good as that for LCG heat removal, simply because of the nature of the methods used and the difficulty associated with determinations of evaporative heat loss rate. Nevertheless, the correlation is still good, and the limitation of evaporative heat loss as reflected by the asymptotic behavior of the data is strongly evident.

Evaporative heat loss rate did not exceed 200 watts and was far less than LCG heat removal rates for the same metabolic rates. Also, the evaporative heat loss rates shown are much lower than corresponding rates that might be expected at the same metabolic rate without an LCG. This

is a reflection of the effect of the LCG in reducing sweat rate and heat strain.

The prediction of the mathematical model is the same as shown in Figure 3-91b, and is reproduced on the clear overlay preceding Figure 4-3. As in the previous correlations, the regression curve fit falls within the band predicted by the model. Therefore, the model is also capable of predicting evaporative heat loss rates at comfort for subjects wearing an LCG. This is particularly gratifying because it again confirms a strong theoretical basis for the behavior expressed by the data.

It should be mentioned that the correlations of Figures 4-2 and 4-3 are really dependent upon the type of LCG used. This is because the comfort zone utilized to affect these relationships was established while using an Apollo-type LCG. Therefore, the heat storage associated with comfort may be quite different for an LCG of a radically different design, such as a head cooling garment. However, for LCGs similar in design to the Apollo-LCG, these correlations are accurate and can be used to express comfort requirements. This also applies for LCGs with improved heat transfer coefficients (Figure 4-6) because these only alter the efficiency of heat removal, not the heat removal requirements for comfort.

One final point pertaining to this and the previous figures concerns the effect of environmental heat exchange. The correlations presented have been generated for conditions of zero environmental heat exchange (neutral environment). As delineated in the results of Series D, the effect of a cold environment would be to provide an alternative to evaporative heat removal. Consequently, sweating would be further reduced in a cold environment. Conversely, a hot environment acts to partially negate the effectiveness of the LCG as an alternate heat removal method

to sweating. Therefore, body temperature rise, sweating and evaporative heat removal must increase to compensate for the decrease in LCG effectiveness. The magnitude of the change required in LCG performance in order to maintain comfort for several environments ranging from hot to cold can be estimated from the results of Series D (Figures 3-94 and 3-95).

The final correlation (Figure 4-4) shows sweat rate and its associated evaporative heat removal rate as a function of metabolic rate at comfort. The data were determined by subtracting evaporative heat loss attributed to respiration and passive diffusion from total evaporative heat loss rate. A regression fit through the data yields a second order fit described by the following equation:

$$\text{Sweat rate at comfort, g/hr} = -.0007\ (\text{Met.Rate})^2 + .655\ (\text{Met.Rate}) - 52.6.$$

The fit has a correlation coefficient of 0.78 and a standard error of $\pm$26 g/hr. Since this correlation depends heavily upon the total evaporative heat loss data of Figure 4-3, it is to be expected that it would suffer from the same sources of error, with the final correlation coefficients being quite similar. Nevertheless, the results are satisfactory, especially considering that determinations of evaporative heat loss rate and sweat rate are tricky propositions at best.

The predictions of the mathematical model are also shown on the clear overlay preceding Figure 4-4. The validity of the relationship expressed by the above comfort sweat equation is enhanced by the fact that the regression curve and the data fit nicely within the band predicted by the model for sweat rate at comfort. Thus, the physiological response of sweating while wearing an LCG under comfort conditions is accurately predicted by the model. Active sweat rate is limited below 100 g/hr over

the entire range of metabolic rates considered and appears to be asymptotic to this value.

This result may be compared with the conclusion of Webb and Annis (159, 160), who set 100 g/hr as a desirable upper limit for total moisture loss consistent with subjective comfort while wearing an LCG. Their data included insensible transpiration and evaporative losses from the lungs, which can amount to one-half the total moisture loss at high metabolic rates. It appears, therefore, that the results of Webb and Annis may have been somewhat lower than the results expressed here. However, these investigators have acknowledged the conservatism of their sweat limits for high rates of work (156). On the other hand, it should be recognized that their experiments were conducted at atmospheric pressure, and under these conditions, evaporation rates are slightly lower than at altitude.

Chambers, Blackaby and Miles (32) also associated subjective comfort at high metabolic rates with sweat rates below 100 g/hr and decreased skin temperatures. Waligora and Michel (149) reported similar findings in an early study utilizing a prototype Apollo-LCG. Shvartz and Benor (124) recorded total moisture loss rates of 156 g/hr for subjects selecting their own inlet temperature and flowrate in accordance with subjective comfort while wearing an Apollo-type LCG at moderate metabolic rates.

In addition, many other investigators have reported significant reductions in sweat rate while wearing a cooling garment other than the Apollo-LCG (54, 77, 99, 122, 123, 165). Many of these authors have utilized a head-cooling garment or a partial body cooling garment, but the reduction or limitation of sweating while using these garments has been a consistent observation.

The Effects of the LCG on Thermal Comfort and Sweating

An important factor which has only been touched upon to this point is a discussion of thermal comfort and sweating for subjects with and without an LCG. Several authors have reported results in which high metabolic rates were presumably achieved with thermal comfort without an LCG. Metabolic heat was removed by convective, radiative and evaporative cooling alone.

Fanger (49,50) developed regression equations correlating thermal comfort with environmental parameters and measured physiological responses. Thermal comfort was based upon a subjective scale and was achieved at moderate work rates and above. This was accomplished by varying room temperature, relative humidity, wall temperature and other factors in such a way as to maximize convective and radiative cooling without limiting sweat rate. Under these conditions, sweat rates in excess of 300 g/hr were observed for sustained work loads on the order of 600 watts, which were consistent with subjective comfort. Fanger's comfort sweat equation is shown graphically in Figure 4-4 and is noticeably higher than the results expressed here with LCG cooling.

In a similar experiment, Webb (155) observed elevated sweat rates associated with comfort for nude subjects working in a room at 25°C. Some of his data are also shown in Figure 4-4.

Chato and Hertig (33) observed sweat rates of approximately 300 g/hr for subjects working at moderate metabolic rates (387 watts) with subjective comfort while wearing only athletic trunks, shoes and socks in a room temperature environment ranging between 13 to 24°C. They also conducted shower studies utilizing subjective control of shower temperature

at heavy workloads to maintain comfort, and concluded that some sweat secretion may be necessary.

Stolwijk, Saltin and Gagge (139) did not observe suppressed sweat rates when room cooling was varied to provide subjective comfort at high metabolic rates. However, none of the preceding studies utilized an LCG and therefore, have no basis for comparison with subjective comfort evaluations while wearing an LCG. The results of these studies are also vulnerable to the previous observation that man is a questionable judge of his own thermal state.

For the studies in which comfort and heat strain were measured and compared directly for subjects working with and without an LCG, the results overwhelmingly support the idea that reduced sweat rates, reduced heat strain and superior thermal comfort are achieved at all metabolic rates while wearing an LCG. Shvartz and Benor (124) showed reduced body heat storage, heart rate, rectal temperature, and sweat rate for subjects wearing an LCG in warm environments compared to the same tests without an LCG.

Gold and Zonitzer (54) have shown dramatic reductions in heat strain as measured by the Craig index of physiological strain for subjects exercising in hot, dry environments with an LCG, following identical runs without one. (The Craig index quantitates heat strain by comparatively weighting the increase in heart rate, rectal temperature and sweat rate). The same authors also noted reduced reddening and sweating of skin regions not directly covered by the cooling garment, and improved subject comfort with the LCG. Waligora and Michel (179) compared cooling characteristics of the Apollo pressure suit incorporating an LCG, with those of a Mercury pressure suit utilizing gas cooling alone. They found that the LCG assumes

the major burden of cooling, with increased comfort over the gas cooling system by reducing sweating.

Kissen, Hall, and Klemm (77) showed reduced heat strain measurements in severe hyperthermic exposure when subjects used a head and neck cooling garment. Williams and Shitzer (165) used a similar garment to demonstrate reductions in weight loss, heat storage, heart rate and other strain indices for subjects working in hot environments. Nunneley, Troutman and Webb (99) also observed reductions in heat stress in studies similar to those of Williams and Shitzer.

Schvartz (123) and Nunnely (98) reviewed the literature on water cooled garments of varying designs and ascertained the ability of the LCG to reduce heat strain and increase comfort. Finally, several years of experience in testing both at sea level and altitude conditions at the Johnson Space Center have firmly established the preference that subjects have for using an LCG to maintain comfort.

The comfort-sweat curve of Figure 4-4 is interesting from yet another standpoint. Although it expresses the asymptotic behavior of sweat rate at comfort, it also shows that some amount of sweating is desirable at moderate metabolic rates and above. In other words, comfort is not commensurate with complete suppression of sweating. In fact, elimination of sweating at moderate and high metabolic rates was associated with uncomfortably cold-sensations and even shivering in Series A

This is in agreement with the findings of Chambers (30) that a pressure suit equipped with an LCG still requires an oxygen ventilation system to maintain comfort by evaporation of sweat at high work rates. In the same study, Chambers also determined skin temperature zones associated with comfort (see Figure 4-7). These zones coincided with

minimal levels of sweat secretion. Zero sweat rates were related to subjectively cold and uncomfortable conditions. Nunneley, in her review of water cooled garments, states that optimum LCG cooling should also include minimal levels of sweat secretion. She summarizes the opinion of several papers that despite variations in environmental conditions or work load, a man wearing an LCG at comfort should never be cold or obviously sweating (30, 156, 160, 161). Waligora and Michel (149) also derived approximate comfort limits based on skin temperature that included provisions for minimal sweating at comfort while wearing an LCG.

On the other hand, it should be emphasized that the relationship of Figure 4-4 represents a delicate sweating balance associated with a heat-storage based comfort band. Therefore, for application in pressure suits, the use of heat rejection systems dependent upon evaporative cooling alone is marginal both from physiological and practical standpoints. Such systems require elevated total body heat storage, and thus increased heat strain, in order to produce the desired sweat and evaporation rates. Futhermore, in consideration of the fact that the maximum evaporative heat removal rate for current pressure suits using a ventilating gas is less than 300 watts (83, 98), systems such as that proposed by Chato and Hertig (33) would require radical departures in design.

The Mathematical Model as an Index of Heat Strain

Throughout this thesis, the value of the heat-storage based comfort band has been underscored. It was shown that the accuracy of the mathematical model predictions was improved when deviations from the comfort zone were small. It was also shown that the model could accurately predict the amount of LCG cooling that a subject would select to maintain comfort.

The model could actually predict the subject's behavioral response by making use of the comfort band. Sweating and evaporative heat loss at comfort were also accurately predicted, and agreed with the results of other investigators. However, in addition to its value as a tool for the preceding correlations, the mathematical model and the comfort band have application as a reference index for physiological stress.

It has long been known that tolerance of stored heat is strictly limited (18, 74, 108, 146). Excess body heat storage at first produces activation of compensatory mechanisms and subjective temperature awareness; then discomfort, deteriorating psychomotor capacity and eventually, collapse leading to death (86, 151). Blockley (18) and Kaufman (74) have shown that the physiological tolerance limit for stored body heat at rest is about 175 watt-hr. Signs of impending collapse include rising rectal temperature, heart rates above 160, flushed skin, inattention to work, and frequent headache, fatigue, and nausea (18, 74, 101, 152).

For tasks involving skilled performance, heat storage must be kept far below the limits described above for tolerance. Blockley (17), Webb (152), and Wing (167) have independently concluded that decrements in psychomotor performance appear when heat storage approaches 3/4 of the tolerance limit. NASA's Johnson Space Center has adopted 88 watt-hr as the permissible limit of body heat storage prior to impairment, and 117 watt-hr as the tolerance limit.

Some controversy continues on the relationship of heat storage limits to performance and tolerance, but the above limits have proven practical and realistic for a multitude of applications involving stressful environments. These limits are deliberately conservative in that they specify the likelihood that only a small percentage of individuals exposed will

experience performance impairment or collapse due to heat stress. The limits for physically fit individuals or those acclimatized to heat would be higher.

The fact that the mathematical model can accurately predict body heat storage in response to metabolism and environmental parameters makes it a valuable tool for assessing the degree of heat stress. This is accomplished by comparing the predicted results with the performance and tolerance limits. Furthermore, when used in conjunction with the comfort zone, the model can predict the degree of deviation from thermal comfort.

For example, the comfort and tolerance bands shown in Figure 4-8 were used with model predictions to generate sweat rate performance envelopes (Figure 4-9). It is observed in Figure 4-9 that at high metabolic rates (600 watts), the comfort band, performance limit, and tolerance limit almost coincide. This is a reflection of the fact that the Apollo-type LCG is not designed to provide adequate heat removal for metabolic rates greater than 600 watts in a neutral environment. On the other hand, it is observed that for lower metabolic rates, considerably higher inlet temperatures than those selected for comfort can be tolerated before performance becomes impaired. For example, at a metabolic rate of 350 watts, 16-20°C inlet water temperatures are required for comfort but performance does not become impaired until water temperature exceeds 27°C.

At first glance, the results of Figure 4-9 may appear paradoxical in that the sweat rate associated with performance impairment or tolerance limits actually decreases as metabolic rate increases. This indicates that an individual would actually sweat less at higher metabolic rates than at lower rates, before encountering thermal stress. However, this

apparent contradiction is explained by a consideration of skin temperature, core temperature, and body heat storage.

The performance and tolera . limits are each based upon a limiting value of body heat storage that is independent of metabolic rate. However, in order to reduce the amount of heat stored in the body at a high metabolic rate to the same level as that of a lower rate, more LCG heat removal is required and, therefore, a lower inlet water temperature is necessary. This means that the skin temperature must be increasingly lowered as metabolic rate increases, in order to keep body heat storage constant and below the performance or tolerance limits.

The decreased skin temperature inhibits the contribution of the peripheral or local response to sweating. This inhibition actually more than offsets the increased central response due to the higher rise in core temperature at the higher metabolic rate. The net result is an inhibition of the local sweating response that overshadows the increased central response and produces a lower sweat rate associated with performance or tolerance limits at higher metabolic rates.

This inhibitory characteristic of skin cooling is predicted by the model but requires additional experimental data for verification. Stolwijk and Hardy have recently performed water immersion experiments at various metabolic rates which tentatively support the idea of a reduced tolerance at colder water temperatures and higher metabolic rates, but additional studies in this area of performance and tolerance are needed.

The dependence of active sweat rate upon heat storage and body temperatures limits the usefulness of sweat rate alone as an index of heat stress. Indicators such as the Belding-Hatch Stress Index or the P4SR are unsafe

to use as a means of predicting sweat rate or stress unless all the conditions are similar to those for which the index was originally derived.

For example, the P4SR was derived from experimental data for subjects wearing limited clothing who were heat acclimatized (103). As a consequence of the latter, the sweat rates associated with tolerance limits are considerably higher than those expressed in Figure 4-9 for unacclimatized subjects. Gillies and Webb (103) do not recommend the use of P4SR for predicting sweat rate, but rather as a means for comparing environments in terms of thermal stress, to be followed by experimental evaluation of the environments, with sweat production being taken as one of several dependent variables.

As mentioned previously, consideration of skin temperature is an important factor when an LCG is used for cooling. Mean skin temperature and its range and distribution are pertinent measurements in the determination of thermal contact. Kerslake (76) has shown that for resting subjects, $\overline{T}_S$ for comfort is about 33°C with a 6°C longitudinal gradient; the head being the warmest and the hands and feet the coolest. Allan (1) and Webb and Annis (159) have shown that as metabolism rises from rest, the mean skin temperature associated with comfort and the absence of sweating falls.

Chambers (32) has derived a subjective comfort zone based on skin temperature, indicated in Figure 4-7, that shows a decrease in skin temperature associated with comfort as metabolic rate increases. Hurrah and Buchberg (62) and Walagora and Michel (149) have presented similar results, shown in the same figure. Data from the results of Series A-D are also shown superposed with the results of these investigators in Figure 4-7, and agreement is good.

The importance of a normal skin distribution for comfort has also been mentioned by British workers designing cooling equipment (23, 25, 26), and the effects of skin temperature on comfort and thermoregulation while wearing an LCG are summarized nicely by Nunneley (98).

> "As the temperature is lowered through the comfort zone there is generalized cutaneous vasoconstriction until conductance is reduced to its minimum value, attributable to tissue heat conduction. Any further temperature decrease involves passive body cooling; when cooling exceeds metabolic heat production, the major defense mechanism is to increase the latter by shivering or voluntary activity. Environmental temperature rising through the zone of vasomotor control produces cutaneous vasodilatation, warming of the skin, a decrease in core-skin temperature gradient and increasing conductance. In heat stress, the cutaneous circulation may demand a significant portion of cardiac output. As the heat load increases beyond one threshold temperature, sweating begins and is gradually increased along with further vasodilatation. The physiological reaction to a given heat load depends partly upon whether the source is internal (metabolic) or external."

The previous discussion has centered upon the importance of skin temperature when LCG cooling is used to provide thermal comfort. However, it is only a part of the story. Several additional factors are equally, if not more, important in determination of comfort and heat stress. These are the rectal temperature, the sweat rate and body heat storage.

The importance of rectal (or tympanic, or head core) temperature and its effects upon sweating and heat stress have been emphasized several times throughout this thesis. It has a stronger influence upon sweat rate and body heat storage than does skin temperature (133-139, 172). It follows then, that its influence upon comfort and heat stress is considerable. Whereas skin temperature was reduced at higher metabolic rates by LCG control consistent with comfort, the same does not hold true for core temperature. When a man begins working, his rectal temperature

rises in spite of comfort LCG cooling at the skin surface (155, 156). Rectal temperature continues to rise until it reaches a plateau associated directly with metabolic rate.

The relationship between core temperature rise and metabolic rate was established in 1938 by Nielson (97). It has been confirmed repeatedly and is also valid when strong LCG cooling is applied. Figure 4-7 shows core temperature versus metabolic rate when subjective comfort was achieved be means of LCG cooling. The results shown are from Webb (155, 156), Harrah and Buchberg (61), and an envelope of data from five other studies (103). Comfort data from Series A are also shown and agree well with the other results. These findings suggest that the body appears to prefer a higher core temperature at higher work levels and probably accomplishes this by adjustment of its internal thermostat or set-point (98).

The relationship of sweat rate and evaporative heat loss to comfort and heat stress has been discussed at length. Sweating results primarily from increases in skin temperature and core temperature, with the latter having a greater weight. The reason that sweating is suppressed to limits below 100-200 g/hr at comfort (see Figure 4-4) is that relatively small increases in core temperature at higher metabolic rates are countered by large decreases in skin temperature brought about by LCG control (as typified by the skin temperature comfort zone of Chambers). It is this simultaneous increase in core temperature and decrease in skin temperature (shown in Figure 4-7) that accounts for sweat suppression.

Such situations, in which central warm reception collides with messages of cold from the skin are paradoxical, but not uncommon. As Benzinger (8) observed in his classic essay, "The Human Thermostat",

"The running athlete in cool weather, the ascending mountaineer, the skier on sunny slopes, all lightly clad, and perhaps the swimmer in tropical waters, experience skin temperatures low enough for cold receptors to be active, while the athletic effort elevates internal cranial temperature above the set point. Cold reception at the skin may then interfere with the thermostatic control and prevent or delay an immediate adjustment of elevated cranial internal temperatures through sweating. However, unnecessary excessive or prolonged evaporative cooling is prevented after termination of the muscular effort.

The opposite condition, central temperature below the set point, combined with a warm skin, has been studied and clarified by experiments in water. It is a transient state of tranquility and subjective comfort in which no thermoregulatory impulses seem to arise at either central or peripheral thermoreceptors. Thus, due to a lack of driving impulses, heat regulation is suspended when the skin is warm and the centers are cool. Likewise, heat regulation is delayed or suspended when the skin is cold and the centers are warm."

Under normal conditions, without an LCG, it is the evaporation of sweat that enables men to work in hot environments. However, even with an LCG, core temperature must [illegible] order for sweating and evaporative heat removal to be adequate at high metabolic rates. This means that the body must store heat in order to sweat, since heat storage is influenced to a greater extent by increases in core temperature than skin temperature. Consequently, there is a certain amount of body heat storage, and therefore, heat stress associated with sweating. This was shown to be the case by Blockley and Roth (19) who demonstrated that the amount of sweating associated with LCG heat removal has a powerful influence on the tolerance time in a stressful environment. Furthermore, high sweat rates can produce fluid and electrolyte imbalances and eventual collapse (56, 79, 86, 154). Providing drinking water to replace lost fluids does not always remedy the situation because paradoxically, excess heat storage has been shown to cause subjects to avoid drinking, with ensuing voluntary, significant dehydration (17, 74, 154).

The previous arguments have led the author to conclude that the best index of comfort and heat strain is one that takes all of the previous factors into consideration; namely, body heat storage. The comfort, performance impairment, and tolerance bands of Figure 4-8 tie together all of the effects of skin temperature, core temperature and sweat rate. The heat-storage based comfort zone, combined with the parametric predictions of the mathematical model, provide relationships for LCG heat removal, sweat rate, rectal temperature and skin temperature. These relationships conform closely to the available experimental data. Similarly, parametric predictions of the mathematical model, combined with the performance and tolerance heat-storage limits resulted in Figure 4-9, which can be used to assess the degree of heat stress and deviation from comfort.

The significance of heat storage is further supported in studies by Webb (155, 156) which show that even with adequate LCG cooling commensurate with subjective comfort, a man working at higher metabolic rates will experience a rectal temperature increase resulting in a net increase in body heat storage, despite a large drop in skin temperature. Whereas this increase in body heat storage (and heat strain) is not apparent from comfort criteria based upon skin temperature or sweat rate, it is taken into account in the heat storage based comfort band of Figure 4-8, since the heat storage associated with comfort while wearing an LCG is shown to increase with metabolic rate.

Accuracy of the Mathematical Model

The discussion now turns to some general comments regarding the accuracy of the mathematical model. It has been shown that model predictions are most accurate for testing conditions near thermal comfort.

The greater the deviation from comfort, the greater the error of the model predictions. This was explained in terms of the increased responses required by the thermoregulatory system in order to return the organism to homeostatic conditions after a large metabolic or environmental step-change; and the difficulty in simulating these complex responses.

For off-comfort conditions, errors generally consisted of underpredictions in LCG heat removal, overpredictions of evaporative heat loss and sweating, and underpredictions of mean skin temperature. This was especially evident for the cold conditions of Series A, where shivering was frequently encountered. The magnitude of the errors, although significant, was not large enough (generally below 10% of metabolic rate) to warrant modifications to the equations simulating the active thermoregulatory system responses (vasodilatation, vasoconstriction, shivering and sweating). This decision resulted in part from the fact that inaccuracies in predictions for off-comfort conditions were just as easily attributed to test data error resulting from test procedures or data management as to improper model simulations.

Considering the relatively small magnitude of the errors and the factors described above, it was not possible to isolate the model as the major source of these errors. Furthermore, modification of the controlling equations seemed improper in light of the good agreement achieved with test data for comfort conditions. On the other hand, it was possible to modify the model to improve predictions of individual skin temperatures. This was accomplished by modifying the equations describing the passive (or controlled) system.

As mentioned in the discussion of the results from Series A, the model is better suited for determining total heat balance relationships

than for the partitioning and distribution of heat among the individual body compartments. That is not to say that the performance of the model was unacceptable for the latter. On the contrary, the largest errors observed in individual skin temperatures at equilibrium were on the order of 2-3°C for comfort conditions and somehwat larger for off-comfort conditions.

However, it was observed that chest (or trunk) temperatures were consistently underpredicted throughout. The chest skin temperature was usually the lowest predicted temperature, followed closely by the leg temperature (the forehead and hand temperatures were usually the warmest). Although the test data also showed leg and chest temperatures as the coldest, chest temperature was not consistently colder than that of the leg skin. Furthermore, predictions of leg skin temperature were often higher than the actual data.

It was decided that the model was extracting too much heat from the trunk area into the LCG and not quite enough from the arms and legs. Modifications were made to the program that consisted of alterations in the partitional heat removal characteristics of the LCG. This resulted in improved predictions of individual skin temperatures with no appreciable effect upon the total heat balance responses of sweating, shivering, blood-flow or heat storage. The effect was simply to redistribute the skin temperature computations to improve agreement with the test data. This was done by altering the percentage heat removal by the LCG assigned to each body area.

The changes made are summarized in Table D8 of Appendix D, and the resulting improvements in individual skin temperature predictions are shown for several cases of Series A and C in Figures D12 and D1 to D4 of

Appendix D. The magnitude of the changes shown in Table D8 was determined largely by trial and error.

The errors described above could just as easily have resulted from an overly large vasoconstriction signal in the model's chest skin region, as opposed to the use of an unrealistically large heat transfer coefficient in the model between the skin of the chest and the LCG. However, because of reluctance to change active thermoregulatory system parameters, it was judged more prudent to modify the latter. Fortunately, these modifications (decreasing the weighting factor for LCG heat extraction from the chest while increasing it for the arms and legs) resulted in improved individual skin temperature predictions without affecting other parameters.

Additional Model Development

Although the performance of the model has exceeded expectations, it is evident that more development needs to be done. However, this should be tempered by the knowledge that any model is, by definition, simpler than the system it attempts to represent. In keeping with this guideline, changes to the equations governing the controlling system are difficult because of the scarcity of off-comfort data. Based upon available data of the total heat balance type, changes in controlling equations of sweat, shiver, and blood-flow rates are not justified.

What is really needed are more detailed data on the blood-flow characteristics, sweat rates, and shiver rates for the individual body compartments of the organism while under stress (such as head, hands, feet, upper and lower arms, trunk, etc.). In addition, more information is required on regional and internal heat generation terms and internal

temperature distributions within body regions (including internal organs). Until such information is determined and made available, changes to the controlling equations of the mathematical model are only speculative and of no real benefit, especially in view of the more than adequate performance of the model in predicting total heat balance data, external skin temperature distributions, and body heat storage and heat stress.

On the other hand, there is considerable room for improvement to the passive or controlled system in the model. To begin with, it is apparent that the number of body compartments needs to be increased. The current version of the model has 10 body compartments (head, trunk, 2 arms, 2 legs, 2 hands, and 2 feet). However, the data of Series A and C indicate that there can be as much as a 7°C difference between the skin temperatures of the abdomen, back, and upper chest while wearing an LCG. Obviously, characterizing these 3 regions by one trunk segment is an oversimplification. Similarly, the test data also show significant temperature differences between the upper and lower leg (calf versus thigh) and upper and lower arm (biceps versus forearm).

These shortcomings will be corrected in a new version of the model which is currently being developed. The technical description and appropriate equations for this new model are presented in Appendix F. For additional information, interested parties should contact the author, care of the Johnson Space Center. The new model will have as many as 19 body compartments, with the trunk being divided longitudinally into several cylindrical regions from the upper to the lower chest and the arms and legs being divided into at least upper and lower segments.

Another problem with the existing model is its failure to account for temperature distributions in any spatial direction other than

radially outward from the center of each body compartment. For most applications, this is perfectly acceptable. However, for applications, in the manned space program, the structure and definition of the model is now being directed at certain unique characteristics or conditions which are deemed of primary importance.

One of these conditions is exposure to widely disparate environments on different sides of the body. This undoubtedly would result in different skin temperatures for those regions of the body exposed to the different environments. The effect of this simultaneous hot and cold environment on comfort is not well known. A study by Hall and Klemm (59) indicates that men exposed to widely disparate radiant environments on opposite sides of the body find the situation comfortable if the mean skin temperature is normal. However, additional data are needed to verify this finding.

The test data of Series A and C indicate that considerable temperature differences are also possible between different sides of the same body compartment when the heat is generated internally by metabolism with a uniform environment rather than externally from a disparate environment. Specifically, temperature differneces of up to 3°C were observed between the chest and the back with uniform test conditions and moderate metabolic rates (See Figure 3-1, Series A Results).

The current model has no provision for such two-dimensional variations in skin temperature. However, the new version of the model will consider spatial temperature variations in both the radial and angular directions (as measured from the centerline of each major body segment) and will prove useful in analyzing the problems discussed above. The added capability of angular temperature variation is built into

the partial dfferential equations describing the passive system in the upcoming model and is also summarized in Appenidx F.

Another error source in the current model is the separation of radial temperature variations into 4 layers (Figure 2-7). Each of the body compartments in the passive system is characterized by only 2 thin layers (skin and fat) and 2 thick layers (muscle and core). This simplified approach, using the so-called lumped parameter finite difference method, can lead to errors during the development of new temperature gradients. This is especially true within the muscle and core layers, which are relatively thick and should have continuous temperature variation across the layer.

Obviously, characterizing each layer as a single lump at one temperature is a simplification that can lead to errors, especially in the transient response of the model. During moderate heat stress, such errors are small because the gradients are small and convective heat transfer by the circulatory system is the major avenue of heat flow (136). However, during exposure to severely stressful environments, or conditions that cause large deviations from comfort, the gradients and their associated errors can become significant.

Also, the use of an LCG causes lowered skin temperatures and reduced convective heat flow by the bloodstream due to vasoconstriction effects. This can lead to large conductive gradients between the core and the skin, resulting in considerable errors in a 4 layer model (although these errors tend to diminish as steady-state is approached).

A simple remedy to the problem consists of introducing additional layers into the controlled system. This is the approach that was followed by Wissler in his one-dimensional model (168), and will be

adopted in the new model, as outlined in Appendix F. The number of layers will be increased and can be selected by the user, depending upon the degree of stress associated with a particular environment. The solution to the equations makes use of the ADI (alternating difference implicit) numerical method technique, and promises increased accuracy. These improvements, of course, increase the complexity and the computer time required to run the model, but should provide overall improved performance, especially for off-comfort conditions.

Before concluding the discussion of model accurancy, one final note should be touched upon. As mentioned previously, any mathematical model of the human body is, by necessity, an oversimplification of the real system. There are effects and counter-effects which, due to their complexity, are beyond the capability of the model to simulate. It is likely that several of these effects have contributed in some form or fashion to the errors observed in this model. Examples of 2 such effects are the recruitment of muscle fibers, and the role of 24-hr rhythms in thermal balance.

The current model assumes that for a step increase in metabolic rate, all the muscles in a given muscle compartment are instantaneously activated and immediately supplied with all of the blood required for oxygen transport. There is no attempt to make allowances for the development or repayment of an oxygen debt, or for the recruitment effect, whereby groups of muscle fibers are activated in a given muscle in proportion to the required load.

The other effect, which has only recently been identified, is the possible existence of a 24-hr rhythm relationship between heat production and heat loss. Paul Webb, in a 1971 study (157), showed a diurnal

rhythm in body heat storage over 24-hr periods in which subjects wore an LCG that was automatically adjusted to maintain comfort throughout the experiment. Total body heat storage was shown to vary sinusoidally with positive values for the 12 wakeful hours and negative, destorage values for the 12 hours encompassing the subject's sleep periods. Body temperatures and total heat storage were unchanged at the end of each 24-hr period and the observed rhythms in heat production, heat dissipation and heat storage appeared to follow a pattern closely related to the diurnal swings in body temperature frequently described in the literature.

The observed variations in heat storage were surprisingly large, with values as high as $\pm$35 watts, despite the fact that the subjects reported complete comfort over the entire experiment. The implications of such a 24-hr rhythm in heat storage are obvious. Many of the errors in the heat balance data of Series A, B, C and D may, in fact not be errors at all, but normal variations in heat storage occurring in a diurnal fashion.

The integration of the thermoregulatory model with simultaneous models of the cardiovascular, respiratory and other physi'gical systems is a project being undertaken by the Biomedical Research C. ce of NASA's Johnson Space Cente . Such an integrated approach may correct some of the shortcomings of the type described above. Fortunately, the applications and requirements of the thermoregulatory model (total heat balance, overall heat loss paths, average skin temperatures, total body heat storage, heat stress and comfort index, etc.) are so relatively coarse as to transcend the errors associated with complex second order effects of the kind just described. This is the single, most important

factor justifying the continuing development of mathematical models for thermoregulation.

Additional Applications of the Model

In addition to its usefulness as a research tool for investigating the physiological responses of the thermoregulatory system, and as an index for heat stress, the mathematical model has several other attractive applications. For example, the model can be used to analyze and predict the effectiveness of the LCG for warming subjects in cold environments. It has been shown (101) that one of the major problems facing divers at great depths is excessive loss of body heat. This can lead to shivering and performance decrements which make the accomplishement of undersea tasks difficult.

Webb (158) has investigated the application of LCGs to rewarm divers by circulating warm water through an LCG after the dive. He found that divers submerged in water ranging from 5 to 15°C for up to an hour required an average of 244 watt-hr of LCG heating to replace the heat lost during the dives. The completion of rewarming was not reliably indicated by rectal, ear canal, or skin temperature measurements; but rather by the release of body heat that had been previously conserved, a rise in heart rate, the restoration of a normal body heat balance, and the return of cutaneous vasomotor control. The mathematical model is currently being used to analyze Webb's results.

More interesting perhaps is the potential application of LCGs to provide a heat balance for subjects during exposure to a cold ervironment. Fig e 4-10 shows the predictions of the mathematical model for the hypothetical case of a clothed individual at a metabolic rate of 200 watts in a cold environment with and without an LCG. The results demonstrate

the usefulness of the model as a guide for selection of LCG parameters (flowrate, inlet temperature, etc.) required for a particular environment. This is shown by the decrease in negative heat storage (and shivering) as LCG heating is increased. The set of inlet temperatures formed by the intersection of the constant inlet temperature lines with the comfort band (darker lines) indicates the amount of LCG heating required at each environment in order to maintain comfort.

As mentioned previously, the mathematical model also shows promise as a tool for designing and analyzing new LCGs. Of special interest in this area is the recent development of head-cooling garments. The results of several investigations (98, 122, 123, 126, 162-166) indicate that the head and neck are probably the most efficient areas for removal of heat by liquid cooling. This apparently results from the absence of significant vasomotor control in these areas. Thus, vasoconstriction, which may significantly reduce LCG heat removal in other regions of the body, is absent in this case. This allows a disproportionately large amount of heat to be extracted from the head and neck.

However, the usefulness of the head-cooling garment remains a controversial subject because some investigators claim that it may subcool the blood supply leading to the hypothalamus, thus inhibiting normal thermoregulatory system responses of sweating and vasodilatation, while providing a false sense of subjective comfort. If this were the case, it would be expected that head core temperatures would decrease, sweat rates would be reduced or remain unchanged and deep body (rectal) temperatures would rise.

In an attempt to investigate these effects, the mathematical model was used to simulate an experiment performed by Williams and Shitzer (165)

in which subjects were exposed to a harsh environment of 47°C at 40° relative humidity at metabolic rates of about 150 watts. Runs were made with no LCG cooling and then with a head-cooling garment supplied with inlet water temperatures of 10-12°C at flowrates of 40 liters/hr. The model predictions and comparisons to avaiable test data are shown in Figure 4-11.

The model results match the available test data well and indicate that significant subcooling of the hypothalamic blood supply is probably not occurring. This is concluded from the fact that rectal temperature and heat storage are both reduced, which implies a reduction rather than an increase in heat strain. The reduction in rectal temperature occurs because a relatively large amount of metabolic heat is being transferred to the head-cooling garment. Consequently, sweat rate is also lowered. On the other hand, the predicted drop in hypothalamic temperature caused by head cooling is not low enough to cause a subcooling effect. This drop is caused by conductive cooling to the LCG at the skin surface rather than direct cooling of the blood supply which would have resulted in a marked decrease in hypothalamic temperature, associated with an increase rather than a drop in rectal temperature.

The mathematical model can also be used to investigate the probable effect of LCG cooling upon the threshold level of thermoregulatory responses such as sweating, shivering and peripheral blood-flow. Figure 4-12 shows the results of simulations made for a subject wearing light clothing and working at various metabolic rates in a room temperature environment (21°C) with and without an LCG. For the case of no LCG, it is seen that at metabolic rates below 160 watts, shivering increases

almost rectilinearly whereas for rates greater than 160 watts, sweating increases in a rectilinear fashion.

The effect of the LCG upon this curve was determined by making simulations using a fixed inlet temperature of 27°C with a flowrate of 109 liters/hr. The results for the fixed inlet temperature have the effect of displacing the no-cooling curve to the right, thus moving the thermoneutral metabolic rate to 215 watts. The same effects are also shown for the vasoconstriction/vasodilatation curve. Here, skin blood-flow is reduced at lower metabolic rates due to constriction and increased at higher metabolic rates due to dilatation. Again, the effect of the LCG is to shift the curve to the right. Note that the thermoneutral point for sweating and shivering occurs at the same metabolic rate as that for vasoconstriction and vasodilatation. This is a consequence of the use of approximately the same core and skin set-points in the equations that characterize these processes in the mathematical model.

Other applications of the model are not necessarily limited to cases in which subjects are wearing an LCG. For example, another use of the model as a strain index is shown in Figure 4-13. Here, runs were made simulating athletic conditioning programs in which subjects jogged at rates of approximately 1 mile every 8 min in hot and humid environments (35°C at 60% R.H.). The results indicate that under such conditions (which are typical of many summer football training sessions), heat storage can reach levels of performance impairment after 4 min, and may reach tolerance levels after 7 min. Although such results are not universally applicable since factors like conditioning, body size and structure, etc., are not taken into account, they do provide a reference that can be used as a worst-case guide for safe exposure time of athletes to sustained exercise

in stressful environments. Incidentally, the results of informal questionnaires concerning the summer jogging programs of NASA test subjects in Houston have provided general credibility to the above predictions.

Another useful application of the model is in the planning of hardware acceptability and human performance tests to ascertain that test conditions are satisfactory from the standpoint of safety. For example, Figure 4-14 shows the predicted time for skin temperature to reach pain threshold limits for subjects exposed to high incident radiation heating sources while wearing clothing with variable insulation properties. The predicted results for nude subjects correlate well with available data in the literature (103). Typically, results like these are used in the design of fire fighting suits; and have also been used to determine the acceptability of NASA space suit designs for providing adequate protection from test conditions simulating severe solar and thermal exposure while on the lunar surface or in deep space.

Another interesting area of application of the mathematical model is in the investigation of the effects of altitude on thermoregulation and heat loss. From the equations of convection and evaporation heat transfer, one would predict that the effect of altitude upon heat loss would be to decrease convective heat loss while increasing evaporation heat loss (see equations 2.15 and 2.24, Appendix B). Total heat loss should remain unchanged. Decreased convective heat loss is predicted because the convective heat transfer coefficient between the skin and the surrounding air decreases due to decreased energy transfer accompanying decreased pressure forces at altitude. Increased evaporation loss is predicted due to an increased mean free path between collisions of water vapor molecules, resulting in an increased mass transfer coefficient.

Although experimental data are not abundant in the literature, several recent studies have verified the above conclusions (53, 60, 67, 85a, 143). In particular, the recent work of Varent et al. (143) is of special interest. Lowlanders (subjects unacclimatized to altitude) were tested at sea-level and then at high-altitude (3800 meters) at metabolic rates of 581 watts in a closed room in which the environmental conditions (other than barometric pressure) were kept constant. The results were then compared to those for acclimatized subjects who were natives at the high-altitude location. Body temperatures and heat loss were measured and the results for the sea-level and high-altitude tests were compared.

Varene et al. found that the effect of altitude was to decrease convective heat loss by about 3% while increasing evaporative heat loss by almost 10% in unacclimatized subjects. They also found that increases in deep-body (core) temperature were not affected by the altitude but that mean skin temperature increased during exercise for unacclimatized subjects at sea level and acclimatized subjects at altitude, but actually decreased for unacclimatized subjects at altitude. The paradoxical drop in mean skin temperature resulted in a slightly lower heat storage rate (3%) for unacclimatized subjects at altitude.

This finding could not be reproduced in the initial simulations of the mathematical model, and evidently resulted from some physiological response of the thermoregulatory system that was not anticipated. (The results of Varene's study and the comparable model predictions are shown in Table 4-1.) In an attempt to explain the results, several model parameters were varied to try to duplicate the experimental result of a decrease in skin temperature during exercise at altitude.

It was found that a 50% reduction in the skin blood-flow rate used in the model produced the necessary decrease in mean skin temperature similar to Varene's experiment. Without the 50% reduction in peripheral circulation, calculated skin temperature increased and more closely matched the data for acclimatized subjects. From this model result, it may be surmised that in unacclimatized subjects at altitude, blood-flow to the skin is probably sacrificed so that more blood is available to assist the working muscles in their hypoxic condition. The decrease in skin blood-flow then accounts for the drop in skin temperature, which, in turn, contributes to the decrease in convective heat loss.

On the other hand, the model results for the experiments with acclimatized subjects indicate that the process of acclimatization to altitude probably involves a restoration of normal skin blood-flow. This is permissible after long term acclimatization because the working muscles then receive adequate oxygen supply due to an increase in the number of red blood cells (polycythemia). This results in an increased arterial oxygen capacity (from 20 to 30 volumes percent). In addition, increased myoglobin levels in the working muscles themselves facilitate oxygen transfer. The latter responses are well known physiological adaptations that accompany acclimatization to altitude (101, 102).

One additional benefit of this study was an improvement in the model's characterization of respiratory heat loss. Initial runs could not produce the same levels of increased evaporative heat loss in unacclimatized subjects that accompanied Varene's data at altitude. It was found that the model was not accounting for the increase in respiratory minute volume produced by hyperventilation in response to hypoxia. The respiratory response curve shown in Figure 4-15 was then added to the model, and

the resulting increase in evaporative heat loss by respiration brought the model predictions into closer agreement.

Another interesting application of the model involves the effects of altitude on heat loss in a deep space environment. On Earth, in a gravity environment, convection and evaporation normally occur by 2 processes -- forced and free convection. Forced convection is heat loss from a forced velocity field, while free convection is heat loss resulting from density gradients in the air, leading to air motion. On earth, differences in temperature between the skin and the surrounding air lead to the air density differences that provide equivalent velocities sufficient to remove heat and water vapor, even if there is no forced air velocity. However, in a gravity-free environment these density gradients cease to be effective; consequently, heat loss by free convection is absent. It therefore becomes necessary to provide a minimum air circulation in order to assure that forced convection and evaporation heat removal will be adequate to prevent potentially serious problems of high body temperature and heat storage. The minimum forced convection velocity required depends upon the spacecraft environmental temperatures and pressure, and the individual's metabolic rate. By using the mathematical model to simulate these variables, it was found (81) that forced air velocities of 25 ft/min or more provide acceptable heat removal for moderate metabolic rates and tolerable heat removal for high work rates. These results are shown in Figure 4-16.

The number of other potential applications for the mathematical model are numerous, however, one is particularly noteworthy. In order even to attempt to understand the complex processes that occur in the body, it is necessary to appreciate the intricate interactions that occur

between the various physiological systems for maintenance of homeostasis. Thus, the thermoregulatory system depends upon and influences the circulatory system, which in turn affects the respiratory system which, in turn affects the excretpru system and nervous systems, ard so on. The mathematical model described here is inadequate in that it does not properly interface with similar models characterizing other physiological processes. For that matter, models of the cardiovascular system, respiratory system, nervous system, etc., are also inadequate if they do not interact with this or similar models. Thus, the integration of this model with those of other physiological systems is an ultimate application which will not only provide more realisti_ boundary conditions for each model, but will also make possible meaningful simulation of whole-organism responses. This goal has yet to be realized but is currently being undertaken by the Environmental Physiology Branch of the Johnson Space Center. The development of such an integrated model could doubtless provide better insight into the interactions between man and his physical environment.

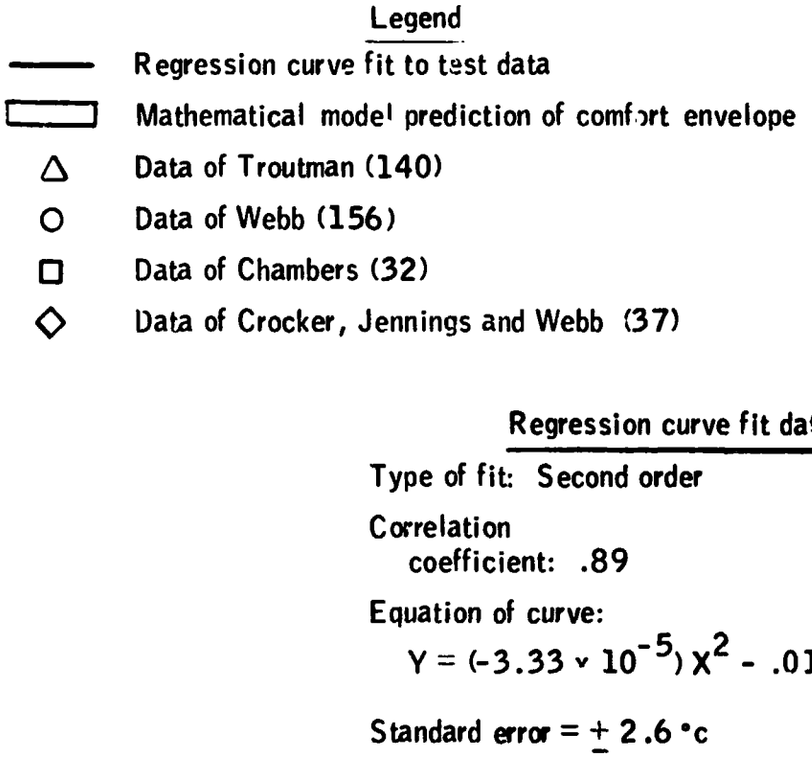

Figure 4-1.- LCG inlet temperatures selected for comfort vs metabolic rate.

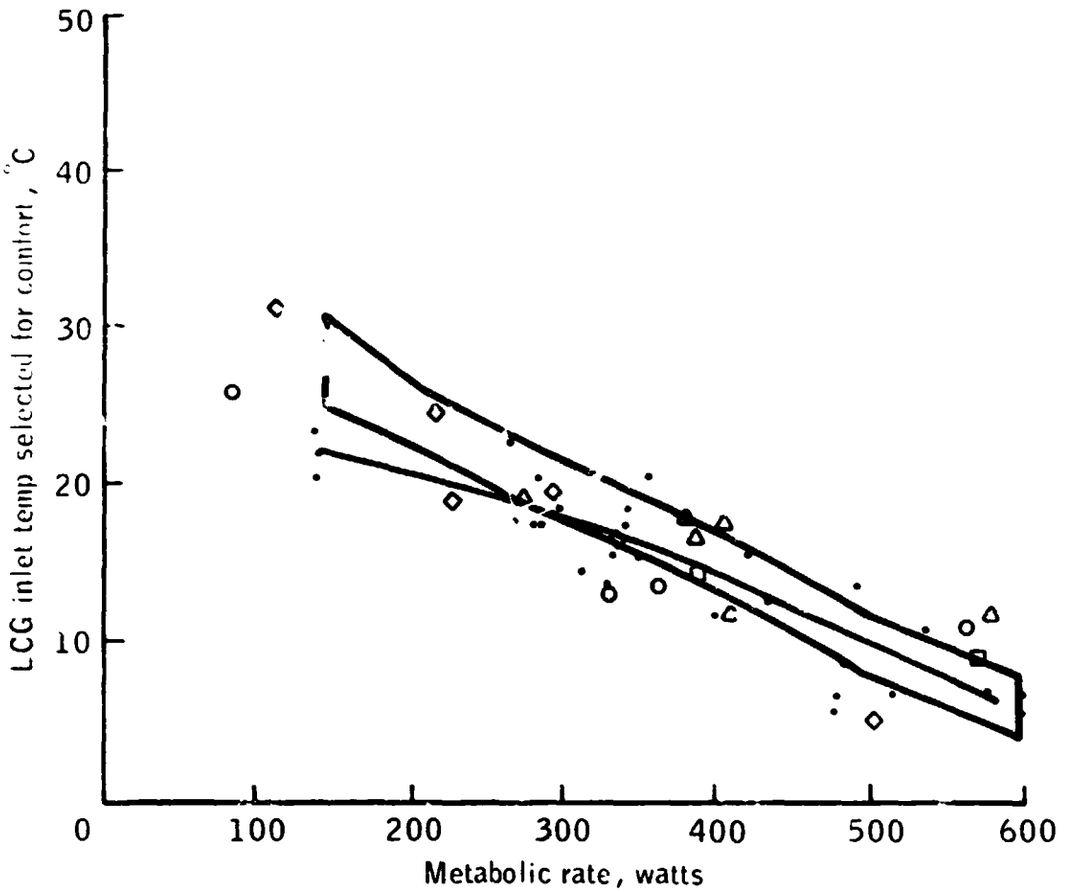

Figure 4-1.- Concluded.

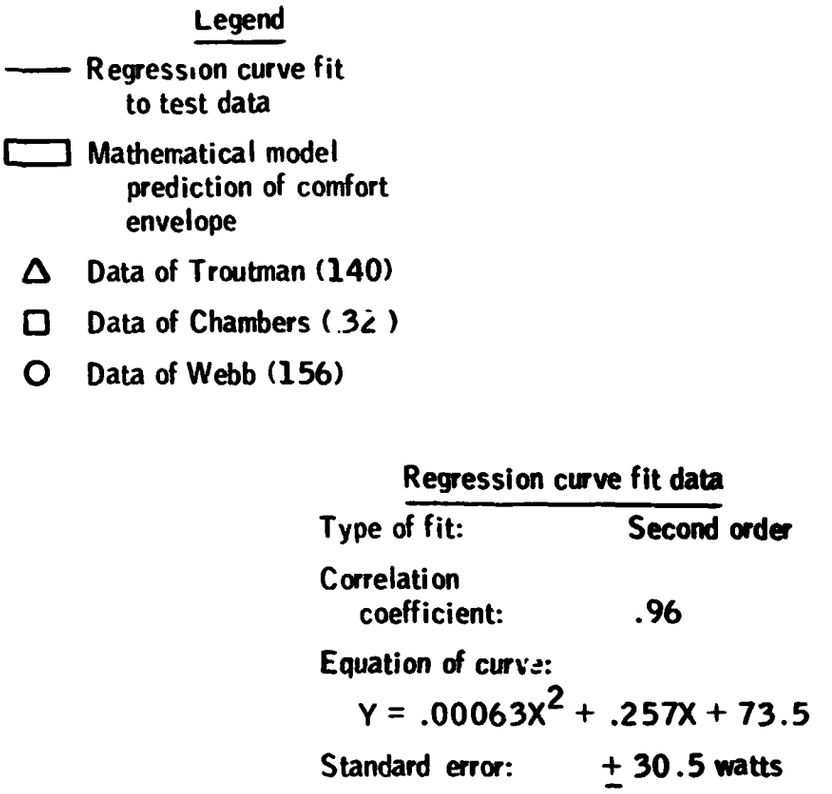

Figure 4-2.- LCG heat removal rate at comfort vs metabolic rate.

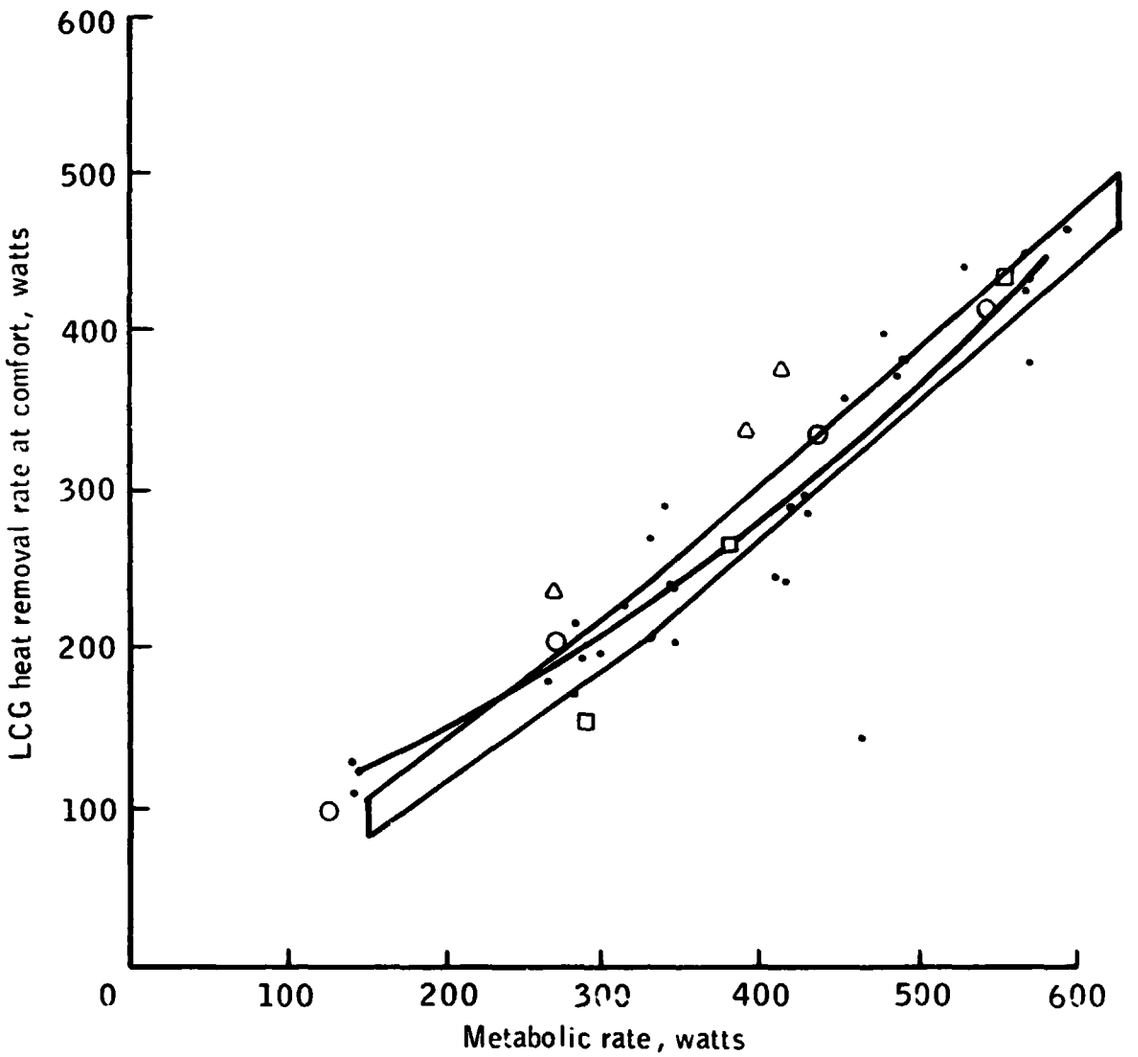

Figure 4-2. Concluded.

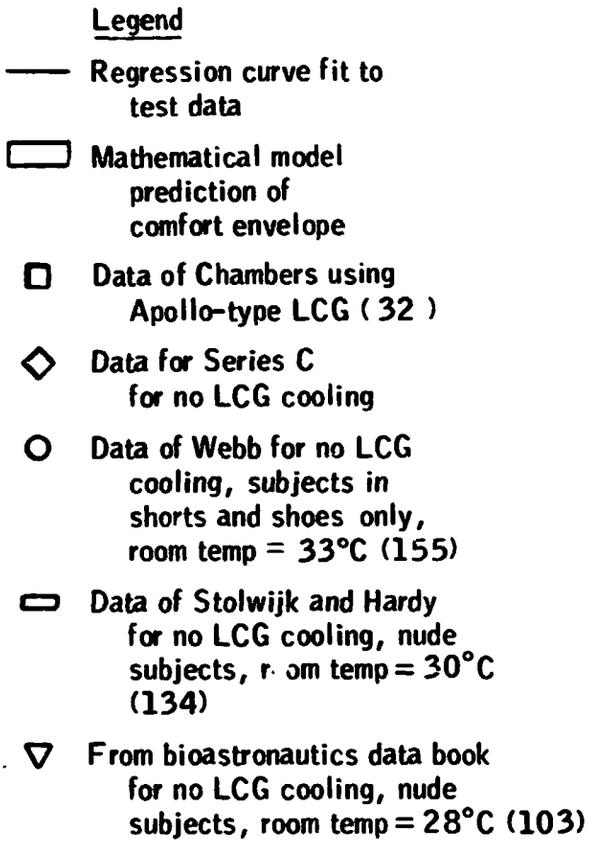

Figure 4-3.- Total evaporative heat loss rate at comfort vs metabolic rate.

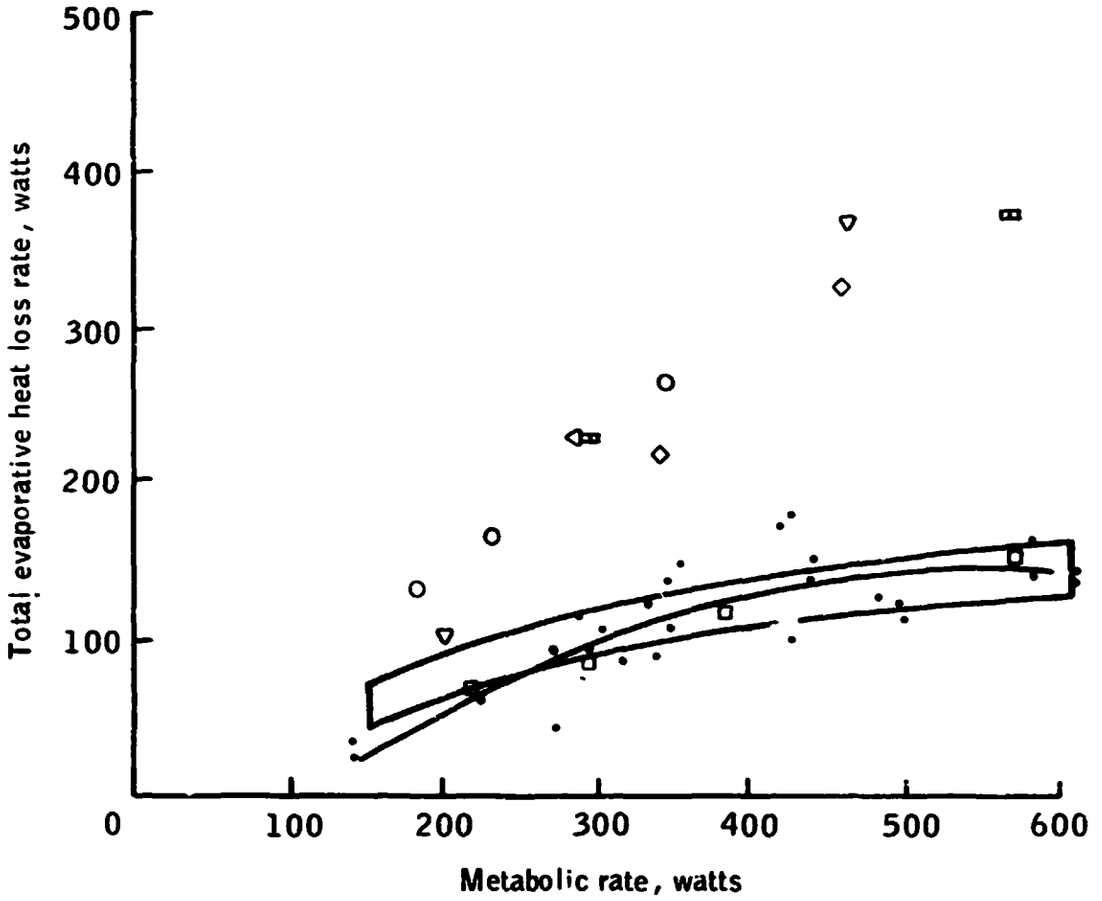

Figure 4-3.- Concluded.

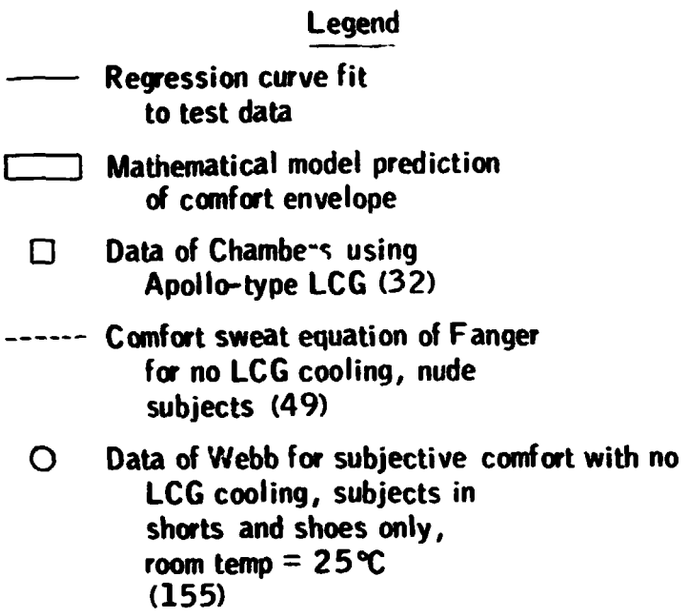

Figure 4-4.- Active sweat rate at comfort vs metabolic rate.

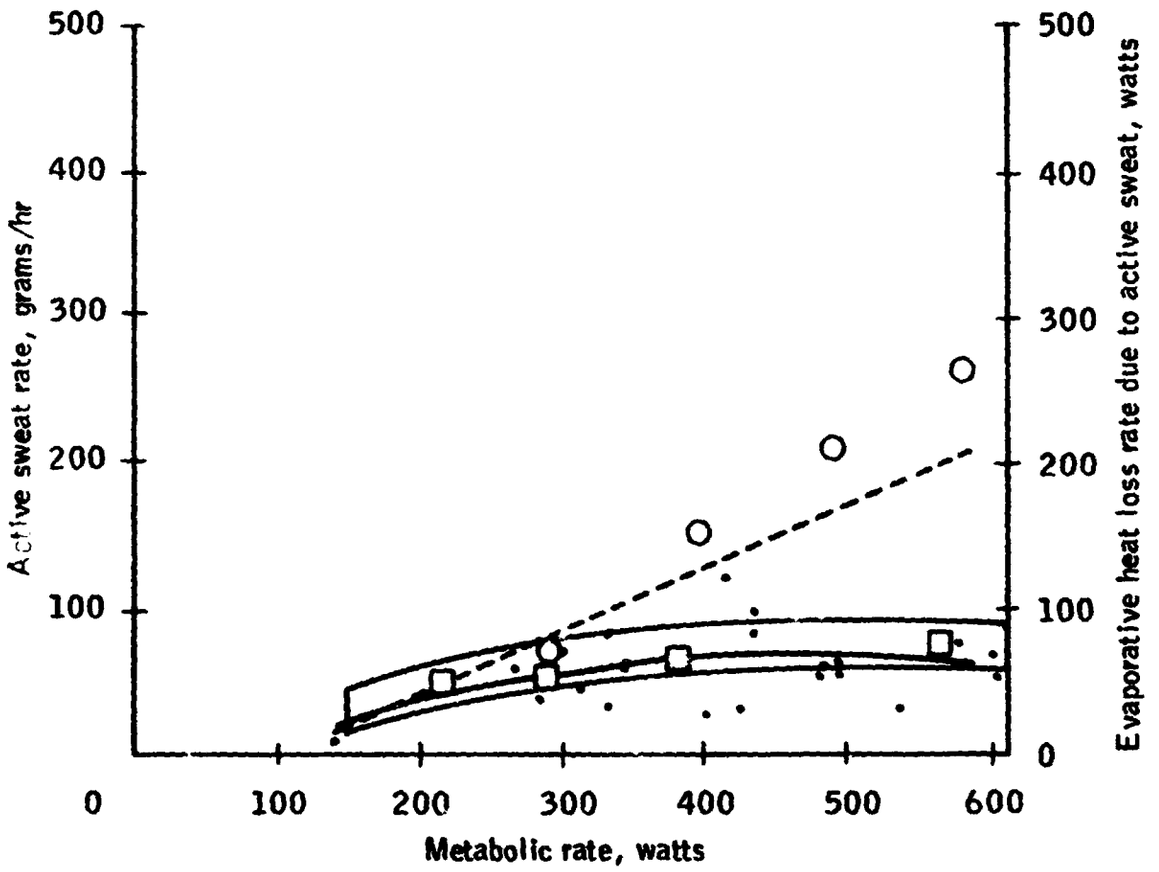

Figure 4-4.- Concluded.

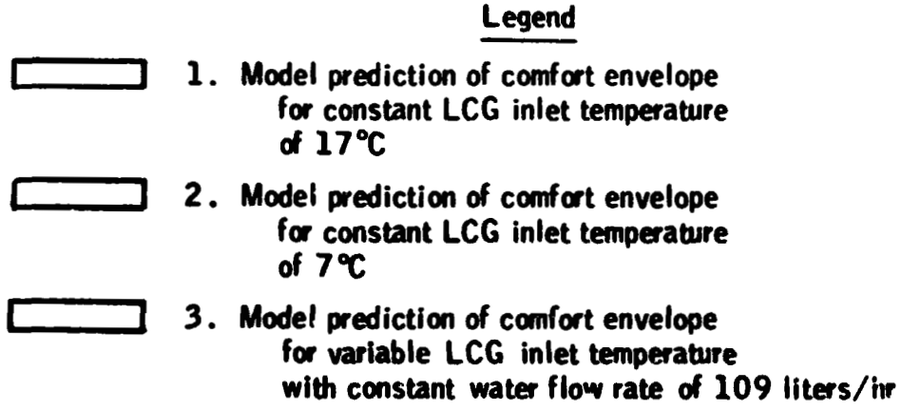

Figure 4-5.- LCG water flowrate selected for comfort vs metabolic rate.

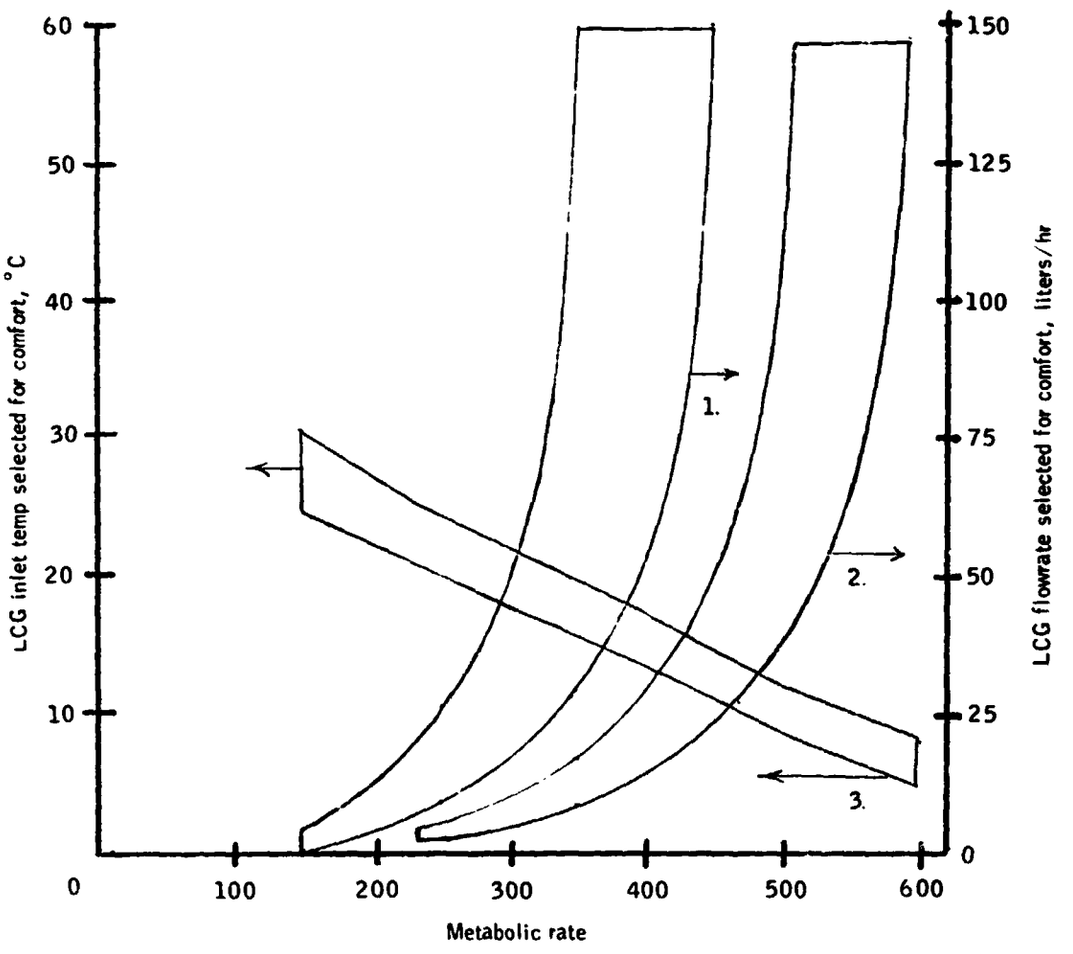

Figure 4-5.- Concluded.

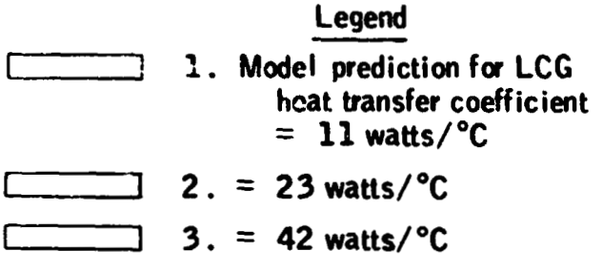

Figure 4-6.- Effect of LCG heat transfer coefficient upon LCG inlet temperature selected at comfort.

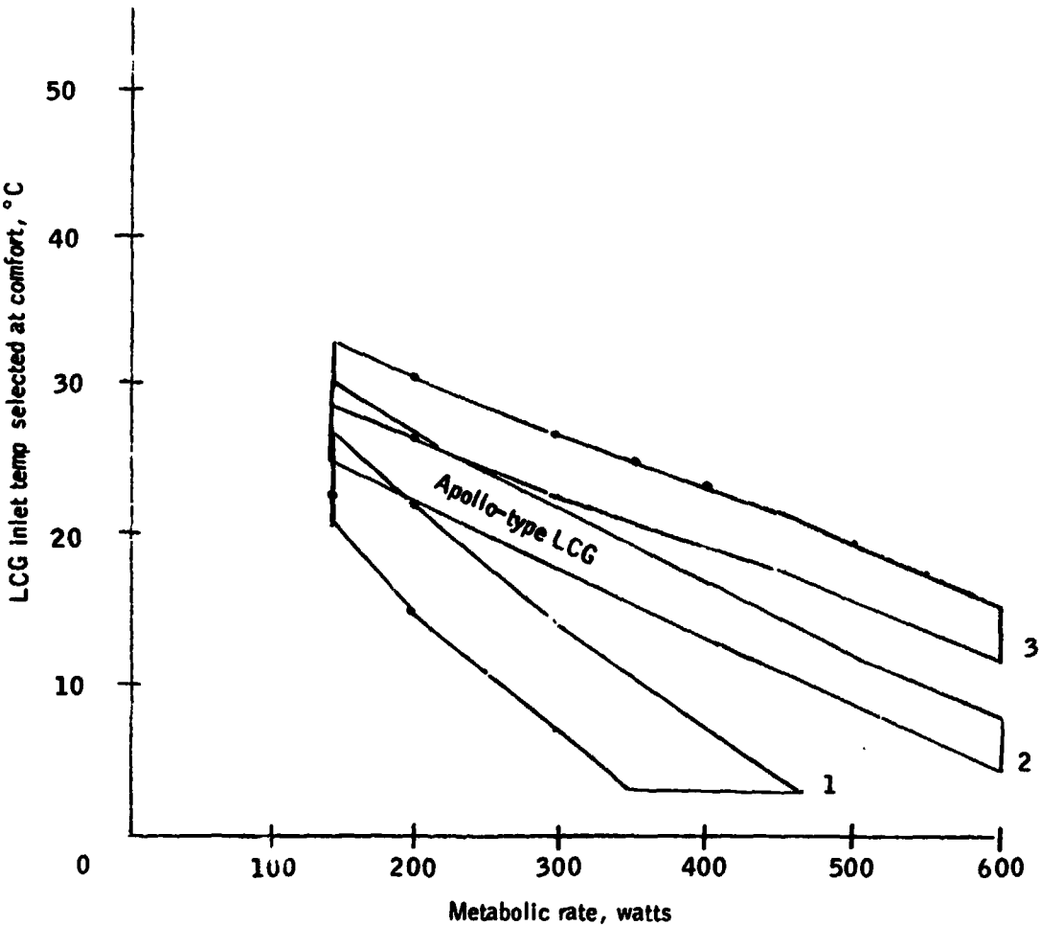

Figure 4-6.- Concluded.

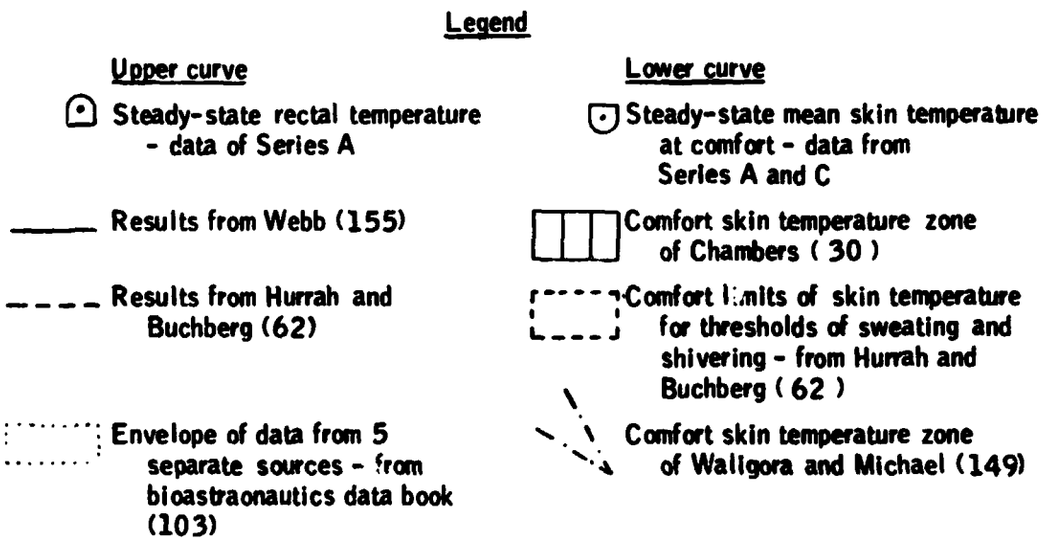

Figure 4-7.- Rectal temperature (upper curve) and zones of mean skin temperature at comfort (lower curve) vs metabolic rate, with LCG cooling.

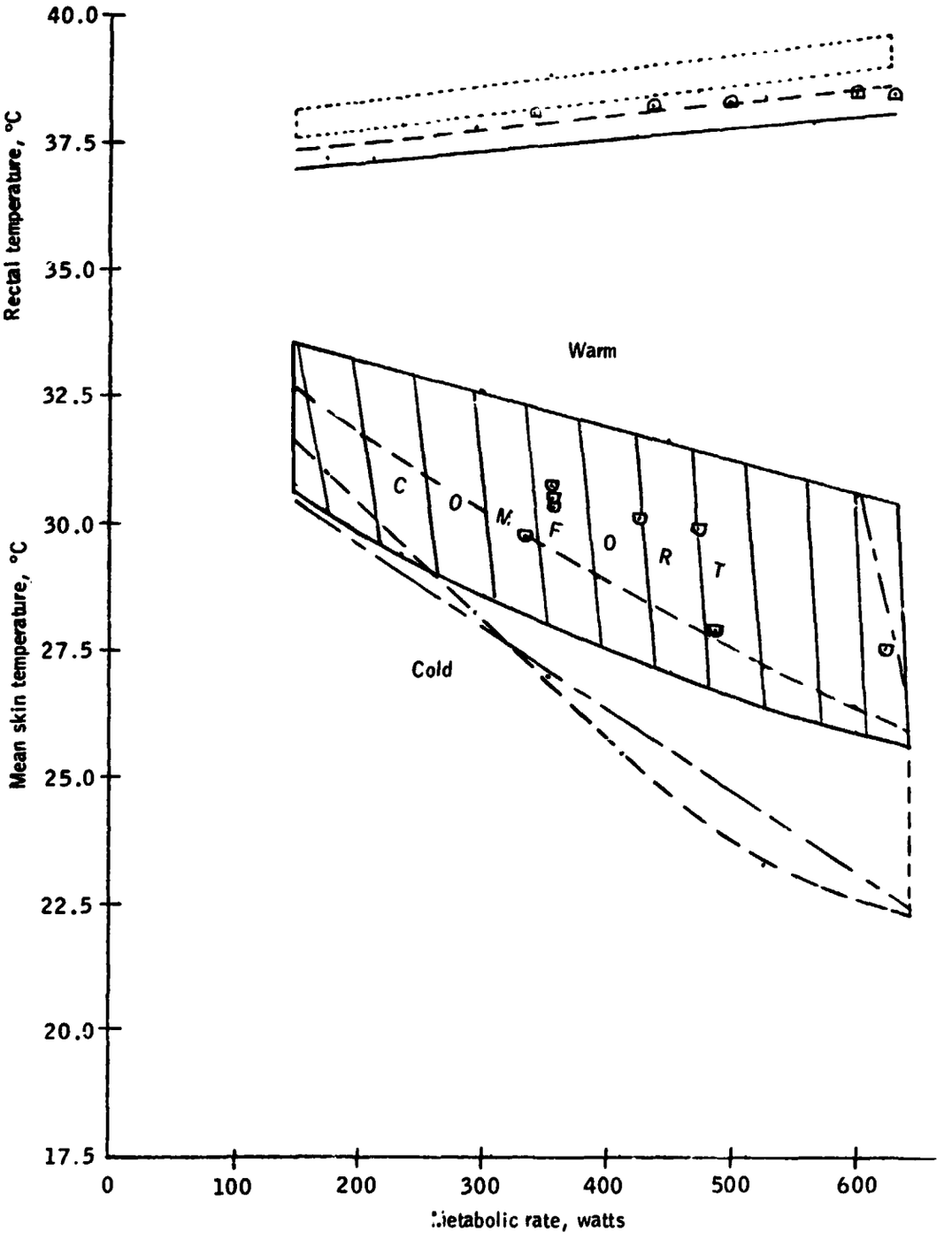

Figure 4-7.- Concluded.

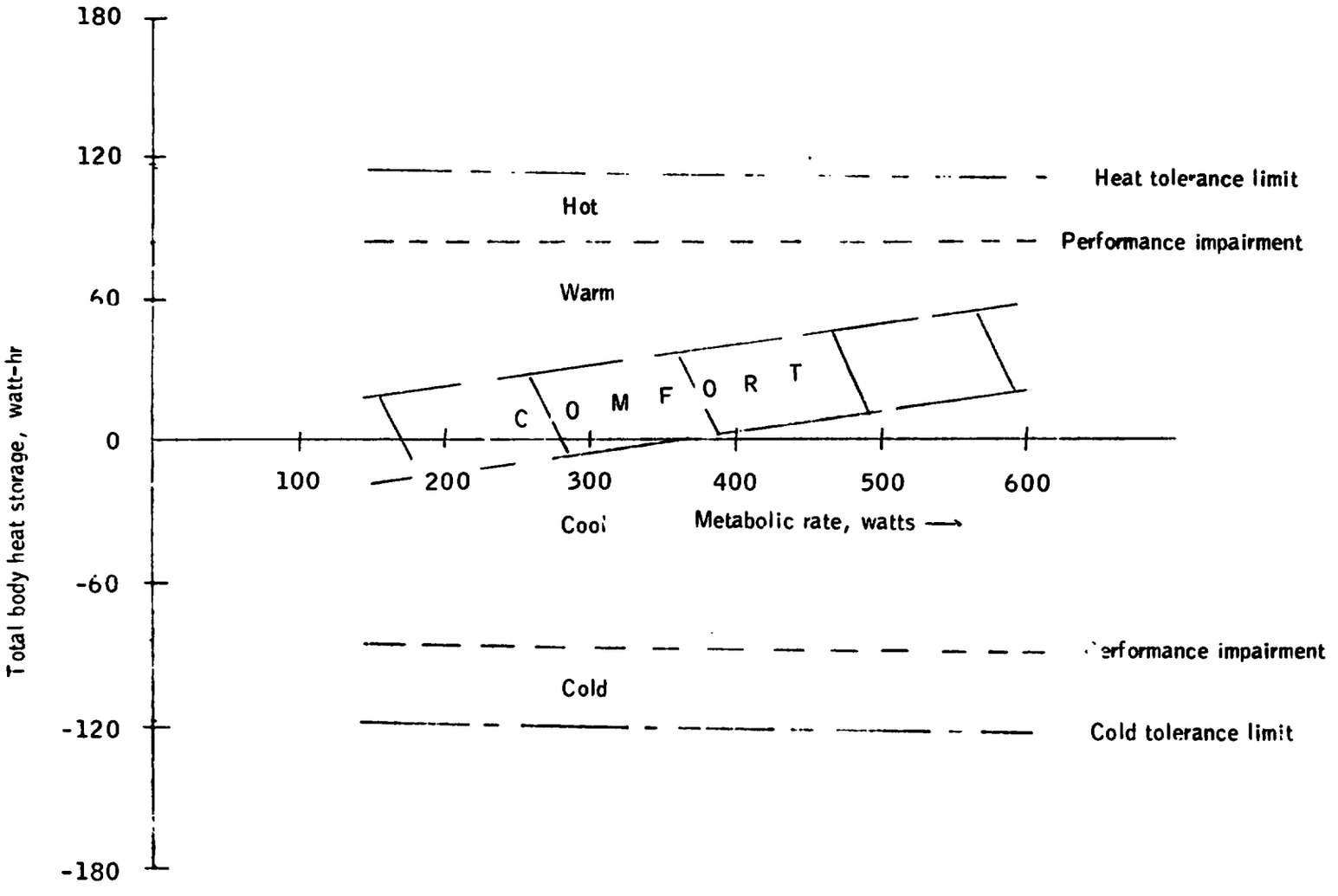

Figure 4-8.- Comfort band with performance and tolerance limits.

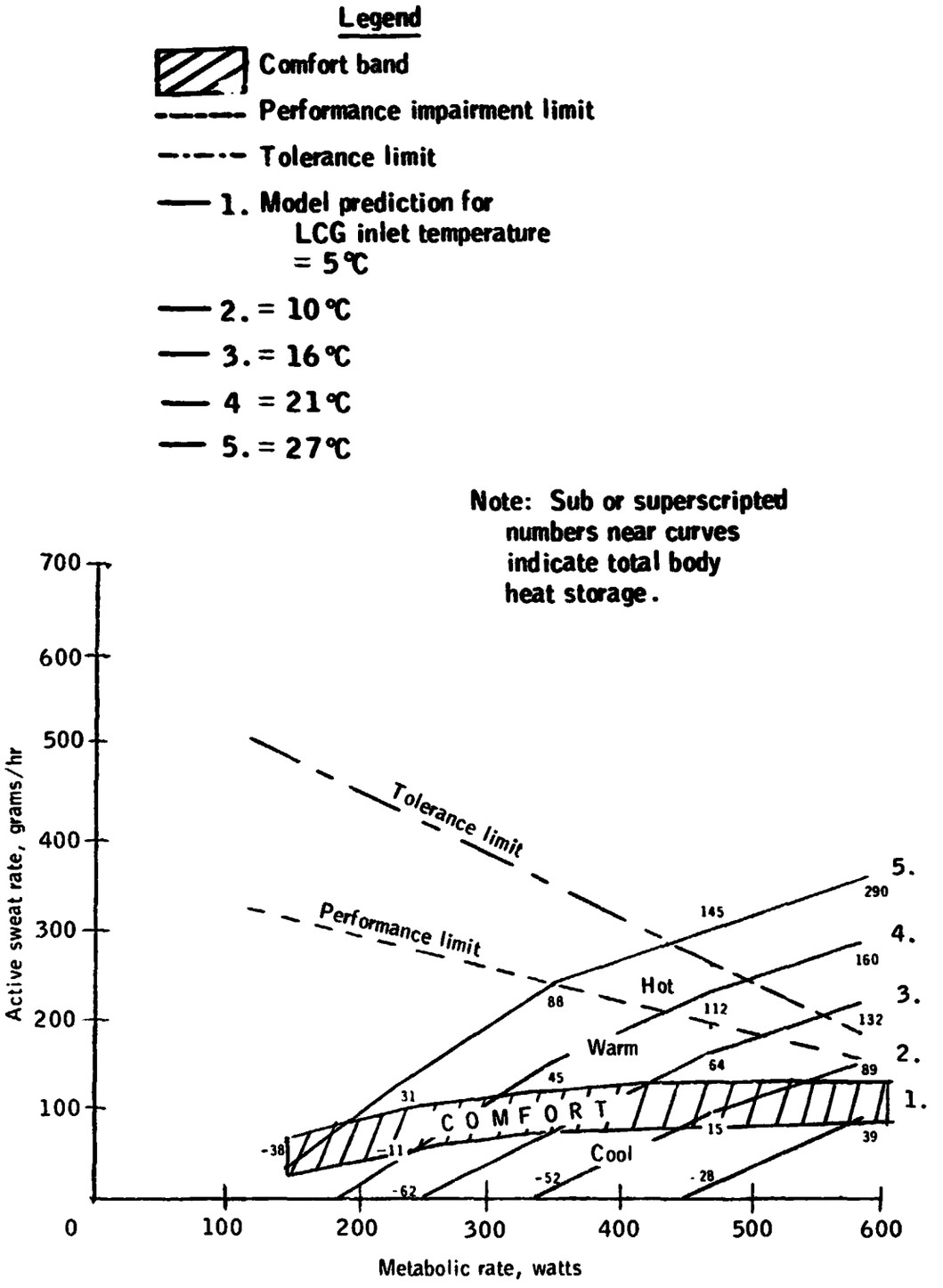

Figure 4-9.- Active sweat rate vs metabolic rate for comfort, performance impairment, and tolerance limits.

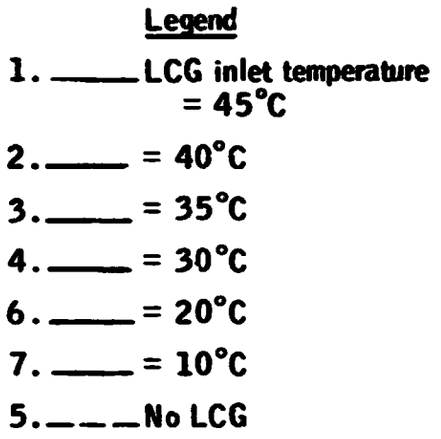

Figure 4-10.- Predicted LCG heating required for comfort at a metabolic rate of 200 watts in cold environments.

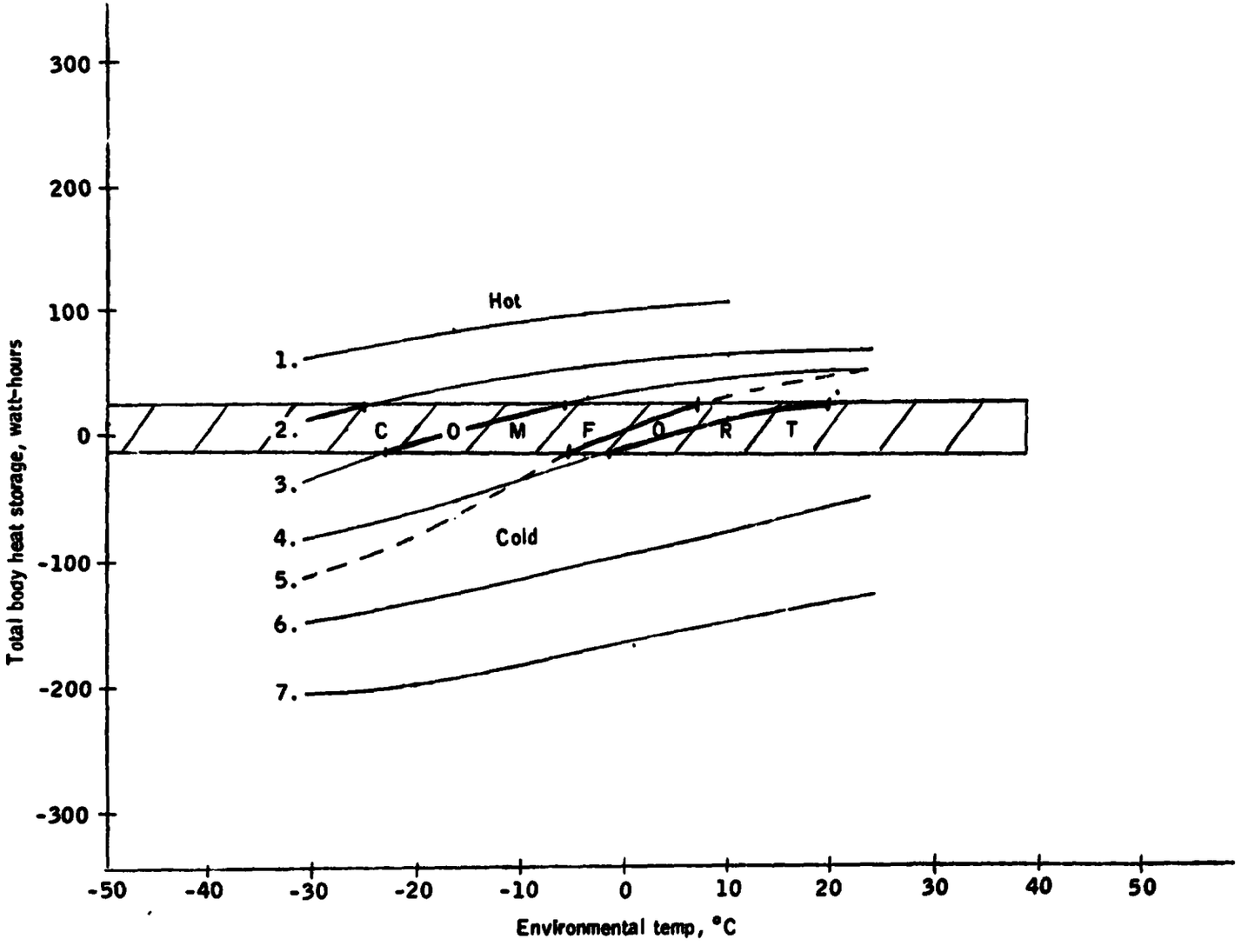

Figure 4-10.- Concluded.

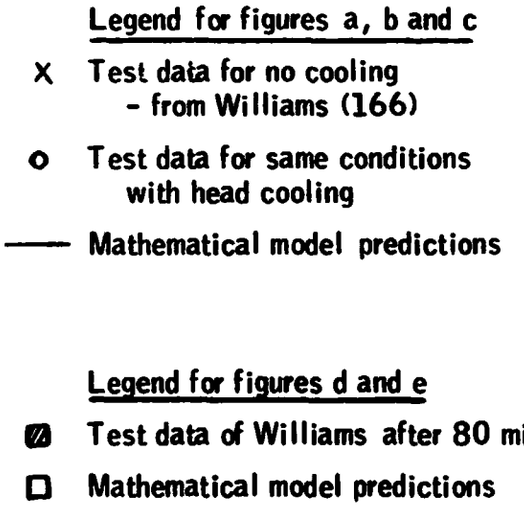

Figure 4-11.- Investigation study of the effects of head cooling.

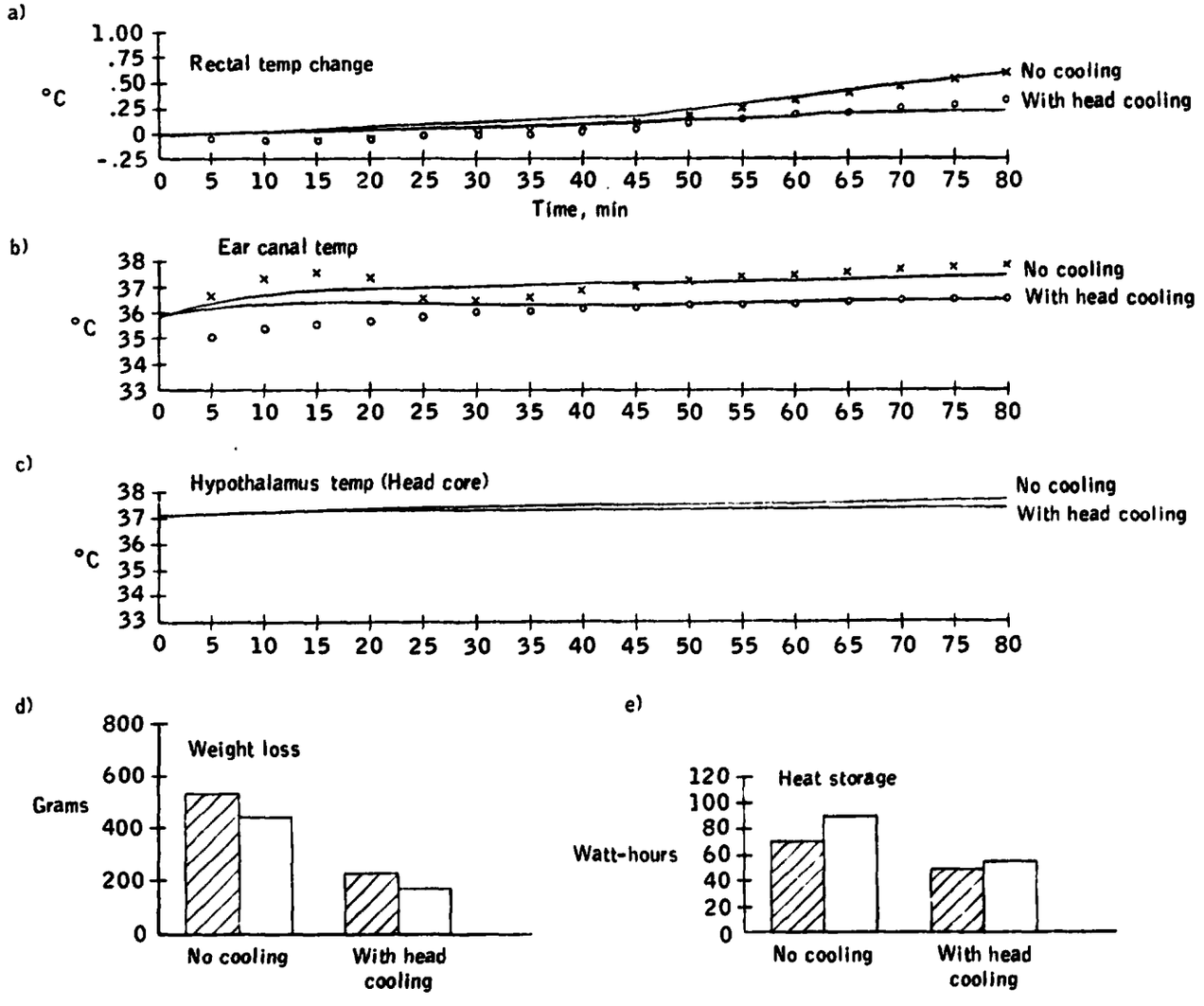

Figure 4-11.- Concluded.

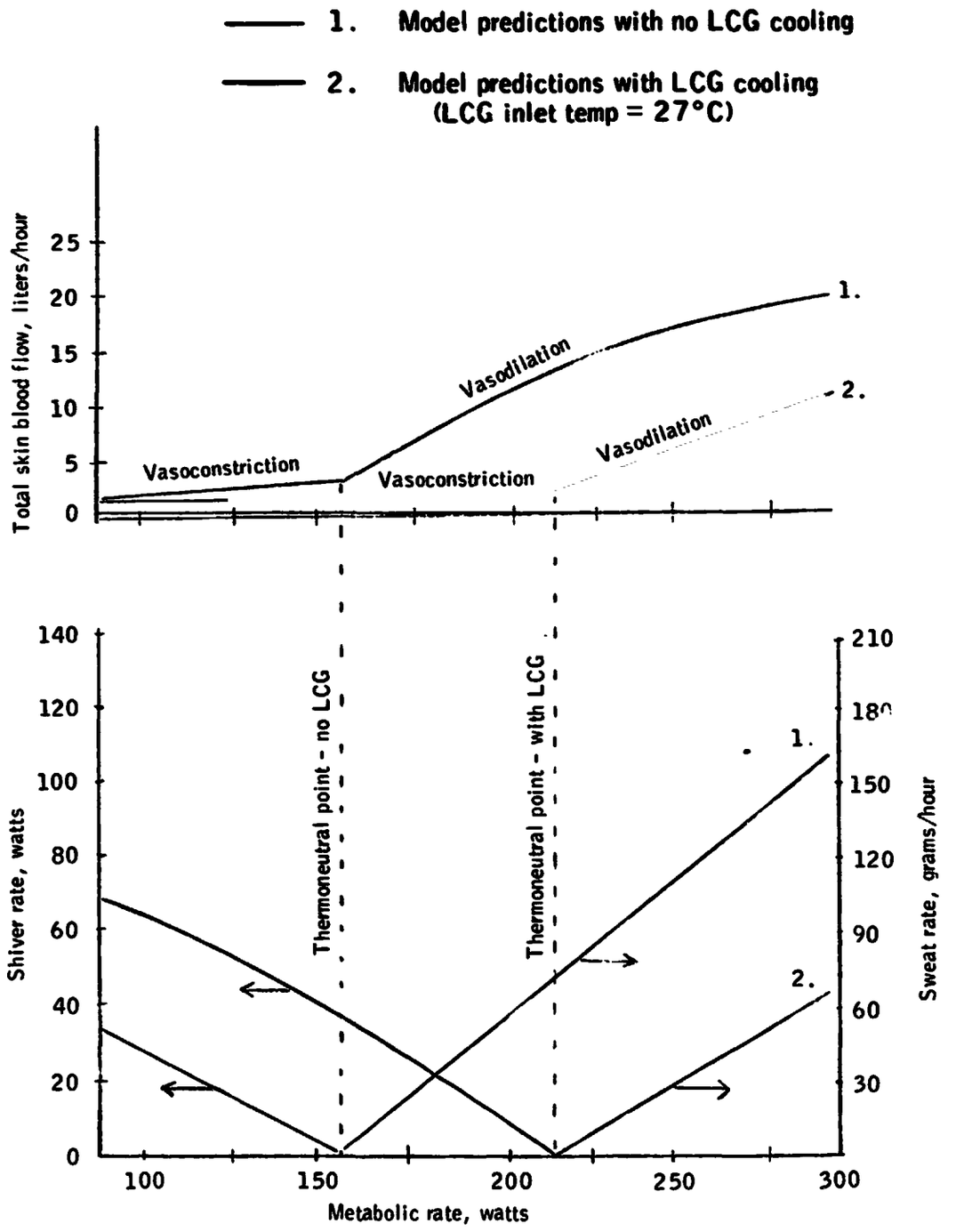

Figure 4-12.- Study of the thermoregulatory effects of the LCG upon skin bloodflow, shivering, and sweating.

Note: For this simulation, the following conditions were utilized:

Metabolic rate = 967 watts
Atmospheric temperature = 35°C
Relative humidity = 60%
Clothing insulation values = shorts and shoes only

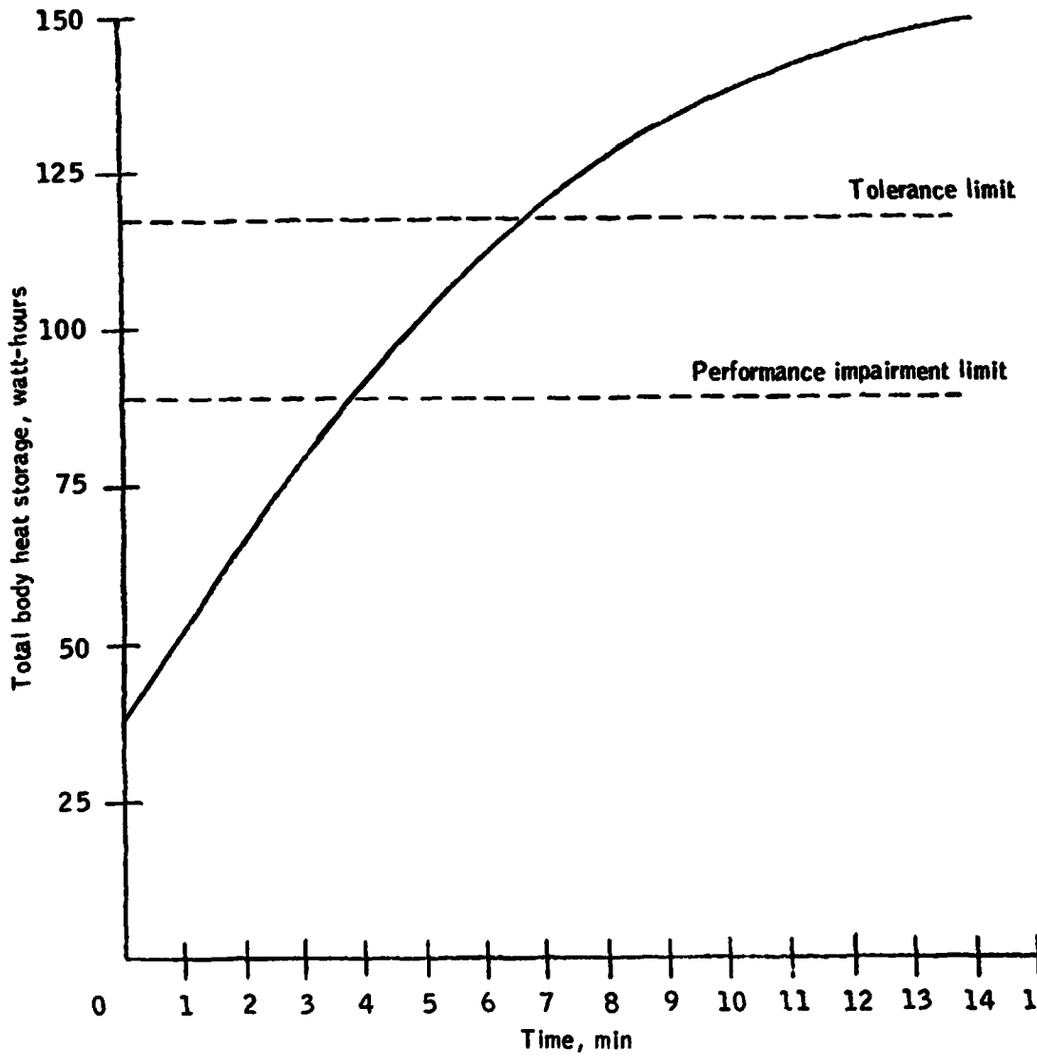

Figure 4-13.- Predicted body heat storage vs time for average subjects running one mile every eight minutes in a hot, humid environment.

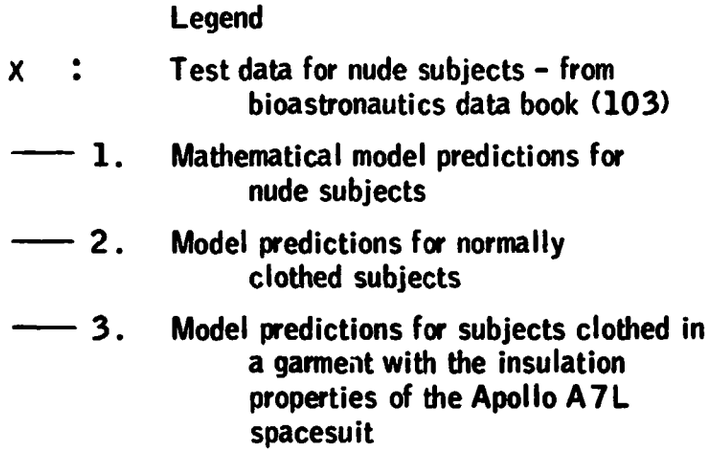

Figure 4-14.- Time required for skin temperature to reach pain threshold of 45°C vs intensity of incident environmental heat flux, for various garment insulation properties.

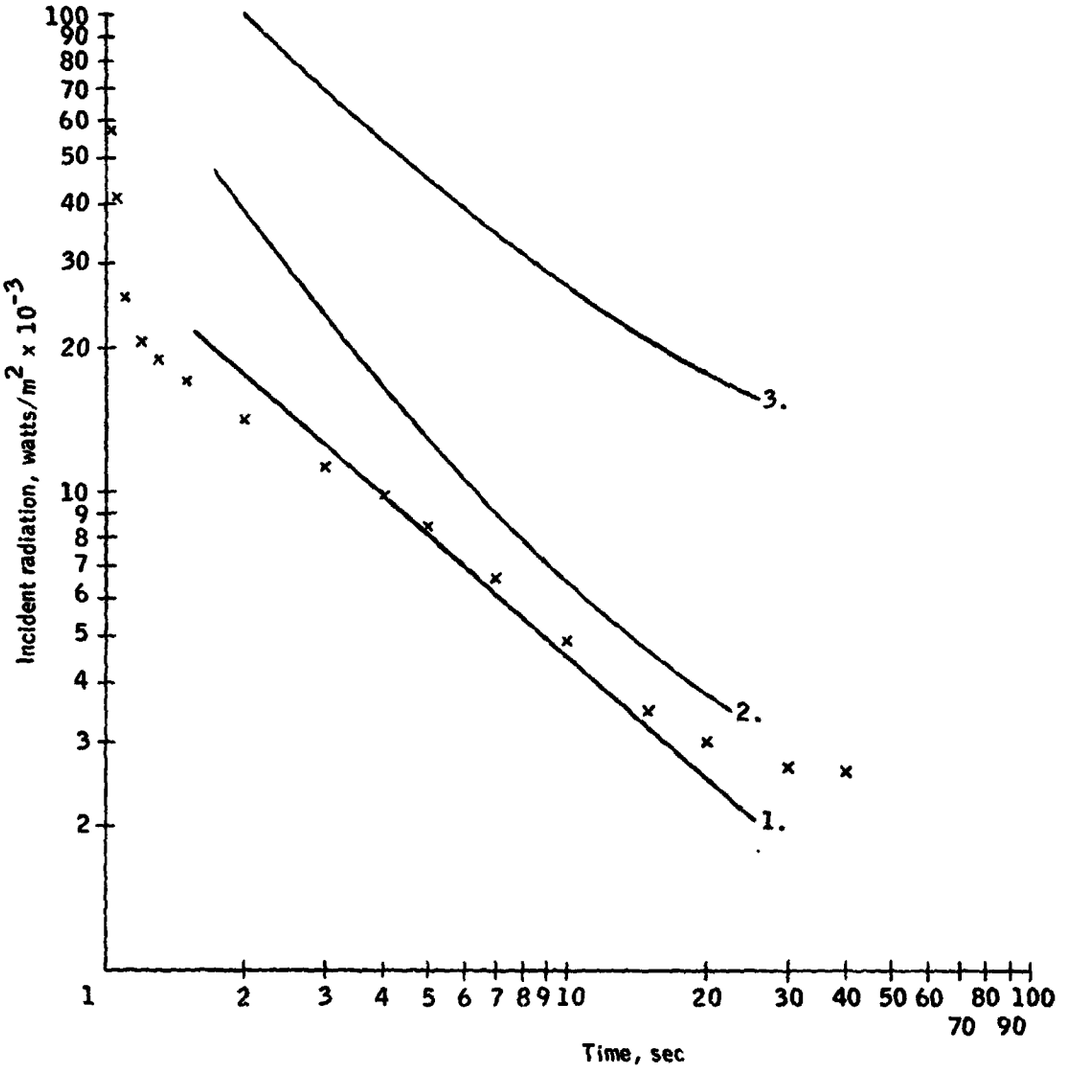

Figure 4-14.- Concluded.

TABLE 4-1. COMPARISON OF PREDICTED AND ACTUAL THERMAL DATA - SEA LEVEL AND ALTITUDE

Parameter	Data of Varene (143)			Mathematical Model Predictions			
	1	2	3	4	5	6	7
Altitude	Sea Level	3800 meters (Non-Acclimatized Lowlanders)	3800 meters (Acclimatized Highlanders)	Sea Level	3800 meters	3800 Meters Increased Respiration Reduced Bloodflow	3800 Meters Increased Respiration Normal Bloodflow
Temperature °F	68°	68°	68°	68°	68°	68°	68°
Dewpoint, °F	42°	42°	42°	42°	42°	42°	42°
Metabolic rate, Kcal/hr (approx.)	500	500	500	500	500	500	500
Exercise period, min	30	30	30	30	30	30	30
Work efficiency, % of metabolic rate	20%	20%	20%	20%	20%	20%	20%
Convective heat loss, % of metabolic rate	--	--	--	11%	8%	8%	8%
Radiation heat loss	--	--	--	22%	22%	22%	22%
Convection & radiation heat loss	29%	26%	24%	32%	30%	30%	30%
Evaporation heat loss	--	--	--	17%	22%	22%	22%
Respiratory evaporation heat loss	--	--	--	15%	15%	18%	18%
Total evaporation loss (+ respiration)	34%	44%	40%	33%	37%	40%	40%
Heat storage rate, % Metabolic rate	17%	14%	16%	15%	13%	13%	13%
Change in core temperature during exercise, °C	+.85°	+.85°	+.98°	+.8°	+.9°	+1.0°	+.9°
Change in mean skin temp. during exercise, °C	+.85°	-.47°	+.41°	+.51°	+.77°	-.1°	+.65°

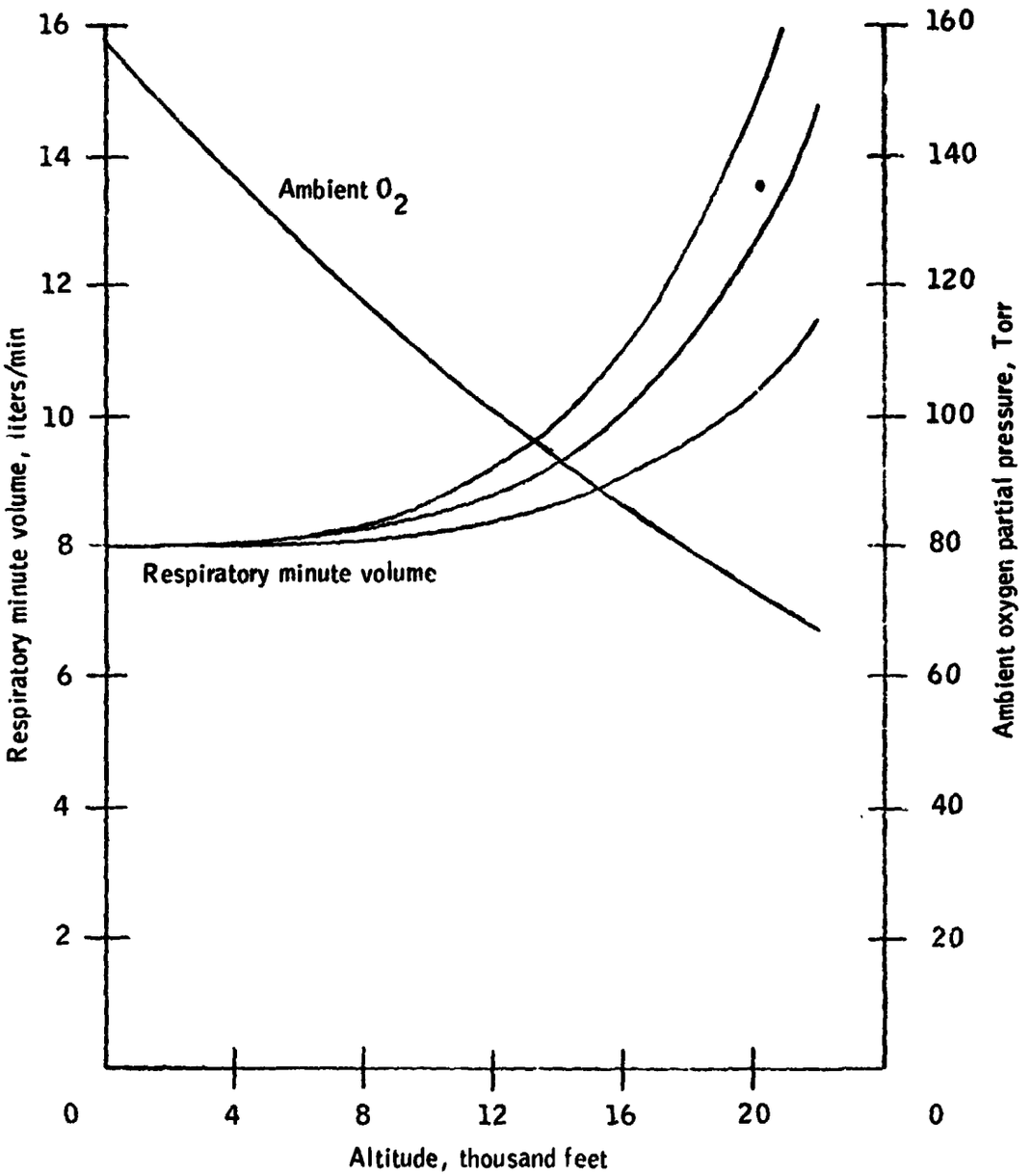

Figure 4-15.- Effect of acute hypoxia (30 minutes) on the respiratory minute volume (100).

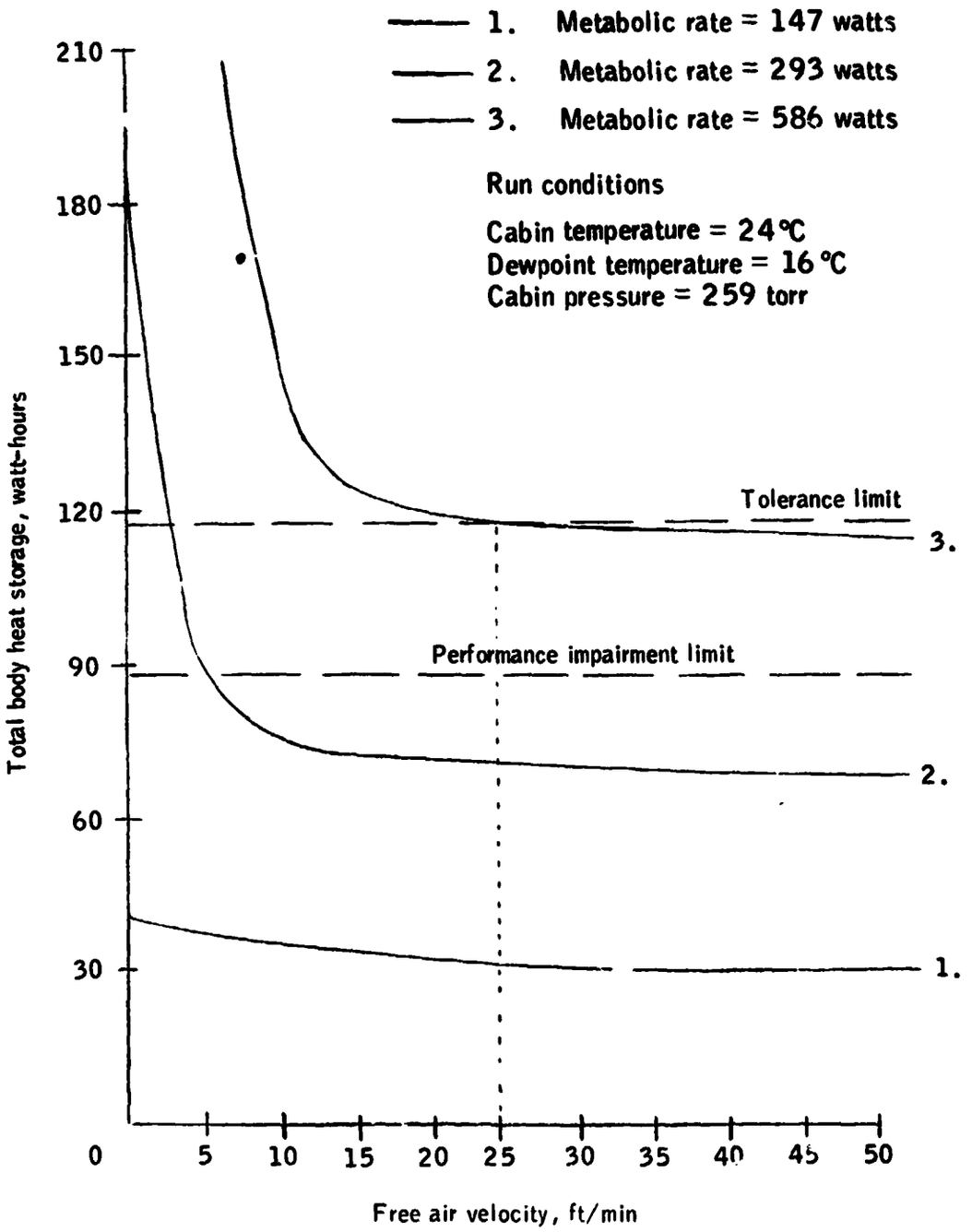

Figure 4-16.- Steady-state body heat storage vs free air velocity in a zero-gravity environment.

5. SUMMARY

Utilizing test data and the results of a mathematical model of the human thermoregulatory system, the control of thermal balance with a liquid circulating garment has been investigated. The test data were generated from 5 series of experiments in which environmental and metabolic conditions were varied parametrically as a function of several independent variables. These included the effects of LCG flowrate, LCG inlet temperature, net environmental heat exchange, surrounding gas ventilation rate, ambient pressure, metabolic rate, and subjective vs. obligatory control of LCG cooling.

It was found that for human test subjects exercising with an LCG, skin temperature was directly related to the LCG water temperature and flowrate rather than metabolic rate. Conversely, rectal or head core temperature was found to vary rectilinearly in response to metabolic rate and was independent of LCG heat removal.

A comfort band based upon total body heat storage was introduced and used with subjective evaluations to assess thermal comfort. It varied linearly from 0 $\pm$ 19 watt-hr stored body heat at a metabolic rate of 146 watts to 40 $\pm$ 19 watt-hr stored body heat at a metabolic rate of 586 watts. This band was shown to be a most effective means of quantitating thermal comfort.

It was found that test conditions associated with thermal comfort produced a monotonically increasing relationship between metabolic rate and LCG heat dissipation that was nearly rectilinear. On the other hand, off-comfort test conditions produced results that were clearly curvilinear or discontinuous. This effect was attributed to the second and higher order responses of the thermoregulatory system when exposed to off-comfort

conditions. These responses included sweating, shivering, vasoconstriction and vasodilatation.

It was found that convective heat removal by a surrounding, circulating gas stream was almost negligible when the majority of metabolic heat was rejected to the LCG. This was found to be the case even when gas flowrate was almost doubled from 170 to 331 liters/min. The latter effect was attributed to countercurrent heat transfer between the LCG and the circulating gas.

It was shown that thermal comfort could be provided either by controlling the LCG flowrate at a fixed inlet temperature or controlling the inlet temperature with a fixed flowrate. However, the latter method was judged to be more effective because it provided greater sensitivity and avoided the problem of a reduced LCG heat transfer coefficient at low water flowrates.

The effect of variations in net environmental heat exchange, or radiation heat transfer, was also investigated. It was demonstrated that for the same water flowrate and inlet temperature, the LCG was less effective at providing thermal comfort when net environmental heat exchange was into the suit and more effective when it was out of the suit. This was manifested by decreased LCG heat removal, increased sweat rates and higher body heat storage for the former condition as compared to the latter. The LCG was shown to absorb (or lose) approximately 40% of an increase (or decrease) in environmental heat exchange. The remaining 60% of the environmental exchange resulted in higher (or lower) sweat rates and evaporative heat loss.

It was demonstrated that the stressful effects of variations in environmental heating or cooling, and changes in other factors such as

metabolic rate, ambient temperature, pressure or humidity could be countered by permitting the subject to control the inlet temperature of the LCG in response to his own thermal comfort.

Test subjects controlled the cooling of their LCGs in such a way as to limit sweat rates below 100 g/hr. For neutral environments (zero net environmental heat exchange), the LCG inlet temperature selected for comfort was shown to be a near-rectilinearly decreasing function of metabolic rate described by the following equation:

$$T_{inlet}\ (°C) \text{ at comfort} = -3.33 \times 10^{-5}\ (\text{Met.Rate})^2 - .0118\ (\text{Met.Rate}) + 25.1.$$

Conversely, the resulting LCG heat removal rate at comfort was shown to be a near-rectilinearly increasing function of metabolic rate. This was described by:

$$\text{LCG heat removal required for comfort (Watts)} = .00063\ (\text{Met.Rate})^2 + .257\ (\text{Met.Rate}) + 73.5.$$

By controlling the LCG heat removal rate in this fashion, the total evaporative heat removal rate was limited. It showed a second order dependence upon metabolic rate and asymptotically approached a limit of 150 Watts. The equation describing this relation was found to be:

$$\text{Total evaporative heat loss rate at comfort (Watts)} = -.00074\ (\text{Met.Rate})^2 + .818\ (\text{Met.Rate}) - 79.5.$$

The greatest portion of the total evaporative heat loss was shown to arise from evaporation of active sweat. The remainder was attributed to evaporative heat loss through the respiratory tract with some small amount

occurring from passive diffusion at the skin surface. Empirical expressions for respiratory heat loss showed that it accounted for approximately 10% of metabolic heat dissipation and was not significantly affected by the presence of the LCG. On the other hand, both total evaporative heat loss rate and active sweat rate at comfort were shown to be limited to far smaller values when the LCG was used to provide a thermal balance as compared to similar results without an LCG. Active sweat rate at comfort was observed to exhibit a second order dependence upon metabolic rate, and asymptotically approached a limit below 100 g/hr. This was described by the following equation:

$$\text{Sweat rate at comfort (g/hr)} = -.0007\ (\text{Met.Rate})^2 + .655\ (\text{Met.Rate}) - 52.6.$$

The usefulness of the mathematical model as a tool for interpreting the test data, and for generating trends and relationships between various physiological variables, was also investigated and verified. Test data were compared to model predictions and the resulting comparisons were used to evaluate test results, or as a basis for adjustment of model parameters in order to enhance the accuracy of the model. Predictions of LCG heat removal, evaporative heat loss, sweat rate, rectal or head core temperature, and mean and individual skin temperatures were compared to the test data and shown to be quite accurate. Based upon these comparisons, adjustment of several passive system parameters of the model resulted in improved predictions of individual skin temperatures.

The parametric relationships between sweat rate, total body heat storage, metabolic rate, and LCG heat transfer rate derived from the model and test studies resulted in a method of predicting body heat storage and

metabolic rate from LCG inlet temperature and heat removal. This correlation was used to evaluate the real-time comfort, metabolic work rate, and life-support system consumables utilization rate of astronauts performing tasks on the lunar surface. The information was then used to assess real-time astronaut well-being and to modify the planned activities of the lunar surface explorations if necessary. Comparisons of the predictions of the above correlation with post-EVA Apollo mission results demonstrated an accuracy of better than 90%.

The use of the model for various practical applications was considered. It was shown that the model could be used as an effective tool for studying the performance and tolerance limits of humans to thermal stress. It was also shown how it could be used to study the effects of altitude, clothing, ambient temperature and humidity, and gravity upon the responses of the human thermoregulatory system.

Finally, from the overall comparisons of the model predictions with the test data, the inadequacies of the current model were i minated and used to formulate the basis of a new model designed to correct these shortcomings. The structure and logic behind the new model was also presented.

Based upon the results of the investigations described above, the following conclusions were drawn:

1. The mathematical model can be used as an accurate simulator of the major physiological variables comprising the human thermoregulatory system, such as sweat rate, skin temperature, core temperature and convective, radiative and evaporative heat loss.

2. The model can also be used to evaluate LCG performance and design.

3. The heat storage based comfort band is a practical and reasonably accurate means of quantitating human thermal comfort.

4. When combined with the comfort band and performance and tolerance limits, the mathematical model can be used as an accurate index of thermal stress and comfort.

5. The current model should be revised to reflect the changes outlined by this investigation. The revised model should produce improved predictions of individual skin temperatures and other physiological parameters.

6. Additional research is needed before further improvements to the equations of the active thermoregulatory system can be made. This should include studies on the internal temperature distribution within the body and possibly organ temperature and local heat generation studies. Additional studies on the response to off-comfort conditions would also be helpful.

6. BIBLIOGRAPHY

1. Allan, J. R.: 1966, The Liquid Conditioned Suit, a Physiological Assessment', Memo 234, Flying Personnel Research Committe, RAF Institute of Aviation Medicine, Farnborough.

2. Allan, J. R.: 1967, 'The Effects of High Ambient Humidity on the Performance of the Liquid Conditioned Suit', FPRC-1265, Flying Personnel Research Committee, RAF Institute of Aviation Medicine, Farnborough.

3. Allan, J. R.: 1970, 'Protection of Air Crew Against Heat', paper presented to Ergonomics Research Society Annual Conference.

4. Ames Research Center: Portable Life Support Systems. A conference held at NASA Ames Research Center, Moffett Field, CA. April 30 - May 2, 1969. NASA SP-234.

5. Ames Research Center: Second Conference on Portable Life Support Systems. May 11 - 13, 1971. NASA SP-302.

6. Apollo 15 Extravehicular Mobility Unit Thermal Vacuum Qualification Test - Detailed Test Procedure. NASA/Johnson Space Center, Houston, Texas, March 1971.

7. Arpaci, Vedat S.: Conduction Heat Transfer, Addison-Wesley Publishing Company, Reading, Mass. 1966.

8. Benzinger, T. H.; and Kitzinger, C.; and Pratt, A. W.: The Human Thermostat. Temperature Regulation, No. 56.

9. Berry, C. A.: Preliminary Clinical Report of the Medical Aspects of Apollos VII and VIII. Aerospace Medicine, March 1969. pp. 245-254.

10. Berry, C. A.: Summary of Medical Experience in the Apollo 7 Through 11 Manned Spaceflights. Aerospace Medicine, May 1970. pp. 500-519.

11. Billingham, J., M. D.: Estimates of Metabolic Rates, Thermal Balance, and Water Requirements for Apollo Crew Members. CSD-A-053. Crew Systems Division, Manned Spacecraft Center. December 23, 1964.

12. Billingham, J., Lt.; and Kerslake, M.: Specification for Thermal Comfort in Aircraft Cabins (proposed as a basis for an official specification). Air Ministry, June 1960.

13. Bird, Byron R., Transport Phenomena, Warren E. Stewart, and Edwin N. Lightfoot. John Wiley & Sons, Inc. New York 1960

14. Bitterly, J. G.: ECGS High-Performance Liquid-Phase-Change Space Suit Garment Cooling System Development. Proceedings of the Symposium on Individual Cooling, Kansas State University, Manhattan, Kansas. March 17-18, pp. 170-204.

15. Edited by Bligh, J., and Moore R. E., Essays on Temperature Regulation, North-Holland Publishing Company, Amsterdam, Holland and American Elsevier Publishing Company, Inc., New York. 1972.

16. Blockley, W. V.: 1963, 'Heat Storage Rate as a Determinant of Tolerance Time and Duration of Unimpaired Performance Above 150°F', Fed. Proc. 22. 887-898.

17. Blockley, W. V.: Human Sweat Response to Activity and Environment in the Compensable Zone of Thermal Stress: A Systematic Study. NASA CR-65260, 1965.

18. Blockley, W. V.; McCuthen, J. W.; and Taylor, C. L.: Prediction of Human Tolerance for Heat in Aircraft: A Design Guide. UCLA for Wright Air Development Center. May 1954.

19. Blockley, W. V.; and Roth, H. P.: Tolerance for Work-Induced Heat Stress in Men Wearing Liquid Cooled Garments. Final Report on Contract NAS 9-10961. December 1971.

20. Brouha, L.: 1960, Physiology in Industry, Pergamon Press, New York.

21. Buchberg, H. and Harrah, C. B., "Conduction Cooling of the Human Body - A Biothermal Analysis," Thermal Problems in Biotechnology, American Society of Mechanical Engineers, pp. 82 - 95 (1968).

22. Burton, A. C., "The Application of the Theory of Heat Flow to the Study of Energy Metabolism," Journal of Nutrition, 7, 497-533, 1934.

23. Burton, D. R.: Performance of Water Conditioned Suits. Aerospace Medicine May 1966.

24. Burton, D. R.: Engineering Aspects of Personal Conditioning. Proceedings of the Symposium on Individual Cooling, Kansas State University, Manhattan, Kansas. March 17-18, 1969, pp. 33-49.

25. Burton, D. R. and Collier, L.: 1964, 'The Development of Water Conditioned Suits', Tech. Note ME-400, Royal Aircraft Establishment, Farnborough.

26. Burton, D. R. and Collier, L.: 1965, 'The Performance of Water Conditioned Suits', Tech. Report No. 65004, Royal Aircraft Establishment, Farnborough.

27. Carpenter, R. and Winter, W. R., "A Flight-Rated Liquid Cooled Garment for Use Within a Full-Pressure Suit," Second Conference on Portable Life Support Systems, NASA SP-302, pp. 237 - 246 (1972).

28. Operational Methods in Applied Mathematics, H. S. Carslaw, and J. C. Jaeger. Oxford University Press, London 1941

29. Chai, C. Y.; and Lin, M. T.: Effects of Heating and Cooling the Spinal Cord and Medulla Oblongata on Thermoregulation in Monkeys. J. Physiol., Vol. 225, 1972. pp. 297-308.

30. Chambers, A. B.: Controlling Thermal Comfort in the EVA Space Suit. ASHRAE Journal, March 1970, pp. 33-38.

31. Chambers, A. B. and Blackaby, J., "A Liquid Cooled Garment Temperature Controller Based on Sweat Rate, "Second Conference on Portable Life Support Systems, NASA SP-302, pp. 283 - 294 (1972).

32. Chambers, A. B.; Blackaby, J. R.; and Miles, J. B.: A Study of the Thermoregulatory Characteristics of a Liquid-Cooled Garment with Automatic Temperature Control Based on Sweat Rate: Experimental Investigation and Biothermal Man-Model Development. NASA TN D-7311, NASA, Washington, D.C., June 1973.

33. Chato, J. C.; and Hertig, B. A.: Regulation of Thermal Sweating in EVA Space Suits. Proceedings of the Symposium on Individual Cooling, Kansas State University, Manhattan, Kansas. March 17-18, 1969, pp. 78-92.

34. Chato, J. C. and Hertig, B. A., "Thermal Behavior of Biological Media," AIAA Paper 70-813, 1970.

35. Chato, J. C.; and Trezek, G. J: Problems of Heat and Mass Tranfer in Biotechnology. Report on a Workshop held at Allerton House of the University of Illinois at Urbana-Champaign, September 16-19, 1973.

36. Clifford, J. M.: 1965b, 'Some Aspects of Personal Cooling in Inadequately Air Conditioned Cockpits', AGARD CP-2, pp. 75-88.

37. Crocker, J. F., Webb, P., and Jennings, D. C.: 1964, 'Metabolic Heat Balances in Working Men Wearing Liquid Cooled Sealed Clothing', AIAA-NASA Third Manned Spaceflight Meeting, AIAA Publication CP-10, pp. 111-117.

38. Darling, R. C., Downey, J. A., Huckaba, C. E. and Myers, S. J.: Thermoregulation in the Spinal Man, Journal of Applied Physiology. Vol 34, No. 6, June 1973, pp. 790-794.

39. Datta, S. R.; and Ramanathan, N. L.: Energy Expenditure in Work Predicted from Heart Rate and Pulmonary Ventilation. Journal of Applied Physiology Vol. 26, No. 3, March 1969. pp. 297-302.

40. Documenta Geige, Scientific Tables 6th Edition, Geige Pharmaceuticals, Ardsley, New York.

41. Drake, R. M.; Funk, J. E.; and Moegling, J. B.: Convective Heat Transfer in the Gemini and Apollo Space Suits. Proceedings of the Symposium on Individual Cooling, Kansas State University, Manhattan, Kansas. March 17-18, 1969, pp. 119-137.

42. Debois; Hardy, J.: Basal Metabolism, Radiation, Convection, and Vaporization. Journal of Nutrition, 15:477, 1938.

43. DuBois, D.; and DuBois, E. F., Clinical Calorimetry: Fifth Paper, The Measurement of Surface Area of Man. ARch. Intern. Med., 15, 868-888, 1915.

44. Eichna, L. W., et al., "The Upper Limits of Heat and Humidity Tolerated by Acclimatized Men Working in Hot Environments," Journal of Industrial Hygiene and Toxicology 27, 59-84, 1945.

45. Elkins, W.; and Williams, W.: Advanced High Efficient Liquid Transport Garments. NASA Ames Research Center. November 1973. AIAA Crew Equipment Systems Conference, Las Vegas, AIAA Paper 73-1334.

46. Ellis, W. E.; Morris, D. W.; and Colburn, J.: Thermal Vacuum Qualification of the Extravehicular Mobility Unit for Apollo G Missions. NASA/MSC-05150, Houston, Texas, 1971.

47. Facility User's Guide, Space Environment Test Division, No. SETD No. 1001, NASA/Johnson Space Center, November 1971.

48. Fan, L. T., Hsu, F. T. and Hwang, C. L., "A Review on Mathematical Models of the Human Thermal System,: IEEE Trans. on Bio-Medical Eng., vol. BME-18, 1971, pp. 218-234.

49. Fanger, P. O.: Calculation of Thermal Comfort: Introduction of a Basic Comfort Equation. Trans. ASHRAE, 73, II, 1967, pp. III.4.1 - III.4.20.

50. Fanger, P. O.; Nevins, R. G.; and McNall, P. E.: Predicted and Measured Heat Losses and Thermal Comfort Conditions for Human Beings. Thermal Problems in Biotechnology, ASME Symposium Series, New York, 1968, pp. 61-81.

51. Gersten, J. W.; Orr, W.; Sexton, A. W.; and Okin, D.: External Work in Level Walking. Journal of Applied Physiology. Vol. 26, No. 3, March 1969. pp. 286-289.

52. Gisolfi, Carl; and Robinson, Sid: Relations between Physical Training, Acclimatization, and Heat Tolerance. Journal of Applied Physiology. Vol. 26, No. 5, May 1969. pp. 530-534.

53. Gleser, M. A.: Effects of Hypoxia and Physical Training on Hemodynamic Adjustments to One-Legged Exercise. Journal of Applied Physiology Vol. 34, No. 5, May 1973, pp. 655-659.

54. Gold, A. J.; and Zornitzer, A.: Effect of Partial Body Cooling on Man Exercising in a Hot, Dry Environment. Aerospace Medicine September 1968.

55. Genin, A. M. and Golovkin, L. G.: 1966, The Problem of Prolonged Autonomous Human Existence in a Space Suit,' NASA TTF-10, p. 413.

56. Gold, A. J. and Zornitzer, A.: 1968, 'Effect of Partial Body Cooling on Man Exercising in a Hot, Dry Environment,' Aerospace Med. 39 944-946.

57. Goodman, A. B.; and Wolf, A. V.: Insensible Water Loss from Human Skin as a Function of Ambient Vapor Concentration. Journal of Applied Physiology. Vol. 26, No. 2, February 1969. pp. 203-207.

58. Griffiths, I. D.; and McIntyre, D. A.: The Balance of Radiant and Air Temperature for Warmth in Older Women. Environmental Research 6, 382-388 (1973). pp. 382-388.

59. Hall, J. F. and Klemm, F. K.: 1969, 'Thermal Comfort in Disparate Thermal Environemnts', J. Appl. Physiol. 27, 601-606, also AMRL-TR-69-46.

60. Hannon, J. P.; and Sudman, D. M.: Basal Metabolic and Cardiovascular. Function of Women during Altitude Acclimatization. Journal of Applied Physiology Vol. 34, No. 4, April 1973, pp. 471-477.

61. Hardy, J.; Stolwijk, J.; and Gagge, R.: Physiological and Behavioral Temperature Regulation. First International Symposium on Temperature Regulation. 1970

62. Harrah, C. B.; and Buchberg, Harry: Prediction of the Skin Temperature Distribution and Gross Body Conductance for Conduction Cooling of the Human Body. Proceedings of the Symposium on Individual Cooling, Kansas State University, Manhattan, Kansas. March 17-18, 1969, pp. 92-100.

63. Edited by Hartnett, James P. and Thomas F. Irvine, Jr., Advances in Heat Transfer, Academic Press, New York. 1967.

64. Hayward, J. S.; Collis, M.; and Eckerson, J. D.: Thermographic Evaluation of Relative Heat Loss Areas of Man during Cold Water Immersion. Aerospace Medicine, Volume 44, July 1973, pp. 708-711.

65. Heath, J. E.; Williams, B. A.; and Mills, S. H.: Interactions of Hypothalamic Thermosensitivity and Body Size in Vertebrates. Int. J. Biometeor. 1971, vol. 15, number 2-4, pp. 254-257.

66. Hertzman, A. B.: 1959, 'Vasomotor Regulation of Cutaneous Circulation,' Physiol. Rev. 39, 280-306.

67. Hill, June R.: The Oxygen Consumption of New-Born and Adult Mammals: Its Dependence on the Oxygen Tension in the Inspired Air and on the Environmental Temperature. J. Physiol. (1959) 149, 346-373.

68. Hill, J. W.: 1970, 'Experience with Water Cooled Clothing in Industry', paper presented to Ergonomics Research Society Annual Conference'.

69. Hills, B. A.: Chemical Facilitation of Thermal Conduction in Physiological Systems. Science, Vol. 182, 1973, pp. 823-825.

70. Hodgdon, J. A., "An Examination of Ambient Temperature and Light-Dark Cycling as Entraining Agents for the Circadian Body Temperature Rhythm in the Pig-tailed Monkey", Ph. D Thesis, University of California, Berkeley, 1975.

71. Howard, D. C.; and Syversen, R. G.: Selection of Astronaut Cooling Systems for Extravehicular Space Missions. AIAA Fourth Thermophysics Conference, San Francisco, California. June 16-18, 1969. AIAA Paper No. 69-617.

72. Janssen, J. E.: Thermal Environment Requirements in Manned Spacecraft. Honeywell Research Center, Hopkins, Minnesota.

73. Jennings, D. C.: 1966, 'Water-Cooled Space Suit', J. Spacecraft, August, 1251-1256.

74. Kaufman, W. C.: 1963, "Human Tolerance Limits for Some Thermal Environments of Aerospace', Aerospace Med. 34, 889-896.

75. Kays, W. M.: Convective Heat and Mass Transfer, McGraw-Hill Book Company, New York 1966.

76. Kerslake, D. Mck.: 1964, 'An Estimate of the Preferred Skin Temperature Distribution in Man', FPRC Memo 213, Flying Personnel Research Committee, RAF Institute of Aviation Medicine, Farnborough.

77. Kissen, A. T.; Hall, J. F.; and Klemm, F. K.: Physiological Responses to Cooling the Head and Neck Versus the Trunk and Leg Area in Severe Hyperthermic Exposure. Aerospace Medicine. August 1971.

78. Principles of Heat Transfer, Frank Kreith, International Textbook Company, Scranton, Pennsylvania 1966.

79. Kuno, Y.: 1956, Human Perspiration, Charles C. Thomas, Springfield Illinois.

80. Kuznetz, L. H., A Model for the Transient Metabolic Response of Man in Space, NASA Internal Note No. - MSC-EC-R-68-4, Johnson Space Center, Houston, Dec. 1968.

81. Kuznetz, L. H., The Effects of Free Stream Gas Velocity upon Astronaut Thermal Comfort, NASA Internal Note No. MSC-EC-R-69-7, Johnson Space Center, Houston, 1969.

82. Kuznetz, L. H., The Real Time Determination of Metabolic Rate, NASA Internal Note No. MSC-EC-R-69-8, Johnson Space Center, Houston, 1969.

83. Kuznetz, L. H., Unpublished Internal NASA Studies, NASA-JSC, Houston, Texas.

84. Kuznetz, L. H.: Radiation Heat Transfer Between the Human Body and a Completely Surrounding Garment. University of California, Berkeley. ME 253 Project, Spring Quarter, 1970.

85. Kuznetz, L. H.: The Effect of Liquid Cooling Garments upon Vasoconstriction, Vasodilation, and Heat Transfer from the Human Arm. Unpublished NASA notes. NASA/Johnson Space Center, EC2/Crew Systems Division. Houston, Texas, 1971.

85a. Kuznetz, L. H.: The Effect of Altitude upon Human Thermoregulation. A seminar report for physiology 232, University of California, Berkeley, Spring Quarter, 1973.

86. Leithead, C. S. and Lind, A. R.: 1964, Heat Stress and Heat Disorders, F. A. Davis, Philadelphia.

87. London, R. C.: A Review of Work in the United Kingdom on Water Cooled Suits. Proceedings of the Symposium on Individual Cooling, Kansas State University, Manhattan, Kansas. March 17-18, 1969, pp. 138-169

88. Major Test Facilities of the Engineering and Development Directorate, MSC-03415, NASA/Johnson Space Center, Houston, Texas. October 1970.

89. Marcus, P.: Some Effects of Radiant Heating of the Head on Body Temperature Measurements at the Ear. Aeropsace Medicine April 1973.

90. Marcus, P.: Some Effects of Cooling and Heating Areas of the Head and Neck on Body Temperature Measurement at the Ear. Aerospace Medicine April 1973.

91. McFarland, Ross A.: Human Factors in Relation to the Development of Pressurized Cabins. Aerospace Medicine, Volume 42, No. 12, December 1971.

92. Merrill, G. L. and Starr, J. B.: 1967, 'Automatic Temperature Control for Liquid-Cooled Flight Suits', NADC-AC-6702. U.S. Naval Air Development Center.

93. Mitchell, D.; Wyndham, C. H.; Vermeulen, A. J.; Hodgson, T; Atkins, A. R.; and Hofmeyr, H. S.: Radiant and Convective Heat Transfer of Nude Men in Dry Air. Journal of Applied Physiology. Vol. 26, No. 1, January 1969. pp. 111-118.

94. Morgan, L., Collett, G., Cook, D., Computer Program Documentation For Al-Node Transient Metabolic Man Program, Doc. No. LEC/672-23-03003, NASA-JSC, Houston, August 1974.

95. Nadel, E. R.; Homer, I.; Bergh, U.; Astrand, P. O.; and Stolwijk, J. A. J.: Thermoregulatory Shivering During Exercise. Life Sciences Vol. 13, pp. 983-989, 1973.

96. NASA No. SETDN 1001 Facility User's Guide. Space Environmental Test Division, November 1971.

97. Nielsen, M.: Die regulation der Korpertemperatur bei Muskelarbeit. Skand. Arch. Physiol., volume 79, 1938, pp. 193-230.

98. Nunneley, Sarah A.: Water Cooled Garments: A Review. Space Life Sciences Volume 2, December 1970, pp. 335-360.

99. Nunneley, S. A.; Troutman, S. J.; and Webb, P.: Head Cooling in Work and Heat Stress. Aerospace Medicine January 1971.

100. Pace, N., Environmental Physiology Syllabus, 4th Edition. Design Enterprises, Berkeley, 1974.

101. Paca, Nello, Notes from Environmental Physiology 132, a course conducted at the University of California, Berkeley, Winter 1972.

102. Paca, Nello, Notes from Space Physiology 232, a course conducted at the University of California, Berkeley, Spring 1970.

103. Bioastronautics Data Book, Edited by James F. Parker, Jr., and Vita R. West. National Aeronautics and Space Administration, Washington, D. C. 1973.

104. Pyschrometric Charts for Oxygen and Air at Various Pressures. NASA Scientific Tables.

105. Rambaut, P. C.; Heidelbaugh, N. D.; Reid, J. M.; and Smith, M. C.: Caloric Balance During Simulated and Actual Space Flight. Aerospace Medicine, November 1973. pp. 1264-1269.

106. Richardson, D. L: Portable Life Support Systems for Extravehicular Activity. Proceedings of the Symposium on Individual Cooling, Kansas State University, Manhattan, Kansas. March 17-18, 1969, pp 50-77.

107. Robinson, S.; Meyer, F. F.; Newton, J. L.; Ts'ao, C. H.; and Folgersen, L. O.: Relations Between Sweating, Cutaneous Blood Flow, and Body Temperature in Work. J. Appl. Physiol., volume 20, 1965, pp. 575-582.

108. Roth, H. P.; and Blockley, W. V.: Limits of Endurance for Heat Stress Arising from Work while Totally Insulated. Final Report on Contract NAS 9-8871. NASA. April 1970.

109. Rowell, L. B., Brengelmann, G. L., Blackmon, J. R., and Murray, J. A.: 1970, 'Redistribution of Blood Flow During Sustained High Skin Temperature in Resting Man', J. Appl. Physiol. 28, 415-420.

110. Rowell, L. B., Brengelmann, G. L., and Murray, J. A.: 1969a, 'Cardiovascular Responses to Sustained High Skin Temperature in Resting Man', J. Appl. Physiol. 27, 673-680.

11. Rowell, L. B., Murray, J. A., Brengelmann, G. L., and Kraining, K. K.: 1969c, 'Human Cardiovascular Adjustments to Rapid Changes in Skin Temperature During Exercise', Circ. Res. 24, 711-724.

112. Santa Maria, L. J.: Determination of Skin Temperature under a Comfort-Controlled Liquid-Cooled Garment in Exercising Subjects. Final Report No. NADC-CS-7118 NASA Defense P[illegible]hase Request T-91349. October 26, 1971.

113. Sawin, C. F.: The Respiratory Function of the Blood of Deer Mice at Sea Level and High Altitude. PH.D Thesis at University of California, 1969.

114. Conduction Heat Tranfer, P. J. Schneider, Addision-Wesley Publishing Company, Inc. Reading, Mass. 1955.

115. Scholander, P. F.: Chemical Analysis of Respiratory Gas Composition. Journal of Biological Chemistry, Vol. 167, No. 1, January 1947.

116. Shitzer, A.: Mathematical Models of Thermoregulation and Heat Transfer in Mammals. NASA Technical Memorandum NASA TM X-62,172. Ames Research Center. July 1972.

117. Shitzer, A.; and Chambers, A. B.: Comparative Study of Patches for Liquid Cooled Garments. Journal of Spacecraft and Rockets, Vol. 10, No. 8, August 1973.

118. Shitzer, A., Chato, J. C. and Hertig, B. A., "A Study of the Thermal Behavior of Biological Tissue with Application to Thermal Control of Protective Suits," NASA-CR-116873, 1971.

119. Shitzer A., Chato, J. C. and Hertig, B. A., "A Study of the Thermal Behavior of Living Biological Tissue With Application to Thermal Control of Protective Suits," Department of Mechanical and Industrial Engineering, University of Illinois at Urbana-Champaign, Urbana, Ill., Technical Report No. ME-TR-207 (1971).

120. Shitzer, A., Chato, J. C. and Hertig, B. A., "Removal of Metabolic Heat From Man Working in a Protective Suit," Second Conference on Portable Life Support Systems, NASA SP-302, pp. 265 - 281 (1972).

121. Shitzer, A.; and Williams, B. A.: A Modular Liquid-Cooled Helmet Liner for Thermal Comfort. Ames Research Center. Aerospace Medicine.

122. Shvartz, E.: Effect of a Cooling Hood on Physiological Responses to Work in a Hot Environment. Journal of Applied Physilogy, Vol. 29, No. 1, July 1970.

123. Shvartz, E., "Efficiency and Effectiveness of Different Water Cooled Suits - A Review," Aerospace Medicine, 43, pp. 488-491, 1972.

124. Shvartz, E. and Benor, D., "Total Body Cooling in Warm Environment," J. Appl. Physiology, 31, pp. 24 - 27 (1971).

125. Smith, T. F.: Thermal Response of Man. NASA/Johnson Space Center Internal Document. Houston, Texas, August 1973.

126. Smith, Theodore F.: Liquid Cooled Garment Design. Paper for NASA/ L. B. Johnson Space Center written by NASA-ASEE Summer Faculty Fellow. August 1974.

127. Smith, Theodore F.: Thermal Response of A Human Being in a Space Suit Environment. NASA/Johnson Space Center Internal Document. Houston, Texas, August 1974.

128. Fundamentals of Statistical Thermodynamics, R. E. Sonntag, and G. J. Van Wylen; John Wiley and Sons, Inc., New York, New York. 1968.

129. Spencer, G. L.; and Grafe, R. L.: Summary Test Report of the EMU Manned Thermal-Vacuum Qualification Test for Apollo J Missions, NASA-MSC-01462, Houston, Texas, 1971.

130. Starr, J. B.· 1970, 'Fluidic Temperature Control for Liquid-Cooled Space Suits', in Portable Life Support Systems, NASA-SP-234, pp. 179-189.

131. Starr, J. B. and Merrill, G. L.: 1968, 'Fluidic Temperature Control for Liquid-Cooled Flight Suits', NADC AC-6818, Naval Air Development Center, Johnsville, Pennsylvainia.

132. Stoll, A. M.; and Chianta, M. A.: Applications of Biophysical Heat Transfer Studies in Protection Systems, NADC-MR-6722. Aerospace Medical Research Department, Department of the Navy. December 1967.

133. Stolwijk, J. A. J.
A Mathematical Model of Physiological Temperature Regulation in Man. John B. Pierce Foundation Laboratory, Report Number NAS-9-9531.

134. Stolwijk, J. A. J.
A Mathematical Model of Physiological Temperature Regulation in Man. NASA CR-1855, 1971.

135. Stolwijk, J. A. J.: A Mathematical Model of Physiological Temperature Regulation in Man. NASA Contractor Report NASA CR-1855 August 1971.

136. Stolwijk, J. A. J.
Mathematical Model of Thermoregulation.
Physiological and Behavioral Temp. Regulation, 1971, pp. 703-721.

137. Stolwijk, J. A. J. and Hardy, J. D.
Temperature Regulation in Man - A Theoretical Study.
Pflugers Archiv., vol. 291, 1966, pp. 129-162.

138. Stolwijk, J. A. J. and Hardy, J. D.
Skin and Subcutaneous Temperature Changes During Exposure to Intense Thermal Radiation. Thermal Problems in Aerospace Medicine, J. D. Hardy ed., 1968, pp. 31-46

139. Stolwijk, J. A. J.; Saltin, B.; and Gagge, [illegible] Physiological Factors Associated with Sweating During [illegible] Aerospace Med., volume 39, 1968, pp. 1101-1105.

140. Troutman, S. J.: Automatic Control of Water Cooling. Proceedings of the Symposium on Individual Cooling, Kansas State University, Manhattan, Kansas. March 17-18, 1969, pp. 262-280.

141. Troutman, S. J.; and Webb, Paul: Automatic Controllers for the Apollo LCG. Final Report on Contract NAS 9-9778. June 1970.

142. Van Der Walt, W. H.; and Wyndham, C. H.: An Equation for Prediction of Energy Expenditure of Walking and Running. Journal of Applied Physiology, Vol. 34, No. 5, may 1973. pp. 559-562.

143. Varene, P.; Jacquemin, C.; Durand, J.; and Raynaud, J.: Energy Balance During Moderate Exercise at Altitude. Journal of Applied Physiology. Vol. 34, No. 5, May 1973. pp. 633-638.

144. Veghte, J. H.: 1965, 'Efficacy of Pressure Suit Cooling System in Hot Environments', Aerospace Med. 36, 964-967.

145. Veghte, J. H.: 1970, 'Efficacy of Ventilating Systems', in Portable Life Support Systems, NASA SP-234, pp. 151-158.

146. Veghte, J. H. and Webb, P.: 1961, 'Body Cooling and Response to Heat', J. Appl. Physiol. 16, 235-238.

147. Waligora, J. M., Hawkins, W. R., Humbert, G. F., Nelson, L. J., Vogel, S. J., and Kuznetz, L. H., Apollo Experience Report - Assessment of Metabolic Expenditures, NASA Technical Note No. JSC-07484, Johnson Space Center, Houston, Texas, Sept. 1974.

148. Waligora, J. M.: Report on Development Tests of a Cooling Garment for Support of the Shuttle Emergency Rescue Sphere. Unpublished internal NASA document. Crew Systems Division, 1974.

149. Waligora, J. M.; and Michel, E. L.: Application of Conductive Cooling for Working Men in a Thermally Isolated Environment. Aerospace Medicine, May 1968, pp. 485-487.

150. Wang Laboratories Inc: N^{th} Order Regression Program, Statistical/ Engineering General Program Library, GLBR 22, 1973 pp. 13-17.

151. Webb, P.: 1959, 'Human Thermal Tolerance and Protective Clothing', Am. Soc. N. Y. Acad. Sci. 82, 714-723.

152. Webb, P.: 1961, 'Temperature Stresses', in Aerospace Medicine (ed. by H. G. Armstrong), pp. 324-344, Williams and Wilkins, Baltimore.

153. Webb, P.: 1966, 'Dissociation of Heat Production and Heat Loss in Working Men', Am. Soc. of Mechanical Engineers, Winter Meeting.

154. Webb, P.: 1967, 'Human Water Exchange in Space Suits and Capsules', NASA CR-804.

155. Webb, Paul: Physiological Effects of Cooling. Proceedings of the Symposium on Individual Cooling, Kansas State University, Manhattan, Kansas. March 17-18, 1969, pp. 1-32.

156. Webb, P.: 1970, 'Automatic Cooling: Strategies, Designs, and Evaluations', in Portable Life Support Systems, NASA SP-234, pp. 159-177.

157. Webb, Paul: Metabolic Heat Balance Data for 24-Hour Periods. Int. J. Biometeor. 1971, vol. 15, number 2-4, pp. 151-155.

158. Webb, Paul: Rewarming After Diving in Cold Water. Aerospace Medicine October 1973.

159. Webb, Paul; and Annis, James A.: Biothermal Responses to Varied Work Programs in Men Kept Thermally Neutral by Water Cooled Clothing. NASA CR-739, 1967.

160. Webb, P. and Annis, J. R.: 1968, 'Cooling Required to Suppress Sweating During Work', J. Appl. Physiol. 25, 489-493.

161. Webb, Paul; Annis, James F.; and Troutman, Samuel J.: Automatic Control of Water Cooling in Space Suits. NASA CR-1085, 1968.

162. Webb, Paul; Annis, James F.; and Troutman, Samuel J.: Human Calorimetry with a Water-Cooled Garment. Journal of Applied Physiology Vol. 32, No. 3, March 1972.

163. Williams, B. A.; and Chambers, A. B.: The Effect of Neck Warming and Cooling on Thermal Comfort. Aerospace Medicine, 43:1972

164. Williams, B. A.; and Chambers, A. B.: Effect of Neck Warming and Cooling on Thermal Comfort. Second Conference on Portable Life Support Systems NASA SP-302 1971.

165. Williams, B. A.; Shitzer, A.: Reduction of Thermal Strain with Head Cooling. Aerospace Medicine 45:1974.

166. Williams, B. A.; Shitzer, A.; and Elkins, W.: A Liquid Cooled Aircrew Helmet Liner for Thermal Comfort. 44th Aerospace Medical Conference Las Vegas, Nev. 1973.

167. Wing, J. F.: 1965, 'Upper Thermal Tolerance Limits for Unimpaired Mental Performance', Aerospace Med. 36, 960-964

168. Wissler, Eugene H.: A Mathematical Model of the Human Thermal System. (Study supported by office of Surgeon General, U. S. Army, under contract # DA49-193-MD-2005.) Bulletin of Mathematical Biophysics, Vol. 26, 1964. pp. 147-166.

169. Wortz, E. C., Edwards, D. K., and Harrington, T. J.: 1964, 'New Techniques in Pressure Suit Cooling', Aerospace Med. 35, 978-984.

170. Wurster, R. D.; Hassler, C. R.; McCook, R. D.; and Randall, W. C.: Reversal in Patterns of Sweat Recruitment. Journal of Applied Physiology, Vol. 26, No. 1, January 1969. pp. 89-94.

171. Wyndham, C. H.; Strydom, N. B; Benade, A. J. S; and Van Rensburg, A. J.: Limiting Rates of Work for Acclimatization at High Wet Bulb Temperatures. Journal of Applied Physiology, Vol. 35, No. 4, October 1973, pp. 454-458.

172. Wyss, C. R.; Brengelmann, Johnson, J. M.; Rowell, L. B.; and Niederberger, M.: Control of Skin Blood Flow, Sweating, and Heart Rate: Role of Skin versus Core Temperature. Journal of Applied Physiology. Vol. 36, No. 6, June 1974.

173. Zuntz and Schumberg, modified by Lusk, G.: Metabolic Rate Determinations from Oxygen Consumptions. Journal of Biological Chemistry. Vol. 59, p. 1. 1924.

APPENDIX A

LEADING PARTICULARS OF THE APOLLO A7L SUIT, THE APOLLO LCG, AND TEST INSTRUMENTATION AND EQUIPMENT

TABLE A1.- LEADING PARTICULARS OF THE A7L EMU

Item	Value	
	A7L PGA with ITMG	PLSS
Weight	41.87 lb	34.33 lb
Operational temperature limitations	+250° F	S/C[a] wall -20° to +150° F
Leak rate at 3.7 psid (max.)	180.00 scc/min (0.0315 lb/hr)	180.00 scc/min (0.0315 lb/hr)
Operating pressure	3.75 ± 0.25 psid	3.75 ± 0.25 psid
Structural pressure	6.00 psid	6.00 psid
Proof pressure	8.00 psid	8.00 psid
Burst pressure	10.00 psid	10.00 psid
Pressure drop		
12 acfm, 3.5 psia. 50° F, and inlet diverter valve open (IV position)	4.70 in. H_2O	4.70 in. H_2O
6 acfm, 3.9 psia, 77° F, and inlet diverter valve closed (EV position)	1.80 in. H_2O	--

[a]Spacecraft.

TABLE A2.- LEADING PARTICULARS OF THE LIQUID-COOLING GARMENT AND MULTIPLE WATER CONNECTOR

Item	Value
Liquid-cooling garment	
Weight (charged)	[a]4.60 lb
Operating pressure	4.20 to 22.0 psid
Structural pressure	28.50 psid
Proof pressure	33.75 psid
Burst pressure	47.50 psid
Pressure drop	
[a]4.0 lb/min and 70° ± 10° F inlet	3.2 psi including both halves of connector
Leak rate	
[a]19.0 psid and 45° F	0.58 cc/hr
Multiple water connector	
Pressure-drop	
[a]4.0 lb/min and 70° ± 10°F, both halves, both directions	1.3 psi

[a]Design value.

TABLE A3.- INSTRUMENTATION AND EQUIPMENT

Equipment	Function	Description	Manufacturer	Location
Thermocouples	Measure wall & air temperatures	Copper-Constantan	Omega Corp. Thermal Electric Co. Conax	
Skin Temperature Thermocouples	Measure skin temperature	Copper-Constantan		
Thermistors	Measure tympanic temperature Measure rectal temperature Measure LCG water inlet & outlet temperatures Measure suit gas inlet & outlet temperatures	Linear precision type	Yellow Springs Instruments	Yellow Springs, Ohio
Dewpointers	Measure suit gas inlet & outlet dew points Measure ambient humidity	Thermoelectric refrigerator or heater & polished mirror	Cambridge Corp. Hastings Corp.	Cambridge, Mass.
Mass Flowmeters	Measure suit gas flowrate	Turbine flowmeter	Quantum Dynamics Corp. Flow Technology Corp.	Tarzana, Cal.
Oxygen Flowmeter	Measure oxygen flowrate	Volume flowmeter	National Instruments-Voluflow	
LCG Water Flowmeter	Measure LCG water flowrate	Turbine flowmeter	Cox Corp. Potter Instruments	Cambridge, Mass. New York, N.Y.
Total Pressure Transducer	Measure total ambient pressure	Variable reluctance type transducer	Pace Corp. Valadyne Corp.	

TABLE A3.- CONTINUED

Equipment	Function	Description	Manufacturer	Location
Gas Analyzers	Measure oxygen partial pressure	Paramagnetic sensor	Beckman Instruments	
		Mass spectrometer	Med Spectrometer	Baltimore, Md.
	Measure CO_2 partial pressure	Infrared detection	Beckman Instruments	
		Mass spectrometer	Med Spectrometer	Baltimore, Md.
	Measure nitrogen partial pressure	Gas ionization	Med Science Corp.	
		Mass spectrometer	Med Spectrometer	Baltimore, Md.
EKG Sensors	Measure EKG and heart rate	Silver chloride electrodes	NASA-JSC Crew Systems Division	Houston, Texas
Douglas Bags	Collect respiratory gases	Rubberized bags with check valves	Warren E. Collins Corp.	Braintree, Mass.
Tissot Spirometer	Measure pulmonary function	Spirometer	Warren E. Collins Corp.	Braintree, Mass.
Bicycle Ergometer	Impose desired workload	Variable Resistance Ergometer	Warren E. Collins Corp.	Braintree, Mass.
Treadmill	Impose desired workload	Variable Speed Treadmill	A. R. Young Corp.	Indianapolis, Ind.
Human Balance	Measure weight loss	Double Beam Balance	Buffalo Corp.	
		Electronic Balance	Toledo Balance Corp.	Toledo, Ohio
NASA-JSC Hypobaric Chambers	Control ambient pressure from sea level to below 10 torr Control ambient temperature and humidity and infrared radiation Provide and recondition ventilating suit gas and LCG water to desired specifications	8' Chamber	Chicago Bridge and Iron Corp.	Chicago, Ill.
		SESL Chamber B		

TABLE A3.- CONTINUED

Equipment	Function	Description	Manufacturer	Location
Xenon Lamps	Provide ultra-violet radiation as desired.	Xenon Vapor Solar Simulators	Spectrolab Corp.	Cal.
Apollo A7L Suit	See Section 2	See Section 2	International Latex Corp.	Dover, Delaware
Apollo LCG	See Section 2	See Section 2	International Latex Corp.	Dover, Delaware
PLSS	See Section 2	See Section 2	Hamilton Standard Division of United Aircraft	Windsor Locks, Comm.

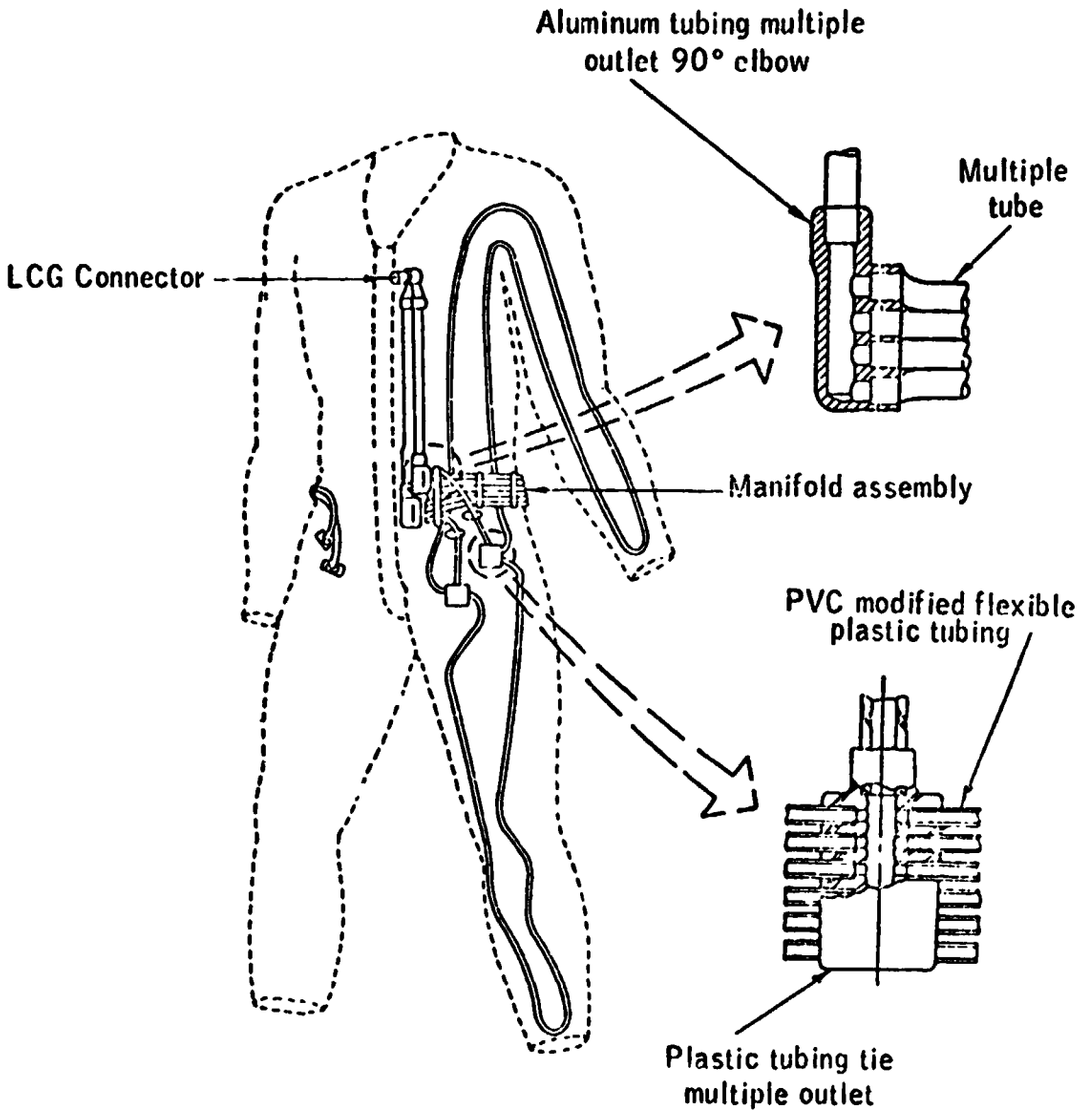

Figure A-1. Coolant system of the LCG.

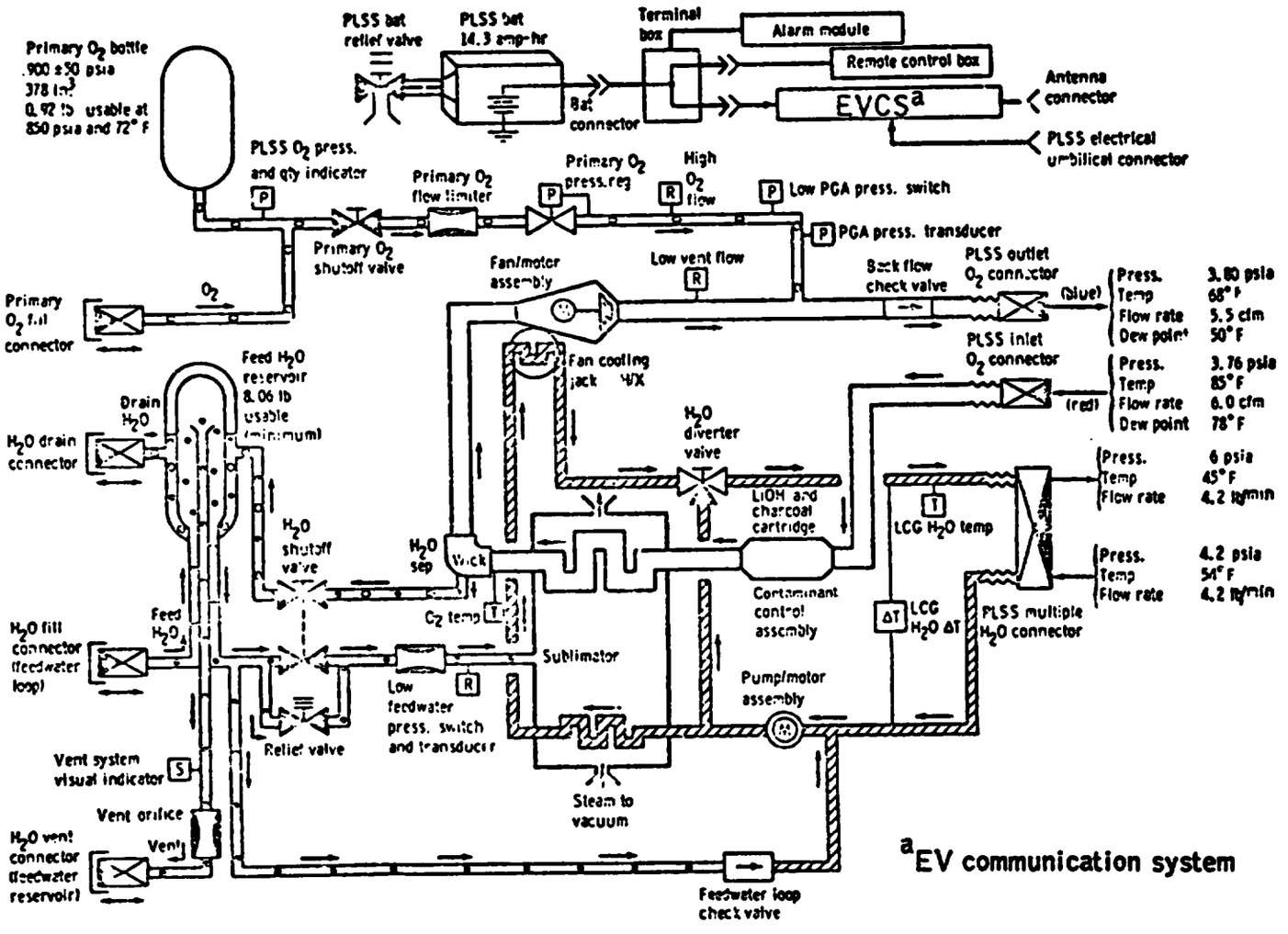

Figure A-2. Detailed schematic of the Portable Life Support System (PLSS).

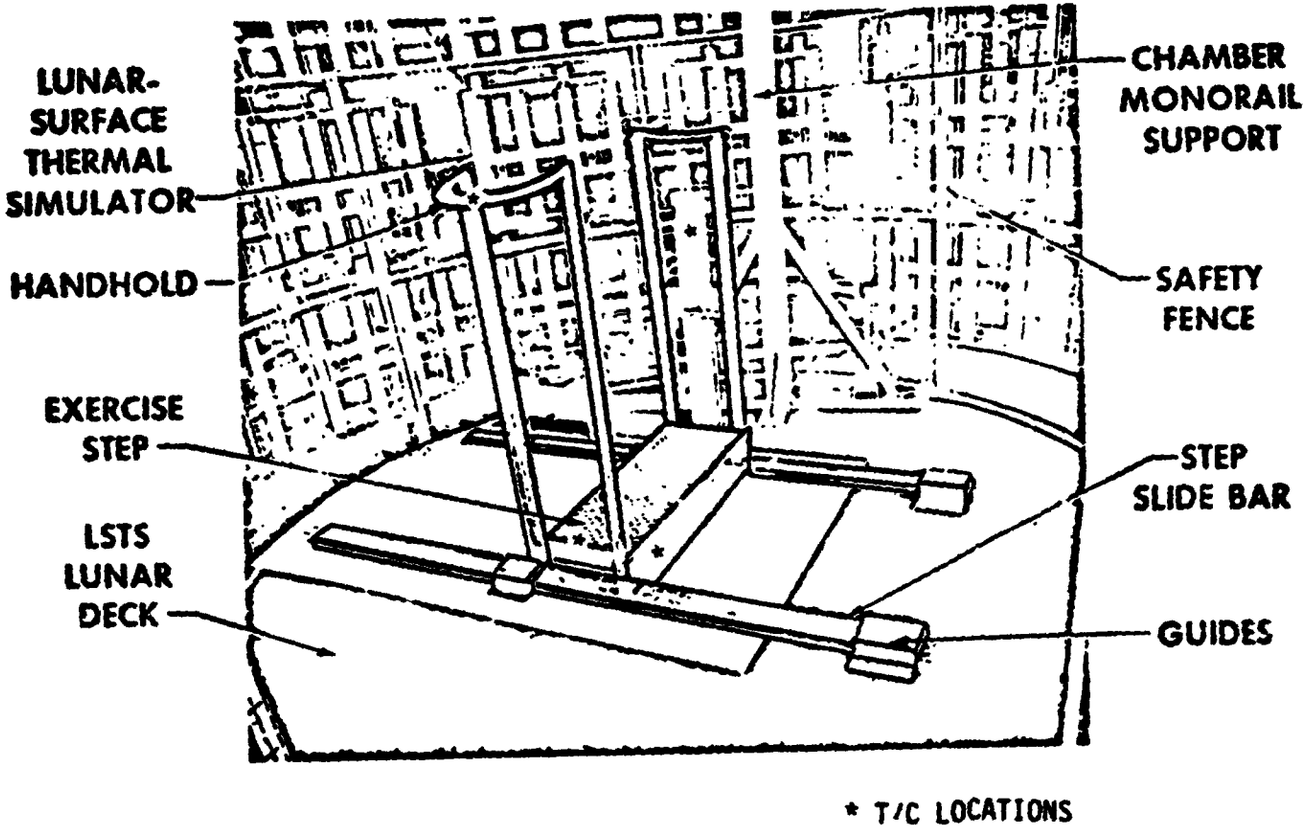

Figure A-3. Exercise stand for test series D.

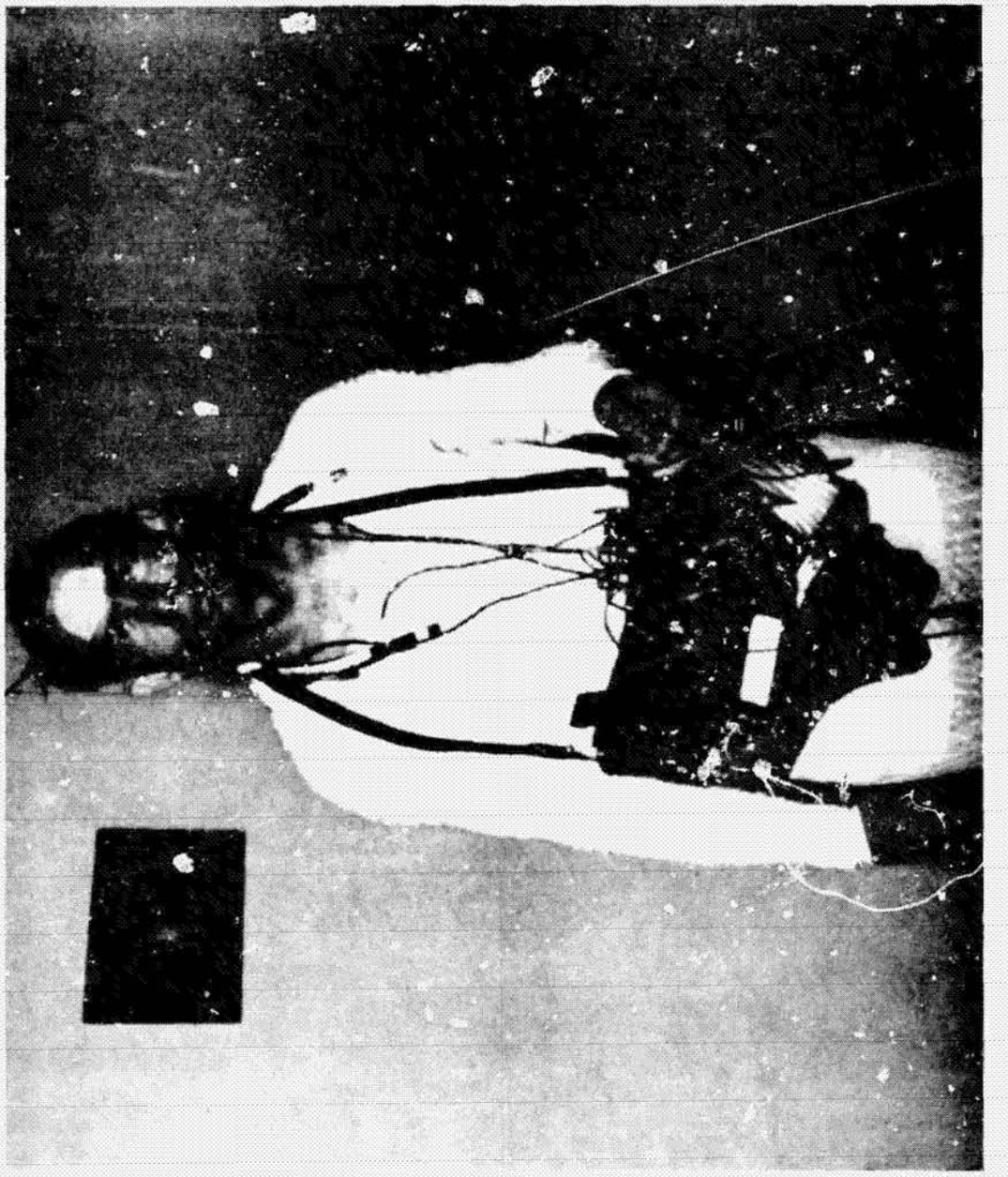

Figure A-4. LCG with bioharness and skin temperature thermocouples.

REPRODUCIBILITY OF THE
ORIGINAL PAGE IS POOR

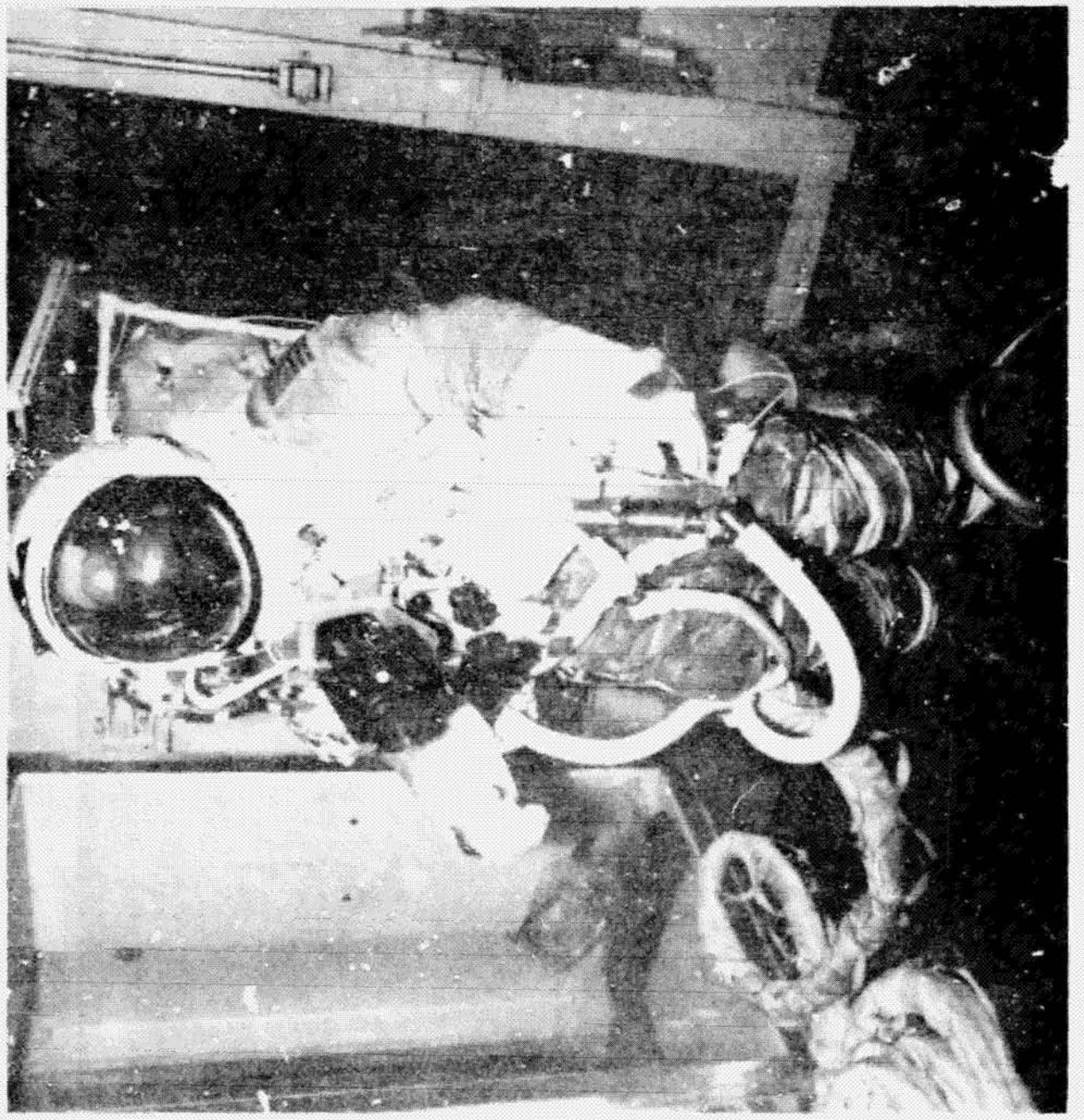

Figure A-5. A7L suit + Apollo LCG + PLSS=(EMU) prior to entering chamber in test series D.

REPRODUCIBILITY OF THE
ORIGINAL PAGE IS POOR

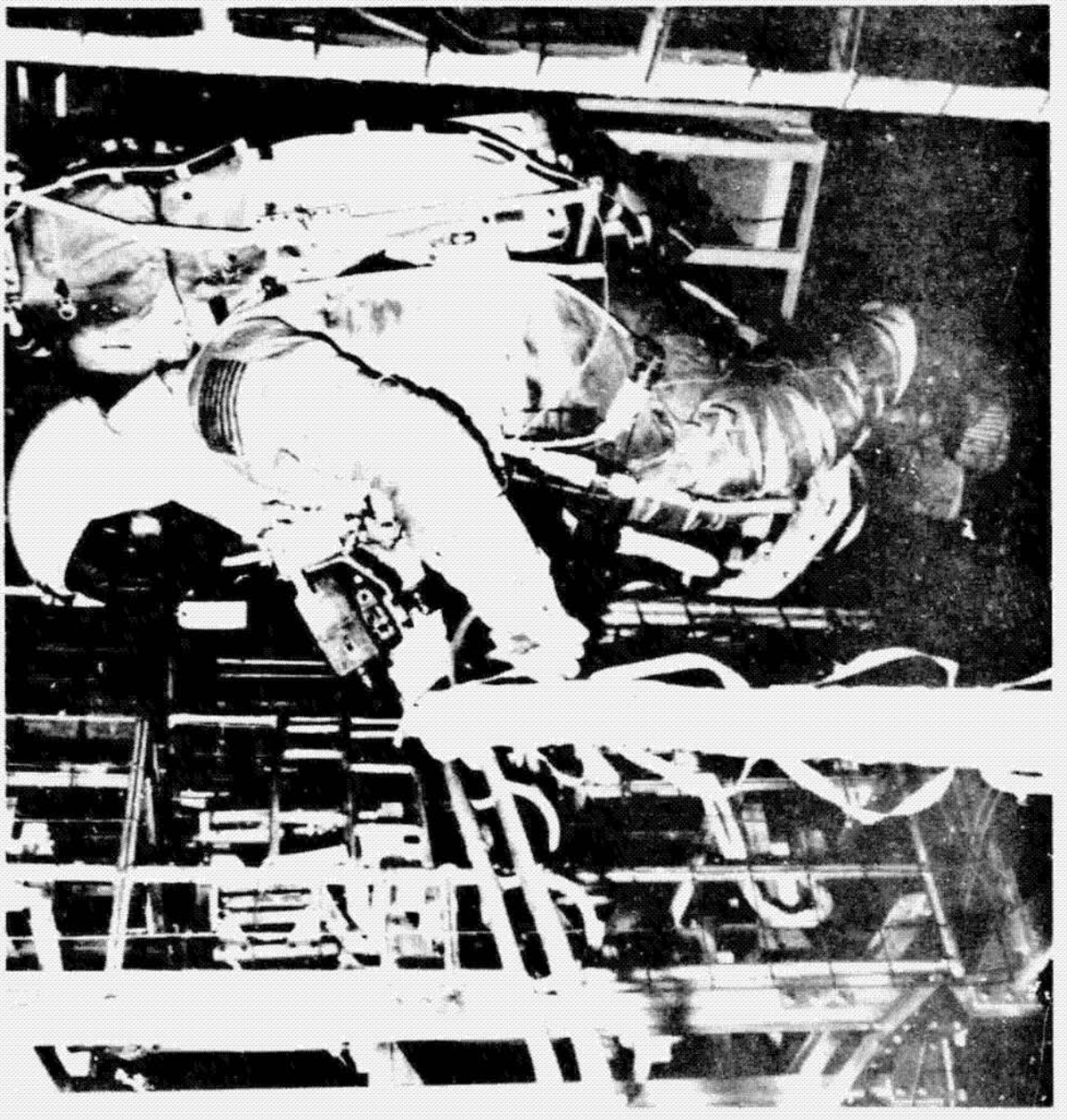

Figure A-6. Side view of EMU showing PLSS and weight relief system.

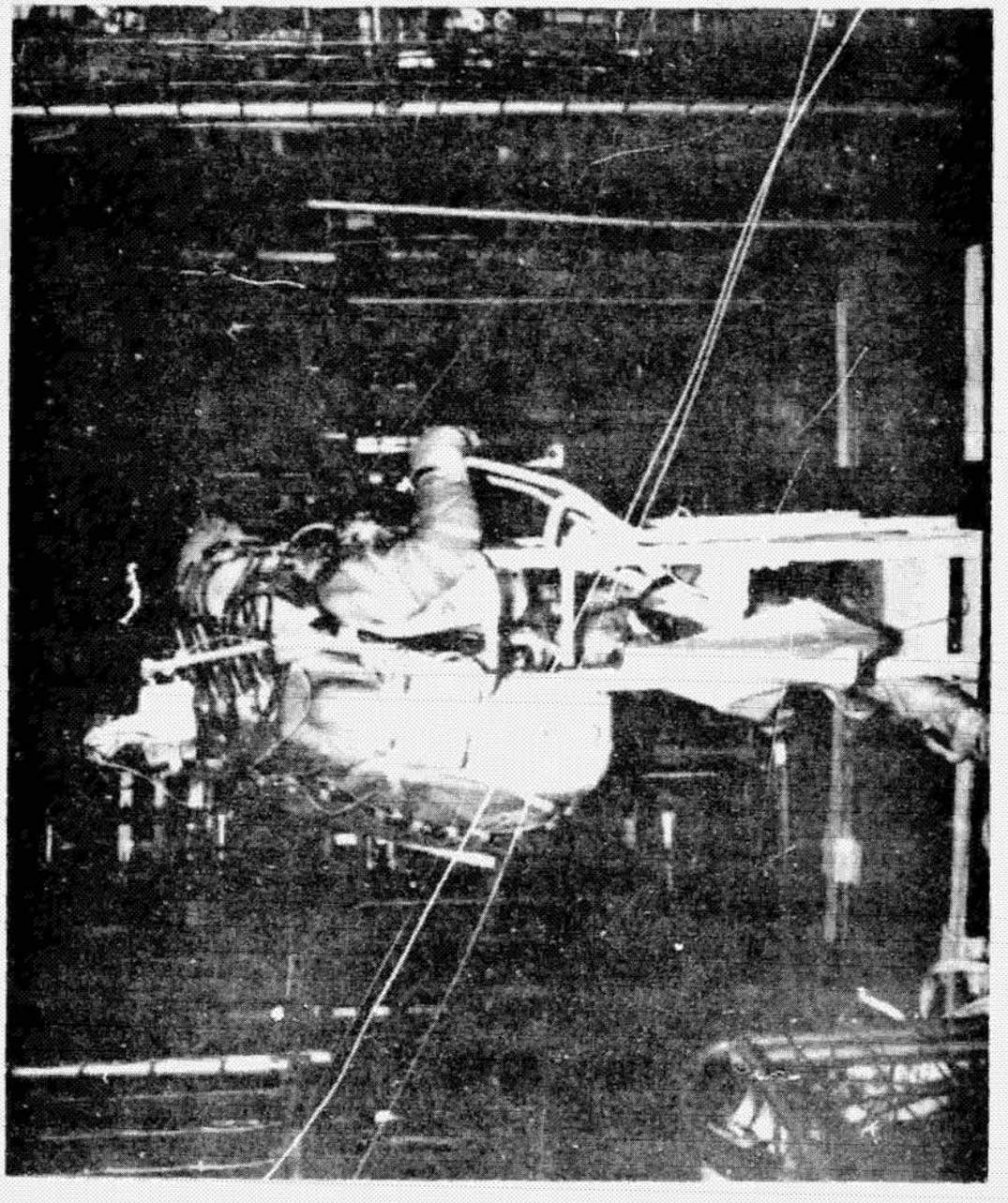

Figure A-7. Subject exercising on step during test series D.

APPENDIX B

TECHNICAL DESCRIPTION

OF THE

MATHEMATICAL MODEL

(80, 83, 125)

NOMENCLATURE

A_s	Skin Area, Ft^2
$A_{s,c}$, $A_{s,r}$	Convective and Radiative Skin Area, Ft^2
B	Heart Output, Pulses per Minute
c	Heat Capacity, Btu/lb_m -°F
c_o, C_t	Cold Sensation Signals, °F
C_{sw}, C_{co}, C_{di}, C_{sh}	Control Coefficients for Sweat, Vasoconstriction, Vasodilation, and Shiver
D	Temperature Difference, °F
E_{max}	Maximum Evaporation, Btu/hr
F	View Factor
G	Dimensionless Gravitational Acceleration
Gr	Grashof number
h	Enthalpy, Btu/lb_m
h_c, h_r	Convective and Radiative Coefficients, $Btu/hr-ft^2-°F$
h_{fg}	Enthalpy of Evaporation, Btu/lb_m
k	Thermal Conductivity, Btu/hr-ft-°F
L	Thickness, ft
m	Mass, lb_m
$\dot{m}$	Mass Flow Rate, lb_m/hr
M	Metabolism, Btu/hr
$\bar{M}_o$, $\bar{M}_w$	Molecular Weight of Oxygen and Water
Nu	Nusselt Number
P	Pressure, psia
Pr	Prandtl Number
P_v	Partial pressure, psia

P_{sw}, P_{co}, P_{di}, P_{sh}	Control Coefficients for Sweat, Vasoconstriction, Vasodilation, and Shiver
Q	Heat Transfer, Btu/hr
Q_{blood}	Blood Flow Heat Transfer, Btu/hr
Q_{cond}	Conductive Transfer, Btu/hr
Q_{conv}	Convective Transfer, Btu/hr
Q_{cool}	Coolant Heat Transfer, Btu/hr
Q_{diff}	Diffusion Heat Transfer, Btu/hr
Q_{evap}	Evaporative Transfer, Btu/hr
Q_{gen}	Heat Generation, Btu/hr
Q_{rad}	Radiative Transfer, Btu/hr
Q_{resp}	Respiratory Heat Transfer, Btu/hr
Q_{shiv}	Shiver Heat Generation, Btu/hr
Q_{stor}	Energy Storage, Btu
Q_{sweat}	Sweat Heat Transfer, Btu/hr
R	Conductance, Btu/hr-°F
Re	Reynolds Number
$\bar{R}_o$	Gas Constant for Oxygen, ft-lb_f/lb_m-°R
S_s, S_c, S_d	Control Signals for Sweat, Vasoconstriction, and Vasodilation
S_{sw}, S_{co}, S_{di}, S_{sh}	Control Coefficients for Sweat, Vasoconstriction, Vasodilation, and Shiver
t	Temperature, °F
$\bar{t}$	Average Temperature, °F
t_i, t_o	Inlet and Outlet Temperature, °F
t_{set}	Set Temperature, °F

T	Temperature, °R
U	Internal Energy, Btu/hr
UA	Overall Conductance, Btu/hr-°F
V	Velocity, ft/min
W	Work, Btu/hr
W_a, W_t	Warm Sensation Signals, °F
α_c, α_d	Vasoconstriction and Vasodilation Distribution
α_g	Garment Area Distribution
α_r	Thermoreceptor Distribution
α_{resp}	Respiratory Heat Transfer Distribution
α_s	Skin Area Distribution
α_{sh}	Shiver Distribution
α_{sw}	Sweat Distribution
α_w	Coolant Distribution
α_{wk}	Work Distribution
ϵ	Emittance
η_e	Ventilation Efficiency
η_m	Mechanical Efficiency
η_n	Net Efficiency
σ	Stefan - Boltzmann Constant, Btu/hr-ft^2-°R^4
ν	Time, hr

Subscripts

b	Blood
c	Core
d	Environment

f	Fat
g	Garment
m	Muscle
o	Basal
r	Radiative
s	Skin
w	Coolant

MODEL DESCRIPTION

The thermal system of man is conveniently analyzed by considering a controlled system and a controlling system [2]†. The controlled system is associated with the various thermal characteristics and energy transfer mechanisms found in man. Body temperature regulation through sweating, shivering, and variable blood flow rate is the function of the controlling system. Energy balances applicable to energy transfer in man are given in Section 1. A description of energy terms introduced in the energy balances is presented in Section 2. Expressions as modeled for the controlling system are discussed in Section 3.

1. ENERGY BALANCES

Analysis of energy transfer mechanisms associated with man begins with the first law of thermodynamics which may be written for steady flow condition as*

$$mc \frac{dt}{d\tau} = M - W - Q + \Delta (\dot{m}h) \qquad (1.1)$$

The term on the left of Eq (1.1) represents the time rate of change of internal energy. M and W denote energy generation and external work, respectively. Energy transfer as heat is denoted by Q. This term includes heat transfer by conduction, convection, radiation, and evaporation within man as well as between him and his environment. Respiratory heat transfer is also included in this term. The Δ - symbol of Eq. (1.1) denotes the difference between the product of mass flow and enthalpy for inlet and outlet conditions. Energy transfer associated with food intake and waste products is included in this term. Except in certain applications, energy content of these materials may be neglected.

†References shown in brackets are presented in the Appendix B References.
*Notation t and T designate temperatures in °F and °R, respectively.

Before conservation of energy can be applied directly to evaluation of the thermal response of man, temperature distribution and material properties of man must be considered. A man at rest may exhibit an internal body tissue temperature approximately 5°F higher than the skin temperature. At higher activity levels, this temperature difference may increase to 10°F. Although these temperature differences are not large in view of certain applications, they are significant for the thermal state of man. The body is composed of heterogeneous material which result in non-uniform physical and thermal properties. Effects of non-uniform temperature distribution and properties are accounted for by subdividing the body into several elements. Each body element has uniform temperature distribution and properties. During the initial development of the thermal model, the body was divided into core and skin layers. However, it became apparent that two segments were insufficient and a finer subdivision was needed. In the present model, 41 nodes are employed. The body is subdivided into ten segments consisting of head, trunk, as well as right and left arms, hands, legs, and feet. Each segment is further divided into core, muscle, fat, and skin layers. An additional segment which remains as a whole is the blood compartment. A spherical shape is assumed for the head with circular cylinders for the remaining segments. Representative surface areas, volumes, and weights for the various segments and layers are given by Stolwijk [2]. Energy balance for each layer is written to include stored energy rate, energy generation due to metabolism, work, and shiver as well as energy exchange by conduction with adjacent layers, by convection with the blood compartment, and by conduction, convection, radiation, and evaporation with the environment. Appropriate energy balances for each layer follow.

1.1 Core Layers

Core layers exchange energy by conduction with muscle layers and by convection with the blood compartment. Head and trunk layers also exchange energy with the respiratory tract. Energy balance for core layers is written as

$$m_c c_c \frac{dt}{d\tau}_c = Q_{gen,c} + Q_{blood,c} - Q_{cond,c} - Q_{resp,c} \qquad (1.2)$$

In Eq. (1.2), $Q_{gen,c}$ represents heat generation due to metabolism, work, and shiver. Convective heat transfer due to blood flow is denoted by $Q_{blood,c}$. $Q_{cond,c}$ designates conduction heat transfer between core and muscle layers. Respiratory tract heat transfer is represented by $Q_{resp,c}$ and is applicable only for the head and trunk core layers. Specific expressions for each energy transfer term are given in Section 2.

1.2 Muscle Layers

Muscle layers exchange energy by conduction with core and fat layers, by convection with the blood compartment, and, for head and trunk layers, with the respiratory tract. Energy balance for muscle layers is expressed as

$$m_m c_m \frac{dt}{d\tau}_m = Q_{gen,m} + Q_{blood,m} + Q_{cond,c} - Q_{cond,m} - Q_{resp,m} \qquad (1.3)$$

where $Q_{cond,m}$ represents conduction between muscle and fat layers. Respiratory heat transfer applies only for the head and trunk muscle layers.

1.3 Fat Layers

Fat layers exchange energy by conduction with muscle and skin layers, by convection with the blood compartment, and, for head layer, with the

respiratory tract. Energy balance for fat layers is

$$m_f c_f \frac{dt_f}{d\tau} = Q_{gen,f} + Q_{blood,f} + Q_{cond,m} - Q_{cond,f} - Q_{resp,f} \qquad (1.4)$$

where $Q_{cond,f}$ denotes conduction between fat and skin layer.

1.4 Skin Layers

Energy transfer mechanisms for skin layers may be more numerous since these layers may exchange energy with the environment by conduction, convection, radiation, and evaporation. Furthermore, a garment or layer of clothing may cover certain skin areas where energy exchange for these skin layers is by conduction to the garment and by evaporation. In some applications, the tubes of a Liquid Conditioning Garment (LCG) are in contact with skin areas. Water circulated through these tubes at various flowrates and temperatures can provide very significant conductive cooling. Skin layers also exchange energy by convection with the blood compartment and by conduction with fat layers. Energy balance for skin layers assumes the form

$$m_s c_s \frac{dt_s}{d\tau} = Q_{gen,s} + Q_{blood,s} + Q_{cond,f} - Q_{cond,s} - Q_{conv,e}$$

$$- Q_{rad,e} - Q_{evap,e} - Q_{LCG} \qquad (1.5)$$

where $Q_{cond,s}$ designates conduction between skin layers and environment or garment. Convection, radiation, and evaporation heat exchange with the environment are represented by $Q_{conv,e}$, $Q_{rad,e}$, and $Q_{evap,e}$, respectively. Heat transfer to an LCG is denoted by Q_{LCG}. Evaporation is actually a mass transfer mechanism, but for convenience is included as a heat transfer mode. Exposed skin areas exchange energy with the environment by all mechanisms with conduction being generally least significant. Convection

and radiation for covered skin areas may be neglected but evaporation may still be important due to moisture permeation of garment.

1.5 Garment Layers

Although garment layers are not directly associated with the body, energy balances are presented. The garment is subdivided into segments corresponding to those for the skin areas. Energy exchange for garment layers occurs by conduction with skin layers as well as by convection and radiation with the environment. Condensation of sweat in garment layers is absent [3]. Furthermore, heat transfer from garment layers to the LCG and the thermal response of the garment are neglected. Energy balance for garment layers is

$$Q_{cond,s} = Q_{rad,\ e} + Q_{conv,\ e} \tag{1.6}$$

This expression applies only to skin areas covered by garment layers.

1.6 Blood Compartment

The blood compartment exchanges energy by convection with all body layers. Energy balance for this compartment is written as

$$m_b c_b \frac{dt_b}{d\tau} = -Q_{blood} \tag{1.7}$$

where Q_{blood} represents total heat transfer by blood flow to all body layers.

2. ENERGY TRANSFER TERMS

Energy transfer in man is associated with energy generation due to metabolism, work, and shiver as well as with conduction between adjacent tissue layers and convection due to blood flow. Man exchanges energy with his environment through conductive, convective, radiative, and evaporative transfer mechanisms. Each energy term introduced in the energy balances is described in the following sections.

2.1 Heat Generation

Heat generation as employed in energy balances refers to energy generation due to metabolism, work, and shiver and represents the M-W term in the generalized conservation of energy equation, EQ (1.1). Metabolism is the product of chemical reactions within the body. At complete rest, the metabolic rate is commonly referred to as basal metabolism with a typical value for the whole body of 278 Btu/hr. Work refers to external mechanical work performed by or on the body. Performance of work causes a change in metabolic rate which may be related through introduction of an efficiency factor as defined later. Shiver is activation of muscle layers and is a control mechanism for maintenance of body temperature in a cold environment.

Metabolic rates for core, fat, and skin layers are taken as those attributed to basal metabolism. Thus, these layers do not contribute to work and shiver. Heat generation for core layers is written as

$$Q_{gen,c} = M_{o,c} \tag{2.1}$$

where $M_{o,c}$ is basal metabolism with typical values for each core layer given in Table 1. Similar expressions for fat and skin layers are applicable with basal metabolism values also listed in Table 1.

As previously noted, work and shiver are assigned to muscle layers. Heat generation for these layers is expressed as

$$Q_{gen,m} = M_{o,m} + \alpha_{wk} (M - M_o - W) + \alpha_{sh} Q_{shiv} \tag{2.2}$$

where $M_{o,m}$ denotes muscle basal metabolism with values given in Table 1. α_{wk} represents distribution of metabolic rate above basal metabolism and of work assigned to each muscle layer. Similarily, α_{sh} is distribution of shiver throughout muscle layers. Values for work and shiver distribution in muscle layers are given in Table 2. It would be expected that work distribution in muscle layers is dependent upon the type of activity performed by man. Further study is needed to define work distribuiton for different activities. Metabolic rate and total basal metabolism are denoted by M and M_o, respectively. Values of metabolic rate for several common activities are given by Fanger [4]. Total basal metabolism has a value of 278 Btu/hr. Work and metabolic rates are combined by introducing mechanical or gross efficiency [4,5] defined as

$$\eta_m = \frac{W}{M} \tag{2.3}$$

Typical values of mechanical efficiency for various activities are given by Fanger [4]. Effects of atmospheric pressure and gravitational acceleration on work and, consequently, mechanical efficiency remain to be evaluated. It is convenient to introduce a quantity called net efficiency [5] defined as

$$\eta_n = \frac{W}{M-M_o} \tag{2.4}$$

Eqs. (2.3) and (2.4) combine to yield the following expression for net efficiency.

TABLE 1.- BODY CAPACITANCES, BASAL METABOLISM, AND BASAL BLOOD FLOW

SEGMENT	CORE			MUSCLE			FAT			SKIN		
	m_c*	M_o+	m_b#	mc	M_o	m_b	mc	M_o	m_b	mc	M_o	m_b
Head	6.67	44.6	105.6	1.488	1.075	0.594	0.496	0.498	0.264	0.535	0.243	3.7
Trunk	20.9	156.3	510.0	34.0	25.4	14.08	9.42	9.32	5.06	2.69	1.222	4.62
Arm	1.382	1.37	0.759	3.35	2.485	1.364	0.644	0.648	0.352	0.484	0.2185	0.55
Hand	0.1568	0.1733	0.11	0.0738	0.0539	0.055	0.0992	0.0997	0.055	0.134	0.0817	2.2
Leg	4.4	4.44	2.32	10.2	7.37	4.07	1.58	1.593	0.088	1.192	0.538	3.135
Foot	0.2645	0.289	0.165	0.0738	0.0539	0.033	0.148	0.1493	0.088	0.247	0.1077	3.3

* mc - Capacitance, Btu/°F, 4.94 Btu/°F for blood compartment

\+ M_o - Basal metabolism, Btu/hr, Total is 278 Btu/hr

\# m_b - Basal blood flow, lb_m /hr, Total is 682.79 lb_m/hr

TABLE 2.- WORK AND SHIVER DISTRIBUTION IN MUSCLES

SEGMENT	α_{wk}	α_{sh}
Head	0.0	0.023
Trunk	0.3	0.948
Arm	0.04	0.00165
Hand	0.005	0.00115
Leg	0.3	0.0095
Foot	0.005	0.00115
Total	0.0	1.0

$$\eta_n = \frac{\eta_m M}{M-M_o} \tag{2.5}$$

Heat generation expression for muscle layers than assumes the form

$$Q_{gen,m} = M_{o,m} + \alpha_{wk} (M-M_o) (1-\eta_n) + \alpha_{sh} Q_{shiv} \tag{2.6}$$

Regulation of shiver is governed by control mechanisms and is discussed in Section 3.

2.2 Blood Flow

Energy transfer due to blood flow is modeled as blood flow from the blood compartment to all body layers. Blood enters a body layer at a temperature equal to that of the blood compartment and leaves with a temperature equal to the layer temperature. Blood flow heat transfer for core layers is given by

$$Q_{blood,c} = (\dot{m}_b c_b)_c (t_b - t_c) \tag{2.7}$$

where $\dot{m}_b$ and c_b represent blood flow rate and heat capacity, respectively. Blood compartment temperature is denoted by t_b. Similar expressions apply for muscle, fat, and skin layers. Specification of blood flow rate for each layer is now examined.

Since core, fat, and skin layers do not contribute to work or shiver, blood flow to these layers is independent of work and shiver. Furthermore, vasconstriction and vasodilation are controlling mechanisms for regulation of blood flow to skin layers. Recognizing these concepts, blood flow rates for core and fat layers are assumed to remain at their basal values. Thus, for core layers

$$\dot{m}_{b,c} = \dot{m}_{o,b,c} \tag{2.8}$$

with similar expression applicable to fat layers. $\dot{m}_{b,o,c}$ is basal blood flow rate for core layers. Blood flow rate for muscle layers is taken as that attributed to basal c ditions plus that due to heat generation. Stolwijk [2] states that the latter contribution can be approximated by assuming that 1 lb_m of blood supplies sufficient oxygen to produce 1 Btu of energy as heat. Hence, for muscle layers

$$\dot{m}_{b,m} = \dot{m}_{o,b,m} + Q_{gen,m} - M_{o,m} \tag{2.9}$$

where heat generation for muscle layers is given by Eq. (2.6).

Vasoconstruction and vasodilation effects in skin layers are modeled as follows

$$\dot{m}_{b,s} = \frac{\dot{m}_{o,b,s} + \alpha_d S_d}{1 + \alpha_c S_c} \tag{2.10}$$

where α_d and α_c are distribution of vasodilation and vasoconstriction, respectively, throughout skin layers. Recommended values are given in Table 3. S_d and S_c are signals for vasodilation and vasoconstriction, respectively, from the controlling system. Strengths of these signals depend on skin temperature levels compared to desired temperature levels. These signals are further discussed in Section 3.

Recommended basal blood flow rates for each body layer are given in Table 1. Blood heat capacity is taken as 1.0 Btu/lb_m - °F. An important parameter related to heart output is the number of pulses or beats per minute required by the heart to pump a given quantity of blood through the physiological system. Number of pulses per minute is given by

$$B = \frac{5.926}{60} \dot{m}_b \tag{2.10}$$

TABLE 3.- VASOCONSTRICTION, VASODILATION, SWEAT, AREA AND RECEPTOR DISTRIBUTION IN SKIN

SEGMENT	α_c	α_d	α_{sw}	α_s	α_r
Head	0.05	0.132	0.081	0.07	0.0827
Trunk	0.15	0.322	0.482	0.3602	0.587
Arm	0.025	0.0475	0.077	0.06705	0.0411
Hand	0.175	0.115	0.0155	0.025	0.011075
Leg	0.025	0.061	0.1095	0.1587	0.093
Foot	0.175	0.05	0.0175	0.0343	0.01995
Total	1.0	1.0	1.0	1.0	1.0

where the average cardiac stroke volume is incorporated in the constant (5.926) and $\dot{m}_b$ is total blood flow rate from the blood compartment.

2.3 Conduction Between Layers

Since adjacent body layers may exhibit different temperatures, there is conductive transfer between the layers. The general form for conduction may be written as

$$Q_{cond} = R\ (t_1 - t_2) \tag{2.11}$$

where R is conductance between adjacent nodes at temperatures of t_1 and t_2. Various formulations [6] may be employed to evaluate conductance for inhomogeneous materials. The method employed here is that attributed to Stolwijk [7] and resultant conductances are given in Table 4.

2.4 Environment

Energy transfer from skin layers to the environment occurs by conduction, convection, radiation, and evaporation. Some skin areas may be covered by a garment where convection and radiation are negligible and conduction is between skin and garment layers. In some applications, the skin is in contact with LCG cooling tubes and energy transfer to the coolant must be considered. Conduction, convection, and radiation are sometimes referred to as sensible heat transfer, whereas evaporation is called latent heat transfer. Furthermore, as is discussed later, respiratory heat transfer may be broken down into sensible and latent components. In the following presentation, each energy transfer mechanism contributing to heat transfer between man and his environment is examined. In order to keep the discussion general, the surrounding atmosphere is referred to as a gas.

TABLE 4.- CONDUCTIVE RESISTANCES*

SEGMENT	CORE TO MUSCLE	MUSCLE TO FAT	FAT TO SKIN
Head	8.85	12.82	22.60
Trunk	3.09	10.70	28.05
Arm	3.18	8.32	22.80
Hand	4.50	8.32	9.41
Leg	5.75	18.70	35.50
Foot	5.54	13.36	11.93

*R-conductance, Btu/hr - °F

Conductive transfer exists when skin layers are in direct contact with an object and, in most applications, may be neglected. A situation which requires further examination is zero gravity with no gas velocity where convection would be zero. Conduction would then occur from skin layers to the surrounding gas.

Convective transfer from skin layers to surrounding gas is given by Newton's "Law of Cooling" [8]

$$Q_{conv,e} = h_c A_{s,c} (t_s - t_e) \tag{2.12}$$

where h_c is convective coefficient and $A_{s,c}$ is skin area. Total skin area is given by

$$A_a = \sum \alpha_s A_{sc} \tag{2.13}$$

where α_s is fraction of skin area on a particular body segment with values given in Table 3. Surrounding gas temperature is denoted by t_e. Specification of the convective coefficient depends on whether the gas flow was induced by forced or free convection effects and whether the motion is laminar or turbulent. For forced convection, data can be conveniently correlated by using the following expression

$$Nu = C\, Re^i\, Pr^j \tag{2.14}$$

where Nu is Nusselt number or dimensionless convective coefficient, Re is Reynolds number, and Pr is Prandtl number. Values of constants C, i, and j depend on the range of Reynolds numbers of interest. The results of a study by Berenson [9] were used to generate values of 0.60, 1/2, and 1/3 for C, i, and j, respectively. This analysis considered forced convection for man as flow perpendicular to a circular cylinder with a

diameter of 1 ft. Properties of the gas were assumed to be those for air at atmospheric pressure. The resultant expression for the convective coefficient is as follows

$$h_c = 0.0212 \ (V_e P_e)^{1/2} \tag{2.15}$$

where V_e is gas velocity and P_e is total gas pressure. Free convection data can be correlated with an expression of the form

$$Nu = C \ (Gr \ Pr)^i \tag{2.16}$$

where Gr is Grashof number. Values of constants C and i depend on the range of the product of Grashof and Prandtl number of interest. For a man, Berenson [9] considered free convection from a vertical cylinder with length equal to 6 ft and used the theoretical expression derived for Nusselt number [8]. Using his results, the following expression was obtained for atmospheric air

$$h_c = 0.06 \ [P_e^{\ 2} \ G \ (t_s - t_e) \ ]^{1/4} \tag{2.17}$$

where G represents the ratio of gravitational acceleration to the corresponding value on earth. In situations were both forced and free convection effects exist, it is recommended that the maximum value of the convective coefficient calculated from Eqs (2.15) and (2.17) be used.

Radiative transfer is evaluated by assuming that skin areas view surrounding walls that are perfect radiators at a temperature of t_r. Radiant exchange between the body segments is approximated by use of an effective radiative skin area, $A_{s,r}$. Radiative transfer to the environment is then expressed as [8]

$$Q_{rad,e} = h_r \ A_{s,r} \ (t_s - t_r) \tag{2.18}$$

where h_r denotes radiative coefficient evaluated from

$$h_r = \alpha \, \varepsilon_s \, F_{sw} \, (T_s^2 + T_r^2)(T_s + T_r) \tag{2.19}$$

In Eq (2.19), σ is Setefan-Boltzmann constant, ε_s is skin emittance, and F_{sw} is view factor between skin and surrounding walls. Typically assumed values for emittance and view factor are 0.9 and 1.0, respectively. Fanger [12] presents view factors for man to different areas of a room that will soon be incorporated in this analysis. This would allow for including effects of non-uniform surrounding wall temperature distribution on the thermal state of man.

Evaporative transfer consists of water vapor diffusion and evaporation of sweat from the skin surface and may be written as

$$Q_{evap,e} = Q_{diff,e} + Q_{sweat,e} \tag{2.20}$$

Each component of evaporative transfer expression has the following general form

$$Q = \dot{m} \, h_{fg} \tag{2.21}$$

where $\dot{m}$ is mass flow of water for diffusion or evaporation, h_{fg} represents latent heat of vaporization at skin temperature with a typical value of 1040 Btu/lb_m. Diffusion is given by the following expression [4]

$$Q_{diff,e} = 6.66 \, A_{s,c} \, (P_{v,s} - P_{v,dew}) \tag{2.22}$$

where $P_{v,s}$ and $P_{v,dew}$ are water vapor partial pressures evaluated at skin and gas dewpoint temperatures, respectively. Sweat is a mechanism for maintaining body temperature in a warm environment. Based on physiological data reported in the literature, the following expression is used for sweat

heat transfer

$$Q_{sweat,e} = \alpha_{sw} S_s 2^{(t_s - t_{set,s})/4} \quad (2.23)$$

where α_{sw} is sweat distribution over skin areas with values given in Table 3. S_s is the sweat signal from the control mechanism and is discussed in Section 3. Skin set temperature is denoted by $t_{set,s}$ with values given in Section 3. Recent results reported by Stolwijk [2] suggest that the factor of 4 be replaced by 10. When skin areas become completelv wetted with swe t, maximum evaporation of sweat occurs and remaining sweat drips off the body and does not contribute to temperature regulation. For forced evaporation, the results of Berenson were utilized to derive the following expression for maximum evaporative heat transfer:

$$E_{max} = 0.126 A_{s,c} T_e^{1.04} \eta e (V_e/P_e)^{1/2} (P_{v,s} - P_{v,dew}) \quad (2.24)$$

similarly, for maximum free evaporation

$$E_{max} = 1.32 A_{s,c} \frac{T_e}{P_e} \left\{ P_e G [0.005 P_e (t_s - t_e) + 1.02 (P_{v,s} - P_{v,dew})] \right.$$
$$\left. (P_{v,s} - P_{v,dew}) \right\} \quad (2.25)$$

In Eq (2.24), η_e represents the ventilation efficiency of the surroundings. Maximum evaporation rates are calculated from Eqs (2.24) and (2.25) and then compared with evaporative transfer given by Eq (2.20) is used unless it exceeds Eqs 2.24 or Eqs 2.25, in which case, the latter expressions are used for evaporative heat removal rate.

Covered skin areas may exhibit conductive energy transfer to a coolant flowing in tubes that are in contact with the skin (LCG). Furthermore, conduction to the garment and evaporation still exist for these skin areas.

Heat transfer to the LCG is estimated by evaluating an average temperature of skin areas covered by cooling tubes from the expression

$$\bar{t}_{s,g} = \frac{\sum \alpha_s \; t_s}{\sum \alpha_s} \tag{2.26}$$

where summation extends over skin areas covered by the LCG. Typically head, hands, and feet skin areas are not covered. Heat transfer from the garment to the coolant is neglected. For a given inlet water temperature $t_{i,w}$, the outlet water temperature is obtained from

$$t_{o,w} = t_{i,w} + [1 - EXP\ (-\frac{UA}{\dot{m}_w\ c_w})](\bar{t}_{s,g} - t_{i,w}) \tag{2.27}$$

Water flow rate and heat capacity are denoted by $\dot{m}_w$ and c_w, respectively. UA represents the LCG overall heat transfer coefficient with a typical value of 43.5 Btu/hr - °F. Heat transfer from the skin to the LCG is given as

$$Q_{LCG} = \alpha_w m_w\ c_w\ (t_{o,w} - t_{i,g}) \tag{2.28}$$

where α_w is percent of water flow assigned to each skin area. Values for coolant flow distribution as used in the program are listed in Table 5.

Conduction from skin to garment is approximated by

$$Q_{cond,s} = A_{s,c}\ \frac{k_g}{L_g}\ (t_s - t_g) \tag{2.29}$$

where k_g and L_g represent garment thermal conductivity and thickness, respectively. The factor of $L_g/(0.88\ k_g)$ is called the Clo value. Convective transfer from the garment is evaluated with skin temperature replaced by garment temperature in Eq. (2.12) and associated expressions for convective coefficient. Similarly, radiative transfer is evaluated

with skin temperature replaced by garment temperature in Eqs (2.18) and (2.19). A garment modifies convective and radiative areas appearing in Eqs (2.12) and (2.18), respectively. Fanger [4] recommends that the nude skin areas be multiplied by factors that account for changes in surface areas when a garment covers the skin. These adjustments in surface areas were incorporated in the program. Diffusion and maximum evaporation rates for covered skin areas are calculated from Eqs. (2.22) and (2.24) as well as (2.25), respectively, with skin temperature and water vapor partial pressure replaced by corresponding values evaluated at garment temperature. The expression for sweat remains unchanged and no condensation is assumed to occur within the garment. Using the garment energy balance, Eq (1.6) and appropriate expressions for conductive, convective, and radiative transfer terms, garment temperature is given as

$$t_g = \frac{h_r\, t_r + h_c\, t_e + (A_{c,s}\, k_g / L_g)\, t_s}{h_r + h_c + (A_{c,s}\, k_g / L_g)} \tag{2.30}$$

Average garment temperature is evaluated from

$$\bar{t}_g = \sum \alpha_g\, t_g \tag{2.31}$$

where α_g represents distribution of garment area for various body segments with values given in Table 5.

Respiratory heat transfer takes place within the respiratory tract and is associated with a change in temperature and water vapor content between inspired and expired gas. Sensible or dry respiratory heat transfer refers to the former heat transfer mechanism and latent or wet respiratory heat transfer to the latter mechanism. Total dry respiratory heat transfer evaluated from physiological measurements is expressed as

$$Q_{resp,d} = \dot{m}_{resp}\, c_e\, (\bar{t}_{resp} - t_e) \tag{2.32}$$

TABLE 5.- COOLANT FLOW AND GARMENT AREA DISTRIBUTION

SEGMENT	α_w	α_g
Head	0.0	0.0
Trunk	0.44	0.3317
Arm	0.085	0.104
Hand	0.0	0.0
Leg	0.195	0.23015
Foot	0.0	0.0
Total	1.0	1.0

and total wet respiratory heat transfer is

$$Q_{resp,w} = \dot{m}_{resp} \left(P_{v,\ t\ resp} - 0.8\ P_{v,dew}\right) \frac{\bar{M}_w}{M_g} \frac{h_{fg}}{P_g} \tag{2.33}$$

Pulmonary mass flow rate is denoted by $\dot{m}_{resp}$ and is evaluated from

$$\dot{m}_{resp} = \frac{0.0418\ (144)\ P_e M}{\bar{R}_o T_e} \tag{2.34}$$

, which incorporates the affect of metabolic rate upon respiratory minute volume. In Eq. (2.32), c_e is gas heat capacity. $\bar{t}_{resp}$ represents the average respiratory tract temperature and is determined from

$$\bar{t}_{resp} = \sum \alpha_{resp}\ t \tag{2.35}$$

where α_{resp} represents distribution of respiratory heat transfer to the various body layers in contact with the respiratory tract with values given in Table 6. The value of t is the corresponding layer temperature. Respiratory heat transfer for these body layers is given as

$$Q_{resp} = \alpha_{resp} \left(Q_{resp,d} + Q_{resp,\ w}\right) \tag{2.36}$$

It should be noted that all constants appropriate to the gas mixture are for oxygen. Fanger [4] reported similar expressions as Eqs (2.32) to (2.34), however, all properties were for air. Appropriate expressions for other gas mixtures are also included in the model.

An important parameter indicative of the thermal response of man is heat storage relative to a desired temperature level. This quantity is expressed as

$$Q_{stor} = \sum m\ c\ (t - t_{set}) \tag{2.37}$$

TABLE 6.- RESPIRATORY TRACT HEAT TRANSFER DISTRIBUTION

SEGMENT	LAYER	α_{RESP}
Head	Core	0.3855
	Muscle	0.0860
	Fat	0.0287
Trunk	Core	0.238
	Muscle	0.2615
Total		1.0

where summation extends over all body layers plus the blood compartment. Values of capacitances defined as the product of mass and heat capacity are given in Table 1 for each body layer and for the blood compartment. Another parameter of interest is storage rate or rate of change of internal energy. This factor is given as

$$U = M - W + Q_{shiv} - (Q_{cond,s} + Q_{conv,e} + Q_{rad,e} + Q_{evap,e} \quad (2.38)$$

$$+Q_{LCG} - (Q_{resp,d} + Q_{resp,w})$$

where summation is for all skin surface areas.

3. CONTROLLING SYSTEM

The body has three primary control mechanisms for physiological temperature regulation:

a. Shivering

b. Blood flow rate through vasoconstriction and vasodilation

c. Sweating

A detailed discussion of each controller is given by Stolwijk [2] and only functions employed in the program are discussed here

The control signal for each mechanism is thought to originate from the difference between the body layer temperature and a desired temperature called a set temperature. Set temperatures represent temperatures observed when there is a minimum of thermal regulation with values for each body layer as well as for the blood compartment given in Table 7. The temperature difference is referred to as an error or test signal and is expressed for each body layer as

$$D = t - t_{set} \quad (3.1)$$

TABLE 7.- SET TEMPERATURES*

SEGMENT	CORE	MUSCLE	FAT	SKIN
Head	98.6	97.6	97.0	96.6
Trunk	98.8	98.3	95.9	94.4
Arm	96.1	95.1	94.1	93.7
Hand	95.9	95.7	95.6	95.5
Leg	97.6	96.5	95.1	94.5
Foot	95.8	95.5	95.7	94.5

t_{set}, °F

Recent experimental results reported by Stolwijk [2] indicate that this signal might also be dependent upon the rate of change of temperature. When the signal is negative, the body senses cold, and shiver as well as vasoconstriction mechanisms are activated. Positive values of this signal indicate warm sensation, and sweating as well as vasodilation mechanisms are initiated. These observations for each body layer are expressed as follows.

Positive D

$$W_a = D, \; C_o = 0 \tag{3.2}$$

Negative D

$$W_a = 0, \; C_o = -D \tag{3.3}$$

where W_a and C_o are warm and cold signals, respectively. Warm and cold sensations are thought to be initiated by thermoreceptors located in skin layers. The strength of the signals is a function of a number of skin receptors. The total or integrated warm and cold signals for only the skin layers are evaluated as follows:

$$W_t = \sum \alpha_r \, W_a \tag{3.4}$$

and

$$C_t = \sum \alpha_r \, C_o \tag{3.5}$$

where α_r is the distribution of skin receptors throughout the various skin areas. Recommended values of skin receptor distribution are given in Table 3.

The control signals for sweating, blood flow, and shivering are expressed as the sum of three terms. Each term represents the product of a control coefficient and a quantity related to warm or cold sensation. The control signals are written as

Sweating

$$= C_{sw} W_{a,c} + S_{sw} W_t + P_{sw} W_{a,c} W_t \quad (3.6)$$

Vasodilation

$$= C_{di} W_{a,c} + S_{di} W_t + P_{di} W_{a,c} W_t \quad (3.7)$$

Vasoconstriction

$$= C_{co} C_{o,c} + S_{co} C_t + P_{co} C_{o,c} C_t \quad (3.8)$$

Shivering

$$Q_{shiv} = C_{sh} C_{o,c} + S_{sh} C_t + P_{sh} C_{o,c} C_t \quad (3.9)$$

where $W_{a,c}$ and $C_{a,c}$ represent warm and cold signals for the head core, respectively. Typical values for the control coefficients are given in Table 8. Negative values of the above signals should be set to zero.

TABLE 8.- CONTROL COEFFICIENTS

REGULATION	C*	S+	F#
Sweating	884.0	0.0	73.4
Vasodilation	183.5	0.0	0.0
Vasocon-striction	5.55	5.55	0.0
Shivering	0.0	0.0	12.22

* Values in column are C_{cw}, C_{di}, C_{co}, and C_{sh}

\+ Values in column are S_{sw}, S_{di}, S_{co}, and S_{sh}

\# Values in column are P_{sw}, P_{di}, P_{co}, and P_{sh}

REFERENCES

1. Morgan, L. W., Collett, G., and Cook, D. W., Jr., "41 Node Transient Metabolic Man Program," Lockheed Electronics Company, LEC/672-23-030031 (1970).

2. Stolwijk, J. A. J., "A Mathematical Model of Physiological Temperature Regulation in Man," NASA CR-1855 (1971).

3. Sibbons, J. L. H., "Coefficients of Evaporative Heat Transfer," Physiological and Behavioral Temperature Regulation, Charles C. Thomas, Springfield, Ill., pp. 108-138 (1970).

4. Fanger, P. O., "Predicted and Measured Heat Losses and Thermal Comfort Conditions for Human Beings." Thermal Problems in Biotechnology, ASME, pp. 61-81 (1968).

5. Ruch, T. C. and Patton, H. D., Physiology and Biophysics, Saunders (1965).

6. Trezek, G. J. and Witwer, J. G., "Finite-Difference Methods for Inhomogeneous Regions," J. Heat Transfer, 94C, pp. 321-323 (1972).

7. Stolwijk, J. A. J. and Hardy, J. D., "Temperature Regulation in Man - A Theoretical Study," Pfugers Arch., 291, pp. 129-162 (1966).

8. Kreith, F., Principles of Heat Transfer, 3rd. ed., Intext Press, New York (1973).

9. Lin, S. H. and Berenson, P. J., "Study of the Thermal Processes for Man-in-Space," NASA CR-216 (1965).

10. Berenson, P. J. and Robertson, W. G., "Temperature," Bioastronautics Data Book, NASA-SP-3006, pp. 65-148 (1973).

11. Rapp, G. M., "Convective Mass Transfer and the Coefficient of Evaporative Heat Loss from Human Skin," Physiological and Behavioral Temperature Regulation, Charles C. Thomas, Springfield, Ill., pp. 55-80 (1970).

12. Fanger, P. O., Thermal Comfort, McGraw-Hill, New York (1970).

13. Eckert, E. R. G. and Drake, R. M. Jr., Heat and Mass Transfer, McGraw-Hill, New York (1959).

14. Reid, R. C. and Sherwood, T. K., The Properties of Gases and Liquids, McGraw-Hill, New York (1966).

15. Cunningham, D. J., "An Evaluation of Heat Transfer Through the Skin in the Human Extremity," Physiological and Behavioral Temperature Regulation, Charles C. Thomas, Springfield, Ill., pp. 302-315 (1970).

SAMPLE RUNS FROM THE MATHEMATICAL MCDEL

SHOWING INPUT/OUTPUR FORMAT

INITIAL CONDITIONS

SHIRTSLEEVES POOL

MAN

METABOLIC ACTIVITY LEVEL, BTU/HR----------	389.000
USEFUL WORK EFFICIENCY, PERCENT----------	.000
CONVECTIVE AREA OF MAN, SQ FT----------	15.500
RADIATIVE AREA OF MAN, SQ FT----------	11.500

CABIN

VIEW FACTOR----------	1.000
CABIN ATMOSPHERIC TEMPERATURE, F----------	74.000
EFFECTIVE WALL TEMPERATURE, F----------	74.000
FREESTREAM VELOCITY, FT/MIN----------	30.000
CABIN PRESSURE, PSIA----------	14.700
DEW POINT TEMPERATURE IN CABIN, F----------	55.000
G ----------	1.000

UNDERGARMENT

THICKNESS OF UNDERGARMENT----------	.028
CONDUCTIVITY OF UNDERGARMENT----------	.046
EMISSIVITY OF UNDERGARMENT----------	.970

24.0	85.91	.059	98.02	81.95	83.56	56.66	-6.99	1076.31	60.79	231.61	-327.91	.00	-91.96
LCG INLET WATER TEMPERATURE			48.000	DF									
LCG OUTLET WATER TEMPERATURE			57.396	DF									
LCG WATER TEMPERATURE DIFFERENCE			9.396	DF									
SUIT INLET DEWPOINT TEMPERATURE			50.000	DF									
SUIT INLET DRY BULB TEMPERATURE			85.000	DF									
OXYGEN USED			.064	LBS									
CO2 PRODUCED			.375	LBS									
TOTAL WATER EVAPORATION FROM BODY			.137	LBS									
FEED WATER USED			.000	LBS									
METABOLIC RATE			1000.000	BTU/HR									
WATER FLOW RATE			120.000	LB/HR									
PARTIAL PRESSURE OF CO2 IN HELMET			3.208139	MM HG									
26.0	85.81	.059	98.90	81.75	83.43	54.89	-6.69	1084.22	57.20	227.80	-312.02	.00	-82.62
LCG INLET WATER TEMPERATURE			48.000	DF									
LCG OUTLET WATER TEMPERATURE			57.260	DF									
LCG WATER TEMPERATURE DIFFERENCE			9.260	DF									
SUIT INLET DEWPOINT TEMPERATURE			50.000	DF									
SUIT INLET DRY BULB TEMPERATURE			85.000	DF									
OXYGEN USED			.072	LBS									
CO2 PRODUCED			.081	LBS									
TOTAL WATER EVAPORATION FROM BODY			.197	LBS									
FEED WATER USED			.000	LBS									
METABOLIC RATE			1000.000	BTU/HR									
WATER FLOW RATE			120.000	LB/HR									
PARTIAL PRESSURE OF CO2 IN HELMET			3.209081	MM HG									
28.0	85.70	.059	98.88	81.56	83.29	54.21	-4.93	1073.80	53.87	224.27	-297.97	.00	-72.76
LCG INLET WATER TEMPERATURE			48.000	DF									
LCG OUTLET WATER TEMPERATURE			57.181	DF									
LCG WATER TEMPERATURE DIFFERENCE			9.181	DF									
SUIT INLET DEWPOINT TEMPERATURE			50.000	DF									
SUIT INLET DRY BULB TEMPERATURE			85.000	DF									
OXYGEN USED			.078	LBS									
CO2 PRODUCED			.087	LBS									
TOTAL WATER EVAPORATION FROM BODY			.164	LBS									
FEED WATER USED			.000	LBS									
METABOLIC RATE			1000.000	BTU/HR									
WATER FLOW RATE			120.000	LB/HR									
PARTIAL PRESSURE OF CO2 IN HELMET			3.209957	MM HG									
30.0	85.60	.053	98.86	81.39	83.19	53.60	-4.32	1063.10	50.80	221.02	-284.12	.00	-62.44
LCG INLET WATER TEMPERATURE			48.000	DF									
LCG OUTLET WATER TEMPERATURE			57.106	DF									
LCG WATER TEMPERATURE DIFFERENCE			9.106	DF									
SUIT INLET DEWPOINT TEMPERATURE			50.000	DF									
SUIT INLET DRY BULB TEMPERATURE			85.000	DF									
OXYGEN USED			.083	LBS									
CO2 PRODUCED			.094	LBS									
TOTAL WATER EVAPORATION FROM BODY			.166	LBS									
FEED WATER USED			.000	LBS									
METABOLIC RATE			1000.000	BTU/HR									
WATER FLOW RATE			120.000	LB/HR									
PARTIAL PRESSURE OF CO2 IN HELMET			3.210765	MM HG									
32.0	85.49	.053	98.84	81.22	82.99	53.07	-3.79	1053.80	47.89	217.92	-271.73	.00	-51.70
LCG INLET WATER TEMPERATURE			48.000	DF									

TIME, MIN	TEMP WATER OUT, F	TEMP HEAD CORE F	AV TEMP SKIN, F	TEMP UNDER-GARMENT F	Q SENSIBLE BTU/HR	Q EVAP BTU/HR	Q LATENT BTU/HR	HEAT STORAGE RATE BTU/HR	SHIVER RATE BTU/HR	TOTAL HEAT STORAGE BTU	CABIN TEMP F	DEW POINT F	CO2 PRESS MM HG
•0	•00	98•60	•00	•00	•00	•00	•00	•00	•00	•00	74•00	55•00	•21
• DIVIDE CHECK AT 027242													
• DIVIDE CHECK AT 027242													
• DIVIDE CHECK AT 027242													
• DIVIDE CHECK AT 027242													
• DIVIDE CHECK AT 027242													
• DIVIDE CHECK AT 027242													
• DIVIDE CHECK AT 027242													
• DIVIDE CHECK AT 027242													
• DIVIDE CHECK AT 027242													
2•0	•00	98•55	94•33	85•53	264•90	•00	84•27	43•53	•21	1•29	74•00	55•00	•21
4•0	•00	98•49	94•15	85•47	261•51	•00	83•86	44•92	•78	2•71	74•00	55•00	•21
6•0	•00	98•43	94•03	85•44	59•48	•00	83•55	47•47	1•50	4•24	74•00	55•00	•21
8•0	•00	98•39	93•95	85•43	257•97	•00	83•32	49•93	2•22	5•86	74•00	55•00	•21
10•0	•00	98•35	93•89	85•42	256•80	•00	83•14	51•96	2•70	7•56	74•00	55•00	•21
12•0	•00	98•32	93•84	85•43	255•87	•00	83•00	53•64	3•50	9•32	74•00	55•00	•21
14•0	•00	98•30	93•81	85•43	255•10	•00	82•88	55•01	3•99	11•14	74•00	55•00	•21
16•0	•00	98•29	93•78	85•44	254•46	-•00	82•79	56•13	4•38	12•99	74•00	55•00	•21
18•0	•00	98•29	93•75	85•45	253•92	•00	82•72	57•03	4•67	14•87	74•00	55•00	•21
20•0	•00	98•29	93•73	85•46	253•47	•00	82•66	57•74	4•86	16•78	74•00	55•00	•21
22•0	•00	98•29	93•72	85•47	253•08	-•00	82•62	58•30	4•99	18•72	74•00	55•00	•21
24•0	•00	98•30	93•71	85•48	252•75	-•00	82•58	58•72	5•05	20•66	74•00	55•00	•21
26•0	•00	98•31	93•69	85•49	252•47	•00	82•56	59•02	5•05	22•63	74•00	55•00	•21
28•0	•00	98•32	93•69	85•49	252•23	•00	82•54	59•22	4•99	24•59	74•00	55•00	•21
30•0	•00	98•33	93•68	85•50	252•04	•00	82•53	59•32	4•89	26•57	74•00	55•00	•21
32•0	•00	98•34	93•67	85•51	251•88	•00	82•53	59•34	4•78	28•54	74•00	55•00	•21
34•0	•00	98•34	93•67	85•52	251•75	•00	82•52	59•29	4•56	30•52	74•00	55•00	•21
36•0	•00	98•37	93•67	85•53	251•65	-•00	82•53	59•18	4•35	32•49	74•00	55•00	•21
38•0	•00	98•39	93•67	85•53	251•57	-•00	82•54	59•01	4•12	34•46	74•00	55•00	•21
40•0	•00	98•40	93•67	85•54	251•52	•00	82•55	58•79	3•87	36•42	74•00	55•00	•21
42•0	•00	98•42	93•67	85•55	251•50	•00	82•56	58•53	3•60	38•37	74•00	55•00	•21
44•0	•00	98•43	93•67	85•56	251•49	•00	82•58	58•24	3•31	40•32	74•00	55•00	•21
46•0	•00	98•45	93•67	85•56	251•50	•00	82•60	57•91	3•01	42•25	74•00	55•00	•21
48•0	•00	98•47	93•68	85•57	251•53	•00	82•62	57•56	2•71	44•17	74•00	55•00	•21
50•0	•00	98•48	93•68	85•58	251•57	•00	82•64	57•18	2•40	46•08	74•00	55•00	•21
52•0	•00	98•50	93•69	85•58	251•63	-•00	82•67	56•79	2•08	47•98	74•00	55•00	•21
54•0	•00	98•51	93•69	85•59	251•70	•00	82•69	56•37	1•76	49•87	74•00	55•00	•21
56•0	•00	98•53	93•70	85•60	251•78	•00	82•72	55•94	1•44	51•73	74•00	55•00	•21
58•0	•00	98•55	93•71	85•60	251•87	•00	82•75	55•50	1•12	53•59	74•00	55•00	•21
60•0	•00	98•56	93•71	85•61	251•97	•00	82•78	55•05	•80	55•43	74•00	55•00	•21
62•0	•00	98•58	93•72	85•62	252•08	•00	82•81	54•59	•48	57•26	74•00	55•00	•21

REPRODUCIBILITY OF THE
ORIGINAL PAGE IS POOR

| | | |

TIME, MIN	TEMP RATED OUT. F	TEMP HEAD CORE F	AV TEMP SKIN, F	TEMP UNDERGARMENT F	Q SENSIBLE BTU/HR	Q EVAP BTU/HR	Q LATENT BTU/HR	HEAT STORAGE RATE BTU/HR	SHIVER RATE BTU/HR	TOTAL HEAT STORAGE Btu	CABIN TEMP F	DEW POINT F	CO2 PRESS MM HG
[illegible]	.00	98.67	93.57	85.50	260.95	50.94	133.78	0.26	.00	70.04	74.00	55.00	.21
[illegible]	.00	98.67	93.56	85.50	259.89	51.54	134.38	3.73	.00	70.19	74.00	55.00	.21
[illegible]	.00	98.67	93.56	85.50	259.92	52.08	134.91	3.[illegible]	.00	70.30	74.00	55.00	.21
104.0	.00	98.67	93.55	85.49	260.76	52.64	135.39	2.[illegible]	.00	70.40	74.00	55.00	.21
108.0	.00	98.67	93.55	85.49	260.78	53.00	135.82	2.[illegible]	.00	70.49	74.00	55.00	.21
112.0	.00	98.67	93.54	85.49	260.65	53.39	136.20	2.[illegible]	.00	70.56	74.00	55.00	.21
116.0	.00	98.67	93.[illegible]	85.48	260.59	53.74	136.55	1.[illegible]	.00	70.63	74.00	55.00	.21
120.0	.00	98.67	93.[illegible]	85.48	260.54	54.06	136.86	1.40	.00	70.68	74.00	55.00	.21
124.0	.00	98.67	93.[illegible]	85.48	260.49	54.34	137.15	1.36	.00	70.73	74.00	55.00	.21
128.0	.00	98.67	93.[illegible]	85.48	260.44	54.60	137.40	1.16	.00	70.77	74.00	55.00	.21
132.0	.00	98.67	93.[illegible]	85.47	260.40	54.83	137.63	.97	.00	70.80	74.00	55.00	.21
136.0	.00	98.67	93.[illegible]	85.47	260.35	55.05	137.84	.81	.00	70.83	74.00	55.00	.21
140.0	.00	98.67	93.51	85.47	260.31	55.24	138.03	.66	.00	70.85	74.00	55.00	.21
144.0	.00	98.67	93.51	85.47	260.27	55.41	138.19	.53	.00	70.87	74.00	55.00	.21
148.0	.00	98.68	93.51	85.47	260.23	55.57	138.35	.41	.00	70.89	74.00	55.00	.21
152.0	.00	98.68	93.50	85.46	260.20	55.71	138.49	.31	.00	70.90	74.00	55.00	.21
156.0	.00	98.69	93.50	85.[illegible]	260.16	55.85	138.62	.22	.00	70.91	74.00	55.00	.21
160.0	.00	98.69	93.50	85.46	260.13	55.96	138.73	.14	.00	70.91	74.00	55.00	.21
164.0	.00	98.69	93.49	85.46	260.10	56.08	138.84	.06	.00	70.91	74.00	55.00	.21
168.0	.00	98.69	93.49	85.46	260.07	56.17	138.93	-.00	.00	70.91	74.00	55.00	.21
172.0	.00	98.69	93.49	85.46	260.04	56.26	139.02	-.06	.00	70.91	74.00	55.00	.21
176.0	.00	98.69	93.49	85.46	260.01	56.35	139.11	-.12	.00	70.91	74.00	55.00	.21
180.0	.00	98.69	93.48	85.46	259.99	56.41	139.17	-.15	.00	70.90	74.00	55.00	.21
184.0	.00	98.68	93.49	85.45	259.96	56.48	139.23	-.19	.00	70.90	74.00	55.00	.21
188.0	.00	98.68	93.[illegible]	85.45	259.94	56.54	139.29	-.24	.00	70.89	74.00	55.00	.21
192.0	.00	98.68	93.48	85.45	259.92	56.60	139.35	-.27	.00	70.88	74.00	55.00	.21
196.0	.00	98.68	93.48	85.45	259.90	56.64	139.39	-.29	.00	70.87	74.00	55.00	.21
200.0	.00	98.68	93.48	85.45	259.88	56.69	139.43	-.31	.00	70.86	74.00	55.00	.21
204.0	.00	98.68	93.47	85.[illegible]	259.86	56.73	139.47	-.33	.00	70.85	74.00	55.00	.21
208.0	.00	98.68	93.47	85.45	259.84	56.77	139.51	-.35	.00	70.84	74.00	55.00	.21
208.7	.00	98.68	93.47	85.[illegible]	259.83	56.78	139.52	-.36	.00	70.83	74.00	55.00	.21

IMPOSED CONDITIONS
EVA MODE

MAN	
METABOLIC ACTIVITY LEVEL, BTU/HR	1000.000
USEFUL WORK EFFICIENCY, PERCENT	.000
CONVECTIVE AREA OF MAN, SQ FT	19.500
RADIATIVE AREA OF MAN, SQ FT	19.500
CABIN	
CABIN ATMOSPHERIC TEMPERATURE, F	75.000
EFFECTIVE WALL TEMPERATURE, F	75.000
FREESTREAM VELOCITY, FT/MIN	15.000
CABIN PRESSURE, PSIA	.000
UNDERGARMENT	
THICKNESS OF UNDERGARMENT	.014
CONDUCTIVITY OF UNDERGARMENT	.094
EMISSIVITY OF UNDERGARMENT	.900
LIQUID COOLED GARMENT	
LIQUID COOLANT FLOW RATE, LB/HR	.000
TEMPERATURE OF LIQUID COOLANT IN	40.000
SPECIFIC HEAT OF COOLANT	1.000
UA OF LIQUID COOLED GARMENT	43.500
PRESSURE SUIT	
Q ABSORBED PER SQ FT	
TORSO	95.900
RIGHT SLEEVE	95.900
LEFT SLEEVE	95.900
RIGHT LEG	95.900
LEFT LEG	95.900
RIGHT GLOVE	95.900
LEFT GLOVE	95.900
RIGHT BOOT	95.900
LEFT BOOT	95.900
HELMET	190.000
SUIT LOOP FLOW, LBM	14.000
SPECIFIC HEAT OF GAS	.220
TEMPERATURE OF GAS INTO SUIT	50.000
DEWPOINT TEMPERATURE AT SUIT INLET, F	50.000
TOTAL SUIT PRESSURE, PSIA IT INLET, F	3.850
PARTIAL PRESSURE OF OXYGEN IN SUIT, PSIA	3.850
RADIATIVE AREA OF SUIT COMPONENTS, SQ FT	
TORSO	7.340
EACH SLEEVE	2.320
EACH LEG	5.070
HELMET	1.470
EACH GLOVE	.420
EACH BOOT	.960
CONVECTIVE AREA OF SUIT COMPONENTS, SQ FT	
TORSO	9.220
EACH SLEEVE	2.910
EACH LEG	6.380
HELMET	1.850

EACH GLOVE	.770
EACH BOOT	1.190
WEIGHT OF SUIT COMPONENTS	
TORSO	15.600
EACH SLEEVE	4.490
EACH LEG	13.020
HELMET	2.750
EACH GLOVE	1.220
EACH BOOT	1.950
SPECIFIC HEAT OF SUIT COMPONENTS	
TORSO	.220
EACH SLEEVE	.220
EACH LEG	.220
HELMET	.300
EACH GLOVE	.220
EACH BOOT	.220
THICKNESS OF SUIT COMPONENTS, FT	
TORSO	.008
EACH SLEEVE	.008
EACH LEG	.008
HELMET	.021
EACH GLOVE	.004
EACH BOOT	.008
CONDUCTIVITY OF SUIT COMPONENTS	
TORSO	.000
EACH SLEEVE	.000
EACH LEG	.000
HELMET	.027
EACH GLOVE	.000
EACH BOOT	.000
EMISSIVITY OF INNER SURFACE OF SUIT COMPONENTS	
TORSO	.900
EACH SLEEVE	.900
EACH LEG	.900
HELMET	.900
EACH GLOVE	.900
EACH BOOT	.900
EMISSIVITY OF OUTER SURFACE OF SUIT COMPONENTS	
TORSO	.910
EACH SLEEVE	.910
EACH LEG	.910
HELMET	.620
EACH GLOVE	.910
EACH BOOT	.910
PURGE FLOW	YES
MAXIMUM RUN TIME, MINUTES	180.000

TIME, MIN	TEMP GAS OUTLET F	S/M AT SUIT OUTLET	TEMP HEAD	TEMP CORE F	AV TEMP SKIN F	AV TEMP INSIDE SUIT F	AV TEMP OUTSIDE SUIT F	Q THRU SUIT BTU/HR	Q SENSIBLE TOTAL BTU/HR	QEVAP BTU/HR	Q LATENT BTU/HR	HEAT STORAGE RATE BTU/HR	SHIVER RATE BTU/HR	TOTAL HEAT STORAGE BTU
.0	85.36	.029	98.04		93.27	81.78	79.26	134.76	242.48	330.81	96.60	.00	.00	163.69
LCG INLET WATER TEMPERATURE						98.000	OF							
LCG OUTLET WATER TEMPERATURE						.000	OF							
LCG WATER TEMPERATURE DIFFERENCE						-98.000	OF							
SUIT INLET DEWPOINT TEMPERATURE						50.000	OF							
SUIT INLET DRY BULB TEMPERATURE						50.000	OF							
OXYGEN USED						.000	LBS							
CO2 PRODUCED						.000	LBS							
TOTAL WATER EVAPORATION FROM BODY						.000	LBS							
FEED WATER USED						.000	LBS							
METABOLIC RATE						1000.000	BTU/HR							
WATER FLOW RATE						.000	LB/HR							
PARTIAL PRESSURE OF CO2 IN HELMET						1.323518	MM HG							
2.0	87.02	.067	99.08		88.82	82.56	75.59	-3.	1548.22	160.35	336.29	-884.51	.00	127.73
LCG INLET WATER TEMPERATURE						98.000	OF							
LCG OUTLET WATER TEMPERATURE						59.978	OF							
LCG WATER TEMPERATURE DIFFERENCE						11.978	OF							
SUIT INLET DEWPOINT TEMPERATURE						50.000	OF							
SUIT INLET DRY BULB TEMPERATURE						85.000	OF							
OXYGEN USED						.006	LBS							
CO2 PRODUCED						.006	LBS							
TOTAL WATER EVAPORATION FROM BODY						.015	LBS							
FEED WATER USED						.000	LBS							
METABOLIC RATE						1000.000	BTU/HR							
WATER FLOW RATE						120.000	LB/HR							
PARTIAL PRESSURE OF CO2 IN HELMET						3.182216	MM HG							
4.0	86.80	.063	99.10		88.71	83.05	72.33	-9.38	1411.89	127.32	302.94	-716.77	.00	101.91
LCG INLET WATER TEMPERATURE						98.000	OF							
LCG OUTLET WATER TEMPERATURE						59.191	OF							
LCG WATER TEMPERATURE DIFFERENCE						11.191	OF							
SUIT INLET DEWPOINT TEMPERATURE						50.000	OF							
SUIT INLET DRY BULB TEMPERATURE						85.000	OF							
OXYGEN USED						.011	LBS							
CO2 PRODUCED						.013	LBS							
TOTAL WATER EVAPORATION FROM BODY						.028	LBS							
FEED WATER USED						.000	LBS							
METABOLIC RATE						1000.000	BTU/HR							
WATER FLOW RATE						120.000	LB/HR							
PARTIAL PRESSURE OF CO2 IN HELMET						3.190519	MM HG							
6.0	86.68	.061	99.11		88.45	83.38	69.53	-12.11	1329.53	119.11	280.53	-618.06	.00	79.39
LCG INLET WATER TEMPERATURE						98.000	OF							
LCG OUTLET WATER TEMPERATURE						56.722	OF							
LCG WATER TEMPERATURE DIFFERENCE						10.722	OF							
SUIT INLET DEWPOINT TEMPERATURE						50.000	OF							
SUIT INLET DRY BULB TEMPERATURE						85.000	OF							
OXYGEN USED						.017	LBS							
CO2 PRODUCED						.019	LBS							
TOTAL WATER EVAPORATION FROM BODY						.040	LBS							
FEED WATER USED						.000	LBS							

METABOLIC RATE ---------- 1000.000 BTU/HR
WATER FLOW RATE ---------- 120.000 LB/HR
PARTIAL PRESSURE OF CO2 IN HELMET 3.194089 MM HG

8.0	86.60	.060	99.11	84.63	83.61	67.07	-13.19	1279.96	106.43	279.01	-953.96	.00	59.88

LCG INLET WATER TEMPERATURE ------- 48.000 DF
LCG OUTLET WATER TEMPERATURE ------ 58.413 DF
LCG WATER TEMPERATURE DIFFERENCE -- 10.413 DF
SUIT INLET DEWPOINT TEMPERATURE --- 50.000 DF
SUIT INLET DRY BULB TEMPERATURE --- 85.000 DF
OXYGEN USED ---------- .022 LBS
CO2 PRODUCED ---------- .026 LBS
TOTAL WATER EVAPORATION FROM BODY - .052 LBS
FEED WATER USED ---------- .000 LBS
METABOLIC RATE ---------- 1000.000 BTU/HR
WATER FLOW RATE ---------- 120.000 LB/HR
PARTIAL PRESSURE OF CO2 IN HELMET 3.194932 MM HG

10.0	86.53	.059	99.10	84.05	83.75	64.92	-13.13	1235.69	98.05	271.03	-906.71	.00	92.29

LCG INLET WATER TEMPERATURE ------- 48.000 DF
LCG OUTLET WATER TEMPERATURE ------ 58.192 DF
LCG WATER TEMPERATURE DIFFERENCE -- 10.192 DF
SUIT INLET DEWPOINT TEMPERATURE --- 50.000 DF
SUIT INLET DRY BULB TEMPERATURE --- 85.000 DF
OXYGEN USED ---------- .028 LBS
CO2 PRODUCED ---------- .031 LBS
TOTAL WATER EVAPORATION FROM BODY - .063 LBS
FEED WATER USED ---------- .000 LBS
METABOLIC RATE ---------- 1000.000 BTU/HR
WATER FLOW RATE ---------- 120.000 LB/HR
PARTIAL PRESSURE OF CO2 IN HELMET 3.198398 MM HG

12.0	86.46	.058	99.08	83.81	83.84	63.04	-12.52	1205.33	91.23	263.75	-869.08	.00	86.81

LCG INLET WATER TEMPERATURE ------- 48.000 DF
LCG OUTLET WATER TEMPERATURE ------ 58.019 DF
LCG WATER TEMPERATURE DIFFERENCE -- 10.019 DF
SUIT INLET DEWPOINT TEMPERATURE --- 50.000 DF
SUIT INLET DRY BULB TEMPERATURE --- 85.000 DF
OXYGEN USED ---------- .033 LBS
CO2 PRODUCED ---------- .037 LBS
TOTAL WATER EVAPORATION FROM BODY - .074 LBS
FEED WATER USED ---------- .000 LBS
METABOLIC RATE ---------- 1000.000 BTU/HR
WATER FLOW RATE ---------- 120.000 LB/HR
PARTIAL PRESSURE OF CO2 IN HELMET 3.200101 MM HG

14.0	86.38	.057	99.05	83.29	83.87	61.38	-11.58	1180.48	84.87	257.09	-837.52	.00	80.93

LCG INLET WATER TEMPERATURE ------- 48.000 DF
LCG OUTLET WATER TEMPERATURE ------ 57.876 DF
LCG WATER TEMPERATURE DIFFERENCE -- 9.876 DF
SUIT INLET DEWPOINT TEMPERATURE --- 50.000 DF
SUIT INLET DRY BULB TEMPERATURE --- 85.000 DF
OXYGEN USED ---------- .039 LBS
CO2 PRODUCED ---------- .044 LBS
TOTAL WATER EVAPORATION FROM BODY - .083 LBS
FEED WATER USED ---------- .000 LBS
METABOLIC RATE ---------- 1000.000 BTU/HR
WATER FLOW RATE ---------- 120.000 LB/HR

PARTIAL PRESSURE OF CO2 IN HELMET 3.201848 MM HG

16.0	86.30	.056	99.02	82.93	83.87	59.93	-10.50	1159.32	79.09	286.69	-410.21	.00	-3.19
LCG INLET WATER TEMPERATURE			48.000	OF								
LCG OUTLET WATER TEMPERATURE			57.799	OF								
LCG WATER TEMPERATURE DIFFERENCE			9.799	OF								
SUIT INLET DEWPOINT TEMPERATURE			50.000	OF								
SUIT INLET DRY BULB TEMPERATURE			85.000	OF								
OXYGEN USED			.044	LBS								
CO2 PRODUCED			.050	LBS								
TOTAL WATER EVAPORATION FROM BODY			.096	LBS								
FEED WATER USED			.000	LBS								
METABOLIC RATE			1000.000	BTU/HR								
WATER FLOW RATE			120.000	LB/HR								
PARTIAL PRESSURE OF CO2 IN HELMET			3.203366	MM HG								
18.0	86.21	.054	99.00	82.65	83.83	58.65	-9.90	1140.81	73.75	296.32	-386.13	.00	-16.99
LCG INLET WATER TEMPERATURE			48.000	OF								
LCG OUTLET WATER TEMPERATURE			57.635	OF								
LCG WATER TEMPERATURE DIFFERENCE			9.635	OF								
SUIT INLET DEWPOINT TEMPERATURE			50.000	OF								
SUIT INLET DRY BULB TEMPERATURE			85.000	OF								
OXYGEN USED			.050	LBS								
CO2 PRODUCED			.054	LBS								
TOTAL WATER EVAPORATION FROM BODY			.104	LBS								
FEED WATER USED			.000	LBS								
METABOLIC RATE			1000.000	BTU/HR								
WATER FLOW RATE			120.000	LB/HR								
PARTIAL PRESSURE OF CO2 IN HELMET			3.204743	MM HG								
20.0	86.12	.055	98.97	82.90	83.76	57.83	-8.33	1129.37	68.99	290.29	-369.66	.00	-28.93
LCG INLET WATER TEMPERATURE			48.000	OF								
LCG OUTLET WATER TEMPERATURE			57.531	OF								
LCG WATER TEMPERATURE DIFFERENCE			9.531	OF								
SUIT INLET DEWPOINT TEMPERATURE			50.000	OF								
SUIT INLET DRY BULB TEMPERATURE			85.000	OF								
OXYGEN USED			.055	LBS								
CO2 PRODUCED			.062	LBS								
TOTAL WATER EVAPORATION FROM BODY			.117	LBS								
FEED WATER USED			.000	LBS								
METABOLIC RATE			1000.000	BTU/HR								
WATER FLOW RATE			120.000	LB/HR								
PARTIAL PRESSURE OF CO2 IN HELMET			3.206988	MM HG								
22.0	86.02	.055	98.94	82.16	83.67	56.59	-7.39	1107.62	64.69	236.79	-345.37	.00	-40.75
LCG INLET WATER TEMPERATURE			48.000	OF								
LCG OUTLET WATER TEMPERATURE			57.435	OF								
LCG WATER TEMPERATURE DIFFERENCE			9.435	OF								
SUIT INLET DEWPOINT TEMPERATURE			50.000	OF								
SUIT INLET DRY BULB TEMPERATURE			85.000	OF								
OXYGEN USED			.061	LBS								
CO2 PRODUCED			.069	LBS								
TOTAL WATER EVAPORATION FROM BODY			.127	LBS								
FEED WATER USED			.000	LBS								
METABOLIC RATE			1000.000	BTU/HR								
WATER FLOW RATE			120.000	LB/HR								
PARTIAL PRESSURE OF CO2 IN HELMET			3.207114	MM HG								

LCG OUTLET WATER TEMPERATURE ------	57.035	OF
LCG WATER TEMPERATURE DIFFERENCE --	9.035	OF
SUIT INLET DEWPOINT TEMPERATURE ---	50.000	OF
SUIT INLET DRY BULB TEMPERATURE ---	85.000	OF
OXYGEN USED ----------	.089	LBS
CO2 PRODUCED ----------	.100	LBS
TOTAL WATER EVAPORATION FROM BODY -	.176	LBS
FEED WATER USED ----------	.000	LBS
METABOLIC RATE ----------	1000.000	BTU/HR
WATER FLOW RATE ----------	120.000	LB/HR
PARTIAL PRESSURE OF CO2 IN HELMET	3.281532	MM HG

34.0 85.38 .052 98.82 81.07 82.83 52.80 -3.34 1045.22 45.04 214.94 -260.16 .00 -100.55

LCG INLET WATER TEMPERATURE -------	48.000	OF
LCG OUTLET WATER TEMPERATURE ------	56.968	OF
LCG WATER TEMPERATURE DIFFERENCE --	9.68	OF
SUIT INLET DEWPOINT TEMPERATURE ---	50.000	OF
SUIT INLET DRY BULB TEMPERATURE ---	85.000	OF
OXYGEN USED ----------	.094	LBS
CO2 PRODUCED ----------	.106	LBS
TOTAL WATER EVAPORATION FROM BODY -	.186	LBS
FEED WATER USED ----------	.000	LBS
METABOLIC RATE ----------	1000.000	BTU/HR
WATER FLOW RATE ----------	120.000	LB/HR
PARTIAL PRESSURE OF CO2 IN HELMET	3.212272	MM HG

APPENDIX C

PHYSIOLOGICAL RELATIONSHIPS

AND EQUATIONS

SYMBOLS AND ABBREVIATIONS USED IN APPENDIX C

A_s = skin surface area

CAL-EVAP = calculation of total evaporative heat loss from body heat balance equation

CAL-RAD = calculation of net environmental heat exchange from PLSS heat balance

C_1, C_2 = constants for respiratory minute volume

C_p = heat capacity of surrounding gas

C_{pw} = heat capacity of water

CO_2 = carbon dioxide proudction rate, gms/minute

D = Diffusion coefficient for water vapor to gas

EVAP = Evaporation heat loss

ELECT = Heat input to PLSS Feedwater from PLSS electronic (LCG pump + fan)

FEED H_2O = Total PLSS Feedwater used

h_{fg} = latent heat of vaporization of water

LiOH = Heat input to PLSS Feedwater from PLSS Lithium Hydroxide Cartridge

$\dot{m}_g$ = gas flowrate

$\dot{m}_r$ = respiratory ventilation rate or minute volume

$\dot{m}_w$ = LCG water flowrate

M.R. = Metabolic Rate, watts

O_2 = Oxygen consumption rate, gms/minute

P = Pressure

QD = Evaporative heat loss from the skin by passive mass diffusion

QRE = Evaporative heat loss through the respiratory tract

QRC = Convective heat loss through the respiratory tract

QR = Total heat loss through the respiratory tract

R = gas constant

RQ = respiratory quotient

T_a = temperature of inspired gas or surrounding gas

T_i = temperature of body compartment i

$\bar{T}_r$ = temperature of the respiratory tract (also = expired gas temperature)

$\bar{T}_s$ = skin temperature (mean)

T_{wi} = LCG water inlet temperature

T_{wo} = LCG water outlet temperature

UA = LCG heat transfer coefficient

$\dot{V}$ = volumetric flowrate

$Wt.$ = Body weight loss or collected water loss

W_a = Specific humidity of inspired gas

$\bar{W}_r$ = Specific humidity of expired gas (saturated at $\bar{T}_r$)

W_s = Specific humidity of water vapor at the skin surface (saturated at $\bar{T}_s$)

α_i = weighting fact or for body compartment

ρ = gas density

ADDITIONAL EQUATIONS UTILIZED IN RESULTS

(1) R.Q. $= CO_2/O_2$

(2) O_2 $= 25.825\ (M.R.)\left\{.0001708 - \left(\frac{R.Q. - .707}{.293}\right)(.0000123)\right\}$

See Figure C1

(3) EVAP $= Wt/h_{fg}$ (assumes that all water is evaporated)

(4) QRS $= \dot{m}_r\ h_{fg}\ (\bar{T}_r - T_a)$

(5) QRG $= \dot{m}_r h_{fg}\ (\bar{w}_r - w_a)$

(6) QR $=$ QRS + QRE See Figure C5

(7) QD $= A_s D\ (W_s - W_a)$ See Figure C6

(8) $\dot{m}_r$ $= C_1\ (M.R.) + C_2$ See Figure C4

(9) $\bar{T}_r$ $= \sum_i \alpha_i\ T_i$ See Table 6, Appendix B

(10) UA $= \dot{m}_w\ C_{pw}\ \ln\ \frac{(T_{wi} - \bar{T}_s)}{T_{wo} - \bar{T}_s}$

(11) ρ $= P/_{RT}$

(12) $\dot{m}_g$ $= \dot{v}$

(13) CAL-EVAP $=$ M.R. - RAD - LCG-CONV - HEAT STORAGE RATE. See Equation 1, Section 2

(14) CAL-RAD $=$ (Feed H_2O) ω_{fg} - M.R. - LiOH - ELECT See Figure 2-3

SAMPLE CALCULATION OF TOTAL EVAPORATIVE HEAT LOSS AND ACTIVE SWEAT RATE

Data from Test Series A - Sequence 5 (see Table D1.)

1. Weight loss = 194 gms/hr

2. Insensible carbon loss

   CO_2 produced = 2.68 gms/minute

   O_2 consumed = 1.95 gms/minute

   Carbon loss = .73 gms/minute x 60 = 44 gms/hr.

3. Total weight loss due to evaporation

   = 194 - 44 = 150 gms/hr

4. Total evaporative heat loss = (weig loss) x (latent heat of vaporization of water)

   = 150 gms/hr x .671 watt-hr/gm = 101 watts

5. Evaporative heat loss by respiration = 54 watts (see Equation 5, Appendix C)

6. Evaporative heat loss by skin diffusion = 15 watts (see Equation 7, Appendix C)

7. Evaporative heat loss by active sweat alone

   = 101 - 54 - 15 = 32 watts (see Equation 8, Section 2)

8. Active sweat rate = 32 watts/.671 $\frac{\text{watt-hr}}{\text{gm}}$ (see Equation 9, Section 2)

   = 48 gms/hr

*Assumes that all perspiration is evaporated.

Figure C-1. Oxygen consumption vs metabolic rate.

Legend

—— 1. RQ = .707

—— 2. RQ = .82

—— 3. RQ = .90

—— 4. RQ = 1.0

Equation of curve

$$\text{Oxygen consumption rate (grams/min)} = 25.825 \times \text{metabolic rate (watts)} \times \left[.0001708 - \left(\frac{RQ - .707}{.293}\right) \times .0000123\right]$$

(173)

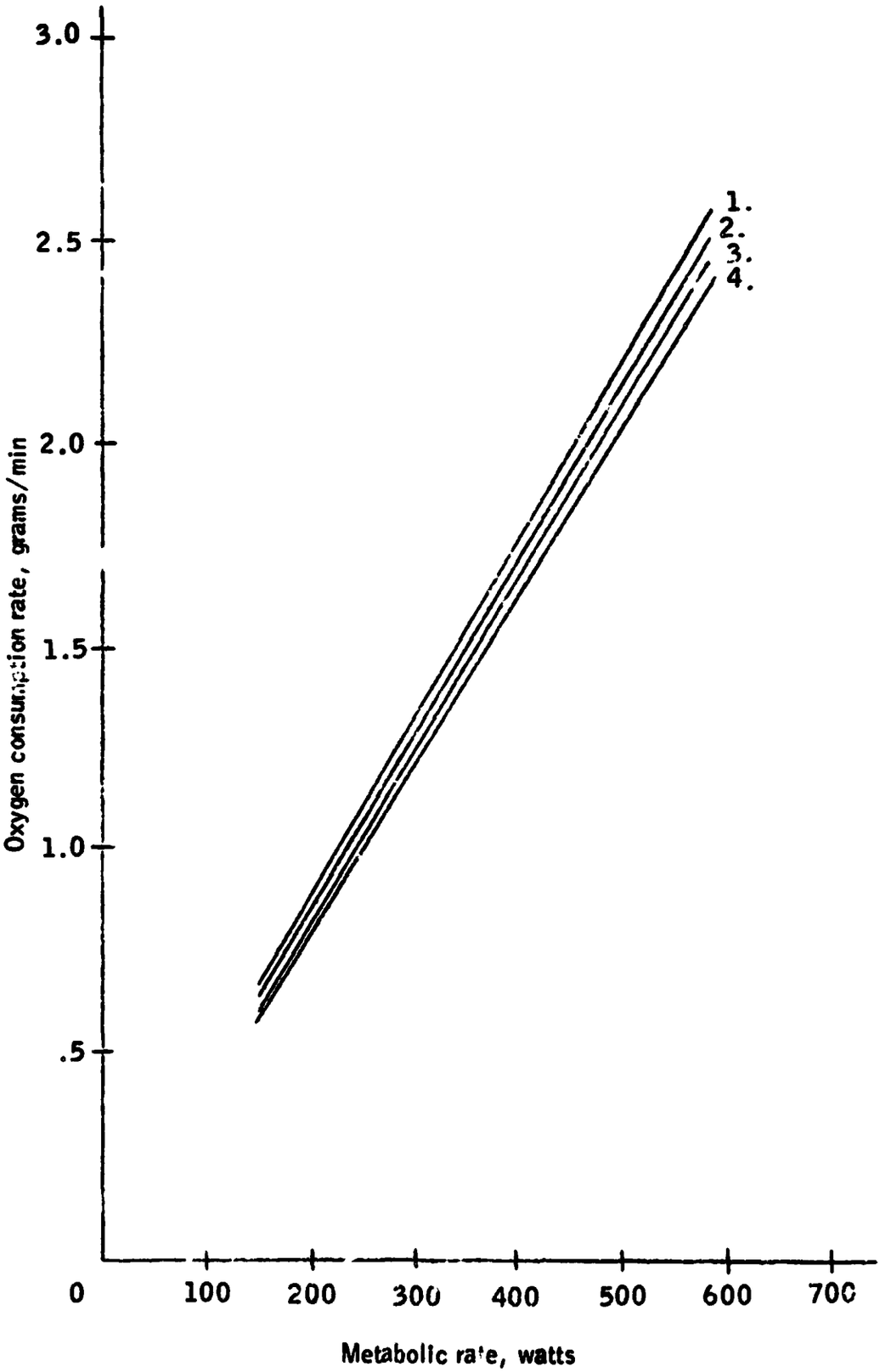
3.0
2.5
2.0
1.5
1.0
.5
0
100
200
300
400
500
600
700
1.
2.
3.
4.
Oxygen consumption rate, grams/min
Metabolic rate, watts

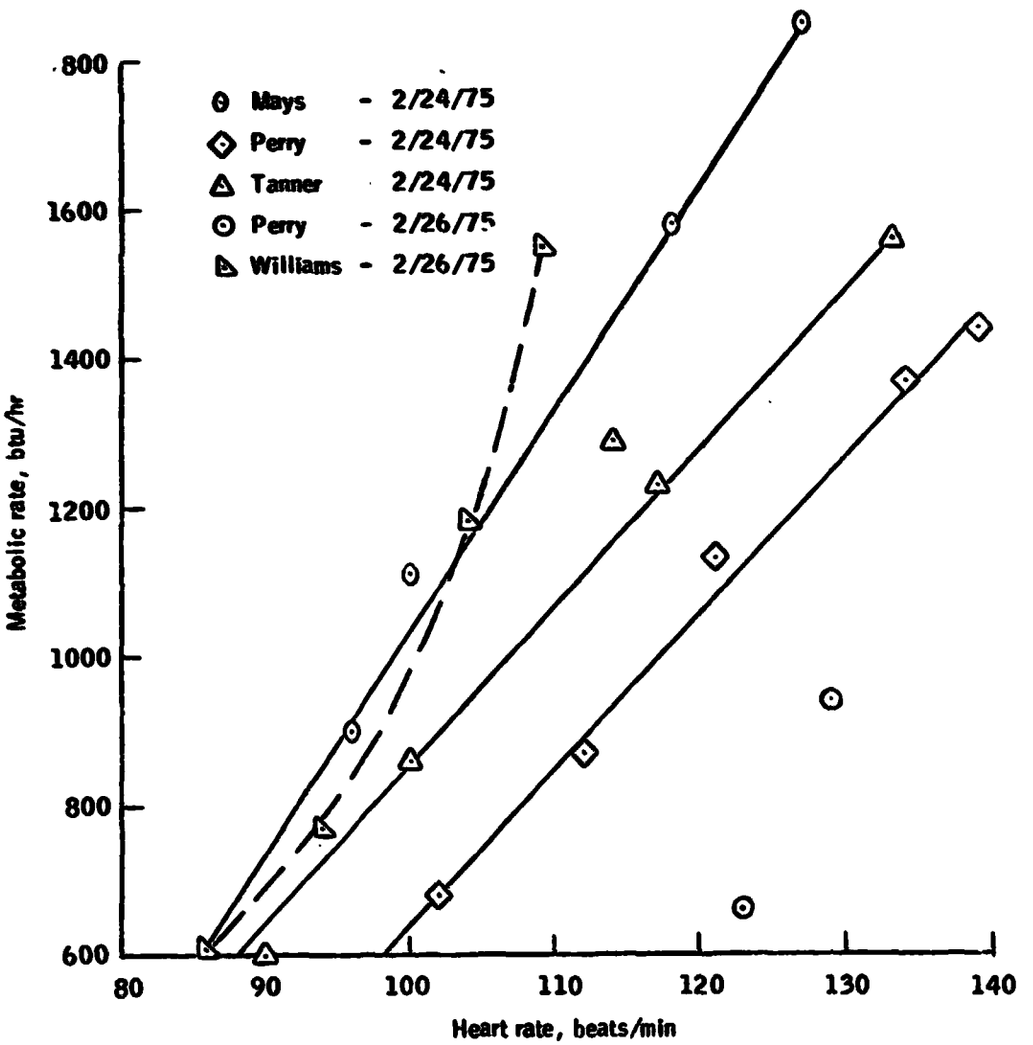
Mays - 2/24/75
Perry - 2/24/75
Tanner 2/24/75
Perry - 2/26/75
Williams - 2/26/75
Metabolic rate, btu/hr
800
1600
1400
1200
1000
800
600
80
90
100
110
120
130
140
Heart rate, beats/min

Figure C-2.

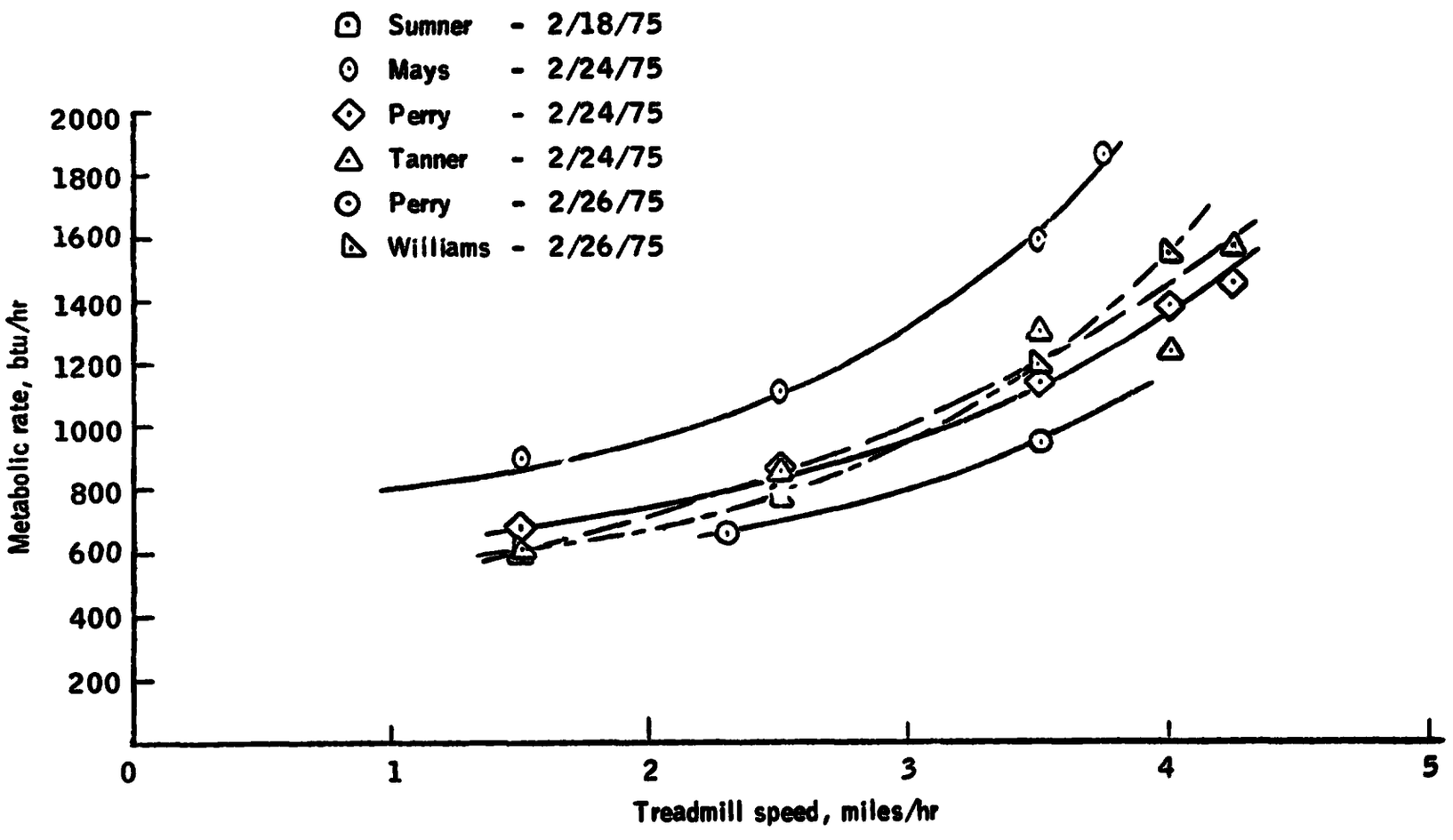
Sumner - 2/18/75
Mays - 2/24/75
Perry - 2/24/75
Tanner - 2/24/75
Perry - 2/26/75
Williams - 2/26/75
Metabolic rate, btu/hr
2000
1800
1600
1400
1200
1000
800
600
400
200
0
1
2
3
4
5
Treadmill speed, miles/hr

Figure C-3.

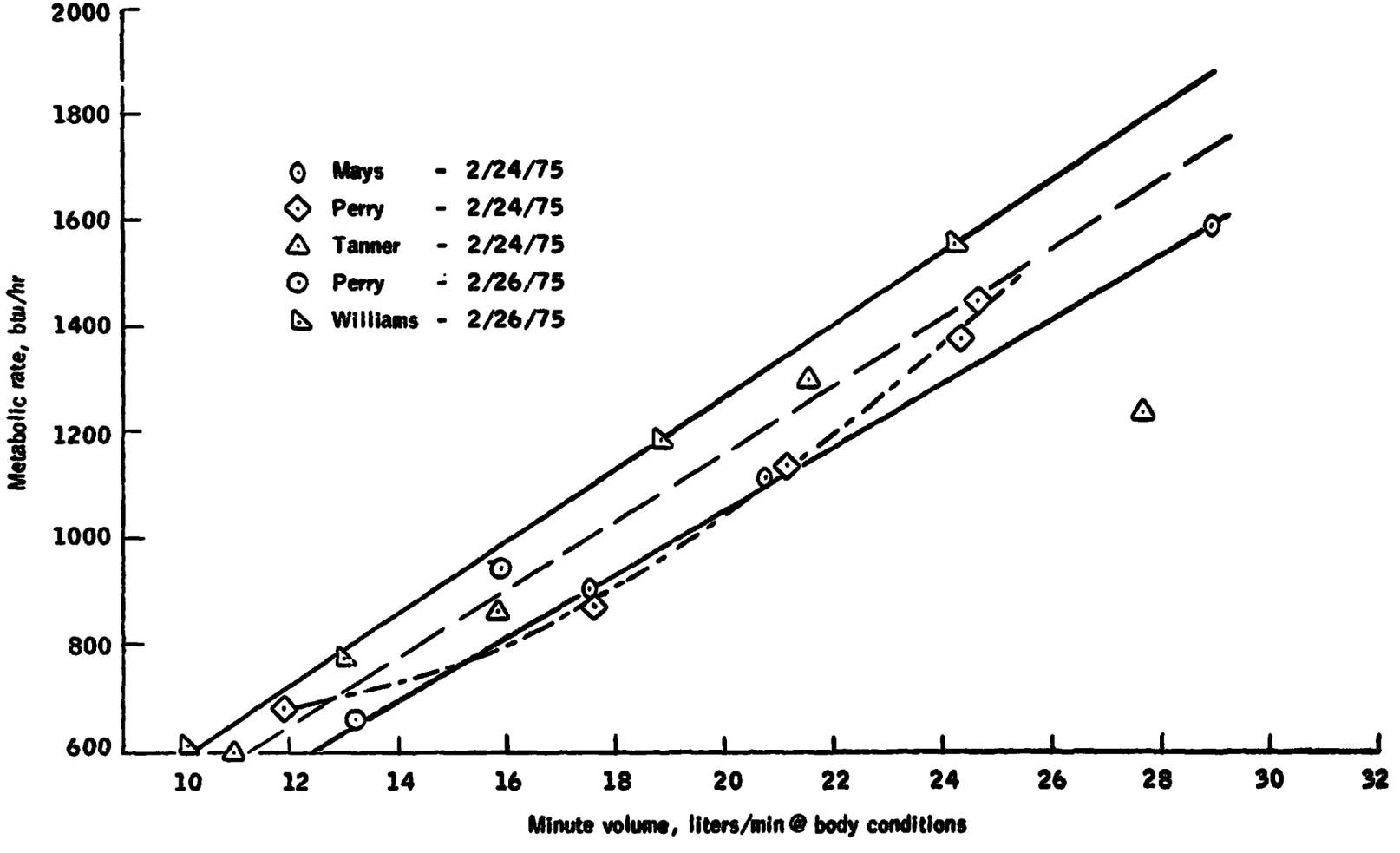
Mays - 2/24/75
Perry - 2/24/75
Tanner - 2/24/75
Perry - 2/26/75
Williams - 2/26/75
Metabolic rate, btu/hr
2000
1800
1600
1400
1200
1000
800
600
10
12
14
16
18
20
22
24
26
28
30
32
Minute volume, liters/min @ body conditions

Figure C-4.

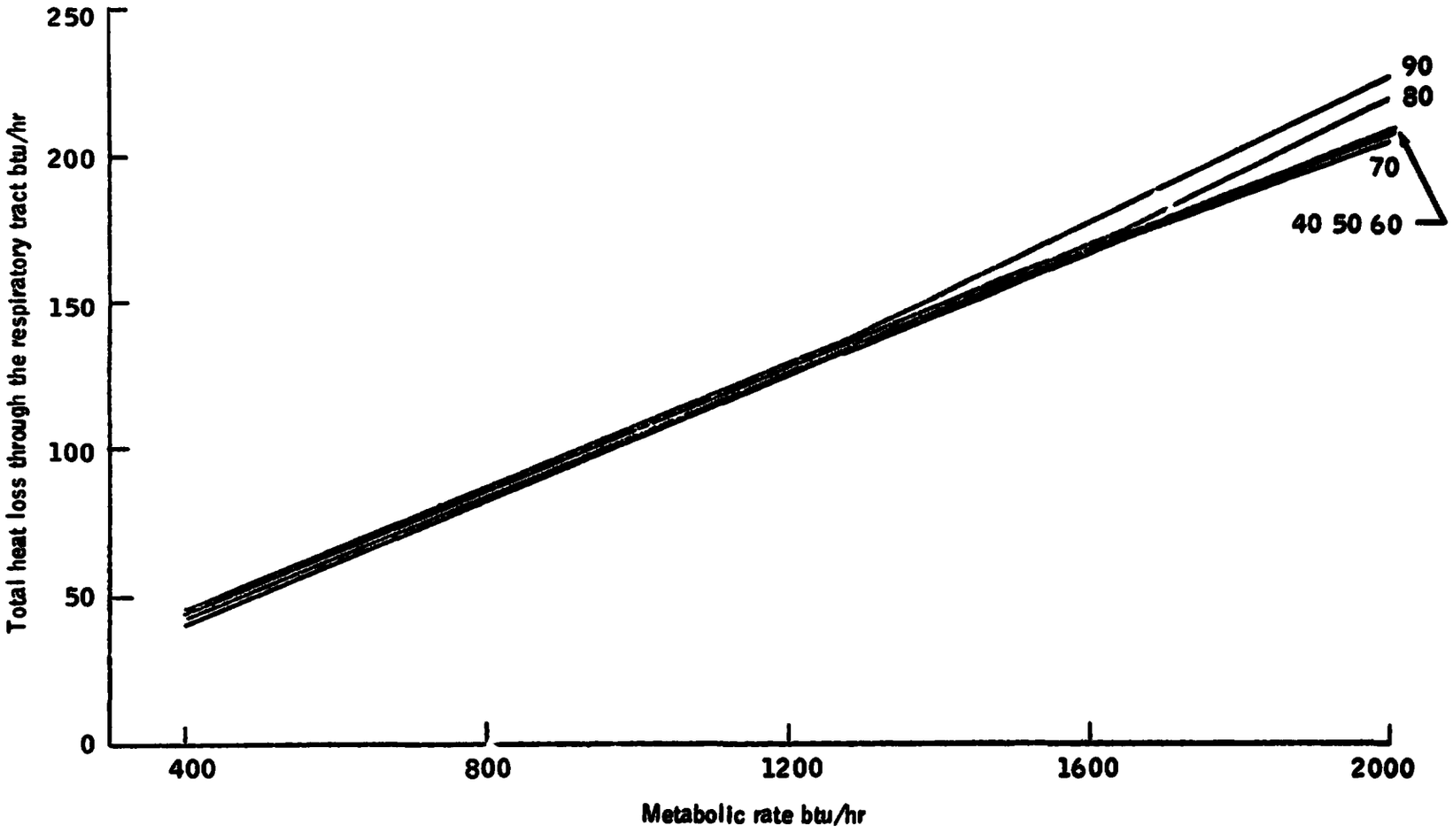

Figure C-5. Sample plot from equation 6, Appendix C for air temp = 80°F dewpoint = 50°F.

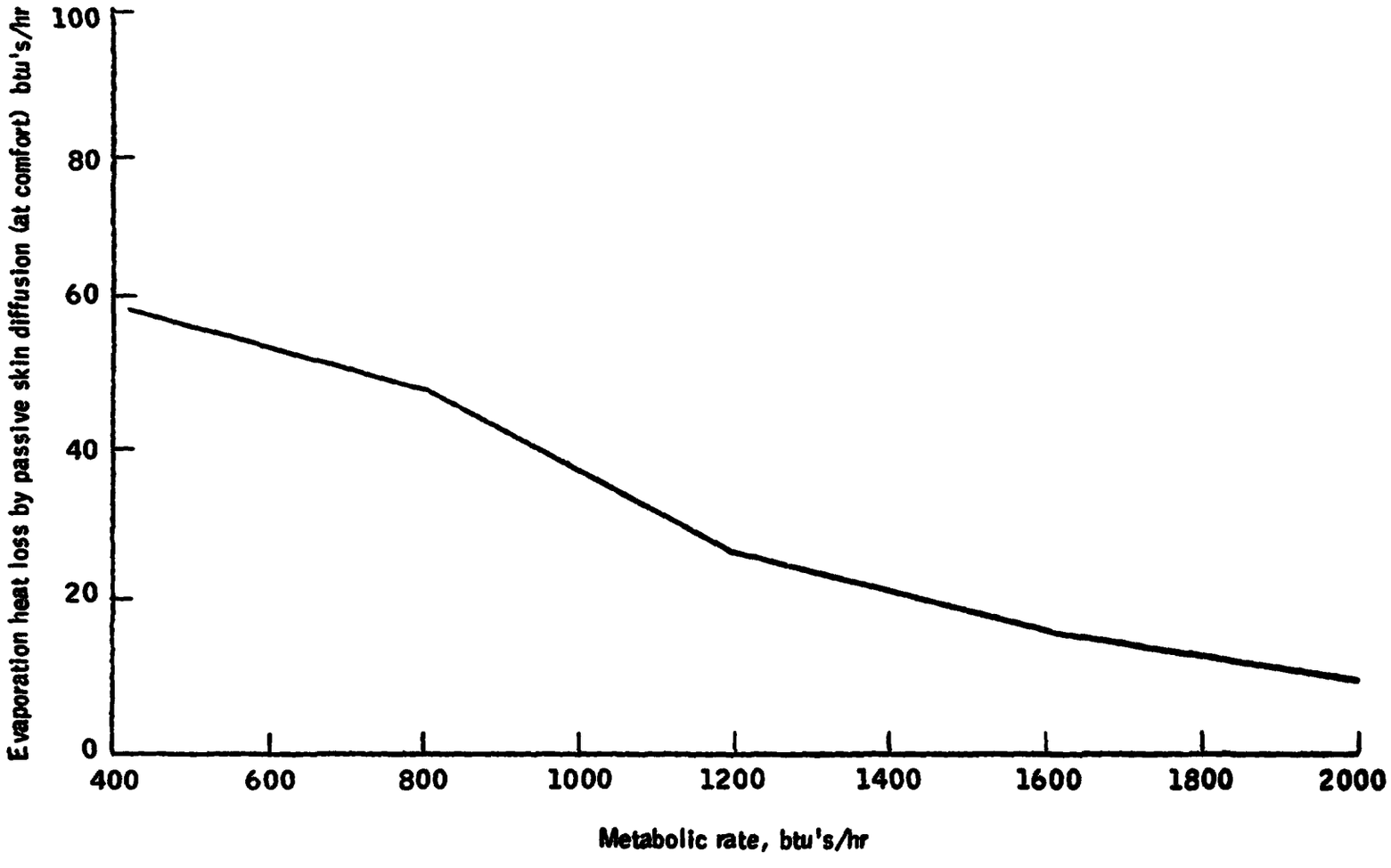

Figure C-6. Sample plot from equation 7, Appendix C for comfort conditions with air temp = 80 °F, dewpoint = 50 °F.

APPENDIX D

RAW DATA

TABLE D1.- SERIES A - RAW DATA

TEST SUBJECT	1/T.W.	2/J.W.	3/R.H.	4/R.H.	5/M.C.	6/J.W.	7/F.D.	8/R.H.	9/R.H.	10/R.H.	11/J.W.
Date	2/11/65	8/3/65	7/27/65	2/2/65	2/4/65	2/16/64	1/15/65	7/29/65	1/21/65	8/4/65	1/13/65
Duration, Minutes	100	120	120	150	180	150	180	120	180	120	120
CO_2 collected, gms/minute[1]	.59	1.15	1.33	1.68	2.68	3.17	1.73	2.15	2.42	2.68	3.33
O_2 collected, gms/minute[1]	.45	.93	1.02	1.42	1.95	2.43	1.53	1.72	1.85	2.01	2.58
RQ	.95	.9	.95	.86	1.0	.95	.82	.91	.95	.97	.94
Metabolic rate, watts[2]	117	228	254	342	433	589	360	413	452	491	618
Weight loss, gms/hr[3]	52	79	96	150	194	287	109	129	164	232	261
Mean skin temperature °C	28	30.1	30.1	29.75	30	32.5	24	28.5	27.5	28	27.2
Rectal temperature	36.75	37.4	36.8	38	38.25	38.5	37.4	37.8	37.25	38.3	38.5
Total body heat storage, watt-hrs	-77	-46	-96	+5	+32	+62	-118	-23	-57	-7	+14
Ambient pressure, torr	760	760	760	760	760	760	760	760	760	760	760
Ambient temperature, °C	25	25	26	24	24	25	26	27	25	24	25
Ambient dewpoint, °C	14	14	13	14	13	13	15	13	12	13	16
LCG water flowrate, liters/hr	109	109	109	109	109	109	109	109	109	109	109
LCG inlet water temperature, °C	16	16	16	16	16	16	7	7	7	7	7
LCG outlet water temperature, °C	17.4	17.5	17.7	17.7	17.9	18.6	9.8	10.0	10.0	10.2	10.8

1. Average of measurements made at 5 minute intervals over the last 60 minutes of each test. 2. See eqn. 2 and Figure C1, Appendix C. 3. Measured over the last 60 minutes of each test. NOTE: All data are steady state values, as measured at the conclusion of each test sequence, unless specified otherwise.

TABLE D2.- SERIES B - RAW DATA

TEST/ SUBJECT / DATE	L/J.W. 1/26/74					2/J.W. 1/26/70							3/C.L. 1/26/70					4/C.L. 8/28/70			
Steady-State Test Condition	A	B	C	D	E	A	B	C	D	E	F	G	A	B	C	D	E	A	B	C	D
Metabolic rate, watts	336	467	435	410	293	528	293	556	308	440	351	497	440	322	296	346	483	278	276	308	467
Duration-Time to reach steady state, minutes	30	→																			
Suit gas (O_2) flowrate, liters/min. pure oxygen	170	→																			
Suit pressure, torr	195																				
Ambient (chamber) pressure, torr	0	→																			
Sui gas inlet temp., °C	20																				
Suit gas outlet temp., °C	23	23	20	20	19	18	17	22	19	23	23	22	16	18	19	25	23	14	19	24	21
Suit gas inlet dewpoint, °C	4	→																			
Suit gas outlet dewpoint, °C	22	22	19	18	16	17	16	21	19	23	23	22	12	14	18	22	23	12	18	22	18
LCG water flow-rate, liters/hr	109	→																			
LCG inlet water temp., °C	25	18	12	12	18	7	13	13	19	19	25	18	7	13	18	24	19	18	23	26	18
LCG outlet water temp., °C	27	21	16	15	20	11	15	17	21	22	23	21	11	16	20	27	21	20	25	27	21

NOTE: All data are equilibrium values, as measured at the conclusion of each test sequence.

TABLE D3.- TEST SERIES C - RAW DATA

TEST/SUBJECT DATE	1/J.B. 1/18/69	2/J.B. 1/18/69	3/J.B. 1/18/69	4/J.B. 1/18/69	5/J.B. 1/18/69	6/J.B. 1/18/69	7/J.B. 1/18/69	8/J.B. 1/18/69	9/J.M. 1/21/69	10/J.M. 1/21/69
Duration, minutes	30	30	30	30	30	30	30	30	30	30
Metabolic rate, watts	352	352	352	352	469	469	469	469	586	586
Mean skin temperature, °C	33.5	30.7	30.5	30.2	33.3	31.1	30.3	29.9	30.9	31.4
Tympanic temperature, °C	36.8	36.75	36.7	36.75	37.3	37.25	37.3	37.25	37.5	37.5
Total body heat storage, watt-hrs.	48	27	30	5	70	59	59	30	65	70
Suit gas (O_2) flowrate, liters/minute	331	331	331	331	331	331	331	331	331	331
Suit pressure, torr	259	259	259	259	259	259	259	259	259	259
Ambient pressure, torr	259	259	259	259	259	259	259	259	259	259
Suit gas inlet temperature, °C	25.1	22.2	22.8	22.9	25.4	27.2	24.7	26.2	23.4	22.9
Suit gas outlet temperature, °C	29.5	25.7	25.7	25.6	30.3	27.9	26.4	26.5	26.8	26.6
Suitgas outlet dewpoint, °C	7.2	8.1	7.2	7.2	7.5	7.2	7.2	7.2	7.2	7.2
Suit gas outlet dewpoint, °C	24.4	18.3	17.8	16.1	28.9	23.9	22.2	21.7	24.2	22.8
LCG water flowrate, liters/hr	0	27	55	82	0	27	55	82	55	82
LCG inlet water temperature, °C	-	18.8	18.9	18.3	-	19.4	18.8	18.4	17.3	16.8
LCG outlet water temperature, °C	-	22.3	21.4	20.6	-	23.8	22.2	21.1	22.2	20.2

NOTE: All data are equilibrium values, as measured at the conclusion of each test sequence.

TABLE D4.- SERIES D - RAW DATA

TEST/SUBJECT	1/D.S.	2/F.H.	3/J.M.	4/J.M.	5/J.M.	6/J.M.	7/K.M.
Date	3/30/71	4/2/71	2/22/69	2/26/69	3/7/69	2/20/69	2/24/69
Duration, hrs	6.98	6.87	3.17	3.43	3.93	3.62	3.52
CO_2 collected, gms	525.0	478.9	303.1	330.1	255.1	298.7	369.2
O_2 produced, gms	523.5	476.5	334.9	349.3	282.8	329.7	408.0
RQ	1.003	1.005	.905	.945	.902	.906	.905
Total metabolic heat produced, watt-hrs	2133	1943	1330	1402	1122	1310	1620
Weight loss, kgms	1.816	1.362	1.021	1.475	1.249	1.589	1.362
Evaporated water collected, kgm	1.125	.842	.549	.558	.400	.749	.833
Unevaporated water, kgms	.691	.520	.472	.917	.849	.840	.529
Average mean skin temperature, °C	30	30	30	28	30	32	29
Average core temperature, °C	37.9	36.8	37.4	37.3	36.4	37.2	36.7
Body heat storage at end of test, watts-hrs	35	-30.5	-22.5	19	-30	9.7	53
Average heat storage during test, watt-hrs	33	1.5	12	13	52	28.5	-1
Suit gas (O_2) flowrate, liters/hr pure oxygen	170	170	170	170	170	170	170
Suit pressure, torr	195	195	195	195	195	195	195
Ambient (chamber	0	0	0	0	0	0	
Ambient (chamber) pressure, torr	0	0	0	0	0	0	0
Average suit gas inlet temperature, °C	30	24	22	22	22	22	22
Average suit gas outlet temperature, °C	31.2	23.6	26	28	22	25	29
LCG water flowrate, liters/hr	109	109	109	109	109	109	109

TABLE D4.- CONTINUED

TEST SUBJECT	1/D.S.	2/F.H.	3/J.M.	4/J.M.	5/J.M.	6/J.M.	7/K.M.
Average LCG inlet water temperature selected, °C	19	22	13.5	11.5	17	23	13
Average LCG outlet water temperature, °C	21.5	23	16	15	19	24.5	17
Average NET environmental heat exchange, watts	+79 into suit	-67 out of suit	+65 into suit	+117 into suit	-35 out of suit	-72 out of suit	+37 into suit

TABLE D5.

TEST NUMBER	TOTAL WATER COLLECTED IN PLSS DUE TO EVAPORATIVE HEAT LOSS, KGMS	TOTAL WATER COLLECTED AS PREDICTED BY INTEGRATION OF EVAPORATIVE HEAT LOSS RATE, KGMS
1	1.125	1.88
2	.842	1.67
3	.549	.70
4	.558	.584
5	.40	.331
6	.749	.736
7	.833	.731

TABLE D. STEADY-STATE (EQUILIBRIUM) DATA FOR TEST SERIES D

TEST	1							2			3			4			5		6			7	
Time during test of steady-state occurrence, hours	.83	1.49	4.0	6.0	.50-2.17	3.92-5.17	4.5-5.17	4.83	1.5-2.5	3.83-5.17	2.23	0-1.17	1.92-2.75	.83	1.5	1.58-2.83	1.25	2.5-3.5	1.25	2.16	1.25-2.75	1.5	1.75-2.5
Metabolic rate, watts	293	504	322	366	353	444	494	431	485	445	615	504	589	340	146	488	146	358	146	583	424	146	548
LCG inlet temp., °C	21	14	15	21	19	13	9	21	19	18	6	16	7	14	15	6	21	16	24	13	21	21	11
Net environmental heat exchange, watts	+79 into suit							-79 out of suit			+65 into suit			+117 into suit			-35 out of suit		-72 out of suit			+137 into suit	
LCG heat removal rate, watts	203	410	264	188	274	335	437	220	214	264	498	413	466	258	249	489	117	192	81	293	219	183	503
Total evaporative heat loss rate, watts	164	170	135	255	156	186	134	141	202	112	179	154	185	196	25	114	25	129	25	218	130	97	179
Evaporative heat loss rate by active sweat, watts	124	109	92	208	111	131	60	88	144	57	107	93	115	152	0	56	0	87	0	149	78	72	114
Mean skin temp., °C	31.2	30.3	30.2	-	31.2	28.6	27.8	30.3	29.0	30.3	28.7	31.8	28.5	27.8	28.5	27.3	20	28.8	33	32	33	30	28.8
Head core (Tympanic) temperature, °C	37.5	37.55	37.5	-	37.8	37.5	37.6	36.8	36.8	36.3	37.9	37	37.5	37.4	36.8	37.5	36.5	36.2	37.2	37.4	37.4	36	36.6
LCG heat transfer coefficient, watts/°C	22	28	19	-	26	23	25	25	25	23	23	28	23	20	19	25	14	15	10	16	20	22	32
Total body heat storage, watts-hours	35	50	16	-	30	15	30	0	5	-20	8	25	5	20	-5	10	-50	-75	38	50	50	-18	35

NOTE: Barred data are time-averaged values.

TABLE D7.- COMFORT POINTS - DATA FROM SERIES A, B, C, &D

METABOLIC RATE, WATTS	LCG INLET TEMP. SELECTED AT COMFORT, °C	LCG HEAT REMOVAL RATE, WATTS	TOTAL EVAPORATIVE HEAT LOSS RATE, WATTS	EVAPORATIVE HEAT LOSS RATE BY ACTIVE SWEAT, WATTS	ACTIVE SWEAT RATE GRAMS/HOUR
293	21	174	117	77	115
504	14	379	123	62	92
322	15	232	87	45	67
494	9	405	86	60	89
354	19	242	109	63	94
445	13	303	139	84	125
424	21	248	174	121	180
340	14	211	126	82	122
146	14	202	25	0	0
499	6	442	59	0	0
431	21	246	181	128	191
146	21	129	25	0	0
548	11	448	97	32	48
505	16	387	115	54	81
615	6	472	140	68	101
589	7	441	146	77	115
146	21	121	25	0	0
358	16	206	150	104	155
445	18	290	152	97	145
146	24	110	34	9	13
410	12	392	75	27	40
293	18	219	75	38	57
528	7	550	66	6	9
308	19	200	107	70	104
296	18	198	97	62	92
278	18	239	44	9	13
276	23	182	93	59	88
342	16	274	90	32	48
433	16	297	101	32	48
589	16	386	163	75	112

TABLE D7.- CONTINUED

METABOLIC RATE, WATTS	LCG INLET TEMP. SELECTED AT COMFORT, °C	LCG HEAT REMOVAL RATE, WATTS	TOTAL EVAPORATIVE HEAT LOSS RATE, WATTS	EVAPORATIVE HEAT LOSS RATE BY ACTIVE SWEAT, WATTS	ACTIVE SWEAT RATE GRAMS/HOUR
491	7	452	129	53	79
618	7	524	145	53	79
352	19	154	192	112	167
352	19	245	192	112	88
352	18	294	139	59	88
469	17	458	293	176	263

TABLE D8

LCG Heat Removal Distribution, %

	OLD (.....)	NEW (_____)
Trunk	44	22.5
Arms	17	25
Legs	39	52.5

Figure D-1. Predicted and actual body temperatures vs time for Series C, sequences 1 - 8.

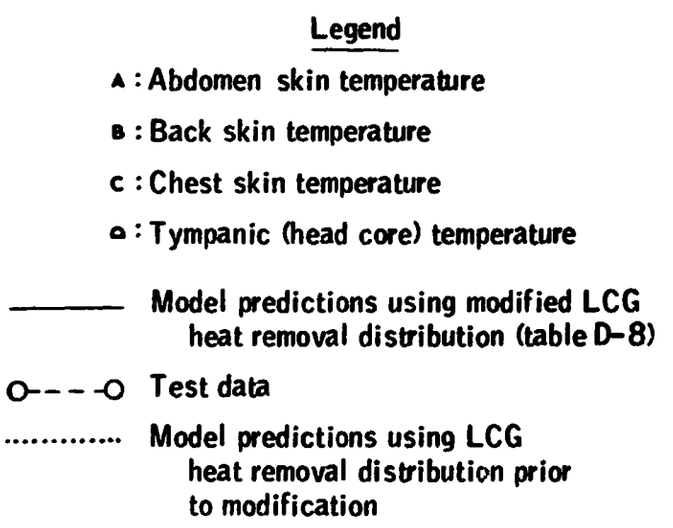

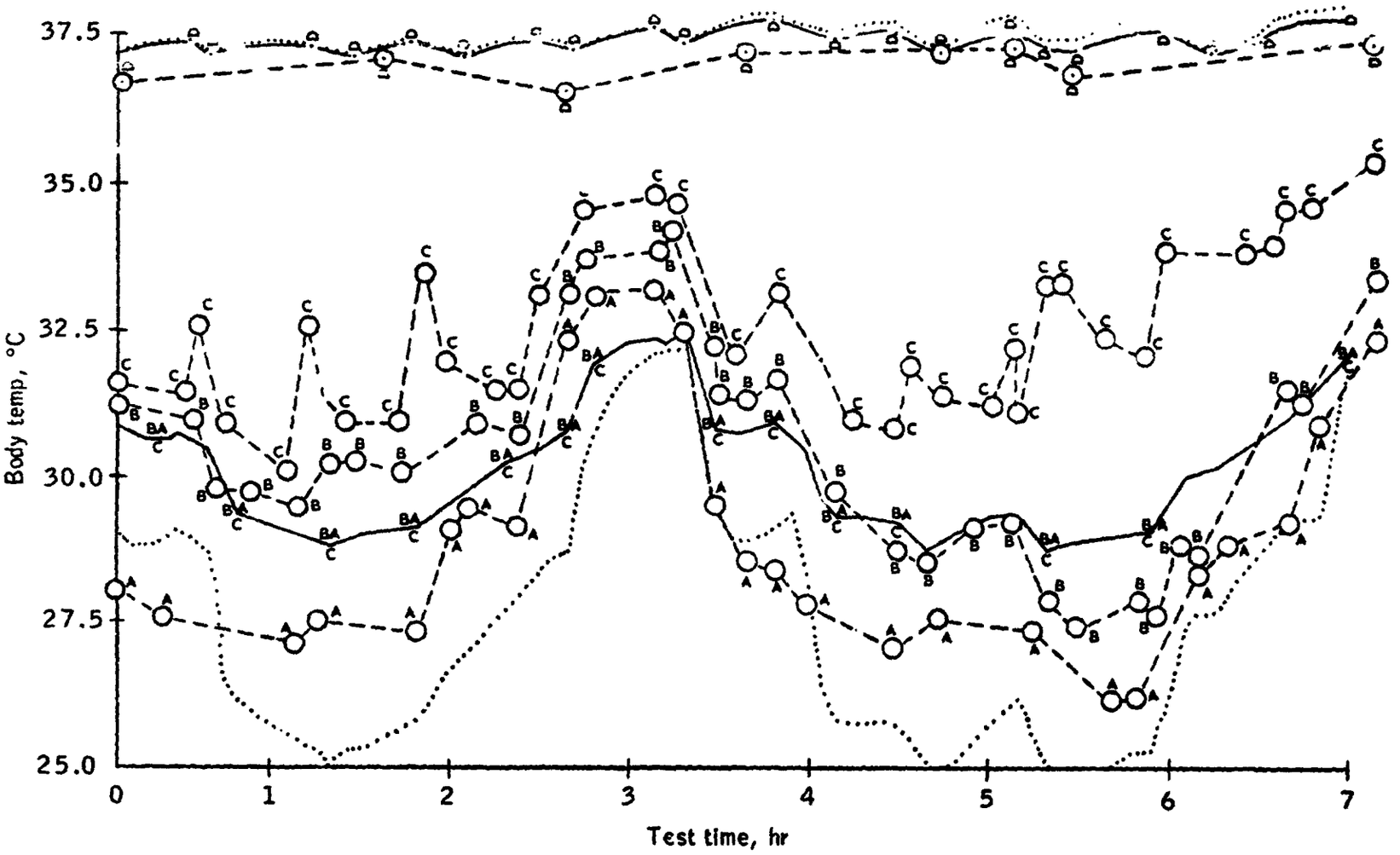
37.5
35.0
32.5
30.0
27.5
25.0
Body temp, °C
0
1
2
3
4
5
6
7
Test time, hr

Figure D-2. Predicted and actual body temperatures vs time for Series C, sequences 1-8.

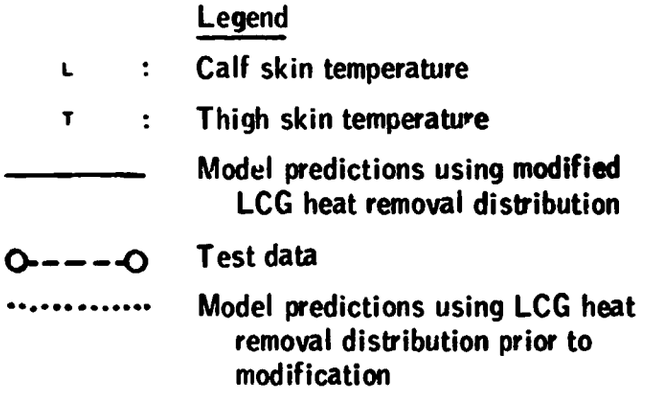

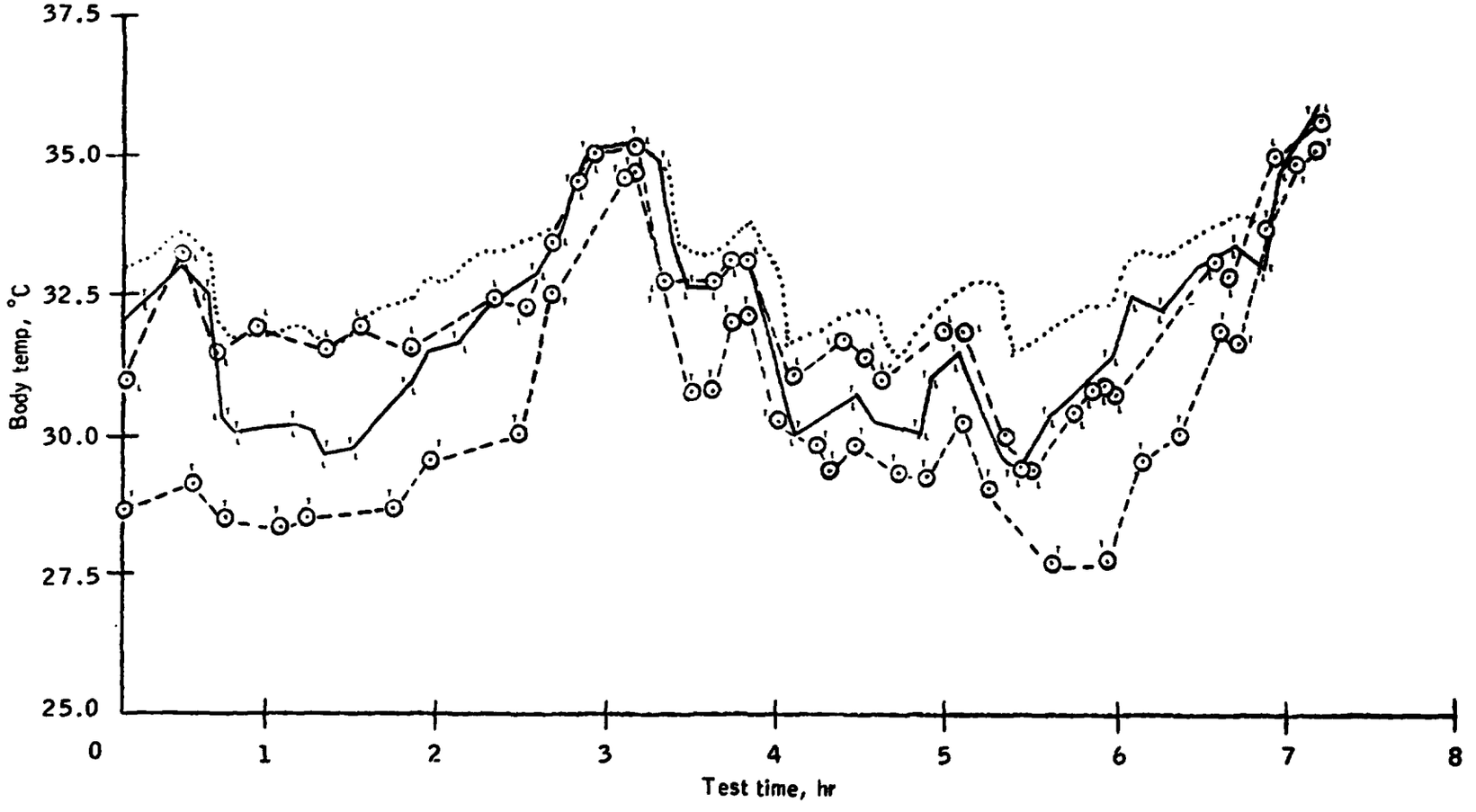
37.5
35.0
32.5
30.0
27.5
25.0
Body temp, °C
0
1
2
3
4
5
6
7
8
Test time, hr

Figure D-3. Predicted and actual body temperatures vs time for Series C, sequences 9 and 10.

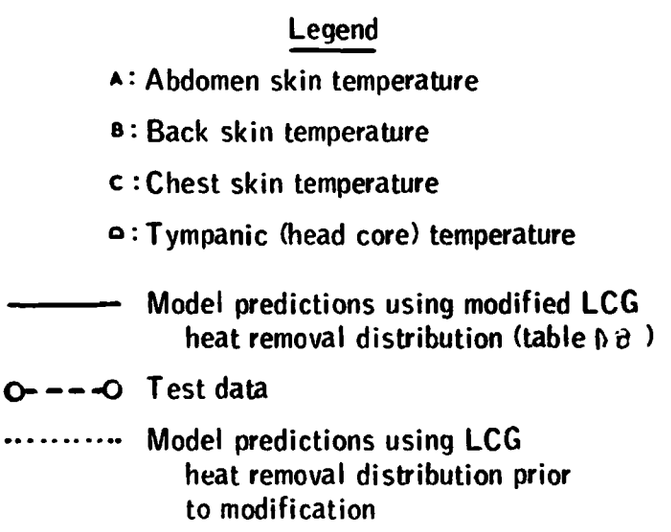

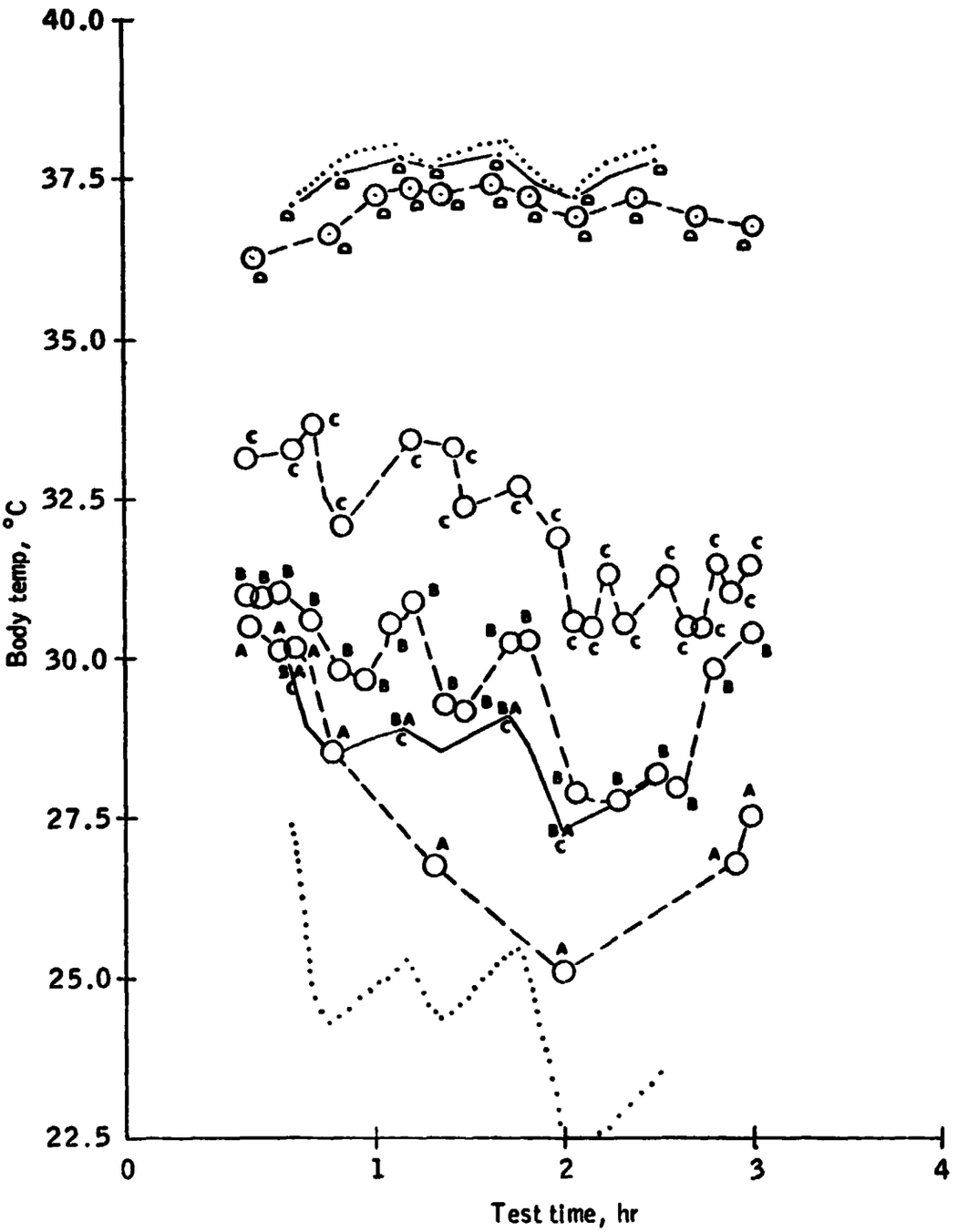
40.0
37.5
35.0
32.5
30.0
27.5
25.0
22.5
Body temp, °C
0
1
2
3
4
Test time, hr

Figure D-4. Predicted and actual body temperatures vs time for Series C, sequences 9 and 10.

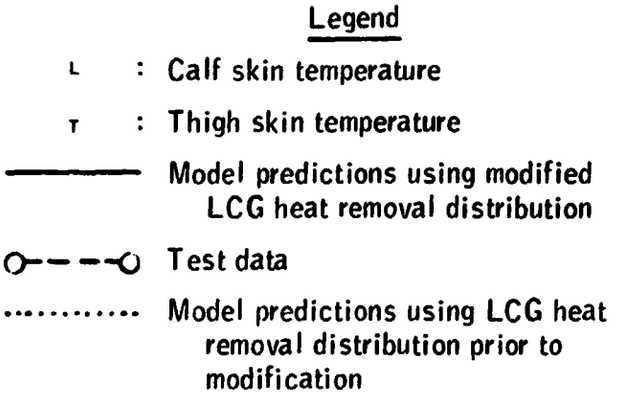

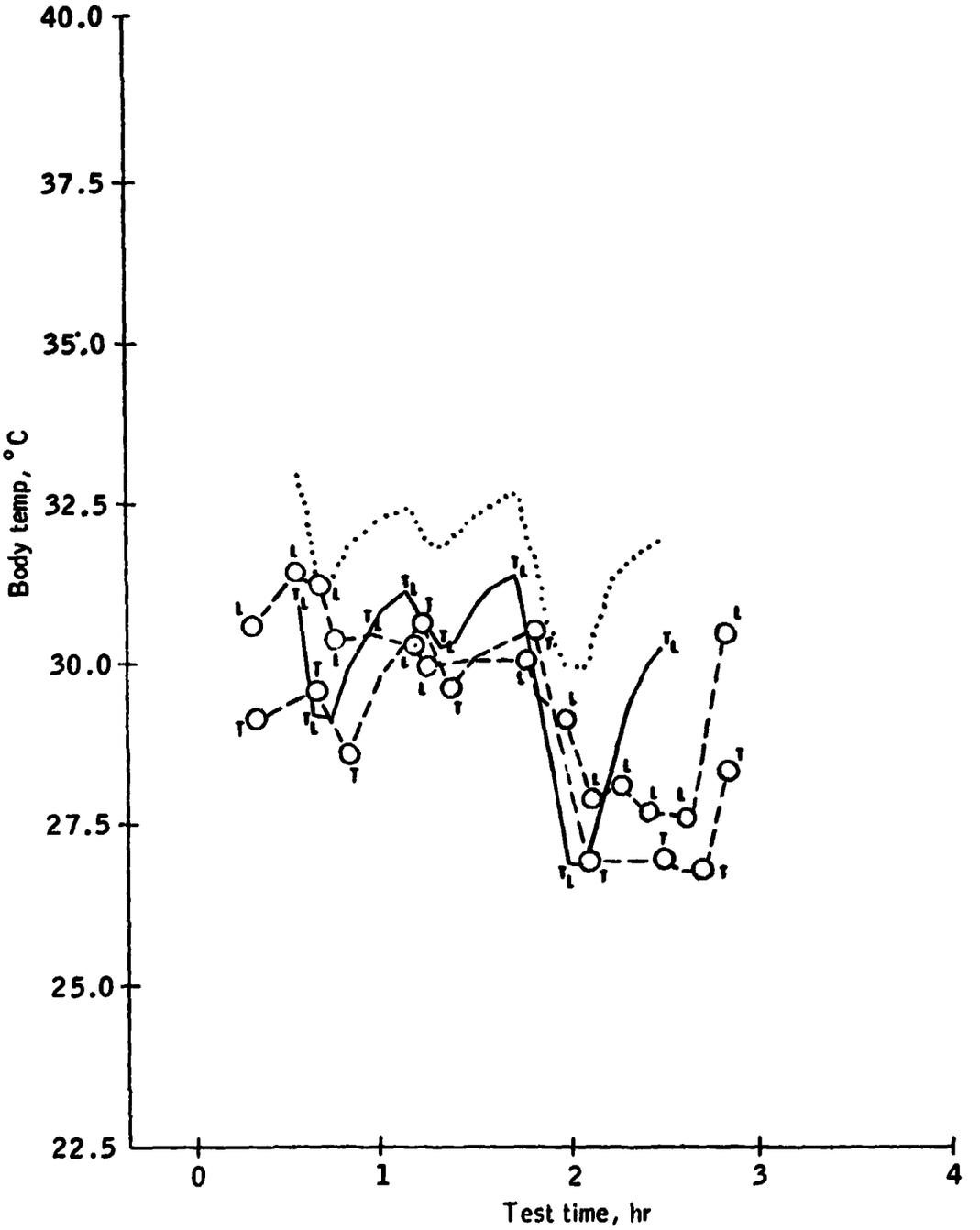
40.0
37.5
35.0
32.5
30.0
27.5
25.0
22.5
Body temp, °C
0
1
2
3
4
Test time, hr

Figure D-5. Predicted and actual skin temperatures vs time for Series D, test no. 1.

Legend

C : Upper chest skin temperature

H : Forehead skin temperature

B : Lower back skin temperature

A : Forearm skin temperature

L : Leg (calf) skin temperature

⊙- - - -⊙ Test data

——— Model predictions

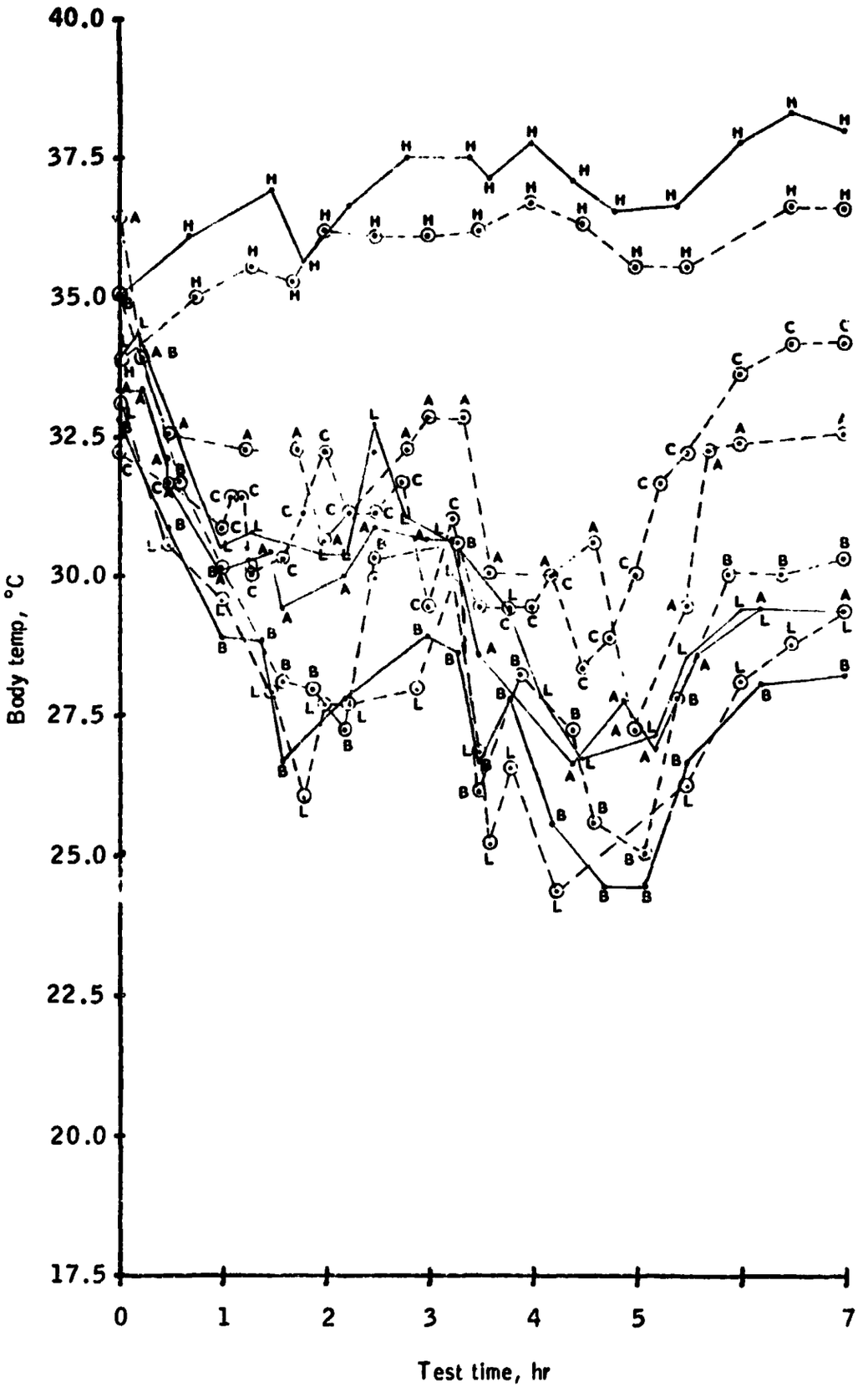
40.0
37.5
35.0
32.5
30.0
27.5
25.0
22.5
20.0
17.5
Body temp, °C
0
1
2
3
4
5
7
Test time, hr

Figure D-6. Predicted and actual skin temperatures vs time for Series D, test no. 2.

Legend

C : Upper chest skin temperature

B : Lower back skin temperature

A : Forearm skin temperature

L : Leg (calf) skin temperature

P : Bicep skin temperature

⊙- - -⊙ Test data

——— Model predictions

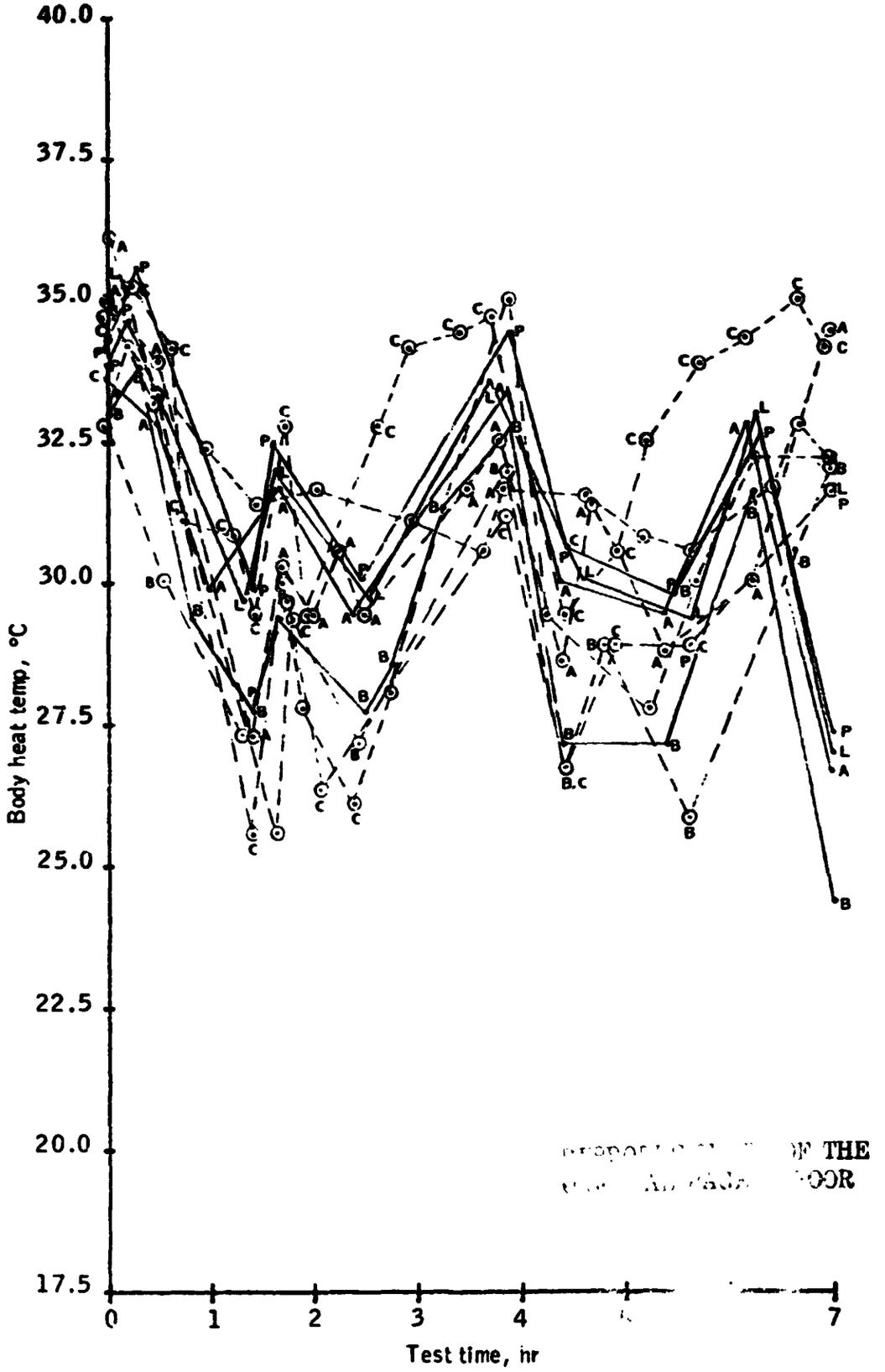
40.0
37.5
35.0
32.5
30.0
27.5
25.0
22.5
20.0
17.5
Body heat temp, °C
0
1
2
3
4
7
Test time, hr

Figure D-7. Predicted and actual skin temperatures for Series D, test no. 3.

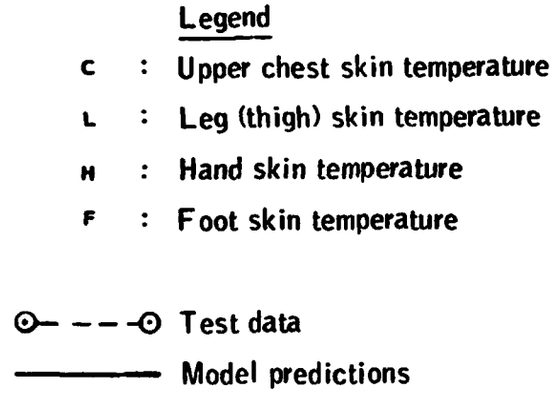

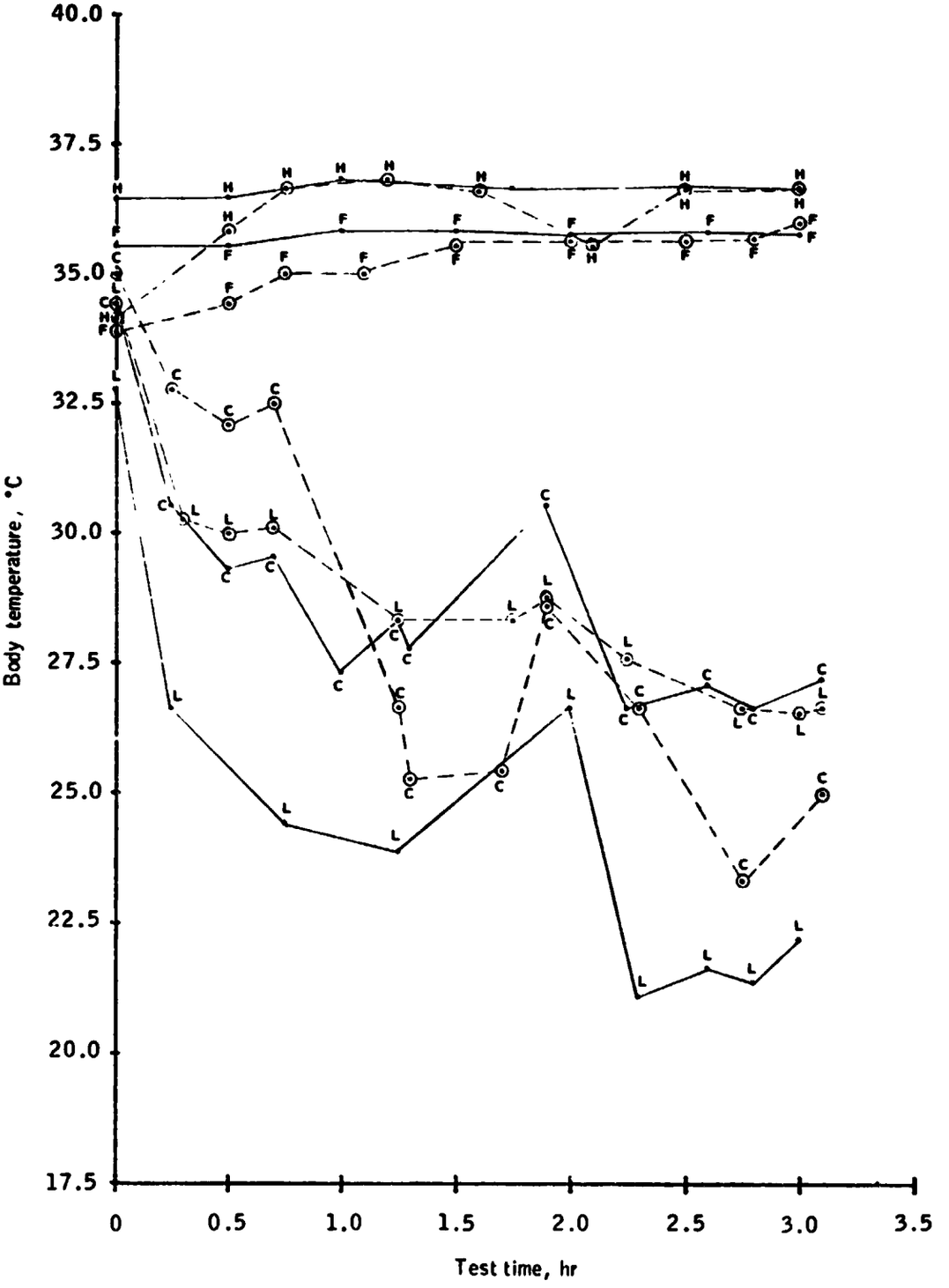
40.0
37.5
35.0
32.5
30.0
27.5
25.0
22.5
20.0
17.5
Body temperature, °C
0
0.5
1.0
1.5
2.0
2.5
3.0
3.5
Test time, hr

Figure D-8. Predicted and actual skin temperatures for Series D, test no. 4.

Legend

C : Upper chest skin temperature

L : Leg (thigh) skin temperature

H : Hand skin temperature

F : Foot skin temperature

⊙ - - - ⊙ Test data

——— Model predictions

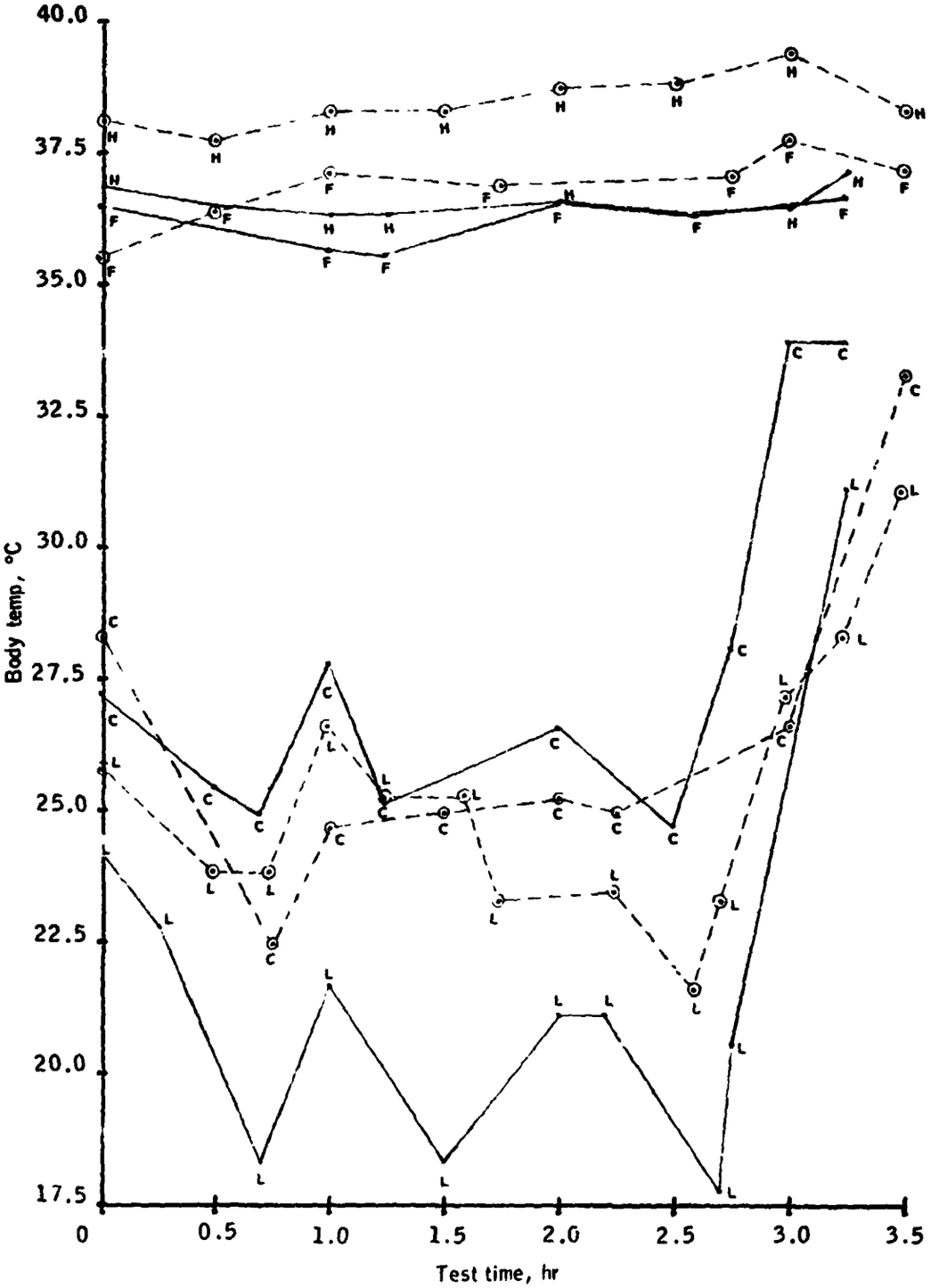
40.0
37.5
35.0
32.5
30.0
27.5
25.0
22.5
20.0
17.5
Body temp, °C
0
0.5
1.0
1.5
2.0
2.5
3.0
3.5
Test time, hr

Figure D-9. Predicted and actual skin temperatures for Series D, test no. 5.

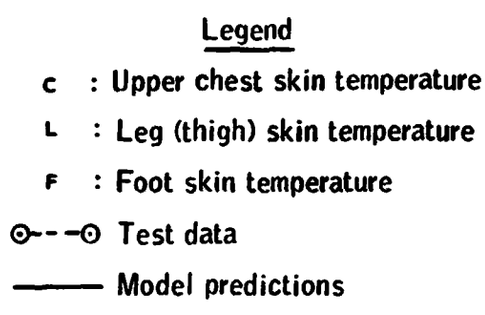

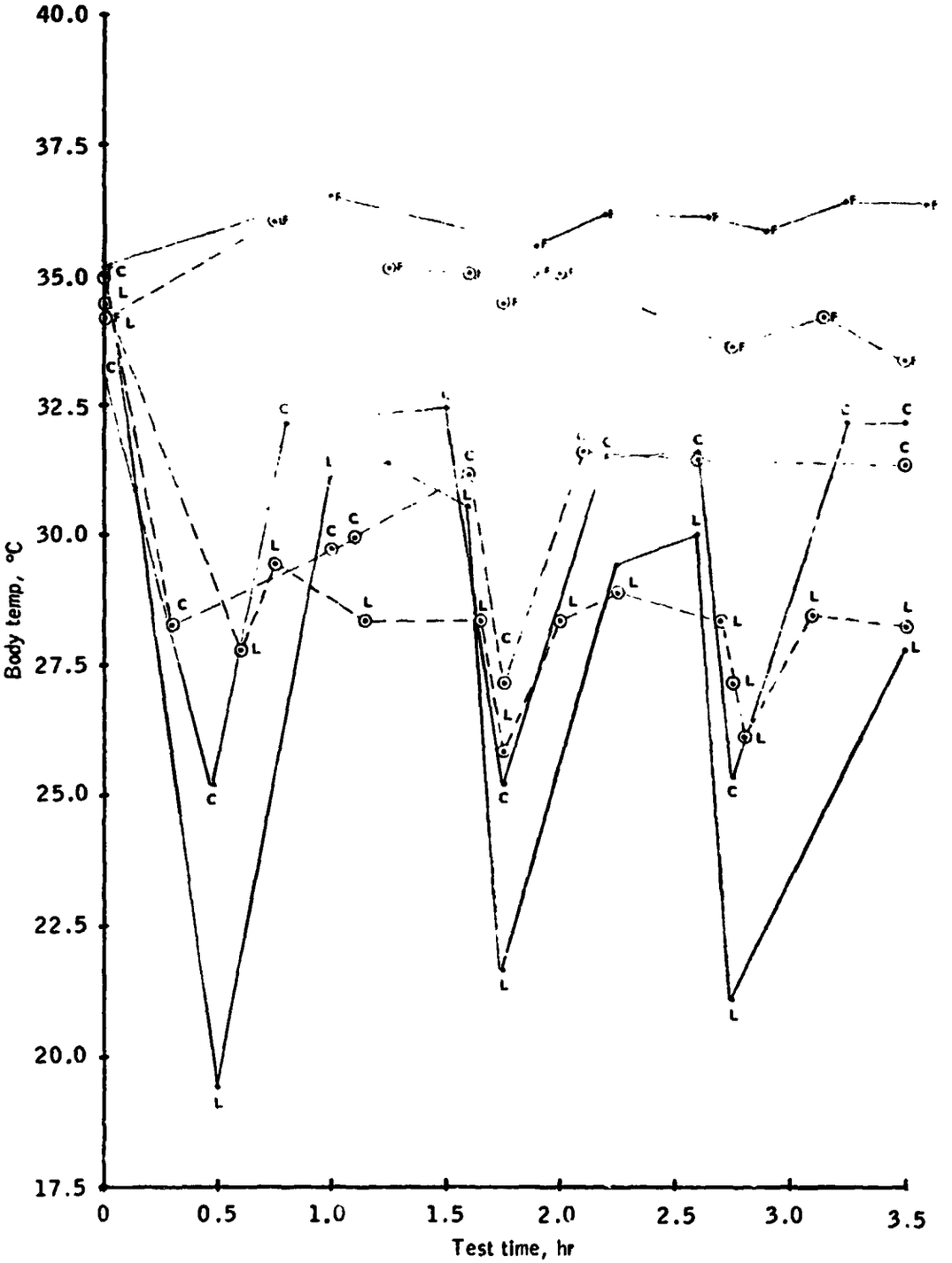
40.0
37.5
35.0
32.5
30.0
27.5
25.0
22.5
20.0
17.5
Body temp, °C
0
0.5
1.0
1.5
2.0
2.5
3.0
3.5
Test time, hr

Figure D-10. Predicted and actual skin temperatures for Series D, test no. 6.

Legend

L : Leg (thigh) skin temperature

H : Hand skin temperature

F : Foot skin temperature

O-- -⊙ Test data

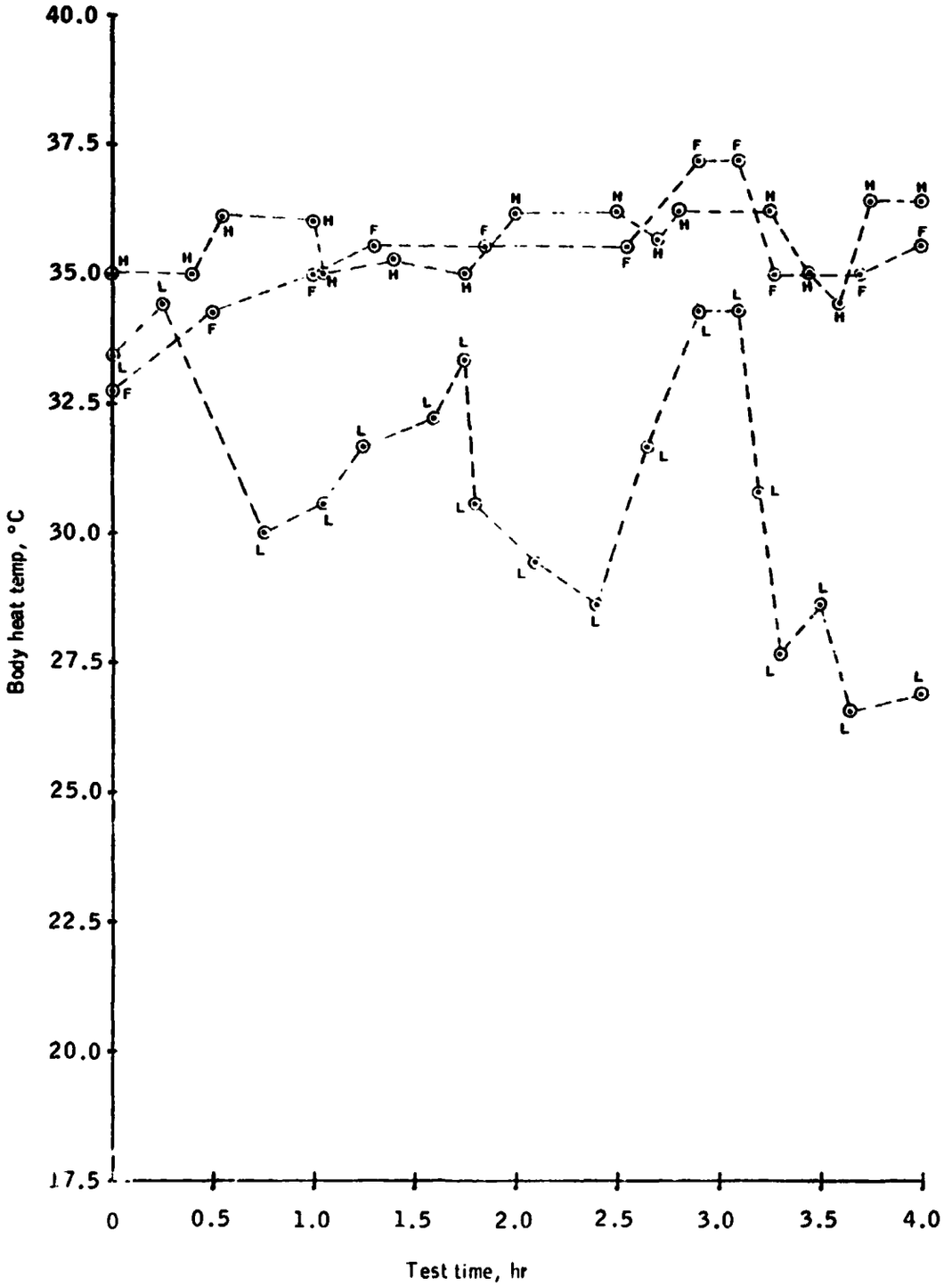
40.0
37.5
35.0
32.5
30.0
27.5
25.0
22.5
20.0
17.5
Body heat temp, °C
0
0.5
1.0
1.5
2.0
2.5
3.0
3.5
4.0
Test time, hr

Figure D-11. Predicted and actual skin temperatures for Series D, test no. 7.

Legend

C : Upper chest skin temperature

L : Leg (thigh) skin temperature

H : Hand skin temperature

F : Foot skin temperature

⊙– – –⊙ Test data

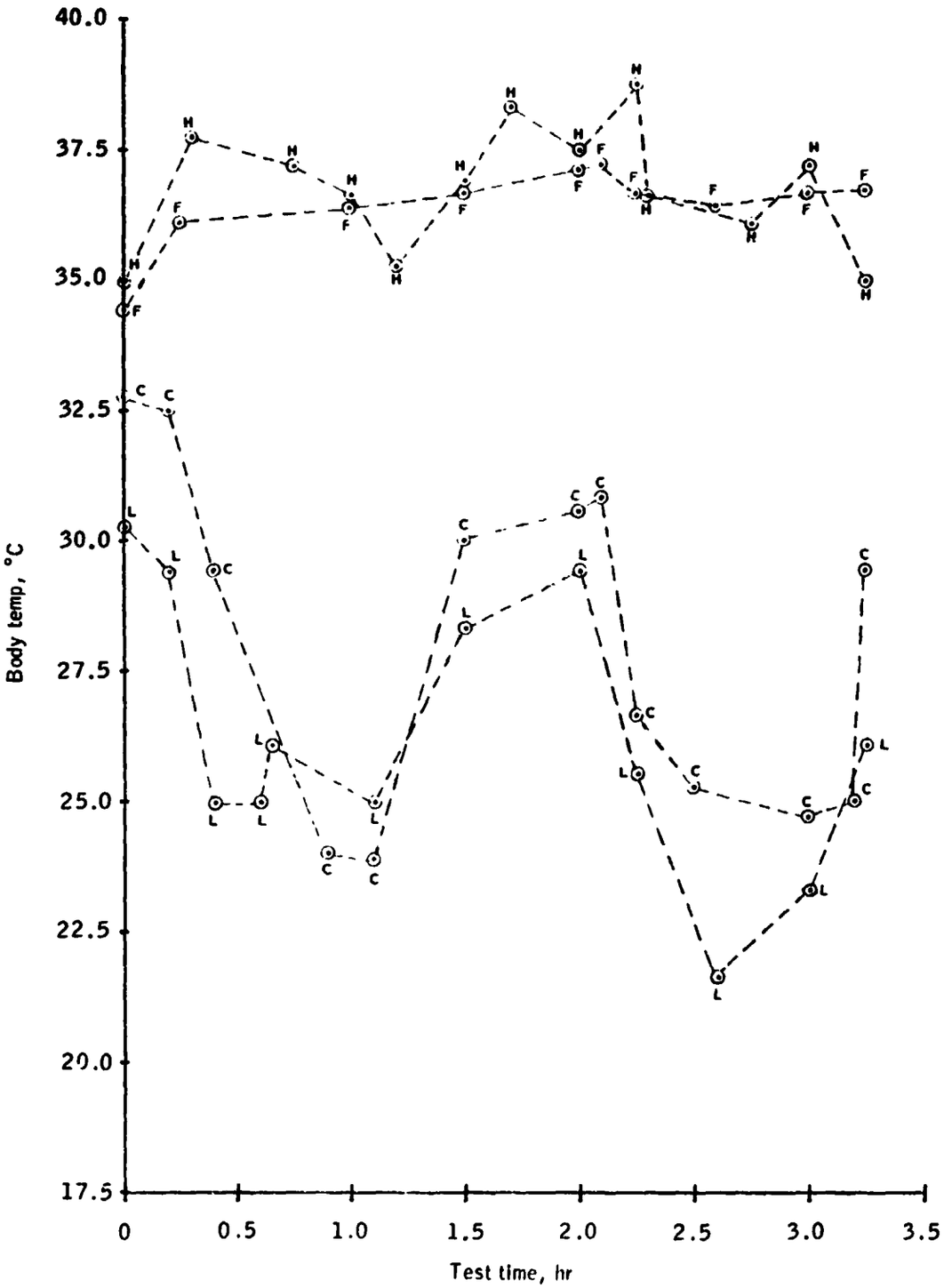
40.0
37.5
35.0
32.5
30.0
27.5
25.0
22.5
20.0
17.5
Body temp, °C
0
0.5
1.0
1.5
2.0
2.5
3.0
3.5
Test time, hr

Figure D-12. Predicted and actual steady-state rectal and mean skin temperature vs metabolic rate for cool and moderate LCG inlet temperatures using modified LCG heat removal distribution - Series A.

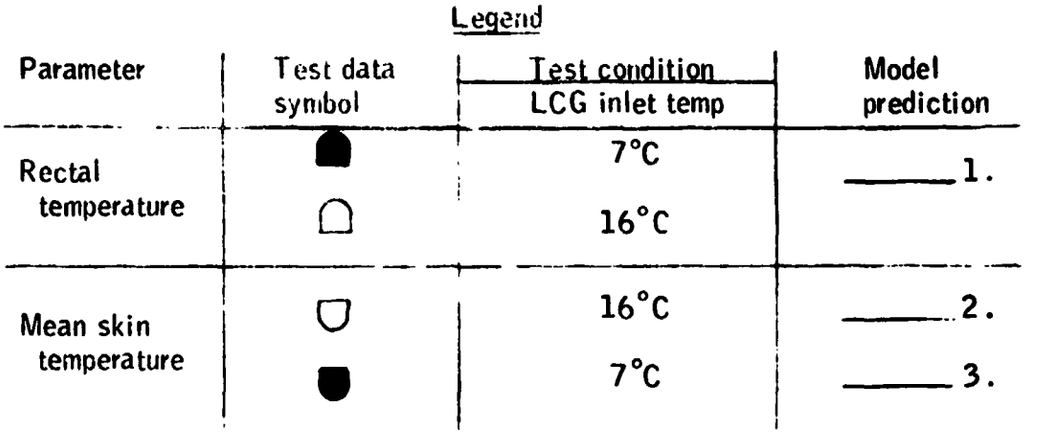

Note: Dotted lines (....) represent model predictions using LCG heat removal distribution prior to modification.

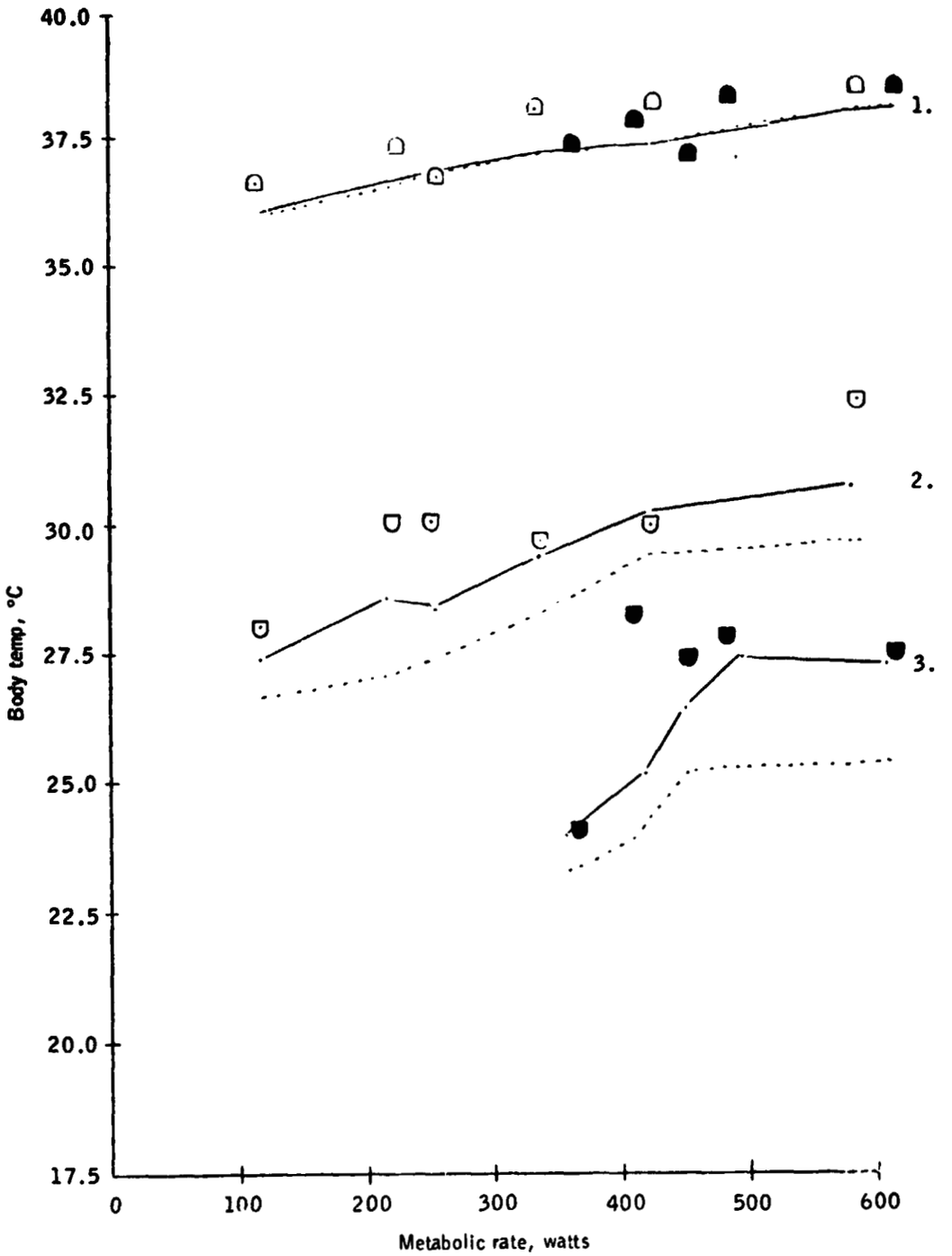
40.0
37.5
35.0
32.5
30.0
27.5
25.0
22.5
20.0
17.5
Body temp, °C
0
100
200
300
400
500
600
Metabolic rate, watts
1.
2.
3.

APPENDIX E

APOLLO EXPERIENCE REPORT

AND LUNAR SURFACE MISSION RESULTS

OPR 3 A2-M0 0 8 YR 7 1

17712 METABOLIC/BIOENVIRONMENTAL SUMMARY 17?A 17:C

BIOMED PARAMETERS CDR		BIOMED PARAMETERS LMP		MED INPUTS	
AVG SAMPLE PRD	19:46 M/S	AVG SAMPLE PRD	19:45 M/S	SAMPLE PRD	4●
AVG HEART RATE	81 BT/M	AVG HEART RATE	105 BT/M	CDR DATA	
MEAN HEART RT	91 BT/M	MEAN HEART RT	92 BT/M	CM SLOPE	39.●
MET RT HRT	1338 B/HR	MET RT HRT	352 B/HR	CC INTEC	−23●●
MET SUB TOT HR	122 BTU	MET SUB TOT HR	84 BTU	QC RQ	●.?●●
MET TOT HRT	1753 BTU	MET TOT HRT	1715 BTU	LC SUIT LK	123
METABOLIC DATA CDR		METABOLIC DATA LMP		AM PRES Δ	15.●
MET RT O2	1●?4 B/HR	MET RT O2	1384 B/HR	ASO QRAD	●.●
MET RT LCG	835 B/HR	MET RT LCG	1?●3 B/HR	FLCGO	25?.●
MET SUB TOT O2	232 BTU	MET SUB TOT O2	232 BTU		S[redacted]
MET SUB TOT LCG	154 BTU	MET SUB TOT LCG	124 BTU	LMP DATA	
MET TOT O2	1772 BTU	MET TOT O2	1430 BTU	LM SLOPE	27.●
MET TOT LCG	1●7? BTU	MET TOT LCG	1352 BTU	CI INTEC	−22●●
PLSS 1 PARAMETERS CDR		PLSS 2 PARAMETERS LMP		QI RQ	●.?●●
PGA PRESSURE	3.6●◇PSID	PGA PRESSURE	LPSID	LI SUIT LP	123
PGA PCO2	●.? MMHG	PGA PCO2	2●.●◇MMHG	AM PRES Δ	15.●
POS O2 P	3?1◇PSIG	POS O2 P	1138 PSIG	ASI QRAD	●.●
PRESS BASE	1052 PSIG	PRESS BASE	1●?? PSIG	FLCG1	25●.●
SUB O2 TEMP	48.8 °F	SUB O2 TEMP	14.3◇ °F		S[redacted]
LCG IN TEMP	64.4 °F	LCG IN TEMP	13.2◇ °F	COMMON	
LCG Δ TEMP	2.7 °F	LCG Δ TEMP	12.3◇ °F	KHO	●.●
FEED H2O PRES	1.?2◇PSIA	FEED H2O PRES	3.●4 PSIA	FLST	5.4●
EVCS SYNC	NO	EVCS SYNC	NO	XM	●.A??
				XI	-11.●
				MT	●.●5●
				MS	●.?●●
				GET	●14? 11A 1?:?●
				S/TOT	??? 1?.●●

Figure E1. - Live data and computation display, during Apollo 16.

OF THE ORIGINAL PAGE IS POOR

REPRODUCIBILITY OF THE ORIGINAL PAGE IS POOR

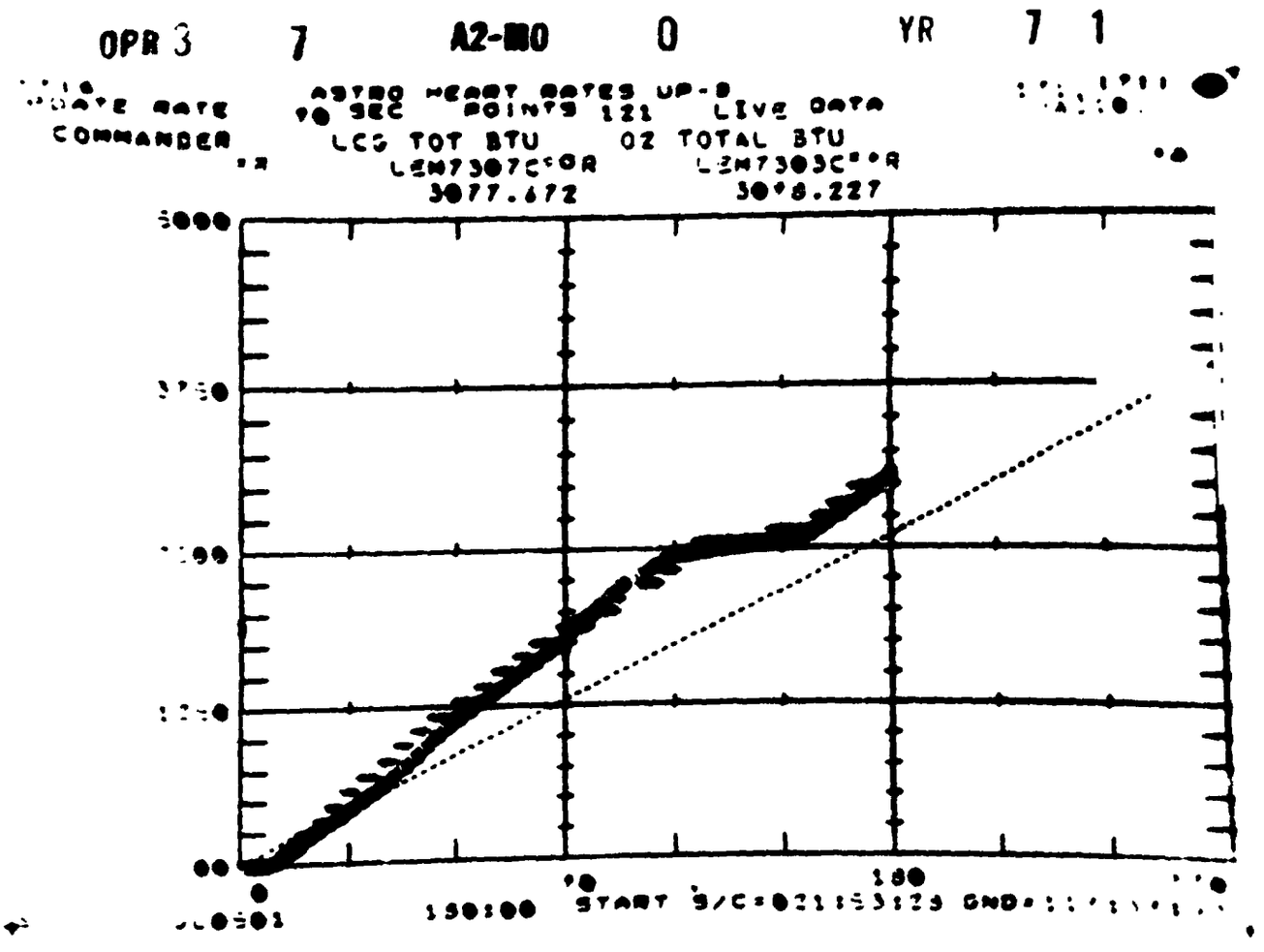

Figure E2. - Live data and computation display, during Apollo 16.

NASA TECHNICAL NOTE

NASA TN D-7883

NASA TN D-7883

APOLLO EXPERIENCE REPORT - ASSESSMENT OF METABOLIC EXPENDITURES

J. M. Waligora, W. R. Hawkins, G. F. Humbert, L. J. Nelson, S. J. Vogel, and L. H. Kuznetz

Lyndon B. Johnson Space Center
Houston, Texas 77058

NATIONAL AERONAUTICS AND SPACE ADMINISTRATION • WASHINGTON, D. C. • MARCH 1975

1 Report No	2 Government Accession No	3 Recipient's Catalog No
NASA TN D-7883		

4 Title and Subtitle	5 Report Date
APOLLO EXPERIENCE REPORT ASSESSMENT OF METABOLIC EXPENDITURES	March 197 6 Performing Organization Code JSC-07484
7 Author(s) J. M. Waligora, W. R. Hawkins, G. F. Humbert, and L. H. Kuznetz, JSC, and L. J. Nelson and S. J. Vogel, Boeing Company	8 Performing Organization Report No JSC S-394
9 Performing Organization Name and Address Lyndon B. Johnson Space Center Houston, Texas 77058	10 Work Unit No 914-50-95-13-72 11 Contract or Grant No
12 Sponsoring Agency Name and Address National Aeronautics and Space Administration Washington, D.C. 20546	13 Type of Report and Period Covered Technical Note 14 Sponsoring Agency Code

15 Supplementary Notes

16 Abstract

A significant effort was made to assess the metabolic expenditure for extravehicular activity on the lunar surface. After evaluation of the real-time data available to the flight controller during extravehicular activity, three independent methods of metabolic assessment were chosen based on the relationship between heart rate and metabolic production, between oxygen consumption and metabolic production, and between the thermodynamics of the liquid-cooled garment and metabolic production. The metabolic assessment procedure is analyzed and discussed. Real-time use of this information by the Apollo flight surgeon is discussed. Results and analyses of the Apollo missions and comments concerning future applications are included.

17 Key Words (Suggested by Author(s))
- Heart Rate
- Oxygen Consumption
- Liquid-Cooled Garment
- Energy Levels
- Extravehicular Activities

18 Distribution Statement
STAR Subject Category:
12 (Astronautics, General)

19 Security Classif (of this report)	20 Security Classif (of this page)	21 No of Pages	22 Price
Unclassified	Unclassified	12	$3.25

* For sale by the National Technical Information Service, Springfield, Virginia 22151

APOLLO EXPERIENCE REPORT

EDITORIAL COMMITTEE

The material submitted for the Apollo Experience Reports (a series of NASA Technical Notes) was reviewed and approved by a NASA Editorial Review Board at the Lyndon B. Johnson Space Center consisting of the following members: Scott H. Simpkinson (Chairman), Richard R. Baldwin, James R. Bates, William M. Bland, Jr., Aleck C. Bond, Robert P. Burt, Chris C. Critzos, John M. Eggleston, E. M. Fields, Donald T. Gregory, Edward B. Hamblett, Jr., Kenneth F. Hecht, David N. Holman (Editor/Secretary), and Carl R. Huss. The prime reviewer for this report was Donald T. Gregory.

APOLLO EXPERIENCE REPORT

ASSESSMENT OF METABOLIC EXPENDITURES

By J. M. Waligora, W. R. Hawkins, G. F. Humbert,
L. J. Nelson,* S. J. Vogel,* and L. H. Kuznetz
Lyndon B. Johnson Space Center

SUMMARY

Before the first Apollo extravehicular activity, the staff of the NASA Lyndon B. Johnson Space Center (formerly the Manned Spacecraft Center) developed operational methods to determine the energy expenditures of the crewmen. These methods were required to allow adequate physiological evaluation of the crewmen, to determine the usage rate of life-support system consumables, and to provide information for real-time activity scheduling and for planning future missions.

Three independent methods were used to determine crewmen energy expenditures. The heart-rate method was based on the direct linear relationship between energy expenditure and heart rate, which was determined before each flight. The oxygen method was based on the proven clinical procedure that relates energy expenditure to oxygen consumption. The liquid-cooled-garment method was based on a modified direct calorimetric approach to energy measurement. Preflight testing of these methods demonstrated inadequacies and inaccuracies that were corrected, and a system was developed that facilitated integration of the three methods into an accurate estimate of energy expenditure.

During each extravehicular activity, this integrated estimate was reported to the mission control flight surgeon and to the life-support system monitors. Thus, the flight surgeon was prepared to make recommendations concerning the immediate and future well-being of the crewmen. Postflight analyses of the results, combined with motion analysis, permitted accurate assessments of energy expenditure for specific lunar surface tasks. It was concluded that these methods provided reliable information on crewmember energy expenditures, which ranged from 822×10^3 to 1267×10^3 J/hr (780 to 1200 Btu/hr) for the Apollo lunar surface extravehicular activities.

---

*Boeing Company.

INTRODUCTION

Information about energy expenditure at the onset of planning for Apollo extravehicular activity (EVA) was meager. The observations made during the Gemini EVA periods indicated that the energy expenditures were greater than expected. The basis for the comparison was the heart rates observed during altitude chamber simulations and those observed during the actual EVA. The greatest deviation between the expected heart rates and the observed heart rates occurred during the Gemini XI EVA. Instead of providing a quantitative measurement of metabolism, these observations only indicated that at times the metabolic rates were more than the life-support system could accommodate. Data were available from 1/6-g trainers of many types; however, there was a general lack of confidence in this type of lunar surface simulation, particularly when the data were applied to energy expenditures for movement on the unknown terrain of the lunar surface.

A measurement of crew metabolic rates was required for several reasons. The basic measurement was important to the flight surgeon because it provided a measure of how closely a crewman was approaching his maximum work rate either acutely, as during a maximum effort when a crewman's maximum oxygen consumption might be exceeded, or chronically, as when a sustained moderately high work rate might lead to exhaustion. The metabolic rate also provided data that could affect the flight surgeon's evaluation of other information regarding a crewman. For example, a heart rate of 130 beats/min would indicate one level of concern for a crewman vigorously at work and another for a crewman at rest.

The metabolic rate measurement was also important to the monitors of the portable life-support system (PLSS) because the useful life of a PLSS on the lunar surface depended on the usage rate of consumables (oxygen, sublimator water supply, and carbon dioxide absorber). The usage rate of these consumables is closely related to metabolic rate; this relationship was particularly significant in the case of the water supply to the sublimator that provided the cooling for the PLSS because there was no measurement of sublimator water supply.

The metabolic rate measurement provided essential information for the lunar surface activity planners who assembled a schedule of crew activities based on preflight estimations of the metabolic expenditure and the time required to perform each activity. These planners were responsible for modifying the crewman's activity in real time if the metabolic expenditures for the activities or the time required to perform the activities deviated from the predicted values.

Before the first Apollo EVA, several groups at the NASA Lyndon B. Johnson Space Center (JSC) (formerly the Manned Spacecraft Center (MSC)) had been concerned with metabolic rates. A medical operations group was responsible for providing metabolic rate estimates for specific tasks and for monitoring the crew during 1/6-g training at MSC; a medical research group provided the metabolic requirements for the design of the life-support system and sponsored several research programs to evaluate various 1/6-g simulations. An engineering group attempted to use heat-loss data from the liquid-cooled garment (LCG) to estimate metabolic rate in calculating the usage of sublimator water supply. In 1969, before the first Apollo EVA (on the Apollo 9 mission),

the Life Sciences Directorate formed a Metabolic Assessment Team that was composed of personnel from the Life Sciences Directorate and a member from the Engineering and Development Directorate, all of whom had been working in the area of metabolism. The team also benefited from support received from the Mission Evaluation Team and other MSC groups. The Metabolic Assessment Team was charged with the responsibility for reviewing and evaluating real-time data that would be available during EVA and for devising procedures to use these data in measuring the crewman's metabolic rates during EVA.

As a result of the team's initial studies, three independent methods based on the most common laboratory methods were implemented:

1. The relationship between heart rate and metabolic rate

2. The relationship between oxygen consumption and metabolic rate

3. The relationship between the heat removed from the crewman by the LCG and metabolic rate

Each method was used during ground-based tests and each was found to provide useful data but to have deficiencies when used alone. The advantages and deficiencies of these methods and the real-time modifications made to improve them are presented in the following sections.

HEART-RATE METHOD

Heart rates were used during Apollo flights to estimate metabolic expenditures during specific extravehicular activities. Because the heart rate is an indicator of total physiological and psychological stress, it is not entirely dependent on metabolic rate. The heart-rate method was, however, the only method with a timelag short enough to allow a minute-by-minute estimate of the energy expenditure.

In addition to the inaccuracies (psychogenic factor, heat storage, and fatigue) usually associated with this method of metabolic-rate estimation, three unique problems were encountered during the Apollo missions: calibration-curve inaccuracies, crewmember deconditioning, and the technique used to determine heart rate. Control of the usual inaccuracies was not considered feasible because insufficient data were available during the EVA; however, as explained in this report, control of the unique sources of inaccuracy was attempted.

Calibration curves (heart rate compared with metabolic rate) for each individual were determined before each mission by using standard ergometric calibration techniques. Heart-rate data were obtained under resting conditions and at several work rates; least-squares analysis was used to determine a linear regression curve. Standard errors as large as 211×10^3 J/hr (200 Btu/hr) were not unusual. Changes in test protocol (more data points at various work rates) did not significantly increase the accuracy, and it was concluded that this modification to the standard laboratory calibration procedures was not worthwhile.

Deconditioning of crewmen between preflight and postflight measurements resulted in a 10- to 35-beats/min increase in heart rate for any given workload experienced before deconditioning. Attempts were made to use this information to correct the EVA heart-rate/metabolic-rate curve by shifting (biasing) the curve. Furthermore, to obtain information that would allow inserting bias into the curve (which was assumed to be progressive with the length of exposure to weightlessness), efforts were made to obtain heart-rate data during successive in-flight sleep periods before the EVA. These corrective efforts improved the estimates only slightly because a wide variation in individual crewmember response contributed greatly to the inaccuracies inherent in this method.

The use of heart rate alone as an independent indicator of metabolic rates under space-flight conditions is not recommended. Errors as large as 80 percent have been noted. However, the use of heart rate as a dependent method was useful when the total metabolic expenditure as measured by oxygen and LCG methods could be used as a reference. After the first Apollo flights, use of the heart-rate method as an independent real-time method was discontinued; the method was then used as a real-time and postflight dependent method. The relationship between heart rate and metabolic rate was based on hourly measurements of the total EVA energy expenditure as determined by the oxygen and LCG measurements. The heart-rate method then allowed real-time and postflight measurement of specific activities on a minute-by-minute basis. An example of the heart-rate method is the measurement of metabolic rate during deployment of the heavy Apollo lunar surface experiments package by the lunar module pilot. This activity took 2 to 3 minutes to accomplish. The response of the oxygen and LCG methods did not allow isolation of this activity, but the heart-rate method responded quickly to this activity and provided the best information on energy expenditure for the activity.

OXYGEN METHOD

The oxygen method involved using the PLSS oxygen bottle pressure decay to estimate oxygen consumption and thereby metabolic rate. The oxygen bottle pressure was telemetered from each EVA crewman and displayed in real time.

Special problems were associated with using this method as a metabolic-rate indicator. For best accuracy of the oxygen method, a measurement of respiratory quotient (RQ) as well as oxygen consumption is required. The RQ is a ratio of the amount of carbon dioxide produced and the amount of oxygen consumed. There was no measurement of carbon dioxide production; therefore, the RQ had to be estimated.

A random noise error was experienced in the telemetered oxygen bottle pressure data. To minimize this error, a metabolic computation was not performed until a significant drop in bottle pressure occurred. Consequently, at lower metabolic rates, updates did not yield information frequently enough during EVA for adequate evaluation of consumables status and crewmember condition.

The suit oxygen leakage rate was variable and had to be estimated. The maximum oxygen leakage rate allowed by the pressure suit specification was equivalent to a metabolic rate of approximately 211×10^3 J/hr (200 Btu/hr).

The following attempts were made to reduce errors associated with the oxygen method. The RQ was determined on several occasions during crew training and during manned tests in the thermal-vacuum facilities; this determination enabled more accurate estimates during missions. A suit-leak check was performed at the NASA John F. Kennedy Space Center before launch readiness to provide an indication of leak rates to be expected during the mission. These leak rates were used as initial values in the oxygen-consumption metabolic program. A pressure integrity check was performed before each lunar surface EVA, and the measured leak rates were used to update the program. Experience indicates that the suit leak will increase during use, especially if activity is vigorous. Accordingly, upward adjustments were made in the program as the EVA progressed.

LIQUID-COOLED-GARMENT METHOD

Because of the limitations of the other methods available to estimate metabolic rate, direct calorimetry was the third method to be considered. All the energy produced by metabolism is accountable either as heat produced or as physical work; direct calorimetry is the measurement of this energy production. A complete energy accounting required measurement of heat removed by the LCG, heat (both sensible and latent) removed by the gas stream, heat leak into or out of the pressure suit, and energy dissipated outside the suit either as work or as heat from frictional work.

The available PLSS data were limited to LCG inlet and outlet temperature and gas inlet temperature and, at first, appeared to be inadequate to calculate an energy balance. However, the availability of a thermal model of man in a pressure suit (ref. 1) together with considerable empirical data on heat removal from man in a pressure suit (ref. 2) allowed estimates of the types of heat loss not directly measured.

An LCG heat-balance computer program was constructed to estimate metabolic rate. Using the thermoregulatory model, a relationship between LCG heat removal and metabolic rate for each LCG inlet temperature (fig. 1) was defined. This estimate of metabolic rate was not dependent on proper crew selection of inlet temperature. The estimate provided valid data on the metabolic rate of a crewman who had

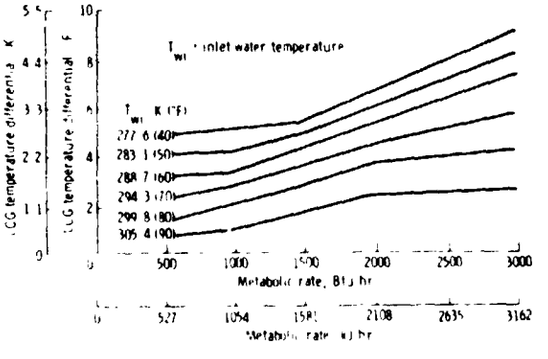

Figure 1. - Example of factor 1 LCG program; metabolic rate plotted as a function of heat picked up by the LCG for each of a family of inlet temperatures. Relationship is based on the assumption that a steady state exists; crewman comfort is not assumed.

not selected a comfortable water temperature (provided he was in or near steady state). This estimate of metabolic rate, based on inlet temperature and the difference between inlet and outlet temperature, was accurate only when the data were rather stable. The estimate was not accurate during a rapid transient of water temperature or metabolic rate. To provide data during transient periods, a simpler estimate of metabolic rate was used that consisted of a linear equation relating metabolic rate to LCG heat removal (fig. 2). This estimate was accurate only when comfortable coolant temperatures were selected by the crewman. A difference in the two estimates over a period of time indicated that the crewman was functioning at either a hotter or cooler body temperature than optimum. On several occasions, this condition led to the flight surgeon's recommendation to change the LCG diverter valve setting.

A manual input, identified as "factor," was made available in the program. When the factor equaled zero, the metabolic rate was based on the estimate using the difference between inlet and outlet temperature; when the factor equaled 1, the metabolic rate was based on the estimate using the difference between inlet and outlet temperature combined with the absolute value of the inlet temperature. An operational procedure was developed for control of the factor input in a consistent manner. Factor 1 was chosen after obtaining two consistent 12-minute readouts. After any transient change, factor zero was reselected. Other real-time inputs to the program included the heat leak into the suit and the LCG flow rate. These values were based on analysis and were provided by the Mission Evaluation Team before flight and, after the Apollo 14 mission, during each EVA by means of a telephone link to the medical science support room.

Because of its analytical nature, the LCG method was of no value until it could be verified with test data from training runs in the MSC Space Environmental Simulation Laboratory chamber. The test data indicated that the LCG method predicted the sublimator water usage and the carbon dioxide absorption in lithium hydroxide canisters as accurately as or more accurately than the other methods and that the method would be of value.

In calculating an estimate of sublimator water usage, the LCG method was of special value because a heat leak into or out of the suit affected both the LCG method and the sublimator water usage. Therefore, the accuracy of the heat-leak estimate was not critical for estimating sublimator water usage, although it was critical for estimating metabolic rate.

Experience with the heat-balance program during early Apollo missions increased confidence in the program and provided familiarity with its strengths and weaknesses. The LCG method provided the best prediction of sublimator water usage when predictions were

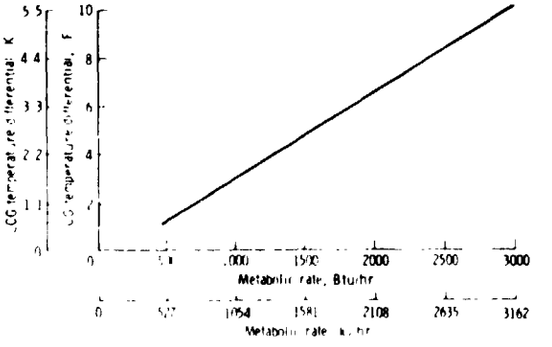

Figure 2. - Example of factor zero LCG program; metabolic rate plotted as a function of heat picked up by the LCG. Relationship is based on the assumption that the crewman is maintaining a comfortable LCG inlet temperature.

compared with measurements of remaining feedwater. Comparisons of LCG and oxygen data indicated that the heat-balance program, as designed, compensated for inappropriate diverter-valve settings; however, accuracy was reduced if comfortable settings were not maintained by the crewman. The response of the heat-balance program was demonstrated to be slow, which was expected, but the program did begin to respond almost immediately to a change in metabolic rate.

INTEGRATION OF METHODS

Because early studies indicated many sources of uncertainty in each method when used individually, the decision was made to use all three methods simultaneously. The metabolic team received all incoming raw data, processed the data in accordance with the best real-time estimates for values of the unmeasurable factors involved, used the results obtained from each of the individual methods to provide correction factors for the other methods, and provided one integrated value for the flight surgeon. It was realized that this process could be iterative and that updates could, as the EVA progressed, cause retrospective changes in values. However after completion of the mission and after complete postflight analysis of the data, the results could be compared with the EVA crewman's subjective evaluation of the workloads; thus, a better base for planning future lunar traverses could be established.

The results obtained from the Apollo 11 mission were used to plan rest periods and to establish limits on heart and respiratory rates (not only absolute limits but also limits for predictions of developing difficulties). These results led to an extension of the lunar surface stay time for the Apollo 12 mission without loss of confidence. Similarly, the experience and information gained from preceding missions were incorporated into the planning for the next mission. The confidence level increased as the information base increased; both stay times and useful work on the lunar surface increased, and a high level of confidence was maintained that safety had not been adversely affected.

During the actual EVA, the flight surgeon had to be ready at all times to make recommendations concerning the advisability of continuing an activity or to aid in planning a deviation in the mission plan. The principal concerns of the flight surgeon were the reserve capacity of the crewman and his physiological status. The physiological status was based on a variety of factors, some of which were historical (e.g., the extent of deconditioning resulting from 3 days of weightlessness during translunar coast, the amount of fatigue, the preflight physical condition of the crewman, the individual crewman response observed during training for specific activities, the amount and kind of exercise used by the crewman during translunar coast, and the amount and depth of sleep obtained by the crewman). Other factors were real time in that they were derived from current activity. Within this context, the flight surgeon required data on both the cumulative and the peak energy demands being experienced by the crewman during the EVA. Data on cumulative energy expenditures are most directly applied in determining the status of consumables and in determining the general physical status and reserve. Excessively high heart rates, hyperventilation, and heat storage can be related to instantaneous peaks of energy expenditure. Therefore, data that tend to quantitate these peaks are evaluated and used as specifics in the total consideration of crew status.

The integration of the three methods has provided both cumulative and peak data. Use of these data during the mission has prevented the crewmen from exceeding preset heart-rate and respiratory-rate limits and has assured that physiological limits for heat storage were not exceeded.

Heart rates higher than those expected were noted during Apollo EVA periods. Because these increases were present during both rest and work periods, it is thought that they resulted from deconditioning experienced during the first 3 days of translunar coast weightlessness. These higher heart rates have been carefully included in all considerations. With more understanding of the biomedical effects of both weightlessness and lunar surface exposure, techniques may be developed to minimize the undesirable changes.

RESULTS AND ANALYSIS

Because of the problems experienced in using each of the three assessment methods, the real-time values reported to the flight surgeon and the PLSS consumables analysts were integrated values. When determining an assessed metabolic rate, the team leader examined the results of all three methods together with all other PLSS telemetry data. After the flight, this integrated result was further updated by comparing the results of actual sublimator water supply measurements, water tank warning tones,[1] PLSS lithium hydroxide canister analysis (Apollo 9 only), and oxygen-method maximum (assuming suit oxygen leakage was zero). Actual sublimator water supply measurements, which were made by the crewmen immediately after the EVA, and water tank warning tones supplied a maximum limit to the integrated results. All errors (such as water spillage) decreased the measured water remaining, increasing the apparent metabolic rate. Total oxygen used also provided an upper limit to the average metabolic rate (assuming suit oxygen leakage was zero). Lithium hydroxide analysis, performed on the Apollo 9 canister, provided a basis for determining carbon dioxide production, thus an assessment of RQ, which was then used to refine the oxygen-method and LCG-method results. The postflight integrated metabolic results for the Apollo Program extravehicular activities are shown in table I. The overall error of integrated metabolic assessments made during the Apollo flights was estimated to be 10 to 15 percent, based on method variability.

[1] On the Apollo 15 to 17 missions, which had auxiliary sublimator water tanks, a warning tone sounded when the main tank was depleted.

TABLE 1. - METABOLIC EXPENDITURES FOR APOLLO LUNAR SURFACE EVA

Apollo mission	EVA	Crewman (a)	Metabolic rate										EVA duration, hr
			ALSEP deployment		Geological station activity		Overhead		Lunar roving vehicle operations		Total for all activities		
			kJ/hr	Btu/hr	kJ/hr	Btu/hr	kJ/hr	Btu/hr	kJ/hr	Btu/hr	kJ/hr	Btu/hr	
11	1	CDR	818	775	1023	969	899	851	--	--	949	900	2.43
		LMP	1267	1200	1471	1393	1269	1202	--	--	1267	1200	
12	1	CDR	864	818	1017	963	1232	1167	--	--	1019	975	3.90
		LMP	1006	953	1028	974	1119	1060	--	--	1054	1000	
	2	CDR	--	--	913	865	902	854	--	--	922	875	3.78
		LMP	-	-	1058	1002	1038	983		-	1054	1000	
14	1	CDR	762	722	1230	1165	920	871	-	-	843	800	4.80
		LMP	947	897	729	690	1084	1027	--	-	980	930	
	2	CDR	494	468	996	943	895	848	--	--	959	910	3.58
		LMP	851	806	1120	1061	894	847	--	--	1054	1000	
15	1	CDR	1182	1119	1153	1092	1417	1342	639	605	1159	1100	6.53
		LMP	1369	1297	778	737	1226	1161	435	412	1033	980	
	2	CDR	1019	965	1227	1162	1202	1138	624	591	1054	1000	7.22
		LMP	1110	1051	792	750	1116	1057	414	392	854	810	
	3	CDR	1095	1037	1013	959	1303	1234	578	547	1086	1030	4.83
		LMP	962	911	788	746	981	929	447	423	854	810	
16	1	CDR	869	823	905	857	1146	1085	725	687	917	870	7.18
		LMP	1081	1024	925	1065	1154	1093	666	631	1065	1010	
	2	CDR	--	--	933	884	1044	989	470	445	822	780	7.38
		LMP	--	--	1023	969	987	935	438	415	874	830	
	3	CDR	--	--	966	915	983	931	518	491	854	810	5.67
		LMP	--	--	1013	959	1107	1048	430	407	864	820	
17	1	CDR	1192	1129	1094	1036	1267	1200	506	479	1150	1090	7.20
		LMP	1166	1104	1255	1189	1193	1130	472	447	1139		
	2	CDR	--	--	1094	1036	1267	1200	506	479	869	820	7.62
		LMP	--	--	1255	1189	1193	1130	472	447	874	830	
	3	CDR	--	--	1094	1036	1267	1200	506	479	980	930	7.25
		LMP	--	--	1255	1189	1193	1130	472	447	990	940	
Mean			1024	970	1024	970	1130	1070	518	490	980	930	
Total time, hr			28.18		52.47		52.83		25.28		158.76		

[a] CDR = commander, LMP = lunar module pilot

CONCLUDING REMARKS

The following conclusions are based on Apollo Program metabolic expenditure measurement estimations. The three methods of metabolic assessment, used with knowledge of their deficiencies, proved to be valuable indicators of crewman metabolic production. The overall average metabolic production of Apollo crewmen during extravehicular activity on the lunar surface ranged from 823×10^3 to 1267×10^3 J/hr (780 to 1200 Btu/hr).

Lyndon B. Johnson Space Center
National Aeronautics and Space Administration
Houston, Texas, September 25, 1974
914-50-95-13-72

REFERENCES

1. Stolwijk, J. A. J.: A Mathematical Model of Physiological Temperature Regulation in Man. NASA CR-1855, 1971.

2. Waligora, James M.; and Michel, Edward L.: Application of Conductive Cooling for Working Men in a Thermally Isolated Environment. Aerospace Med., vol. 39, no. 5, May 1968, pp. 485-487.

NASA-Langley, 1975 S-394

NATIONAL AERONAUTICS AND SPACE ADMINISTRATION
WASHINGTON, D C 20546

OFFICIAL BUSINESS
PENALTY FOR PRIVATE USE $300

SPECIAL FOURTH-CLASS RATE BOOK

POSTAGE AND FEES PAID
NATIONAL AERONAUTICS AND SPACE ADMINISTRATION
451

U.S.MAIL

POSTMASTER If Undeliverable (Section 158 Postal Manual) Do Not Return

"The aeronautical and space activities of the United States shall be conducted so as to contribute . . . to the expansion of human knowledge of phenomena in the atmosphere and space. The Administration shall provide for the widest practicable and appropriate dissemination of information concerning its activities and the results thereof."

—NATIONAL AERONAUTICS AND SPACE ACT OF 1958

NASA SCIENTIFIC AND TECHNICAL PUBLICATIONS

TECHNICAL REPORTS Scientific and technical information considered important, complete, and a lasting contribution to existing knowledge.

TECHNICAL NOTES Information less broad in scope but nevertheless of importance as a contribution to existing knowledge

TECHNICAL MEMORANDUMS Information receiving limited distribution because of preliminary data, security classification, or other reasons. Also includes conference proceedings with either limited or unlimited distribution.

CONTRACTOR REPORTS Scientific and technical information generated under a NASA contract or grant and considered an important contribution to existing knowledge.

TECHNICAL TRANSLATIONS Information published in a foreign language considered to merit NASA distribution in English

SPECIAL PUBLICATIONS Information derived from or of value to NASA activities. Publications include final reports of major projects, monographs, data compilations, handbooks, sourcebooks, and special bibliographies

TECHNOLOGY UTILIZATION PUBLICATIONS Information on technology used by NASA that may be of particular interest in commercial and other non-aerospace applications Publications include Tech Briefs, Technology Utilization Reports and Technology Surveys

Details on the availability of these publications may be obtained from:

SCIENTIFIC AND TECHNICAL INFORMATION OFFICE

NATIONAL AERONAUTICS AND SPACE ADMINISTRATION

Washington, D.C. 20546

TABLE E1.- SUMMARY OF APOLLO G-MISSION LUNAR SURFACE EMU[1] POST FLIGHT THERMAL ANALYSIS RESULTS

		APOLLO 11		APOLLO 12				APOLLO 14			
		EVA 1		EVA 1		EVA 2		EVA 1		EVA 2	
		CDR[2]	LMP[3]	CDR	LMP	CDR	LMP	CDR	LMP	CDR	LMP
	EVA TIME, MIN.	150		226		224		288		276	
THERMAL ANALYSIS RESULTS	ASTRONAUT METABOLIC RATE IMPOSED ON EMU, BTU/HR	900	1200	975	1000	875	1000	800	930	910	1000
	EMU HEAT LEAKAGE, BTU/HR	-25	-25	-100	-100	0	0	-140	-140	135	135
	EMU OXYGEN LEAKAGE, LB/HR							0.001	0.041	0.024	0.025
CONSUM-ABLE ANALYSIS RESULTS	USABLE OXYGEN REMAINING, %							40	8	20	9
	USABLE FEEDWATER REMAINING, %							38	27	20	11
	POWER REMAINING, %							15	12	17	18
	LiOH REMOVAL CAPACITY REMAINING, %							66	62	62	59

[1] EMU = Extravehicular Mobility Unit (NASA Apollo A7LB Space Suit + LCG + PLSS)

[2] CDR = Mission Commander

[3] LMP = Lunar Module Pilot

TABLE E1.- CONTINUED

		APOLLO 15						APOLLO 16					
		EVA 1		EVA 2		EVA 3		EVA 1		EVA 2		EVA 3	
		CDR	LMP	CDR	LMP	CDR	LMP	CDR	LMP	CDR	LMP	DCR	LMP
	EVA TIME, MIN	392		433		290		398		436		336	
THERMAL ANALYSIS RESULTS	ASTRONAUT METABOLIC RATE IMPOSED ON EMU, BTU/HR	1100	980	1000	810	1030	810	870	1010	780	830	810	820
	EMU HEAT LEAKAGE, BTU/HR	30	30	120	120	175	175	135	135	220	220	295	295
	EMU OXYGEN LEAKAGE, LB/HR	0.032	0.011	0.028	0.018	0.051	0.023	0.019	0.013	0.021	0.020	0.020	0.020
CONSUMABLE ANALYSIS RESULTS	USABLE OXYGEN REMAINING, %	7	15	9	25	33	46	33	17	24	20	45	37
	USABLE FEEDWATER REMAINING, %	18	17	14	30	42	45	30	9	24	20	34	33
	POWER REMAINING, %	21	20	12	18	39	41	28	23	10	12	31	34
	LiOH REMOVAL CAPACITY REMAINING, %	4	11	25	49	50	57	49	2	59	48	60	58

		APOLLO 17					
		EVA 1		EVA 2		EVA 3	
		CDR	LMP	CDR	LMP	CDR	LMP
	EVA TIME, MIN	432		457		435	
THERMAL ANALYSIS RESULTS	ASTRONAUT METABOLIC RATE IMPOSED ON EMU, BTU/HR	1090	1080	820	830	930	940
	EMU HEAT LEAKAGE, BTU/HR	15	15	185	185	305	305
	EMU OXYGEN LEAKAGE, LB/HR		0.029	0.006	0.026	0.006	0.029
CONSUMABLE ANALYSIS RESULTS	USABLE OXYGEN REMAINING, %		7	13	12	12	8
	USABLE FEEDWATER REMAINING, %		8	11	18	5	13
	POWER REMAINING, %		8	15	4	19	8
	LiOH REMOVAL CAPACITY REMAINING, %		9	44	47	33	33

TABLE E2. SELECTED LIVE APOLLO EVA DAT/

/ND RTCC METABOLIC RATE COMPUTATIONS

MISSION	EVA TIME, MIN	ASTRONAUT	LCG ΔT, °C	LCG INLET TEMP., °C	LCG HEAT REMOVAL RATE, WATTS	REAL-TIME METABOLIC RATE, WATTS
APOLLO 11, EVA 1	+24	CDR	1.1	26	141	220
	+24	LMP	3.5	7.2	437	542
	+48	CDR	1.5	21.5	185	210
	+48	LMP	2.1	16	267	293
APOLLO 12, EVA 2	+42	CDR	0.67	25	135	161
	+42	LMP	1.3	21	200	256
	+93	CDR	2.8	18.5	352	501
		CDR	0.8	23	175	192
	+201	LMP	1.9	13	306	350
APOLLO 15, EVA 1	+36	CDR	1.8	20	237	337
	+180	CDR	1.7	19.5	275	388
	+180	LMP	1.4	17.5	247	276
	+270	CDR	1.5	18	267	327
	+270	LMP	1.4	16	250	259
APOLLO 17, EVA 1	+90	CDR	1.6	19	249	304
	+90	LMP	1.7	19	287	385
	+210	LMP	1.7	15.5	275	336
	+270	LMP	1.8	17	290	386
	+360	CDR	1.3	20	205	254

APPENDIX F

FORMULATION OF THE NEW MATHEMATICAL MODEL

KEY TO MATHEMATICAL SYMBOLS FOR THE PASSIVE SYSTEM

A_J	Area of skin element $_J$
B	Radiosity
ε_J	Emissivity of skin element $_J$
F_{JW}	Configuration factor
H	Irradiation
h	Heat transfer coefficient
h_D	Mass transfer coefficient
I	Index for internal temperature locations
J	Index for skin temperature locations
k	Thermal conductivity of tissue element
(mc)	Product of mass and specific heat of tissue element
$(\dot{m}c)_b$	Product of local bloodflow rate and specific heat of blood
q_c	Convective heat transfer rate at the skin surface
q_m	Local tissue heat generation rate
q_{Rad}	Radiative heat transfer rate at the skin surface
q_s	Evaporative heat transfer rate at the skin surface
r	Radius
T	Temperature of tissue element
t	Time
T_b	Temperature of the central bloodstream
VPP(T)	Vapor pressure at temperature T
θ	Angle
ρ_J	Reflectivity of skin element $_J$

1. TECHNICAL DESCRIPTION OF A NEW MATHEMATICAL MODEL

a. Passive Model

The body will be divided into cylindrical segments representing the head, torso, abdomen, and both arms, hands, legs, and feet. The primary objective of this effort will be the description of the temperature field angularly as well as radially (see Figure 1). Thus, the pertinent equation in cylindrical coordinates is:

$$(mc)\frac{\partial T}{\partial t} = k\left\{\frac{\partial^2 T}{\partial r^2} + \frac{1}{r}\frac{\partial T}{\partial r} + \frac{1}{r^2}\frac{\partial^2 T}{\partial \theta^2}\right\} + (\dot{m}c)_b(T-T_b) + q_m \qquad (1)$$

Where the term on the left hand side represents heat stored in the tissues, the bracketed term on the right hand side is heat transferred by conduction to other tissue elements, the second term on the right hand side is heat transferred from the tissue to the bloodstream by convection, and the last term, q_m, represents metabolic heat generation.

Each of the major segments will be further divided into subsegments. The subsegments will be chosen in such a way that the physical properties and temperatures in the longitudinal direction are constant. Thus, for example, subsegments B and C in Figure 2 contain the heart and lungs and subsegment E contains the liver. The actual number of subsegments to be considered will depend upon the number of major organs for which data is obtainable and will be decided at the conclusion of a literature search.

It should be noted that the bloodflow rate to each element, $(mc)_b$, is variable and controlled by the active thermoregulatory system. The temperature of the central blood pool, T_b, is also variable and is determined by a heat balance of the form:

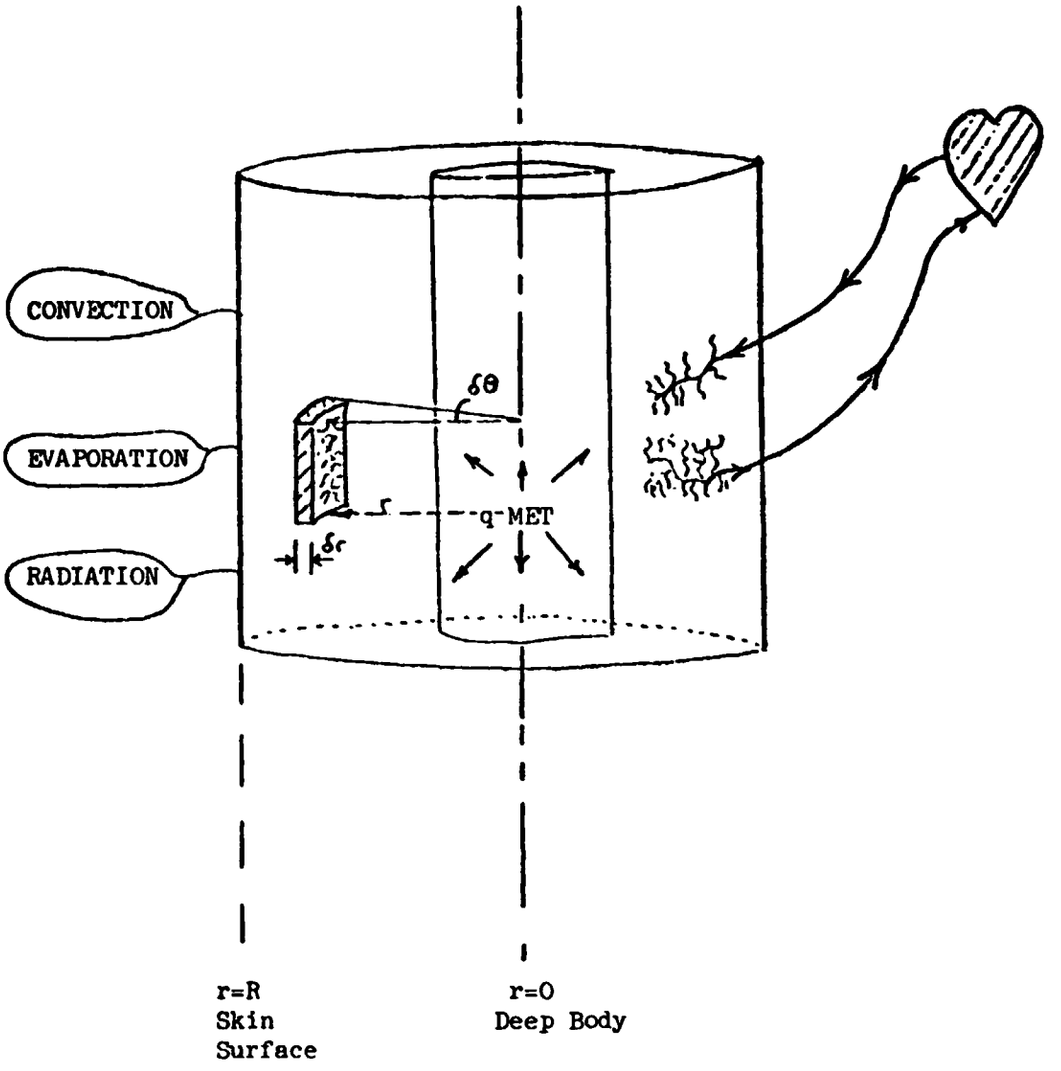

HEAT CONDUCTED BETWEEN TISSUE ELEMENTS RADIALLY AND ANGULARLY + HEAT TRANSFERRED BY CONVECTION TO THE BLOODSTREAM + METABOLIC HEAT GENERATED = HEAT STORED IN THE TISSUE ELEMENT.

Figure 1. - Internal tissue element heat balance.

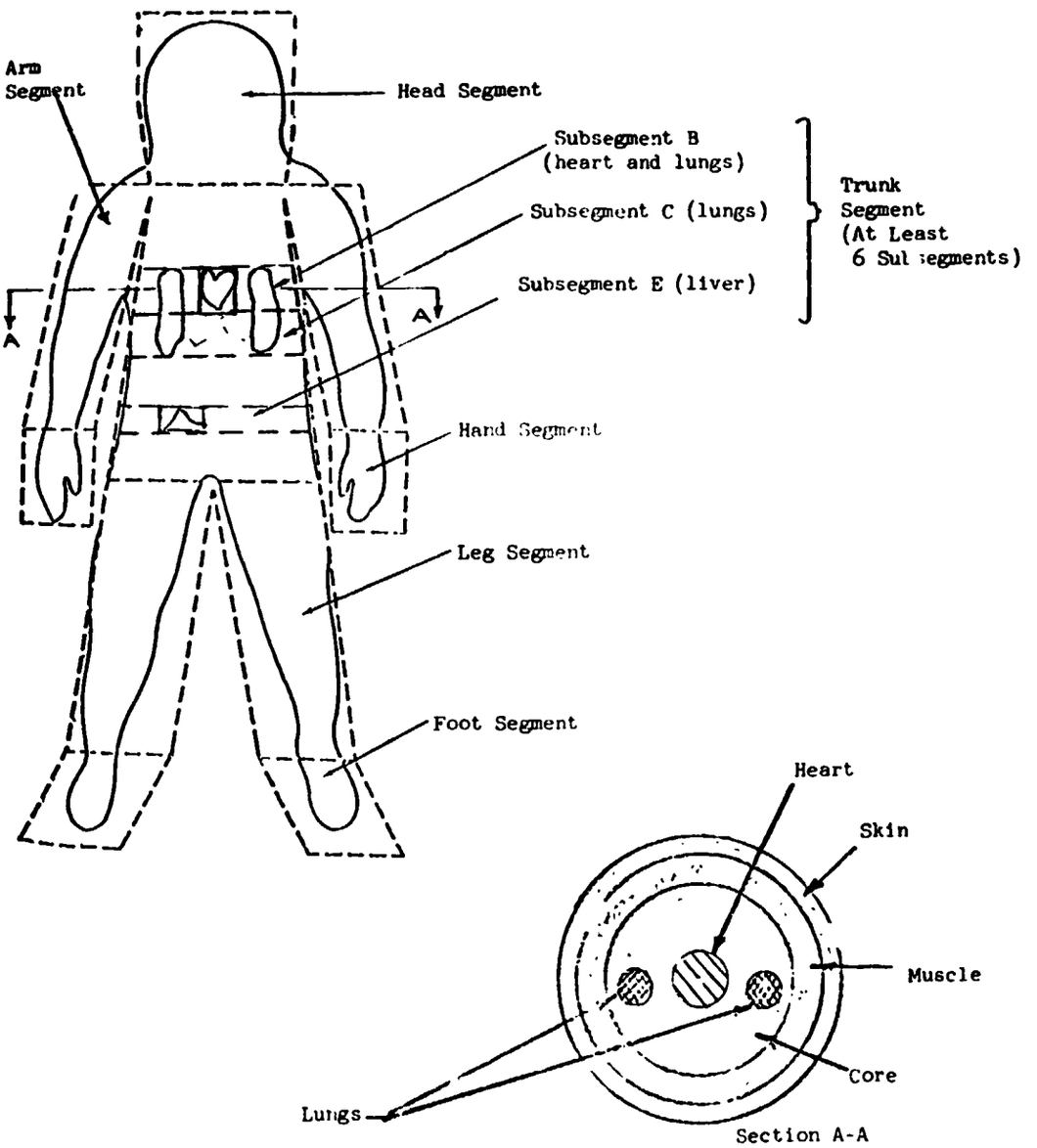
Arm Segment
Head Segment
Subsegment B (heart and lungs)
Subsegment C (lungs)
Subsegment E (liver)
Trunk Segment (At Least 6 Subsegments)
A
A
Hand Segment
Leg Segment
Foot Segment
Heart
Skin
Muscle
Core
Lungs
Section A-A

Figure 2.

$$(mc)_b \frac{dT_b}{dt} = \sum_{I=1}^{N} (\dot{m}c)_{b_I} (T_b - T_1) \quad (2)$$

The boundary condition to be imposed at the skin surface of each of the subsegments is:

$$-k \frac{\partial T}{\partial r} = q_c + q_s + q_{Rad}. \quad (3)$$

Where q_c, q_{Rad}, and q_s are the rates of heat transfer by convection, radiation, and evaporation at the skin surfaces.

Convective Heat Transfer

The amount of heat transferred by convection from the various skin surfaces to the air surrounding a man is

$$q_c = hA_J (T_J - T_{air}) \quad (4)$$

Where T_J is the skin temperature of segment $_J$. The heat transfer coefficient, h, is determined from the solution of the equations of momentum and energy for the specific physical system considered. Treating the skin surfaces as a flat plate with air flowing parallel to it leads to the resulting expression for h:

$$\frac{hL}{k} = Nu = .662\ Re^{1/2} Pr^{1/3} \quad (5)$$

Solving the same equations for air flowing perpendicular to a vertical cylinder leads to a similar result. In either case, the magnitude of h for normal surrounding environments is usually low enough so that convective heat transfer at the skin surface by itself is not adequate to remove internal body heat generation. Solution of the equations governing free convection leads to a similar conclusion.

Radiative Heat Transfer

The heat transferred by radiation at the skin surface to the surrounding environment is:

$$q_{Rad} = B - H \tag{6}$$

where B = radiosity

H = Irradiation

Utilizing expressions for radiosity and irradiation for diffuse-diffuse (skin-wall surface) interchange, we derive:

$$q_{Rad} = \frac{A_J \varepsilon_J \sigma}{1-\varepsilon_J} \left\{ T_J^4 - \frac{\varepsilon_J T_J^4 + \rho_J F_{J\omega} \varepsilon_\omega T_\omega^4}{1-\rho_J \rho_\omega F_{J\omega}^2 A_J/A_\omega} \right\} \tag{7}$$

Where A_J = area of skin element $_J$

ε_J = emissivity of skin element $_J$

ρ_J = reflectivity of skin element $_J$

F_{JW} = configuration factor between skin element $_J$ and surroundings (wall)

For the general case of a man in a large room (Aw >> A_J), equation 7 reduces to:

$$q_{Rad} = A_J \varepsilon_J \sigma \ (T_J - \varepsilon_w F_{Jw} T_w^4) \tag{8}$$

This is the radiation boundary condition for each skin surface subsegment.

Evaporative Heat Transfer

The quantity of heat transferred by evaporation of water from the skin surface to the environment is highly variable and under the control of the active thermoregulatory system. Water (sweat) is a

normal byproduct of the body's metabolic processes. Since the partial pressure of water vapor at the surface of the skin is usually greater (due to these processes) than the partial pressure of water vapor in the surrounding atmosphere, diffusion occurs. However, if the metabolic rate, and consequently heat generation, is increased due to heavy workloads, etc., diffusion, radiation, and sensible convection may not be enough to dissipate the excessive production of heat. If this occurs, body temperatures begin to rise. If these temperatures increase appreciably above certain control values, geometrically distributed sweat glands pour excessive water, resulting from the increased metabolic rate, onto the skin surface. The sweat on the surface of the skin will then absorb heat as it evaporates. As long as the environment remains within certain bounds, all of the sweat on the skin compartment surface will be evaporated. However, if the environment is such that the maximum amount of sweat that can be evaporated is less than the amount being produced, the body will not be able to dissipate the difference, and, consequently, will store heat.

This maximum evaporative capacity, EMAX, is the mass transfer expression

$$EMAX = h_D A_J \left(VPP(T_J) - VPP\ (T_{dew})\right) \tag{9}$$

where h_D is a mass transfer coefficient, A is the skin compartment area, and VPP(T) and $VPP(T_{dew})$ are partial water vapor pressures evaluated at the skin surface and in the air stream, respectively. The mass transfer coefficient h_D, is determined by applying the heat-mass transfer analogy to the convective heat transfer coefficient

previously discussed. The amount of sweat generated at the skin surface, SWEAT, is determined by thermoregulatory control. Thus, the quantity of heat transferred by evaporation at the skin surface is

$$q_s = \begin{cases} SWEAT & SWEAT < EMAX \\ EMAX & EMAX < SWEAT \end{cases}$$

Summarizing then, equations 1, 2, and 3 are the basic equations necessary to describe the human temperature system. These equations will be utilized with equations 4 - 9 for each major subsegment. The number of subsegments will be chosen based on data availability.

b. Active Thermoregulatory Control System

The controlling system for this mathematical model is identical to that described in Section 2 and Appendix B for the current model.

2. NUMERICAL METHOD

The basic equations that must be solved numerically to determine the temperature field are:

$$(mc)\frac{\partial T}{\partial t} = k\left\{\frac{\partial^2 T}{\partial r^2} + \frac{1}{r}\frac{\partial T}{\partial r} + \frac{1}{r^2}\frac{\partial^2 T}{\partial \theta^2}\right\} + q_m + (\dot{m}c)_b(T-Tb) \qquad (1)$$

$$(mc)_b \frac{dT_b}{dt} = \sum_{J=1}^{n} (\dot{m}c)_{b_1} (T-T_b) \qquad (2)$$

$$-k\frac{\partial T}{\partial r} = q_{Rad} + q_s + q_c \qquad (3)$$

Since a large matrix of equations are to be handled, an implicit scheme will be employed in order to reduce computer run time and minimize stability problems. Central difference approximations will be used were feasible to reduce error. Utilizing the Taylor series approximations for the derivatives in equations 1, 2, and 3,:

$$\frac{\partial^2 T}{\partial r^2} = \frac{T_{r+i,\theta} + T_{r-1,\theta} - 2T_{r,\theta}}{(\Delta r)^2} \quad + \text{4th and higher order terms}$$

$$\frac{\partial T}{\partial r} = \frac{T_{r+i,\theta} - T_{r-i,\theta}}{2\Delta r} \quad + \text{3rd and higher order terms} \qquad (10)$$

$$\frac{\partial^2 T}{\partial \theta^2} = \frac{T_{r,\theta+1} + T_{r,\theta-1} - 2T_{r,\theta}}{(\Delta\theta)^2} \quad + \text{4th and higher order terms}$$

$$\frac{\partial T}{\partial t} = \frac{T^{t+1}_{r,\theta} - T^{t}_{r,\theta}}{\Delta t} \quad + \text{2nd and higher order terms}$$

Substituting these expressions (and neglecting 2nd and higher order terms), the numerical approximation for equation 1 is:

$$(mc)\frac{T^{t+1}_{r,\theta} - T^{t}_{r,\theta}}{\Delta t} = k\left\{\frac{T^{t+1}_{r+1,\theta} + T^{t+1}_{r-1,\theta} - 2T^{t+1}_{r,\theta}}{(\Delta r)^2} + \frac{T^{t+1}_{r+1,\theta} - T^{t+1}_{r-1,\theta}}{2r\Delta r}\right.$$

$$\left. + \frac{T^{t+1}_{r,\theta+1} + T^{t+1}_{r,\theta-1} - 2T^{t+1}_{r,\theta}}{r^2(\Delta\theta)^2}\right\} + q_{m_{r,\theta}} \qquad (11)$$

$$+ (\dot{m}c)_b\,(T^{t+1}_{r,\theta} - T^{t+1}_{b}) \qquad \text{- Internal Temperature Field}$$

The derivation of equation 11 assumes that the thermal properties are fairly constant over the entire internal field. If this is not the case, then discontinuities must be taken into account. For example, if there is a discontinuity in the conductivity, k, at the muscle-skin boundary (Figure 3), then equation 11 can be applied within the skin annulus, and

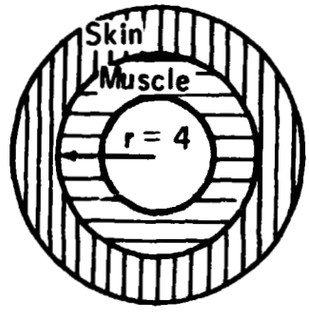

Figure 3

also within the muscle annulus, but not at the interface between them. At the skin-muscle interface, an additional boundary condition must be considered - flux equality. Thus, for example at r = 4,

$$-k_m \frac{\partial T}{\partial r} = -k_s \frac{\partial T}{\partial r} \qquad (12)$$

Utilizing the appropriate numerical approximation,

$$\frac{k_m\left(T^{t+1}_{r,\theta} - T^{t+1}_{r-1,\theta}\right)}{\Delta r} = \frac{k_s\left(T^{t+1}_{r+1,\theta} - T^{t+1}_{r,\theta}\right)}{\Delta r} \quad \text{at}_{r=4} \tag{13}$$

Another problem arises along the central axis of a subsegment. The determination of the central axis temperature presents a unique problem because equation 11 cannot be evaluated at r = 0. This problem is circumvented by choosing the grid spacing so that the temperature at the axis is never actually calculated. This objective can be accomplished by spacing the last grid point one-half an increment removed fromthe boundary as shown in Figure 4. In this arrangement, the temperature one-half an increment on either side of the center line is calculated. These are then related by the periodicity boundary condition:

$$\begin{matrix} T_{r=0_1} = T_{r=1_1} \\ \theta=\theta_2 \quad \theta=\theta_1+\Pi \end{matrix} \tag{14}$$

The fictious temperature, T_θ, is then eliminated by approximating the boundary condition at the skin surface by a central difference expression:

$$-k\frac{\partial T}{\partial r} = -k\left(\frac{T_{R+1/2} - T_{R-1/2}}{\Delta r}\right) + \text{3rd and higher order terms} \tag{15}$$

at
r=R

Therefore, neglecting the higher order terms.

$$-k\left(\frac{T_{6,\theta_1} - T_{5,\theta_1}}{\Delta r}\right) = q_{Rad} + q_c + q_s \tag{16}$$

and

$$T_{R,\theta_1} = \frac{T_{5,\theta_1} + T_{6,\theta_1}}{2} \tag{17}$$

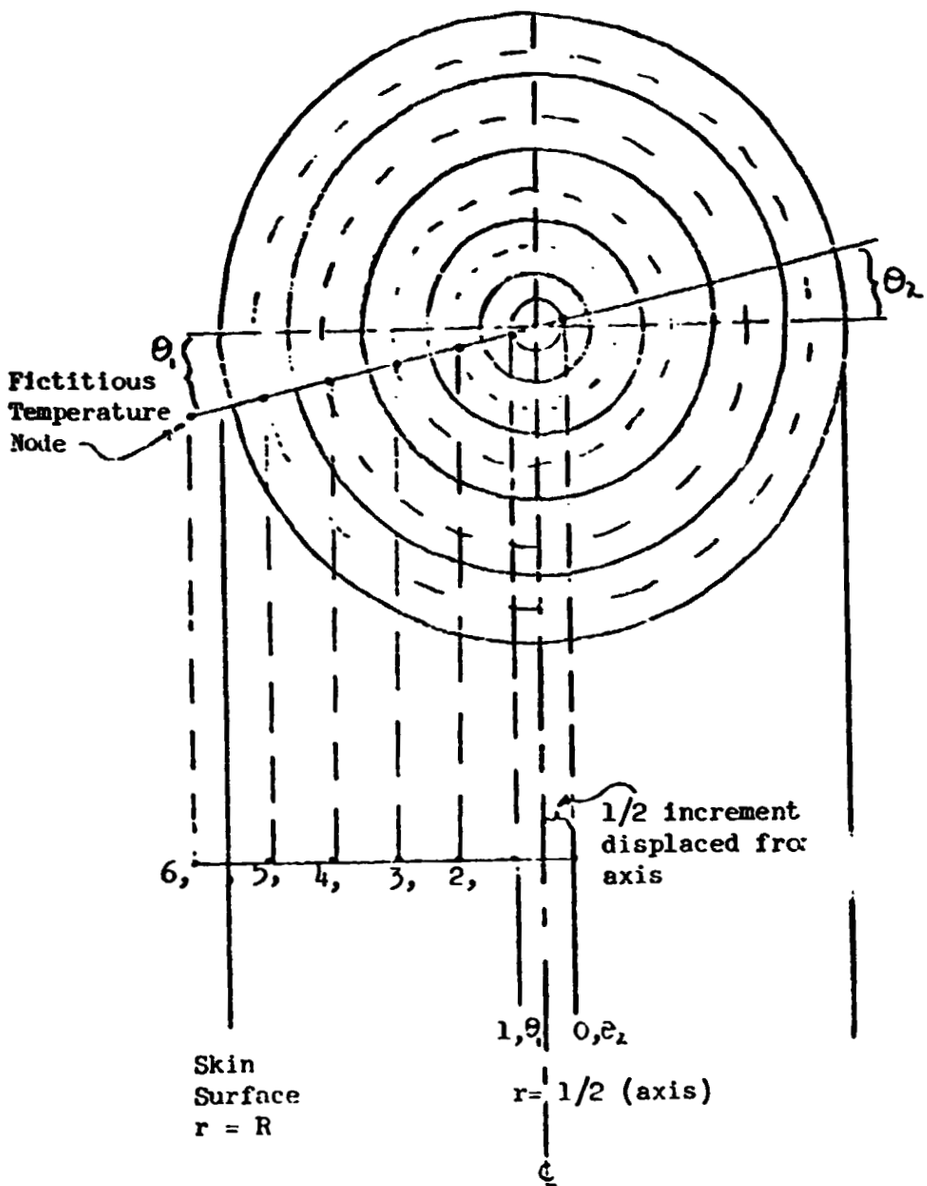
θ_2
θ_1
Fictitious
Temperature
Node
1/2 increment
displaced from
axis
6,
5,
4,
3,
2,
1, θ_1
0, θ_2
Skin
Surface
r = R
r= 1/2 (axis)
℄

Figure 4.

The temperature of the central blood pool is found from:

$$(mc)_b \frac{\left(T_b^{t+1} - T_b^t\right)}{\Delta\tau} = \sum_{\text{all } r,\theta} (\dot{m}_{r,\theta} c)_b \left(T_{r,\theta}^{t+1} - T_b^{t+1}\right) \tag{18}$$

Equations 11, 13, 16, and 18 are then the finite difference equations that must be solved for each subsegment in order to specify the temperature field of the human body. A most convenient means of solving this large matrix of equations is the alternating difference implicit technique (ADI). In this scheme, a matrix of the form shown in Figure 5 is used.

The temperature field is solved implicitly in the radial direction at time t + 1/2 using explicit values for the derivatives in the θ direction. The field is then determined implicitly in the angular direction at time t + 1 using explicit values of the derivatives in the radial direction calculated at time t + 1/2. Thus, for example

$$(mc)_{r,\theta} \frac{\left(T_{r,\theta}^{t+1/2} - T_{r,\theta}^{t}\right)}{\Delta t/2} = k_{r,\theta} \left\{ \frac{T_{r+1,\theta}^{t+1/2} \quad T_{r-1,\theta}^{t+1/2} - 2T_{r,\theta}^{t+1/2}}{(\Delta r)^2} + \frac{T_{r+1,\theta}^{t+1/2} - T_{r-1,\theta}^{t+1/2}}{2r\Delta r} \right.$$

$$\left. + \frac{T_{r,\theta+1}^{t} + T_{r,\theta-1}^{t} - 2T_{r,\theta}}{r^2(\Delta\theta)^2} \right\} + q_{m_{r,\theta}}$$

$$+ (\dot{m}c)_{r,\theta} \left(T_{r,\theta}^{t+1/2} - T_b^{t+1/2}\right)$$

The values of $T_{r,\theta}^{t+1/2}$ thus determined throughout the matrix are ther used explicitly in the same equation. Except now, variations in the θ direction

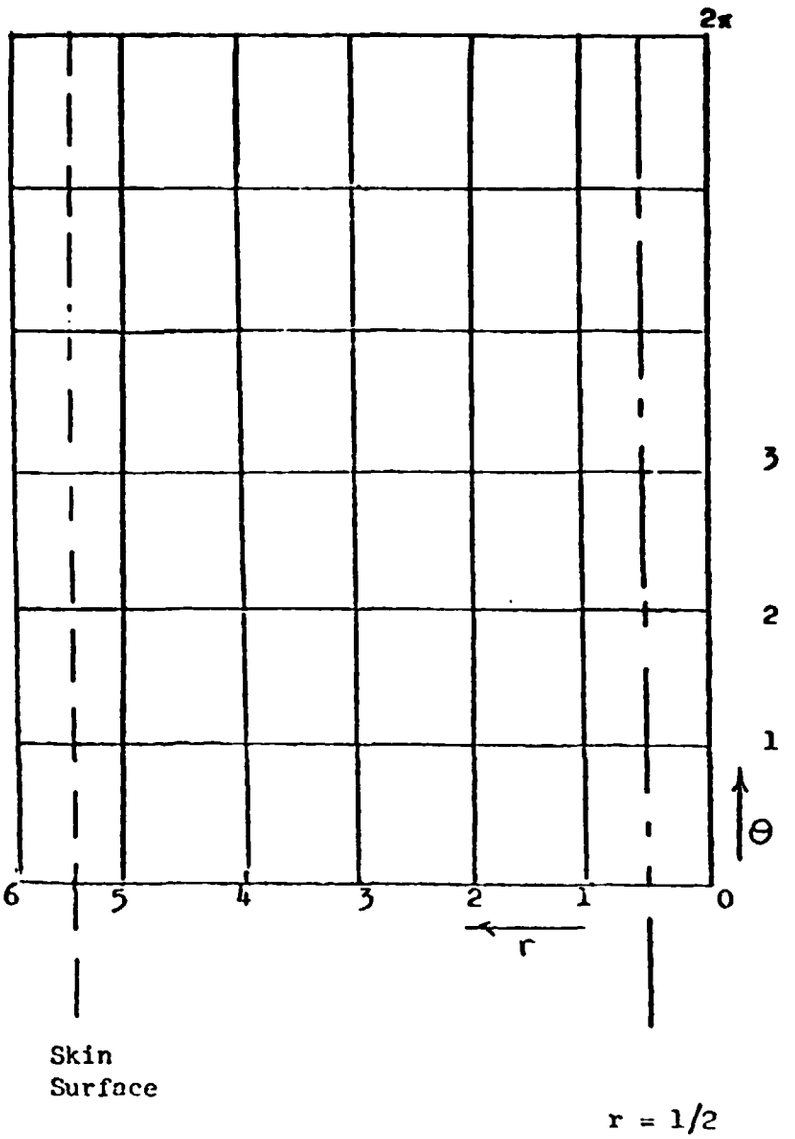

Figure 5. - Solution grid for ADI method.

are treated implicitly to determine $T_{r,\theta}^{t+1}$. This marching procedure is repeated for each full time step until all matrix temperatures are known for all time and the temperature field is thus specified.

It is proposed to check the accuracy of this numerical approximation by comparing the results with those for which a closed form solution is obtainable.